frontiers | Research Topics

Improving our understanding of the management and pathogenesis of rare and neglected tumors of the central and peripheral nervous system

Edited by
Laura Gatti, Ignazio Gaspare Vetrano and Pierpaolo Alongi

Published in
Frontiers in Oncology
Frontiers in Neurology

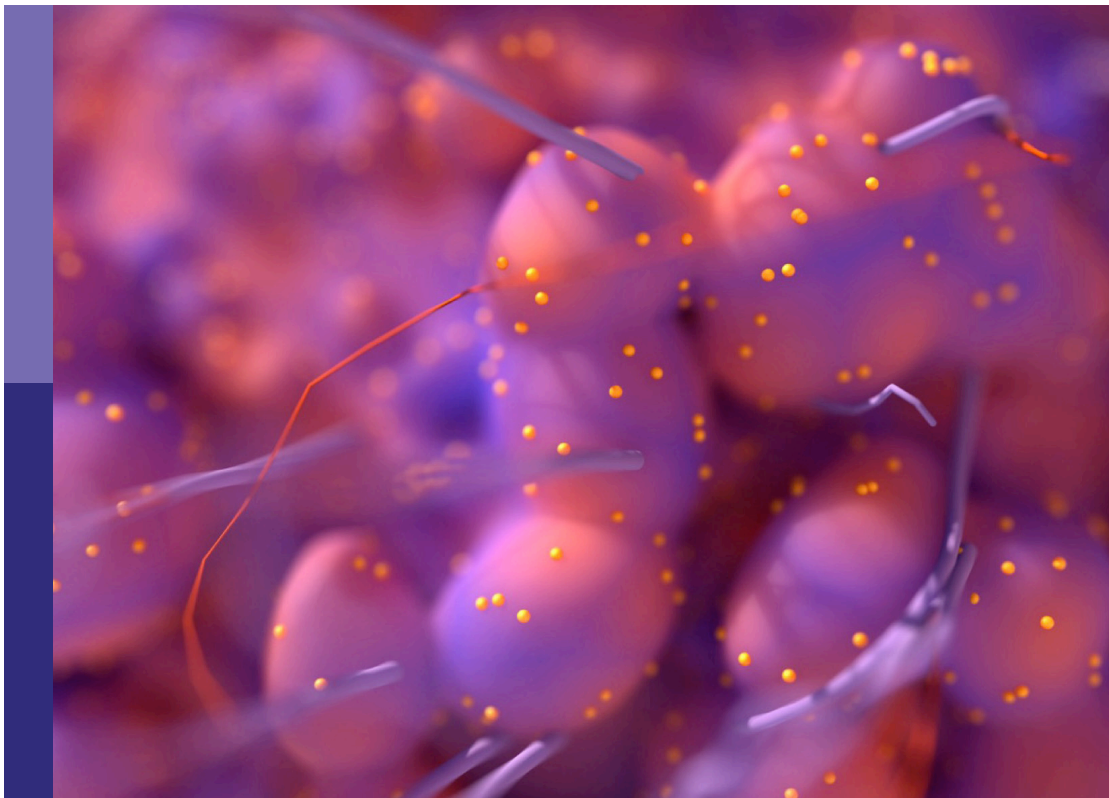

ISSN 1664-8714
ISBN 978-2-83252-071-0
DOI 10.3389/978-2-83252-071-0

About Frontiers

Frontiers is more than just an open access publisher of scholarly articles: it is a pioneering approach to the world of academia, radically improving the way scholarly research is managed. The grand vision of Frontiers is a world where all people have an equal opportunity to seek, share and generate knowledge. Frontiers provides immediate and permanent online open access to all its publications, but this alone is not enough to realize our grand goals.

Frontiers journal series

The Frontiers journal series is a multi-tier and interdisciplinary set of open-access, online journals, promising a paradigm shift from the current review, selection and dissemination processes in academic publishing. All Frontiers journals are driven by researchers for researchers; therefore, they constitute a service to the scholarly community. At the same time, the *Frontiers journal series* operates on a revolutionary invention, the tiered publishing system, initially addressing specific communities of scholars, and gradually climbing up to broader public understanding, thus serving the interests of the lay society, too.

Dedication to quality

Each Frontiers article is a landmark of the highest quality, thanks to genuinely collaborative interactions between authors and review editors, who include some of the world's best academicians. Research must be certified by peers before entering a stream of knowledge that may eventually reach the public - and shape society; therefore, Frontiers only applies the most rigorous and unbiased reviews. Frontiers revolutionizes research publishing by freely delivering the most outstanding research, evaluated with no bias from both the academic and social point of view. By applying the most advanced information technologies, Frontiers is catapulting scholarly publishing into a new generation.

What are Frontiers Research Topics?

Frontiers Research Topics are very popular trademarks of the *Frontiers journals series*: they are collections of at least ten articles, all centered on a particular subject. With their unique mix of varied contributions from Original Research to Review Articles, Frontiers Research Topics unify the most influential researchers, the latest key findings and historical advances in a hot research area.

Find out more on how to host your own Frontiers Research Topic or contribute to one as an author by contacting the Frontiers editorial office: frontiersin.org/about/contact

Improving our understanding of the management and pathogenesis of rare and neglected tumors of the central and peripheral nervous system

Topic editors

Laura Gatti — IRCCS Carlo Besta Neurological Institute Foundation, Italy
Ignazio Gaspare Vetrano — Department of Neurosurgery, IRCCS Carlo Besta Neurological Institute Foundation, Italy
Pierpaolo Alongi — ARNAS Ospedali Civico Di Cristina Benfratelli, Italy

Citation

Gatti, L., Vetrano, I. G., Alongi, P., eds. (2023). *Improving our understanding of the management and pathogenesis of rare and neglected tumors of the central and peripheral nervous system*. Lausanne: Frontiers Media SA.
doi: 10.3389/978-2-83252-071-0

Table of contents

frontiers | Frontiers in Oncology

TYPE Editorial
PUBLISHED 17 March 2023
DOI 10.3389/fonc.2023.1162728

OPEN ACCESS

EDITED AND REVIEWED BY
David D. Eisenstat,
Royal Children's Hospital, Australia

*CORRESPONDENCE
Ignazio G. Vetrano
ignazio.vetrano@istituto-besta.it

SPECIALTY SECTION
This article was submitted to Neuro-Oncology and Neurosurgical Oncology, a section of the journal Frontiers in Oncology

RECEIVED 09 February 2023
ACCEPTED 06 March 2023
PUBLISHED 17 March 2023

CITATION
Vetrano IG, Alongi P and Gatti L (2023) Editorial: Improving our understanding of the management and pathogenesis of rare and neglected tumors of the central and peripheral nervous system. *Front. Oncol.* 13:1162728. doi: 10.3389/fonc.2023.1162728

Editorial: Improving our understanding of the management and pathogenesis of rare and neglected tumors of the central and peripheral nervous system

Ignazio G. Vetrano[1,2]*, Pierpaolo Alongi[3] and Laura Gatti[4]

[1]Department of Neurosurgery, Fondazione IRCCS Istituto Neurologico Carlo Besta, Milan, Italy, [2]Department of Biomedical Sciences for Health, Università degli Studi di Milano, Milan, Italy, [3]Nuclear Medicine Unit, A.R.N.A.S Ospedale Civico Di Cristina e Benfratelli, Palermo, Italy, [4]Neurobiology Laboratory, Fondazione IRCCS Istituto Neurologico Carlo Besta, Milan, Italy

KEYWORDS

DIPG (diffuse infiltrative pontine gliomas), intracranial lymphomas, MPNST (malignant peripheral nerve sheath tumors), pleomorphic xanthoastrocytomas, sodium fluorescein (SF), solitary fibrous tumor (SFT), astroblastoma, peripheral nerve sheath tumors

Editorial on the Research Topic
Improving our understanding of the management and pathogenesis of rare and neglected tumors of the central and peripheral nervous system

The Frontiers Research Topic titled "*Improving our Understanding of the Management and Pathogenesis of Rare and Neglected Tumors of the Central and Peripheral Nervous System*" includes 22 articles published from May 2022 to February 2023. This collection comprises 13 original research articles, 7 case reports, and 2 reviews, with the common aim to collect information about clinical and surgical management, new diagnostic techniques (pre-, post-, and intraoperative), innovative therapeutic therapies, as well as preclinical studies based on genetic, cellular, molecular, or omic approaches, dedicated to rare tumors of the central and peripheral nervous system in both pediatric and adult populations. Although uncommon compared to other tumors, primary Central Nervous System (CNS) and Peripheral Nervous System (PNS) cancers can cause severe morbidity and mortality across all populations. Despite the efforts and care improvement dedicated to the most prevalent brain and spine tumors (such as glioblastomas, metastases, or meningiomas), some of these diseases still lack defined management plans or specific preclinical assessment of their cellular/molecular features, thus affecting patients' management.

While CNS tumors can now be much more precisely characterized than a few years ago, the translation of this increased knowledge into more effective treatments is still seriously lagging behind, in particular considering specific populations such as children or the elderly. This is particularly true for pediatric CNS tumors. In a large series of 80 children, Zhang et al. confirmed that Diffuse Intrisic Pontine Glioma (DIPG, included in Diffuse Midline Gliomas, H3K27 altered) display a broad spectrum of clinical and imaging

features; whereas surgery could play a role in addition to adjuvant therapies, H3K27 alteration was the independent prognostic influencing factor. Falco et al. analyzed the role of intraoperative fluorescent dyes in the surgical management of pleomorphic xanthoastrocytoma (PXA), a rare brain tumor most commonly affecting children and young adults. Surgical resection is the mainstay of treatment, and the extent of resection is associated with improved survival. Among the twelve patients included, comprising three pediatric patients, sodium fluorescein helped distinguish tumors from viable tissue in all cases. Their data suggest a role in improving the extent of resection during surgery of PXA. Merchant et al. presented a case of Oligodendroglioma IDH-mutant and 1p/19q-codeleted associated with a germline mutation in PMS2 like Lynch Syndrome, to evaluate the role of germline PMS2 mutations in gliomas, and highlighted the importance of genetic testing in neuro-oncology. Frederico et al. elegantly analyzed the heterogenicity among adult patients harboring MN1-altered CNS tumors. These uncommon lesions were recently added to the 2021 WHO classification under the name Astroblastoma, MN1-altered. Thought to occur most commonly in children and predominantly in females, MN1-altered CNS tumors are associated with typical (whereas not pathognomonic) histological patterns, with a distinct DNA methylation profile and recurrent fusions implicating the MN1 (meningioma 1) gene. The authors emphasize the diagnostic challenges, considering that most cases with morphological features of astroblastoma (but not all) show these molecular features, whereas not all tumors with MN1 fusions show astroblastoma morphology. From a clinical point of view, there is significant variability in reported outcomes: multiple recurrences are frequent, despite multimodality treatments. Additionally, the authors propose a standardized model for patient-reported outcomes. Pavlova et al. evaluated, in the preclinical setting, the effect of radiation therapy on patient-derived glioblastoma cells to evaluate the contribution of homologous recombination and nonhomologous end in DNA break repair after exposure to different radiation doses.

Solitary fibrous tumor (SFT), previously known as hemangiopericytoma or SFT/hemangiopericytoma, is a rare intracranial malignancy thought to originate from pericyte cells lining the capillary walls. These tumors represent less than 1% of intracranial tumors and are frequently mistaken for meningiomas on imaging. Unlike most meningiomas, however, SFT has a propensity for local recurrence and extracranial metastasis after resection. Surgery usually represents the pivotal therapeutic point, but the role of adjuvant treatment is often unclear. Three papers analyzed the impact of radiation therapy in the management of SFT. Liu et al. evaluated 38 patients with SFT, confirming that patients with high WHO-grade SFT have an impaired PFS and reduced OS, which appears even more negatively affected by a subtotal resection. Postoperative radiotherapy increases the local control rate in patients with WHO grade 3 tumors. Gou et al. focused on the role of postoperative stereotactic radiosurgery or intensity-modulated radiotherapy; this second option seems to increase disease-free survival compared to radiosurgery. Finally, Allen et al. proposed for the first time the use of a mixed-modality, multi-fraction radiosurgery technique to treat recurrent SFT, to maximize radiation dose to the targets while minimizing complication risk after resection.

Three papers analyzed different aspects of intracranial lymphomas, considering that intracranial lymphomas can mimic different brain tumors. Yang et al. evaluated the impact of risk factors such as age, Ann Arbor stage, and treatment in the prognosis of primary intracranial malignant lymphomas. Cheng et al. evaluated a series of primary ventricular lymphomas, an extremely rare and frequently misdiagnosed disease, with high mortality (median survival time of 15 months). Wang et al. evaluated the case of a suspected pituitary apoplexy, in which the diagnosis was lymphoblastic lymphoma derived from B-cells.

Other papers investigated different CNS tumors, included within a wide spectrum of embryonal origin and clinical behaviors. Li et al. evaluated a *de novo* mutation in von Hippel–Lindau (VHL) syndrome, performing whole-exon gene analysis to improve the understanding of the diagnosis. Early recognition and treatment of VHL syndrome can also be available with genetic testing technology in case of a negative familial history. Strengthening the understanding of this complex genetic disease and improving the diagnostic rate of VHL syndrome is helpful for personalized treatments. Xu et al. assessed clinicopathological characteristics, prognostic factors, and outcomes in a series of 17 children harboring embryonal tumors with multilayered rosettes (C19MC-altered or not elsewhere classified). They confirmed the aggressive behaviors of such tumors: for patients receiving chemotherapy, the median overall survival time was 7.4 months, while those who did not receive chemotherapy was 1.2 months. Children older than four years tend to have a higher rate of metastasis.

Kim et al. evaluated the impact of Gamma-Knife radiosurgery for vestibular schwannomas in neurofibromatosis type 2 patients. Longitudinal volumetric analyses showed that most treated lesions showed effective tumor control up to 85% at 60 months, whereas unirradiated lesions progressed with a relative volume increase of 14.0% (7.8-27.0) per year during the observation period. However, 29% of cases showed pseudoprogression with significant volume expansion in the early follow-up period, which practically reduced the tumor control rate to 57% at 24 months, and the short-term effects of this treatment are not highly advantageous in terms of hearing preservation. Therefore, careful patients selection is necessary for such treatment.

Fang et al. presented a gene expression evaluation of adamantinomatous craniopharyngioma (ACP), an epithelial tumor arising from Rathke's pouch remains. They screened for differentially expressed genes (DEGs) to identify key signaling pathways. Hierarchical clustering showed that the DEGs could precisely distinguish the ACP group from the control group, suggesting that E-cadherin (*CDH1*) may play a relevant role in the pathways in cancer signaling pathway that regulates ACP development, and it could be a target suitable for precision medicine.

Feng et al. conducted a Surveillance, Epidemiology, and End Results population-based study for the elderly with malignant meningiomas, a rare form of a relatively common CNS tumor,

with poor survival. The multivariable analysis among this specific population revealed that surgical resection is recommended for elderly patients with malignant meningiomas (if surgery is not contraindicated for systemic, patient-specific factors). However, gross-total resection does not significatively impact patients' survival, compared to subtotal resection in older patients. Also, Serratrice et al. evaluated meningiomas but focused on spinal forms. They reviewed the fundamental epidemiological and clinical aspects of spinal meningiomas, their histological and genetic characteristics, and their management, including updated surgical advancements.

The remainder of the accepted manuscripts studied PNS tumors, from preclinical studies to clinical and surgical points of view. The special issue comprises six papers based on Peripheral Nerve Sheath Tumors (PNST). Gu et al. performed a preclinical assessment of MEK inhibitors for Malignant PNST (MPNSTs), rare soft-tissue sarcomas refractory to standard therapies. The majority of MPNSTs show inactivation of NF1 and upregulation of RAS/RAF/MEK/ERK signaling pathways. The authors evaluated different MEK inhibitors in terms of efficacy, safety, and mechanism of adaptive response in the case of MPNSTs. Using a tissue microarray, they identified p-ERK as a biomarker for predicting the prognosis of MPNST patients as well as an effective therapeutic target. Trametinib consequentially appeared as the most potent MEK inhibitor for treating MPNSTs. Globally, reduced reactivation of the MAPK pathway and compensatory activation of the parallel pathways contributed to better efficacy.

Imaging differentiation among benign and malignant PNST is pivotal in Neurofibromatosis type 1. Liu et al. reviewed different non-invasive image-based diagnostic common findings. Moreover, the addition of novel technologies like radiogenomics can introduce future perspectives that ultimately can contribute to the radiology image-based clinical screening of MPNST in NF1 patients. Bonomo et al. provided a new case of sporadic spinal psammomatous malignant melanotic Nerve Sheath Tumor (SSP-MMNST), a rare subgroup of PNST arising along the spine, with only a few reports described. The literature review identified 21 eligible studies assessing 23 patients, with a mean onset age of 41 years and a slight male gender predominance. In all cases, resection is the treatment of choice in all amenable cases, followed in selected cases with residual tumors by adjuvant radiotherapy or chemotherapy.

Nevertheless, the metastatic and recurrence rates were 31.58% and 36.8%, respectively. Wei et al. focused on the differential diagnosis of tuberous sclerosis and neurofibromatosis type 1. The treatments for the two diseases vary significantly, and misdiagnoses can seriously threaten the patient's health. Finally, Nazzi et al. assessed the role of sodium fluorescein in PNST, evaluating a comprehensive series of 142 cases submitted to fluorescein-guided surgery. In fact, surgery is the mainstay of treatment for PNST, but sometimes distinguishing between intact functional nerve and the fibers from whence the PNST arose may not always be easy to perform, constituting the most relevant risk factor in determining a worsening neurological condition. Intraoperative fluorescein characteristics and postoperative neurological and radiological outcomes were analyzed and compared with a historical series. Bright fluorescence was present in all schwannomas and neurofibromas, although with a less homogeneous pattern, whereas it was significantly less evident for MPNST. The authors concluded that SF is a valuable method for safe fluorescence-guided resection of PNST and mimicking lesions, with a positive effect mainly in plexiform neurofibromas, suggesting a possible role in improving the functional and oncological outcome of these lesions.

In summary, the special issue provides great information on different, rare central and peripheral nervous system tumors. The editors hope that this collection of knowledge can be exploited to help improve knowledge and research on neuro-oncology.

Author contributions

All authors listed have made a substantial, direct, and intellectual contribution to the work and approved it for publication.

Acknowledgments

We are very grateful to all the authors who contributed to this Research Topic and for the interest shown by the scientific community.

Conflict of interest

The authors declare that the research was conducted in the absence of any commercial or financial relationships that could be construed as a potential conflict of interest.

Publisher's note

frontiers | Frontiers in Oncology

ORIGINAL RESEARCH
published: 13 May 2022
doi: 10.3389/fonc.2022.913254

Prognostic Factors and Treatment Strategies for Elderly Patients with Malignant Meningioma: A SEER Population-Based Study

Songshan Feng[1,2,3,4], Jing Li[5], Fan Fan[1], Zeyu Wang[1], Qian Zhang[6], Hao Zhang[1], Ziyu Dai[1], Xun Zhang[1], Peng Luo[7], Zaoqu Liu[8], Jian Zhang[7], Zhuoyi Liu[6] and Quan Cheng[1,2,9]**

[1] Department of Neurosurgery, Xiangya Hospital, Central South University, Changsha, Hunan, China, [2] National Clinical Research Center for Geriatric Disorders, Xiangya Hospital, Central South University, Changsha, China, [3] Xiangya Cancer Center, Xiangya Hospital, Central South University, Changsha, China, [4] Key Laboratory of Molecular Radiation Oncology Hunan Province, Changsha, China, [5] Department of Rehabilitation, the Second Xiangya Hospital, Central South University, Changsha, China, [6] Department of Anesthesiology, Xiangya Hospital, Central South University, Changsha, China, [7] Department of Oncology, Zhujiang Hospital, Southern Medical University, Guangzhou, China, [8] Department of Interventional Radiology, The First Affiliated Hospital of Zhengzhou University, Zhengzhou, China, [9] Department of Clinical Pharmacology, Xiangya Hospital, Central South University, Changsha, China

Objective: Malignant meningioma (MM) is a relatively rare disease with poor survival. Few studies had focused on MM in the elderly population. This study aims to explore the prognostic factors and optimal therapeutic strategy in elderly patients with MM.

Methods: We took advantage of the Surveillance, Epidemiology, and End Results (SEER) database to include 275 adult patients with histologically confirmed MM between 2011 and 2018. The Kaplan–Meier curves were plotted by different covariates to reveal the survival probability. Univariate and multivariable Cox proportional hazard regression analyses were applied to identify prognostic factors for cancer-specific survival (CSS).

Results: The multivariable analysis in the elderly group revealed that when compared with patients receiving gross total resection (GTR), patients receiving biopsy had significantly worse CSS (HR = 3.72; 95% CI: 1.35–10.21; P = 0.011), whereas patients receiving subtotal resection (STR) had nearly the same CSS (HR = 0.83; 95% CI: 0.37–1.86; P = 0.653). Meanwhile, postoperative radiotherapy (PORT) showed no significant association with CSS in the elderly patient group (HR = 0.94; 95% CI: 0.42–2.12; P = 0.888).

Conclusion: Surgical resection is recommended for elderly patients with MM in the absence of surgical contraindications, but GTR does not present survival benefit in the elderly patients compared with STR. Additional large-scale clinical studies are needed to explore the survival benefit of PORT applied in patients with MM.

Keywords: malignant meningioma, elderly patient, treatment strategy, SEER, patient prognosis

OPEN ACCESS

Edited by:
Ignazio Gaspare Vetrano, Carlo Besta Neurological Institute Foundation (IRCCS), Italy

Reviewed by:
Manuela Caroli, Fondazione Politecnico di Milano, Italy
Silvia Schiavolin, Carlo Besta Neurological Institute Foundation (IRCCS), Italy

***Correspondence:**
Quan Cheng
chengquan@csu.edu.cn
Zhuoyi Liu
zhuoyiliu@csu.edu.cn

Specialty section:
This article was submitted to Neuro-Oncology and Neurosurgical Oncology, a section of the journal Frontiers in Oncology

Received: *05 April 2022*
Accepted: *14 April 2022*
Published: *13 May 2022*

Citation:
Feng S, Li J, Fan F, Wang Z, Zhang Q, Zhang H, Dai Z, Zhang X, Luo P, Liu Z, Zhang J, Liu Z and Cheng Q (2022) Prognostic Factors and Treatment Strategies for Elderly Patients with Malignant Meningioma: A SEER Population-Based Study. Front. Oncol. 12:913254. doi: 10.3389/fonc.2022.913254

INTRODUCTION

Meningioma is the most common primary neoplasm of the central nervous system, accounting for 38.3% of all brain tumors (1). According to the most recent report from the Central Brain Tumor Registry of the United States, malignant meningioma (MM) composes 1.04% of all meningiomas with an incidence of 0.09 per 100,000 people (1). There is evidence that age-specific incidence rates of meningiomas increase in both men and women, with a median age at diagnosis of 65 and 66 years old for malignant and non-malignant meningiomas, respectively (1, 2). As far as we know, most studies on MMs did not take the elderly (≥65 years old) as an independent patient group to describe (3). There were reports revealing that older age was associated with worse patient survival (4–7). Several studies suggested that craniotomy for resection of meningioma in the elderly patients carried higher risk of mortality and morbidity compared with younger patients (8, 9). Other studies reported that no significant difference was detected in the mortality rate after surgery for elderly versus non-elderly patients, but more elderly patients presented postoperative complications and neurological deterioration (10–12). At present, there is still a lack of consensus on the surgical outcome of elderly patients with MM, and the specific treatment strategies need to be further explored. Furthermore, it is expected that the average human life expectancy continues to increase and more elderly patients with MM will be diagnosed (10). Therefore, we conducted this study aiming to explore the prognostic factors and figure out the optimal therapeutic strategy, especially in elderly patients with MM.

MATERIALS AND METHODS

Study Population

Given the low incidence of MM, we took advantage of the Surveillance, Epidemiology, and End Results (SEER) database and retrospectively analyzed 275 patients diagnosed with histologically confirmed MM between 2011 and 2018. The subgroup analysis for elderly and younger patients was performed with respect to extent of surgical resection (EOR), postoperative radiotherapy (PORT), and their influence on long-term patient survival. All records of intracranial MM with positive histology between 2004 and 2018 were initially extracted from the SEER database, which provides patient demographics, tumor characteristics, treatment methods, and survival status with de-identified records. WHO grade 3 meningioma was defined as MM, which included the ICD-O-3 histology and behavior records of 9530/3 (Meningioma, malignant), 9531/3 (Meningiothelial meningioma, malignant), 9532/3 (Fibrous meningioma, malignant), 9534/3 (Angiomatous meningioma, malignant), 9535/3 (Hemangioblastic meningioma, malignant), 9537/3 (Transitional meningioma, malignant), 9538/3 (Papillary meningioma), and 9539/3 (Meningeal sarcomatosis) according to existing studies (13, 14). Patients with unknown information of marital status, race, tumor size, laterality, cancer-specific survival (CSS) status, and age<18 years old were excluded. Patients with recurrent MM were also excluded, which had at least one prior record of WHO grade 1 or WHO grade 2 meningioma in the SEER database. The detailed protocol was provided by the SEER*Stat tutorial naming "case listing exercise 1b: view patient histories" (https://seer.cancer.gov/seerstat/tutorials/case-listings.html). Surgery code 0 (no surgery of primary site; autopsy only), code 10 (no specimen sent to pathology), code 22 (resection of tumor of spinal cord or nerve), and code 90 (surgery, not otherwise specified) were excluded. In addition, the small part of patients treated with radiotherapy prior to surgery, intraoperative radiotherapy, radioactive implants, radioisotopes, and unknown method were excluded. **Supplementary Table 1** showed that the records of surgery code changed significantly since 2011, which revealed the advancement in surgical techniques. To provide the most up-dated evidence, the patient diagnosed before 2011 were excluded, and little parts of patients with surgery code 40 (partial resection of lobe of brain) and 55 (gross total resection of lobe of brain) were also excluded (n = 20). The final study population included 275 adult patients diagnosed between 2011 and 2018 recorded as surgery code 20 (local excision, biopsy), 21 [subtotal resection (STR) of tumor], and 30 [radical, total, gross resection of tumor (GTR)] (**Figure 1**).

Covariates Included

The following demographic information was included for analysis: age group (<65 and ≥65 years), gender (male and female), race (other, black, and white), and marital status (single, divorced, married, and widowed). The following tumor characteristics were analyzed: tumor site (cerebral meninges and other), laterality (unilateral, bilateral, and midline), histology (9530/3 and other), tumor size (≥4.9 and <4.9 cm, the best cutoff was defined by x-tile software) (15), and other tumor(s) (before MM, and after MM, defined by the record of "sequence number" in SEER*Stata). EOR includes code 20 (biopsy), code 21 (STR), and code 30 (GTR). Concerning adjuvant therapy, PORT (no/unknown and beam radiation), and chemotherapy (no/unknown and yes) were included for analysis. CSS was defined as the event of interest in this study.

Statistical Methods

The distribution of the baseline characteristics between different age groups was compared by the chi-squared test (categorical variables with all cell counts>5) or the Fisher's exact test (categorical variables with cell counts ≤5). The Kaplan–Meier curves in the entire cohort were plotted by all covariates to reveal the CSS probability of different groups, which were compared by log-rank test. Univariate and multivariable Cox proportional hazard regression analyses were applied to identify prognostic factors from all covariates for CSS. The baseline characteristics between groups receiving different EOR were compared by the chi-squared test, Fisher's exact test, or one-way ANOVA test (continuous variable). The Kaplan–Meier curves by EOR and PORT were plotted in elderly and younger patient group. Furthermore, univariate and multivariable Cox proportional hazard regression analyses were also applied to assess the survival benefits provided by EOR and PORT for younger and elderly patients, respectively. $P < 0.05$ was considered statistically

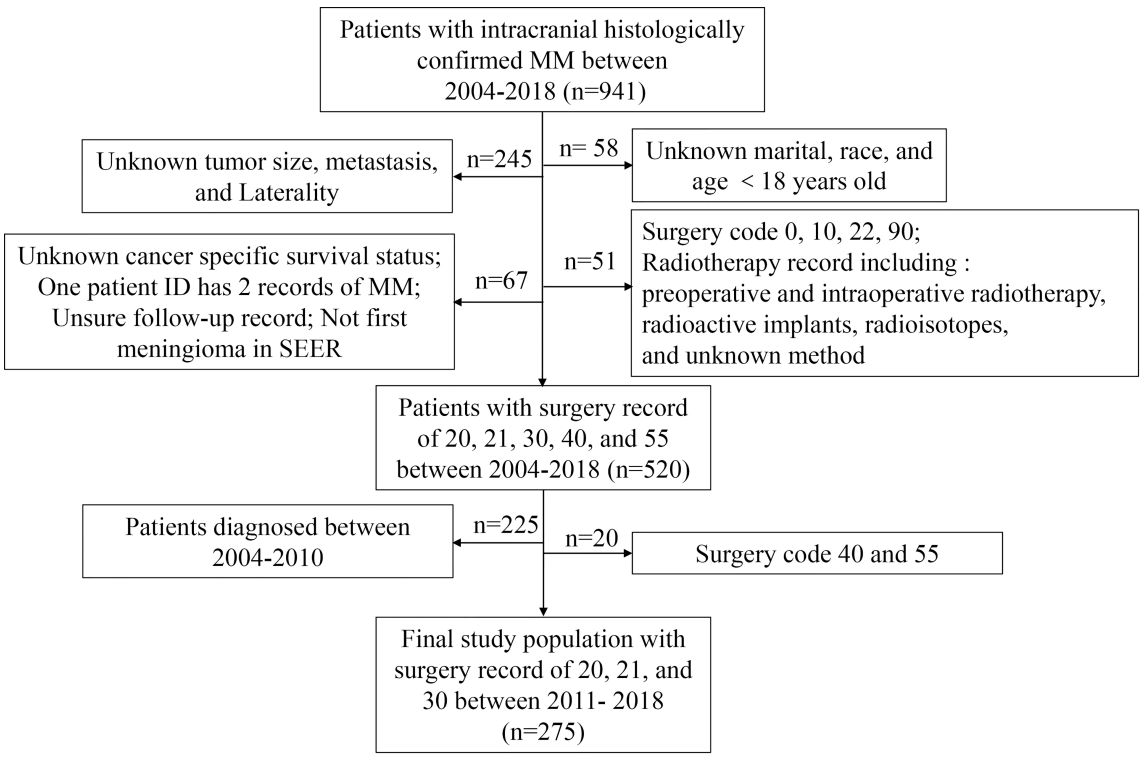

FIGURE 1 | Flow chart of patient selection criteria with *de novo* MM between 2011 and 2018.

significant. All statistical analyses were performed in R version 3.5.1 (http://www.r-project.org/).

RESULTS

Baseline Characteristics

The median age was 62 years old, and median survival time was 28 months. At the time of data collected, 183 cases were alive, 56 cases died of MM, and 36 cases died of other causes. The 1-, 2-, and 5-year CSS rates were 88.5%, 80.7%, and 52.1%, respectively. The baseline characteristics were compared between age groups in **Table 1**. The marital status showed a significant difference, whereas race and gender showed no difference between age groups. The majority of patients had tumor larger than 4.9 cm, tumor located in cerebral meninges, unilateral tumor, tumor with histology 9530/3, tumor without metastasis, and no other tumor(s). Tumor characteristics including tumor size, site, laterality, histology, metastasis, and other tumor(s) showed no significant difference between different age groups ($P > 0.05$). Concerning treatment methods, the results revealed that the GTR rate was 52.4% in the entire cohort, 51.3% in the younger group, and 53.7% in the elderly group. Compared with patients in the younger group, more patients received biopsy only and fewer patients received STR in the elderly group. A total of 149 patients received PORT and 12 patients received postoperative chemotherapy, which showed no significant difference between age groups.

Prognostic Factors of CSS in the Entire Cohort

Kaplan–Meier curves indicated that patients in the elderly group, with tumor size>4.9 cm, receiving biopsy only, and receiving chemotherapy had significantly worse survival probability. In addition, the Kaplan–Meier curves by PORT, gender, race, marital status, histology, tumor site, laterality, metastasis, and other tumor(s) showed no significant difference (**Figure 2** and **Supplementary Figure 1**). The results of univariate analysis revealed that patients in elderly group (HR = 2.73; 95% CI: 1.57–4.74; P = 3.56e−4), with tumor size>4.9 cm (HR = 1.77; 95% CI: 1.04–3.04; P = 0.036), receiving biopsy only (HR = 2.62; 95% CI: 1.29–5.31; P = 0.007), and receiving chemotherapy (HR = 3.69; 95% CI: 1.75–7.81; P = 6.3e−4) presented significantly worse CSS. PORT, gender, race, marital status, histology, tumor site, laterality, metastasis, and other tumor(s) were not significantly associated with CSS ($P > 0.05$) (**Table 2** and **Supplementary Table 2**). Consistently, the results of the multivariable analysis revealed that patients in the elderly group (HR = 3.41; 95% CI: 1.86–6.23; P = 6.81e−5), with tumor size>4.9 cm (HR = 1.78; 95% CI: 1.01–3.16; P = 0.048), receiving biopsy only (HR = 3.03; 95% CI: 1.43–6.44; P = 0.004), and receiving chemotherapy (HR = 4.19; 95% CI: 1.77–9.90; P =

TABLE 1 | Patient demographics, tumor characteristics, and treatment options of 275 patients with MM from 2011 to 2018 in different age groups.

	Overall [n (%)]	<65 years [n (%)]	≥65 years [n (%)]	P-value
No.	275 (100)	152 (100)	123 (100)	
Gender				0.052
Male	133 (48.4)	65 (42.8)	68 (55.3)	
Female	142 (51.6)	87 (57.2)	55 (44.7)	
Race				0.85
Other	33 (12.0)	17 (11.2)	16 (13.0)	
Black	43(15.6)	23 (15.1)	20 (16.3)	
White	199 (72.4)	112 (73.7)	87 (70.7)	
Marital				<0.001†
Single	64 (23.3)	48 (31.6)	16 (13.0)	
Divorced	29 (10.5)	12 (7.9)	17 (13.8)	
Married	159 (57.8)	86 (56.6)	73 (59.3)	
Widowed	23 (8.4)	6 (3.9)	17 (13.8)	
Site				0.506
Meninges	267 (97.1)	149 (98.0)	118 (95.9)	
Other	8 (2.9)	3 (2.0)	5 (4.1)	
Laterality				0.182
Unilateral	253 (92.0)	136 (89.5)	117 (95.1)	
Bilateral	2 (0.7)	1 (0.7)	1 (0.8)	
Midline	20 (7.3)	15 (9.9)	5 (4.1)	
Histology				0.577
9530/3	216 (78.5)	117 (77.0)	99 (80.5)	
Other	59 (21.5)	35 (23.0)	24 (19.5)	
Other tumors				0.068
One primary	203 (73.8)	120 (78.9)	83 (67.5)	
Before MM	51 (18.5)	21 (13.8)	30 (24.4)	
After MM	21 (7.6)	11 (7.2)	10 (8.1)	
Size				0.998
>4.9cm	133 (48.4)	73 (48.0)	60 (48.8)	
≤4.9cm	142 (51.6)	79 (52.0)	63 (51.2)	
Metastasis				0.627
No	268 (97.5)	147 (96.7)	121 (98.4)	
Yes	7 (2.5)	5 (3.3)	2 (1.6)	
Surgery code				0.04†
GTR	144 (52.4)	78 (51.3)	66 (53.7)	
Biopsy	38 (13.8)	15 (9.9)	23 (18.7)	
STR	93 (33.8)	59 (38.8)	34 (27.6)	
Chemotherapy				0.607
Yes	12 (4.4)	8 (5.3)	4 (3.3)	
No/Unknown	263 (95.6)	144 (94.7)	119 (96.7)	
PORT				0.237
Beam radiation	149 (54.2)	77 (50.7)	72 (58.5)	
No/Unknown	126 (45.8)	75 (49.3)	51 (41.5)	

†*P < 0.05, statistically significant.*

EOR, extent of surgery; GTR, gross total resection; STR, subtotal resection; PORT, postoperative radiotherapy; MM, malignant meningioma.

0.001) showed significant worse CSS. Meanwhile, PORT, gender, race, marital status, histology, tumor site, laterality, metastasis, and other tumor(s) were not significantly associated with CSS (P > 0.5) (**Table 2** and **Supplementary Table 2**).

The Survival Benefits of EOR and PORT in Subgroups

The subgroup analysis of elderly and younger patients was conducted to assess the survival benefits of EOR and PORT. First, the Kaplan–Meier curves in the younger group indicated that patients receiving biopsy presented the worst survival probability, and patients receiving GTR had a slightly better survival probability than that receiving STR (P = 0.055). The Kaplan–Meier curves in the elderly group showed that the survival probability of patients receiving different EOR had no significant difference (P = 0.22). The Kaplan–Meier curves in both age groups suggested that PORT did not affect survival probability (**Figure 3**). The univariate analysis in the younger group showed that when compared with patients receiving GTR, patients receiving biopsy had significantly worse CSS (HR = 4.23; 95% CI: 1.13–15.81; P = 0.032) and patients receiving STR had slightly worse CSS (HR = 2.66; 95% CI: 0.93–7.69; P = 0.069). Meanwhile, the univariate analysis in the elderly group illustrated that when compared with patients receiving GTR, patients receiving biopsy had slightly worse CSS (HR = 2.07; 95% CI: 0.89–4.82; P = 0.091), but patients receiving STR possessed nearly the same CSS (HR = 1.09; 95% CI: 0.51–2.35; P = 0.808). The results of univariate analysis revealed that PORT presented no significant association with CSS in both younger group and

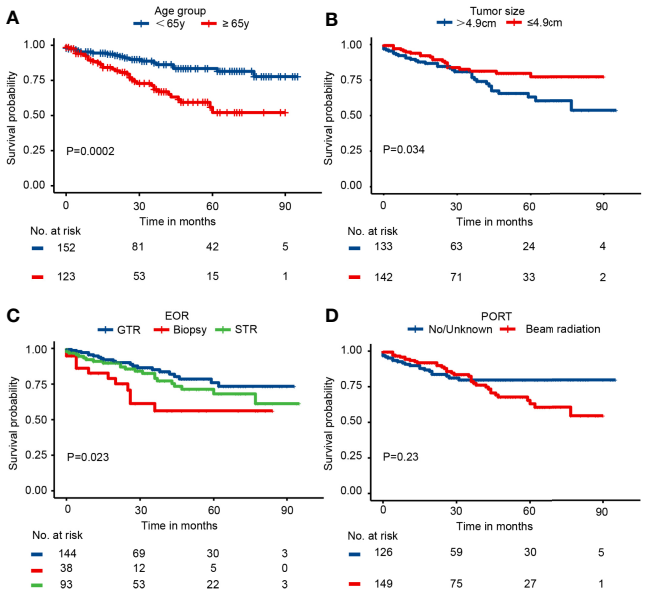

FIGURE 2 | The Kaplan–Meier curves by **(A)** age group, **(B)** tumor size, **(C)** EOR, and **(D)** PORT in the entire cohort.

TABLE 2 | Results of univariate and multivariable Cox proportional regression analysis of age group, tumor size, EOR, and PORT in the entire study population.

	Univariate Analysis		Multivariable Analysis	
	HR (95% CI)	**P-value**	**HR (95% CI)**	**P-value**
Age				
<65 years	1 [Reference]		1 [Reference]	
≥65 years	2.73 (1.57–4.74)	3.56×10^{-4}†	3.41 (1.86–6.23)	6.81×10^{-5}†
Size				
≤4.9cm	1 [Reference]		1 [Reference]	
>4.9cm	1.77 (1.04–3.04)	0.036†	1.78 (1.01–3.16)	0.048†
Extent of resection				
GTR	1 [Reference]		1 [Reference]	
Biopsy	2.62 (1.29–5.31)	0.007†	3.03 (1.43–6.44)	0.004†
STR	1.40 (0.77–2.53)	0.262	1.23 (0.67–2.27)	0.497
PORT				
No/Unknown	1 [Reference]		1 [Reference]	
Beam radiation	1.29 (0.81–2.38)	0.235	0.81 (0.44–1.49)	0.503

†*P < 0.05, statistically significant.*

EOR, extent of surgery; GTR, gross total resection; STR, subtotal resection; PORT, postoperative radiotherapy.

elderly group (**Table 3**). Consistently, the multivariable analysis in the younger group suggested that when compared with patients receiving GTR, patients receiving biopsy had significantly worse CSS (HR = 6.47; 95% CI: 1.42–29.44; P = 0.018) and patients receiving STR had slightly worse CSS (HR = 2.77; 95% CI: 0.81–9.48; P = 0.103). The multivariable analysis in the elderly group revealed that when compared with patients receiving GTR, patients receiving biopsy had significantly worse CSS (HR = 3.72; 95% CI: 1.35–10.21; P = 0.011) and patients receiving STR had nearly the same CSS (HR = 0.83; 95% CI: 0.37–1.86; P = 0.653). At the same time, the results of multivariable analysis illustrated that PORT showed no significant association with CSS in both younger group and elderly group (**Table 3**). The results of univariate and multivariable analyses of gender, race, marital, tumor size, histology, site, laterality, metastasis, other tumor(s), and chemotherapy in different age groups were presented in **Supplementary Table 3** (<65 years) and **Supplementary Table 4** (≥65 years), respectively.

The baseline characteristics of patients were compared between groups receiving different EOR in **Supplementary Table 5** (<65 years) and **Supplementary Table 6** (≥65 years), respectively. The results suggested that the patient demographics and tumor characteristics such as age, gender, tumor size, and tumor location presented no significant difference between elderly patients receiving different EOR.

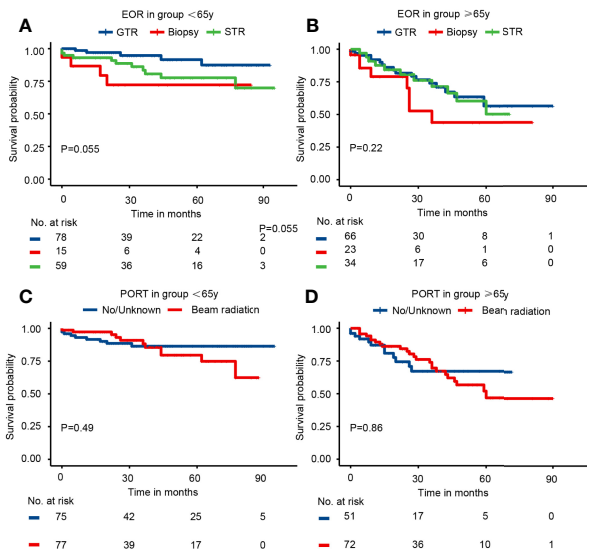

FIGURE 3 | The Kaplan–Meier curves by EOR and PORT in different age groups. **(A)** EOR in group <65 years. **(B)** EOR in group ≥65 years. **(C)** PORT in group <65 years. **(D)** PORT in group ≥65 years.

TABLE 3 | Results of univariate and multivariable Cox proportional regression analysis of EOR and PORT in different age groups.

Patient groups			Univariate Analysis		Multivariable Analysis	
			HR (95% CI)	P-value	HR (95% CI)	P-value
EOR	<65 years	GTR	1 [Reference]		1 [Reference]	
		Biopsy	4.23 (1.13–15.81)	0.032†	6.47 (1.42–29.44)	0.018†
		STR	2.66 (0.93–7.69)	0.069	2.77 (0.81–9.48)	0.103
	≥65 years	GTR	1 [Reference]		1 [Reference]	
		Biopsy	2.07 (0.89–4.82)	0.091	3.72 (1.35–10.21)	0.011†
		STR	1.09 (0.51–2.35)	0.808	0.83 (0.37–1.86)	0.653
PORT	<65 years	No/unknown	1 [Reference]		1 [Reference]	
		Beam radiation	1.36 (0.56–3.31)	0.493	2.29 (0.27–19.05)	0.442
	≥65 years	No/unknown	1 [Reference]		1 [Reference]	
		Beam radiation	1.06 (0.53–2.13)	0.865	0.94 (0.42–2.12)	0.888

†*P < 0.05, statistically significant.*

EOR, extent of surgery; GTR, gross total resection; STR, subtotal resection; PORT, postoperative radiotherapy.

DISCUSSION

Because of the prolongation of life expectancy, the treatment strategy of meningiomas in elderly patients has become a more and more important issue. Thus, we utilized the SEER database and retrospectively analyzed 275 patients diagnosed as MM with long-term outcome results, aiming to explore the prognostic factors and figure out the optimal therapeutic strategy for this specific population.

Elderly patients are more likely to be accompanied by other diseases, resulting in poor physical condition before surgery. Considering the risk of surgery and the corresponding surgical morbidity and mortality, conservative treatment may be a reasonable choice for elderly patients. However, it was reported that elderly patients who received conservative treatment had increased tumor-related mortality compared with patients who underwent surgical resection (16). Furthermore, both the univariate and multivariable analysis in our study suggested that biopsy was significantly associated with worse CSS in elderly patients. The European Association of Neuro-Oncology guidelines suggested surgical resection followed by PORT for the treatment of patients with MM (17). However, the specific surgical benefits and the choice of surgical patterns need to be further discussed.

There were studies reporting that meningioma surgery in elderly patients presented a higher risk of mortality and morbidity compared to intracranial tumor surgery in general (8, 18). Steinberger et al. revealed in their study that old age was an independent predictor of morbidity and mortality in patients undergoing craniotomy for resection of meningioma (9). Ferroli et al. reported in their retrospective cohort study that postoperative complications and surgical complexity could significantly influence the early outcome in elderly patients undergoing brain tumor surgery, and postoperative complications was the only factor with a strong correlation to postoperative worsening at the 3-month follow-up (19). In another study, the authors reported that no significant difference was

discovered regarding the 30-day mortality rate for elderly versus non-elderly patients, whereas elderly patients had a significantly higher complication rate compared with non-elderly patients (10). Boviatsis et al. also revealed that the mortality rate between the elderly group and the younger group was not significant, but more elderly patients were discharged having deteriorated neurologically in comparison to their preoperative status (11). Hence, although there is dispute on whether the surgical resection would increase the mortality rate or not, it is generally recognized that the incidence of postoperative complications is higher in elderly patients.

Regarding the EOR and its influence on the long-term patient survival, several studies revealed that GTR was a favorable factor for patient survival in the general population (20, 21). Other studies indicated that GTR was not significantly associated with patient survival (22, 23). One particular study suggested that the overall survival of patients treated with near total resection was better than patients treated with GTR (24). Taking age into consideration, Brokinkel et al. reported that the progression-free interval of patients undergoing GTR was distinctly prolonged as compared with STR and emphasized the importance of achieving maximum safe resection in elderly patients (25). Another study also reported that the EOR had no influence on the functional outcome of elderly patients (26). However, D'Andrea et al. indicated that radical resection could increase postoperative morbidity in elderly patients (27). In another study, Chen et al. suggested that the aggressive resection of meningiomas in elderly patients could increase the morbidity and mortality, and survival with residual tumor was acceptable in this specific population (28). Our results revealed that GTR only improved CSS in younger patients compared with STR but did not present survival benefit in elderly patients. Therefore, we believe that surgeons should take into account the factors that the elderly are more prone to surgical complications when formulating surgical strategy for this special patient group, and a more balanced choice should be made in the pursuit of GTR and preservation of neurological function, so as to improve the postoperative functional status and survival of elderly patients.

Generally, PORT is recommended after tumor resection for the treatment of MM (17). There was supporting evidence revealing that PORT improved the survival of patients with MM (29, 30). Orton reported that PORT improved the overall survival of patients with MM undergoing both GTR and STR (4). However, another study illustrated that patients with MM did not benefit from PORT (20). For elderly patients with MM specifically, Zhou et al. and Achey et al. both suggested that PORT could not provide survival benefits after GTR (6, 31). The results of univariate analysis and multivariable analysis in our study showed that PORT exhibited no significant association with CSS in both younger group and elderly group. However, there may be a selection bias that those patients considered to possess a higher risk of recurrence or with more aggressive tumors are more likely to receive PORT. In addition, the information about PORT is not complete in the SEER database, which may affect the accuracy of the conclusion. We believe that additional large-scale clinical studies are needed to explore the survival benefit of PORT applied in patients with MM.

We are aware of the limitations of this study. The patients extracted from the SEER database may not represent the general patient cohort. For the elderly population, the concomitant disease before surgery, the complications, and functional status after surgery are important factors and may affect patient survival largely, which could not be obtained through the SEER database. Furthermore, the records of Simpson grades of resection and the exact radiotherapy information are also not available. Moreover, the insufficient number of patients may affect the analysis results and lead to selection bias.

CONCLUSION

Surgical resection is recommended for elderly patients with MM in the absence of surgical contraindications, but GTR do not present survival benefit in the elderly patients compared with STR. Meanwhile, PORT exhibits no significant association with CSS in elderly group. Additional large-scale clinical studies are needed to explore the survival benefit of PORT applied in patients with MM. Despite several limitations, we believe that this study would help clinicians evaluate the prognosis of patients with MM and optimize treatment strategies for elderly patients specifically.

DATA AVAILABILITY STATEMENT

The original contributions presented in the study are included in the article/**Supplementary Material**. Further inquiries can be directed to the corresponding authors.

AUTHOR CONTRIBUTIONS

SF, ZYL, and QC made substantial contributions to the design of this study. SF, JL, FF, ZW, ZQL, and QC carried out the analysis and interpreted the data. SF, ZD, HZ, and JL made contributions to the drafting of the manuscript. ZD, QZ, PL, JZ, and XZ made contributions to the review of previous literature. SF, ZYL, and QC contributed substantially to the revision of the manuscript. All authors contributed to the article and approved the submitted version.

FUNDING

This work was supported by the National Natural Science Foundation of China (Nos. 82102848, 82073893, and 81703622), China Postdoctoral Science Foundation (No. 2018M633002), Hunan Provincial Natural Science Foundation of China (Nos. 2018JJ3838 and 2020JJ8111), and Xiangya Hospital Central South University postdoctoral foundation.

ACKNOWLEDGMENTS

All authors thank SEER database for providing the worthy patient cohort for research.

SUPPLEMENTARY MATERIAL

The Supplementary Material for this article can be found online at: https://www.frontiersin.org/articles/10.3389/fonc.2022.913254/full#supplementary-material

REFERENCES

1. Ostrom QT, Patil N, Cioffi G, Waite K, Kruchko C, Barnholtz-Sloan JS. CBTRUS Statistical Report: Primary Brain and Other Central Nervous System Tumors Diagnosed in the United States in 2013-2017. *Neuro Oncol* (2020) 22 (12 Suppl 2):iv1–96. doi: 10.1093/neuonc/noaa200
2. Wiemels J, Wrensch M, Claus EB. Epidemiology and Etiology of Meningioma. *J Neurooncol* (2010) 99:307–14. doi: 10.1007/s11060-010-0386-3
3. Meehan TP, Fine MJ, Krumholz HM, Scinto JD, Galusha DH, Mockalis JT, et al. Quality of Care, Process, and Outcomes in Elderly Patients With Pneumonia. *JAMA* (1997) 278:2080–4. doi: 10.1001/jama.1997.03550230056037
4. Orton A, Frandsen J, Jensen R, Shrieve DC, Suneja G. Anaplastic Meningioma: An Analysis of the National Cancer Database From 2004 to 2012. *J Neurosurg* (2018) 128:1684–9. doi: 10.3171/2017.2.JNS162282
5. Champeaux C, Jecko V, Houston D, Thorne L, Dunn L, Fersht N, et al. Malignant Meningioma: An International Multicentre Retrospective Study. *Neurosurgery* (2019) 85:E461–9. doi: 10.1093/neuros/nyy610
6. Achey RL, Gittleman H, Schroer J, Khanna V, Kruchko C, Barnholtz-Sloan JS. Nonmalignant and Malignant Meningioma Incidence and Survival in the Elderly, 2005-2015, Using the Central Brain Tumor Registry of the United States. *Neuro Oncol* (2019) 21:380–91. doi: 10.1093/neuonc/noy162
7. Barthelemy E, Loewenstern J, Konuthula N, Pain M, Hall J, Govindaraj S, et al. Primary Management of Atypical Meningioma: Treatment Patterns and Survival Outcomes by Patient Age. *J Cancer Res Clin Oncol* (2018) 144:969–78. doi: 10.1007/s00432-018-2618-4
8. Konglund A, Rogne SG, Lund-Johansen M, Scheie D, Helseth E, Meling TR. Outcome Following Surgery for Intracranial Meningiomas in the Aging. *Acta Neurol Scand* (2013) 127:161–9. doi: 10.1111/j.1600-0404.2012.01692.x
9. Steinberger J, Bronheim RS, Vempati P, Oermann EK, Ladner TR, Lee NJ, et al. Morbidity and Mortality of Meningioma Resection Increases in Octogenarians. *World Neurosurg* (2018) 109:e16–23. doi: 10.1016/j.wneu.2017.09.021
10. Connolly ID, Cole T, Veeravagu A, Popat R, Ratliff J, Li G. Craniotomy for Resection of Meningioma: An Age-Stratified Analysis of the MarketScan Longitudinal Database. *World Neurosurg* (2015) 84:1864–70. doi: 10.1016/j.wneu.2015.08.018
11. Boviatsis EJ, Bouras TI, Kouyialis AT, Themistocleous MS, Sakas DE. Impact of Age on Complications and Outcome in Meningioma Surgery. *Surg Neurol* (2007) 68:407–11; discussion 411. doi: 10.1016/j.surneu.2006.11.071
12. Poon MT, Fung LH, Pu JK, Leung GK. Outcome Comparison Between Younger and Older Patients Undergoing Intracranial Meningioma Resections. *J Neurooncol* (2013) 114:219–27. doi: 10.1007/s11060-013-1173-8
13. Moreau JT, Hankinson TC, Baillet S, Dudley RWR. Individual-Patient Prediction of Meningioma Malignancy and Survival Using the Surveillance, Epidemiology, and End Results Database. *NPJ Digit Med* (2020) 3:12. doi: 10.1038/s41746-020-0219-5
14. Dolecek TA, Dressler EV, Thakkar JP, Liu M, Al-Qaisi A, Villano JL. Epidemiology of Meningiomas Post-Public Law 107-206: The Benign Brain Tumor Cancer Registries Amendment Act. *Cancer* (2015) 121:2400–10. doi: 10.1002/cncr.29379
15. Camp RL, Dolled-Filhart M, Rimm DL. X-Tile: A New Bio-Informatics Tool for Biomarker Assessment and Outcome-Based Cut-Point Optimization. *Clin Cancer Res* (2004) 10:7252–9. doi: 10.1158/1078-0432.CCR-04-0713
16. Arienta C, Caroli M, Balbi S. Intracranial Meningiomas in Patients Over 70 Years Old. Follow-Up in Operated and Unoperated Cases. *Aging (Milano)* (1992) 4:29–33. doi: 10.1007/BF03324059
17. Goldbrunner R, Minniti G, Preusser M, Jenkinson MD, Sallabanda K, Houdart E, et al. EANO Guidelines for the Diagnosis and Treatment of Meningiomas. *Lancet Oncol* (2016) 17:e383–91. doi: 10.1016/S1470-2045(16)30321-7
18. Eksi MS, Canbolat C, Akbas A, Ozmen BB, Akpinar E, Usseli MI, et al. Elderly Patients With Intracranial Meningioma: Surgical Considerations in 228 Patients With a Comprehensive Analysis of the Literature. *World Neurosurg* (2019) 132:e350–65. doi: 10.1016/j.wneu.2019.08.150
19. Ferroli P, Vetrano IG, Schiavolin S, Acerbi F, Zattra CM, Schiariti M, et al. Brain Tumor Resection in Elderly Patients: Potential Factors of Postoperative Worsening in a Predictive Outcome Model. *Cancers (Basel)* (2021) 13 (10):2320. doi: 10.3390/cancers13102320
20. Choi Y, Lim DH, Jo K, Nam DH, Seol HJ, Lee JI. Efficacy of Postoperative Radiotherapy for High Grade Meningiomas. *J Neurooncol* (2014) 119:405–12. doi: 10.1007/s11060-014-1507-1
21. Zhang GJ, Zhang YS, Zhang GB, Li D, Zhang LW, Wu Z, et al. Prognostic Factors and the Management of Anaplastic Meningioma. *Clin Neurol Neurosurg* (2018) 170:13–9. doi: 10.1016/j.clineuro.2018.03.028
22. Champeaux C, Dunn L. World Health Organization Grade II Meningioma: A 10-Year Retrospective Study for Recurrence and Prognostic Factor Assessment. *World Neurosurg* (2016) 89:180–6. doi: 10.1016/j.wneu.2016.01.055
23. Rosenberg LA, Prayson RA, Lee J, Reddy C, Chao ST, Barnett GH, et al. Long-Term Experience With World Health Organization Grade III (Malignant) Meningiomas at a Single Institution. *Int J Radiat Oncol Biol Phys* (2009) 74:427–32. doi: 10.1016/j.ijrobp.2008.08.018
24. Sughrue ME, Sanai N, Shangari G, Parsa AT, Berger MS, McDermott MW. Outcome and Survival Following Primary and Repeat Surgery for World Health Organization Grade III Meningiomas. *J Neurosurg* (2010) 113:202–9. doi: 10.3171/2010.1.JNS091114
25. Brokinkel B, Holling M, Spille DC, Hess K, Sauerland C, Bleimuller C, et al. Surgery for Meningioma in the Elderly and Long-Term Survival: Comparison With an Age- and Sex-Matched General Population and With Younger Patients. *J Neurosurg* (2017) 126:1201–11. doi: 10.3171/2016.2.JNS152611
26. Cohen-Inbar O, Soustiel JF, Zaaroor M. Meningiomas in the Elderly, the Surgical Benefit and a New Scoring System. *Acta Neurochir (Wien)* (2010) 152:87–97; discussion 97. doi: 10.1007/s00701-009-0552-6
27. D'Andrea G, Roperto R, Caroli E, Crispo F, Ferrante L. Thirty-Seven Cases of Intracranial Meningiomas in the Ninth Decade of Life: Our Experience and Review of the Literature. *Neurosurgery* (2005) 56:956–61; discussion 956-61. doi: 10.1227/01.NEU.0000158303.28823.E9
28. Chen ZY, Zheng CH, Tang L, Su XY, Lu GH, Zhang CY, et al. Intracranial Meningioma Surgery in the Elderly (Over 65 Years): Prognostic Factors and Outcome. *Acta Neurochir (Wien)* (2015) 157:1549–57; discussion 1557. doi: 10.1007/s00701-015-2502-9
29. Modha A, Gutin PH. Diagnosis and Treatment of Atypical and Anaplastic Meningiomas: A Review. *Neurosurgery* (2005) 57:538–50; discussion 538-50. doi: 10.1227/01.NEU.0000170980.47582.A5
30. Dziuk TW, Woo S, Butler EB, Thornby J, Grossman R, Dennis WS, et al. Malignant Meningioma: An Indication for Initial Aggressive Surgery and Adjuvant Radiotherapy. *J Neurooncol* (1998) 37:177–88. doi: 10.1023/A:1005853720926
31. Zhou H, Bai HX, Chan L, Zhang PJ, Karakousis G, Huang R, et al. Survival Benefit of Adjuvant Radiotherapy in Elderly Patients With WHO Grade III Meningioma. *World Neurosurg* (2019) 131:e303–11. doi: 10.1016/j.wneu.2019.07.140

Conflict of Interest: The authors declare that the research was conducted in the absence of any commercial or financial relationships that could be construed as a potential conflict of interest.

frontiers | Frontiers in Oncology

REVIEW
published: 23 May 2022
doi: 10.3389/fonc.2022.898971

Image-Based Differentiation of Benign and Malignant Peripheral Nerve Sheath Tumors in Neurofibromatosis Type 1

Jun Liu[1†], Jing-Ning Huang[1†], Ming-Han Wang[1†], Zhen-Yang Ni[2], Wei-Hao Jiang[2], Manhon Chung[3], Cheng-Jiang Wei[3] and Zhi-Chao Wang[3*]*

[1] School of Medicine, Shanghai Jiao Tong University, Shanghai, China, [2] School of Electronic Information and Electrical Engineering, Shanghai Jiao Tong University, Shanghai, China, [3] Department of Plastic and Reconstructive Surgery, Shanghai Ninth People's Hospital, School of Medicine, Shanghai Jiao Tong University, Shanghai, China

Neurofibromatosis type 1 (NF1) is a dominant hereditary disease characterized by the mutation of the *NF1* gene, affecting 1/3000 individuals worldwide. Most NF1 patients are predisposed to benign peripheral nerve sheath tumors (PNSTs), including cutaneous neurofibromas (CNFs) and plexiform neurofibromas (PNFs). However, 5%-10% of PNFs will ultimately develop into malignant peripheral nerve sheath tumors (MPNSTs), which have a poor prognosis. Early and reliable differentiation of benign and malignant tumors in NF1 patients is of great necessity. Pathological evaluation is the "gold standard" for a definite diagnosis, but the invasive nature of the biopsy procedure restricts it from applying as a screening tool during the decades-long follow-up of these patients. Non-invasive image-based diagnostic methods such as CT and MRI are often considered essential screening tools for multiple types of tumors. For NF1 patients' lifelong regular follow-ups, these radiological methods are currently used for tumor evaluation. However, no consensus was established on screening the malignant transformation of benign PNSTs. Moreover, novel technologies like radiogenomics and PET-MRI have not been well evaluated and fully adopted for NF1 patients. This review summarizes current studies of different imaging methods for differentiating benign and malignant tumors in NF1. Meanwhile, we discussed the prospects of the usage of new tools such as radiogenomics and PET-MRI to distinguish MPNST from benign PNSTs more precisely. Summarizing these findings will help clarify the directions of future studies in this area and ultimately contribute to the radiology images-based clinical screening of MPNST in NF1 patients and finally improve the overall survival rates of these patients.

Keywords: neurofibromatosis type 1 (NF1), malignant peripheral nerve sheath tumors (MPNST), differential diagnosis, medical radiology image methods, future prospectives

OPEN ACCESS

Edited by:
Ignazio Gaspare Vetrano, Carlo Besta Neurological Institute Foundation (IRCCS), Italy

Reviewed by:
Marco Moscatelli, Carlo Besta Neurological Institute Foundation (IRCCS), Italy
Nora F. Dengler, Charité Universitätsmedizin Berlin, Germany

***Correspondence:**
Cheng-Jiang Wei
616813512@qq.com
Zhi-Chao Wang
shmuwzc@163.com;
wangzhichao@sh9hospital.org.cn

[†]These authors have contributed equally to this work and share first authorship

Specialty section:
This article was submitted to Neuro-Oncology and Neurosurgical Oncology, a section of the journal Frontiers in Oncology

Received: *18 March 2022*
Accepted: *18 April 2022*
Published: *23 May 2022*

Citation:
Liu J, Huang J-N, Wang M-H, Ni Z-Y, Jiang W-H, Chung M, Wei C-J and Wang Z-C (2022) Image-Based Differentiation of Benign and Malignant Peripheral Nerve Sheath Tumors in Neurofibromatosis Type 1. Front. Oncol. 12:898971. doi: 10.3389/fonc.2022.898971

INTRODUCTION

Neurofibromatosis type 1 (NF1), a hereditary disorder that primarily affects the peripheral nervous system, has a prevalence of approximately 1:2500 to 1:3500 in individuals worldwide (1). NF1 is caused by the mutation of the *NF1* gene, and the classic clinical characteristics include café-au-lait macules, skinfold freckling, benign neurofibromas, brain tumors, iris hamartomas, and typical bony lesions (2). Among those symptoms, benign neurofibromas, including cutaneous neurofibroma (CNF) and plexiform neurofibroma (PNF), are among the most common features of NF1. Approximately 30%-50% of patients with NF1 have plexiform neurofibromas. As a benign tumor, disability and deformity are common for these patients due to the vast tumor volume. Moreover, 5%-10% of these PNFs have the capacity for transformation into malignant peripheral nerve sheath tumors (MPNSTs), which have a poor overall survival rate of typically less than 5 years (1). Early diagnosis of MPNST is essential for early treatment, which will ultimately improve the prognosis of the patients. Tissue biopsy is considered the definitive diagnostic method for these patients, but as an invasive method, it cannot serve as a screening tool to be applied throughout the lifelong follow-up of patients with NF1. There is an urgent need for non-invasive, widely-used, and economical tools for these patients.

Medical radiology methods such as computed tomography (CT), magnetic resonance imaging (MRI), and positron emission tomography-computed tomography (PET-CT) played significant roles in various types of tumors. Unlike biopsy, these image-based methods are noninvasive and more suitable screening tools. One of the main functions of medical imaging methods is to distinguish benign lesions from malignant tumors. A report suggested that ultrasound-based differentiation of malignant and benign thyroid nodules has promising potential for clinical use (3). Meanwhile, another study showed that Cone-beam CT was proposed as a novel approach to predict breast lesion malignancy (4). Actually, in NF1-PNSTs and NF1-related MPNSTs, these image-based methods are also considered essential and widely adopted in tumor diagnosis and evaluation. The above studies on other types of tumors suggest the potential of image-based methods serving as efficient, noninvasive, inexpensive, and widely available tools in the differentiation of benign PNF and MPNST (5). However, as NF1 tumors are relatively rare, clear indications of image-based distinction between benign and malignant NF1 have not yet been fully defined.

To identify current studies and possible future directions in this area, we conducted a systematic review of the literature on radiology image-based differentiation of benign and malignant tumors in NF1. This review comprehensively summarizes different image-based methods used in distinguishing benign from malignant NF1 tumors, including CT, MRI, PET-CT, and ultrasound. This review also discusses the combination of radiology images and multiple-omics disciplines, such as the potential of clinical usage of radiogenomics in this field. On this basis, we further discuss possible future directions of radiology image methods in NF1. Better clarification of these will contribute to the early differential diagnosis of MPNST from PNF and eventually improve the overall survival of these patients.

MATERIALS AND METHODS

Search Strategy and Information Sources

This review was in line with recommendations from the Preferred Reporting Items for Systematic Reviews and Meta-Analyses (PRISMA) statement. The publications were identified by comprehensive searching of PubMed and our own reference library. Search terms included combinations of "Neurofibromatosis type 1," "Malignant peripheral nerve sheath tumors," "magnetic resonance imaging," "Computed Tomography," "PET imaging," "ultrasound," and "radiogenomics."

Study Selection, Data Collection, and Exclusion/Inclusion Criteria

Selection of material was limited to papers published in English. All of the publications were checked by at least two investigators. Patents, books and documents, case reports, and conferences were excluded. Also studies regarding only neurofibromatosis type 2 (NF2) or other unconcerned diseases were excluded. Studies related to differential diagnosis of benign and malignant tumors based on imaging characteristics, and correlation of genomics and radiology, are the inclusion criteria.

RESULTS

Using the search strategies mentioned above, 3203 records were presented, and among which 39 records met this review criteria. After applying the exclusion criteria, 3165 publications were removed, including; (a) 1977 records, such as patents, books and documents, case reports, and conferences; (b) 672 records did not relate to NF1; (c) 407 records did not relate to differential diagnosis and radiogenomics; and (d) 108 records did not meet the inclusion criteria. A flowchart (**Figure 1**) demonstrates the screening process and study selection.

Magnetic Resonance Imaging (MRI)

MRI is currently the preferred radiology image method for NF1. Compared to CT images, the MRI has a better resolution for this soft-tissue tumor. Based on the scarce clinical consensus, multiple current studies have already described the potential of MRI in the differential diagnosis of MPNST from NF1.

Benign neurofibroma is a well-defined mass with high intensity on T2-weighted MRI images. A central area of low intensity (the "target sign") in PNF lesions is sometimes observed, which is due to the presence of myxoid material peripherally and fibrous tissue centrally (**Figure 2**). Studies demonstrated that although not all benign tumors showed a "target sign," it indicated the lesion as benign PNF once it occurred (6). Compared with PNFs, MPNSTs on T2 sequences were more extensive with an infiltrative margin. Moreover, the

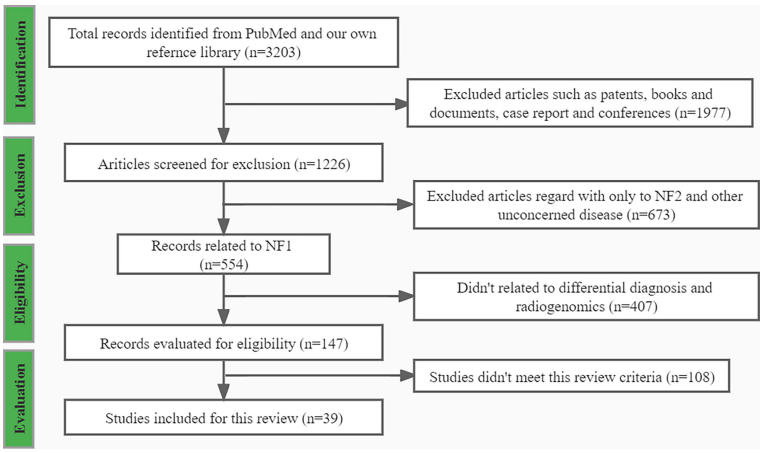

FIGURE 1 | The flowchart of publications screening process.

invasive growth of this malignant tumor resulted in a perifocal edema reaction which presented as "feathery" outside the tumor pseudo capsule (7). On T1-weighted images, it is hard to distinguish benign neurofibromas from MPNSTs due to the isointensity to adjacent muscles, but neurofibromas showed central focal enhancement and MPNSTs showed peripheral enhancement on T1-enhanced sequence after gadolinium (Gd) administration (7, 8). The underlying pathological mechanisms were that malignant transition of the tumor occurred with necrosis, hemorrhage, or both, leading to intratumoral cystic changes, accompanied by heterogeneity on MRI, but this rarely happens in neurofibroma (9) (**Figure 3**). In general, several key features mentioned above can be used to distinguish MPNST from benign neurofibroma, including the largest dimension of the mass, signal features of TI-weighted images and T2-weighted images, enhancement pattern, and cystic changes (**Table 1**). Junji Wasa et al. reported that the presence of two or more of the four features (the largest dimension of the mass, peripheral enhancement pattern, perilesional edema like zone, and intratumoral cystic lesion) had indicated malignant peripheral nerve sheath tumors with a sensitivity of 61% and a specificity of 90% (7). A meta-analysis of the included lesions involving at least 300 patients with NF1 (616 in total, some with NF1 features were not reported) showed that pooled and weighted sensitivity, specificity, and AUC values for MRI in detecting MPNSTs were 68%, 93%, and 0.89 when using feature combination, with specificity of perilesional edema and irregular being 94% and 90%, respectively (10).However, it is worth noting that morphological identification based on MRI is highly subjective. Furthermore, not all patients have the typical signs mentioned above on MRI images, and the scarcity of "atypical patients" also restricts the clinical usage and popularization of these features.

Beyond morphological features on MRI, functional MRI (fMRI), especially the diffusion-weighted image (DWI) based fMRI, has recently played an essential role in identifying MPNST as an auxiliary diagnostic technique. Well L et al. acquired axial

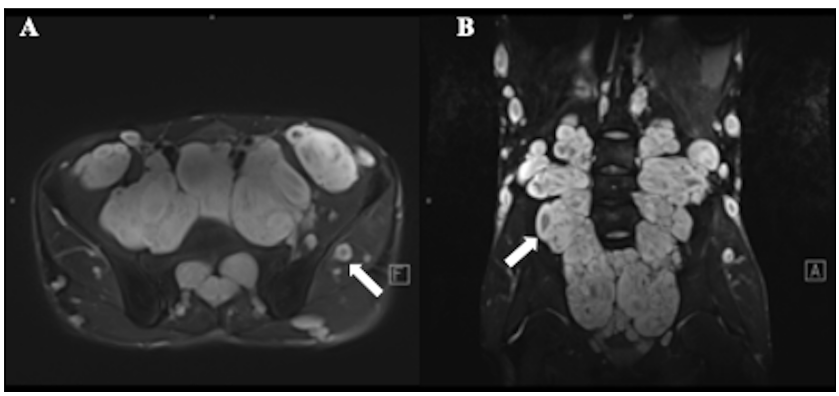

FIGURE 2 | A 17-year-old male with plexiform neurofibroma (PNF) who presented multiple masses throughout the body. T2-weighted MR image showed a target sign (arrow) with peripheral area of high intensity and central area of low intensity. **(A)** Multiple nodules and lumps in the walking area of the bilateral femoral nerve, sciatic nerve, and obturator nerve; **(B)** Multiple nodules and lumps in the epidermis, subcutaneous and soft tissues of the abdomen and pelvis.

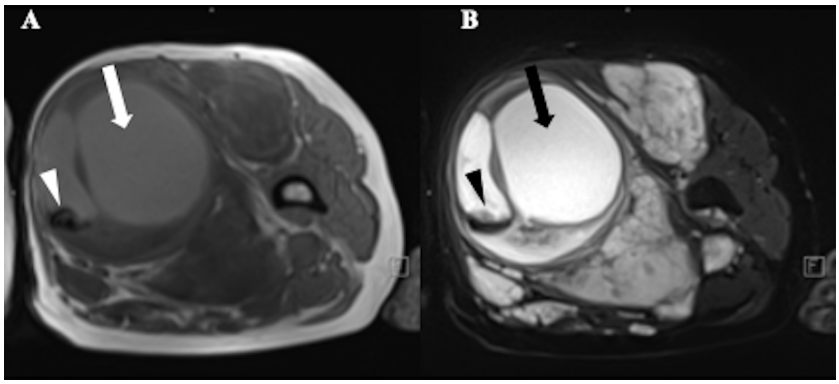

FIGURE 3 | A 52-year-old female with Neurofibromatosis type 1 (NF1) who presented with a large mass in soft tissue of upper left thigh. MRI showed a heterogeneous signal with cystic change (arrows) and hemorrhage (arrowheads) in the mass, suggestive of malignant transformation. **(A)** T1-weighted MR image;**(B)** T2-weighted MR image.

respiratory-triggered echo-planar sequences with 11 diffusion gradient b-values and used DWI-derived parameters (e.g., ADC, IVIM) for diagnosis (6). They found that DWI exhibited better performance in the differentiation of benign and malignant peripheral nerve sheath tumors (MPNSTs) in patients with NF1 compared with only using morphological features determined by MRI (6). Ahlawat S et al. further found that the "target sign" was more frequently visible on high b-values DWI images and ADC images than on anatomic sequences (11). They thought that the absence of a "target sign" on DWI might further indicate a neurogenic neoplasm as a malignant lesion, but this study lacked histological confirmation in benign cases and failed to assess and explain the histological architecture of the "target sign" (11). The meta-analysis mentioned above reported ADCmin or ADCmean with or without feature combination had sensitivity of 88%, specificities of 94%, and AUC values of 0.97 (10). A further study has found that DWI/ADC mapping specificity is likely to be another valuable method for MPNST differential diagnosis (12).

Another essential point about NF1 is that patients with neurofibromas may have tumors all over the body, and whole-body tumor burden is another indicator for the risk of malignant transformation (13). Whole-body MRI is an efficient tool for the whole-body tumor burden evaluation. A study demonstrated its suitability as a tool for identifying concealed MPNST (14). Wenli Cai et al. used the dynamic-threshold (DT) level set three-dimensional segmentation method to perform whole-body MRI and calculated volume, breaking the shackles of traditional two-dimensional methods (15). This 3D method allowed us to analyze the number and volume of tumors, which can be more effective for reliably assessing the patients' tumor burden (15). In addition, whole-body MRI can better track the occurrence and progression of tumors to assist doctors in better understanding the dynamic changes from PNF to MPNST (16). The regular surveillance by this method is especially essential for children because most PNF growth occurred at a young age, not in adulthood (17). By using whole-body MRI, various complications of tumors can be detected and treated before symptoms further developed and irreversible damage occurred (18).

Computed Tomography (CT)

CT is an ideal examination method for observing bone, joint, and soft tissue lesions. Advanced computed tomography (CT)

TABLE 1 | Features of Neurofibroma and MPNST on MRI.

	Neurofibroma	MPNST
Lesion size	small	Large
Margin	well defined	Invasive or ill-defined
Signal features of T1-weighted images T2-weighted images	peripheral high with central low on the T2-WI (target sign) Heterogeneous on T1-WI	peritumoral edema reaction show feathery outside the tumor a hyperintense signal on the T2-WI Heterogeneous on the T1-WI
Enhancement Pattern (Gd administration)	central enhancement on the T1WI	peritumoral edema presents edge enhancement on T2WI peripheral enhancement on the T1WI
cystic changes	few cystic changes	necrosis or hemorrhage
Whole-body MRI	/	more internal tumors larger volume
DW-MRI	/	lower diffusivity higher perfusion fraction

methods, such as CT perfusion and dual-energy CT, can help distinguish benign lesions from malignant head and neck tumors (19). However, there were no definitive CT diagnostic features reported that can be used to differentiate MPNST from benign PNF among NF1 patients until now (20). Nevertheless, our team developed a machine learning approach based on CT images that has recently shown great potential in differentiating MPNST from benign NF1 (20). This model, developed by combining machine learning technology with CT images, accurately distinguished malignancy-transformed lesions from benign neurofibromas of the head and neck. However, the limitation in training cohort hinders the accuracy of this model when applied to other parts of the body (20).

PET Imaging

Positron emission tomography (PET) scan is an imaging method using a radioactive medium like 18F-FDG to show the metabolic activity of different tissues to reveal the metabolic or biochemical function. PET/CT, the most popular PET-imaging mode at present, combines PET and CT and can simultaneously show the pathophysiological changes and morphological structure of the lesion, offering more information for the early diagnosis and differential diagnosis of tumors. Cook, G. J. R. and his colleagues found that 18F-FDG PET uptake was higher in MPNSTs than in benign neurofibromas, and the heterogeneity was more pronounced in MPNSTs. The first-order heterogeneity parameter was discriminatory in SUVmax, which exhibited significant differences in benign and malignant lesions of neurofibromas (21) (**Figure 4**). Further studies showed that high-order features could distinguish benign from malignant tumors, but the discriminatory ability was weaker compared with the usage of SUVmax (21). One of the limitations of FDG-PET/CT is that there is a significant overlap of the SUV values between benign and malignant lesions. A prospective trial on this problem demonstrated that although the SUVmax values of benign and malignant lesions overlapped, the FDG uptake of all malignant lesions was greater than 3.15 (22). Another clinical study showed that the detection sensitivity of SUV value for asymptomatic malignant lesions was 100%, the negative predictive value was 100%, and the specificity was 45.1% (23). Consistent with those findings, another study further analyzing early and delayed imaging found similar accuracy at differentiating MPNSTs from benign NF1 but better sensitivity for delayed acquisition (24). In addition, some novel PET/CT tracers have also been used in the differentiation of benign from malignant NF1. The 68Ga-PSMA in cutaneous neurofibromas can be clearly visualized on PET/CT images and showed some differences in different lesions, suggesting the potential of 68Ga-PSMA PET/CT in the surveillance of neurofibromatosis type 1 (25). Furthermore, the addition of 11C methionine to PET/CT improved its specificity in equivocal NF1 cases (26). Among these, a study suggested amino acid preparations with half-lives and novel tracers for measuring DNA or cell membrane synthesis should also be considered (27).

However, CT imaging is not the first choice for detecting soft-tissue tumors, as MRI has higher soft-tissue resolution and provides better anatomical information than CT images in these diseases. As a result, PET/MRI, combining PET and MRI imaging, might have higher accuracy in tumor screening and diagnosis than PET/CT. Reinert, C. P. et al. analyzed FDG-PET/MRI data in patients with neurofibromatosis type 1 and found that SUV values were significantly higher in the MPNST group than in the PNF group (28). Meanwhile, there was a significant difference in the ratio of lesion SUVmean-to-liver SUVmean between MPNSTs and PNFs (28).

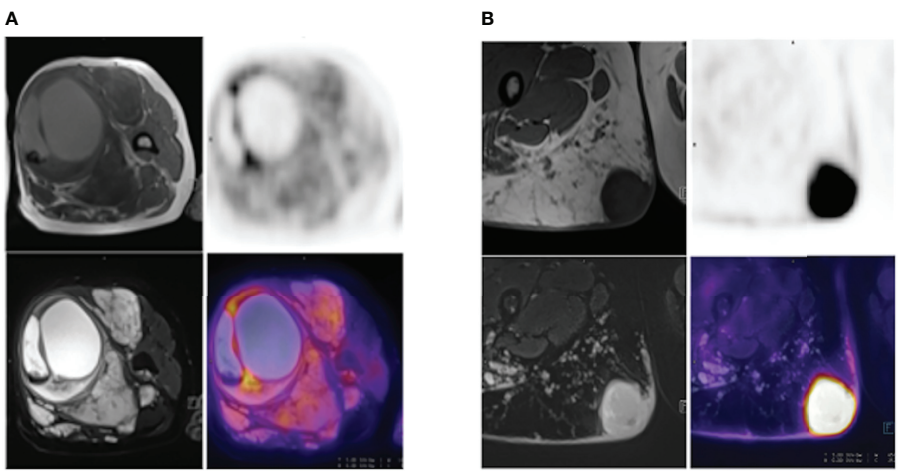

FIGURE 4 | **(A)** A 52-year-old NF1 patient with benign PNF lesions, particularly in the left thigh. The lesion was located in the soft tissue of the upper segment of the left thigh, was approximately 8.7 cm-9.5 cm in size, with clear boundary, heterogeneous internal signal, visible cystic degeneration with hemorrhage, and increased FDG uptake at the septa, SUVmax=4.9. **(B)** A 28-year-old NF1 patient with a MPNST in the upper segment of the right thigh, measuring 3.9 cm – 3.8 cm, with well-defined borders and increased FDG uptake, SUVmax=14.4.

Ultrasound

Ultrasound is used as an alternative regular approach to determine the peripheral neuropathic characteristics in NF1, providing valuable guidance in making a diagnosis and an operative plan (29). Beyond this, it is also considered as a potential tool for the differential diagnosis of MPNST from NF1. Peripheral neuropathies in NF1 are classified into four types by ultrasound: multiple nodular class, plexiform class, diffuse class, and mixed class (30). The multiple nodular class presents as multiple ovoids, lobulated nodes with clear boundaries, characterized by hypoechoic mixed echo in ultrasound. The plexiform class presents with thickening of long range of peripheral nerve trunks and loss of normal nerve tract structure, characterized by a pampiniform and beaded hypoechoity. The diffuse class has thickened subcutaneous tissue and fat layers, with a nodular hypoechoity. The mixed class has the diffuse class coexisting with the multiple nodular class and hypoechoic masses, often in subcutaneous muscular layers (30). When the benign neurofibroma transformed into MPNST, the ultrasound features presented as recurrence of lobulated tumors, characterized by heterogeneous echo, with plentiful blood flow signals (29). In addition, MPNST may sometimes occur in areas where peripheral neuropathies were not found previously (31).

The characteristics of benign and malignant peripheral neuropathies were further summarized manifesting in seven aspects in a study of high-resolution ultrasound: (1) The size of a benign tumor mostly was below 5 centimeters while that of MPNSTs was generally above 5 centimeters; (2) Most benign tumors grew slowly for years, while MPNSTs grew fast over weeks to months; (3) The margins of benign tumors were regular with no peritumoral edema, while the margins of MPNST were irregular and the peritumoral edema is presented; (4) Benign tumors were characterized by homogenous echo, while MPNSTs were characterized by heterogeneous echo; (5) Benign tumors were often solitary, but the MPNSTs were infiltrative; (6) Regarding to vascularization, benign tumors presented as hierarchic, and MPNSTs presented as stenotic, occlusive, trifurcated, and archaic vascular pattern; (7) In contrast-enhanced ultrasonography, no enhancement was seen in benign tumors, while peripheral enhancement with central nonenhancement presented in MPNSTs (32).

Radiogenomics

In recent years, scientists have focused on combining imaging technology with other biological information and managed to provide imaging parameters biological explanations. Radiogenomics is a specific example of combining imaging features and genomic profiles (33). Neurofibromatosis type 1 (NF1) is an autosomal dominant disorder (1), which means that the occurrence and development of NF1 are tightly related to the gene mutation. It was reported that loss of the *CDKN2A* locus at 9p21 and mutation of the *TP53* gene might lead to the malignant transformation to MPNST. Also the loss-of-function mutations in EED and SUZ12 genes was related to MPNST, resulting in the loss of expression of trimethylated histone 3 at lysine residue 27 (H3K27me3) (34). Several studies recently have focused on the relationship between genetic phenotypes and imaging characteristics of NF1. Liu Y et al. divided the *NF1* mutations into five mutation domains (MDs) according to their biochemical functions. They also categorized the MRI features into six groups, including histogram statistics features, image gradient features, run-length (RL) texture features, gray level co-occurrence matrix texture features, shape-based features, and second-order moment features (35). Clinical characteristics were also added, and the study suggested a strong association among phenotypes, image feature patterns, and *NF1* mutation type and domains (35). Another study found that a special imaging feature of some NF1 patients on MRI, the neurofibromatosis type 1 bright objects (NBOs), was correlated with the mutation type of the *NF1* gene (36). NBOs were more likely to appear in the NF1 patients with frameshift variants than splicing or missense variants (36).

DISCUSSION AND FUTURE DIRECTIONS

Malignant transformation of patients with NF1 can be detected by various methods, such as clinical manifestations and pathological characteristics. Three clinical symptoms, pain, enlargement of the mass, and neurological symptoms, were reported as worth evaluating (37). However, in multivariate analysis, only peripheral nerve sheath tumor enlargement remained an independent high-risk factor for malignant transformation (37). Clinical features provided primary evidence for malignant transformation in NF1 patients, but there is a great need for further evidence to confirm these associations. Under these circumstances, histopathological examination is used as the gold standard for diagnosis. Moreover, NF1 could be divided into six diagnostic categories: neurofibroma (NF), neurofibroma with atypia, cellular neurofibroma, ANNUBP, low-grade MPNST, and high-grade of MPNST according to the pathological characteristics of the tumor (34). However, tissue biopsy is an invasive process that is not suitable for every follow-up of NF1 patients during their lifetime. Therefore, reliable, noninvasive, and widely available tools are in great need.

Many studies have been devoted to the development of various image-based techniques to distinguish malignant lesions from benign NF1 tumors, including MRI, CT, PET, and ultrasound.

MRI, as a mature radiological method, has high potential in the clinical practice for differentiation of NF1 and MPNST. The "target sign" is the particular sign of benign tumors in T2-weighted imaging (11). In addition, the number of tumors, the peripheral enhancement pattern, the perilesional edema-like zone, and the presence or absence of intratumoral cystic lesions are also the key points in distinguishing benign and malignant tumors (7). However, current reported experiences-based differentiation is highly subjective, which

are hard to popularize for the NF1 which is a relatively rare type of tumor. There is an urgent need for establishing objective standards for distinguishing MPNST from benign NF1. Noticing the current research highlights in radiomics and artificial intelligence-assisted diagnosis in multiple types of cancer, we propose extracting high-throughput MRI imaging features from NF1 and MPNST patients and applying deep learning methods. A machine learning model developed to automatically identify benign and malignant neurofibromas might achieve the purpose of early screening of patients with MPNST by a relatively objective and easily popularized tool.

CT is commonly used to observe bone, joint, and soft tissue lesions. Advanced computed tomography (CT), such as CT perfusion and dual-energy CT, helped distinguish multiple types of malignant tumors from benign head and neck lesions (19). However, this anatomic imaging method was proven to be ineffective to distinguish MPNST from benign NF1 (22). With the development of computer technology, the application of deep learning and artificial intelligence models has provided new possibilities for CT in the differential diagnosis of MPNST from benign NF1.

Compared to CT and MRI imaging, PET/CT combines anatomical, functional, and metabolic information of the lesion. At present, there are many clinical studies on PET/CT in differentiating benign and malignant neurofibromas based on significant differences in parameters such as SUVmax and 18F-FDG uptake (21–23). However, MRI has higher soft-tissue resolution and provides better anatomical information than CT images in these diseases, suggesting PET/MRI might have higher accuracy in tumor screening and diagnosis. Clinical studies have also reported defects of these methods: MRI had limited sensitivity for detecting MPNST, while the metabolic activity of MPNST was not always a reliable indicator of histopathologic tumor grade (38). Moreover, clinical studies of PET/MRI in differentiating benign from malignant neurofibromas are rare. But this technique is still believed to have a prosperous future in clinical usage for NF1 patients, which need more explorations in the future.

Ultrasound is a reliable, convenient, and cost-effective method for the differentiation of benign from malignant NF1, The characteristics of benign and malignant peripheral neuropathies were further summarized manifesting in seven aspects in a study of high-resolution ultrasound (32), offering a sort of differential standard for malignant transformation in individuals with NF1. Though ultrasound is not well suited for whole-body tumor volume evaluation, it is highly valuable in the diagnosis and clinical assessment of NF1 and related MPNST. Compared to PET-CT and whole-body MRI, ultrasound is radiotoxicity-free and relatively economical. In addition, ultrasound might contribute to distinguishing features of interest for investigation by MRI (29). Despite the above, ultrasound is not currently widely applied in the clinic. One reason might be the scarcity of sufficient clinical studies in this area, causing a lack of universal clinical guidelines. With the increasing clinical application of this method in the future, ultrasound might become a convenient and reliable screening method to differentiate MPNST from benign PNF.

In conclusion, multiple imaging modalities play essential roles in distinguishing MPNST from benign NF1. All these methods have their own strengths and weaknesses, such as limited sensitivity, high cost, or difficulties in whole-body assessment. More importantly, the results are not convincing enough due to the limited number of recruited patients in current studies.

Further studies are needed to solve these problems, and we recommend the following aspects be taken into consideration in future studies: (1) Combination of different imaging methods. Different imaging methods have their tendencies, and the combination could better exploit their strengths and circumvent their weaknesses. (2) Combination of computer technologies such as artificial intelligence with these imaging methods. As neurofibromatosis type 1 is a relatively rare disease, most clinical doctors, especially those in remote areas, have limited experience in reading radiological images of NF1 patients. AI models could acquire and analyze the information quickly and even exhibited better performance than doctors. The development of AI models could easily spread, which would be convenient and efficient for NF1 patients' lifelong follow-up at their local hospital. (3) Association between radiological images and other omics. One of the directions of current studies in radiology imaging is how to explain the image parameters such as grey value differences with biological significance. In this article, we searched for the possible relationship between NF1 radiology images and genomic profiles and the results are presented. The combination of the two could probably be applied to the early discovery or even early prevention of MPNST developing from benign neurofibroma of NF1 patients. Though current studies are superficial, we believe further studies will improve our understanding of radiogenomics. In addition, the combination of radiology and histopathology is worth exploring. Although no study has completely explained the correlation of histology and radiology in NF1, a retrospective study analyzing the three-dimensional T1-weighted MR images of NF1 patients suggested that patients with NF1 had higher subcortical volumes and thicker cortices in selected regions, particularly in the hippocampus, amygdalae, cerebellar white matter, ventral diencephalon, thalamus, and occipital cortex (39). This study demonstrated the histological changes as part of the reasons for the variation on radiological images.

CONCLUSION

A summary diagram of image-based characteristics of differentiation of benign and malignant peripheral nerve sheath tumors in individuals with NF1 is presented (**Figure 5**). Although studies in this area are still in the early stages and mostly lack of large cohorts, current data have implicated the exciting potential roles of medical radiological imaging in the differential diagnosis of MPNST from benign NF1 at early stage and have even promoted further understanding and evaluation of this disease. With further studies in the future, we are confident in the prospect of a more significant role of these radiological imaging methods in

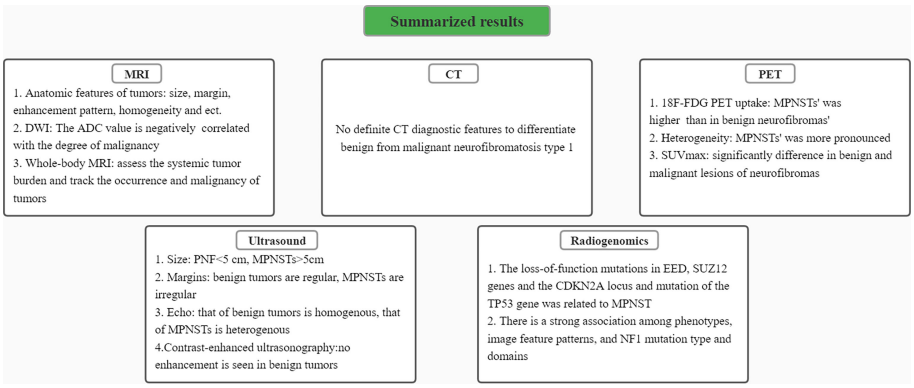

FIGURE 5 | A summary diagram of results. Characteristics of differentiating benign peripheral nerve sheath tumors from malignant ones in MRI, CT, PET, ultrasound images and radiogenomics were respectively presented.

the clinical diagnosis, follow-up, and treatment of NF1 and related tumors.

AUTHOR CONTRIBUTIONS

JL, J-NH, M-HW, and C-JW contributed to the conception of the study and wrote the manuscript. JL, J-NH, and M-HW contributed significantly to collection and assembly of data. W-HJ, Z-YN, C-JW, MC, and Z-CW help with the writing-review, editing and supervision. All authors read and approved the final manuscript.

FUNDING

This work was supported by grants from The 15th undergraduate training program for innovation of Shanghai Jiao Tong University school of medicine (1521X311); "Chenguang Program" supported by Shanghai Education Development Foundation (SHEDF) (19CG18); Shanghai Rising Star Program supported by Science and Technology Commission of Shanghai Municipality (20QA1405600); Science and Technology Commission of Shanghai Municipality (19JC1413); Natural Science Foundation of Shanghai (22ZR1422300); Shanghai Municipal Key Clinical Specialty (shslczdzk00901); Innovative research team of high-level local universities in Shanghai (SSMU-ZDCX20180700). National Natural Science Foundation of China (82102344)

ACKNOWLEDGMENTS

We sincerely appreciate the support from the 15th undergraduate training program for innovation of Shanghai Jiao Tong University school of medicine.

REFERENCES

1. Anderson JL, Gutmann DH. Neurofibromatosis Type 1. *Handb Clin Neurol* (2015) 132:75–86. doi: 10.1016/B978-0-444-62702-5.00004-4
2. Ferner RE, Gutmann DH. Neurofibromatosis Type 1 (NF1): Diagnosis and Management. *Handb Clin Neurol* (2013) 115:939–55. doi: 10.1016/B978-0-444-52902-2.00053-9
3. Xia J, Chen H, Li Q, Zhou M, Chen L, Cai Z, et al. Ultrasound-Based Differentiation of Malignant and Benign Thyroid Nodules: An Extreme Learning Machine Approach. *Comput Methods Programs BioMed* (2017) 147:37–49. doi: 10.1016/j.cmpb.2017.06.005
4. Uhlig J, Uhlig A, Kunze M, Beissbarth T, Fischer U, Lotz J, et al. Novel Breast Imaging and Machine Learning: Predicting Breast Lesion Malignancy at Cone-Beam CT Using Machine Learning Techniques. *AJR Am J Roentgenol* (2018) 211(2):W123–31. doi: 10.2214/AJR.17.19298
5. Salamon J, Mautner VF, Adam G, Derlin T. Multimodal Imaging in Neurofibromatosis Type 1-Associated Nerve Sheath Tumors. *Rofo* (2015) 187(12):1084–92. doi: 10.1055/s-0035-1553505
6. Well L, Salamon J, Kaul MG, Farschtschi S, Herrmann J, Geier KI, et al. Differentiation of Peripheral Nerve Sheath Tumors in Patients With Neurofibromatosis Type 1 Using Diffusion-Weighted Magnetic Resonance Imaging. *Neuro Oncol* (2019) 21(4):508–16. doi: 10.1093/neuonc/noy199
7. Wasa J, Nishida Y, Tsukushi S, Shido Y, Sugiura H, Nakashima H, et al. MRI Features in the Differentiation of Malignant Peripheral Nerve Sheath Tumors and Neurofibromas. *AJR Am J Roentgenol* (2010) 194(6):1568–74. doi: 10.2214/AJR.09.2724
8. Ogose A, Hotta T, Morita T, Yamamura S, Hosaka N, Kobayashi H, et al. Tumors of Peripheral Nerves: Correlation of Symptoms, Clinical Signs, Imaging Features, and Histologic Diagnosis. *Skeletal Radiol* (1999) 28 (4):183–8. doi: 10.1007/s002560050498
9. Levine E, Huntrakoon M, Wetzel LH. Malignant Nerve-Sheath Neoplasms in Neurofibromatosis: Distinction From Benign Tumors by Using Imaging Techniques. *AJR Am J Roentgenol* (1987) 149(5):1059–64. doi: 10.2214/ajr.149.5.1059
10. Wilson MP, Katlariwala P, Low G, Murad MH, McInnes MDF, Jacques L, et al. Diagnostic Accuracy of MRI for the Detection of Malignant Peripheral Nerve Sheath Tumors: A Systematic Review and Meta-Analysis. *AJR Am J Roentgenol* (2021) 217(1):31–9. doi: 10.2214/AJR.20.23403
11. Ahlawat S, Fayad LM. Imaging Cellularity in Benign and Malignant Peripheral Nerve Sheath Tumors: Utility of the "Target Sign" by Diffusion Weighted Imaging. *Eur J Radiol* (2018) 102:195–201. doi: 10.1016/j.ejrad.2018.03.018
12. Ahlawat S, Blakeley JO, Rodriguez FJ, Fayad LM. Imaging Biomarkers for Malignant Peripheral Nerve Sheath Tumors in Neurofibromatosis Type 1. *Neurology* (2019) 93(11):E1076–84. doi: 10.1212/WNL.0000000000008092

13. Nguyen R, Jett K, Harris GJ, Cai W, Friedman JM, Mautner VF., et al. Benign Whole Body Tumor Volume is a Risk Factor for Malignant Peripheral Nerve Sheath Tumors in Neurofibromatosis Type 1. *J Neurooncol* (2014) 116 (2):307–13. doi: 10.1007/s11060-013-1293-1
14. Ahlawat S, Fayad LM, Khan MS, Bredella MA, Harris GJ, Evans DG, et al. Current Whole-Body MRI Applications in the Neurofibromatoses: NF1, NF2, and Schwannomatosis. *Neurology* (2016) 87(7 Suppl 1):S31–9. doi: 10.1212/WNL.0000000000002929
15. Cai W, Kassarjian A, Bredella MA, Harris GJ, Yoshida H, Mautner VF, et al. Tumor Burden in Patients With Neurofibromatosis Types 1 and 2 and Schwannomatosis: Determination on Whole-Body MR Images. *Radiology* (2009) 250(3):665–73. doi: 10.1148/radiol.2503080700
16. Hirbe AC, Gutmann DH. The Management of Neurofibromatosis Type 1-Associated Malignant Peripheral Nerve Sheath Tumors: Challenges, Progress, and Future Prospects. *Expert Opin Orphan Drugs* (2017) 5(8):623–31. doi: 10.1080/21678707.2017.1348294
17. Nguyen R, Dombi E, Widemann BC, Solomon J, Fuensterer C, Kluwe L, et al. Growth Dynamics of Plexiform Neurofibromas: A Retrospective Cohort Study of 201 Patients With Neurofibromatosis 1. *Orphanet J Rare Dis* (2012) 7:75. doi: 10.1186/1750-1172-7-75
18. Legius E, Brems H. Genetic Basis of Neurofibromatosis Type 1 and Related Conditions, Including Mosaicism. *Childs Nerv Syst* (2020) 36(10):2285–95. doi: 10.1007/s00381-020-04771-8
19. Abdel Razek AAK, Gamaleldin OA, Elsebaie NA. Peripheral Nerve Sheath Tumors of Head and Neck: Imaging-Based Review of World Health Organization Classification. *J Comput Assist Tomogr* (2020) 44(6):928–40. doi: 10.1097/RCT.0000000000001109
20. Wei CJ, Yan C, Tang Y, Wang W, Gu YH, Ren JY, et al. Computed Tomography-Based Differentiation of Benign and Malignant Craniofacial Lesions in Neurofibromatosis Type I Patients: A Machine Learning Approach. *Front Oncol* (2020) 10. doi: 10.3389/fonc.2020.01192
21. Cook GJR, Lovat E, Siddique M, Goh V, Ferner R, Warbey VS., et al. Characterisation of Malignant Peripheral Nerve Sheath Tumours in Neurofibromatosis-1 Using Heterogeneity Analysis of F-18-FDG PET. *Eur J Nucl Med Mol Imaging* (2017) 44(11):1845–52. doi: 10.1007/s00259-017-3733-1
22. Tovmassian D, Abdul Razak M, London K. The Role of [(18)F]FDG-PET/CT in Predicting Malignant Transformation of Plexiform Neurofibromas in Neurofibromatosis-1. *Int J Surg Oncol* (2016) 2016:6162182. doi: 10.1155/2016/6162182
23. Azizi AA, Slavc I, Theisen BE, Rausch I, Weber M, Happak W, et al. Monitoring of Plexiform Neurofibroma in Children and Adolescents With Neurofibromatosis Type 1 by [(18) F]FDG-PET Imaging. Is it of Value in Asymptomatic Patients? *Pediatr Blood Cancer* (2018) 65(1):e26733. doi: 10.1002/pbc.26733
24. Chirindel A, Chaudhry M, Blakeley JO, Wahl R. F-18-FDG PET/CT Qualitative and Quantitative Evaluation in Neurofibromatosis Type 1 Patients for Detection of Malignant Transformation: Comparison of Early to Delayed Imaging With and Without Liver Activity Normalization. *J Nucl Med* (2015) 56(3):379–85. doi: 10.2967/jnumed.114.142372
25. Gulhane B, Ramsay S, Fong W. 68ga-PSMA Uptake in Neurofibromas Demonstrated on PET/CT in a Patient With Neurofibromatosis Type 1. *Clin Nucl Med* (2017) 42(10):776–8. doi: 10.1097/RLU.0000000000001777
26. Bredella MA, Torriani M, Hornicek F, Ouellette HA, Plamer WE, Williams Z, et al. Value of PET in the Assessment of Patients With Neurofibromatosis Type 1. *AJR Am J Roentgenol* (2007) 189(4):928–35. doi: 10.2214/AJR.07.2060
27. Fisher MJ. The Use of PET in the Evaluation of Tumors in Children With Neurofibromatosis Type 1. *Pet Clinics* (2008) 3(4):531–49. doi: 10.1016/j.cpet.2009.04.005
28. Reinert CP, Schuhmann MU, Bender B, Gugel I, la Fougere C, Schafer J, et al. Comprehensive Anatomical and Functional Imaging in Patients With Type I Neurofibromatosis Using Simultaneous FDG-PET/MRI. *Eur J Nucl Med Mol Imaging* (2019) 46(3):776–87. doi: 10.1007/s00259-018-4227-5
29. Winter N, Rattay TW, Axer H, Schaffer E, Decard BF, Gugel I, et al. Ultrasound Assessment of Peripheral Nerve Pathology in Neurofibromatosis Type 1 and 2. *Clin Neurophysiol* (2017) 128(5):702–6. doi: 10.1016/j.clinph.2017.02.005
30. Telleman JA, Stellingwerff MD, Brekelmans GJ, Visser LH. Nerve Ultrasound: A Useful Screening Tool for Peripheral Nerve Sheath Tumors in NF1? *Neurology* (2017) 88(17):1615–22. doi: 10.1212/WNL.0000000000003870
31. Telleman JA, Stellingwerff MD, Brekelmans GJ, Visser LH. Nerve Ultrasound in Neurofibromatosis Type 1: A Follow-Up Study. *Clin Neurophysiol* (2018) 129(2):354–9. doi: 10.1016/j.clinph.2017.11.014
32. Winter N, Dohrn MF, Wittlinger J, Loizides A, Gruber H, Grimm A. Role of High-Resolution Ultrasound in Detection and Monitoring of Peripheral Nerve Tumor Burden in Neurofibromatosis in Children. *Childs Nerv Syst* (2020) 36(10):2427–32. doi: 10.1007/s00381-020-04718-z
33. Bodalal Z, Trebeschi S, Nguyen-Kim TDL, Schats W, Beets-Tan R. Radiogenomics: Bridging Imaging and Genomics. *Abdom Radiol (NY)* (2019) 44(6):1960–84. doi: 10.1007/s00261-019-02028-w
34. Miettinen MM, Antonescu CR, Fletcher CDM, Kim A, Lazar AJ, Quezado MM, et al. Histopathologic Evaluation of Atypical Neurofibromatous Tumors and Their Transformation Into Malignant Peripheral Nerve Sheath Tumor in Patients With Neurofibromatosis 1-a Consensus Overview. *Hum Pathol* (2017) 67:1–10. doi: 10.1016/j.humpath.2017.05.010
35. Liu Y, Jordan JT, Bredella MA, Erdin S, Walker JA, Vangel M, et al. Correlation Between NF1 Genotype and Imaging Phenotype on Whole-Body MRI: NF1 Radiogenomics. *Neurology* (2020) 94(24):e2521–31. doi: 10.1212/WNL.0000000000009490
36. Hazan F, Gursoy S, Unalp A, Yilmaz U, Demirag B, Aydin Koker S, et al. Evaluation of Clinical Findings and Neurofibromatosis Type 1 Bright Objects on Brain Magnetic Resonance Images of 60 Turkish Patients With NF1 Gene Variants. *Neurol Sci* (2021):2045–57. doi: 10.1007/s10072-020-04988-0
37. Valeyrie-Allanore L, Ismaili N, Bastuji-Garin S, Zeller J, Wechsler J, Revuz J, et al. Symptoms Associated With Malignancy of Peripheral Nerve Sheath Tumours: A Retrospective Study of 69 Patients With Neurofibromatosis 1. *Br J Dermatol* (2005) 153(1):79–82. doi: 10.1111/j.1365-2133.2005.06558.x
38. Derlin T, Tornquist K, Munster S, Apostolova I, Hagel C, Friedrich RE, et al. Comparative Effectiveness of 18F-FDG PET/CT Versus Whole-Body MRI for Detection of Malignant Peripheral Nerve Sheath Tumors in Neurofibromatosis Type 1. *Clin Nucl Med* (2013) 38(1):e19-25. doi: 10.1097/RLU.0b013e318266ce84
39. Barkovich MJ, Tan CH, Nillo RM, Li Y, Xu D, Glastonbury CM, et al. Abnormal Morphology of Select Cortical and Subcortical Regions in Neurofibromatosis Type 1. *Radiology* (2018) 289(2):499–508. doi: 10.1148/radiol.2018172863

Conflict of Interest: The authors declare that the research was conducted in the absence of any commercial or financial relationships that could be construed as a potential conflict of interest.

frontiers | Frontiers in Oncology

CASE REPORT
published: 26 May 2022
doi: 10.3389/fonc.2022.907324

Recurrent Solitary Fibrous Tumor (Intracranial Hemangiopericytoma) Treated With a Novel Combined-Modality Radiosurgery Technique: A Case Report and Review of the Literature

Alexander J. Allen[1]*, *Dominic Angelo Labella*[1], *K. Martin Richardson*[1], *Jason P. Sheehan*[2] *and Charles R. Kersh*[1]

[1] Chesapeake Regional, Riverside & University of Virginia Radiosurgery Center, Riverside Regional Medical Center, Newport News, VA, United States, [2] Department of Neurological Surgery, University of Virginia Health System, Charlottesville, VA, United States

OPEN ACCESS

Edited by:
Pierpaolo Alongi,
ARNAS Ospedali Civico Di Cristina Benfratelli, Italy

Reviewed by:
Pantaleo Romanelli,
CDI, Italy
Mirza Pojskic,
University Hospital of Giessen and Marburg, Germany

***Correspondence:**
Alexander J. Allen
ajallen583@gmail.com

Specialty section:
This article was submitted to Neuro-Oncology and Neurosurgical Oncology, a section of the journal Frontiers in Oncology

Received: 29 March 2022
Accepted: 22 April 2022
Published: 26 May 2022

Citation:
Allen AJ, Labella DA, Richardson KM, Sheehan JP and Kersh CR (2022) Recurrent Solitary Fibrous Tumor (Intracranial Hemangiopericytoma) Treated With a Novel Combined-Modality Radiosurgery Technique: A Case Report and Review of the Literature. Front. Oncol. 12:907324. doi: 10.3389/fonc.2022.907324

Solitary Fibrous Tumor (SFT) is a rare and aggressive mesenchymal malignancy of the dura with a predilection for recurrence after treatment. We report a case of a SFT initially treated with subtotal surgical resection followed by a combination of Gamma Knife (GK) and linear accelerator-based radiosurgery. Forty-four days post-resection, the tumor had demonstrated radiographic evidence of recurrent disease within the post-operative bed. GK radiosurgery treatment was delivered in a "four-matrix" fashion targeting the entire surgical cavity as well as three nodular areas within this wide field. This treatment was delivered in one fraction with a stereotactic head frame for immobilization. A consolidation radiosurgery treatment course was then delivered over three additional fractions to the resection bed using a linear accelerator and mesh mask for immobilization. The total biologically effective dose (BED) was calculated as 32.50 Gy to the surgical bed and approximately 76.50 Gy to each nodular area. Almost three years post-operatively, the patient is alive and without radiographic or clinical evidence of disease recurrence. To our knowledge, no prior experiences have documented treatment of SFT using a mixed-modality, multi-fraction radiosurgery technique like the method detailed in this report. Our experience describes a combined modality, multi-fraction radiosurgery approach to treating recurrent SFT that maximizes radiation dose to the targets while minimizing complication risk. We believe this novel radiosurgery method should be considered in cases of grade II SFT post-resection.

Keywords: gamma knife (GK), solitary fibrous tumor (SFT), intracranial hemangiopericytoma, stereotactic radiosurgery (SRS), recurred cancer

INTRODUCTION

Solitary fibrous tumor (SFT), known as hemangiopericytoma prior to the updated 2016 World Health Organization (WHO) guidelines, is a rare intracranial malignancy thought to originate from pericyte cells lining the capillary walls. These tumors constitute 2.5% of meningeal tumors and less than 1% of intracranial tumors (1, 2). They are usually attached to the dura, and are thus frequently mistaken for meningiomas on imaging. Unlike meningiomas, SFT are malignant and have a propensity for local recurrence and extracranial metastasis after resection (3). SFT are classified as WHO grade I or II neoplasms with some anaplastic variants classified as grade III (high grade) (4). The mean age of occurrence is 43 years and men are slightly more often affected than women (male/female ratio 1.4:1) (2).

While resection is the most common initial therapy for SFT, stereotactic radiosurgery (SRS), specifically Gamma Knife (GK) radiosurgery, has emerged as a promising adjuvant treatment. Multiple studies have suggested a likely survival benefit of adjuvant SRS for SFT compared to resection alone (5–7). However, published data still show high recurrence rates of SFT despite adjuvant radiosurgery, implying a need for more effective treatment plans (5). There is evidence suggesting that higher cumulative radiation dose from adjuvant GK correlates with significantly improved progression free survival (PFS) for SFT (6, 8). However, delivering higher doses of radiation can increase risk of adverse effects, and dividing treatment across multiple fractions requires multiple invasive headframe placements for most GK systems. We describe treating a case of grade II SFT post-resection using a single-fraction GK treatment with multiple treatment volumes followed by a multi-fraction consolidation radiosurgery treatment using a linear accelerator (**Figure 1**). Most of the literature documenting radiosurgery treatment for SFT focuses on single-fraction GK specifically. To our knowledge, there are no published studies documenting adjuvant SRS treatment of SFT administered in multiple fractions using two different radiotherapy delivery systems.

CASE DESCRIPTION

A 61-year-old male with a past medical history of hypertension initially presented to the emergency room after experiencing a sudden episode of expressive aphasia for one minute while resting at home. His symptoms had completely resolved upon arrival to the emergency department. He denied any nausea, vomiting, vision changes, or witnessed seizure-like activity. Neurological exam in the emergency department was non-focal.

Subsequent magnetic resonance imaging (MRI) of the brain revealed a 5.2 x 5.6 cm low T1, high FLAIR, high T2, homogenously enhancing dural-based mass in the posterior frontal lobe. The mass extended across the midline with invasion and transgression of the interhemispheric fissure and superior sagittal sinus with minimal surrounding vasogenic edema. After neurosurgical evaluation, dexamethasone and levetiracetam were started and the patient was scheduled for surgery. The patient underwent craniotomy and resection of the presumed meningioma 17 days after initial presentation. The tumor was dissected from within the sagittal sinus. However, the tumor was only partially resected as the visible disease could not be fully excised from the patent sinus anteriorly or posteriorly. The patient tolerated surgery without complications.

Surgical pathology was consistent with a malignant Hemangiopericytoma/Solitary Fibrous Tumor (SFT), World Health Organization (WHO) grade II/III, Ki67 2%, and diffusely *STAT6* positive. A brain MRI performed 44 days post-operatively revealed post-surgical encephalomalacia in the high right posterior region with marginal nodular enhancement along the left lateral and posterior surgical bed. These findings were compatible with recurrent disease. Due to the low likelihood of achieving a complete resection in a subsequent operation, as well as patient preference, repeat surgery was deferred in favor of radiosurgery. We sought to deliver a high cumulative dose to the resection bed based on the literature showing better outcomes in treating SFT with higher overall radiation doses from adjuvant SRS. However, due to the large size of the treatment area, we could not achieve an adequate cumulative dose in a single headframe-based Gamma Knife (GK) radiosurgery treatment without risking significant complications. The decision was thus made to pursue a hypofractionated radiotherapy regimen, with each treatment separated by at least one week. Because our institution at the time was equipped with a GK Perfexion™ system that only allowed for headframe-based treatment, we opted for a combination technique of GK followed by stereotactic body radiotherapy (SBRT) with a linear accelerator.

The patient underwent GK to the tumor bed using a four-matrix paradigm: the broad, post-operative region was treated with 8 Gy to the 50% isodose line while three radiographically enhancing, nodular foci within this region were simultaneously treated with 20 Gy each to the 50% isodose line (**Figure 2**).

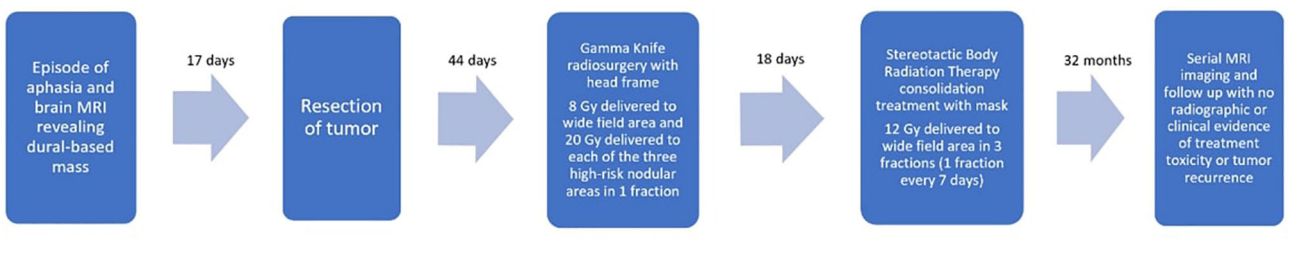

FIGURE 1 | Clinical and Treatment Timeline.

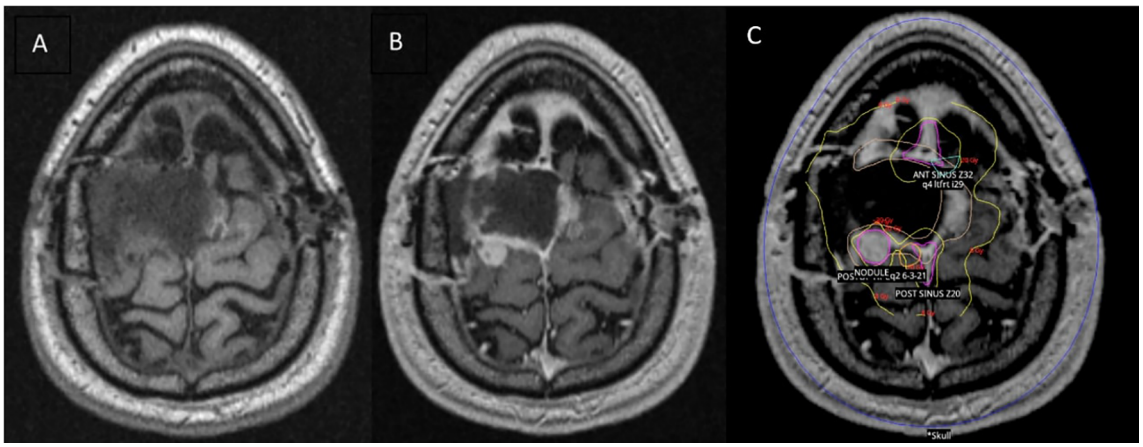

FIGURE 2 | Brain MRI performed 44 days post-operatively and overlying radiotherapy treatment plan. **(A)** MRI T1 pre-contrast. **(B)** MRI T1 post-contrast showing peripheral nodular enhancement on the left lateral and posterior surgical bed. **(C)** Gamma Knife (GK) radiosurgery treatment plan overlying T1 post-contrast MRI brain. The wide post-operative area is represented by the yellow contour. The pink contours delineate the three nodular, high-risk areas.

A stereotactic head frame was attached to the calvarium prior to treatment, and the treatment was delivered in one fraction. SBRT consolidation treatment to the area was then performed with a Varian Edge™ linear accelerator and a thermoplastic mesh mask for immobilization. The treatment plan was transferred from the GammaPlan™ planning system to the ARIA™ linear accelerator planning software. The first fraction of consolidation SBRT was delivered 18 days after initial GK treatment. This consolidation plan consisted of treating the broad, post-operative area to 12 Gy in 3 fractions, one fraction every seven days. The three high-risk nodular areas were contoured, and each received 14-16 Gy during the consolidation treatment. After completion of both the GK and consolidation treatment, each high-risk area in the tumor bed had received a total dose equivalent to 34-36 Gy, corresponding to a biologically effective dose (BED) of 76.25-76.50 Gy. The field encompassing the surgical bed received a total dose of 20 Gy, corresponding to a BED of 32.50 Gy.

A brain MRI three months after completion of consolidative SBRT demonstrated a subdural fluid collection and a focus of nodular dural enhancement overlying the posterior right frontal lobe measuring 0.3 x 0.7 cm. Neurosurgical follow-up at that same time revealed no clinical changes. Brain MRI and clinical follow-up roughly every 3 months thereafter demonstrated no new evidence of recurrent disease and gradual resolution of the enhancement. The most recent brain MRI performed 34 months after completing the radiosurgery treatment course showed only expected gliosis, post-surgical changes, and no enhancing foci or evidence of recurrent tumor (**Figure 3**). The patient has remained asymptomatic and without any functional deficits since completing treatment.

DISCUSSION

Solitary Fibrous Tumor (SFT) is a rare and aggressive intracranial mesenchymal malignancy. Prior to 2016, SFTs were defined as benign mesenchymal tumors that were clinically and pathologically distinct from hemangiopericytomas (HPCs). Recent evidence has shown that SFTs and intracranial HPCs both share the immunohistochemical features of *NAB2* and *STAT6* gene fusion as well as *STAT6* overexpression. This finding prompted the World Health Organization (WHO) to classify both conditions under the umbrella term of *solitary fibrous tumor* in their updated 2016 guidelines (9). Given the rarity of SFTs, there is no gold standard for treatment, and most evidence regarding management comes from small studies and case series. Surgical resection is the most common and most widely accepted initial treatment; however, resection alone has been shown to provide poor long-term control. While complete resections have been associated with improved survival, they are very difficult to achieve given the tendency of SFTs to infiltrate adjacent vascular structures (10). The recurrence rate of SFTs after surgery alone is estimated at 88-100% as soon as 12 months post-resection, suggesting a need for adjuvant therapy (5–7). Adjuvant chemotherapy has shown only minimal benefit, and adjuvant conventionally fractionated radiotherapy has shown mixed results in the literature (5, 6).

There is minimal data evaluating treatment of SFT that accounts for all tumors now included under the updated 2016 WHO definition. Sung et al. identified a cohort of patients diagnosed with SFT or HPC, reclassified them according to these new guidelines, and analyzed clinical outcomes. They found that adjuvant radiotherapy (RT) was associated with improved progression-free survival, but not overall survival (OS) for grade II SFT. Of those receiving adjuvant RT, 31% received single-fraction Gamma Knife (GK) radiosurgery treatments, although the authors did not specifically compare the outcomes for GK versus conventional RT (1). Shin et al. performed a similar study in 2021, which showed resection to be superior to radiosurgery as an initial treatment. They showed no statistically significant benefit in OS or recurrence-free survival

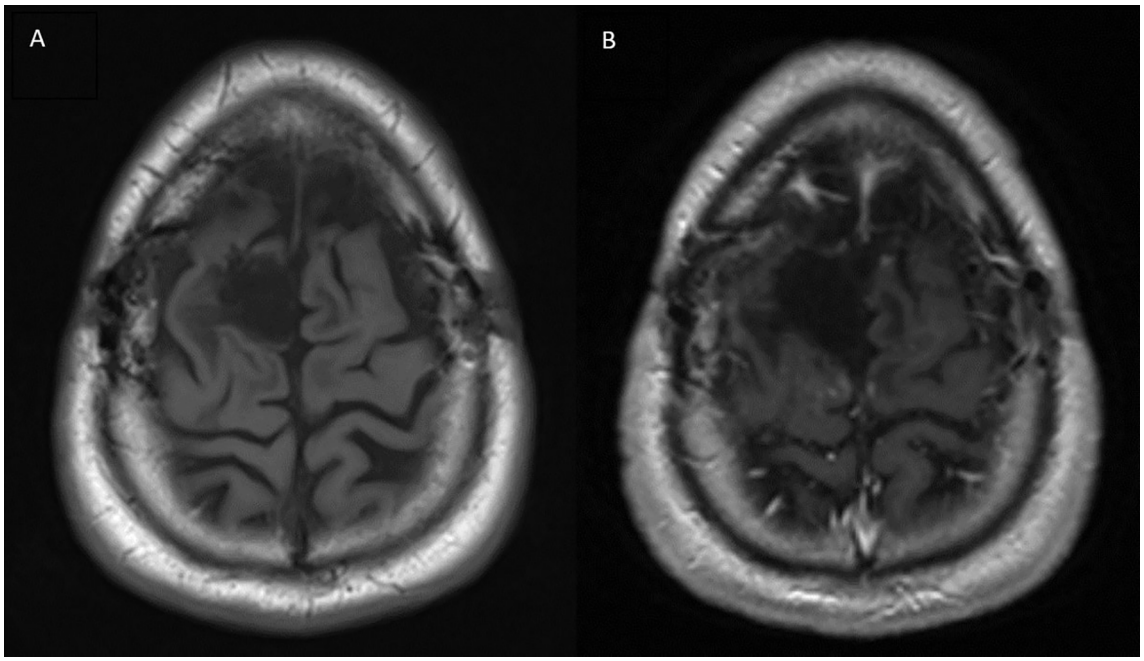

FIGURE 3 | Brain MRI performed 34 months after completion of radiotherapy treatment. **(A)** T1 pre-contrast **(B)** T1 post-contrast showing no areas of peripheral or nodular enhancement.

(RFS) for patients receiving adjuvant RT versus resection alone, although most of these patients received hyperfractionated regimens rather than radiosurgery (9). Since 2016 there has been scant evidence evaluating multi-fraction radiosurgery's utility in treating SFT, although the available results have been encouraging. One 2021 report described an 87-year-old woman who received fractionated GK radiosurgery for SFT of the sella turcica that recurred after partial resection. After completion of GK, the patient's visual field deficits resolved and she has been without recurrence for 15 months (11).

Stereotactic radiosurgery (SRS), specifically GK, has emerged as a promising post-operative treatment modality for SFT in the past decade. Multiple case series have demonstrated a likely survival benefit of adjuvant SRS compared to resection alone, with 3-year progression-free survival (PFS) of SFT treated with surgery and adjuvant SRS ranging from 60-92% in the literature (**Table 1**) (5–7). However, even with this PFS benefit, local recurrence after adjuvant radiosurgery remains prevalent (5, 6). Therefore, a need for more effective post-surgical treatment methods remains. Some studies, such as the 20-patient series by Kano et al. and the multi-center study by Cohen-Inbar et al., have found that higher cumulative radiation dose from adjuvant GK correlates with improved PFS for treatment of SFT (6–8).

However, increasing cumulative dose in a single GK fraction to intracranial targets can be problematic, as it confers a greater risk of brain radiation necrosis, especially for larger treatment volumes (15). Increasing total GK dose by spreading treatment over multiple fractions is often avoided as it requires multiple stereotactic head frame placements for most systems. Head frame placement procedures are invasive and involve surgically securing an aluminum stereotactic head frame to the calvarium using screws or pins, which serves to enhance precision of

TABLE 1 | Previous studies on post-operative radiosurgery for recurrent or residual hemangiopericytoma.

Investigator, year	Patients (n)	Total tumors (n)	Margin dose (Gy)	Median target volume (mL)	Median follow-up (mos)	Tumor control at last FU	5 year OS (%)	1 year PFS (%)	3 year PFS (%)
Kano, 2008 (6)	20	29	15	4.5	37.9	72.4	85.9	89	66.7
Kim, 2010 (16)	9	17	18.1	2.2	33.8	82.4	NA	100	NA
Olson, 2010 (5)	21	28	17	4.6	68	46.4	81	60	60.3
Veeravagu, 2011 (15)	14	24	21.2	9.2	37	81.8	81	95	71.5
Tsugawa, 2014 (7)	7	10	16.5	4.1	52.1	70	85.7	100	92
Cohen-Inbar 2017 (8)	90	133	15	4.9	59	55	82	92	70
Kim, 2017 (14)	18	40	NA	NA	134.7	80	85.6	NA	NA

NA, Not available.

radiation delivery. Our experience was unique in that we pursued an unconventional post-operative radiotherapy course consisting of a single-fraction GK treatment followed by a multi-fraction radiosurgery consolidation treatment with a linear accelerator. The GK treatment was delivered to four treatment volumes that included the entire resection cavity and three discrete tumor nodules at the cavity margins. The consolidation treatment was delivered to the entire resection cavity, and the enhancing tumor nodules were contoured. In total, the wide post-operative field received a cumulative dose of 20 Gy, while each radiographically high-risk area noted on initial MRI received 34-36 Gy. We were thus able to deliver a concentrated dose to high-risk areas that was significantly greater than the mean dose of 17-20 Gy described in most published case series of SRS-treated SFT (5–7). We achieved this while reducing the burden of invasive procedures for the patient, as stereotactic head frame placement was required for only one treatment session.

It is important to note that our experience occurred prior to the inception of the recently developed GK Icon™ and eXtend™ technologies, which do not require head frame placement and thus allow for multi-fraction treatment regimens. The GK Icon™ system allows for headframe and mask-based immobilization during treatment while the eXtend™ system uses a vacuum-sealed dental bite-tray and electronic probes to maintain inter and intra-fraction patient positioning (15, 16). These recently developed iterations of GK treatment are advantageous over our described treatment technique in that they do not require the interfraction transfer of treatment data from one system to another. Additionally, each of these systems incorporates cutting edge intrafraction motion management and interfraction repositioning systems, which allow for submillimeter targeting accuracy that cannot be achieved with linear accelerator-based treatment (15, 16). However, our described technique has some benefits over these systems. For example, because of the bite-tray based immobilization in the eXtend™ system, poor dentition or hypersensitive gag reflex can be barriers to treatment. It is also broadly thought that, despite the impressive precision of mask and bite tray-based systems, they are still not as precise as rigid, frame-based fixation (15). Additionally, most institutions with GK still only have access to headframe-based Perfexion™ systems, making our combination technique that incorporates this older system clinically relevant due to wider availability.

This case report is limited by a relatively short follow-up time, and further serial imaging and follow-up for this patient are necessary to more accurately assess this treatment method's long-term efficacy. However, the lack of disease recurrence and the patient's high quality of life several years post-treatment are very encouraging. We also believe our experience is a valuable contribution to the literature given the paucity of data describing treatment options for SFT as defined by the 2016 WHO guidelines. We hope that our reporting of this new radiosurgery paradigm may better inform the management of this uncommon and aggressive cancer.

CONCLUSIONS

Post-resection Gamma Knife radiosurgery with multiple treatment volumes to target radiographically high-risk areas, followed by multi-fraction radiosurgery using a linear accelerator, could be a safe and effective way to treat recurrent, grade II SFT without significantly compromising patient quality of life.

DATA AVAILABILITY STATEMENT

The original contributions presented in the study are included in the article/supplementary material. Further inquiries can be directed to the corresponding author.

ETHICS STATEMENT

Written informed consent was obtained from the individual(s) for the publication of any potentially identifiable images or data included in this article.

AUTHOR CONTRIBUTIONS

AA and DL contributed to the conceptualization, design, and writing of the original draft of this report. KR, JS, and CK contributed to the conceptualization and design of this report. All authors contributed to the reviewing and editing of this report. All authors contributed to the article and approved the submitted version.

REFERENCES

1. Sung KS, Moon JH, Kim EH, Kang S, Kim SH, Suh C, et al. Solitary Fibrous Tumor/Hemangiopericytoma: Treatment Results Based on the 2016 WHO Classification. *J Neurosurg JNS* (2019) 130(2):418–25. doi: 10.3171/2017.9.JNS171057
2. Prado C, Navarro-Martin A, Lucas A, Macià M, Guedea F. Adjuvant Fractionated Radiotherapy After Resection of Intracranial Hemangiopericytoma. *Rep Pract Oncol Radiother* (2012) 17(4):237–42. doi: 10.1016/j.rpor.2012.03.005
3. Schiariti M, Goetz P, El-Maghraby H, Tailor J, Kitchen N. Hemangiopericytoma: Long-Term Outcome Revisited. *J Neurosurg JNS* (2011) 114(3):747–55. doi: 10.3171/2010.6.JNS091660
4. Rutkowski MJ, Jian BJ, Bloch O, Chen C, Sughrue ME, Tihan T, et al. Intracranial Hemangiopericytoma: Clinical Experience and Treatment Considerations in a Modern Series of 40 Adult Patients. *Cancer* (2012) 118 (6):1628–36. doi: 10.1002/cncr.26411
5. Olson C, Yen CP, Schlesinger D, Sheehan J. Radiosurgery for Intracranial Hemangiopericytomas: Outcomes After Initial and Repeat Gamma Knife Surgery. *J Neurosurg* (2010) 112(1):133–9. doi: 10.3171/2009.3.JNS0923

6. Kano H, Niranjan A, Kondziolka D, Flickinger JC, Lunsford LD. Adjuvant Stereotactic Radiosurgery After Resection of Intracranial Hemangiopericytomas. *Int J Radiat Oncol Biol Phys* (2008) 72:1333–9. doi: 10.1016/j.ijrobp.2008.03.024
7. Tsugawa T, Mori Y, Kobayashi T, Hashizume C, Shibamoto Y, Wakabayashi T. Gamma Knife Stereotactic Radiosurgery for Intracranial Hemangiopericytoma. *J Radiosurg SBRT Vol* (2014) 3:29–35.
8. Cohen-Inbar O, Lee C, Mousavi SH, Kano H, Mathieu D, Meola A, et al. Stereotactic Radiosurgery for Intracranial Hemangiopericytomas: A Multicenter Study. *J Neurosurg JNS* (2017) 126(3):744–54. doi: 10.3171/2016.1.JNS152860
9. Shin DW, Kim JH, Chong S, Song SW, Kim YH, Cho YH, et al. Intracranial Solitary Fibrous Tumor/Hemangiopericytoma: Tumor Reclassification and Assessment of Treatment Outcome via the 2016 WHO Classification. *J Neuro-Oncol* (2021) 154(2):171–8. doi: 10.1007/s11060-021-03733-7
10. Melone AG, D'Elia A, Santoro F, Salvati M, Delfini R, Cantore G, et al. Intracranial Hemangiopericytoma – Our Experience in 30 Years: A Series of 43 Cases and Review of the Literature. *World Neurosurg* (2014) 81:556–62. doi: 10.1016/j.wneu.2013.11.009
11. Thapa S, Fujio S, Kitazono I, Yonenaga M, Masuda K, Kuroki S, et al. Solitary Fibrous Tumor or Hemangiopericytoma of the Sella in an Older Patient Treated With Partial Removal Followed by Fractionated Gamma Knife Radiosurgery. *NMC Case Rep J* (2021) 8(1):697–703. doi: 10.2176/nmccrj.cr.2021-0103
12. Kim JW, Kim DG, Chung HT, Paek SH, Kim YH. Gamma Knife Stereotactic Radiosurgery for Intracranial Hemangiopericytomas. *J Neurooncol*. (2010) 99 115–22
13. Veeravagu A, Jiang B, Patil CG, Lee M, Soltys SG, Gibbs IC, et al. CyberKnife Stereotactic Radiosurgery for Recurrent, Metastatic, and Residual Hemangiopericytomas. *J Hematol Oncol* (2011) 4:26. doi: 10.1186/1756-8722-4-26
14. Kim BS, Kong DS, Seol HJ, Nam DH, Lee JI. Gamma Knife Radiosurgery for Residual or Recurrent Intracranial Hemangiopericytomas. *J Clin Neurosci* (2017) 35:35–41. doi: 10.1016/j.jocn.2016.10.002
15. Sayer FT, Sherman JH, Yen C, Schlesinger DJ, Kersh R, Sheehan JP. Initial Experience With the Extend System: A Relocatable Frame System for Multiple-Session Gamma Knife Radiosurgery. *World Neurosurg* (2011) 75:665–72. doi: 10.1016/j.wneu.2010.12.051
16. Bush A, Vallow L, Ruiz-Garcia H, Herchko S, Reimer R, Ko S, et al. Mask-Based Immobilization in Gamma Knife Stereotactic Radiosurgery. *J Clin Neurosci* (2021) 83:37–42. doi: 10.1016/j.jocn.2020.11.033

Conflict of Interest: The authors declare that the research was conducted in the absence of any commercial or financial relationships that could be construed as a potential conflict of interest.

Publisher's Note: All claims expressed in this article are solely those of the authors and do not necessarily represent those of their affiliated organizations, or those of the publisher, the editors and the reviewers. Any product that may be evaluated in this article, or claim that may be made by its manufacturer, is not guaranteed or endorsed by the publisher.

frontiers | Frontiers in Oncology

ORIGINAL RESEARCH
published: 30 May 2022
doi: 10.3389/fonc.2022.915273

Clinical Features, Management, and Prognostic Factors of Intracranial Solitary Fibrous Tumor

Jingdian Liu†, Sisi Wu†, Kai Zhao, Junwen Wang, Kai Shu* and Ting Lei*

Department of Neurosurgery, Tongji Hospital, Tongji Medical College, Huazhong University of Science and Technology, Wuhan, China

Background: Because of the low incidence and the constantly changing diagnostic and classification criteria, the clinical features, management, and prognostic factors of intracranial solitary fibrous tumor (ISFT) remain unclear and were thus analyzed in this study.

Method: A total of 38 patients with ISFTs who were diagnosed in our institution were enrolled in this study. Patient data including age, gender, clinical presentation, histopathological features, immunohistochemistry staining, tumor location, tumor size, treatment methods, and prognosis were extracted and retrospectively analyzed.

Results: The median age at diagnosis was 45.5 years (range 28–66 years) and the male-to-female ratio was 1:1.53 in our series. The 3-, 5-, and 10-year progression-free survival (PFS) rate was 82.2%, 62.8%, and 21.4%, respectively; and the 3-, 5-, and 10-year overall survival rate was 97.1%, 86.9%, and 64.2%, respectively. Patients with high WHO grade (grade 3) ISFTs experienced impaired PFS ($p < 0.05$) and OS ($p < 0.01$). Subtotal resection (STR) was associated with worse PFS and OS ($p < 0.001$, respectively). Postoperative radiotherapy (PORT) improved PFS, especially local control rate, in patients with WHO grade 3 ISFTs ($P = 0.025$) or STR ($p = 0.027$). Moreover, CD34-negative immunostaining and a high Ki-67 index (>10%) were associated with impaired PFS in ISFTs.

Conclusion: Our study provides evidence that high tumor grade, subtotal tumor resection, CD34 negative immunostaining, and high Ki-67 index (>10%) were independent predictors for the poor prognosis of ISFTs. PORT can improve local control rate, and should be recommended for patients with high-grade ISFTs or STR.

Keywords: intracranial solitary fibrous tumor, clinical outcome, prognostic factors, radiotheapy, surgery treatment

OPEN ACCESS

Edited by:
Ignazio Gaspare Vetrano, Carlo Besta Neurological Institute Foundation (IRCCS), Italy

Reviewed by:
Francesco Acerbi, Carlo Besta Neurological Institute Foundation (IRCCS), Italy
Lorenzo Giammattei, Centre Hospitalier Universitaire Vaudois (CHUV), Switzerland

***Correspondence:**
Kai Shu
kshu@tjh.tjmu.edu.cn
Junwen Wang
jwwang@tjh.tjmu.edu.cn

†These authors have contributed equally to this work and share first authorship

Specialty section:
This article was submitted to Neuro-Oncology and Neurosurgical Oncology, a section of the journal Frontiers in Oncology

Received: *07 April 2022*
Accepted: *27 April 2022*
Published: *30 May 2022*

Citation:
Liu J, Wu S, Zhao K, Wang J, Shu K and Lei T (2022) Clinical Features, Management, and Prognostic Factors of Intracranial Solitary Fibrous Tumor. Front. Oncol. 12:915273. doi: 10.3389/fonc.2022.915273

INTRODUCTION

Solitary fibrous tumor (SFT) was first described as a rare mesenchymal neoplasm arising from pleura by Klemperer and Rabin in 1931 (1). Although this type of tumor has been identified in nearly every anatomic site of the body, the intracranial origin is less common. Intracranial SFT (ISFT) comprises less than 1% of all primary brain tumors (2). Originally, ISFTs and hemangiopericytomas (HPC) were regarded as two separate neoplasms due to their distinct

biological behaviors. With the development of sequencing technologies, the NGFI-A–binding protein 2 signal transducer and activator of transcription 6 (NAB2-STAT6) fusion gene was detected in both SFT and HPC (3). The special NAB2-STAT6 fusion protein can drive tumor growth by activating the EGR gene (3). The discovery resulted in the combination of these two diseases into a single entity, and the combined term "solitary fibrous tumor/hemangiopericytoma" was proposed in the 2016 World Health Organization (WHO) classification of central nervous system (CNS) tumors (4). According to the latest version in 2021, the term "hemangiopericytoma" has been removed to conform fully with soft tissue pathology nomenclature, with the tumor now termed only "SFT" (5).

ISFTs are difficult to distinguish radiologically from meningiomas because of their overlapping imaging features (6). Traditionally, some immunohistochemistry markers (for example, CD34 and CD99) were employed for the diagnosis of ISFTs. However, this can be problematic because these markers can be also detected in other brain tumors (7). After the discovery of NAB2-STAT6 fusion gene, accumulating evidence has found that STAT6 nuclear staining is extremely sensitive and specific in ISFTs, which made STAT6 immunohistochemistry a powerful diagnostic modality (8).

Because of the low incidence and the changes in WHO classification and diagnostic criteria over the years, the knowledge of natural course and prognostic factors of ISFTs is still limited. Hitherto, little information about ISFTs has been reported in the literature. Most previous reports either exhibited small patient series or confused HPCs with SFTs as the same tumors (9–11). In this present study, we included 38 patients with ISFTs and analyzed their clinical characteristics and follow-up outcomes to gain novel insight into the management of this disease.

MATERIALS AND METHODS

From March 2008 to September 2020, 38 patients with primary ISFT underwent surgical treatments in the neurosurgery department of Tongji Hospital, Huazhong University of Science and Technology. Patients with any other cancers or severe chronic basic diseases were excluded. Patient information including age at the time of surgery, gender, clinical manifestation, histopathologic features, tumor location, imaging features, treatment methods, survival status, and survival time were retrospectively collected. This study was approved by local ethical authorities in accordance with the Helsinki Criteria. Written informed consent was obtained from each individual patient or from family members of those who had died.

The extent of tumor resection was determined by surgical notes and postoperative neuro-imaging findings. Gross total resection (GTR) was equivalent to Simpson grades I and II, whereas others were considered subtotal resection (STR). The selection of adjuvant radiotherapy depended on the patient's willingness, extent of surgery resection, WHO grade, and clinical presentation. Progression-free survival (PFS) was determined as the time interval from the date of surgery to the time of tumor progression or recurrence, which was identified by follow-up magnetic resonance imaging (MRI) after surgery for patients. Tumor recurrence was classified as local, regional, or distant. Local recurrence referred to an event within 2 cm (the maximum margin for the clinical target volume (CTV) from gross tumor volume in patients with PORT) from surgical area. Regional recurrence was defined as a remote intracranial recurrence beyond primary tumor site. Distant recurrence meant extracranial metastasis of the tumor. Survival time was calculated from the date of the surgery to the time of death. Surviving patients were censored at the time of last follow-up. The first postoperative MRI was performed 1 month after surgery, and then, the follow-up interval was extended to 3 months. Survival data of patients were obtained through outpatient and telephone follow-up.

The diagnosis was confirmed by neuropathology experts through postoperative genetic and histopathologic examination of tumor samples. In addition, three most common primer pairs were designed and employed to identify the NAB2-STAT6 fusion subtypes by reverse transcriptase polymerase chain reaction (RT-PCR) in 33 samples (12) (**Supplementary Table S1**). Five other tissues were excluded due to poor tissue preservation. As described previously, immunohistochemistry staining was performed to detect expression of STAT6, CD34, S-100, Ki-67, vimentin (VIM), epithelial membrane antigen (EMA), and glial fibrillary acidic protein (GFAP) (13).

Quantitative variables and categorical variables were compared by Student's t-test and chi-square test (or Fisher's exact test), respectively. The effects of each factor on PFS and OS were evaluated by Kaplan–Meier method and univariate/multivariate cox regression method. A p-value < 0.05 was considered significantly different. R software (version 4.0.2) was used for performing all statistical analysis and graphing.

RESULTS

The clinical and histopathological characteristics of 38 patients with ISFTs were summarized in **Table 1**. The median age of patients at the first surgery after diagnosis was 45.5 years (range, 28–66 years). Fifteen patients were male (39.5%), and 23 were female (60.5%) with a male-to-female ratio of 1:1.53. The majority of the tumors (63.2%) were supratentorial, whereas 14 were located in the infratentorial region. The average size (maximum diameter) of tumors was 5.1 cm. The most common symptom was headache which occurred in 27 patients (71.1%). Other symptoms included epilepsy (n = 5, 13.2%), limb weakness (n = 7, 18.4%), visual impairment (n = 5, 13.2%), and paresthesia (n = 3, 7.9%). Two patients (5.3%) were asymptomatic, and the tumors were detected by routine clinical examinations. According to postoperative histopathological findings, nine (23.7%) patients were diagnosed with WHO grade 3, 17 (44.7%) with WHO grade 2, and 12 (31.6%) with WHO grade 1.

TABLE 1 | Characteristics of 38 patients.

Characteristics		Numbers (%)
Age (years)		
20–40		11 (28.9%)
41–60		24 (63.2%)
>61		3 (7.9%)
Median		45.5
Range		28–66
Gender		
Male		15 (39.5%)
Female		23 (60.5%)
Location of tumor		
Supratentorial		24 (63.2%)
Infratentorial		14 (36.8%)
Size		
<5 cm		17 (44.7%)
≥5 cm		21 (55.3%)
Mean		5.1 ± 2.2
Extent of surgery		
GTR		29 (76.3%)
STR		9 (23.7%)
Radiotherapy		
Yes	GTR (range, 55–62 Gy; 1.8–2.3 Gy/fractionation)	6 (15.8%)
	STR (range, 53–65 Gy; 1.8–2.2 Gy/fractionation)	5 (13.2%)
	Total	11 (28.9%)
No		27 (71.1%)
WHO grade		
1		12 (31.6%)
2		17 (44.7%)
3		9 (23.7%)
Ki-67 index		
1-5%		21 (55.3%)
6-10%		9 (23.7%)
>10%		8 (21.1%)
CD34		
Positive		28 (73.7%)
Weak positive		5 (13.2%)
Negative		5 (13.2%)
Recurrence		
Local		13 (34.2%)
Regional		3 (7.9%)
Distant		2 (5.3%)

Figure 1 exhibited the representative MRI images of ISFTs. Generally, the signal intensity of the tumor mass was heterogeneous mixed isointense and hypointense on non-contrast T1 and T2 MRI sequences, and marked and heterogeneous enhancement on T1 with gadolinium contrast (T1-Gd) MRI scan.

Figure 2 presented the intraoperative images for tumor resection of a recurrent ISFT. A STR was finally performed in this case due to the tumor invasion of skull base bone and sellar construction with a serious intraoperative bleeding (about 1,000 ml).

All 38 patients underwent long-term follow-up after the first surgery, and the mean follow-up period was 66.6 months (range, 12–165 months). Five patients experienced postoperative complications: three patients got cerebrospinal fluid leakage, one patient had incision infection, and one patient developed hydrocephalus, which was subsequently cured by ventriculo-peritoneal shunt. Eighteen cases suffered from recurrence during follow-up period, and seven patients elapsed. Recurrence was determined as local in 13 patients, regional in three patients (one patient with grade 3 and two patients with grade 2), and distant in two patients (two patients with grade 3). The 3-, 5-, and 10-year PFS rate was 82.2%, 62.8%, and 21.4%, respectively. Overall survival (OS) rate was 97.1% for 3 years, 86.9% for 5 years, and 64.2% for 10 years.

On the basis of the Kaplan–Meier survival analysis, patients with WHO high-grade ISFTs had a lower PFS (median PFS 42 vs. 88 months, $p = 0.031$) and OS (median OS 63 vs. 152 months, $p = 0.0059$) compared with lower-grade counterparts (**Figures 3A, B**). Moreover, a markedly decreased recurrence or progression rate and prolonged survival were observed in patients with GTR (median PFS 88 vs. 36 months, $p < 0.0001$; median OS 152 vs. 60 months, $p = 0.00069$) (**Figures 3C, D**). In addition, univariate/multivariate Cox regression analysis was performed to further verify this result, as shown in **Table 2**. Patient age, gender, tumor location (infratentorial or supratentorial), and tumor size were not correlated with prognosis (**Table 2**).

GTR was achieved in 29 patients (76.3%), whereas others underwent STR due to illegible boundary between tumor mass and surrounding normal tissues. In our series, none of the cases received chemotherapy. Postoperative radiotherapy (PORT) (11 patients were treated) was performed predominately in patients with high-grade tumors or STR (range, 53–65 Gy; 1.8–2.3 Gy/fractionation). The median margin for the CTV) was 10 mm (range, 5–20 mm) from gross tumor volume (GTV). Five of nine patients treated with STR received PORT, whereas six of nine diagnosed with WHO grade 3 ISFTs received PORT, and three patients refused due to personal financial reasons or opposition of their families. The effect of radiotherapy on prognosis is not significant when the analysis was performed across all patients (**Table 2**), but in patients with WHO grade 3 ISFTs, PORT remarkably suppressed the progression/recurrence of tumors but did not improve OS (median PFS: 58 vs. 35 months, $p = 0.025$; median OS: 63 vs. 113 months, $p = 0.19$) (**Figures 4A, B**). In addition, an improvement of PFS could be observed in patients treated with PORT in the STR subgroup (median PFS: 42 vs. 28.5 months, $p = 0.14$) (**Figure 4C**); however, no statistical differences were established, owing to the small case series. The impact of PORT on OS of patients with STR was not observed (Median OS: 60 vs. 68.5 months, $p = 0.74$) (**Figure 4D**). Furthermore, we also analyzed the impact of surgical extent and PORT on different patterns of recurrence (**Table 3**). Local recurrence was the main progression type (26.1% after GTR and 100% after STR, respectively) in the subgroup of patients without radiotherapy. According to the results of Kaplan–Meier analysis, GTR significantly decreased the local recurrence (**Figure 5A**). Moreover, PORT significantly suppressed the local recurrence in patients with WHO grade 3 ISFTs or in those with STR (**Figures 5B, C**).

According to the results of IHC staining, the positive rate of STAT6, VIM, S-100, EMA, and GFAP was 92.1%, 94.7%, 39.4%, 23.7%, and 5.3%, respectively. The level of expression of CD34 was classified as follows: diffuse positive (28 cases, 73.7%), weakly

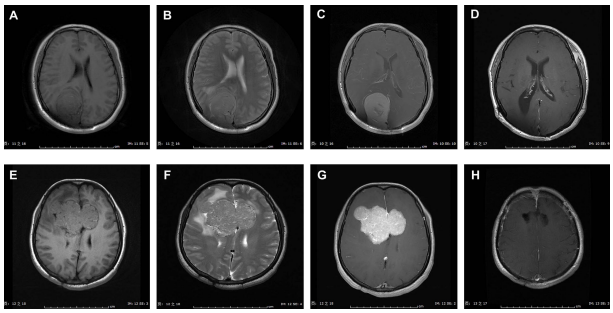

FIGURE 1 | Representative MRI scans of ISFTs in our series. Generally, the signal intensity of the tumor mass was heterogeneous mixed isointense and hypointense on non-contrast T1 and T2 MRI sequences, and marked and heterogeneous enhancement on T1 with gadolinium contrast (T1-Gd) MRI scan. **(A–D)** MRI scans of a 47-year-old female with ISFT lesion located in right occipital lobe. **(A–C)** Preoperative axial T1, T2, and T1-Gd MRI scans. **(D)** Postoperative T1-Gd MRI scan showed a GTR resection. **(E–H)** MRI scans of a 44-year-old female with ISFT mass originated from callosum and invaded into both sides of frontal lobe. **(E–G)** Preoperative axial T1, T2, and T1-Gd MRI scans. **(H)** Postoperative T1-Gd MRI scan demonstrated a GTR resection.

(focal) positive (five cases, 13.2%), and negative (five cases, 13.2%). The mean value of Ki-67 index was 8.5% (range, 1%–30%). The CD34 expression and WHO grade showed a significant negative correlation ($p = 0.011$) (**Table 4**). Moreover, high-grade ISFTs had a higher Ki-67 index compared with low-grade tumors (average value: 13.4% for grade 3 vs. 8.2% for grade 2 vs. 5.3% for grade 1, $p = 0.034$).

The NAB2-STAT6 fusion subtypes were detected and summarized in **Table 5**. NAB2ex4–STAT6ex2, NAB2ex6–STAT6ex16, and NAB2ex6–STAT6ex17 fusion variants were detected in 5, 12, and 9 cases, respectively. Seven cases could not be distinguished by the aforementioned NAB2–STAT6 fusion. Notably, three STAT6-negative ISFTs were confirmed to harbor NAB2ex6–STAT6ex16 fusion. No statistical differences were established for the prognosis between variable fusion subtypes in this study.

Tumors with a higher Ki-67 index (>10%) were associated with worse PFS (median PFS: 58 vs. 92 months, $p = 0.0164$) but not OS (**Figures 6A, B**). In addition, absent/low expression of CD34 in ISFTs portended an unfavorable prognosis (median PFS: 42 vs. 88 months, $p = 0.039$; median OS: 89 vs. 152 months, $p = 0.37$) (**Figures 6C, D**).

DISCUSSION

Although SFTs and HPCs have been consolidated into a single disease according to the 2013 (fourth edition) and 2020 (fifth

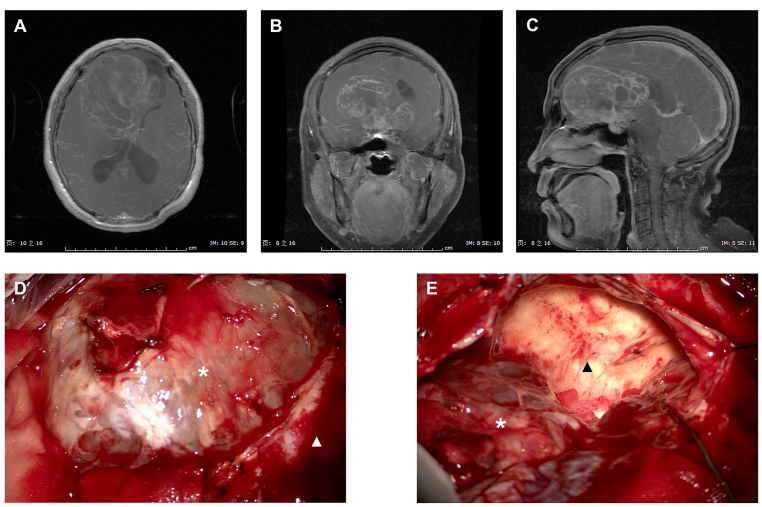

FIGURE 2 | Intraoperative images for tumor resection of a recurrent ISFT. **(A–C)** Preoperative axial, coronal, and sagittal T1-Gd MRI scans of a huge recurrent ISFT tumor mainly located in the right frontal skull base, showing a marked and heterogeneous enhancement. **(D, E)** Intraoperative images revealed a red solid tumor mass (black arrow), which was not clearly distinguishable from the normal brain tissue during tumor resection (white arrow). Finally, a subtotal resection was performed due to the tumor invasion of skull base bone and sellar construction with a serious intraoperative bleeding (about 1,000 ml).

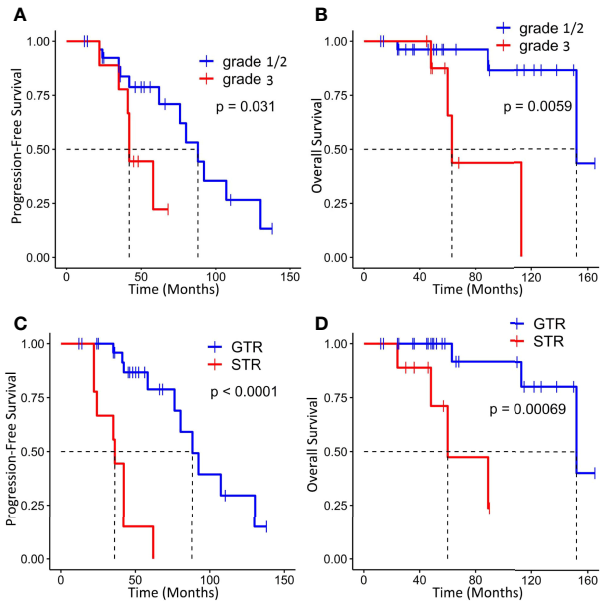

FIGURE 3 | Kaplan–Meier survival curves for progression-free survival and overall survival based on WHO grade **(A, B)** and extent of resection **(C, D)**.

edition) WHO classification of tumors of soft tissue and bone, the term "hemangiopericytoma" is still used widely by neuropathologists (14). Traditionally, ISFTs were considered to be benign with a low possibility of relapse and an indolent course, whereas HPCs exhibited a local aggressive behavior (15). However, some SFTs with malignant features were continuously reported (16). Thus, the misdiagnosis between SFTs and HPCs occurs frequently during the past years. The distinction between the two types was no longer clinically significant due to the pronounced clinical and histopathological overlap. In the 2021 WHO classification of CNS tumors, the term "hemangiopericytoma" was removed with the tumor named only "SFT" (5). Because of the constantly changing classification criteria in recent years, the clinical features and management guidelines of ISFTs remain unclear. To fill this gap, we conducted this retrospective study by analyzing the clinical and follow-up data of 38 patients with ISFTs.

Unlike other types of brain tumors, patients with ISFTs usually have a younger onset age, with a peak in the 40–60 years (7). The patients aged 41–60 years in our department

TABLE 2 | Results of univariate and multivariate cox regression analysis. .

	PFS-Univariate Analysis			PFS-Multivariate Analysis		
Factors	**HR**	**95%CI**	**P-value**	**HR**	**95%CI**	**P-value**
Age	1.00	0.95–1.05	0.960	–	–	–
Gender (female vs. male)	1.05	0.40–2.80	0.916	–	–	–
Location (Infratentorial vs. Supratentorial)	1.08	0.41–2.85	0.876	–	–	–
Size (≥5 cm *vs.* <5 cm)	0.47	0.17–1.29	0.134	–	–	–
WHO grade (3 vs. 1/2)	3.36	1.07–10.6	0.044*	4.24	1.29–13.91	0.017*
The extent of surgery (STR vs. GTR)	11.94	3.50–40.85	<0.001*	13.55	3.90–47.03	<0.001*
Radiotherapy (Yes vs. No)	1.57	0.60–4.15	0.368	–	–	
	OS-Univariate analysis			**OS-Multivariate analysis**		
Factors	**HR**	**95%CI**	**P-value**	**HR**	**95%CI**	**P-value**
Age	1.02	0.93–1.10	0.703	–	–	–
Gender (female vs. male)	1.16	0.20–6.47	0.866	–	–	–
Location (Infratentorial vs. Supratentorial)	1.80	0.36–8.98	0.479	–	–	–
Size (≥5 cm vs. <5 cm)	0.82	0.18–3.69	0.796	–	–	–
WHO grade (3 vs. 1/2)	8.38	1.44–48.7	0.014*	18.71	1.81–193.4	0.014*
The extent of surgery (STR vs. GTR)	16.75	1.85–151.4	0.004*	35.52	2.447–515.6	0.009*
Radiotherapy (Yes vs. No)	1.56	0.34–7.12	0.570	–	–	–

P values are statistically significant. HR, hazard ratio; CI, confidence interval.*

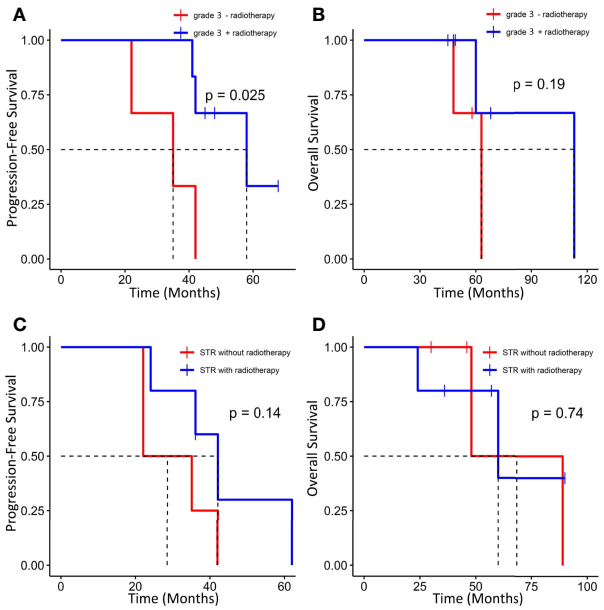

FIGURE 4 | Kaplan–Meier survival curves for progression-free survival and overall survival based on PORT. **(A, B)** Effect of PORT on PFS and OS in patients with WHO grade 3 ISFTs. **(C, D)** Effect of PORT on PFS and OS in patients with STR.

occupied up to nearly 64%. Early perspectives thought that ISFTs were more predominant in men, whereas the opposite trend was observed in this study (17). In addition, approximately equal gender distribution was recently reported by a population-based study (18). The symptoms of patients with ISFTs are non-specific in our cohort, which is aligned with other studies (9). Headache is the most common presentation in brain tumors due to the tissues compression or increased intracranial pressure caused by tumor growth. Other neurologic symptoms including epilepsy, limb weakness, paresthesia, and visual impairment are associated with tumor location and nerves invasion. In addition, previous studies reported some uncommon symptoms covering anosmia, memory loss, dysphasia, hyponatremia, amenorrhea, and hypoglycemia (9).

In the majority of previous studies, WHO grade and the extent of resection are commonly reported as prognostic factors of ISFTs, which is in line with ours (10, 11). Multivariate analysis indicated that GTR remarkably prolonged OS and PFS of patients, regardless of tumor grade and other confounders. For the vast majority of benign ISFTs, GTR is independently sufficient to achieve clinical cure. Notwithstanding, in our cohort, two of 10 patients with WHO grade 1 ISFT receiving GTR still developed local recurrences at 9 and 11 years after surgery, respectively. Moreover, a recent study reported that longer recurrence intervals along with malignant transformation occurred in some WHO grade 1 ISFTs (19). For this reason, long-term follow-up should be warranted irrespective of the grade of ISFTs. In terms of higher grade ISFTs, frequent recurrence occurred after GTR due to higher mitotic activity and with microscopic residual disease (18).

Many researchers reported that patients could benefit from radiotherapy after surgery (18, 20). However, the benefit may be specific to patients with STR or high grade ISFTs and be highly confined to local control. In our series, the effect of radiotherapy on PFS and OS was not significant when the analysis was performed across all patients (**Table 2**). In STR subgroup, the

TABLE 3 | Patterns of recurrence according to the type of treatment.

		n	Local	Regional	Distant
GTR	**PORT (+)**	6	1 (16.7%)	1 (16.7%)	1 (16.7%)
	PORT (–)	23	6 (26.1%)	1 (4.3%)	0
STR	**PORT (+)**	5	2 (40%)	1 (20%)	1 (20%)
	PORT (–)	4	4 (100%)	0	0
p-value			0.026*	0.340	0.149

*Chi-square test (or Fisher's exact test). *P < 0.05.*

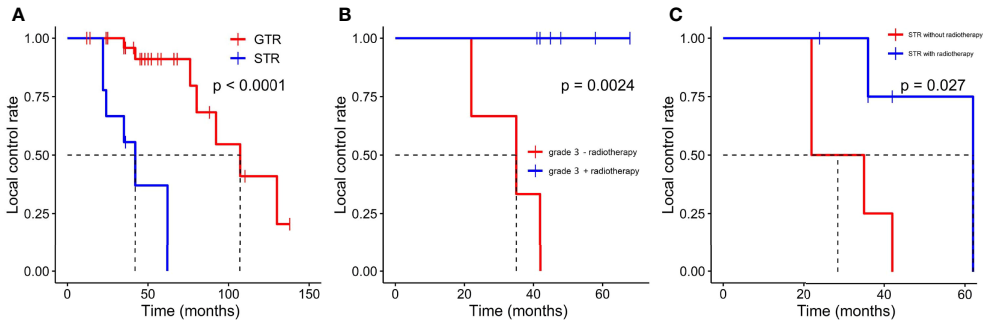

FIGURE 5 | Kaplan–Meier survival curves for local control rate. **(A)** The effect of resection extension on local control rate. **(B)** The effect of PORT on local control rate in patients with WHO grade 3 ISFTs. **(C)** the effect of PORT on local control rate in patients with STR.

TABLE 4 | Correlation analysis between IHC markers and WHO grade.

	WHO 1/2	WHO 3	P-value
STAT6			–
Positive	26	9	
Negative	3	0	
VIM			0.423
Positive	28	8	
Negative	1	1	
S-100			0.273
Positive	13	2	
Negative	16	7	
EMA			–
Positive	9	0	
Negative	20	9	
GFAP			–
Positive	2	0	
Negative	27	9	
CD34			0.011*
Positive	23	5	
Weakly positive	5	0	
Negative	1	4	

P values are statistically significant.*

TABLE 5 | NAB2-STAT6 fusion subtypes in 33 patients with ISFTs.

NAB2-STAT6 Fusion Type	N	%
EX4-EX2	5	15.2%
EX6-EX17	9	27.3%
EX6-EX16	12	36.4%
Not applicable	7	21.2%
Total	33	100%

PFS of patients with STR + PORT was improved compared with those who received STR alone, although the effect was also not significant (**Figure 4C**). Taking into consideration that the patients without PORT had a higher local recurrence rate (**Table 3**), we analyzed the effect of PORT on local control rate. Interestingly, PORT significantly improved the local control rate in patients with STR (**Figure 5C**). It is odd that the patients receiving PORT had much higher regional and distant recurrence rates in this cohort. This might be because the majority (55%) of patients with PORT were diagnosed as WHO grade 3 ISFTs, which generally had more malignant phenotypes.

Little literature reported the effect of radiotherapy on GTR subgroup. A recent study reported that patients with GTR can benefit from PORT (20). Unfortunately, this issue was difficult to be evaluated in our series, because of the small case series and the selection bias that the vast majority of people with RT in GTR subgroup were the patients with WHO grade 3 ISFTs. Recently, two based-population studies found that GTR with radiation significantly improved disease-free survival compared with GTR alone in borderline malignant or malignant ISFTs (18, 21). Our results also suggested that PORT can improve PFS and local control rate for patients who were diagnosed with WHO grade 3 tumors. In contrast, the clinical value of PORT in benign ISFTs is still debatable. Moritani et al. reported that progression and dedifferentiation of an ISFT were probably related to the application of radiation therapy (22). In addition, in five patients with lower-grade ISFTs in which malignant transformation occurred, two cases underwent RT after initial surgery (19). However, the association between radiotherapy and malignant transformation of benign ISFTs needs further confirmation. Altogether, PORT should be recommended primarily for patients with high grade ISFTs or those with STR. For the patients with benign ISFTs who underwent GTR, the role of PORT requires further evaluation in the future.

Shin et al. assessed the significance of preoperative radiotherapy in ISFTs (23). They observed a worse RFS and OS in patients who received radiotherapy before resection though further validation would be required. On the other hand, it is also difficult to selectively implement preoperative radiotherapy only for the patients with high-grade tumors, because of the plight of identification of tumor histological type and tumor grade before resection.

IHC staining characterized by mainly STAT6 is the key to the diagnosis of ISFTs. Although ISFTs were confused with meningiomas on imaging, the STAT6 immunostaining is

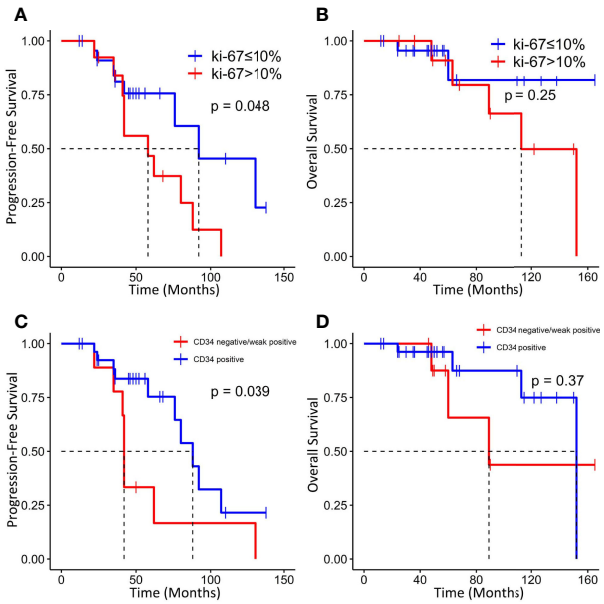

FIGURE 6 | Kaplan–Meier survival curves for progression-free survival and overall survival based on Ki-67 index **(A, B)** and CD34 **(C, D)**.

totally negative in meningiomas (7). However, absence of STAT6 nuclear expression by IHC staining may not exclude the possibility of SFT. The sensitivity of STAT6 for ISFTs was reported to be 96.6% by analysis of a literature review, resembling a 92.1% positive rate in the present study (7). For diagnosis of STAT6-negative ISFTs, combination with other IHC markers is helpful, although their specificities for ISFTs are not so high as STAT6 (24). In addition, molecular diagnostic techniques such as RT-PCR could be helpful for STAT6-negative SFTs by detecting the NAB2–STAT6 fusion (12, 25). As a transmembrane glycoprotein, CD34 was identified in hematopoietic stem and progenitor cells, fibroblast-related mesenchymal cells, and endothelial cells (26). Before the discovery of STAT6-NAB2 fusion gene, positive expression of CD34 was regarded as the most prominent characteristic of ISFTs and was often used for differential diagnosis (27). However, 5%–10% of SFTs were negative for CD34 (7, 28). A study found that the absence of CD34 may be related to dedifferentiation of SFT (29). In addition, a recent clinicopathologic study of 25 cases with loss of CD34 reported that CD34-negative SFTs are more likely to exhibit malignant behaviors, compared with their CD34-positive counterparts (28). Although the authors reported the correlation between prognosis of patients with SFTs and CD34, the majority of the reported cases are extracranial and the significance of CD34 in ISFTs is still unclear (28). As indicated in the results section, we found that reduced/absent expression of CD34 was associated with degree of malignancy of ISFT and tumor progression. Similarly, Yamashita et al. described that expression level of CD34 gradually decreased with increased malignancy of tumors in 163 patients with ISFTs (7). A low expression rate (<10%) of CD34 also was reported in 60% of recurrent cases by Bertero and his colleagues (10). Moreover, some studies found that loss of $CD34^+$-fibrocytes was frequently observed in other types of invasive carcinoma (e.g., invasive lobular carcinoma of the breast and invasive cervical carcinoma) (30, 31). As one type of antigen-presenting cells, loss of $CD34^+$-fibrocytes may promote immune evasion of tumor (32). A high Ki-67 (a proliferation marker) index was also identified as a risk factor for tumor recurrence in our study and others (33).

In conclusion, we assessed the clinical feature and prognosis of 38 patients with ISFTs in this study. The results suggested that tumor grade and extent of surgery resection are independent prognostic factors of ISFTs. PORT could improve PFS, especially decreased local recurrence for patients with high grade ISFTs or those with STR. Moreover, CD34-negative ISFT or a high Ki-67 index might be a prediction of poor prognosis.

DATA AVAILABILITY STATEMENT

The original contributions presented in the study are included in the article/**Supplementary Material**. Further inquiries can be directed to the corresponding authors.

ETHICS STATEMENT

The studies involving human participants were reviewed and approved by the ethics committee of Tongji Hospital, Tongji

Medical College. The patients/participants provided their written informed consent to participate in this study.

AUTHOR CONTRIBUTIONS

JL and SW contributed equally in this work. KS and TL designed and conducted this project. JL, SW, KZ, and JW collected the data and run statistical analysis. JL and SW wrote the original manuscript. KS and JW revised the manuscript. All authors contributed to the article and approved the submitted version.

FUNDING

Natural Science Foundation of Hubei Province (2020CFB657).

SUPPLEMENTARY MATERIAL

The Supplementary Material for this article can be found online at: https://www.frontiersin.org/articles/10.3389/fonc.2022.915273/full#supplementary-material

REFERENCES

1. Klemperer P, Coleman BR. Primary Neoplasms of the Pleura. A Report of Five Cases. *Am J Ind Med* (1992) 22:1–31. doi: 10.1002/ajim.4700220103
2. Dho YS, Jung KW, Ha J, Seo Y, Park CK, Won YJ, et al. An Updated Nationwide Epidemiology of Primary Brain Tumors in Republic of Korea, 2013. *Brain Tumor Res Treat* (2017) 5:16–23. doi: 10.14791/btrt.2017.5.1.16
3. Robinson DR, Wu YM, Kalyana-Sundaram S, Cao X, Lonigro RJ, Sung YS, et al. Identification of Recurrent NAB2-STAT6 Gene Fusions in Solitary Fibrous Tumor by Integrative Sequencing. *Nat Genet* (2013) 45:180–5. doi: 10.1038/ng.2509
4. Louis DN, Perry A, Reifenberger G, von Deimling A, Figarella-Branger D, Cavenee WK, et al. The 2016 World Health Organization Classification of Tumors of the Central Nervous System: A Summary. *Acta Neuropathol* (2016) 131:803–20. doi: 10.1007/s00401-016-1545-1
5. Louis DN, Perry A, Wesseling P, Brat DJ, Cree IA, Figarella-Branger D, et al. The 2021 WHO Classification of Tumors of the Central Nervous System: A Summary. *Neuro Oncol* (2021) 23:1231–51. doi: 10.1093/neuonc/noab106
6. Clarencon F, Bonneville F, Rousseau A, Galanaud D, Kujas M, Naggara O, et al. Intracranial Solitary Fibrous Tumor: Imaging Findings. *Eur J Radiol* (2011) 80:387–94. doi: 10.1016/j.ejrad.2010.02.016
7. Yamashita D, Suehiro S, Kohno S, Ohue S, Nakamura Y, Kouno D, et al. Intracranial Anaplastic Solitary Fibrous Tu-Mor/Hemangiopericytoma: Immunohistochemical Markers for Definitive Diagnosis. *Neurosurg Rev* (2021) 44:1591–600. doi: 10.1007/s10143-020-01348-6
8. Berghoff AS, Kresl P, Bienkowski M, Koelsche C, Rajky U, Hainfellner JA, et al. Validation of Nuclear STAT6 Immunostaining as a Diagnostic Marker of Meningeal Solitary Fibrous Tumor (SFT)/Hemangiopericytoma. *Clin Neuro-pathol* (2017) 36(2017):56–9. doi: 10.5414/NP300993
9. Gopakumar S, Srinivasan VM, Hadley CC, Anand A, Daou M, Karas PJ, et al. In-Tracranial Solitary Fibrous Tumor of the Skull Base: 2 Cases and Systematic Review of the Literature. *World Neurosurg* (2021) 149:e345–59. doi: 10.1016/j.wneu.2021.02.026
10. Bertero L, Anfossi V, Osella-Abate S, Disanto MG, Mantovani C, Zenga F, et al. Pathological Prognostic Markers in Central Nervous System Solitary Fibrous Tu-Mour/Hemangiopericytoma: Evidence From a Small Series. *PloS One* (2018) 13:e0203570. doi: 10.1371/journal.pone.0203570
11. Zeng L, Wang Y, Wang Y, Han L, Niu H, Zhang M, et al. Analyses of Prognosis-Related Factors of Intracranial Solitary Fibrous Tumors and Hemangiopericytomas Help Understand the Relationship Between the Two Sorts of Tumors. *J Neurooncol* (2017) 131:153–61. doi: 10.1007/s11060-016-2282-y
12. Tai HC, Chuang IC, Chen TC, Li CF, Huang SC, Kao YC, et al. NAB2-STAT6 Fusion Types Account for Clinicopathological Variations in Solitary Fibrous Tumors. *Mod Pathol* (2015) 28:1324–35. doi: 10.1038/modpathol.2015.90
13. Wang J, Zhao K, Han L, Jiao L, Liu W, Xu Y, et al. Solitary Fibrous Tumor/Hemangiopericytoma of Spinal Cord: A Retrospective Single-Center Study of 16 Cases. *World Neurosurg* (2019) 123:e629–38. doi: 10.1016/j.wneu.2018.12.004
14. Jo VY, Fletcher CD. WHO Classification of Soft Tissue Tumors: An Update Based on the 2013 (4th) Edition. *Pathology* (2014) 46:95–104. doi: 10.1097/PAT.0000000000000050
15. Tihan T, Viglione M, Rosenblum MK, Olivi A, Burger PC. Solitary Fibrous Tumors in the Central Nervous System. A Clinicopathologic Review of 18 Cases and Comparison to Meningeal Hemangiopericytomas. *Arch Pathol Lab Med* (2003) 127:432–9. doi: 10.5858/2003-127-0432-SFTITC
16. Ogawa K, Tada T, Takahashi S, Sugiyama N, Inaguma S, Takahashi SS, et al. Malignant Solitary Fibrous Tumor of the Meninges. *Virchows Arch* (2004) 444:459–64. doi: 10.1007/s00428-004-0991-7
17. Rutkowski MJ, Sughrue ME, Kane AJ, Aranda D, Mills SA, Barani IJ, et al. Predictors of Mortality Following Treatment of Intracranial Hemangiopericytoma. *J Neurosurg* (2010) 113:333–9. doi: 10.3171/2010.3.JNS091882
18. Kinslow CJ, Bruce SS, Rae AI, Sheth SA, McKhann GM, Sisti MB, et al. Solitary-Fibrous Tumor/Hemangiopericytoma of the Central Nervous System: A Population-Based Study. *J Neurooncol* (2018) 138:173–82. doi: 10.1007/s11060-018-2787-7
19. Apra C, Mokhtari K, Cornu P, Peyre M, Kalamarides M. Intracranial Solitary Fibrous Tumors/Hemangiopericytomas: First Report of Malignant Progression. *J Neurosurg* (2018) 128:1719–24. doi: 10.3171/2017.1.JNS162593
20. Schiariti M, Goetz P, El-Maghraby H, Tailor J, Kitchen N. Hemangiopericytoma: Long-Term Outcome Revisited. Clinical article. *J Neurosurg* (2011) 114(3):747–55. doi: 10.3171/2010.6.JNS091660
21. Lee JH, Jeon SH, Park CK, Park SH, Yoon HI, Chang JH, et al. The Role of Postoperative Radiotherapy in Intracranial Solitary Fibrous Tumor/Hemangiopericytoma: A Multi-Institutional Retrospective Study (KROG 18-11). *Cancer Res Treat* (2021) 54(1):65-74. doi: 10.4143/crt.2021.142
22. Moritani S, Ichihara S, Hasegawa M, Takada S, Takahashi T, Kato E, et al. Dedifferentiation and Progression of an Intracranial Solitary Fibrous Tumor: Autopsy Case of a Japanese Woman With a History of Radiation Therapy of the Head During Infancy. *Pathol Int* (2011) 61:143–9. doi: 10.1111/j.1440-1827.2010.02627.x
23. Shin DW, Kim JH, Chong S, Song SW, Kim YH, Cho YH, et al. Intracranial Solitary Fibrous Tu-Mor/Hemangiopericytoma: Tumor Reclassification and Assessment of Treatment Outcome *via* the 2016 WHO Classification. *J Neurooncol* (2021) 154:171–8. doi: 10.1007/s11060-021-03733-7
24. Macagno N, Figarella-Branger D, Mokthari K, Metellus P, Jouvet A, Vasiljevic A, et al. Differential Diagnosis of Meningeal SFT-HPC and Meningioma: Which Immunohistochemical Markers Should Be Used? *Am J Surg Pathol* (2016) 40:270–8. doi: 10.1097/PAS.0000000000000526
25. Zhang P, Xiong K, Lv P, Zhang H, Wang Y, Yang Z, et al. Malignant Solitary Fibrous Tumor Occurring in the Mediastinal Pleura Showing NAB2ex4-STAT6ex2 Fusion and Negative STAT6 Immunohistochemistry: A Case Report. *Thorac Cancer* (2020) 11:1344–9. doi: 10.1111/1759-7714.13395
26. Sidney LE, Branch MJ, Dunphy SE, Dua HS, Hopkinson A. Concise Review: Evidence for CD34 as a Common Marker for Diverse Progenitors. *Stem Cells* (2014) 32:1380–9. doi: 10.1002/stem.1661
27. Bisceglia M, Galliani C, Giannatempo G, Lauriola W, Bianco M, D'Angelo V, et al. Solitary Fibrous Tumor of the Central Nervous System: A 15-Year Literature Survey of 220 Cases (August 1996-July 2011). *Adv Anat Pathol* (2011) 18:356–92. doi: 10.1097/PAP.0b013e318229c004
28. Dermawan JK, Rubin BP, Kilpatrick SE, Gjorgova Gjeorgjievski S, Fritchie KJ, Goldblum JR, et al. CD34-Negative Solitary Fibrous Tumor: A Clinicopathologic Study of 25 Cases and Comparison With Their CD34-

Positive Counterparts. *Am J Surg Pathol* (2021) 45(12):1616-25. doi: 10.1097/PAS.0000000000001717
29. Zhao C, Fan X, Gao W, Zhang F, Lv H, Jiang X, et al. De-Differentiation Associated With Drop Metastasis of a Recurrent Intracranial Solitary Fibrous Tumor: A Case Report and Literature Review. *Int J Neurosci* (2020) 30:1–7. doi: 10.1080/00207454.2020.1846532
30. Westhoff CC, Jank P, Jacke CO, Albert US, Ebrahimsade S, Barth PJ, et al. Prognostic Relevance of the Loss of Stromal CD34 Positive Fibroblasts in Invasive Lobular Carcinoma of the Breast. *Virchows Arch* (2020) 477:717–24. doi: 10.1007/s00428-020-02835-3
31. Aijaz M, Alam K, Maheshwari V, Hakim S, Kamal M. Clinicopathological Study of Role of CD34 Expressions in the Stroma of Premalignant and Malignant Lesions of Uterine Cervix. *Ann Diagn Pathol* (2019) 38:87–92. doi: 10.1016/j.anndiagpath.2018.11.007
32. Barth PJ, Westhoff CC. CD34+ Fibrocytes: Morphology, Histogenesis and Function. *Curr Stem Cell Res Ther* (2007) 2:221–7. doi: 10.2174/157488807781696249
33. Shukla P, Gulwani HV, Kaur S, Shanmugasundaram D. Reappraisal of Morphological and Immunohistochemical Spectrum of Intracranial and Spinal Solitary Fibrous Tumors/Hemangiopericytomas With Impact on Long-Term Follow-Up. *Indian J Cancer* (2018) 55:214–21. doi: 10.4103/ijc.IJC_631_17

Conflict of Interest: The authors declare that the research was conducted in the absence of any commercial or financial relationships that could be construed as a potential conflict of interest.

Publisher's Note: All claims expressed in this article are solely those of the authors and do not necessarily represent those of their affiliated organizations, or those of the publisher, the editors and the reviewers. Any product that may be evaluated in this article, or claim that may be made by its manufacturer, is not guaranteed or endorsed by the publisher.

frontiers | Frontiers in Neurology

ORIGINAL RESEARCH
published: 06 June 2022
doi: 10.3389/fneur.2022.920505

Clinical Features, Diagnosis, and Treatment of Primary Intraventricular Lymphoma: Insights From a Monocentric Case Series

*Lidong Cheng, Hongtao Zhu, Jing Wang, Guanghui Wang, Xiaoyu Ma, Kai Zhao, Junwen Wang and Kai Shu**

Department of Neurosurgery, Tongji Hospital, Tongji Medical College, Huazhong University of Science and Technology, Wuhan, China

OPEN ACCESS

Edited by:
Ignazio Gaspare Vetrano, IRCCS Carlo Besta Neurological Institute Foundation, Italy

Reviewed by:
Giulio Bonomo, IRCCS Carlo Besta Neurological Institute Foundation, Italy
Jacopo Falco, IRCCS Carlo Besta Neurological Institute Foundation, Italy

***Correspondence:**
Kai Shu
kshu@tjh.tjmu.edu.cn

Specialty section:
This article was submitted to Neuro-Oncology and Neurosurgical Oncology, a section of the journal Frontiers in Neurology

Received: *14 April 2022*
Accepted: *03 May 2022*
Published: *06 June 2022*

Citation:
Cheng L, Zhu H, Wang J, Wang G, Ma X, Zhao K, Wang J and Shu K (2022) Clinical Features, Diagnosis, and Treatment of Primary Intraventricular Lymphoma: Insights From a Monocentric Case Series. Front. Neurol. 13:920505. doi: 10.3389/fneur.2022.920505

Objective: Primary ventricular lymphoma (PVL) is an extremely rare and commonly misdiagnosed disease. Previous studies were predominantly case reports, and literature regarding the diagnosis and treatment of PVL is limited. Therefore, this study aimed to evaluate the characteristics of patients with PVL.

Methods: The data of patients with pathologically confirmed PVL were assessed. Epidemiological data, imaging findings, surgery, pathological results, and prognosis were retrospectively analyzed. A systematic review of relevant literature was also conducted.

Results: A total of eight patients with PVL were identified. The main symptom was increased intracranial pressure. Radiographically, five patients had single lesion and three had multiple lesions; typical findings on magnetic resonance imaging included hypointensity on T1- and T2-weighted imaging, adjacent brain edema, and homogeneous enhancement on contrast-enhanced T1-weighted images. Preoperatively, six cases were misdiagnosed and two cases did not get a definite diagnosis. Craniotomy was performed on all patients, and four achieved gross total resection. Hydrocephalus was relieved after surgical resection in four patients. Pathology revealed diffuse large B-cell lymphoma in all patients. Only one patient had a severe complication. A total of three patients received concomitant adjuvant treatment, whereas five patients refused any adjuvant therapy. At the time of follow-up, the median survival time of patients was 15 months.

Conclusion: Primary ventricular lymphoma mainly presented with symptoms of increased intracranial pressure and had several imaging characteristics for the diagnosis, but the condition still tends to be misdiagnosed. Surgical resection is a feasible treatment for patients with isolated nodules, especially those with acute obstructive hydrocephalus.

Keywords: primary central nervous system lymphoma, intraventricular, clinical features, diagnosis, treatment, case reports, review

INTRODUCTION

Primary central nervous system lymphoma (PCNSL) refers to lymphoma that grows solely within the brain, spinal cord, and eyes, without systemic involvement. PCNSL is a relatively rare and highly invasive extra-nodal non-Hodgkin's lymphoma, accounting for ∼2–5% of intracranial tumors and 4–6% of extra-nodal lymphomas (1, 2). The disease is common in patients with immunodeficiency, but recent literature has reported an increasing incidence of PCNSL in populations with normal immunity (3). PCNSL is associated with poor clinical outcomes and has a median progression-free survival time of 12 months and a median overall survival time of ∼3 years (4). More than 90% of PCNSLs are located in the brain parenchyma of the cerebral hemispheres, whereas primary lymphomas in the ventricle are extremely rare. Notably, there is a paucity of information on the diagnosis, treatment experience, and patient characteristics in PCNSL. In this study, we report the on cases of primary ventricular lymphoma (PVL) at our center and summarize the clinical characteristics and therapeutic effects of PVL based on a literature review.

METHODS

Study Patients

We performed a thorough review and analysis of the clinical data of patients with PCNSL admitted to our center from January 2010 to December 2020. The inclusion criteria were pathological findings confirming lymphoma, lesion located solely in the intraventricular system, and normal immune function. Patients with other systemic lymphomas or brain parenchymal lymphoma invading the cerebral ventricular system were excluded. A total of eight of 198 patients with PCNSL were included in this study, and their epidemiological data, imaging findings, surgical conditions, and pathological results were analyzed. A follow-up was conducted to evaluate patient's prognosis. This study was approved by the Ethics Committee of Tongji Hospital affiliated with Tongji Medical College of Huazhong University of Science and Technology. Because of the retrospective nature of the study, patient consent was not required.

Literature Search

A thorough literature screening of the PubMed and Web of Science databases for case reports on PCNSL in the ventricle was conducted according to the guidelines of the Preferred Reporting Items for Systematic Reviews and Meta-Analyses (PRISMA) using the following terms: "lymphoma" or "PCNSL" and "ventricle," "lateral ventricle," "third ventricle," or "fourth ventricle." The references of the reports were also reviewed. In total, 38 relevant articles were analyzed, 46 patients with a diagnosis were identified, 6 lacked sufficient data, and 1 patient had immunodeficiency; finally, 34 studies for qualitative synthesis were included (**Figure 1**).

RESULTS

Case Series

Epidemiological data, imaging findings, surgery, pathological results, radiotherapy and chemotherapy outcomes, and postoperative survival times of patients are presented in **Table 1**. Of the eight patients, two were women and six were men, and their age ranged from 35 to 69 years (mean, 55±13 years). The most common symptoms included increased intracranial pressure and impaired cerebellar balance perception. A total of five patients experienced headache and dizziness, three presented with nausea and vomiting, two exhibited walking instability, and one presented with memory loss. The onset of disease varied from 1 week to 2 months.

Preoperative magnetic resonance imaging (MRI) examination revealed single lesions in five cases and multiple lesions in three cases (37.5%). A total of four cases were confined to the fourth ventricle, two cases exhibited involvement of the lateral ventricle, and two cases presented with simultaneous involvement of the lateral and fourth ventricles (patients 2 and 8). The maximum diameter of lesions was 1.8–7.0 cm (average, 3.5 cm). A total of four patients exhibited varying degrees of hydrocephalus. There are several radiological features; typical MRI revealed hypointensity on T1- and T2-weighted imaging, with adjacent brain edema, and homogeneous enhancement on contrast-enhanced T1-weighted images, with cluster-like lesion in two patients (patients 2 and 6) and diffuse growth along the choroid plexus and ventricular wall in one patient (patient 8). Preoperatively, the suspected radiological diagnosis of four patients was medulloblastoma or ependymoma, the radiological diagnosis of two patients was meningioma (patients 5 and 6), and the other two patients did not have a definitive diagnosis.

Craniotomy was performed on all eight patients: 4 (50%) achieved gross total resection (GTR), 1 (12.5%) achieved subtotal resection (STR), and 3 (37.5%) achieved partial resection (PTR). Only one patient experienced complications with pulmonary infection, and one presented with minimal subdural hematoma; both patients recovered after treatment. The most serious complication was observed in patient 7, who presented with respiratory failure after surgery. Postoperatively, this patient received tube incision and respiratory support treatment; however, the patient died 10 days later after his family opted to discontinue treatment. None of the other patients presented with serious complications, and all patients recovered well after the surgery. Patient 3 underwent postoperative protocol chemotherapy with high-dose methotrexate (HDX)+temozolomide in addition to locally enhanced radiotherapy in the whole cerebellum. Patients 4 and 5 underwent HDX regimen chemotherapy and whole-brain radiotherapy. Other patients refused chemotherapy and radiotherapy after the surgery.

Postoperative pathology revealed diffuse large B-cell lymphoma (DLBCL), with immunohistochemically related positive indicators, including CD20, CD79a, LCA, MUM-1, PAX5, C-MYC, BCL-2, and BCL-6, in all patients. Only CD20 in patient 5 was negative. The Ki-67 marker index was 70–100%, with an average of 88%. Molecular pathology was performed in

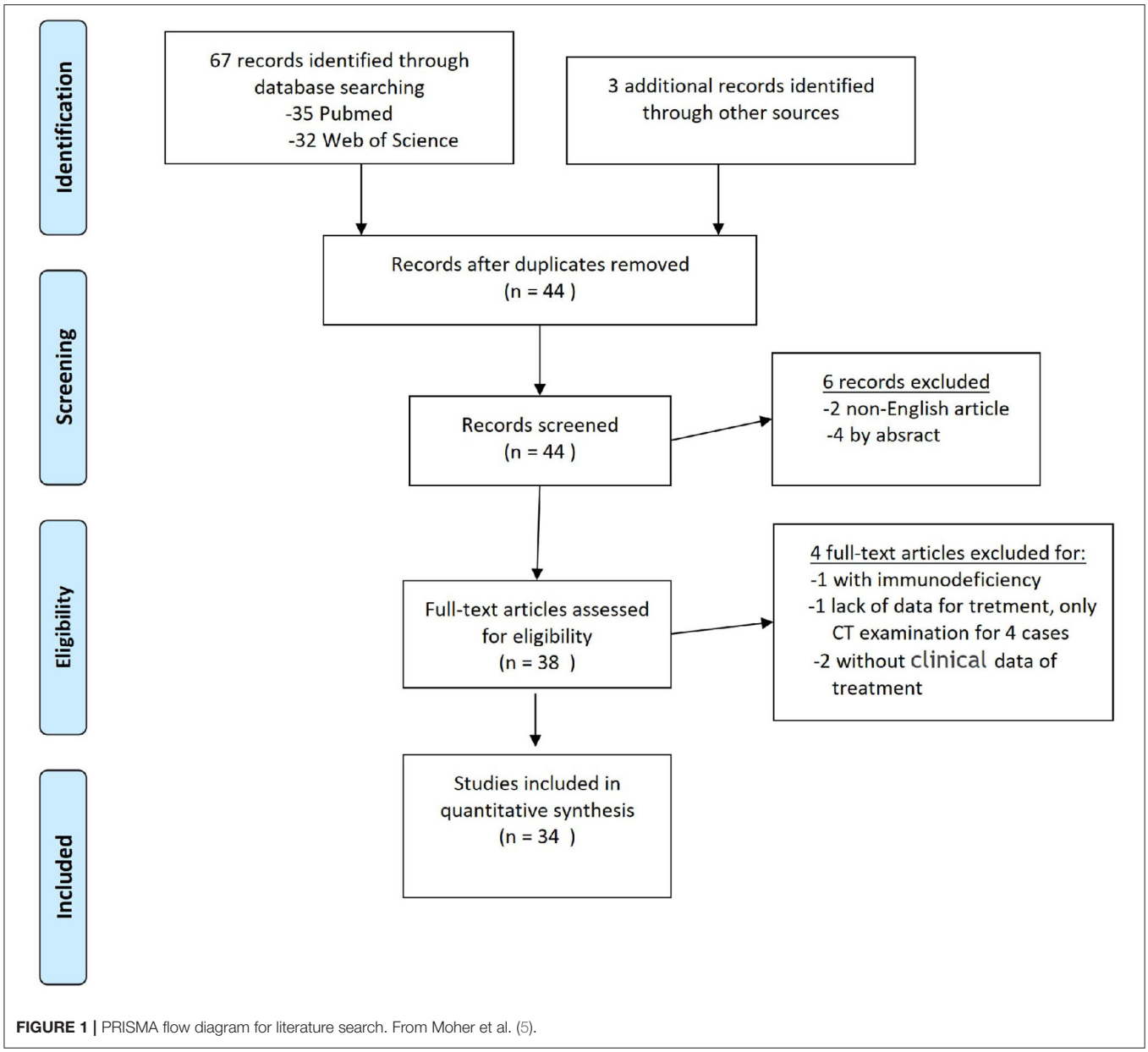

FIGURE 1 | PRISMA flow diagram for literature search. From Moher et al. (5).

five patients, and EBV-encoded small RNA chromogenic *in situ* hybridization was negative in five patients (**Table 2**).

With the exception of patient 7, who discontinued treatment 10 days after surgery, all other patients recovered and were discharged from the hospital. The survival time of patients ranged from 1 month to 4 years. Patients 3 and 5 were still alive during the reporting of this study. At the time of follow-up, the median survival time of patients was 15 months.

Combined Cases and Systematic Review

A total of thirty-nine patients were included in this study through a systematic review (**Supplementary Table 1**) (6–39). In total, 47 patients with PCNSL in the ventricle were identified, including in our series and previous articles. Of all patients, 27.7% were women, and the mean age was 55 ± 18 years (**Supplementary Table 2**). The most common symptoms were headache, nausea, and vomiting (28/47, 59.6%). Moreover, 25.5% patients presented with hemiplegia, ataxia, gait instability, and other motor disorders; 23.4% presented with dizziness or vertigo; 6 (12.8%) exhibited diplopia; 6 presented with memory deficits; 8 presented with rare symptoms, such as seizures, speech disturbance, and confusion. Among the patients, 59.6% had single lesions and 40.4% had multiple lesions. Lesions were confined to the lateral ventricle in 9 (19.1%) patients, third ventricle in 7 (14.9%) patients, and fourth ventricle in 17 (36.2%) patients. Lesions involving multiple ventricles were observed in 14 (29.8%) patients (including one with intraspinal metastasis). Solitary nodular growth was the most common growth pattern

TABLE 1 | Characteristics of the 8 patients included in the series.

Case no.	Age (yrs), sex	Presenting signs	Location	Size (cm)	HD	Growth pattern	Extent of resection	Complication	Adjuvant therapy	FU (mos), status
1	69, F	Headache, dizziness	4th V	4.0	Y	Solitary nodular	GTR	Lung infection	ND	15, died
2	35, M	Dizziness, vomiting	LV, 4th V	7.0	Y	Cluster like	PTR	N	ND	2, died
3	52, M	Unsteady gait	4th V	3.0	N	Solitary nodular	STR	N	CMT+RT	36, alive
4	68, M	Dizziness, vomiting	4th V	3.1	Y	Solitary nodular	GTR	N	CMT+RT	18, died
5	39, M	Headache	LV	3.0	N	Solitary nodular	GTR	Subdural hematoma	CMT+RT	48, alive
6	64, M	Decline in memory,	LV	3.2	N	Cluster like	PR	N	ND	4, died
7	52, M	Dizziness, unsteady gait, vomiting	4th V	3.1	Y	Solitary nodular	GTR	Respiratory failure	ND	Give up treatment
8	67, M	Unsteady gait	LV, 4th V	1.2	N	Diffuse type	PTR	N	ND	1, died

M, male; F, female; 4th V, fourth ventricle; LV, lateral ventricle; HD, hydrocephalus; Y, yes; N, no; GTR, gross total resection; STR, subtotal resection; PTR, partial resection; CMT, chemotherapy; RT, radiotherapy; ND, not did; FU, follow-up.

TABLE 2 | Pathological features of 8 patients.

Case no.	CD20	LCA	CD79a	PAX5	MUM-1	BCL-2	BCL-6	C-MYC	Ki67(%)	EBER CISH
1	+	+	ND	ND	+	ND	+	ND	80	ND
2	+	+	+	+	−	+	+	+	95	−
3	+	+	+	−	+	ND	+	+	90	ND
4	+	ND	+	+	−	+	+	ND	90	ND
5	_	ND	+	+	−	−	+	+	100	−
6	+	ND	ND	+	+	+	−	+	95	−
7	+	ND	ND	+	+	+	+	−	70	−
8	+	ND	ND	+	+	+	+	+	90	−

EBER CISH, EBV-encoded small RNAs chromogenic in situ hybridization.

(25/47, 53.2%) (**Figure 2**). Multiple nodules and cluster-like growth patterns (**Figure 3**) were observed in 5 (10.6%) and 4 (8.5%) patients, respectively. Diffuse growth along the choroid plexus and ventricular wall was also common (21.3%, 10/47) (**Figure 4**). A total of fifteen (31.9%) patients had hydrocephalus, of whom 7 had acute hydrocephalus. According to radiological data, 38 (80.9%) patients were misdiagnosed and 9 (19.1%) cases did not get a definite diagnosis.

A total of seven (14.9%) patients underwent urgent external ventricular drain for acute hydrocephalus, and 26 (55.3%) underwent surgical resection, of whom half (50%) achieved GTR and the remaining half (50%) achieved STR or PTR; 40.4% (19/47) were confirmed by biopsy, 2.1% (1/47) was confirmed using cerebrospinal fluid (CSF) cytopathology, and 2.1% (1/47) was confirmed based on postmortem autopsy. According to pathology, BCL was the most common (74.5%, 35/47), followed by Burkitt lymphoma (8.5%, 4/47), T-cell lymphoma (6.4%, 3/47), and small lymphocytic lymphoma (4.3%, 2/47). A total of three patients were pathologically unclassified. After diagnosis, 29.8% (14/47) of the patients received chemotherapy only, 6.4% (3/47) received radiotherapy only, 27.7% (13/47) received concomitant radiotherapy and chemotherapy, 2.1% (1/47) received immunotherapy, and 34.0% (16/47) did not receive any adjuvant therapy.

At the time of reporting, 25.5% (12/47) of the patients had died, with a median survival time of 7.0 ± 7.2 months (range, 1–18 months), and 59.6% (28/47) of the patients were still alive, with a follow-up time of 12.4 ± 10.3 months (range, 0.5–48 months). The prognosis of 7 patients was not reported.

Case Examples

Case 1

A 69-year-old woman presented with headache and dizziness for 2 months, and weakness in both legs 1 week before

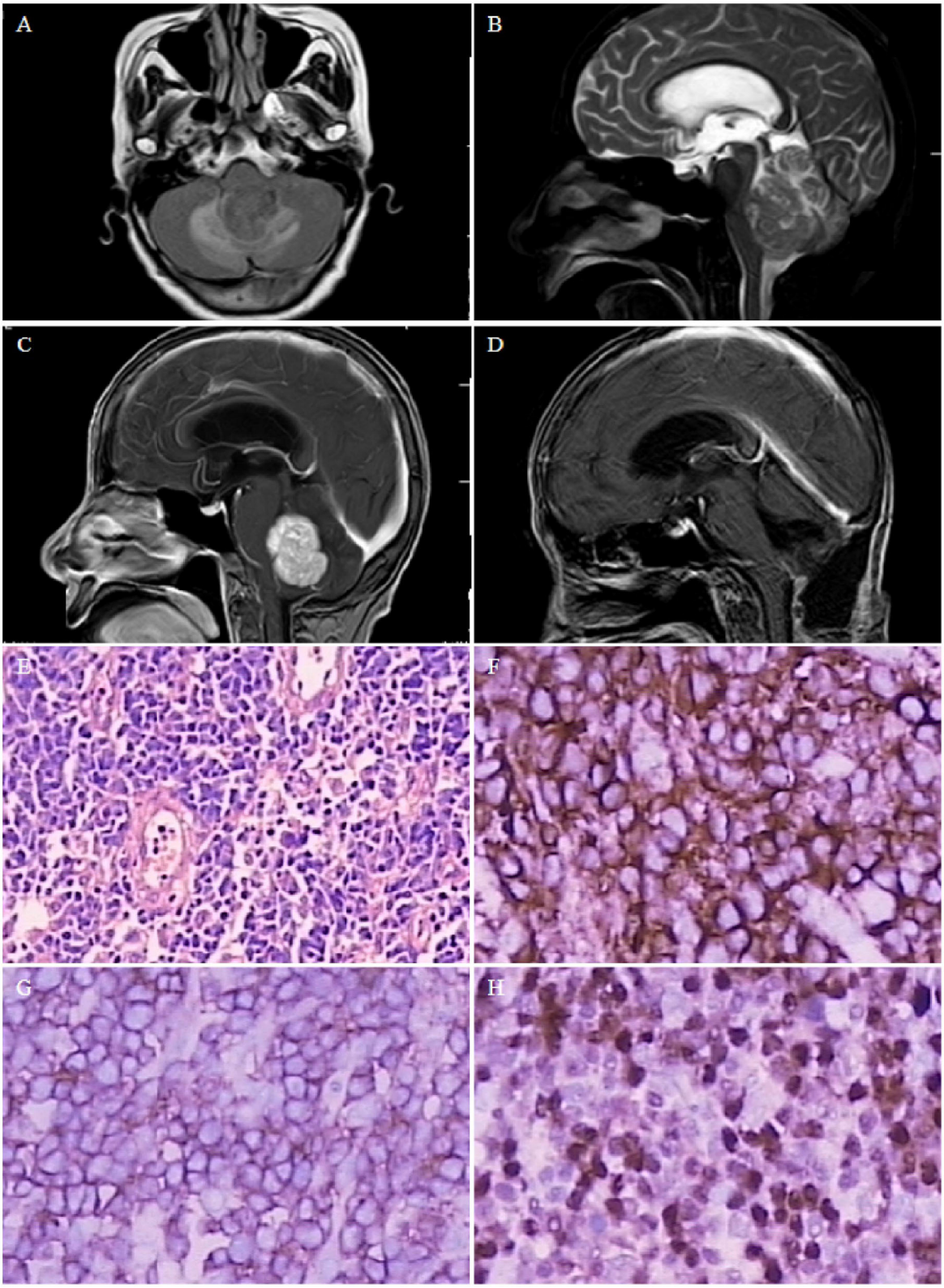

FIGURE 2 | Case 1. Magnetic resonance image of a 4.0×2.8-cm solid mass in the fourth ventricle, with supratentorial hydrocephalus. **(A)** T1-weighted image showing low signal. **(B)** T2-weighted image showing low signal. **(C)** Homogeneous enhancement on contrast-enhanced T1-weighted images. **(D)** Postoperative magnetic resonance image showing no residual lesion, and obstructive hydrocephalus is relieved. Pathological microscopic examination shows diffuse large B-cell infiltration [**(E)** hematoxylin and eosin, 200× magnification], including CD20- [**(F)**, 400× magnification], LCA- [**(G)**, 400× magnification], and MUM-positive [**(H)**, 400× magnification] lesions.

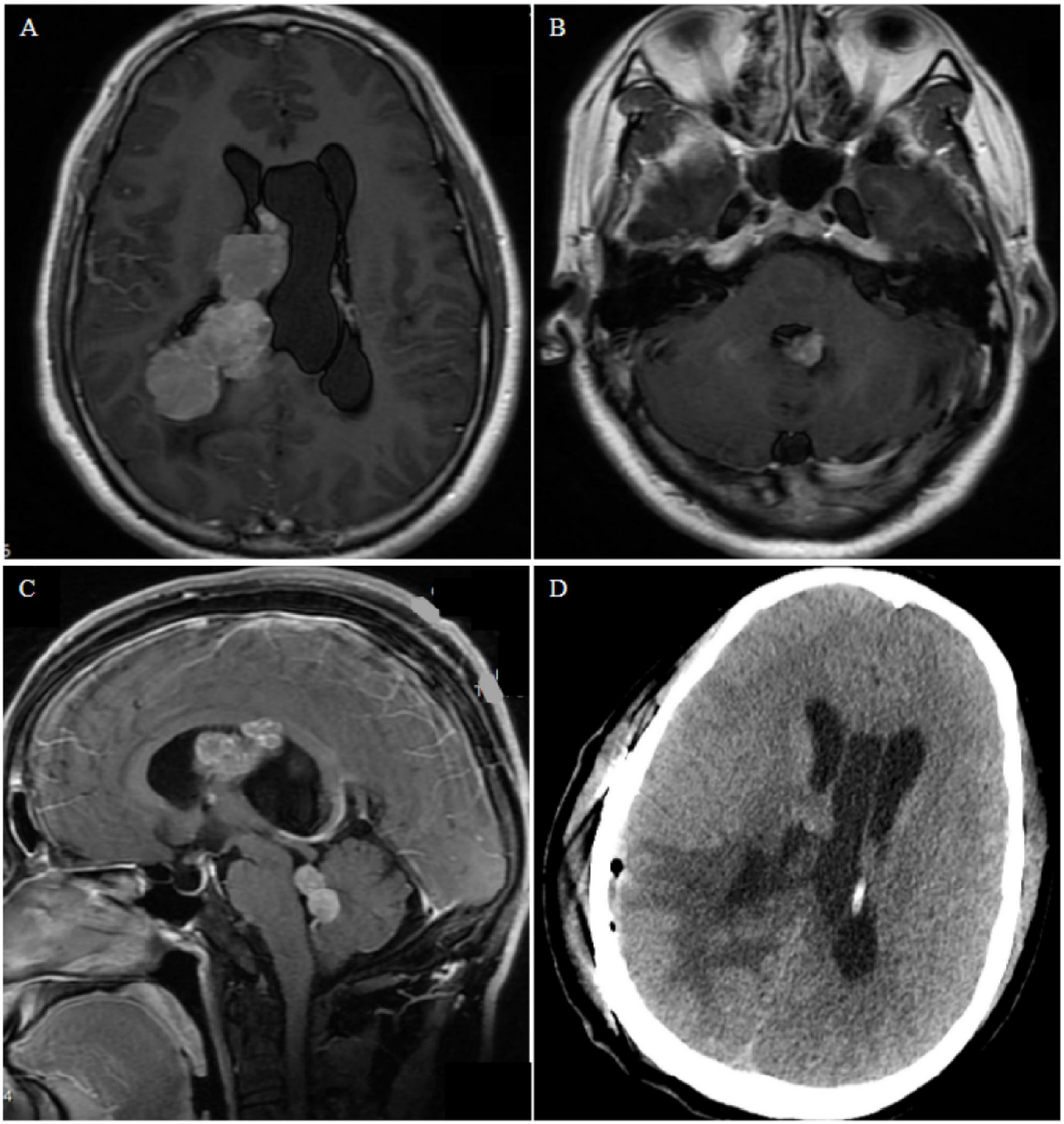

FIGURE 3 | Case 2. **(A,B)** Contrast-enhanced T1-weighted axial images show nodular bead-like lesions in the right and fourth ventricles. **(C)** Sagittal magnetic resonance images showing multiple lesions occupying the midbrain aqueduct and fourth ventricle. **(D)** Postoperative computed tomography shows edema of brain tissue and no bleeding in the operative cavity.

admission. The patient had previously developed ocular fundus pigmentation, resulting in blindness in both eyes. No immune deficiency or other underlying diseases were noted. The patient underwent head imaging 4 months before admission, which only indicated white matter thinning. Physical examination revealed no obvious positive signs. Brain MRI revealed a 4.0×2.8-cm solid mass in the fourth ventricle (**Figure 2**), which was considered a medulloblastoma or solid hemangioblastoma. The patient and her family opted for surgical resection. The surgery was performed *via* a prone postero-medial approach. During the operation, the tumor was observed to originate from the lateral orificium choroid plexus of the fourth ventricle with an abundant blood supply. Complete tumor resection was achieved under electrophysiological monitoring. Histopathological examination

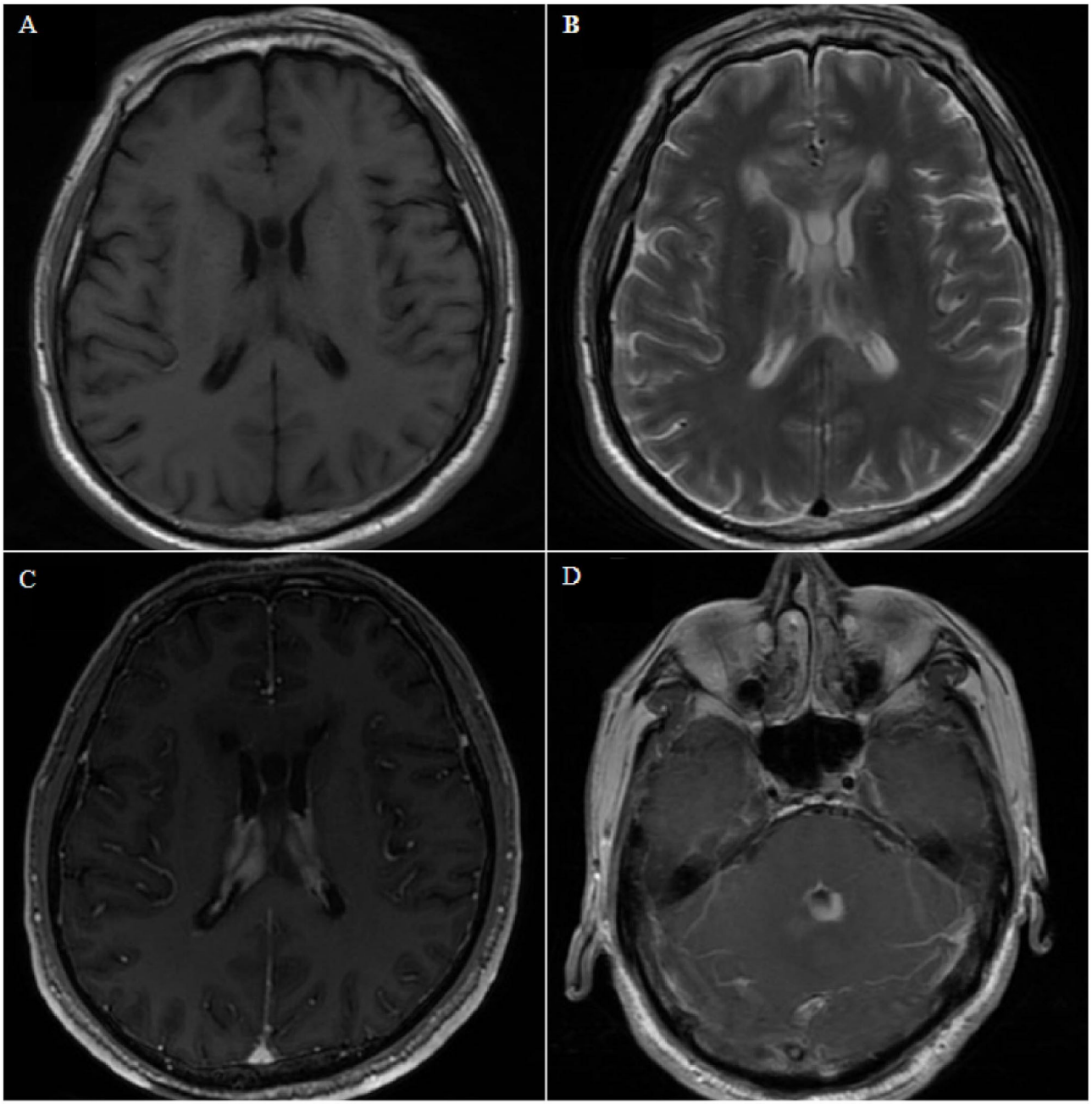

FIGURE 4 | Case 8. Axial magnetic resonance image showing bilateral and fourth ventricle lesions, diffuse growth along the choroid plexus and ventricle wall, low signal on T1- and T2-weighted images **(A,B)**, and homogeneous enhancement on contrast-enhanced T1-weighted images **(C,D)**.

revealed diffuse large B-cell infiltration (**Figure 2E**), with positive immunochemical staining for CD20, LCA, and MUM (**Figures 2F–H**, respectively). The diagnosis was primary DLBCL of the fourth ventricle. The patient developed complications of pulmonary infection, recovered, and was discharged after 2 months of antibiotic treatment. The patient refused further chemoradiotherapy and died 15 months after surgery due to tumor recurrence.

Case 2

A 35-year-old man presented with dizziness, nausea, and vomiting for 2 months. No obvious abnormalities were noted on physical examination, and no past underlying diseases were identified. Magnetic resonance imaging (MRI) examination revealed multiple lesions in the right lateral ventricle, middle cerebral aqueduct, and fourth ventricle, some of which were cluster-like, accompanied by hydrocephalus, with avid

enhancement (**Figure 3**). Preoperative diagnosis could not be performed, considering the possibility of metastases. Most of the intraventricular tumors were resected *via* the temporo-occipital approach. During the operation, the lesions were observed to originate from the choroid plexus. Microsurgical resection was uneventful, and postoperative pathology revealed diffuse large BCL, with no significant postoperative complications. The patient refused further radiotherapy and chemotherapy and died 2 months later.

Case 8

A 67-year-old man presented with gait instability for 20 days, and he had no history of underlying diseases. MRI examination revealed lesions in bilateral ventricles and the fourth ventricle (**Figure 4**), which could not be diagnosed clearly before surgery. After microsurgical resection, the lateral ventricular lesion was partially resected. Postoperative pathology revealed diffuse large BCL. Postoperative systemic examination revealed no other systemic lymphoma. The family refused further chemotherapy, and the patient died 1 month later.

DISCUSSION

Primary central nervous system lymphoma is predominantly located in the deep periventricular parenchyma, such as the corpus callosum and basal ganglia. Lesions may be single or multiple (∼34%) (40), and some lesions may extend into the ventricles. Up to 40–100% of parenchymatous subependymal lesions extend to ependymal surfaces (11). However, PCNSL with lesions purely located in the ventricular system is extremely rare. Previous studies were predominantly the case reports. Indeed, we only identified 39 patients with complete information. This study aimed to improve our current understanding of the diagnosis and treatment of PVL, and to this end, we summarized the epidemiological data, clinical manifestations, and imaging characteristics of PVL in detail based on our cohort and previous literature.

Epidemiology

The average diagnostic age of PCNSL was 65 years, and the male-to-female ratio was ∼1.2:1.7. Studies in the last 10 years have reported that the incidence of PCNSL is higher in elderly patients, especially in the population aged 70–79 years (41). In this study, the average age of patients with PVL was 54 years, which was similar to the overall age of PCNSL onset. Most cases were adults (91.5%, 43/47), and only 4 cases were children (<18 years). The male-to-female ratio was ∼2.6 (34:13), and PVL was more common in men.

Presenting Signs

Clinical symptoms of cerebral parenchymal lymphoma varied, with 70% presenting with focal neurologic deficits and 32–43% presenting with mental and behavioral changes; meanwhile, symptoms of increased intracranial pressure were less common than other intracranial tumors (∼32–33%), and epilepsy was less common (∼11%) (4, 42). PVL typically presented with headache, nausea, vomiting, and other symptoms of increased intracranial pressure, which comprised its main clinical features. Increased intracranial pressure was the reason for medical visits in up to 59.6% of patients. In addition to the mass effect caused by the lesion, intraventricular lymphoma readily blocked the CSF circulation pathway, resulting in hydrocephalus and aggravation of increased intracranial pressure. In our group, four of the eight patients presented with various degrees of hydrocephalus. Focal symptoms caused by lesion compression of adjacent nerves or brain tissue were relatively rare in PVL, accounting for 25.5% of patients. For example, lateral ventricular tumor compression of the thalamus resulted in limb hemiplegia; fourth ventricular tumor compression of the cerebellum induced balance abnormalities, resulting in gait imbalance or ataxia. Other common symptoms included dizziness or vertigo, diplopia, and memory loss. Epilepsy was rare in patients with this disease, with only 2 (4.2%) patients identified. Disturbance of consciousness was observed in a few patients with acute intracranial hypertension or lesions severely compressing the brainstem. Collectively, our findings indicate that increased intracranial pressure is the main clinical symptom of PVL, but this is often nonspecific.

Imaging Features

More than half of patients with AIDS have multiple lesions, whereas in ∼25% of immunocompetent patients, single lesions are more common (43). Of all patients with PCNSL, 87% were supratentorial, and a single lymphoma located in the infratentorial area was extremely rare in patients with normal immune function. PVL with solitary nodules was common, but the proportion of cases with multiple lesions was also high (40.4%). This may be associated with the spread of tumor cells *via* CSF. Furthermore, PVL of the fourth ventricle was common, and the occurrence of single lesions in the fourth ventricle was as high as 36.2%.

Combined with our series of cases and literature review, we classified the growth patterns of PVL into single-nodular type (**Figure 2**), cluster-like type (**Figure 3**), multiple-nodular type (19, 28, 30, 39), and diffuse growth type (**Figure 4**). The single-nodular type was the most common (53.2%), lacked imaging characteristics, and was easily misdiagnosed. The diffuse growth type was also common (21.3%), with lesions growing mainly along the choroid plexus and ventricular wall. This growth pattern may be considered the characteristic growth pattern of PVL. The cluster-like type was rare in other tumors and was also a characteristic of PVL. Multiple nodules were often considered as metastatic tumors, and this growth pattern was mostly due to the metastasis of tumor cells to other ventricles *via* CSF. Brozovich et al. reviewed a group of primary fourth ventricle lymphomas and reported that 50% of patients exhibited metastasis to other ventricles, which further confirmed the spread of PVL *via* CSF (34). Based on these data, we suggest that the presence of multiple lesions in the ventricle, especially those with cluster-like or diffuse growth along the choroid plexus and ventricular wall, is highly likely to be PVL.

Diagnosis and Differential Diagnosis

Primary ventricular lymphomas in the lateral ventricle are more likely to be misdiagnosed as meningioma, choroid plexus papilloma, or glioma. In contrast, in the fourth ventricle,

PVL is more likely to be misdiagnosed as medulloblastoma (in children), ependymoma, or astrocytoma. Multiple lesions are easily misdiagnosed as metastatic tumors or subependymal giant cell astrocytoma (SEGA). The imaging characteristic for diagnosis of PVL, in addition to characteristic growth patterns on MRI examination, is hypointensity on T1- and T2-weighted imaging; contrast enhancement typically shows homogeneous enhancement, with modest surrounding edema, and diffusion-weighted imaging usually shows uniform restricted diffusion (44). Multifocality of meningioma is rare, and choroid plexus papilloma usually presents a cystic, isointense T1-weighted image, and both have a clear boundary and slowly progression (45, 46); medulloblastoma and glioma are typically have high signal on T2-weighted imaging, and contrast enhancement tends to be heterogeneous (47); metastases with a pure intraventricular location are rare, usually with severe brain edema, and SEGA, which commonly occurs in younger patients, is almost always located in the vicinity of the foramen of Monro, with high-density calcification on CT examination (48). CSF is widely used in the diagnosis of PCNSL, including conventional cytology analysis, flow cytometry, polymerase chain reaction, detection of monoclonal B cells, and the recently reported detection of microRNA and interleukin-10 levels, which facilitate the diagnosis of PCNSL (49). However, only 15% of patients with PCNSL with CSF involvement are detectable by CSF examination (4). Patients with PVL may have a higher risk of spread *via* CSF. As a low-risk method, the value of this approach needs further investigation.

Because of the rarity of PVL, noninvasive diagnosis is difficult, and all eight patients in this group were misdiagnosed or could not be diagnosed before surgery. Therefore, obtaining pathological examination through biopsy or surgery is still a necessary means for diagnosing PVL. After a definite diagnosis of intracranial lesions, systemic examinations, including thoracic and abdominal bone marrow punctures, are also necessary for excluding systemic lymphomas involving the central nervous system (50).

Treatment

Considering the rarity of PVL in clinical practice, there is a lack of systematic experience in the treatment of PVL, and treatment is mostly performed according to the principles of PCNSL, including chemotherapy, radiation, and immunotherapy. HDX-based induction chemotherapy is currently the first-line therapy (51). Whole-brain radiotherapy for PCNSL remains controversial (52). As PCNSL has an infiltrative growth pattern, some lesions are multiple and deep, making surgery difficult. Studies have demonstrated that surgical resection did not significantly prolong survival time in patients (53). As a result, surgical resection was not included in the standard treatment plan and was limited to biopsy. With the recent progress in surgical techniques, such as the innovative use of fluorescein sodium, safe resection has been increasingly performed in patients with PCNSL (54). Furthermore, studies have demonstrated that, compared with biopsy, GTR and STR significantly prolong progression-free survival and overall survival time in patients with PCNSL (55). Some researchers propose that, for PCNSL with solitary nodules, superficial position, or acute cerebral hernia, surgical resection should be incorporated into treatment strategies (50). In this study, 26 (55.3%) of 47 patients underwent surgical resection and 50% (13/26) achieved GTR. Only one patient who underwent surgery in our center developed respiratory failure after surgery, and no other patients experienced serious complications; thus, surgery is safe. PVL in the third and fourth ventricles, lesions that easily blocked the CSF circulation pathway and led to obstructive hydrocephalus, and ventriculoperitoneal shunt increased the risk of tumor cell implantation metastasis (56). Surgery not only can gain tumor tissue for pathological diagnosis but also can discharge obstructive hydrocephalus. Hence, for solitary PVL, especially in patients with acute obstructive hydrocephalus, surgical resection is a feasible treatment. For cluster-like lesions that can be completely resected, surgical resection may also be considered. Given the established and wide application of endoscopic technology, endoscopic resection can be considered, as reported in the literature (37). A biopsy is recommended as the first choice for patients with diffuse growth and multinodular growth. In patients with partial lesions invading the medial thalamus, brainstem, and other critical functional areas, surgery should be considered with caution.

Studies have confirmed that prognosis is poorer in patients with PCNSL treated with surgical resection alone than in those treated with postoperative radiotherapy and chemotherapy, with a median survival time of only 4.6 months (57, 58). Among our eight patients, five did not receive any postoperative adjuvant therapy, and all of them relapsed and died, except for one patient who discontinued treatment due to complications, the median survival time was only 5.5 months. Radiotherapy and chemotherapy were considered essential for the treatment of PVL.

Limitations

The sample size of this study was small, and the literature was mainly based on case reports. The study lacked a large sample size and detailed follow-up. In particular, only the survival status of patients was followed up in the literature, and the follow-up time was too short to analyze the factors influencing patient prognosis.

CONCLUSION

Primary ventricular lymphoma is a rare disease that manifests clinically as increased intracranial pressure, but this symptom is nonspecific. Because of noninvasive diagnosis, the condition is commonly misdiagnosed. Cluster-like growth along the choroid plexus and diffuse growth along the ventricular wall constitute key imaging characteristics. For localized lesions, especially in patients with acute obstructive hydrocephalus, surgical resection is feasible, and postoperative adjuvant radiation and chemotherapy are necessary.

DATA AVAILABILITY STATEMENT

The original contributions presented in the study are included in the article/**Supplementary Material**, further inquiries can be directed to the corresponding author/s.

ETHICS STATEMENT

The studies involving human participants were reviewed and approved by Ethics Committee of Tongji Hospital affiliated with Tongji Medical College of Huazhong University of Science and Technology. Written informed consent for participation was not required for this study in accordance with the national legislation and the institutional requirements.

AUTHOR CONTRIBUTIONS

LC and KS concepted and designed the study. HZ, JiW, GW, and XM contributed to acquisition of data. KZ and JuW contributed to analysis and interpretation of data. LC drafted the article. KS approved the final version of the manuscript on behalf of all authors and contributed to study supervision. All authors critically revised the article and reviewed submitted version of the manuscript.

FUNDING

This work was supported by the Natural Science Foundation of Hubei Province (Grant No. 2020CFB657).

SUPPLEMENTARY MATERIAL

The Supplementary Material for this article can be found online at: https://www.frontiersin.org/articles/10.3389/fneur.2022.920505/full#supplementary-material

REFERENCES

1. Villano JL, Koshy M, Shaikh H, Dolecek TA, McCarthy BJ. Age, gender, and racial differences in incidence and survival in primary CNS lymphoma. *Br J Cancer.* (2011) 105:1414–8. doi: 10.1038/bjc.2011.357
2. Dolecek TA, Propp JM, Stroup NE, Kruchko C. Cbtrus statistical report: primary brain and central nervous system tumors diagnosed in the United States in 2005–2009. *Neuro Oncol.* (2012) 14:v1–49. doi: 10.1093/neuonc/nos218
3. Rubenstein J, Ferreri AJ, Pittaluga S. Primary lymphoma of the central nervous system: epidemiology, pathology and current approaches to diagnosis, prognosis and treatment. *Leuk Lymphoma.* (2008) 49:43–51. doi: 10.1080/10428190802311441
4. Korfel A, Schlegel U. Diagnosis and treatment of primary cns lymphoma. *Nat Rev Neurol.* (2013) 9:317–27. doi: 10.1038/nrneurol.2013.83
5. Moher D, Liberati A, Tetzlaff J, Altman DG. The PRISMA Group (2009). Preferred reporting items for systematic reviews and meta-analyses: the PRISMA statement. *PLoS Med*. (2009) 6:e1000097. doi: 10.1371/journal.pmed.1000097
6. Werneck LC, Hatschbach Z, Mora AH, Novak EM. [Meningitis caused by primary lymphoma of the central nervous system. report of a case]. *Arq Neuropsiquiatr.* (1977) 35:366–72. doi: 10.1590/s0004-282x1977000400010
7. Bogdahn U, Bogdahn S, Mertens HG, Dommasch D, Wodarz R, Wunsch PH, et al. Primary non-hodgkin's lymphomas of the Cns. *Acta Neurol Scand.* (1986) 73:602–14. doi: 10.1111/j.1600-0404.1986.tb04607.x
8. Haegelen C, Riffaud L, Bernard M, Morandi X. Primary isolated lymphoma of the fourth ventricle: case report. *J Neurooncol.* (2001) 51:129–31. doi: 10.1023/a:1010790325692
9. Pascual JM, Gonzalez-Llanos F, Roda JM. Primary hypothalamic-third ventricle lymphoma. case report and review of the literature. *Neurocirugia (Astur).* (2002) 13:305–10. doi: 10.1016/s1130-1473(02)70605-2
10. Kelley TW, Prayson RA, Barnett GH, Stevens GH, Cook JR, Hsi ED. Extranodal marginal zone b-cell lymphoma of mucosa-associated lymphoid tissue arising in the lateral ventricle. *Leuk Lymphoma.* (2005) 46:1423–7. doi: 10.1080/10428190500205895
11. Park SW, Yoon SH, Cho KG. An endoscopically proven ventriculitis-type, cyst-like intraventricular primary lymphoma of the central nervous system. *Acta Neurochir (Wien).* (2006) 148:981–4. doi: 10.1007/s00701-006-0797-2
12. Jung TY, Jung S, Lee MC, Lee KH. Extranodal marginal zone b-cell lymphoma mimicking meningioma in lateral ventricle: a case report and possible pathogenesis. *J Neurooncol.* (2006) 80:63–7. doi: 10.1007/s11060-006-9153-x
13. Terasaki M, Abe T, Tajima Y, Fukushima S, Hirohata M, Shigemori M. Primary choroid plexus t-cell lymphoma and multiple aneurysms in the Cns. *Leuk Lymphoma.* (2006) 47:1680–2. doi: 10.1080/10428190600612503
14. Cecchi PC, Billio A, Colombetti V, Rizzo P, Ricci UM, Schwarz A. Primary high-grade b-cell lymphoma of the choroid plexus. *Clin Neurol Neurosurg.* (2008) 110:75–9. doi: 10.1016/j.clineuro.2007.08.019
15. Hill CS, Khan AF, Bloom S, McCartney S, Choi D. A rare case of vomiting: fourth ventricular b-cell lymphoma. *J Neurooncol.* (2009) 93:261–2. doi: 10.1007/s11060-008-9765-4
16. Gu Y, Hou YY, Zhang XB, Hu F. Primary central nervous system burkitt lymphoma as concomitant lesions in the third and the left ventricles: a case study and literature review. *J Neurooncol.* (2010) 99:277–81. doi: 10.1007/s11060-010-0122-z
17. Sasani M, Bayhan M, Sasani H, Kaner T, Oktenoglu T, Cakiroglu G, et al. Primary central nervous system lymphoma presenting as a pure third ventricular lesion: a case report. *J Med Case Rep.* (2011) 5:213. doi: 10.1186/1752-1947-5-213
18. Jiang M, Zhu J, Guan YS, Zou LQ. Primary central nervous system burkitt lymphoma with non-immunoglobulin heavy chain translocation in right ventricle: case report. *Pediatr Hematol Oncol.* (2011) 28:454–8. doi: 10.3109/08880018.2011.566599
19. Brar R, Prasad A, Sharma T, Vermani N. Multifocal lateral and fourth ventricular b-cell primary cns lymphoma. *Clin Neurol Neurosurg.* (2012) 114:281–3. doi: 10.1016/j.clineuro.2011.10.020
20. Yakupoglu H, Onal MB, Civelek E, Kircelli A, Aygun MS, Aygun FM. Primary diffuse choroid plexus t-cell lymphoma: case report. *J Neuroradiol.* (2012) 39:116–8. doi: 10.1016/j.neurad.2011.03.002
21. Rao RN, Mishra D, Agrawal P, Kumar R. Primary B-cell central nervous system lymphoma involving fourth ventricle: a rare case report with review of literature. *Neurol India.* (2013) 61:450–3. doi: 10.4103/0028-3886.117608
22. Bokhari R, Ghanem A, Alahwal M, Baeesa S. Primary isolated lymphoma of the fourth ventricle in an immunocompetent patient. *Case Rep Oncol Med.* (2013) 2013:614658. doi: 10.1155/2013/614658
23. Liao CH, Lin SC, Hung SC, Hsu SP, Ho DM, Shih YH. Primary large b-cell lymphoma of the fourth ventricle. *J Clin Neurosci.* (2014) 21:180–3. doi: 10.1016/j.jocn.2013.02.036
24. Fabiano AJ, Syriac S, Fenstermaker RA, Qiu J. Primary fourth ventricular b-cell lymphoma in an immunocompetent patient. *Clin Neuropathol.* (2014) 33:94–7. doi: 10.5414/NP300658
25. Grossman R, Nossek E, Shimony N, Raz M, Ram Z. Intraoperative 5-aminolevulinic acid-induced fluorescence in primary central nervous system lymphoma. *J Neurosurg.* (2014) 120:67–9. doi: 10.3171/2013.9.JNS131076
26. Alabdulsalam A, Zaidi SZ, Tailor I, Orz Y, Al-Dandan S. Primary burkitt lymphoma of the fourth ventricle in an immunocompetent young patient. *Case Rep Pathol.* (2014) 2014:630954. doi: 10.1155/2014/630954
27. Funaro K, Bailey KC, Aguila S, Agosti SJ, Vaillancourt C. A case of intraventricular primary central nervous system lymphoma. *J Radiol Case Rep.* (2014) 8:1–7. doi: 10.3941/jrcr.v8i3.1361

28. Zhu Y, Ye K, Zhan R, Tong Y. Multifocal lateral and fourth ventricular primary central nervous system lymphoma: case report and literature review. *Turk Neurosurg.* (2015) 25:493–5. doi: 10.5137/1019-5149.JTN.10496-14.1
29. Hsu HI, Lai PH, Tseng HH, Hsu SS. Primary solitary lymphoma of the fourth ventricle. *Int J Surg Case Rep.* (2015) 14:23–5. doi: 10.1016/j.ijscr.2015.07.006
30. Suri V, Mittapalli V, Kulshrestha M, Premlani K, Sogani SK, Suri K. Primary intraventricular central nervous system lymphoma in an immunocompetent patient. *J Pediatr Neurosci.* (2015) 10:393–5. doi: 10.4103/1817-1745.174433
31. Cellina M, Fetoni V, Baron P, Orsi M, Oliva G. Unusual primary central nervous system lymphoma location involving the fourth ventricle and hypothalamus. *Neuroradiol J.* (2015) 28:120–5. doi: 10.1177/1971400915576671
32. Qin JZ, Wu YK, Yang ZJ, Lv J, Dang YY, Zhang HT, et al. Endoscopic biopsy of a b-cell lymphoma involving the entire ventricular system: a case report. *Exp Ther Med.* (2016) 11:325–7. doi: 10.3892/etm.2015.2861
33. Liu H, Hou H, Cheng J. Primary burkitt lymphoma of the fourth ventricle mimicking a medulloblastoma in a child. *J Neurooncol.* (2016) 127:205–7. doi: 10.1007/s11060-015-2023-7
34. Brozovich A, Ewing D, Burns E, Hatcher C, Acosta G, Khan U, et al. Primary Cns lymphoma arising from the 4(th) ventricle: a case report and review of the literature. *Case Rep Oncol Med.* (2019) 2019:2671794. doi: 10.1155/2019/2671794
35. Wang D, Su M, Xiao J. A rare case of primary ventricular lymphoma presented on Fdg Pet/Ct. *Clin Nucl Med.* (2020) 45:156–8. doi: 10.1097/RLU.0000000000002876
36. Haddad R, Alkubaisi A, Al Bozom I, Haider A, Belkhair S. Solitary primary central nervous system lymphoma mimicking third ventricular colloid cyst-case report and review of literature. *World Neurosurg.* (2019) 123:286–94. doi: 10.1016/j.wneu.2018.12.026
37. Guo R, Zhang X, Niu C, Xi Y, Yin H, Lin H, et al. Primary central nervous system small lymphocytic lymphoma in the bilateral ventricles: two case reports. *BMC Neurol.* (2019) 19:200. doi: 10.1186/s12883-019-1430-3
38. Ball MK, Morris JM, Wood AJ, Meyer FB, Kaszuba MC, Raghunathan A. Ventricle-predominant primary cns lymphomas: clinical, radiological and pathological evaluation of five cases and review of the literature. *Brain Tumor Pathol.* (2020) 37:22–30. doi: 10.1007/s10014-019-00354-x
39. Khanna G, Ahlawat S, Garg N, Gupta R, Patir R. A rare case of isolated intraventricular primary central nervous system lymphoma in an 85-year-old man. *Asian J Neurosurg.* (2021) 16:623–5. doi: 10.4103/ajns.AJNS_551_20
40. Correia CE, Schaff LR, Grommes C. Central nervous system lymphoma: approach to diagnosis and treatment. *Cancer J.* (2020) 26:241–52. doi: 10.1097/PPO.0000000000000449
41. Mendez JS, Ostrom QT, Gittleman H, Kruchko C, DeAngelis LM, Barnholtz-Sloan JS, et al. The elderly left behind-changes in survival trends of primary central nervous system lymphoma over the past 4 decades. *Neuro Oncol.* (2018) 20:687–94. doi: 10.1093/neuonc/nox187
42. Bataille B, Delwail V, Menet E, Vandermarcq P, Ingrand P, Wager M, et al. Primary intracerebral malignant lymphoma: report of 248 cases. *J Neurosurg.* (2000) 92:261–6. doi: 10.3171/jns.2000.92.2.0261
43. Fine HA, Mayer RJ. Primary central nervous system lymphoma. *Ann Intern Med.* (1993) 119:1093–104. doi: 10.7326/0003-4819-119-11-199312010-00007
44. Cheng G, Zhang J. Imaging features (ct, mri, mrs, and pet/ct) of primary central nervous system lymphoma in immunocompetent patients. *Neurol Sci.* (2019) 40:535–42. doi: 10.1007/s10072-018-3669-7
45. Teng H, Liu Z, Yan O, He W, Jie D, Qie Y, et al. Lateral ventricular meningiomas: clinical features, radiological findings and long-term outcomes. *Cancer Manag Res.* (2021) 13:6089–99. doi: 10.2147/CMAR.S320651
46. Lin H, Leng X, Qin CH, Du YX, Wang WS, Qiu SJ. Choroid plexus tumours on mri: similarities and distinctions in different grades. *Cancer Imaging.* (2019) 19:17. doi: 10.1186/s40644-019-0200-1
47. Citterio G, Reni M, Gatta G, Ferreri AJM. Primary central nervous system lymphoma. *Crit Rev Oncol Hematol.* (2017) 113:97–110. doi: 10.1016/j.critrevonc.2017.03.019
48. Beaumont TL, Limbrick DD, Smyth MD. Advances in the management of subependymal giant cell astrocytoma. *Childs Nerv Syst.* (2012) 28:963–8. doi: 10.1007/s00381-012-1785-x
49. Schroers R, Baraniskin A, Heute C, Vorgerd M, Brunn A, Kuhnhenn J, et al. Diagnosis of leptomeningeal disease in diffuse large b-cell lymphomas of the central nervous system by flow cytometry and cytopathology. *Eur J Haematol.* (2010) 85:520–8. doi: 10.1111/j.1600-0609.2010.01516.x
50. Hoang-Xuan K, Bessell E, Bromberg J, Hottinger AF, Preusser M, Ruda R, et al. Diagnosis and treatment of primary cns lymphoma in immunocompetent patients: guidelines from the european association for neuro-oncology. *Lancet Oncol.* (2015) 16:e322–32. doi: 10.1016/S1470-2045(15)00076-5
51. Yang H, Xun Y, Yang A, Liu F, You H. Advances and challenges in the treatment of primary central nervous system lymphoma. *J Cell Physiol.* (2020) 235:9143–65. doi: 10.1002/jcp.29790
52. Ferreri AJ, DeAngelis L, Illerhaus G, O'Neill BP, Reni M, Soussain C, et al. Whole-brain radiotherapy in primary cns lymphoma. *Lancet Oncol.* (2011) 12:118–9; author reply 9–20. doi: 10.1016/S1470-2045(11)70018-3
53. Schellekes N, Barbotti A, Abramov Y, Sitt R, Di Meco F, Ram Z, et al. Resection of primary central nervous system lymphoma: impact of patient selection on overall survival. *J Neurosurg.* (2021) 135:1016–25. doi: 10.3171/2020.9.Jns201980
54. Schebesch KM, Hoehne J, Hohenberger C, Acerbi F, Broggi M, Proescholdt M, et al. Fluorescein sodium-guided surgery in cerebral lymphoma. *Clin Neurol Neurosurg.* (2015) 139:125–8. doi: 10.1016/j.clineuro.2015.09.015
55. Weller M, Martus P, Roth P, Thiel E, Korfel A, German PSG. Surgery for primary cns lymphoma? challenging a paradigm. *Neuro Oncol.* (2012) 14:1481–4. doi: 10.1093/neuonc/nos159
56. Chen F, Guo H, Mao C, Jiang X, Liu S, Huang L, et al. Unusual relapse of primary central nervous system lymphoma both inside and outside central nervous system in patient with ventriculoperitoneal shunt. *World Neurosurg.* (2019) 127:625–8. doi: 10.1016/j.wneu.2019.01.277
57. Wang H, Wang M, Wei J, Wang L, Mao L, Jin J. Primary central nervous system lymphoma: retrospective analysis of 34 cases in a single centre. *J Int Med Res.* (2018) 46:883–94. doi: 10.1177/03000605177 34395
58. Henry JM, Heffner RR, Dillard SH, Earle KM, Davis RL. Primary malignant lymphomas of the central nervous system. *Cancer.* (1974) 34:1293–302.

Conflict of Interest: The authors declare that the research was conducted in the absence of any commercial or financial relationships that could be construed as a potential conflict of interest.

frontiers | Frontiers in Oncology

ORIGINAL RESEARCH
published: 07 July 2022
doi: 10.3389/fonc.2022.903177

Preclinical Assessment of MEK Inhibitors for Malignant Peripheral Nerve Sheath Tumors Reveals Differences in Efficacy and Adaptive Response

Yihui Gu[1†], Wei Wang[1†], Yuehua Li[1†], Haibo Li[2†], Zizhen Guo[1], Chengjiang Wei[1], Manmei Long[3], Manhon Chung[1], Rehanguli Aimaier[1], Qingfeng Li[1] and Zhichao Wang[1*]*

[1] Department of Plastic and Reconstructive Surgery, Shanghai Ninth People's Hospital, Shanghai Jiao Tong University School of Medicine, Shanghai, China, [2] Department of Plastic Surgery, The Third Xiangya Hospital, Central South University, Changsha, China, [3] Department of Pathology, Shanghai Ninth People's Hospital, Shanghai Jiao Tong University School of Medicine, Shanghai, China

Malignant peripheral nerve sheath tumors (MPNSTs) are rare soft-tissue sarcomas refractory to standard therapies. Inactivation of *NF1* and subsequent upregulation of RAS/RAF/MEK/ERK signaling exist in the majority of MPNSTs. However, the lack of preclinical assessment of MEK inhibitors in MPNSTs hinders the clinical application as well as the development of combination therapy. To guide further clinical studies, we evaluated different MEK inhibitors in terms of efficacy, safety, and mechanism of adaptive response in treating MPNSTs. Using a MPNST tissue microarray, we found that p-ERK could serve as a biomarker for predicting the prognosis of MPNST patients as well as an effective therapeutic target. Through *in vitro* and *in vivo* experiments, we identified trametinib as the most potent MEK inhibitor for the treatment of MPNSTs. Mechanistically, reduced reactivation of the MAPK pathway and compensatory activation of the parallel pathways contributed to better efficacy. Our results provide a basis for the further clinical application of MEK inhibitors as single agents or combinational therapies.

Keywords: neurofibromatosis type 1, malignant peripheral nerve sheath tumors (MPNST), mek inhibitor, trametinib, target therapy

OPEN ACCESS

Edited by:
Laura Gatti,
IRCCS Carlo Besta Neurological Institute Foundation, Italy

Reviewed by:
Elisabetta Vergani,
National Cancer Institute Foundation (IRCCS), Italy
Cristina Corno,
National Cancer Institute Foundation (IRCCS), Italy

****Correspondence:***
Zhichao Wang
shmuwzc@163.com;
dr_wangzhichao@163.com
Qingfeng Li
liqingfeng@shsmu.edu.cn;
dr_liqingfeng9@163.com

[†]These authors have contributed equally to this work

Specialty section:
This article was submitted to Neuro-Oncology and Neurosurgical Oncology, a section of the journal Frontiers in Oncology

Received: *24 March 2022*
Accepted: *07 June 2022*
Published: *07 July 2022*

Citation:
Gu Y, Wang W, Li Y, Li H, Guo Z, Wei C, Long M, Chung M, Aimaier R, Li Q and Wang Z (2022) Preclinical Assessment of MEK Inhibitors for Malignant Peripheral Nerve Sheath Tumors Reveals Differences in Efficacy and Adaptive Response. Front. Oncol. 12:903177. doi: 10.3389/fonc.2022.903177

INTRODUCTION

Malignant peripheral nerve sheath tumors (MPNSTs) are aggressive soft tissue sarcomas arising in patients with neurofibromatosis type 1(NF1) or sporadically. MPNSTs are refractory to standard therapies (1, 2), and extended resection is currently the only potential curative management for MPNSTs, which is not suitable for advanced MPNST patients. In addition, the local recurrence rate remains high after surgical resection and traditional chemo/radio therapies show mild benefits (3–6). The overall 5-year survival rate has remained poor at only 16-52% for decades, mainly owing to the lack of effective treatments. Therefore, there is an unmet clinical demand to discover novel therapeutic strategies, particularly targeted therapies, to treat advanced MPNSTs.

Genomic profiling of MPNST cohorts revealed that mutation in Neurofibromin 1(*NF1)* occurred in 100% of NF1-associated MPNSTs and 82% of other types of MPNSTs. As a RAS GTPase–activating protein, inactivation of *NF1* leads to uncontrolled activation of RAS and subsequent upregulation of downstream signaling pathways including mitogen-activated protein kinase (MAPK), PI3K/Akt, and Ral-GEF pathways (7–12). Among these dysregulated signaling contributing to the occurrence and progression of MPNSTs, MAPK is the most well-studied signaling pathway which is critical for cell proliferation, differentiation, and survival, suggesting that this pathway is a promising therapeutic target in MPNST treatment. In addition, MAPK signaling pathway is also an effective therapeutic target for a variety of human cancers, including melanoma and NSCLC (13–15).

MEK inhibitors, such as trametinib and cobimetinib, are highly specific, non-ATP competitive, small-molecule inhibitors of MEK1/2. MEK inhibitors have shown promising therapeutic efficacy in RAS-driven tumors including plexiform neurofibroma (pNF), the precancerous lesion of MPNSTs (13, 16–20). In clinical trials, the MEK inhibitor selumetinib led to clinical responses in up to 70% of children with inoperable pNF and subsequently gained FDA approval for this indication (17, 21). However, the efficacy of MEK inhibitors in the treatment of MPNSTs remains controversial. Currently, the research related to MEK inhibitors mainly focused on the development of effective combinational strategies. Several combinational therapies including MEK inhibitors in combination with mTOR inhibitors, MET inhibitors, and others were evaluated in preclinical studies and clinical trials (22–24). However, clinically sufficient combinational therapies still do not exist.

We found that the efficacy of different MEK inhibitors as single agents and the mechanism underlying the difference in treatment response are poorly investigated in preclinical studies. In addition, the low incidence of MPNSTs makes the recruitment of clinical trials extremely difficult. These deficiencies and challenges hinder the implications of MEK inhibitors in MPNST therapy. Therefore, a comprehensive preclinical evaluation of MEK inhibitors is necessary to guide further clinical studies.

In this study, we evaluated different MEK inhibitors in terms of efficacy, safety, and mechanism of adaptive response in treating MPNSTs. We assessed the expression and clinical relevance of MAPK pathway in MPNST patients using a tissue microarray. The efficacy and safety of different MEK inhibitors were evaluated *in vivo* and *in vitro*. In addition, the mechanism of adaptive response in 8 MEK inhibitors was also explored. This study provided a basis for the further clinical application of MEK inhibitors as single agents or combinational therapies.

MATERIALS & METHODS

Cell Lines and Reagents

The $NF1^{+/-}$ Schwann cell line (sNF02.3 2λ) was obtained from the American Type Culture Collection (ATCC). NF1-associated (ST88-14, T265, S462, and S462TY) and sporadic (STS-26T) MPNST lines were kindly granted by Prof. Vincent Keng and Prof. Jilong Yang (**Table S1**). All MPNST cell lines were maintained in high-glucose DMEM supplemented with 10% fetal bovine serum (FBS) and 1% penicillin/streptomycin in a 37°C, 5% CO_2 incubator, sNF02.3 2λ cells were cultured under the same conditions with 1% L-glutamine added.

Reagents and antibodies used in this article are described in **Supplementary Table S2**.

Immunohistochemical Staining

A tissue microarray (TMA) was constructed using 57 paraffin-embedded MPNST specimens obtained from 49 patients who underwent surgical treatment at Shanghai Ninth People's Hospital, Shanghai Jiao Tong University School of Medicine in Shanghai, China. IHC staining was performed as previously described (25). The assessment of TMA IHC staining was accomplished by two qualified pathologists independently. The score was assigned according to the proportion of positive cells within carcinomatous areas so that no staining, <25% of malignant cells staining, 25%-50% of malignant cells staining, >50% of malignant cells staining were recorded as 0, 1, 2, 3. Clinical information was collected through electronic medical records and telephone follow-ups. Twenty-eight of 49 patients were lost to follow-up and were not able to be contacted through multiple methods.

Cell Line-Based Assays

A Cell Counting Kit-8 (CCK-8) assay was implemented to assess cytotoxicity. A total of $1*10^3$ or $3*10^3$ cells per well were seeded into 96-well culture plates and treated with 0.1% DMSO or the indicated drug. After 72 h or 96 h, 10 μL CCK-8 solution (Dojindo, Japan) dispersed in 90 μL DMEM was added per well to measure the 450 nm OD value after a 2 h incubation. Percentage cell viability was calculated as 100% × (OD of drug-treated cells - OD of background control)/(OD of untreated cells - OD of background control). The IC50 of indicated drugs was calculated by Prism 8.4.0 using [inhibitor] vs. normalized response – Variable slope analysis.

Annexin V–FITC and propidium iodide (PI) assays were implemented to detect cell apoptosis. MPNST cells were seeded into 6-well culture plates and treated with DMSO or the indicated MEKi for 24 h or 48 h. Afterwards, MPNST cells were stained with annexin V–FITC and PI at room temperature in the dark for 15 minutes, followed by analysis using a flow cytometer (CytoFLEX LX, Beckman Coulter, Shanghai) equipped with CytExpert software (Beckman Coulter, Shanghai).

A cell cycle assay was implemented to monitor the cell cycle. MPNST cells treated as described above were fixed with cold 70% ethanol, stained with PI/RNase solution, and analyzed on a flow cytometer as described above.

Western Blot Analysis

Cells were lysed in RIPA buffer (Beyotime, China) with protease and phosphatase inhibitor cocktails (Beyotime, China). Proteins separated by SDS-PAGE were transferred onto PVDF membranes and blocked in 3% bovine serum. Afterwards, membranes were incubated overnight in primary antibody solution at 4°C, followed by incubation with an HRP-conjugated secondary antibody for 1 h

at room temperature. Band signals were detected using an Amersham Imager 600 (General Electric Company, Boston, MA, United States), and quantification was performed using ImageJ software after normalization to GAPDH.

Xenografts

Four-week-old male NOD-SCID IL-2 receptor gamma-null mice were purchased from Shanghai Model Organisms Co., Ltd. (Shanghai, China). A total of 5×10^6 S462TY cells suspended in 100 µL phosphate-buffered saline was engrafted subcutaneously into the armpit of each mouse. Tumor volume (based on caliper measurements) was calculated by the modified ellipsoidal formula: tumor volume = 1/2 length* width^2. When tumors reached a volume of approximately 100 mm^3, mice were randomly assigned to treatment with vehicle (n=4), trametinib (0.3 mg/kg, daily gavage, n=4), TAK-733 (2.4 mg/kg, daily gavage, n=4) or selumetinib (15.2 mg/kg, 2 times daily gavage, n=4). After 3 weeks of treatment, mice were sacrificed, and grafts were removed, weighed, and photographed. Grafts were stained with p-ERK, Ki-67, c-MYC, and cleaved Caspase 3 for histological analysis according to standard protocols.

Statistics

Data are presented as the mean ± standard error of the mean (SEM) or standard deviation (SD). Statistical analysis was conducted using Prism 8.4 (GraphPad Software, San Diego, CA). Statistical analyses were performed using the student's t-test, the log-rank test, and the Pearson correlation analysis. P-values < 0.05 were considered to indicate statistical significance, and asterisks (*) are used to indicate significant differences between two specified groups. * indicates a P-value < 0.05, ** indicates a P-value < 0.01, *** indicates a P-value < 0.001.

Ethics Approval and Consent to Participate

The study was approved by the Ethics Committee of Shanghai Ninth People's Hospital, Shanghai Jiao Tong University School of Medicine, and informed consent was achieved from patients under institutional reviewer board protocols.

RESULTS

High Expression of p-ERK Correlates With Dismal Prognosis in MPNSTs

To evaluate the expression of MAPK pathway in MPNSTs, we performed IHC staining of p-ERK using a TMA containing 57 MPNST specimens (**Table S3**). The levels of p-ERK in tumor tissues were classified as score 0 (negative, 20.8%), 1 (low positive, 28.3%), 2 (medium positive, 32.1%) or 3 (high positive, 18.9%) (**Figure 1A**). The expression of p-ERK was positively correlated with that of p-MEK, Ki-67, and CD34 (**Table 1**; **Figures S1A–C**). Analysis of clinicopathological correlations indicated that MPNST patients with high p-ERK expression had a shorter overall survival duration than the p-ERK low expression patients (p = 0.007, **Figure 1B**).

Screening 8 MEK Inhibitors in MPNST Cells Revealed Differences in Efficiency and the Adaptive Response

After identifying p-ERK as a potential therapeutic target for MPNSTs, we screened 8 different MEK inhibitors, trametinib, TAK-733, PD0325901, cobimetinib, pimasertib, refametinib, binimetinib and selumetinib, to investigate their efficacy in MPNSTs. We performed cell viability assays in S462 cells with loss of heterozygosity (LOH) at the NF1 locus. While STS26T with the oncogenic V600E mutation in BRAF served as a control since the BRAF V600E mutation has been shown to be associated with resistance to MEK inhibitors (26). The cell viability curves and corresponding IC50 values of these two cell lines are presented in **Figure 2**. Trametinib and TAK-733 were the most efficient due to having the lowest IC50 values. At the same time, the IC50 values of Trametinib and TAK-733 in S462 were significantly lower than those in STS26T.

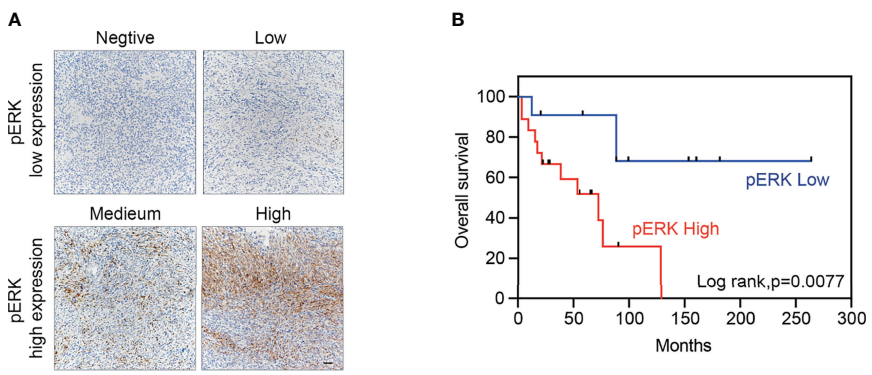

FIGURE 1 | High expression of p-ERK correlates with dismal prognosis in MPNSTs. **(A)** Typical images of p-ERK in MPNST tissues following immunohistochemical staining, scored as 0 (negative), 1 (low positive), 2 (medium positive), and 3 (high positive). Scale bar = 50 µm **(B)** Kaplan–Meier curves for cumulative survival according to the p-ERK level in the MPNST cohort with available follow-up data (n = 29, p = 0.007 by the log-rank test). Negative and low positive were defined as low expression, while medium and high positive were defined as high expression.

TABLE 1 | Pathological parameter with p-ERK expression.

Markers	Correlation coefficients	95% confidence interval	p-value
p-MEK	0.5519	0.3358 to 0.7128	0.0001***
CD34	0.3695	0.1156 to 0.5781	0.0055**
Ki67	0.4105	0.1629 to 0.6094	0.0019**

***p<0.01, ***p<0.001 (Pearson correlation analysis, n= 55)*

To explore the mechanism underlying the difference in efficacy, we next assessed the alterations in protein expression, including p-ERK and p-MEK in the MAPK signaling pathway, the downstream MEK/ERK effector cyclin D1, and p-AKT in the parallel PI3K/AKT pathway. P-ERK levels decreased with increasing concentrations of MEK inhibitors. Trametinib and TAK-733 were the most potent inhibitors, as p-ERK was not detected in S462 cells following 24 h of treatment with 0.01 μM. Selumetinib was the least effective in reducing p-ERK levels. A similar variation tendency in cyclin D1 expression was observed. As demonstrated in previous studies, MEK inhibition could reactivate MAPK signaling or upregulate parallel signaling pathways, particularly, the PI3K pathway, resulting in reduced efficacy of MEK inhibitors (27). It was also observed in S462 cells that compensatory increases in p-MEK and p-AKT occurred after 24 h of MEK inhibitor treatment. Trametinib and TAK-733 induced upregulation of p-MEK less obvious than other MEK inhibitors (**Figure 3**, **Figure S2**).

Inhibition of p-ERK Induced Cell Cycle Arrest and Apoptosis in MPNST Cells

We next explored the efficiency and safety of MEK inhibitors in a variety of MPNST cell models. We selected the most potent MEK inhibitors trametinib and TAK-733, as well as selumetinib, the first FDA-approved MEK inhibitor for the treatment of pediatric PNFs, for further investigations. Cell viability assays were conducted in 4 NF1-MPNST cell lines S462, T265, ST88-14, S462TY, and schwann cell line 02.3 2λ. As shown in **Figure 4A**, trametinib inhibited all the MPNST cells most efficiently with submicromolar IC50 values. In addition, MEK inhibitors trametinib, TAK-733, and selumetinib were more efficient in MPNST cell lines compared with healthy Schwann cell line 02.3 2λ (**Figure S3**).

Furthermore, alterations in cell proliferation, apoptosis, and p-ERK expression following trametinib treatment were also explored in these MPNST cells. All the MPNST cell lines showed a high apoptosis ratio after trametinib treatment in a time-dependent manner (**Figure 4B**, **S4**). Significant blockage of the G0/G1 phase was observed in S462, T265, and S462TY cells while blockage of the G2/M phase was observed in ST88-14 cells (**Figure 4C**). As shown in **Figure 4D** and **Figure S5**, MEK inhibitor trametinib induced a significant reduction of p-ERK expression in S462, T265, ST88-14, and S462TY at a concentration of 0.01μM. The p-ERK expression in 02.3 2λ cells was significantly inhibited only at a higher concentration of 0.1μM (**Figure S6**).

MEK Inhibitors Significantly Inhibited the Growth of MPNST Xenograft Without Inducing Apoptosis

The MEK inhibitors trametinib and TAK-733 and selumetinib were further evaluated *in vivo*. Following the successful establishment of S462TY xenografts, mice were gavaged with trametinib, TAK-733, or selumetinib for 3 weeks. As shown in **Figures 5A, B**, all the three MEK inhibitors reduced the tumor weight and tumor volume significantly. The inhibition in tumor volume persisted from the beginning to the end of administration with no obvious toxicity (**Figure S7**). Immunohistochemical analysis of the MPNST xenografts demonstrated that the three MEK inhibitors induced a robust decrease in p-ERK, Ki-67, and C-MYC at the protein level. However, no obvious alteration of cleaved Caspase 3 expression was observed (**Figure 5C**).

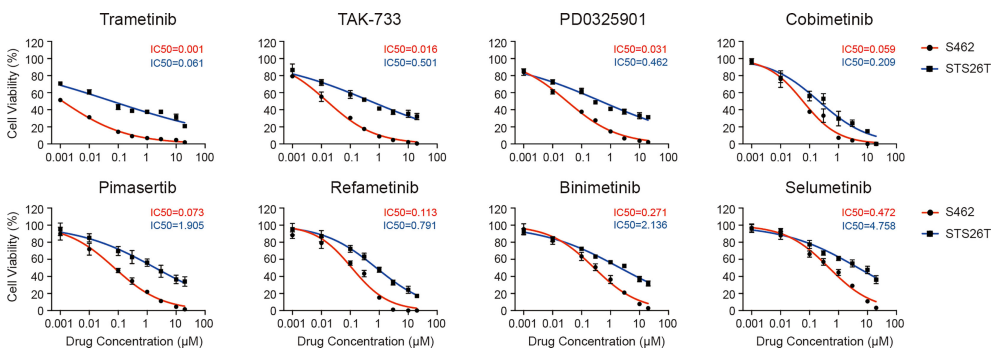

FIGURE 2 | Different efficacy of MEK inhibitors in reducing the viability of MPNST cells. Cell viability of MPNST cell line S462 (the NF1-deficient human MPNST cell line) and STS26T (the NF1-wild-type human MPNST cell line with BRAF V600E and PTEN loss) after treated with MEK inhibitors for 96 h.

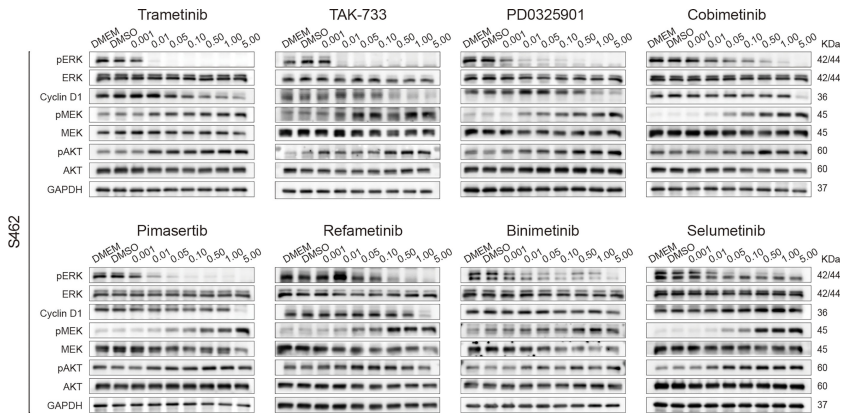

FIGURE 3 | Screening 8 MEK inhibitors in MPNST cells revealed differences in adaptive response. Expression of p-ERK, ERK, cyclin D1, p-MEK, MEK, p-AKT, AKT, and GAPDH in S462 cells treated with different MEK inhibitors at the indicated concentrations for 24h.

DISCUSSION

In this study, we investigated the efficacy of 8 different MEK inhibitors in treating MPNST using cell lines and xenograft models. We identified p-ERK as a biomarker for predicting the prognosis of MPNST patients as well as an effective therapeutic target. Moreover, we identified trametinib as the most potent MEK inhibitor for MPNST and demonstrated that the reduced reactivation of the MAPK pathway and activation of the parallel pathways contributed to better efficacy.

According to previous studies, genetic alterations including loss of NF1, EED, and SUZ12, have been demonstrated to activate the RAS/MAPK pathway in various human cancers including MPNSTs (7, 28, 29). Our findings also confirmed the overactivation of the MAPK pathway in MPNSTs as evidenced by the detection of p-ERK expression. In addition, our result first identified p-ERK as an indicator of a worse prognosis, indicating that the MAPK pathway could serve as a potential target in MPNSTs.

Inhibiting the RAS/MAPK pathway using MEK inhibitors has emerged as an effective strategy in a variety of cancers (30–34), as indicated in several clinical trials. However, the low incidence of MPNSTs added difficulties to the recruitment of clinical trials evaluating MEK inhibitors for MPNSTs. Therefore, we evaluated a panel of MEK inhibitors in various MPNST models and investigated the mechanism underlying the difference in efficacy. We included all the FDA-approved MEK inhibitors, and several

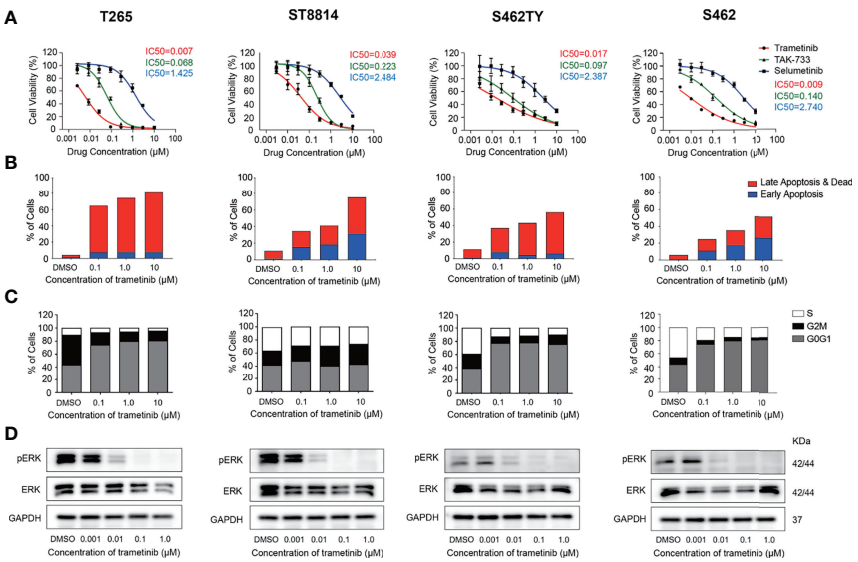

FIGURE 4 | Inhibition of p-ERK induced cell cycle arrest and apoptosis in MPNST cells. **(A)** Cell viability of MPNST cell lines T265, ST8814, S462, S462TY, and Schwann cell line 02.3 2λ treated with MEK inhibitors for 72h. **(B)** apoptosis ratios of MPNST cell lines treated with MEK inhibitor trametinib for 48h. **(C)** Cell cycle and **(D)** p-ERK/ERK expression levels of MPNST cell lines treated with MEK inhibitor trametinib for 24h.

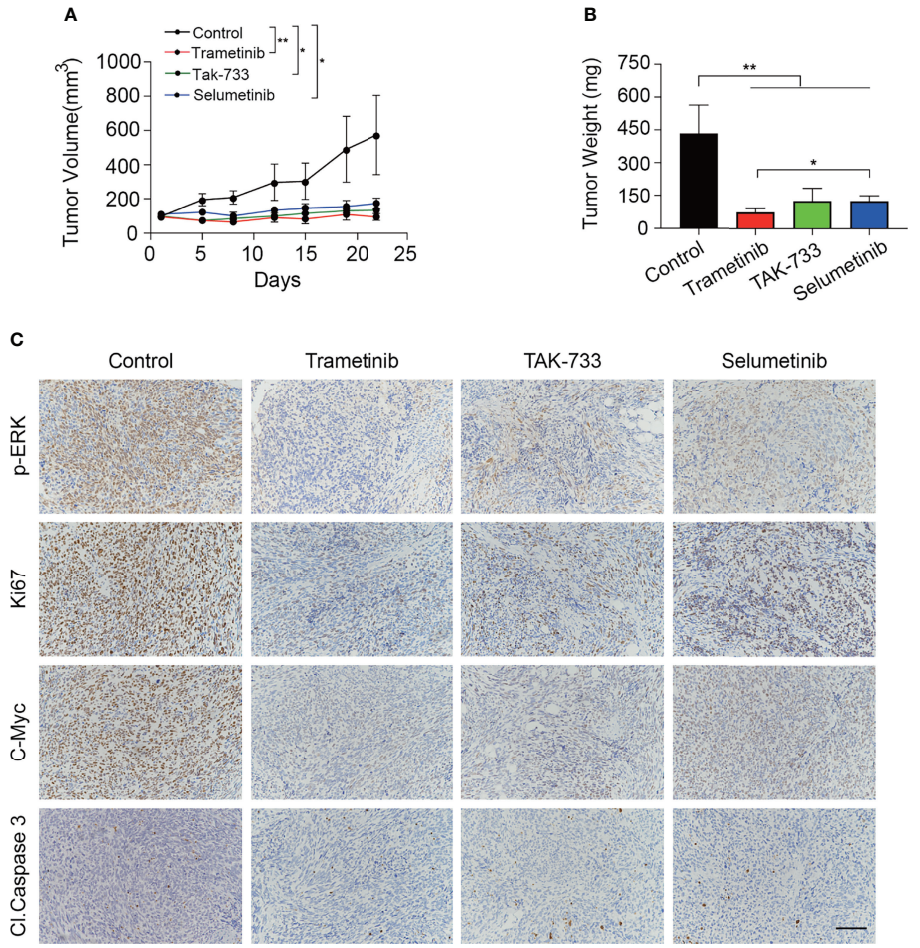

FIGURE 5 | MEK inhibitors significantly inhibited the growth of MPNST xenograft without inducing apoptosis. **(A, B)** Tumor growth curves **(A)** and tumor weight **(B)** of mice treated with control, trametinib, TAK-733 or selumetinib for three weeks. Each point or column represents Mean ± SEM (n = 4). * Represents $p < 0.05$, and ** represents $p < 0.01$ compared with control group (Student's t-test). **(C)** Representative images of p-ERK, Ki67, C-Myc, and Cl. Caspase3 immunohistochemical staining from the extracted tumor tissues in the four groups (scale bar = 100 μm).

potent MEK inhibitors proved to be efficient in clinical trials. Among the 8 inhibitors evaluated *in vitro*, trametinib was the most effective, likely from the significant reduction in p-ERK and downstream cyclin D1 levels. In addition, trametinib induced the lowest increase of p-MEK in S462 cells because it uniquely blocked Raf-dependent MEK phosphorylation, resulting in its potent efficacy in MAPK inhibition. Our *in vivo* experiments also confirmed the efficiency of MEK inhibitors. According to the results above, trametinib turned out to be the optimal choice for clinical application considering its excellent anti-tumor capacity *in vitro* and *in vivo*, as well as its mild reactivation of the MAPK pathway. As demonstrated by a recent case report, trametinib resulted in sustained complete response in an NF1 patient with recurrent and metastatic MPNST (35). In addition, trametinib has been approved by FDA for the treatment of malignant melanoma. Studies are being carried out to evaluate the effectiveness and to screen combinational drugs of MEK inhibitors in cancers including ovarian cancer and lung cancer (19, 32, 36–38).

Despite the potent efficacy of MAPK inhibition, trametinib caused significant activation of PI3K/Akt, a parallel pathway of MAPK signaling. It has been demonstrated in a variety of cancers that parallel pathways, especially the PI3K/Akt signaling pathway, could promote tumor growth and result in adaptive resistance after inhibition of the MAPK signaling (39, 40). Concurrent inhibition of MAPK and PI3K/Akt signaling using combinational therapies increased the efficacy of MEK inhibitors in multiple RAS-driven cancer models including MPNSTs (41, 42). Currently, a clinical trial is being carried out to test the effectiveness of selumetinib (AZD6244) and the mTOR inhibitor sirolimus in patients with unresectable or metastatic MPNST(NCT03433183).

Selumetinib is an FDA-approved MEK inhibitor that has shown excellent therapeutic efficacy in the treatment of pNF, the precursor lesion of MPNSTs. Compared to trametinib, selumetinib induced a more robust compensatory increase in p-MEK levels, indicating the occurrence of reactivation of the MAPK pathway, which might explain the less effective tumor-killing capacity. Wang et al. reported

that in liver cancer, combinational therapy of sorafenib and selumetinib could increase the anti-tumor effectiveness through the synergistic inhibition of p-ERK (43). This combinational therapy might also improve the efficacy of selumetinib in MPNSTs.

It is also worth noticing that the MEK inhibitors inhibited the growth of MPNST xenografts without inducing tumor shrinkage or tumor cell apoptosis *in vivo*. It was inconsistent with the findings in Annexin V/PI assays showing that MEK inhibitors induced cell apoptosis significantly *in vitro*. It could be speculated that the tumor microenvironment including immune cells and extracellular matrix played an important role in limiting the efficacy of MEK inhibitors. Previous studies have suggested that microenvironment components are associated with drug resistance and are considered key obstacles that limit the efficacy of targeted therapy (44–49). For example, fibroblast-derived ECM abrogated anti-proliferative responses to BRAF/MEK inhibition in BRAFV600-mutated advanced melanoma and pharmacological targeting of key molecules could overcome drug resistance (50). Therefore, the role of the tumor microenvironment in limiting the efficacy of MEK inhibitors in treating MPNSTs and the underlying mechanisms deserve further investigation.

In conclusion, the variety of MEK inhibitors and the lack of evaluation of their efficacy in MPNSTs limited the research progress and clinical application of MEK inhibitors in MPNSTs. This study identified the most promising MEK inhibitor trametinib, for the treatment of MPNSTs and clarified the mechanism underlying the difference in efficacy. Our results provide a basis for the further investigation of MEK inhibitors for treating MPNSTs.

DATA AVAILABILITY STATEMENT

The original contributions presented in the study are included in the article/**Supplementary Material**. Further inquiries can be directed to the corresponding authors.

ETHICS STATEMENT

The studies involving human participants were reviewed and approved by Ethics Committee of Shanghai Ninth People's Hospital, Shanghai Jiao Tong University School of Medicine. The patients/participants provided their written informed consent to participate in this study. The animal study was reviewed and approved by Ethics Committee of Shanghai Ninth People's Hospital, Shanghai Jiao Tong University School of Medicine.

AUTHOR CONTRIBUTIONS

YG, WW, YL, and HL generated and analyzed the data. ZG, CW, ML, MC, and RA assessed the TMA IHC staining and collected the clinical information. YG, WW, YL, and HL interpreted the results and wrote the manuscript. QL and ZW supervised the study and revised the manuscript. All authors contributed to the article and approved the submitted version.

FUNDING

This work was supported by grants from National Natural Science Foundation of China (82102344; 82172228); Shanghai Rising Star Program supported by Science and Technology Commission of Shanghai Municipality (20QA1405600); Science and Technology Commission of Shanghai Municipality (19JC1413); Natural Science Foundation of Shanghai (22ZR1422300); "Chenguang Program" supported by Shanghai Education Development Foundation (SHEDF) (19CG18); Shanghai Municipal Key Clinical Specialty (shslczdzk00901); Innovative research team of high-level local universities in Shanghai (SSMU-ZDCX20180700); the Project of Biobank (YBKA201901) from Shanghai Ninth People's Hospital, Shanghai Jiao Tong University School of Medicine.

ACKNOWLEDGMENTS

The authors would like to thank Prof. Vincent Keng and Prof. Jilong Yang for providing cell lines.

SUPPLEMENTARY MATERIAL

The Supplementary Material for this article can be found online at: https://www.frontiersin.org/articles/10.3389/fonc.2022.903177/full#supplementary-material

REFERENCES

1. Farid M, Demicco EG, Garcia R, Ahn L, Merola PR, Cioffi A, et al. Malignant Peripheral Nerve Sheath Tumors. *Oncol* (2014) 19(2):193–201. doi: 10.1634/theoncologist.2013-0328
2. Gutmann DH, Ferner RE, Listernick RH, Korf BR, Wolters PL, Johnson KJ. Neurofibromatosis Type 1. *Nat Rev Dis Primers* (2017) 3(1):17004. doi: 10.1038/nrdp.2017.4
3. Kolberg M, Holand M, Agesen TH, Brekke HR, Liestol K, Hall KS, et al. Survival Meta-Analyses for >1800 Malignant Peripheral Nerve Sheath Tumor Patients With and Without Neurofibromatosis Type 1. *Neuro Oncol* (2013) 15 (2):135–47. doi: 10.1093/neuonc/nos287
4. Vitolo V, Fiore MR, Barcellini A, Vischioni B, Iannalfi A, Facoetti A, et al. Carbon Ion Radiotherapy in the Management of the Tumors of the Peripheral Nervous System. *Anticancer Res* (2019) 39(2):909–13. doi: 10.21873/anticanres.13193
5. Widemann BC. Current Status of Sporadic and Neurofibromatosis Type 1-Associated Malignant Peripheral Nerve Sheath Tumors. *Curr Oncol Rep* (2009) 11(4):322–8. doi: 10.1007/s11912-009-0045-z
6. Blakeley JO, Plotkin SR. Therapeutic Advances for the Tumors Associated With Neurofibromatosis Type 1, Type 2, and Schwannomatosis. *Neuro Oncol* (2016) 18(5):624–38. doi: 10.1093/neuonc/nov200

7. Lee W, Teckie S, Wiesner T, Ran L, Prieto Granada CN, Lin M, et al. PRC2 Is Recurrently Inactivated Through EED or SUZ12 Loss in Malignant Peripheral Nerve Sheath Tumors. *Nat Genet* (2014) 46(11):1227–32. doi: 10.1038/ng.3095
8. Rahrmann EP, Watson AL, Keng VW, Choi K, Moriarity BS, Beckmann DA, et al. Forward Genetic Screen for Malignant Peripheral Nerve Sheath Tumor Formation Identifies New Genes and Pathways Driving Tumorigenesis. *Nat Genet* (2013) 45(7):756–66. doi: 10.1038/ng.2641
9. Mowery A, Clayburgh D. Malignant Peripheral Nerve Sheath Tumors: Analysis of the National Cancer Database. *Oral Oncol* (2019) 98:13–9. doi: 10.1016/j.oraloncology.2019.09.010
10. Schulte A, Ewald F, Spyra M, Smit DJ, Jiang W, Salamon J, et al. Combined Targeting of AKT and mTOR Inhibits Proliferation of Human NF1-Associated Malignant Peripheral Nerve Sheath Tumour Cells *In Vitro* But Not in a Xenograft Mouse Model *In Vivo*. *Int J Mol Sci* (2020) 21(4):1548. doi: 10.3390/ijms21041548
11. Bodempudi V, Yamoutpoor F, Pan W, Dudek AZ, Esfandyari T, Piedra M, et al. Ral Overactivation in Malignant Peripheral Nerve Sheath Tumors. *Mol Cell Biol* (2009) 29(14):3964–74. doi: 10.1128/MCB.01153-08
12. Endo M, Yamamoto H, Setsu N, Kohashi K, Takahashi Y, Ishii T, et al. Prognostic Significance of AKT/mTOR and MAPK Pathways and Antitumor Effect of mTOR Inhibitor in NF1-Related and Sporadic Malignant Peripheral Nerve Sheath Tumors. *Clin Cancer Res* (2013) 19(2):450–61. doi: 10.1158/1078-0432.CCR-12-1067
13. Barbosa R, Acevedo LA, Marmorstein R. The MEK/ERK Network as a Therapeutic Target in Human Cancer. *Mol Cancer Res* (2021) 19(3):361–74. doi: 10.1158/1541-7786.MCR-20-0687
14. Ney GM, McKay L, Koschmann C, Mody R, Li Q. The Emerging Role of Ras Pathway Signaling in Pediatric Cancer. *Cancer Res* (2020) 80(23):5155–63. doi: 10.1158/0008-5472.CAN-20-0916
15. Butler E, Schwettmann B, Geboers S, Hao G, Kim J, Nham K, et al. Functional Imaging of RAS Pathway Targeting in Malignant Peripheral Nerve Sheath Tumor Cells and Xenografts. *Pediatr Blood Cancer* (2020) 67(12):e28639. doi: 10.1002/pbc.28639
16. Flaherty KT, Infante JR, Daud A, Gonzalez R, Kefford RF, Sosman J, et al. Combined BRAF and MEK Inhibition in Melanoma With BRAF V600 Mutations. *N Engl J Med* (2012) 367(18):1694–703. doi: 10.1056/NEJMoa1210093
17. Dombi E, Baldwin A, Marcus LJ, Fisher MJ, Weiss B, Kim A, et al. Activity of Selumetinib in Neurofibromatosis Type 1-Related Plexiform Neurofibromas. *N Engl J Med* (2016) 375(26):2550–60. doi: 10.1056/NEJMoa1605943
18. Jessen WJ, Miller SJ, Jousma E, Wu J, Rizvi TA, Brundage ME, et al. MEK Inhibition Exhibits Efficacy in Human and Mouse Neurofibromatosis Tumors. *J Clin Invest* (2013) 123(1):340–7. doi: 10.1172/JCI60578
19. Han J, Liu Y, Yang S, Wu X, Li H, Wang Q. MEK Inhibitors for the Treatment of non-Small Cell Lung Cancer. *J Hematol Oncol* (2021) 14(1):1. doi: 10.1186/s13045-020-01025-7
20. Kim C, Giaccone G. MEK Inhibitors Under Development for Treatment of Non-Small-Cell Lung Cancer. *Expert Opin Investig Drugs* (2018) 27(1):17–30. doi: 10.1080/13543784.2018.1415324
21. Gross AM, Wolters PL, Dombi E, Baldwin A, Whitcomb P, Fisher MJ, et al. Selumetinib in Children With Inoperable Plexiform Neurofibromas. *N Engl J Med* (2020) 382(15):1430–42. doi: 10.1056/NEJMoa1912735
22. Ahsan S, Ge Y, Tainsky MA. Combinatorial Therapeutic Targeting of BMP2 and MEK-ERK Pathways in NF1-Associated Malignant Peripheral Nerve Sheath Tumors. *Oncotarget* (2016) 7(35):57171–85. doi: 10.18632/oncotarget.11036
23. Wang J, Pollard K, Allen AN, Tomar T, Pijnenburg D, Yao Z, et al. Combined Inhibition of SHP2 and MEK Is Effective in Models of NF1-Deficient Malignant Peripheral Nerve Sheath Tumors. *Cancer Res* (2020) 80(23):5367–79. doi: 10.1158/0008-5472.CAN-20-1365
24. Fischer-Huchzermeyer S, Dombrowski A, Wilke G, Stahn V, Streubel A, Mautner VF, et al. MEK Inhibitors Enhance Therapeutic Response Towards ATRA in NF1 Associated Malignant Peripheral Nerve Sheath Tumors (MPNST) in-Vitro. *PloS One* (2017) 12(11):e0187700. doi: 10.1371/journal.pone.0187700
25. Castellsague J, Gel B, Fernandez-Rodriguez J, Llatjos R, Blanco I, Benavente Y, et al. Comprehensive Establishment and Characterization of Orthoxenograft Mouse Models of Malignant Peripheral Nerve Sheath Tumors for Personalized Medicine. *EMBO Mol Med* (2015) 7(5):608–27. doi: 10.15252/emmm.201404430
26. Kun E, Tsang YTM, Ng CW, Gershenson DM, Wong KK. MEK Inhibitor Resistance Mechanisms and Recent Developments in Combination Trials. *Cancer Treat Rev* (2021) 92:102137. doi: 10.1016/j.ctrv.2020.102137
27. Wang J, Pollard K, Calizo A, Pratilas CA. Activation of Receptor Tyrosine Kinases Mediates Acquired Resistance to MEK Inhibition in Malignant Peripheral Nerve Sheath Tumors. *Cancer Res* (2021) 81(3):747–62. doi: 10.1158/0008-5472.CAN-20-1992
28. Rasmussen SA, Overman J, Thomson SA, Colman SD, Abernathy CR, Trimpert RE, et al. Chromosome 17 Loss-Of-Heterozygosity Studies in Benign and Malignant Tumors in Neurofibromatosis Type 1. *Genes Chromosomes Cancer* (2000) 28(4):425–31. doi: 10.1002/1098-2264(200008)28:4<425::AID-GCC8>3.0.CO;2-E
29. Sohier P, Luscan A, Lloyd A, Ashelford K, Laurendeau I, Briand-Suleau A, et al. Confirmation of Mutation Landscape of NF1-Associated Malignant Peripheral Nerve Sheath Tumors. *Genes Chromosomes Cancer* (2017) 56(5):421–6. doi: 10.1002/gcc.22446
30. Caunt CJ, Sale MJ, Smith PD, Cook SJ. MEK1 and MEK2 Inhibitors and Cancer Therapy: The Long and Winding Road. *Nat Rev Cancer* (2015) 15(10):577–92. doi: 10.1038/nrc4000
31. Fuse MA, Dinh CT, Vitte J, Kirkpatrick J, Mindos T, Plati SK, et al. Preclinical Assessment of MEK1/2 Inhibitors for Neurofibromatosis Type 2-Associated Schwannomas Reveals Differences in Efficacy and Drug Resistance Development. *Neuro Oncol* (2019) 21(4):486–97. doi: 10.1093/neuonc/noz002
32. Chesnokov MS, Khan I, Park Y, Ezell J, Mehta G, Yousif A, et al. The MEK1/2 Pathway as a Therapeutic Target in High-Grade Serous Ovarian Carcinoma. *Cancers (Basel)* (2021) 13(6):1369. doi: 10.3390/cancers13061369
33. Banerjee A, Jakacki RI, Onar-Thomas A, Wu S, Nicolaides T, Young Poussaint T, et al. A Phase I Trial of the MEK Inhibitor Selumetinib (AZD6244) in Pediatric Patients With Recurrent or Refractory Low-Grade Glioma: A Pediatric Brain Tumor Consortium (PBTC) Study. *Neuro Oncol* (2017) 19(8):1135–44. doi: 10.1093/neuonc/now282
34. Robert C, Grob JJ, Stroyakovskiy D, Karaszewska B, Hauschild A, Levchenko E, et al. Five-Year Outcomes With Dabrafenib Plus Trametinib in Metastatic Melanoma. *N Engl J Med* (2019) 381(7):626–36. doi: 10.1056/NEJMoa1904059
35. Nagabushan S, Lau LMS, Barahona P, Wong M, Sherstyuk A, Marshall GM, et al. Efficacy of MEK Inhibition in a Recurrent Malignant Peripheral Nerve Sheath Tumor. *NPJ Precis Oncol* (2021) 5(1):9. doi: 10.1038/s41698-021-00145-8
36. Liu S, Zou Q, Chen JP, Yao X, Guan P, Liang W, et al. Targeting Enhancer Reprogramming to Mitigate MEK Inhibitor Resistance in Preclinical Models of Advanced Ovarian Cancer. *J Clin Invest* (2021) 131(20):e145035. doi: 10.1172/JCI145035
37. Planchard D, Besse B, Groen HJM, Souquet PJ, Quoix E, Baik CS, et al. Dabrafenib Plus Trametinib in Patients With Previously Treated BRAF (V600E)-Mutant Metastatic non-Small Cell Lung Cancer: An Open-Label, Multicentre Phase 2 Trial. *Lancet Oncol* (2016) 17(7):984–93. doi: 10.1016/S1470-2045(16)30146-2
38. Kauko O, O'Connor CM, Kulesskiy E, Sangodkar J, Aakula A, Izadmehr S, et al. PP2A Inhibition Is a Druggable MEK Inhibitor Resistance Mechanism in KRAS-Mutant Lung Cancer Cells. *Sci Transl Med* (2018) 10(450):eaaq1093. doi: 10.1126/scitranslmed.aaq1093
39. Irvine M, Stewart A, Pedersen B, Boyd S, Kefford R, Rizos H. Oncogenic PI3K/AKT Promotes the Step-Wise Evolution of Combination BRAF/MEK Inhibitor Resistance in Melanoma. *Oncogenesis* (2018) 7(9):72. doi: 10.1038/s41389-018-0081-3
40. Turke AB, Song Y, Costa C, Cook R, Arteaga CL, Asara JM, et al. MEK Inhibition Leads to PI3K/AKT Activation by Relieving a Negative Feedback on ERBB Receptors. *Cancer Res* (2012) 72(13):3228–37. doi: 10.1158/0008-5472.CAN-11-3747
41. Watson AL, Anderson LK, Greeley AD, Keng VW, Rahrmann EP, Halfond AL, et al. Co-Targeting the MAPK and PI3K/AKT/mTOR Pathways in Two Genetically Engineered Mouse Models of Schwann Cell Tumors Reduces Tumor Grade and Multiplicity. *Oncotarget* (2014) 5(6):1502–14. doi: 10.18632/oncotarget.1609
42. Arozarena I, Wellbrock C. Overcoming Resistance to BRAF Inhibitors. *Ann Transl Med* (2017) 5(19):387. doi: 10.21037/atm.2017.06.09

43. Wang C, Jin H, Gao D, Lieftink C, Evers B, Jin G, et al. Phospho-ERK is a Biomarker of Response to a Synthetic Lethal Drug Combination of Sorafenib and MEK Inhibition in Liver Cancer. *J Hepatol* (2018) 69(5):1057–65. doi: 10.1016/j.jhep.2018.07.004
44. Yang XH, Flores LM, Li Q, Zhou P, Xu F, Krop IE, et al. Disruption of Laminin-Integrin-CD151-Focal Adhesion Kinase Axis Sensitizes Breast Cancer Cells to ErbB2 Antagonists. *Cancer Res* (2010) 70(6):2256–63. doi: 10.1158/0008-5472.CAN-09-4032
45. Yu Q, Xiao W, Sun S, Sohrabi A, Liang J, Seidlits SK. Extracellular Matrix Proteins Confer Cell Adhesion-Mediated Drug Resistance Through Integrin Alpha V in Glioblastoma Cells. *Front Cell Dev Biol* (2021) 9:616580. doi: 10.3389/fcell.2021.616580
46. Cho C, Horzempa C, Jones D, McKeown-Longo PJ. The Fibronectin III-1 Domain Activates a PI3-Kinase/Akt Signaling Pathway Leading to Alphavbeta5 Integrin Activation and TRAIL Resistance in Human Lung Cancer Cells. *BMC Cancer* (2016) 16:574. doi: 10.1186/s12885-016-2621-6
47. Ye Y, Zhang R, Feng H. Fibronectin Promotes Tumor Cells Growth and Drugs Resistance Through a CDC42-YAP-Dependent Signaling Pathway in Colorectal Cancer. *Cell Biol Int* (2020) 44(9):1840–9. doi: 10.1002/cbin.11390
48. Gao Y, Li X, Zeng C, Liu C, Hao Q, Li W, et al. CD63(+) Cancer-Associated Fibroblasts Confer Tamoxifen Resistance to Breast Cancer Cells Through Exosomal miR-22. *Adv Sci (Weinh)* (2020) 7(21):2002518. doi: 10.1002/advs.202002518
49. Kieffer Y, Hocine HR, Gentric G, Pelon F, Bernard C, Bourachot B, et al. Single-Cell Analysis Reveals Fibroblast Clusters Linked to Immunotherapy Resistance in Cancer. *Cancer Discovery* (2020) 10(9):1330–51. doi: 10.1158/2159-8290.CD-19-1384
50. Berestjuk I, Lecacheur M, Carminati A, Diazzi S, Rovera C, Prod'homme V, et al. Targeting Discoidin Domain Receptors DDR1 and DDR2 Overcomes Matrix-Mediated Tumor Cell Adaptation and Tolerance to BRAF-Targeted Therapy in Melanoma. *EMBO Mol Med* (2022) 14(2):e11814. doi: 10.15252/emmm.201911814

Conflict of Interest: The authors declare that the research was conducted in the absence of any commercial or financial relationships that could be construed as a potential conflict of interest.

Publisher's Note: All claims expressed in this article are solely those of the authors and do not necessarily represent those of their affiliated organizations, or those of the publisher, the editors and the reviewers. Any product that may be evaluated in this article, or claim that may be made by its manufacturer, is not guaranteed or endorsed by the publisher.

frontiers | Frontiers in Oncology

TYPE Case Report
PUBLISHED 02 August 2022
DOI 10.3389/fonc.2022.954879

OPEN ACCESS

EDITED BY
Laura Gatti,
IRCCS Carlo Besta Neurological Institute Foundation, Italy

REVIEWED BY
Angela Mastronuzzi,
Bambino GesùChildren's Hospital (IRCCS),
Italy
Yujie Chen,
Army Medical University, China

*CORRESPONDENCE
Jing Wu
jing.wu3@nih.gov

SPECIALTY SECTION
This article was submitted to Neuro-Oncology and Neurosurgical Oncology, a section of the journal Frontiers in Oncology

RECEIVED 27 May 2022
ACCEPTED 30 June 2022
PUBLISHED 02 August 2022

CITATION
Merchant M, Raygada M, Pang Y, Quezado M, Raffeld M, Xi L, Kim J, Tyagi M, Abdullaev Z, Kim O, Sergi Z, Pillai T, Ozer B, Zaghloul K, Heiss JD, Armstrong TS, Gilbert MR, Aldape K and Wu J (2022) Case report: Oligodendroglioma, IDH-mutant and 1p/19q-codeleted, associated with a germline mutation in *PMS2*. *Front. Oncol.* 12:954879. doi: 10.3389/fonc.2022.954879

Case report: Oligodendroglioma, IDH-mutant and 1p/19q-codeleted, associated with a germline mutation in *PMS2*

Mythili Merchant[1], Margarita Raygada[1], Ying Pang[1], Martha Quezado[2], Mark Raffeld[2], Liqiang Xi[2], Jung Kim[2], Manoj Tyagi[2], Zied Abdullaev[2], Olga Kim[1], Zach Sergi[1], Tina Pillai[1], Byram Ozer[1], Kareem Zaghloul[3], John D. Heiss[3], Terri S. Armstrong[1], Mark R. Gilbert[1], Kenneth Aldape[2] and Jing Wu[1*]

[1]Neuro-Oncology Branch, Center for Cancer Research, National Cancer Institute, Bethesda, MD, United States, [2]Laboratory of Pathology, Center for Cancer Research, National Cancer Institute, Bethesda, MD, United States, [3]Surgical Neurology Branch, National Institute of Neurological Disorders and Stroke, Bethesda, MD, United States

Most tumors, including brain tumors, are sporadic. However, a small subset of CNS tumors are associated with hereditary cancer conditions like Lynch Syndrome (LS). Here, we present a case of an oligodendroglioma, IDH-mutant and 1p/19q-codeleted, and LS with a germline pathogenic *PMS2* mutation. To our knowledge, this has only been reported in a few cases in the literature. While the family history is less typical of LS, previous studies have indicated the absence of a significant family history in patient cohorts with *PMS2* mutations due to its low penetrance. Notably, only a handful of studies have worked on characterizing *PMS2* mutations in LS, and even fewer have looked at these mutations in the context of brain tumor development. This report aims to add to the limited literature on germline *PMS2* mutations and oligodendrogliomas. It highlights the importance of genetic testing in neuro-oncology.

KEYWORDS

lynch syndrome, *PMS2*, CNS, oligodendroglioma, IDH-mutant and 1p/19q-codeleted

Introduction

Oligodendroglioma, IDH-mutant and 1p/19q-codeleted, is a subset of diffuse gliomas that primarily develop sporadically. Very few patients with oligodendroglioma have been associated with a hereditary cancer predisposition syndrome. According to the most recent CBTRUS Statistical Report, these tumors have an adjusted annual incidence rate estimated at 0.11 cases per 100,000 population and account for 0.4% of all primary brain tumors (1). The most recent WHO classification of Central Nervous System (CNS) Tumors defines oligodendrogliomas as a diffusely infiltrating glioma with an *isocitrate dehydrogenase* (*IDH*) mutation and codeletion of chromosomes 1p and 19q (CNS WHO grade 2 or 3) (2).

Brain tumors have been associated with several hereditary syndromes including Lynch Syndrome (LS), which has an autosomal dominant inheritance pattern (3–5). In a study conducted to compare the incidence of brain tumors in families with LS versus that of the general population, it was found that the brain tumor incidence in LS families was 3.35% by the age of 85, compared to 0.47% in the general population (6). LS is caused by germline mutations in DNA mismatch repair (MMR) genes like *MLH1, MSH2, MSH6, PMS1*, and *PMS2*. Individuals that carry mutations in these genes have an increased susceptibility to cancers of the colon, endometrium, stomach, ovary, urinary tract, brain, skin, and many more (7–9). *PMS2* accounts for approximately 5% of the pathogenic variants involved in LS and has a lower penetrance than the other MMR genes (9–11). There is limited validated data on germline monoallelic *PMS2* mutations and, therefore, a lack of clinical and biological phenotype associations (10).

Case presentation

The patient is a 65-year-old gentleman diagnosed with a recurrent oligodendroglioma, IDH-mutant and 1p/19q-codeleted, CNS WHO grade 3. He was initially found to have a non-enhancing lesion in the left posterior temporal lobe at the age of 30. As illustrated in Figure 1, he received a craniotomy with tumor resection about thirty-six years ago. Pathological exam revealed an oligodendroglioma, grade 2. Following three years of clinical observation, he underwent a second tumor resection and received a course of radiation therapy following the surgery. His tumor remained stable until the disease progressed again twenty-three years after the initial diagnosis. At this time, the tumor was confirmed to be a recurrent oligodendroglioma, IDH-mutant and 1p/19q-codeleted, CNS WHO grade 3 after a tumor biopsy. He then received his first chemotherapy regimen, which involved 18 cycles of temozolomide. Approximately ten years later, the MRI findings were suggestive of disease progression (Figure 2A). He underwent a left temporoparietal craniotomy with resection of the tumor. Pathology demonstrated oligodendroglioma, IDH-mutant and 1p/19q-codeleted, CNS WHO grade 3 (Figure 2B). DNA methylation profiling was consistent with the diagnosis of oligodendroglioma, IDH-mutant and 1p/19q-codeleted (Figure 2C). He received his second regimen of chemotherapy with 6 cycles of temozolomide. The patient has been under clinical monitoring and has remained clinically stable since he completed the second round of chemotherapy.

After his most recent tumor recurrence, matched Tumor/Normal Whole Exome Sequencing (T/N WES; NCI-COMPASS-NIH) revealed that he carries a pathogenic germline mutation in *PMS2* (c.251-2A>T splice variant) (Figure 3A). This splice alteration affects a canonical splice acceptor at nucleotide position -2, upstream of coding exon 4 in *PMS2*. Despite the germline *PMS2* mutation, it did not cause a complete loss of PMS2 protein expression, and all MMR proteins were positively expressed (Figure 3B). While his family history is less characteristic of LS, he has a brother with colon cancer (Figure 4). The patient, however, is unable to recall further details regarding the diagnosis, including age of the diagnosis. His father also had multiple myeloma, but there are no other known cancers or hereditary syndromes in the family.

The patient was counseled on the implications of the *PMS2* germline mutation, and he was advised to undergo a colonoscopy as surveillance in accordance with the new germline finding. Although he does not have children, the patient believed that it was important for him to share the information with his brother who had a diagnosis of colon

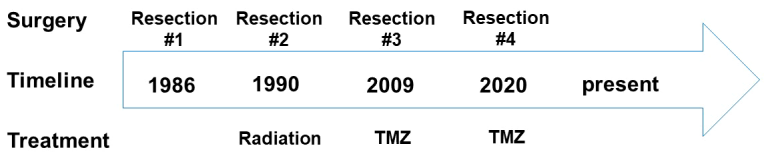

FIGURE 1
Timeline of the disease history and management. TMZ, Temozolomide.

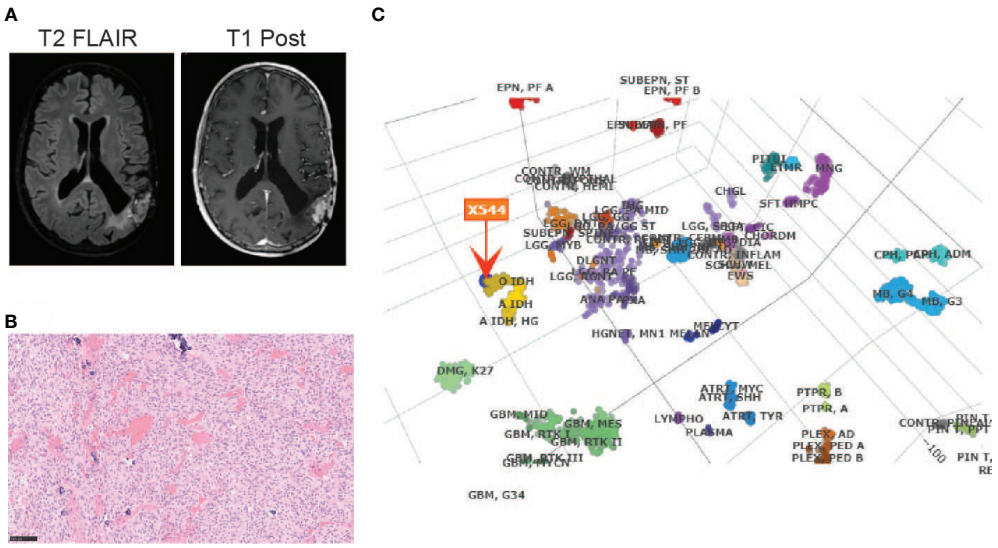

FIGURE 2
Diagnosis of an oligodendroglioma, IDH-mutant and 1p/19q co-deleted, CNS WHO grade 3 by **(A)** MRI before the most recent tumor resection; **(B)** H&E staining (20X) and **(C)** DNA methylation profiling of the tumor sample from the most recent tumor resection.

cancer. He also planned to share his genetic testing results with his primary care physician so that his medical care can be customized to this condition.

Discussion

In this case report, we describe the case of a 65-year-old man diagnosed with a recurrent oligodendroglioma, IDH-mutant and 1p/19q co-deleted, CNS WHO grade 3. The tumor also harbored a pathogenic mutation in *PMS2*, a DNA MMR gene, which was determined to be a germline mutation. *PMS2* is associated with LS and in turn, with a predisposition to several types of cancers, including brain tumors.

Although uncommon, several types of brain tumors are associated with hereditary cancer syndromes like LS. Specifically, LS confers a 4-fold increased risk of developing brain tumors (12, 13). While glioblastoma is the most frequent histological subtype of brain tumors that are found in LS families (56%), other diffuse astrocytomas (22%) and oligodendrogliomas (9%) are also often found (12). Previous studies that have looked at the association between brain tumors and LS have found that 68% of patients have mutations in *MSH2*, 15% had mutations in *MLH1*, 15% in *MSH6*, and 2% in *PMS2* (12), with most showing a loss of corresponding protein expression.

Due to the reduced penetrance and genetic testing complications of monoallelic *PMS2* mutations, biallelic *PMS2* mutations are more commonly detected and better

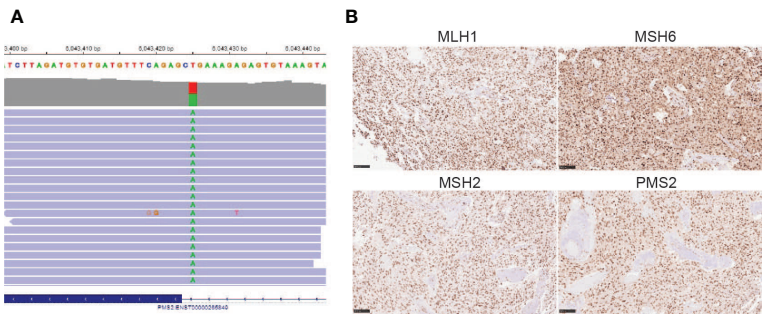

FIGURE 3
(A) *PMS2* mutation found in the proband (c.251-2A>T); **(B)** Immunohistochemistry staining of MMR proteins, including MLH1, MSH6, MSH2, and PMS2 (20X) using the tumor sample from the most recent tumor resection.

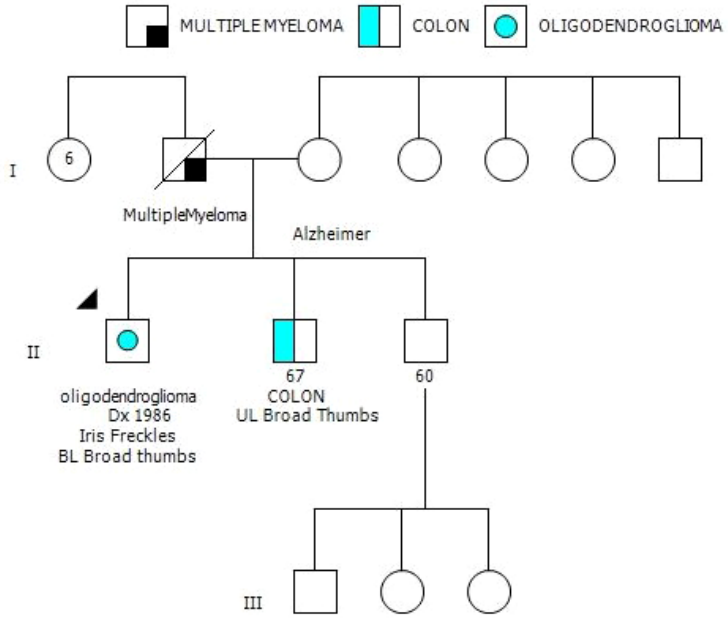

FIGURE 4
Three-generation family history pedigree.

characterized, especially in constitutional MMR deficiency (CMMRD) syndrome (14–16). Several studies have examined the association between biallelic *PMS2* mutations and brain tumors (16–18). One such study reported a case of two affected sisters, one who died of a grade 3 oligodendroglioma and colorectal tumor (the proband), and the other who died of a neuroblastoma at a very early age, with no history of tumors in their parents. The proband was compound heterozygous for *PMS2* (19). Another study in a five-generation Pakistani family revealed six affected individuals who died of brain tumors at very young ages, of which three had biallelic *PMS2* mutations (20).

Carriers of monoallelic *PMS2* mutations are at an increased risk for cancer, however, less is known about monoallelic *PMS2* mutations and their association with brain tumors (21). A report focused on characterizing monoallelic *PMS2* mutations found that only 6.2% of the class 4/5 variant carriers had a family history that fulfilled the Amsterdam diagnosis criteria (10). Another study that aimed to explore the clinical phenotype of germline *PMS2* mutations uncovered that if clinicians relied solely on Amsterdam criteria to identify potential *PMS2* mutation carriers, 90.9% of the mutation carriers in their study would not have been identified, or if clinicians relied on revised Bethesda guidelines alone, 25% of the mutation carriers in their study would have been missed (22). Our patient also did not have a clear family history suggestive of LS. Despite the *PMS2* germline mutation, there was still positive protein expression in the proband, potentially describing why the patient did not have a strong LS phenotype. Moreover, retained protein expression of PMS2 also makes it hard to exclude the possibility of a coincidence in the occurrence of two moderately rare but unrelated diseases. Senter et al. further demonstrated that *PMS2*-associated LS presents highly variable clinical characteristics. For example, the age of the first LS-associated tumor in monoallelic *PMS2* carriers varies from 23-77 years (22). Since half of the carriers are diagnosed with cancer before the age of 45, the general population screening recommendations for colon cancer beginning at the age of 45 would not be adequate for families with a *PMS2* mutation.

The specific *PMS2* mutation in the patient reported here has a gnomAD allele frequency of 0.0004%, underscoring its rarity. To date, it has only been previously reported in few other cases – in an individual with suspected LS (23), in a patient with colorectal cancer and LS (10), and in a 75-year-old patient with sarcoma (24). There are multiple layers of rarity in our case – the low incidence of oligodendrogliomas diagnosed with LS, the rare association of monoallelic *PMS2* mutations with brain tumors, and the extremely low gnomAD allele frequency of the c.251-2A>T mutation in *PMS2*.

These findings emphasize that despite the uncommon nature of hereditary cancer syndromes in neuro-oncology, genetic testing and counseling can help identify genetic conditions that may require specific surveillance regimens, in

turn improving patient care. Since early detection could lead to early intervention and routine surveillance, brain imaging may be indicated in some patients with LS.

Data availability statement

The data analyzed in this study is subject to the following licenses/restrictions: a. The reported PMS2 mutation in this manuscript is from the germline whole exome sequencing. Other than this alteration, the rest of the dataset cannot be shared with the public, even by request. b. Requests to access these datasets should be directed to Jing Wu, jing.wu3@nih.gov.

Ethics statement

The studies involving human participants were reviewed and approved by the Institutional Review Board of the National Institutes of Health. The participant provided the written informed consent to participate in this study.

Author contributions

MM, MRay, YP, OK, ZS, and JW drafted the manuscript. MQ, MRaf, LX, JK, MT, ZA, and KA performed pathologic and molecular diagnostic testing. TP, BO, KZ, JH, TA, MG, and JW were involved in patient care. All authors contributed to the article and approved the submitted version.

Funding

This research was supported by the NIH Intramural Research Program and Lasker Clinical Research Scholar Program. Clinical genetics and genetic counseling were supported by the NCI-CONNECT program.

Conflict of interest

The authors declare that the research was conducted in the absence of any commercial or financial relationships that could be construed as a potential conflict of interest.

Publisher's note

References

1. Ostrom QT, Cioffi G, Waite K, Kruchko C, Barnholtz-Sloan JS. CBTRUS statistical report: Primary brain and other central nervous system tumors diagnosed in the united states in 2014-2018. *Neuro Oncol* (2021) 23(12 Suppl 2): iii1–iii105. doi: 10.1093/neuonc/noab200

2. Louis DN, Perry A, Wesseling P, Brat DJ, Cree IA, Figarella-Branger D, et al. The 2021 WHO classification of tumors of the central nervous system: a summary. *Neuro Oncol* (2021) 23(8):1231–51. doi: 10.1093/neuonc/noab106

3. Lynch HT, de la Chapelle A. Genetic susceptibility to non-polyposis colorectal cancer. *J Med Genet* (1999) 36(11):801–18.

4. de Jong AE, Hendriks YM, Kleibeuker JH, de Boer SY, Cats A, Griffioen G, et al. Decrease in mortality in lynch syndrome families because of surveillance. *Gastroenterology* (2006) 130(3):665–71. doi: 10.1053/j.gastro.2005.11.032

5. Haraldsdottir S, Rafnar T, Frankel WL, Einarsdottir S, Sigurdsson A, Hampel H, et al. Comprehensive population-wide analysis of lynch syndrome in Iceland reveals founder mutations in MSH6 and PMS2. *Nat Commun* (2017) 8:14755. doi: 10.1038/ncomms14755

6. Vasen HF, Sanders EA, Taal BG, Nagengast FM, Griffioen G, Menko FH, et al. The risk of brain tumours in hereditary non-polyposis colorectal cancer (HNPCC). *Int J Cancer* (1996) 65(4):422–5. doi: 10.1002/(SICI)1097-0215(19960208)65:4<422::AID-IJC4>3.0.CO;2-Z

7. Aarnio M, Sankila R, Pukkala E, Salovaara R, Aaltonen LA, de la Chapelle A, et al. Cancer risk in mutation carriers of DNA-mismatch-repair genes. *Int J Cancer* (1999) 81(2):214–8. doi: 10.1002/(SICI)1097-0215(19990412)81:2<214::AID-IJC8>3.0.CO;2-L

8. Watson P, Riley B. The tumor spectrum in the lynch syndrome. *Fam Cancer* (2005) 4(3):245–8. doi: 10.1007/s10689-004-7994-z

9. Talseth-Palmer BA, McPhillips M, Groombridge C, Spigelman A, Scott RJ. MSH6 and PMS2 mutation positive Australian lynch syndrome families: novel mutations, cancer risk and age of diagnosis of colorectal cancer. *Hered Cancer Clin Pract* (2010) 8(1):5. doi: 10.1186/1897-4287-8-5

10. Wang Q, Leclerc J, Bougeard G, Olschwang S, Vasseur S, Cassinari K, et al. Characterisation of heterozygous PMS2 variants in French patients with lynch syndrome. *J Med Genet* (2020) 57(7):487–99. doi: 10.1136/jmedgenet-2019-106256

11. ten Broeke SW, Brohet RM, Tops CM, van der Klift HM, Velthuizen ME, Bernstein I, et al. Lynch syndrome caused by germline PMS2 mutations: delineating the cancer risk. *J Clin Oncol* (2015) 33(4):319–25. doi: 10.1200/JCO.2014.57.8088

12. Therkildsen C, Ladelund S, Rambech E, Persson A, Petersen A, Nilbert M. Glioblastomas, astrocytomas and oligodendrogliomas linked to lynch syndrome. *Eur J Neurol* (2015) 22(4):717–24. doi: 10.1111/ene.12647

13. Koornstra JJ, Mourits MJ, Sijmons RH, Leliveld AM, Hollema H, Kleibeuker JH. Management of extracolonic tumours in patients with lynch syndrome. *Lancet Oncol* (2009) 10(4):400–8. doi: 10.1016/S1470-2045(09)70041-5

14. Wimmer K, Kratz CP, Vasen HF, Caron O, Colas C, Entz-Werle N, et al. Diagnostic criteria for constitutional mismatch repair deficiency syndrome: suggestions of the European consortium 'care for CMMRD' (C4CMMRD). *J Med Genet* (2014) 51(6):355–65. doi: 10.1136/jmedgenet-2014-102284

15. Ramchander NC, Ryan NA, Crosbie EJ, Evans DG. Homozygous germ-line mutation of the PMS2 mismatch repair gene: a unique case report of constitutional mismatch repair deficiency (CMMRD). *BMC Med Genet* (2017) 18(1):40. doi: 10.1186/s12881-017-0391-x

16. De Vos M, Hayward BE, Charlton R, Taylor GR, Glaser AW, Picton S, et al. PMS2 mutations in childhood cancer. *J Natl Cancer Inst* (2006) 98(5):358–61. doi: 10.1093/jnci/djj073

17. Kruger S, Kinzel M, Walldorf C, Gottschling S, Bier A, Tinschert S, et al. Homozygous PMS2 germline mutations in two families with early-onset

haematological malignancy, brain tumours, HNPCC-associated tumours, and signs of neurofibromatosis type 1. *Eur J Hum Genet* (2008) 16(1):62–72. doi: 10.1038/sj.ejhg.5201923

18. Agostini M, Tibiletti MG, Lucci-Cordisco E, Chiaravalli A, Morreau H, Furlan D, et al. Two PMS2 mutations in a turcot syndrome family with small bowel cancers. *Am J Gastroenterol* (2005) 100(8):1886–91. doi: 10.1111/j.1572-0241.2005.50441.x

19. De Rosa M, Fasano C, Panariello L, Scarano MI, Belli G, Iannelli A, et al. Evidence for a recessive inheritance of turcot's syndrome caused by compound heterozygous mutations within the PMS2 gene. *Oncogene* (2000) 19(13):1719–23. doi: 10.1038/sj.onc.1203447

20. Baig SM, Fatima A, Tariq M, Khan TN, Ali Z, Faheem M, et al. Hereditary brain tumor with a homozygous germline mutation in PMS2: pedigree analysis and prenatal screening in a family with constitutional mismatch repair deficiency (CMMRD) syndrome. *Fam Cancer* (2019) 18(2):261–5. doi: 10.1007/s10689-018-0112-4

21. Goodenberger ML, Thomas BC, Riegert-Johnson D, Boland CR, Plon SE, Clendenning M, et al. PMS2 monoallelic mutation carriers: the known unknown. *Genet Med* (2016) 18(1):13–9. doi: 10.1038/gim.2015.27

22. Senter L, Clendenning M, Sotamaa K, Hampel H, Green J, Potter JD, et al. The clinical phenotype of lynch syndrome due to germ-line PMS2 mutations. *Gastroenterology* (2008) 135(2):419–28. doi: 10.1053/j.gastro.2008.04.026

23. Yurgelun MB, Allen B, Kaldate RR, Bowles KR, Judkins T, Kaushik P, et al. Identification of a variety of mutations in cancer predisposition genes in patients with suspected lynch syndrome. *Gastroenterology* (2015) 149(3):604–13 e20. doi: 10.1053/j.gastro.2015.05.006

24. Shirts BH, Casadei S, Jacobson AL, Lee MK, Gulsuner S, Bennett RL, et al. Improving performance of multigene panels for genomic analysis of cancer predisposition. *Genet Med* (2016) 18(10):974–81. doi: 10.1038/gim.2015.212

frontiers | Frontiers in Oncology

TYPE Original Research
PUBLISHED 04 August 2022
DOI 10.3389/fonc.2022.912741

OPEN ACCESS

EDITED BY
Laura Gatti,
IRCCS Carlo Besta Neurological Institute Foundation, Italy

REVIEWED BY
Valentina Pinzi,
IRCCS Carlo Besta Neurological Institute Foundation, Italy
Jiadong Wang,
Health Science Centre, Peking University, China

*CORRESPONDENCE
Galina Pavlova
lkorochkin@mail.ru

SPECIALTY SECTION
This article was submitted to Neuro-Oncology and Neurosurgical Oncology, a section of the journal Frontiers in Oncology

RECEIVED 04 April 2022
ACCEPTED 08 July 2022
PUBLISHED 04 August 2022

CITATION
Pavlova G, Belyashova A, Savchenko E, Panteleev D, Shamadykova D, Nikolaeva A, Pavlova S, Revishchin A, Golbin D, Potapov A, Antipina N and Golanov A (2022) Reparative properties of human glioblastoma cells after single exposure to a wide range of X-ray doses. *Front. Oncol.* 12:912741. doi: 10.3389/fonc.2022.912741

Reparative properties of human glioblastoma cells after single exposure to a wide range of X-ray doses

Galina Pavlova[1,2,3]*, Alexandra Belyashova[1], Ekaterina Savchenko[1], Dmitri Panteleev[2], Dzhirgala Shamadykova[2], Anna Nikolaeva[1], Svetlana Pavlova[2], Alexander Revishchin[2], Denis Golbin[1], Alexander Potapov[1], Natalia Antipina[1] and Andrey Golanov[1]

[1]Nikolay Nilovich (N.N.) Burdenko National Medical Research Center of Neurosurgery (NMRCN), Moscow, Russia, [2]Laboratory of Neurogenetics and Genetics Development, Institute of Higher Nervous Activity and Neurophysiology of Russian Academy of Sciences, Moscow, Russia, [3]Department of Medical Genetics, Sechenov First Moscow State Medical University, Moscow, Russia

Radiation therapy induces double-stranded DNA breaks in tumor cells, which leads to their death. A fraction of glioblastoma cells repair such breaks and reinitiate tumor growth. It was necessary to identify the relationship between high radiation doses and the proliferative activity of glioblastoma cells, and to evaluate the contribution of DNA repair pathways, homologous recombination (HR), and nonhomologous end joining (NHEJ) to tumor-cell recovery. We demonstrated that the GO1 culture derived from glioblastoma cells from Patient G, who had previously been irradiated, proved to be less sensitive to radiation than the Sus\fP2 glioblastoma culture was from Patient S, who had not been exposed to radiation before. GO1 cell proliferation decreased with radiation dose, and MTT decreased to 35% after a single exposure to 125 Gγ. The proliferative potential of glioblastoma culture Sus\fP2 decreased to 35% after exposure to 5 Gγ. At low radiation doses, cell proliferation and the expression of RAD51 were decreased; at high doses, cell proliferation was correlated with Ku70 protein expression. Therefore, HR and NHEJ are involved in DNA break repair after exposure to different radiation doses. Low doses induce HR, while higher doses induce the faster but less accurate NHEJ pathway of double-stranded DNA break repair.

KEYWORDS

human glioblastoma cell cultures, radiation therapy, Rad51, Ku70, Ku80

10.3389/fonc.2022.912741

Introduction

Glioblastoma

Glioblastoma is one of the most common primary tumors of the brain with poor prognosis. The yearly incidence rate of glioblastoma is about 3.2 per 100,000 persons (1). More radical surgery and aggressive chemo- and radiation therapy insignificantly improve prognosis in terms of overall and disease-free survival. In the great majority of cases (up to 95%), a recurrent tumor occurs 2–3 cm from the primary tumor within several months after surgery. New approaches to glioma therapy are being explored to also reduce tumor-cell recovery. Radiation therapy is a critical component of the current combined approach to the treatment of both primary and secondary glioblastomas, increasing the lifespan of patients, which is further improved by targeted therapy. Radiation therapy induces double-stranded DNA breaks in tumor cells, which eventually kills them. At the same time, a fraction of malignant glioma cells are known to be resistant to radiation, and these particular cells prime further tumor growth. The identification of molecular targets of radioresistance mechanisms involving DNA repair can improve the therapeutic efficacy of radiation therapy (2). To date, two DNA repair pathways are involved in tumor-cell recovery, homologous recombination (HR) and nonhomologous end joining (NHEJ) (3). Some researchers claim that HR dominates in radiation-induced DNA damage in glioblastoma cells. This is confirmed by an increased radiosensitivity of glioma cells with inhibited HR, while the inhibition of NHEJ was not as efficient (4, 5). At the same time, many publications indicated the involvement of NHEJ in the repair of radiation-induced DNA damage in glioma cells (6–8). The contribution of these DNA repair pathways to the recovery of glioblastoma cells after radiation therapy remains obscure.

Homologous recombination (HR)

DNA break repair by HR, typical for normal S and G2 cells, is considered to be more accurate than using nonhomologous end joining (NHEJ) is. One of the main factors of this process is the Rad51 recombinase (38 kDa), which was initially identified in yeast and proved to be an ortholog of the bacterial recombinase A (RecA) (9). The human Rad51 gene was localized to the q arm of chromosome 15 (15.1). Rad51, with a number of factors including Rad52, Rad54, BRCA2, and Rad51 paralogs (XRCC2, XRCC3, Rad51B, Rad51C, and Rad51D), associates with DNA, which allows for error-free break repair. Rad51 displaces replication protein A from long 3'-single-stranded DNA using the mediator proteins Rad52 and Rad55-Rad57 to form a long helical nucleoprotein. Rad51 searches the genome for a homologous target, then Rad51 catalyzes strand invasion forming D-loop, the broken 3'-end fuses with intact homologous template. The broken 3'-end is extended by DNA polymerases using homologous DNA as a template to repair DNA around the break site (10). Rad51 expression levels proved to be higher in tumors than they were in normal cells (11). Rad51 inhibition in human glioma cells substantially increased their radiosensitivity and favored their apoptotic death (2, 5, 12). In addition, the G2 phase was substantially elongated in radioresistant glioblastoma cells exposed to 4 Gγ. And Balbous et al. (2) explored the efficacy of radiation time in contrast to their study using different radiation doses. These studies complement each other in understanding HR significance for cell survival after X-radiation (13).

Nonhomologous end joining (NHEJ)

A number of different publications claim that NHEJ plays a key role in the repair of radiation-induced double-stranded DNA breaks. In contrast to HR, this repair mechanism can function throughout the cell cycle (14). Normally, NHEJ contributes to the repair of double-stranded DNA breaks in postmitotic cells (15). A variety of proteins are involved in NHEJ, but two play a major role, Ku70 (69 kDa) and Ku80 (83 kDa). Ku70 is encoded by the XRCC6 gene localized on chromosome 22q13.2. The gene has 13 exons and is expressed in nearly all tissue types. Ku80, a subunit of ATP-dependent DNA helicase II, is encoded by XRCC5, localized on chromosome 2q35 (16). These two proteins form a circular heterodimer with the inner diameter corresponding to the DNA double-helix diameter. The Ku70/80 complex has high affinity for double-stranded DNA. After a double-stranded DNA break is formed, the Ku70/80 complex rapidly binds DNA ends, and recruits and activates DNA-PKcs protein kinase to the damage site (17). NHEJ is mediated by at least six major factors, and four, namely, Ku80, Ku70, Ligase IV, and XRCC4, are highly conserved from yeast to mammals. NHEJ is critical for DNA double-strand break (DSB) repair, and thus for genome-stability maintenance. Mice with targeted mutations that inactivate these genes demonstrate phenotypes incapable of such repair (18). All NHEJ-deficient mice suffer from severe combined immunodeficiency. At the same time, deficiencies in NHEJ proteins Ku70 and Ku80 are correlated with the radiosensitivity and high incidence of spontaneous genomic instability. Some researchers claim that NHEJ is more significant for double-stranded DNA repair after the radiation therapy of tumor cells, considering that NHEJ restores double-stranded breaks throughout the cell cycle, while HR is largely limited to the late S/G2 phase (19).

It was proposed that HR and NHEJ are involved in DNA repair in tumor cells after different X-ray doses (20, 21). After low radiation doses (below 40 m Gγ/min), cells use slower but more reliable homologous recombination. As the radiation dose increases, the contribution of HR decreases, and faster but less accurate NHEJ predominates (22).

The goal of this study was to reveal the relationship between high radiation doses and cell proliferation, activation of different repair pathways, and apoptosis.

Materials and methods

Glioblastoma cell cultures derived from human tumors

Primary cultures were obtained from human postoperative glioblastoma complying with all formal requirements of the Russian Federation. This study was approved by the Ethics Committee of Burdenko Neurosurgical Institute, Russian Academy of Medical Sciences (№_12/2020). All subjects gave written informed consent in accordance with the Declaration of Helsinki.

Human glioma samples were transported to the laboratory within 1 h after surgery in DMEM/F12. Samples were transferred to a Petri dish, dissected, released from vessels, washed with Versene, and incubated with 0.25% trypsin (PanEko, Russia) at 37°C with agitation for 40 min. After dissociation for three times, the supernatant was centrifuged at 1000 rpm for 5 min. Filtered and centrifuged cells were cultured in DMEM/F12 (Gibco, Germany) with 10% FBS (HyClone, USA) and plated in flasks. One day later, unattached cells were removed, and fresh medium was added. Subsequently, the medium was replaced once in 3 days. L-glutamine (PanEko, Russia) was added to the DMEM/F12 medium at 300 mg/l. Cell cultures were incubated at 37°C with 5% CO2. Cultures were maintained for up to 20 passages, and a fraction of cells were cryopreserved at each stage.

Immunocytochemistry

Neurospheres of glioblastoma cells were washed twice in PBS (pH 7.3). Staining was performed using the following primary antibodies: rabbit polyclonal Nestin antibody (dilution 1:200, Chemicon, USA), mouse monoclonal Vimetntin antibody (dilution 1:100, Sigma-Aldrich, USA). The primary antibodies were dissolved in PBS with 0.3% Triton X100 (Sigma-Aldrich, USA), plus 2% donkey serum (Jackson Immunoresearch, UK), and were incubated for 2 h at room temperature. A solution with 1% FBS and 2% donkey serum was used as a negative control. After washing three times for 5 min with PBS (pH 7.3), cells were incubated for 1 h with the following secondary antibodies: donkey anti-rabbit antibodies conjugated with Alexa Fluor 594 (dilution 1:100, #711-545-152, Jackson Immunoresearch, UK), donkey anti-mouse antibodies conjugated with DyLight-488 (dilution 1:100, #705-585-147, Jackson Immunoresearch, UK). Then, neurospheres were washed with PBS (pH 7.3) and stained with bisbenzimide (Sigma- Aldrich, USA) for 5 minutes at room temperature. The cells were washed with PBS (pH 7.3), covered with glycerin, and analyzed by fluorescent microscopy. An Olympus IX81 (Olympus corp., Japan) microscope was used for visualization with a computer-controlled motorized stage (Märzhäuser, Wetzlar) and an Olympus DP72 digital camera (Olympus, Münster, Germany).

X-radiation

For each beam parameter, a 96-well plate, two flasks, and a dish were irradiated using linear accelerator TrueBeam STx (Varian, USA), commonly used in medical practice and receiving regular technical maintenance. Phantoms were exposed to a single vertical bremsstrahlung radiation with a rated energy of 6 MeV and a power of 600 dose rate/min. Field size of 32 × 32 cm provided for uniform radiation of the entire culture. The SSD was 98 cm. Radiation doses varied from 1 to 250 Gγ. Exposure duration depended on the dose and varied from 10 s (1 Gγ) to 43 min (250 Gγ). Control cells were not exposed to radiation but kept under the same conditions, including transportation.

MTT

Colorimetric MTT test was used to estimate cell viability; 96-well plates with 3 × 103 cells per well were incubated at 37° C for 24 h. After X-ray irradiation, plates were incubated for five days. Then, 20 µl of 5 mg/ml 3-(4,5-dimethylthiazol-2-yl)-2,5-diphenyltetrazolium bromide (Sigma-Aldrich, USA) was added, and plates were incubated at 37°C for 2 h. After removal of the medium, 60 µl/well of DMSO (PanEko, Russia) was added, stirred for 15 min, and A 540 nm was measured with a Tecan plate reader (Switzerland). The background with MTT for nonirradiated cells was subtracted, and the mean ± SEM of five replications was used.

Reverse transcription and qPCR assay

Expression levels of XRCC5, XRCC6, and RAD51 in primary glioma cultures were quantified by real-time PCR. Total RNA was isolated from glioma cells using RNAzol solution (MRC, USA) according to the manufacturer's protocol. cDNA was

synthesized from isolated total RNA using the MMLV RT kit (Evrogen, Russia) according to the manufacturer's protocol. cDNA was amplified on a CFX96 Real-Time PCR Detection System (Bio-Rad, USA) using a kit with the SYBR Green I dye (Syntol, Russia). PCR was carried out in a volume of 25 µl containing 2.5 µl dNTPs (2.5 mM each), 1xPCR buffer B, primers (0.25 mM each), and 1 U of Taq DNA polymerase. PCR conditions were as follows (41 cycles): (1) denaturation at 94°C for 20 s, (2) annealing 61°C for 20 s, and (3) 30 s extension at 72°C. Fluorescence was recorded after Step 3. Melting curves were generated after amplification to confirm the homogeneity of the PCR product. RT-PCR data were analyzed using the software supplied with the CFX96 System (Bio-Rad, USA). Primers were selected from RTPrimerDB and using Primer-Blast (NCBI). The efficiency of the selected primers (specificity, dimerization, etc.) was evaluated by the agarose gel electrophoresis of PCR products. Housekeeping gene HPRT was used as the control.

The following primers were used:
Rad51_F 5'-CAGCTGGGAACTGCAACTCA-3'
Rad51_R 5'-ACCGTGAAATGGGTTGTGGG-3'
XRCC5_F 5'-TGACTTCCTGGATGCACTAATCG-3'
XRCC5_R 5'-CCTAAGCGAAAGGGGCCAT-3'
XRCC6_F 5'-GTTGATGCCTCCAAGGCTATG-3'
XRCC6_R 5'-CCCCTTAAACTGGTCAAGCTCTA-3'
HPRT_F 5'-TGAGGATTTGGAAAGGGTGT-3'
HPRT_R 5'-GAGCACACAGAGGGCTACAA-3'

Western blotting

Studied cells were harvested by 0.25% trypsin, washed twice with PBS, and lysed in buffer containing 8 M urea, 1% (v/v) Triton X-100, and 50 mM DTT. After centrifugation at 21,000g for 20 min, the supernatant was transferred to a new tube and used as a stock solution. Aliquots of the stock solution were supplemented with 5 volumes of Laemmli buffer and analyzed by electrophoresis in 10% acrylamide gel. The transfer to a nitro-cellulose membrane (Bio-Rad, USA) was performed using a Mini Trans-Blot System (Bio-Rad, USA) in a buffer containing 25 mM Tris, 192 mM glycine, and 20% (v/v) ethanol. The membrane was incubated in 1% Blocking reagent (Roche #11 096 176 001, Germany) for 50–60 min. Then, the membrane was incubated overnight with Cell Signaling antibodies: aRad51 (d4810), 1/10000; aKu70 (d35), 1/2000; aKu80, 1/8000; and beta-tubulin (9F3), 1/2000. The membrane was washed thrice with TBS-T and exposed to the secondary horseradish peroxidase-conjugated antibodies (aRb*HRP Santa Cruz sc-2030; 1/10000) for 1 h. The signal was detected using the ECL system (Amersham). Western blot data were analyzed by ImageJ according to the software instructions (https://imagej.nih.gov/ij/download.html).

Flow cytofluorometry

Cell death (apoptosis and necrosis) was evaluated using the Annexin V-FITC kit (Biolegend, USA) in accordance with the manufacturer's instructions. Apoptotic events were detected on a BD Accuri C6 flow cytometer (BD, USA). Data were processed using CFlow software (BD, USA). After applying the standard fluorescence-compensation technique, the percentage populations of Annexin V +/PI + cells in the scatter plot with two parameters were used for statistical analysis (30,000 events were collected in each probe designated as "target cells" in the FSC-SSC chart).

Statistical analysis

Results were expressed as mean ± standard error of the mean (SEM). The statistical evaluation was performed by Mann-Whitney test. Each value is the mean of ≥3 independent experiments ± SEM.

Results

Experiments were carried out on two cell cultures derived from supratentorial glioblastoma patients.

Patient S, female, 60 years old, had a short medical history. Headaches and amnestic disorders appeared and progressed within two weeks, and a mass lesion was found in the left temporal lobe with a circular magnetic resonance tomography (MRT) pattern (Figure 2), after which subtotal removal of the tumor was performed. Sanger sequencing indicated IDH1/2 wild type. A continuous cell culture Sus\fP2 for up to 20 passages was derived from the tumor. The patient received chemoradiation therapy with a total radiation dose of 60 Gγ and subsequent administration of temozolomide, which was canceled after two courses due to hematological toxicity. Eight months after chemoradiation therapy, clinicoradiological analysis demonstrated progressive tumor growth, and chemotherapy and targeted second-line treatment (bevacizumab) were administered. However, the patient died of tumor progression at 19 months after diagnosis (Figure 1).

Patient G, male, 37 years old, had a sudden epileptic seizure. MRT (Figure 2) demonstrated a typical ring-shaped gadolinium enhancement in the left frontal lobe with typical ring gadolinium enhancement, after which subtotal removal of an IDH1/2 wild-type glioblastoma was performed. The patient received chemoradiation therapy with a total radiation dose of 66 Gγ and subsequent administration of temozolomide. Twenty-four months after the first surgery, the patient was reoperated due to a locally recurrent tumor. Cell culture GO1 for up to 20 passages was derived from the tumor. Chemoradiation treatment with a total radiation dose of 66 Gγ, combined with temozolomide, bevacizumab, and irinotecan was performed. The patient died of tumor progression at 41 months

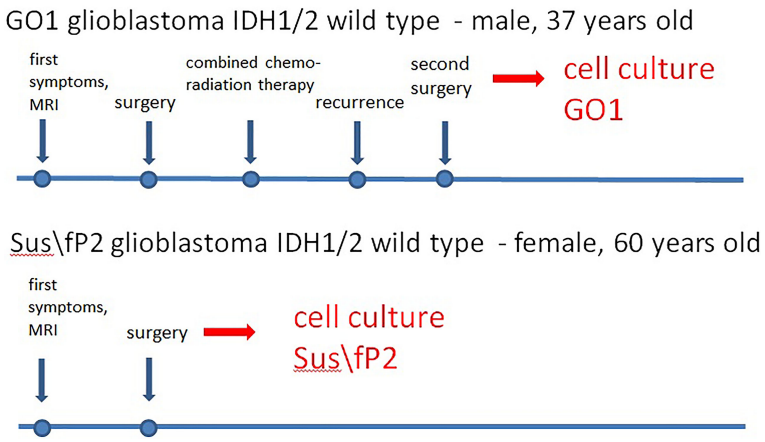

FIGURE 1
Characteristics of glioblastoma cell cultures.

after the first diagnosis or at 17 months after the second operation and cell-culture preparation (Figure 1).

Thus, the Sus\fP2 cell culture was derived from a glioblastoma not exposed to radiation, while the GO1 culture was derived from a recurrent glioblastoma after X-ray therapy.

Both cell cultures were able to form neurospheres with positive staininf for Nestin and Vimentin (Figures 3, 4). Cell cultures were characterized with an expression of the critical genes of human glioblastomas (Supplementary Figure 1).

Effect of radiation on cell proliferation

The obtained cell cultures were maintained for up to 10–20 passages. These cultures were heterogeneous, which distinguishes them from most experimental cell cultures. This brings our experiment closer to *in vivo* processes going into actual tumors exposed to radiation.

The goal of this study was to investigate the effect of single exposure to a wide range of X-ray doses (from 0 to 250 Gγ) of glioblastoma cultures derived from excised primary tumors. Changes in DNA repair capacity were studied under these conditions. The second goal was to investigate the susceptibility of glioma cells to fractionated radiation (two fractions). A special phantom was designed and fabricated from water-equivalent material with a size of 30 × 30 × 3 cm composed of two 1.5 cm plates, with the required number of pockets coinciding with the cell-culture vessel. The Hounsfield value of the phantom material was 110. Uneven exposure in the build-up region was excluded by two solid water slabs with a total thickness of 2 cm on the top and a 5 cm solid water slab on the bottom. Exposure was carried out using a clinical unit with a high dose rate and up-to-date beam characteristics for

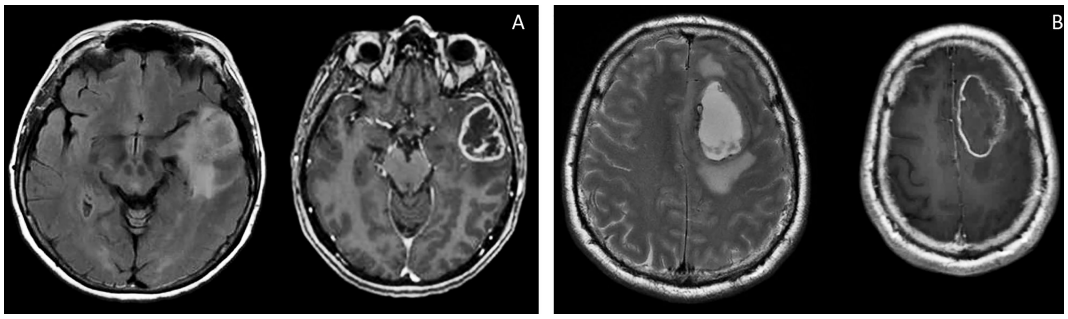

FIGURE 2
Brain MRI, T2 FLAIR, and T1 images of patients S **(A)** and G **(B)**. There are the same typical heterogenic changes of the signal with a ring-like contrast enhancement and a signal typical for edema around the tumors.

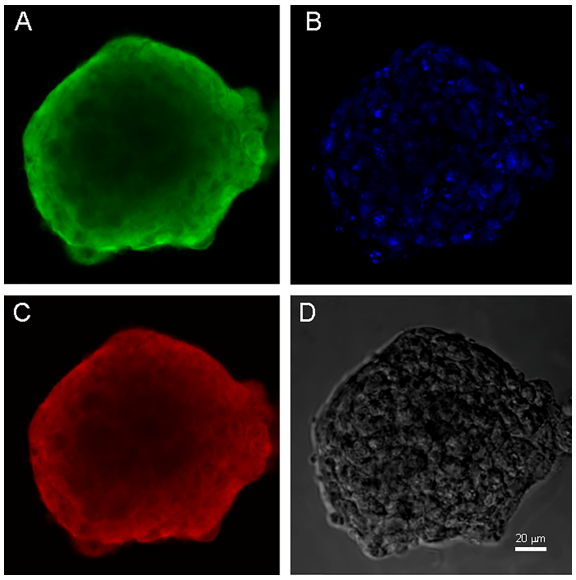

FIGURE 3
Neurospheres of glioblastoma cell culture of GO1. **(A)** antibody staining for Vimentin. **(B)** staining for bisbenzimid, **(C)** antibody staining for Nestin, **(D)** neurospheres in phase contrast. Scale bar is 20 µm.

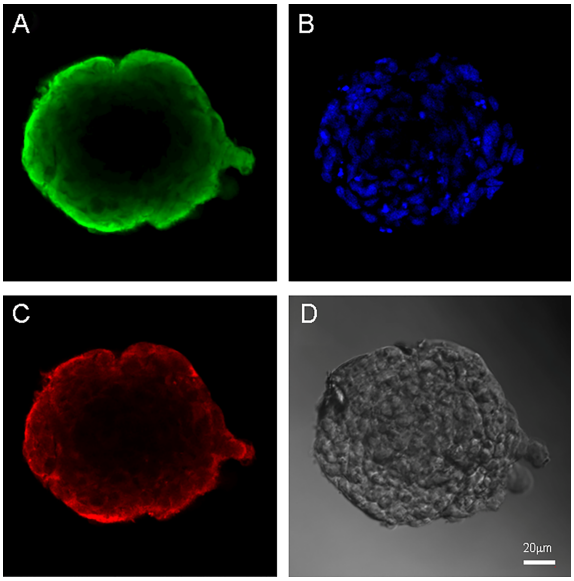

FIGURE 4
Neurospheres of glioblastoma cell culture of Sus\fP2. **(A)** antibody staining for Vimentin. **(B)** staining for bisbenzimid, **(C)** antibody staining for Nestin, **(D)** neurospheres in phase contrast. Scale bar is 20 µm.

glioblastoma radiation therapy. Exposure planning and performance approximated clinical radiation procedures (23).

At the first stage, single exposure was used to analyze the effect of radiation on cell proliferation in the culture and on the DNA repair capacity of cells, using the MTT assay. Both the major HR pathway of DNA repair involving Rad51 and the NHEJ pathway involving the Ku proteins were studied. The population of proliferating cells decreased with the dose of single exposure (Figure 5). GO1 and Sus\fP2 cells not exposed to radiation served as control.

Obtained data demonstrated a sharp decrease in the proliferative activity of Sus\fP2 cells in the dose range from 1 to 40 Gγ relative to GO1 cells. As the dose was increased to 250 Gγ, the proportion of viable cells remained stable at the level of about 30%. This indicated that a pool of cells highly resistant to radiation was stably maintained.

In contrast to Sus\fP2, the proliferative activity of the GO1 culture decreased more smoothly with the radiation dose up to 100 Gy. At a dose of 150–250 Gγ, the proportion of metabolically active cells was about 20%.

The revealed sharp decrease in Sus\fP2 proliferative activity as opposed to G01 prompted us to further test the exposure of Sus\fP2 cells to radiation below 5 Gγ in smaller steps (Figure 5C).

This supplementary experiment confirmed the decrease in Sus \fP2 proliferative activity as the radiation dose increased from 0 to 5 Gγ. The significance of apoptosis and necrosis in cell death after

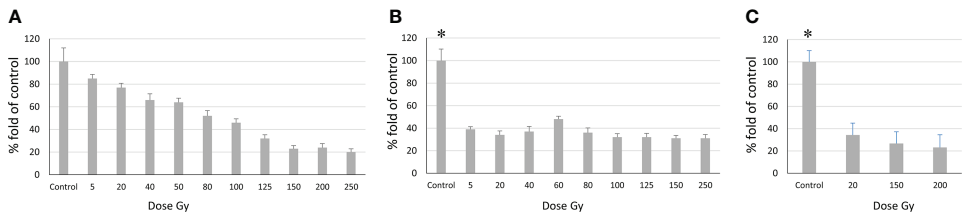

FIGURE 5
Relationship between the number of proliferating cells and radiation dose according to the MTT assay. **(A)** Sus\fP2 cells; **(B)** GO1 cells, **(C)** Sus \fP2 cells exposed to radiation below 5 Gγ. Each value is the mean of ≥3 independent experiments ± Standard Error of the Mean (SEM). Control values on **(B, C)** (denoted with *) significantly exceeded the experimental ones at any radiation doses with p<0.01 according to the Mann-Whitney test.

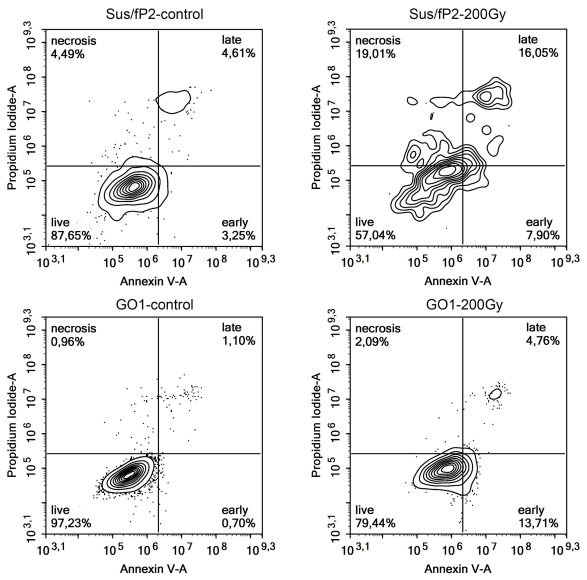

FIGURE 6
Analysis of apoptosis and necrosis in Sus\fP2 and GO1 cell cultures exposed to 200 Gγ.

radiation was evaluated using a high dose of 200 Gγ. After 7 days, cell death was evaluated using flow cytofluorometry. The necrotic and apoptotic indices of cultures substantially differed (Figure 6).

The proportion of Sus\fP2 cells that died *via* apoptosis was insignificantly higher than that *via* necrosis. In the GO1 culture, the proportion of apoptotic cells was much higher than that of necrotic cells (which were close to 0%). Both cultures included cell populations not responding to radiation by self-destruction.

The relationship between DNA repair and radiation dose was studied. In the case of HR typical for DNA repair in both irradiated and nonirradiated tumor cells, the expression level of the primary gene involved, RAD51, and the level of its protein product were studied in irradiated and nonirradiated tumor cells. In the case of NHEJ, the expression levels of the major genes involved, XRCC6 and XRCC5, and the levels of their products, Ku70 and Ku80 were analyzed.

Evaluation of DNA repair by homologous recombination

As the radiation dose increased to 250 Gγ, RAD51 transcription in GO1 cells varied insignificantly (except a significant burst at 20 Gγ; Figure 7A). Analysis of RAD51 transcription revealed no dose-dependent effect; however, its level was higher than that in the control in all samples. The level of RAD51 protein showed a dose-dependent decrease (Figures 7B, C). The increased gene activity can be attributed to alternative splicing producing proteins not recognized by antibodies against RAD51 in Western blotting. The decreased level of the RAD51 protein can indicate that high radiation doses decrease the rate of HR-mediated DNA repair. The second studied culture, Sus\fP2, demonstrated significant growth in RAD51 transcription at doses exceeding 100 Gγ. RAD51 proved most sensitive to doses of 3 and 5 Gγ, as confirmed by both RT-PCR and Western blotting. The same doses substantially de-creased proliferation in this culture

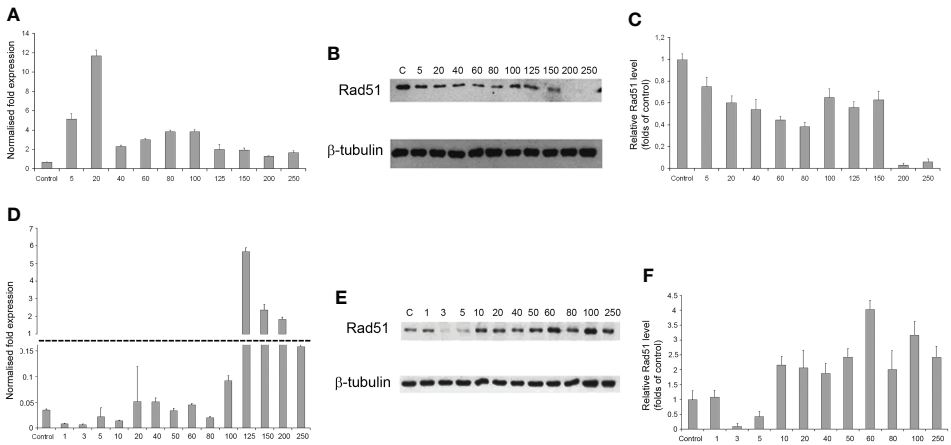

FIGURE 7
The dependence of RAD51 mRNA and protein levels on radiation dose in GO1 **(A–C)** and Sus\fP2 **(D–F)** glioblastoma cell cultures. **(A, D)** mRNA expression; **(B, E)** Western blotting; **(C, F)** Quantification RAD51 protein levels by ImageJ.

(Figure 5A). Conversely, a further increase in radiation promotes an increase in RAD51 expression.

Thus, the patterns of RAD51 expression were significantly different in tumor-cell cultures pre-exposed (GO1) or not pre-exposed (Sus\fP2) to radiation (Figures 7D–F).

Evaluation of DNA repair by nonhomologous end joining

The expression of genes and proteins is involved in DNA repair *via* NHEJ after exposure to different radiation doses. Ku70 and Ku80 are critical factors in this pathway; accordingly, the expression of these proteins and their genes, XRCC6 and XRCC5, was investigated (Figure 8). The expression of Ku80 in GO1 proved insensitive to radiation dose (Figures 8D–F), as indicated by insignificant variations in the levels of both XRCC5 mRNA and the Ku80 protein.

Exposure to radiation doses from 1 to 40 Gγ decreased the protein expression of Ku70 (Figures 8A–C). Doses from 40 to 150 Gγ induced minor variations on the protein level; however, this was lower than that in the control. Doses from 200 to 250 Gγ increased protein synthesis. Analysis of XRCC6 mRNA demonstrated no significant variations on its level. RT-PCR detects the expression of all XRCC6 transcripts; thus, the steady mRNA level could be attributed to alternative splicing decreasing the proportion of mRNA species translated into Ku70.

NHEJ analysis in a tumor-cell culture not pre-exposed to radiation (Sus\fP2) demonstrated no significant changes in the expression of proteins Ku70 and Ku80 (Figures 8G–L).

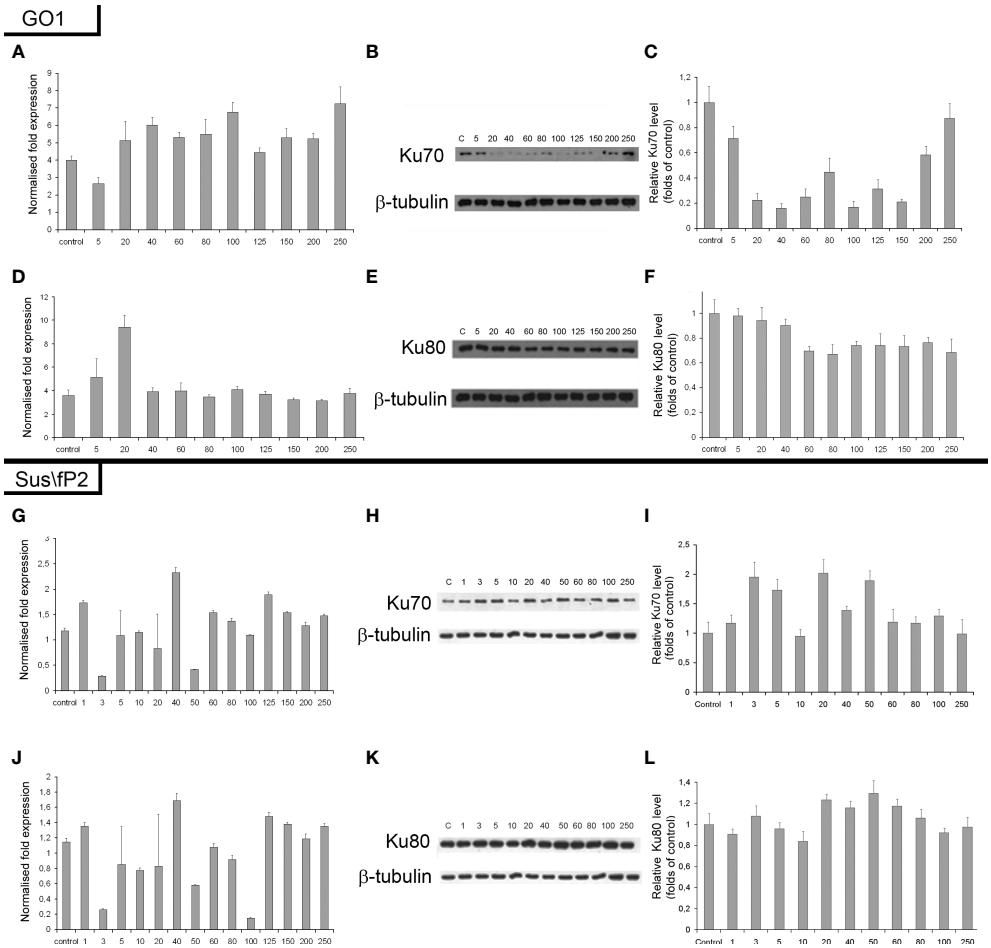

FIGURE 8
Expression of XRCC6 gene **(A)** and its product Ku70 **(B, C)** as a function of radiation dose in glioblastoma GO1 cell culture. Expression of XRCC5 gene **(D)** and its product Ku80 **(E, F)** as a function of radiation dose in GO1 cell culture. Expression of XRCC6 gene **(G)** and its product Ku70 **(H, I)** as a function of a single radiation dose from 5 to 250 Gγ in glioblastoma Sus\fP2 cell culture. Expression of XRCC5 gene **(J)** and its product Ku80 **(K, L)** as a function of a single radiation dose from 5 to 250 Gγ in Sus/fP2 cells.

Considering our previous data indicating that decreased RAD51 expression is correlated with decreased proliferation of Sus\fP2 cells after exposure to up to 10 Gγ, the role of NHEJ in tumor-cell survival seems insignificant.

Discussion

Radiation therapy is a critical component of the current combined approach to the treatment of glioblastomas. An important impact of radiation on living cells is DNA breaks. Significant DNA damage by double-stranded breaks can be expected to induce apoptosis and cell death. However, DNA repair in damaged cells allows for them to survive. DNA repair should be studied in the recovery of glioblastoma cells to reveal pathways critical for their survival and the dose dependency of their effect. It is common knowledge that two DNA repair pathways are involved in tumor-cell recovery after radiation therapy. The homologous recombination (HR) pathway is considered critical for the normal development and functioning of the body, and for the repair of damaged DNA in tumor cells after radiation or chemotherapy. One of the main proteins involved in HR is RAD51, and we studied its mRNA and protein expression here. Another mechanism of DNA break repair that is considered more typical for tumor cells (8) is nonhomologous end joining (NHEJ). The major components of NHEJ are the Ku70 and Ku80 proteins encoded by the XRCC5 and XRCC6 genes, respectively. Ku70 and Ku80 form a circular heterodimer with a central barrel that can cradle the DNA helix (24). Holoenzyme Ku70/80 is the heterodimeric component of DNA-dependent protein kinase (DNA-PK). A number of studies not dealing with cancer-cell irradiation showed that inactivation of DNA-PK yielded a higher level of radioresistance even after 24–72 h of repair. A number of factors were identified that interfere with DNA-PK interactions and increase radiosensitization (25).

Here, we studied changes in the expression of these proteins and genes as a function of radiation doses in the range from 1 to 250 Gγ. We found no publications on DNA repair in glioblastoma cells exposed to a similar dose range. Experiments were carried out on two cell cultures derived from human patients diagnosed with glioblastoma. These are not cell lines, i.e., not uniform. We tried to preserve their heterogeneity, and they were not maintained for more than 20 passages. One of these cultures (GO1) was derived from a recurrent tumor that was exposed to radiation, unlike Sus\fP2. Analysis of their proliferative activity after exposure to 1 to 250 Gγ demonstrated higher sensitivity of Sus\fP2 to radiation; the proliferative capacity of its cells decreased much faster to reach the bottom at 40 Gγ. Significantly, this notable proliferative decline was accompanied by the decreased expression of HR protein factor RAD51 (Figure 9A). GO1 proliferative activity decreased much slower and reached the bottom at 150 Gγ, which could indicate the higher radioresistance of cells acquired after the preceding exposure. Similar dose dependence was observed for the expression of the RAD51 protein.

While many researchers (19) indicated an insignificant role of HR in DNA repair in tumor cells, we observed a correlation between the proliferative activity of cells and the expression level of the main factor of HR-mediated DNA repair, RAD51.

Analysis of proliferative activity in two studied cell cultures in the context of the expression of proteins Ku70 and Ku80, markers of NHEJ involvement in tumor-cell survival after radiation, demonstrated no increase in Ku80 protein level with a radiation dose in both cultures. Considering that the Ku70/Ku80 heterodimer is involved in NHEJ, and Ku80 is always excessive, it cannot be used as a marker in this case. No clear relationship between the proliferative activity of Sus\fP2 and GO1 cells, and Ku70 protein expression was revealed.

Comparison of the dose–effect curves for the expression of proteins critical for HR- and NHEJ-mediated DNA repair and proliferative activity (MTT) further confirmed our observations.

Obtained data after radiation of a cell culture not pre-exposed to X-ray therapy corroborate the proposal by Sasaki et al. (20) that cell proliferation varies with the expression of the RAD51 protein. Hence, it is critical for DNA repair at doses below 40 Gγ, which is apparent in Figure 9 for doses below 10 Gγ. As the dose increases above 40 Gγ, the proliferative activity of cells varies with the protein levels of NHEJ factors Ku70 and Ku80, but no such relationship was observed between proliferative activity and RAD51 expression, which suggests that NHEJ is the main DNA repair pathway at high radiation doses. Mladenov made the same suggestion when using lower doses (26). However, they found a switch of HR-mediated DNA repair to NHEJ, which could be explained with using linear low-diversity cancer cells A549, HA-AsiSI-ER-U2OS, HCT116, and U2OS (γ27).

Different patterns of HR and NHEJ involvement in DNA repair were observed in the tumor pre-exposed to radiation. GO1 cell proliferation tended to decrease with radiation dose in a way similar to that for the expression of the RAD51 protein. No such pattern was observed for the expression of the Ku70 and Ku80 proteins (Figure 8B). This means that HR plays the leading role in DNA repair in this case, and this pattern is no longer observed only after high radiation doses (above 100 Gγ). GO1 cells demonstrate high radiation resistance, and their proliferative activity decreases slowly with radiation doses.

Thus, we demonstrated an important role of RAD51, and hence HR, in DNA repair in cells after low-dose therapy radiation (for Sus\fP2, up to 40 Gγ; for GO1, up to 80 Gγ). RAD51 is considered to mediate only the slow repair of double-stranded DNA breaks and is critical for DNA replication (27). However, our data confirmed the proposal of Short et al. (28) that the level of RAD51 protein is relevant for the radioresistance of glioblastoma cells, which could be modulated by decreasing the cellular level of the RAD51

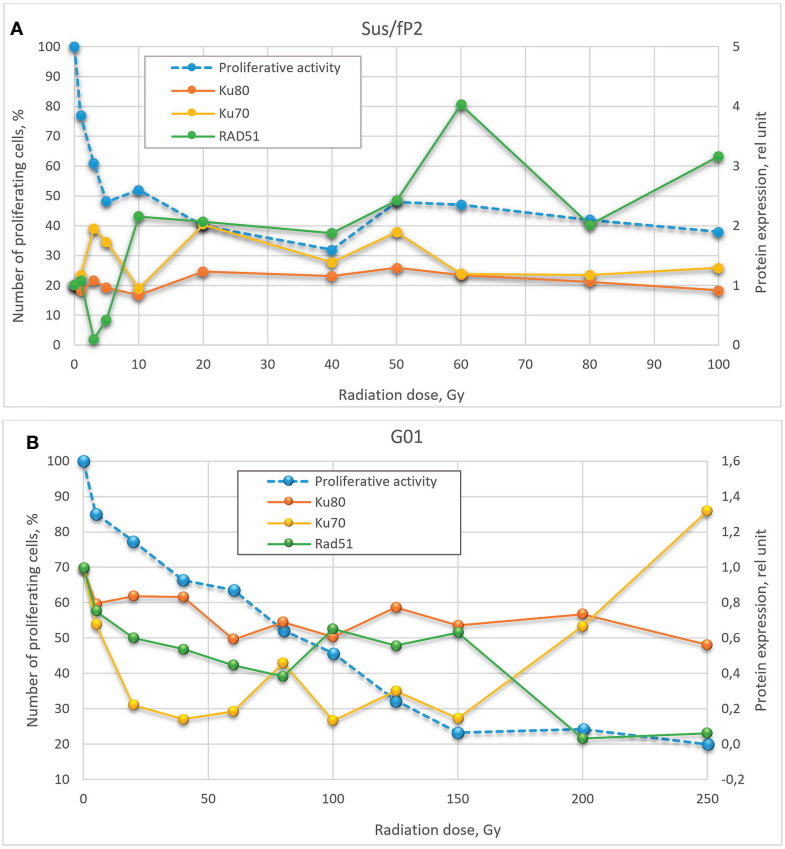

FIGURE 9
Dose-effect relationship between Sus\fP2 **(A)** and GO1 **(B)** proliferative activity and expression of RAD51, Ku70, and Ku80 proteins.

protein (12). Zhong et al. (29) (came to similar conclusions concerning nonsmall cell lung cancer. The latter publication also demonstrated that RAD51 knockdown enhances the radiation-induced degradation of tumor cells and induces their apoptosis.

The significance of RAD51, and hence HR, decreases with high doses of radiation, and cell proliferation starts to depend on Ku70 expression, which indicates the increasing importance of the NHEJ pathway. The radiation dose switching from HR to NHEJ substantially differs in tumor cells pretreated and not pretreated with radiation.

We have applied glioblastoma-derived cell cultures to demonstrate, for the first time, changes of sensitivity of tumor-cell to radiation dose. We have shown that different glioblastomas respond differently to radiation therapy, and this could be due to their peculiarities. For example, a sensitivity of tumor cells to radiation could change if the patient has previously received radiation therapy. Other characteristics of the tumor could also modulate either resistance or sensitivity to radiation therapy. Nevertheless, it becomes possible to choose a more effective dose of radiation for a patient's tumor studying the corresponding individual cell cultures. Our data could justify an individual approach to radiation therapy for a patient.

The significance of a patient-specific approach was confirmed by several publications, e.g., a recent one describing the radiation effect on apoptosis and necrosis in prostate cancer cell lines (30), which demonstrated that low and high radiation doses efficiently induce apoptosis and necrosis, respectively. The exposure of Sus\fP2 to a high dose (200 Gγ) corroborates this conclusion: most cells underwent necrosis. A similar experiment on a cell culture derived from a tumor pre-exposed to radiation demonstrated a different pattern: most dying cells underwent apoptosis. Hence, cell-death processes can vary with treatment conditions and individual neoplasm properties.

Our second observation is that tumor cells pre-exposed to radiation can be more radiation-resistant, which is mediated by HR and hence RAD51. This agrees with the proposal of Short et al. (28) that RAD51 is more significant for DNA repair in tumor cells exposed to radiation than Ku70/Ku80 is. We found the importance of HR repair at irradiation doses

from 1 to 40 Gγ for a glioblastoma cell culture without preliminary irradiation and from 1 to 100 Gγ for a culture with preliminary irradiation.

Our study agrees with the viewpoint that the control of HR processes in human glioma cells is more efficient than the inhibition of the main alternative pathway of DNA repair, NHEJ (4, 5, 31).

Conclusion

Radiation therapy is a critical component of the current approach to glioblastoma (GBM) treatment. However, some GBM cells recover after this exposure and initiate tumor growth. The substantial point is to evaluate a contribution of DNA repair pathways, homologous recombination (HR) and nonhomologous end joining (NHEJ) to a restoration of GBM tumor cells. There is a need to understand to what degree GBM cells change in their sensitivity to radiation during repeated radiation exposure. The point is to conduct this kind of studies not on linear GBM cells, but on primary cell cultures from patient tumors, paying attention to the small number of passages. We used GBM-derived cell cultures to demonstrate, for the first time, changes in tumor-cell sensitivity to radiation doses in the range of 1–250 Gγ. We also suggested an important role of RAD51, and hence HR, in DNA repair in cells after radiation therapy (up to 80 Gγ). The significance of RAD51 and hence HR, decreases with high doses of radiation, and cell proliferation begins to depend on Ku70 expression, which indicates the increasing importance of the NHEJ pathway. Radiation dose switching a mechanism (reparative process) from HR to NHEJ substantially differs for two cell cultures, possibly due to a status of being either pre-treated with radiation or not pre-treated one.

Data availability statement

The original contributions presented in the study are included in the article/Supplementary Material. Further inquiries can be directed to the corresponding author.

Ethics statement

The study involving human participants (cell cultures) was conducted according to the guidelines of the Declaration of Helsinki and was approved by the Local Ethics Committee of Burdenko Neurosurgery Center (protocol code №12/2020, 15.12.2020) and with the 1964 Helsinki declaration and its later amendments or comparable ethical standards. The patients/participants provided their written informed consent to participate in this study.

Author contributions

GP, AB, and AG contributed to the whole conception and design of this project. AP worked as the neurosurgeon to collect cases and analyze the clinical data. DG selected the tissue of human glioblastoma for preparing cell cultures from the Biobank that he directs. ES was responsible for the preparation of glioblastoma cell cultures derived from human tumors for research and MTT. AB, AN, and NA performed X-radiation; DS: reverse transcription and qPCR assay; DP and AR: Western blotting; AR and ES: flow cytofluorometry. GP completed the manuscript and figures and formed the concept of the article; AR helped in figure design. All authors were involved in the writing of the manuscript at the draft and revision stages and have read and approved the final version. All authors have read and agreed to the published version of the manuscript.

Funding

This research was funded by the Ministry of Science and Higher Education of the Russian Federation, grant number 075-15-2020-809 (13.1902.21.0030).

Acknowledgments

We are grateful to Marina Ryzhova (N.N. Burdenko NMRCN) for evaluating IDH mutations in cell cultures.

Conflict of interest

The authors declare that the research was conducted in the absence of any commercial or financial relationships that could be construed as a potential conflict of interest.

Publisher's note

Supplementary material

The Supplementary Material for this article can be found online at: https://www.frontiersin.org/articles/10.3389/fonc.2022.912741/full#supplementary-material

References

1. Ostrom QT, Bauchet L, Davis FG, Deltour I, Fisher JL, Langer CE, et al. The epidemiology of glioma in adults: a "state of the science" review. *Neuro-Oncology* (2014) 16:896–913. doi: 10.1093/neuonc/nou087

2. Balbous A, Cortes U, Guilloteau K, Rivet P, Pinel B, Duchesne M, et al. A radiosensitizing effect of RAD51 inhibition in glioblastoma stem-like cells. *BMC Cancer* (2016) 16:604. doi: 10.1186/s12885-016-2647-9

3. Helleday T, Petermann E, Lundin C, Hodgson B, Sharma RA. DNA Repair pathways as targets for cancer therapy. *Nat Rev Cancer* (2008) 8:193–204. doi: 10.1038/nrc2342

4. Lim YC, Roberts TL, Day BW, Stringer BW, Kozlov S, Fazry S, et al. Increased sensitivity to ionizing radiation by targeting the homologous recombination pathway in glioma initiating cells. *Mol Oncol* (2014) 8:1603–15. doi: 10.1016/j.molonc.2014.06.012

5. Short SC, Giampieri S, Worku M, Alcaide-German M, Sioftanos G, Bourne S, et al. Rad51 inhibition is an effective means of targeting DNA repair in glioma models and CD133+ tumor-derived cells. *Neuro-Oncology* (2011) 13:487–99. doi: 10.1093/neuonc/nor010

6. Bouchaert P, Guerif S, Debiais C, Irani J, Fromont G. DNA-PKcs expression predicts response to radiotherapy in prostate cancer. *Int J Radiat Oncol - Biol - Phys* (2012) 84:1179–85. doi: 10.1016/j.ijrobp.2012.02.014

7. Lee S-W, Cho K-J, Park J-H, Kim SY, Nam SY, Lee B-J, et al. Expressions of Ku70 and DNA-PKcs as prognostic indicators of local control in nasopharyngeal carcinoma. *Int J Radiat Oncol - Biol - Phys* (2005) 62:1451–7. doi: 10.1016/j.ijrobp.2004.12.049

8. Pinel B, Duchesne M, Godet J, Milin S, Berger A, Wager M, et al. Mesenchymal subtype of glioblastomas with high DNA-PKcs expression is associated with better response to radiotherapy and temozolomide. *J Neuro-Oncol* (2017) 132:287–94. doi: 10.1007/s11060-016-2367-7

9. Aboussekhra A, Chanet R, Adjiri A, Fabre F. Semidominant suppressors of Srs2 helicase mutations of saccharomyces cerevisiae map in the RAD51 gene, whose sequence predicts a protein with similarities to procaryotic RecA proteins. *Mol Cell Biol* (1992) 12:3224–34. doi: 10.1128/mcb.12.7.3224-3234.1992

10. Roy U, Greene EC. The role of the Rad55-Rad57 complex in DNA repair. *Genes* (2021) 12:1390. doi: 10.3390/genes12091390

11. Raderschall E, Stout K, Freier S, Suckow V, Schweiger S, Haaf T. Elevated levels of Rad51 recombination protein in tumor cells. *Cancer Res* (2002) 62:219–25.

12. Russell JS, Brady K, Burgan WE, Cerra MA, Oswald KA, Camphausen K, et al. Gleevec-mediated inhibition of Rad51 expression and enhancement of tumor cell radiosensitivity. *Cancer Res* (2003) 63:7377–83.

13. Tachon G, Cortes U, Guichet PO, Rivet P, Balbous A, Masliantsev K, et al. Cell cycle changes after glioblastoma stem cell irradiation: the major role of RAD51. *Int J Mol Sci* (2018) 19:3018. doi: 10.3390/ijms19103018

14. Rothkamm K, Lobrich M. Evidence for a lack of DNA double-strand break repair in human cells exposed to very low x-ray doses. *Proc Natl Acad Sci United States America* (2003) 100:5057–62. doi: 10.1073/pnas.0830918100

15. Enokido Y, Tamura T, Ito H, Arumughan A, Komuro A, Shiwaku H, et al. Mutant huntingtin impairs Ku70-mediated DNA repair. *J Cell Biol* (2010) 189:425–43. doi: 10.1083/jcb.200905138

16. Koike M, Matsuda Y, Mimori T, Harada YN, Shiomi N, Shiomi T. Chromosomal localization of the mouse and rat DNA double-strand break repair genes Ku p70 and Ku p80/XRCC5 and their mRNA expression in various mouse tissues. *Genomics* (1996) 38:38–44. doi: 10.1006/geno.1996.0589

17. Bassing CH, Alt FW. The cellular response to general and programmed DNA double strand breaks. *DNA Repair (Amsterdam)* (2004) 3:781–96. doi: 10.1016/j.dnarep.2004.06.001

18. Ferguson DO, Alt FW. DNA Double strand break repair and chromosomal translocation: lessons from animal models. *Oncogene* (2001) 20:5572–9. doi: 10.1038/sj.onc.1204767

19. Couedel C, Mills KD, Barchi M, Shen L, Olshen A, Johnson RD, et al. Collaboration of homologous recombination and nonhomologous end-joining factors for the survival and integrity of mice and cells. *Genes Dev* (2004) 18:1293–304. doi: 10.1101/gad.1209204

20. Sasaki MS, Takata M, Sonoda E, Tachibana A, Takeda S. Recombination repair pathway in the maintenance of chromosomal integrity against DNA interstrand crosslinks. *Cytogenet Genome Res* (2004) 104:28–34. doi: 10.1159/000077463

21. Takata M, Sasaki MS, Sonoda E, Morrison C, Hashimoto M, Utsumi H, et al. Homologous recombination and non-homologous end-joining pathways of DNA double-strand break repair have overlapping roles in the maintenance of chromosomal integrity in vertebrate cells. *EMBO J* (1998) 17:5497–508. doi: 10.1093/emboj/17.18.5497

22. Soni A, Murmann-Konda T, Siemann-Loekes M, Pantelias GE, Iliakis G. Chromosome breaks generated by low doses of ionizing radiation in G2-phase are processed exclusively by gene conversion. *DNA Repair (Amsterdam)* (2020) 89:102828. doi: 10.1016/j.dnarep.2020.102828

23. Antipina NA, Smirnov GY, Nikolaeva AA, Belyashova AS, Pavlova GV, Golanov AV. Physicotechnical aspects of an experimental study of the effect of high radiation doses on human glioblastoma cell culture. *Med Phys* (2019) 2:51–7.

24. Walker JR, Corpina RA, Goldberg J. Structure of the Ku heterodimer bound to DNA and its implications for double-strand break repair. *Nature* (2001) 412:607–14. doi: 10.1038/35088000

25. Peddi P, Loftin CW, Dickey JS, Hair JM, Burns KJ, Aziz K, et al. Et.al. DNA-PKcs deficiency leads to persistence of oxidatively induced clustered DNA lesions in human tumor cells. *Free Radical Biol Med* (2010) 48:1435–43. doi: 10.1016/j.freeradbiomed.2010.02.033

26. Mladenov E, Staudt C, Soni A, Murmann-Konda T, Siemann-Loekes M, Iliakis G. Strong suppression of gene conversion with increasing DNA double-strand break load delimited by 53BP1 and RAD52. *Nucleic Acids Res* (2020) 48:1905–24. doi: 10.1093/nar/gkz1167

27. Beucher A, Birraux J, Tchouandong L, Barton O, Shibata A, Conrad S, et al. ATM And Artemis promote homologous recombination of radiation-induced DNA double-strand breaks in G2. *EMBO J* (2009) 2009(28):3413–27. doi: 10.1038/emboj.2009.276

28. Short SC, Martindale C, Bourne S, Brand G, Woodcock M, Johnston P. DNA Repair after irradiation in glioma cells and normal human astrocytes. *Neuro-Oncology* (2007) 9:404–11. doi: 10.1215/15228517-2007-030

29. Zhong X, Luo G, Zhou X, Luo W, Wu X, Zhong R, et al. Rad51 in regulating the radiosensitivity of non-small cell lung cancer with different epidermal growth factor receptor mutation status. *Thorac Cancer* (2016) 7:50–60. doi: 10.1111/1759-7714.12274

30. Petragnano F, Pietrantoni I, Di Nisio V, Fasciani I, Del Fattore A, Capalbo C, et al. Modulating the dose-rate differently affects the responsiveness of human epithelial prostate- and mesenchymal rhabdomyosarcoma-cancer cell line to radiation. *Int J Radiat Biol* (2020) 96:823–35. doi: 10.1080/09553002.2020.1739774

31. King HO, Brend T, Payne HL, Wright A, Ward TA, Patel K, et al. Et.al. RAD51 is a selective dna repair target to radiosensitize glioma stem cells. *Stem Cell Rep* (2017) 8:125–39. doi: 10.1016/j.stemcr.2016.12.005

frontiers | Frontiers in Oncology

TYPE Original Research
PUBLISHED 16 September 2022
DOI 10.3389/fonc.2022.996186

OPEN ACCESS

EDITED BY
Ignazio Gaspare Vetrano,
IRCCS Carlo Besta Neurological Institute Foundation, Italy

REVIEWED BY
Valentina Pinzi,
IRCCS Carlo Besta Neurological Institute Foundation, Italy
Enrico Gambatesa,
University of Milan, Italy
Mahmoud Messerer,
Centre Hospitalier Universitaire Vaudois (CHUV), Switzerland

*CORRESPONDENCE
Young-Hoon Kim
justin527@hanmail.net

SPECIALTY SECTION
This article was submitted to Neuro-Oncology and Neurosurgical Oncology, a section of the journal Frontiers in Oncology

RECEIVED 17 July 2022
ACCEPTED 23 August 2022
PUBLISHED 16 September 2022

CITATION
Kim J, Byeon Y, Song SW, Cho YH, Hong C-K, Hong SH, Kim JH, Lee DH, Park JE, Kim HS and Kim Y-H (2022) Vestibular schwannoma associated with neurofibromatosis type 2: Clinical course following stereotactic radiosurgery. *Front. Oncol.* 12:996186. doi: 10.3389/fonc.2022.996186

Vestibular schwannoma associated with neurofibromatosis type 2: Clinical course following stereotactic radiosurgery

Junhyung Kim[1], Yukyeng Byeon[1], Sang Woo Song[1], Young Hyun Cho[1], Chang-Ki Hong[1], Seok Ho Hong[1], Jeong Hoon Kim[1], Do Heui Lee[1], Ji Eun Park[2], Ho Sung Kim[2] and Young-Hoon Kim[1]*

[1]Department of Neurological Surgery, Asan Medical Center, University of Ulsan College of Medicine, Seoul, South Korea, [2]Department of Radiology, Asan Medical Center, University of Ulsan College of Medicine, Seoul, South Korea

Objective: A lack of understanding of the clinical course of neurofibromatosis type 2 (NF2)-associated vestibular schwannoma (VS) often complicates the decision-making in terms of optimal timing and mode of treatment. We investigated the outcomes of stereotactic radiosurgery (SRS) in this population.

Methods: We retrospectively analyzed NF2 patients treated with Gamma-Knife SRS for VS in our tertiary referral center. A total of 41 treated lesions from 33 patients were collected with a follow-up period of 69.1 (45.0-104.8) months. We reviewed the treatment history, hearing function, and other treatment-related morbidities in individual cases. We also analyzed pre- and post-treatment tumor volumes *via* imaging studies. Longitudinal volumetric analyses were conducted for the tumor volume response of the 41 treated lesions following SRS. The growth pattern of 22 unirradiated lesions during an observation period of 83.4 (61.1-120.4) months was separately evaluated.

Results: Most treated lesions showed effective tumor control up to 85% at 60 months after SRS, whereas unirradiated lesions progressed with a relative volume increase of 14.0% (7.8-27.0) per year during the observation period. Twelve (29%) cases showed pseudoprogression with significant volume expansion in the early follow-up period, which practically reduced the rate of tumor control to 57% at 24 months. Among the patients with serviceable hearing, two (20%) cases lost the hearing function on the treated side during the early follow-up period within 24 months.

Conclusions: Progressive NF2-associated VS can be adequately controlled by SRS but the short-term effects of this treatment are not highly advantageous in terms of preserving hearing function. SRS treatment candidates should therefore be carefully selected.

KEYWORDS

neurofibromatosis type 2 (NF2), vestibular schwannoma (acoustic neuroma), stereotactic radiosurgery (SRS), tumor control, hearing preservation

Introduction

Neurofibromatosis type 2 (NF2) refers to a rare neoplastic syndrome of the nervous system, characterized by the presence of multiple schwannomas, meningiomas, or gliomas. NF2 results from the genomic aberrations in the *NF2* tumor suppressor gene, which regulates the production of merlin/schwannomin protein. More than half of the affected individuals are sporadic while some others are inherited in an autosomal dominant pattern. Currently, NF2 is clinically defined by the consensus diagnostic criteria without genetic testing. Most NF2 patients harbor vestibular schwannomas (VS), which often arise bilaterally and are more progressive at a younger age compared with sporadic cases.

For NF2-associated VS patients, the optimal timing and mode of treatment are still the subject of debate due to a biologic behavior that is distinct from their sporadic counterparts. Current clinical guidelines recommend diverse treatment options for individual cases, and stereotactic radiosurgery (SRS) is widely accepted as a viable therapeutic option (1, 2). However, a lack of understanding of the clinical course of NF2-associated VS often complicates the decision-making with regards to treatment. Some experts have insisted that a conservative observational approach (a wait-and-see strategy) is appropriate, especially in specific age groups (3, 4). In contrast, some others suggested early interventions with a treatment modality selected for each case (5). Several studies have reported that SRS is a valid and favorable treatment option that is as effective against VS in NF2 patients as in sporadic cases (6, 7).

We have here investigated the clinical outcomes of an SRS intervention for NF2-associated VS in a cohort from our institution. We evaluated the tumor growth patterns of individual cases and compared treated and untreated lesions.

Materials and methods

Study population

This study was a retrospective review of a case series of NF2 patients who underwent Gamma-Knife SRS treatment for VS between 1991 and 2021 at our tertiary referral center. All available clinical information and neuroimaging data were collected under the approval of our institutional review board. The study patients with NF2 had been identified *via* a clinical diagnosis that was based on the Manchester criteria (8). In cases with bilateral disease, each treated lesion was included as an individual case. Cases missing magnetic resonance image (MRI) data or a lack of detailed reports on the SRS treatment were excluded from the study. Cases lost to follow-up prior to 12 months from the date of the initial treatment were also excluded.

Treatment modality and outcome assessment

The study patients were treated using the Leksell Gamma-Knife Perfection (Elekta, Stockholm, Sweden). In each case, 1 mm- or 1.5 mm-sectioned T1-weighted MRIs with gadolinium enhancement and 2 mm- or 3 mm-sectioned T2-weighted MRI scans were acquired for treatment planning. Doses were calculated using Leksell GammaPlan v5.34-11.3.1 (Elekta, Stockholm, Sweden) software. All patients were typically followed up initially at 3-, 6-, and 12-month intervals after the treatment, and then annually or biannually thereafter depending on their clinical course. Pretreatment screening and follow-up MRIs usually included 3 mm-sectioned axial and coronal postcontrast T1-weighted images, which were used for volumetric assessments of the tumor. The volumetric assessment was conducted by manual segmentation using 3D Slicer v5.10 (NA-MIC, Boston, MA), and the median value of the volume measurements from distinct sequences in each study session was used in the analyses.

For outcome assessments, tumor control, hearing preservation, and other treatment-related comorbidities were investigated. Tumor progression or recurrence was defined as a more than 10% increase in the tumor volume compared with pretreatment volume. Tumor pseudoprogression, or an early transient increase in the tumor volume after SRS, was not separately evaluated since it cannot be differentiated from true

tumor progression in the first five years of follow-up (9, 10). Tumor control was defined as the arrest of tumor growth without progression or a decrease in the tumor volume. Hearing function was evaluated using pure tone audiometry and speech discrimination scoring for the patients who had serviceable hearing on the affected side prior to treatment. Hearing preservation was defined as retention of serviceable hearing (corresponding to a Gardner-Robertson grade I or II) at the last available audiometric follow-up.

Statistics

Descriptive statistics were shown as a frequency with percentages for categorical data and as a median value with interquartile ranges (IQR) for continuous data. Differences between distinct phenotype groups were compared using the Chi-square test for categorical variables and the Wilcoxon-Mann-Whitney U-test for continuous variables. For the subset of patients with bilateral disease, tumor growth patterns were compared between the treated and untreated lesions. In generating tumor growth curves, the logarithmic relative tumor volumes were fitted by linear regression for individual cases, with an assumption of which would follow an exponential function as follows:

$$dV/dt = \delta \ V$$

$$d(\ln V)/dt = \delta,$$

where δ is the effective growth rate.

All results were considered statistically significant if a two-tailed p-value was less than 0.05. All statistical analyses were performed using R v4.2.0 (R Foundation for Statistical Computing, Vienna, Austria).

Results

Baseline characteristics of the study subjects

A total of 33 NF2 patients were reviewed in this study (Figure 1). Bilateral VS was found in 26 (79%) patients in this case series, where 8 (24%) patients underwent SRS on both sides. Among the other cases with bilateral diseases, four (12%) underwent tumor resection without adjuvant SRS for the contralateral lesion, while 14 (42%) patients left one side untreated. Thereby, 41 lesions treated with SRS were included in the outcome assessment (Table 1).

While none of the current study patients were identified as inherited cases, only three of these patients received genetic counseling for NF2. One of these cases was shown to have a deletion of the *NF2* gene in a multiplex ligation-dependent probe amplification study. Based on a historical phenotypic categorization (6, 11, 12), 22 patients (27 lesions) were

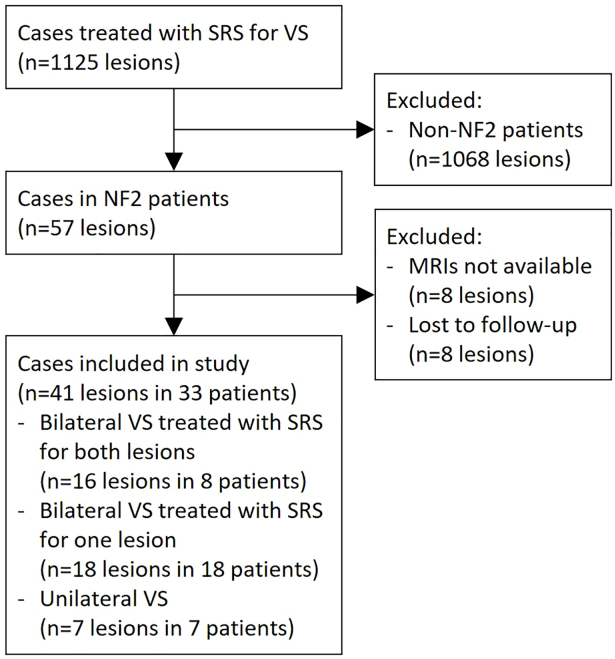

FIGURE 1
Selection of study subjects. NF2, neurofibromatosis type 2; MRI, magnetic resonance imaging; SRS, stereotactic radiosurgery.

10.3389/fonc.2022.996186

TABLE 1 Baseline characteristics of the study patients.

	VS (n=41) in NF2 patients
Age at treatment (year)	37 [29, 50]
≥ 30	29 (71)
Sex	
Male	21 (51)
Criteria for NF2 diagnosis	
Bilateral VS	34 (83)
Unilateral VS with other multiple tumors	7 (17)
Phenotype	
Wishart	27 (66)
Feiling-Gardner	14 (34)
Laterality	
Left	17 (41)
Indication for treatment	
Primary	
Tumor growth	13 (32)
Tumor volume	21 (51)
Adjuvant or secondary (prior surgery)	7 (17)
Hearing function before SRS (Gardner-Robertson grade)	
I	2 (5)
II	8 (20)
III	3 (7)
IV or V	28 (68)

Values are numbers (%) or a median [range]. Data are given for each treated case. VS, vestibular schwannoma; NF2, neurofibromatosis 2; SRS, stereotactic radiosurgery.

deemed to have the Wishart phenotype. The relationship between the presence of bilateral disease and specific phenotypes was not significant (p=0.292), whereas the age at the first treatment was significantly different between the two phenotypes: Wishart, 32 (23-42) years vs. Feiling-Gardner, 50 (43-56) years (p=0.002).

Most of the cases in our current series were treated with Gamma-Knife SRS as a primary intervention. Six cases received SRS as an adjuvant or secondary treatment after tumor resection. No patients were treated with bevacizumab during the follow-up period. More than half of our cases were treated due to a large tumor volume and had a non-serviceable hearing function at the time of their therapy. No other case of a cranial nerve impairment related to the target lesion was observed.

Gamma-Knife SRS was prescribed for a median tumor volume of 2.80 (0.70-5.90) cm^{-3} (Table 2). The majority of the treated lesions were Koos grade II (37%) or III (39%) with a maximal diameter of 2.0 (1.0-2.3) cm. Most cases in our case series underwent a single SRS procedure except three cases with fractionation. The single fraction SRS was was mostly performed with a marginal dose of 12.0 to 13.0 Gy to the 50% isodose lines. The fractionated SRS procedures were performed with a marginal dose of 25.6 Gy over 5 fractions or 20.0 Gy over 3 fractions to the 50% isodose lines.

Tumor growth patterns and tumor volume response to stereotactic radiosurgery

To identify the natural course of the NF2-associated VS lesions in our present series, we conducted a longitudinal volumetric analysis of these tumors during the observation period before the initial irradiation. Among the individuals with bilateral disease, 8 cases that were later treated for the second lesion and 14 cases with untreated contralateral lesions were assessed with available pre-treatment MRI data from at least three different time points during the observation period of 83.4 (61.1-120.4) months. The lesions progressed with a relative volume increase of 14.0% (7.8-27.0) per year (Figure 2). For those 8 cases with both lesions being treated, SRS was performed

TABLE 2 Treatment factors and outcomes.

	VS (n=41) in NF2 patients
Maximal extrameatal diameter (cm)	2.0 [1.1, 2.3]
Extrameatal extension (Koos grade)	
I	5 (12)
II	15 (37)
III	16 (39)
IV	5 (12)
Target volume (cc)	3.06 [1.00, 6.00]
Number of fractions	
Single	39 (93)
Fractionated	3 (7)
Marginal dose (Gy) per fraction	12.0 [12.0, 12.5]
Less than 12.0	5 (12)
12.0-13.0	35 (86)
More than 13.0	1 (2)
Tumor control	
At 12 months	24 (59)
At 24 months (n=36)	21 (58)
At 36 months (n=35)	26 (74)
At 60 months (n=27)	23 (85)
At 120 months (n=11)	9 (82)
Pseudoprogression (n=12)	
Peak volume increase (%)	29.2 [22.4, 36.6]
Time-to-peak volume (month)	17.3 [11.0, 35.4]
Hearing preservation (n=10)	
Serviceable	8 (80)
Non-serviceable	2 (20)
Other comorbidities	
Vestibulopathy	.
Facial nerve palsy	.
Trigeminal neuralgia	.
Symptomatic hydrocephalus (n=33)	1 (3)

Values are numbers (%) or a median [range]. Percentages are based on the total number of treated lesions (n=41), unless otherwise specified. VS, vestibular schwannoma; NF2, neurofibromatosis 2.

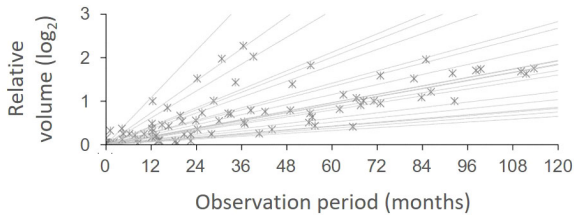

FIGURE 2
Growth patterns of unirradiated vestibular schwannomas. The relative volume change during the observation period was fitted using linear regression for each case [R^2, 0.965 (IQR, 0.937-0.991)]. The volume of unirradiated lesions exponentially expanded with a doubling time of 62.2 (IQR, 30.6-92.3) months, which corresponds to a relative volume increase of 14.0% (IQR, 7.8-27.0%) per year.

for the second lesion at a median of 113.7 (40.8-185.2) months from the initial treatment. The decision to conduct this latter treatment was made after the lesion had grown to 3.57 (2.67-6.19) times its initial volume. No clinical factors were significantly associated with the growth rate.

We next investigated the tumor volume responses to the SRS procedure. We categorized each study patient into distinct treatment response groups in accordance with their individual tumor growth curves derived from longitudinal volumetric measurements (Figure 3A). Half (19 of 41) of these cases exhibited continuous volume shrinkage without pseudoprogression after the treatment (group I). Among the others who had significant volume expansion, 8 (20%) patients showed early pseudoprogression mostly within the first two years (group II; Figures 3B–D), whereas four (10%) cases showed late pseudoprogression with a peak volume at three or four years (group III; Figures 3E–G). Four (10%) cases where true tumor progression was suspected showed sequential tumor growth (group IV; Figures 3H–J) as found in the untreated lesions. Six cases were undetermined with respect to their response groups due to a follow-up period shorter than five years.

Clinical course following stereotactic radiosurgery

The treated lesions were followed up for a median of 69.1 (45.0-104.8) months after SRS. Although four (10%) of our cases displayed failed tumor control at the time of the last imaging study, no cases required salvage surgery during the follow-up period (Table 2). The rate of tumor control varied across different time points from 56% at 12 months to 84% at 60 months. This rate was slightly lower in the earlier follow-up period within two years due to several cases presenting with pseudoprogression. Among the 12 cases that we identified as having pseudoprogression, the tumor volumes were found to have increased to 1.29 (1.22-1.37) times their initial volume. The time to peak volume was 17.3 (11.0-35.4) months. Nevertheless, the tumor volume had recovered to within the control limit in 34.5 (25.8-51.8) months in these cases.

In the context of functional outcomes, hearing preservation was achieved in most (8 of 10) of our current study cases. One unilateral VS patient presented hearing loss on the treated side from Gardner-Robertson grade II to grade IV during early transient progression in 24 months (Figure 4). Another bilateral VS patient who had already lost hearing function on the contralateral side presented hearing impairment in 20 months, but the patient's hearing recovered to Gardner-Robertson grade II after cochlear implantation. Our case series also included three patients with borderline function (Gardner-Robertson grade III), but none of them showed hearing improvement during the audiometric follow-up and two eventually lost their function (Gardner-Robertson grade IV/V) in 12 and 24 months, respectively. No cases presented with any of other cranial nerve dysfunction during follow-up. One subject presented with symptomatic communicating hydrocephalus.

Discussion

VS is a common benign tumor and the basis of its treatment at present is focused on functional outcomes (1). Accordingly, optimal timing for the intervention and the treatment modality itself are important issues for practitioners. Previous studies have consistently reported on VS tumor growth and the risk of hearing loss in affected patients who undergo observation only without treatment. A prior nationwide cohort study revealed that untreated VS lesions usually grow within five years after their initial diagnosis, and 25-40% of them are still capable of growth after 10 years (13). Another large cohort study reported that 43% of NF2 patients start treatment for VS within five years of its diagnosis (3). The five-year mortality of NF2 patients has been reported to be up to 6% in previous articles (3, 14). The previous meta-analysis has also found that patients on an initial observation management plan have a higher risk of early hearing deterioration (15). Considering these circumstances, observation only may no longer be appropriate if there is any suspicion of interval tumor growth.

SRS is a possible good treatment option with an expectation of tumor control without facial palsy, in both non-NF2 (16) and NF2 (2) populations. There are however some concerns regarding the efficacy of this treatment, as some authors have suggested that the reported rates of tumor control have likely been overestimated due to a liberal definition and that SRS had no discernable volume reduction effects (17). Most previous studies have presented an excellent tumor control rate of more than 80% with SRS (6, 7, 12, 18, 19), but these numbers should be carefully assessed because they might overlook the clinical significance of pseudoprogression during the early follow-up

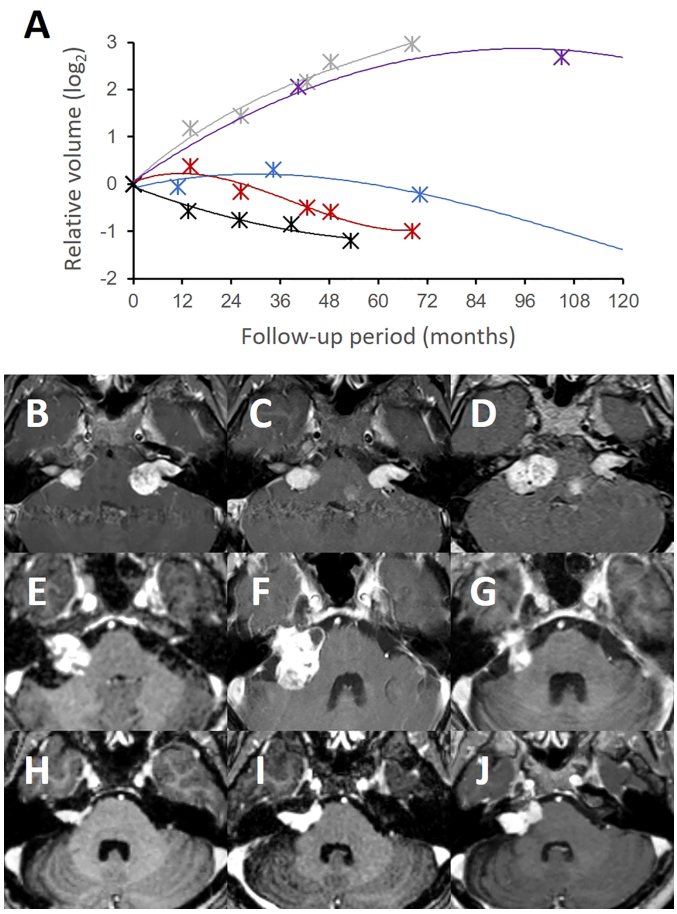

FIGURE 3
Tumor volume response patterns following stereotactic radiosurgery.The tumor volumes of the treated lesions showed distinct patterns in several treatment response groups **(A)**. Group I (black) refers to a typical volume response to SRS without significant pseudoprogression. Group II (red) volume responses had early pseudoprogression on the treated side compared to the contralateral untreated side (grey). Group III (blue) showed a slower response to SRS with delayed pseudoprogression. Group IV (purple) showed a failed tumor control with an exponential tumor growth pattern that was similar to untreated lesions (grey). A group I bilateral NF2-associated VS **(B–D)** showed favorable tumor control on the treated side (left). Notably, however, the contralateral untreated lesion (right) rapidly grew during the same follow-up period. A group III case **(E)** exhibited a slow treatment response, but successful tumor control over a long-term follow-up. This tumor had delayed pseudoprogression **(F)** up to three years post-treatment but eventually regressed without further treatment at 10 years **(G)**. A group IV case **(H)** was resistant to the SRS treatment and consistently grew over three years **(I)** and thereafter **(J)**.

period. In our present case series, 85% of the patients achieved mid- to long-term VS tumor control following SRS, which was comparable to the results described in previous reports (20). However, we also found in our present analyses that one-third of the VS lesions had expanded in volume to a considerably high level and that the tumor control rates at the early time points, i.e., within two years, were practically less than 60%. Nevertheless, in the NF2 population where VS tumors grow more rapidly than in sporadic cases, even an arrest of tumor growth could be advantageous. Currently, a combined treatment strategy of attempted subtotal resection followed by adjuvant SRS in large VS patients is widely accepted with satisfactory outcomes for facial and cochlear functions (21). These concepts for optimal tumor control can be also utilized in NF2 populations depending on the individual patient's condition.

In the context of functional outcomes, the role of SRS has been limited due to the controversial results regarding hearing preservation (22). Most NF2 patients eventually present deafness in their lifetime, and most treatment modalities are rarely effective to revert the natural course of hearing dysfunction. It has been reported that NF2-associated VS is associated with a lower probability of hearing preservation following SRS treatment than sporadic VS (12, 18, 19). We also experienced a couple of cases in our current series in which hearing function was not maintained but in fact rapidly worsened during the early follow-up period. In our study, several cases showed considerably high volume

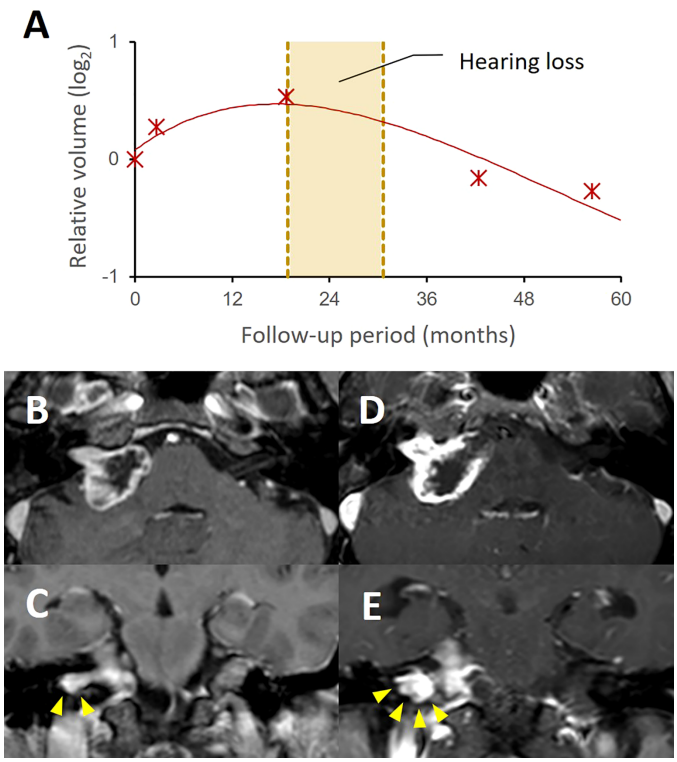

FIGURE 4
A case with progressive hearing loss during pseudoprogression after stereotactic radiosurgery. A group II case showed a typical tumor volume response pattern with transient volume increase up to 42.5% of initial volume after SRS **(A)**. The patient presented progressive hearing loss during pseudoprogression (yellow box). The follow-up MRI **(D, E)** showed a significant volume expansion, compared to the pretreatment MRI **(B, C)**. In this case, the increased extent of the intracanalicular part of the tumor was notable as shown in the coronal images (**E**, arrowheads), which possibly caused cochlear nerve compression in the internal auditory canal.

expansion following the SRS treatment. It has been reported that a recent rapid progression with a greater growth rate is timely difficult to reverse using SRS (23). In addition, there might be other oncological or neuromodulatory mechanisms from the SRS procedure that possibly cause hearing deterioration. Hence, SRS should be carefully considered if hearing preservation is important for the patient. Further investigations that involve longitudinal volumetric analysis and physiologic characterization of VS among the NF2 population might provide better insights into the selection of candidates for SRS.

Conclusions

Progressive NF2-associated VS can be well controlled by SRS, which restricts the growth of these tumors compared to patients who are not treated. Notably, however, the short-term treatment effects of SRS in these cases are not highly advantageous to preserving hearing functions. NF2 candidates should therefore be more carefully selected for this intervention than sporadic VS cases.

Data availability statement

The original contributions presented in the study are included in the article/supplementary material. Further inquiries can be directed to the corresponding author.

Ethics statement

The studies involving human participants were reviewed and approved by the institutional review board in Asan Medical Center. Written informed consent for participation was not required for this study in accordance with the national legislation and the institutional requirements.

Author contributions

JK and Y-HK contributed to the conception and design of the study. JK performed the data analysis and wrote the first

draft of the manuscript. All authors contributed to manuscript revision, read, and approved the submitted version.

Conflict of interest

The authors declare that the research was conducted in the absence of any commercial or financial relationships that could be construed as a potential conflict of interest.

Publisher's note

References

1. Goldbrunner R, Weller M, Regis J, Lund-Johansen M, Stavrinou P, Reuss D, et al. EANO guideline on the diagnosis and treatment of vestibular schwannoma. *Neuro Oncol* (2020) 22(1):31–45. doi: 10.1093/neuonc/noz153

2. Chung LK, Nguyen TP, Sheppard JP, Lagman C, Tenn S, Lee P, et al. A systematic review of radiosurgery versus surgery for neurofibromatosis type 2 vestibular schwannomas. *World Neurosurg* (2018) 109:47–58. doi: 10.1016/j.wneu.2017.08.159

3. Forde C, King AT, Rutherford SA, Hammerbeck-Ward C, Lloyd SK, Freeman SR, et al. Disease course of neurofibromatosis type 2: A 30-year follow-up study of 353 patients seen at a single institution. *Neuro Oncol* (2021) 23(7):1113–24. doi: 10.1093/neuonc/noaa284

4. Goutagny S, Bah AB, Parfait B, Sterkers O, Kalamarides M. Neurofibromatosis type 2 in the elderly population: clinical and molecular features. *Am J Med Genet A* (2013) 161A(4):667–70. doi: 10.1002/ajmg.a.35851

5. Kim BS, Seol HJ, Lee JI, Shin HJ, Park K, Kong DS, et al. Clinical outcome of neurofibromatosis type 2-related vestibular schwannoma: treatment strategies and challenges. *Neurosurg Rev* (2016) 39(4):643–53. doi: 10.1007/s10143-016-0728-5

6. Kruyt IJ, Verheul JB, Hanssens PEJ, Kunst HPM. Gamma knife radiosurgery for treatment of growing vestibular schwannomas in patients with neurofibromatosis type 2: A matched cohort study with sporadic vestibular schwannomas. *J Neurosurg* (2018) 128(1):49–59. doi: 10.3171/2016.9.JNS161463

7. Shinya Y, Hasegawa H, Shin M, Sugiyama T, Kawashima M, Takahashi W, et al. Long-term outcomes of stereotactic radiosurgery for vestibular schwannoma associated with neurofibromatosis type 2 in comparison to sporadic schwannoma. *Cancers (Basel)* (2019) 11(10). doi: 10.3390/cancers11101498

8. Evans DG, Trueman L, Wallace A, Collins S, Strachan T. Genotype/phenotype correlations in type 2 neurofibromatosis (NF2): Evidence for more severe disease associated with truncating mutations. *J Med Genet* (1998) 35(6):450–5. doi: 10.1136/jmg.35.6.450

9. Fouard O, Daisne JF, Wanet M, Regnier M, Gustin T. Long-term volumetric analysis of vestibular schwannomas following stereotactic radiotherapy: Practical implications for follow-up. *Clin Transl Radiat Oncol* (2022) 33:1–6. doi: 10.1016/j.ctro.2021.12.003

10. Meijer OW, Weijmans EJ, Knol DL, Slotman BJ, Barkhof F, Vandertop WP, et al. Tumor-volume changes after radiosurgery for vestibular schwannoma: Implications for follow-up MR imaging protocol. *AJNR Am J Neuroradiol* (2008) 29(5):906–10. doi: 10.3174/ajnr.A0969

11. Ragge NK. Clinical and genetic patterns of neurofibromatosis 1 and 2. *Br J Ophthalmol* (1993) 77(10):662–72. doi: 10.1136/bjo.77.10.662

12. Sun S, Liu A. Long-term follow-up studies of gamma knife surgery for patients with neurofibromatosis type 2. *J Neurosurg* (2014) 121 Suppl:143–9. doi: 10.3171/2014.8.GKS141503

13. Reznitsky M, Petersen M, West N, Stangerup SE, Caye-Thomasen P. The natural history of vestibular schwannoma growth-prospective 40-year data from an unselected national cohort. *Neuro Oncol* (2021) 23(5):827–36. doi: 10.1093/neuonc/noaa230

14. Goshtasbi K, Abouzari M, Yasaka TM, Soltanzadeh-Zarandi S, Sarna B, Lin HW, et al. Treatment analysis and overall survival outcomes of patients with bilateral vestibular schwannoma. *Otol Neurotol* (2021) 42(4):592–7. doi: 10.1097/MAO.0000000000002984

15. Leon J, Lehrer EJ, Peterson J, Vallow L, Ruiz-Garcia H, Hadley A, et al. Observation or stereotactic radiosurgery for newly diagnosed vestibular schwannomas: A systematic review and meta-analysis. *J Radiosurg SBRT* (2019) 6(2):91–100. doi: 10.1016/j.wneu.2021.11.083

16. Savardekar AR, Terrell D, Lele SJ, Diaz R, Keesari PR, Trosclair K, et al. Primary treatment of small to medium (<3 cm) sporadic vestibular schwannomas: A systematic review and meta-analysis on hearing preservation and tumor control rates for microsurgery versus radiosurgery. *World Neurosurg* (2022) 160:102–13.e112. doi: 10.1016/j.wneu.2021.11.083

17. Battaglia A, Mastrodimos B, Cueva R. Comparison of growth patterns of acoustic neuromas with and without radiosurgery. *Otol Neurotol* (2006) 27(5):705–12. doi: 10.1097/01.mao.0000226302.59198.87

18. Spatola G, Carron R, Delsanti C, Thomassin JM, Roche PH, Regis J. Long-term results of gamma-knife stereotactic radiosurgery for vestibular schwannomas in patients with type 2 neurofibromatosis. *Neurochirurgie* (2018) 64(5):355–63. doi: 10.1016/j.neuchi.2016.03.005

19. Mallory GW, Pollock BE, Foote RL, Carlson ML, Driscoll CL, Link MJ. Stereotactic radiosurgery for neurofibromatosis 2-associated vestibular schwannomas: Toward dose optimization for tumor control and functional outcomes. *Neurosurgery* (2014) 74(3):292–300. doi: 10.1227/NEU.0000000000000264

20. Tosi U, Maayan O, An A, Lavieri MET, Guadix SW, DeRosa AP, et al. Stereotactic radiosurgery for vestibular schwannomas in neurofibromatosis type 2 patients: A systematic review and meta-analysis. *J Neurooncol* (2022) 156(2):431–41. doi: 10.1007/s11060-021-03910-8

21. Starnoni D, Giammattei L, Cossu G, Link MJ, Roche PH, Chacko AG, et al. Surgical management for large vestibular schwannomas: a systematic review, meta-analysis, and consensus statement on behalf of the EANS skull base section. *Acta Neurochir (Wien)* (2020) 162(11):2595–617. doi: 10.1007/s00701-020-04491-7

22. Watanabe S, Yamamoto M, Kawabe T, Koiso T, Yamamoto T, Matsumura A, et al. Stereotactic radiosurgery for vestibular schwannomas: Average 10-year follow-up results focusing on long-term hearing preservation. *J Neurosurg* (2016) 125(Suppl 1):64–72. doi: 10.3171/2016.7.GKS161494

23. Killeen DE, Tolisano AM, Isaacson B, Kutz JW, Barnett S, Wardak Z, et al. Vestibular schwannoma tumor size and growth rate predict response with gamma knife stereotactic radiosurgery. *J Neurol Surg B Skull Base* (2022) 83(1):11–8. doi: 10.1055/s-0040-1716677

frontiers | Frontiers in Oncology

TYPE Original Research
PUBLISHED 28 September 2022
DOI 10.3389/fonc.2022.994335

OPEN ACCESS

EDITED BY
Laura Gatti,
Carlo Besta Neurological Institute Foundation, (IRCCS), Italy

REVIEWED BY
Morgan Broggi,
Carlo Besta Neurological Institute Foundation, (IRCCS), Italy
Salvatore Chibbaro,
Neurosurgery Department Strasbourg University Hospital, France

*CORRESPONDENCE
Ping Ai
aiping00222@163.com

†These authors have contributed equally to this work

SPECIALTY SECTION
This article was submitted to Neuro-Oncology and Neurosurgical Oncology, a section of the journal Frontiers in Oncology

RECEIVED 14 July 2022
ACCEPTED 06 September 2022
PUBLISHED 28 September 2022

CITATION
Gou Q, Xie Y and Ai P (2022) Intracranial solitary fibrous tumor/hemangiopericytoma: Role and choice of postoperative radiotherapy techniques. *Front. Oncol.* 12:994335. doi: 10.3389/fonc.2022.994335

Intracranial solitary fibrous tumor/hemangiopericytoma: Role and choice of postoperative radiotherapy techniques

Qiheng Gou[1†], Yuxin Xie[2,3†] and Ping Ai[1*]

[1]Department of Radiation Oncology and Department of Head & Neck Oncology, Cancer Center, West China Hospital, Sichuan University, Chengdu, China, [2]Department of Medical Oncology of Cancer Center, West China Hospital, Sichuan University, Chengdu, China, [3]Laboratory of Molecular Diagnosis of Cancer, Clinical Research Center for Breast, West China Hospital, Sichuan University, Chengdu, China

Background: Intracranial solitary fibrous tumor/hemangiopericytoma (SFT/HPC) is a novel rare disease after the 2016 WHO reclassification. Surgery is the main treatment. Postoperative adjuvant radiotherapy is often used, but the effects of different radiotherapy techniques are still unclear. The purpose of this study was to analyze the effects of postoperative radiotherapy (PORT) and different radiotherapy methods on the efficacy of patients with intracranial SFT/HPC.

Materials and methods: We retrospectively analyzed 42 patients with intracranial SFT/HPC who underwent surgical treatment from 2008 to 2022, 20 of whom were treated with postoperative intensity-modulated radiotherapy (IMRT) and 22 with postoperative stereotactic radiosurgery (SRS). The Kaplan–Meier method was used to analyze the disease-free survival (DFS) of all the 42 patients receiving postoperative radiotherapy and the time to progression (TTP) of 22 of these patients experiencing recurrence. A multivariate Cox proportional hazards model was used to detect prognostic factors of survival.

Results: In the analysis of PORT patients, the median DFS was 8.33 years for PORT IMRT patients and 3.04 years for PORT SRS patients. The 10-year DFS incidence was 46.0% in the PORT IMRT group and 27.5% in the SRS group. Among the 22 patients who relapsed, the median TTP of other patients was 1.25 years, of which 3 received radiotherapy alone and 1 received symptomatic treatment, while the median TTP of surgical and surgical combined with radiotheray patients were 1.83 and 2.49 years, respectively (p=0.035).

Conclusion: PORT IMRT could prolong DFS compared with PORT SRS. It indicated that PORT IMRT radiotherapy technology was a feasible option for

SFT/HPC. Moreover, TTP results of relapsed patients showed that, surgery and surgery combined with radiotherapy treatments have no significant difference on TTP in relapsed patients, but both of them were better than other treatments.

KEYWORDS

intracranial solitary fibrous tumor/hemangiopericytoma (SFT/HPC), postoperative radiotherapy, intensity-modulated radiotherapy (IMRT), *stereotactic radiosurgery (SRS)*, time to progression

Introduction

Hemangiopericytoma (HPC) and solitary fibrous tumor (SFT) are rare primary intracranial tumors. HPC accounts for only 1% of all intracranial tumors (1, 2). Approximately 15% of SFTs show malignant biological behavior, and the others show benign and mesenchymal tumors (3). Recently, researchers found that the Nab2 and STAT6 genes formed a new fusion gene in SFT and HPC samples. This discovery combined the two tumors into a new category, which was named SFT/HPC in the central nervous system (CNS) classification of the World Health Organization (WHO) in 2016 (4). Although several reports have been published describing the pathological characteristics, clinical characteristics and survival outcomes of SFT/HPC (5–8), there is still a lack of sufficient clinical data for this newly defined SFT/HPC.

In addition, previous studies mainly discussed the treatment strategy and prognosis of HPC. Some researchers believe that for HPC, complete surgical resection followed by postoperative radiotherapy (PORT) to the bed is the best strategy (9, 10). Others believed that external irradiation of the tumor bed after surgery appeared to delay recurrence (11).Moreover, PORT was considered the main treatment for HPC. However, a previous study showed that PORT did not improve the local control and survival of HPC. The local control rates after intensity-modulated radiotherapy (IMRT) and stereotactic radiosurgery (SRS) were similar, even though the biological dose of IMRT was much higher than that of SRS (12).

In general, the new classification lacks reliable clinical data, especially leading to doctors' confusion about treatment strategies. We analyzed the clinical features of 42 patients with SFT/HPC who underwent surgical resection and PORT in our institution. The purpose of this study was to analyze the therapeutic effects of different PORT techniques (IMRT vs. SRS) on 42 patients with SFT/HPC.

Abbreviations: SFT, solitary fibrous tumor; HPC, hemangiopericytoma; DFS, disease-free survival; TTP, time to progression; PORT, postoperative radiotherapy; GTR, gross tumor resection; STR, subtotal tumor resection; CTV, clinical target volume; BED, biological effective dose. WHO, World Health Organization; IMRT, intensity-modulated radiotherapy; SRS, stereotactic radiosurgery.

Methods

Patients and diagnosis

A single-institution, retrospective analysis was performed. We conducted a chart review of primary intracranial malignant tumor cases between January 2008 and December 2022 at West China Hospital, Sichuan University, China. The patients selected for this study should be histologically proven to have primary intracranial SFT/HPC who had surgery as the first therapy. We collected complete clinical data on these patients, including medical history, imaging, pathology, treatment and follow-up. Our study was approved by the Clinical Test and Biomedical Ethics Committee at West China Hospital, Sichuan University (reference number 2022-788). Consent forms were obtained from all participants.

Treatment

We retrospectively evaluated 42 patients with SFT/HPC treated with PORT by means of IMRT or SRS. Surgical resection methods include gross tumor resection (GTR) and subtotal tumor resection (STR). The treatment after surgical resection included IMRT and SRS. Moreover, disease recurrence occurred in 22 of these patients. Subsequently, different treatment methods were adopted in these 22 patients, including surgery alone, surgery combined with radiotherapy and others. There were only 4 patients with other treatment methods, of whom 3 cases received radiation alone and 1 case received symptomatic treatment. The symptomatic treatment included analgesia, intravenous infusion of 20% mannitol and glucocorticoids.

Twenty patients received fractionated IMRT after surgery with a median prescription dose of 60 Gy (range 40-63 Gy). IMRT is provided with 6 MV photons by a linear accelerator. The clinical target volume (CTV) was defined as the tumor cavity or residual mass plus 1-2 cm margin. An additional 3-5 mm was added to the CTV to plan the target volume (PTV). Twenty-two patients were treated with SRS gamma knife. The single dose at the tumor margin was 11-15 Gy, and the equal dose curve was 40%-50%. In this study, the choice mainly depended on the joint decision of the attending physician and patients.

Statistics

The characteristics of patients were described by descriptive statistics. Kaplan–Meier analysis was used to estimate OS, and the log rank test was used to evaluate the difference between groups. All statistical variables in univariate analysis were analyzed by the Cox proportional hazards model. OS was defined as the time from diagnosis to patient death. If less than 0.05, the p value was considered significant. All statistical analyses were performed using SPSS version 25.0 (IBM, USA).

Result

Participants

Data and clinical follow-up data were collected from a total of 42 patients with intracranial SFT/HPC diagnosed by PORT (Table 1). There were 25 men and 17 women. Supratentorial lesions accounted for 71.43%. There were 22 cases of pathological grade II (52.38%) and 20 cases of grade III (47.62%). Gross tumor resection (GTR) was performed in 22 cases (52.38%), and subtotal tumor resection (STR) was performed in 15 cases (35.71%). In Table 1, among these patients, a total of 22 patients achieved GTR, of whom 13 patients (56.52%) adopted PORT IMRT and 9 (47.37%) adopted PORT SRS. Among the STR group, 7 patients (30.43%) adopted PORT IMRT and 8 (42.11%) adopted PORT SRS. There were 5 patients with unknown resection types, including 3 patients with PORT IMRT (13.04%) and 2 patients with PORT SRS (10.53). There was no significant difference between the PORT groups.

Patients with SFT/HPC tend to relapse. Among them, 22 patients experienced relapse. Thirteen cases (30.95%) recurred once, 4 cases (9.52%) recurred twice, and 5 cases (11.90%) recurred more than three times. In contrast, SFT/HPC is not prone to distant metastasis. Only 1 patient had liver metastasis, and 3 patients had bone metastasis. All 42 patients accepted radiotherapy; among them, 20 patients used IMRT alone, and 22 patients used SRS alone.

The median follow-up time of all patients was 96 months. The difference between the two groups was related to the recurrence times. In addition, compared with the SRS group, the recurrence frequency of IMRT patients after PORT was significantly reduced ($p<0.001$) (Table 1). There was no significant difference in other clinical characteristics (including tumor resection range and tumor grade) between the PORT-IMRT group and the PORT-SRS group.

Histological findings

The pathological diagnosis of SFT/HPC largely depended on the immunohistochemical (IHC) staining results of CD99, CD34, Ki-67 and STAT6. STAT6 positive status is the basis of the new SFT/HPC classification. We performed STAT6 staining again in all patients who were diagnosed with HPC or SPF and underwent surgical resection and PORT. Therefore, all 42 patients included in our study confirmed STAT6 expression by IHC. After applying the 2016 WHO classification, they were reclassified as follows: 22 WHO grade II SFT/HPC patients and 20 WHO grade III SFT/HPC patients. The pathological specimens of all 42 patients were stained with hematoxylin & eosin (H&E), showing extensive vascularization and cellular tumors. The tumor cells were dense and uniform, with a large number of small vascular cavities and dense reticular fibers. The nuclear division, cell morphological heterogeneity and Ki67 percentage of high-grade HPC were more prominent (Figure 1).

Outcome data

The median DFS was 8.33 years for PORT IMRT patients and 3.04 years for PORT SRS patients. The 10-year DFS incidence was 46.0% in the PORT IMRT group and 27.5% in the SRS group. The results showed that DFS in patients with PORT IMRT was better than that in patients with PORT SRSs (Figure 2).

Among the 22 patients who relapsed, the median TTP of other patients was 1.25 years, of which 3 received radiotherapy alone and 1 received symptomatic treatment, while the median TTP of surgical patients and surgical combined with radiotherapy patients were 1.83 and 2.49 years, respectively ($p=0.035$). (Figure 3)

Main results

All 42 patients received surgery and postoperative radiotherapy. Among them, 22 patients had relapse, of whom 10 received simple surgery, 8 received surgery combined with radiotherapy again, 3 received simple radiotherapy, and 1 received symptomatic treatment such as mannitol and glucocorticoids, as shown in Table 2.

In Cox regression analysis, factors related to DFS in SFT/HPC patients receiving postoperative radiotherapy showed that

TABLE 1 Characteristics of patients with SFT/HPC receiving postoperative radiotherapy divided by radiotherapy technique.

	All(n=42)	IMRT (n=20)	SRS (n=22)	*P*
	No. (%)	No. (%)	No. (%)	
Age at diagnosis (years)				0.976
≤ 40	20 (47.62)	11 (47.83)	9 (47.37)	
> 40	22 (52.38)	12 (52.17)	10 (52.63)	
Sex				0.408
Male	25 (59.52)	15 (65.22)	10 (52.63)	
Female	17 (40.48)	8 (34.78)	9 (47.37)	
Pathology grade				0.976
II	22 (52.38)	12 (52.17)	10 (52.63)	
III	20 (47.62)	11 (47.83)	9 (47.37)	
Intracranial location				0.211
Supratentorial	30 (71.43)	19 (82.61)	11 (57.89)	
Infratentorial	6 (14.29)	2 (8.7)	4 (21.05)	
Both	6 (14.29)	2 (8.7)	4 (21.05)	
Extent of resection				0.629
GTR	22 (52.38)	13 (56.52)	9 (47.37)	
STR	15 (35.71)	7 (30.43)	8 (42.11)	
Unknown	5 (11.90)	3 (13.04)	2 (10.53)	
Recurrence times				< 0.001*
0	20 (47.62)	18 (78.26)	2 (10.53)	
1	13 (30.95)	3 (13.04)	10 (52.63)	
2	4 (9.52)	1 (4.35)	3 (15.79)	
≥ 3	5 (11.90)	1 (4.35)	4 (21.05)	
Liver metastasis				0.265
No	41 (97.62)	23 (100)	18 (94.74)	
Yes	1 (2.38)	0 (0)	1 (5.26)	
Bone metastasis				0.667
No	39 (92.86)	21 (91.3)	18 (94.74)	
Yes	3 (7.14)	2 (8.7)	1 (5.26)	
Other metastasis				0.890
No	40 (95.24)	22 (95.65)	18 (94.74)	
Yes	2 (4.76)	1 (4.35)	1 (5.26)	

IMRT, intensity-modulated radiotherapy; SRS, stereotactic radiosurgery; GTR, gross total resection; STR, subtotal resection.
*P values are statistically significant.

PORT IMRT obtained better DFS than PORT SRS (HR 14.17 [1.78-112.63], p=0.012). On the other hand, sex is a factor influencing DFS. We found that DFS was longer in women than in men (HR 0.24[0.08-0.79], p=0.019). Furthermore, tumor location, pathological grade and recurrence time had no significant relationship with DFS.

Moreover, among the 22 patients who relapsed, Cox regression analysed factors related to progression time in patients with recurrent SFT/HPC. We found no significant correlation with progression time (including age, sex, tumor location and pathological grade). The TTP results of surgery or surgery combined with radiotherapy were better than those of other treatments, including radiotherapy alone and symptomatic treatment (HR 10.93 [1.01–117.91], p=0.049).

Although the median TTP time of surgery combined with radiotherapy was not significantly different from that of surgery alone (HR 0.18 [0.02–1.64], p=0.129), the median TTP time of surgery combined with radiotherapy was longer than that of surgery alone (2.49 vs.1.83 years) (Table 3). However, there were limited number of patients in each group, and further validation is needed.

Discussion

SFT/HPC is a rare disease that is also very rare in the literature because no study has a large number of cases and satisfactory follow-up time. Some studies revealed that the range of tumor resection was crucial. Complete tumor resection plays a

10.3389/fonc.2022.994335

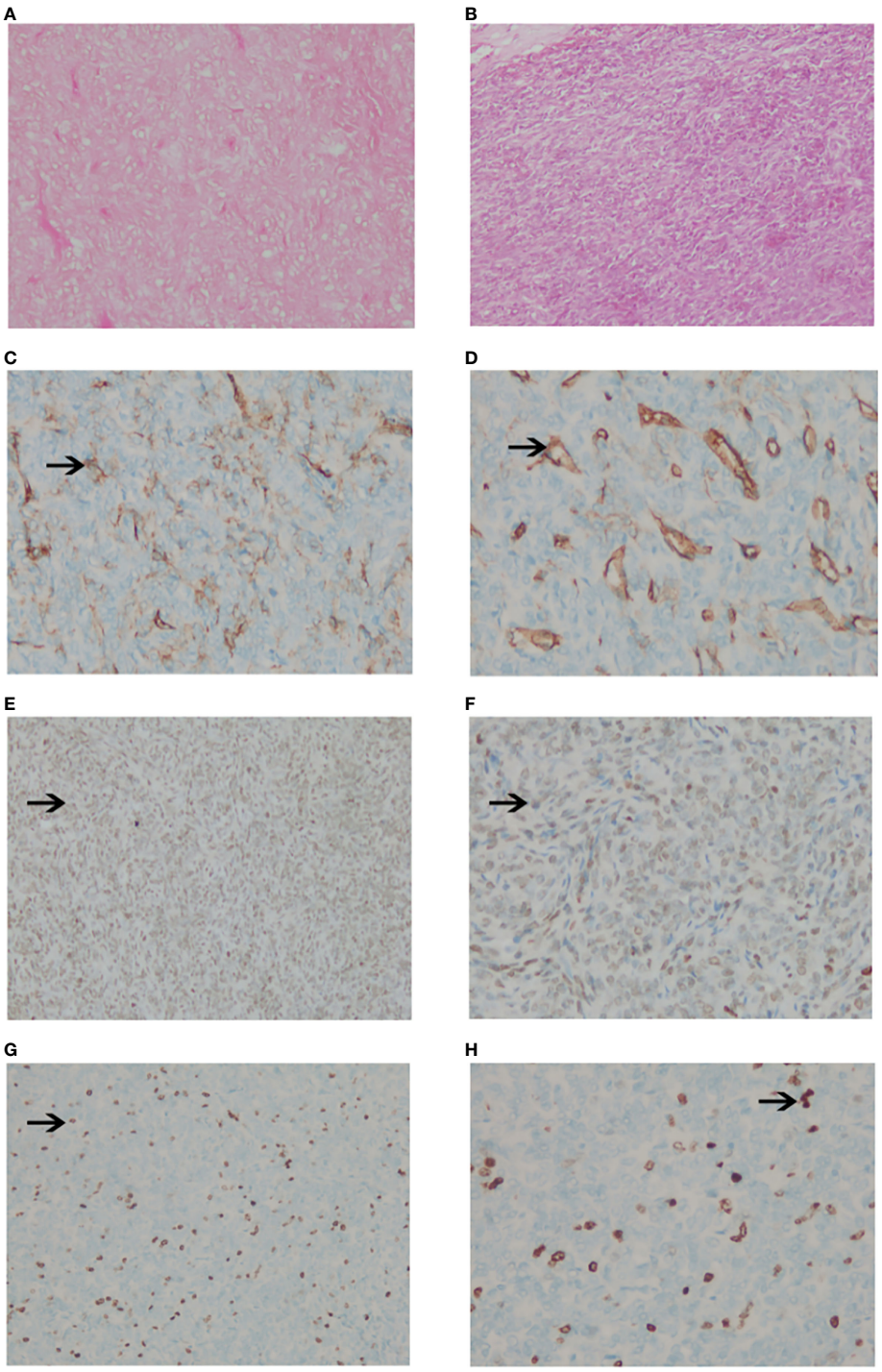

FIGURE 1
Pathological images of intracranial SPF/HPC. **(A, B)**. The tumor showed compact and uniform cells with a large number of small vascular cavities and compact reticular fibers with hematoxylin and eosin stain HEx100 **(A)** and ×200 **(B)**. **(C, D)**. The positive staining of CD34 was brown granular in the cytoplasm (×100) **(C)** and (×200) **(D)**. **(E, F)**. The positive staining of STAT6 was brown granular in the cytoplasm (×100) **(E)** and (×200) **(F)**. **(G, H)**. Negative staining of Ki67 in tumor cells (×100) **(G)** and (×200) **(H)**.

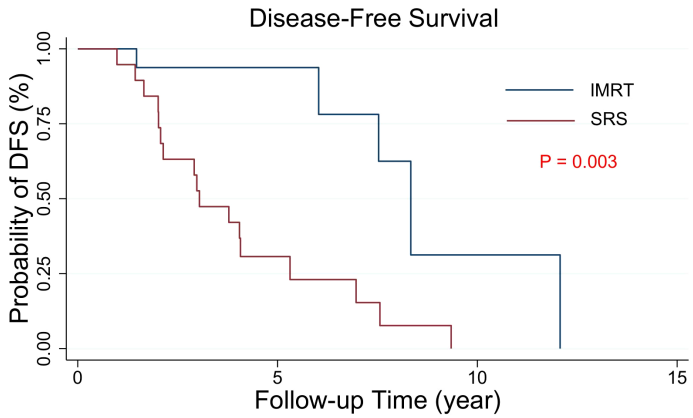

FIGURE 2
Kaplan–Meier estimates of the DFS curves in intracranial SFT/HPC patients with PORT. The DFS of the two groups with different radiotherapy techniques was significantly different (p = 0.003).

key role in local control and survival (13–15). There is no relevant recommendation on the choice of PORT technology. The choice mainly depends on the joint decision of the attending physician and patients in our study. The results showed that PORT IMRT was helpful to prolong DFS in patients compared with PORT SRS. In our study, surgical resection and PORT were both superior to other types of treatment strategies.

Brunori et al. found that, unlike meningiomas, the incidence rate of SFT/HPC was higher in men than in women (16). A meta-analysis of 523 patients showed that the incidence rate in male patients was higher than that in female patients under the age of 45, while the trend was the opposite for patients aged 45 and above (17). In our study, there was no significant difference between groups in age or sex at baseline.

In a previous study that included 191 patients, male patients with HPC had a recurrence risk more than 8 times that of female patients (18), while Damodaran et al. showed that male patients

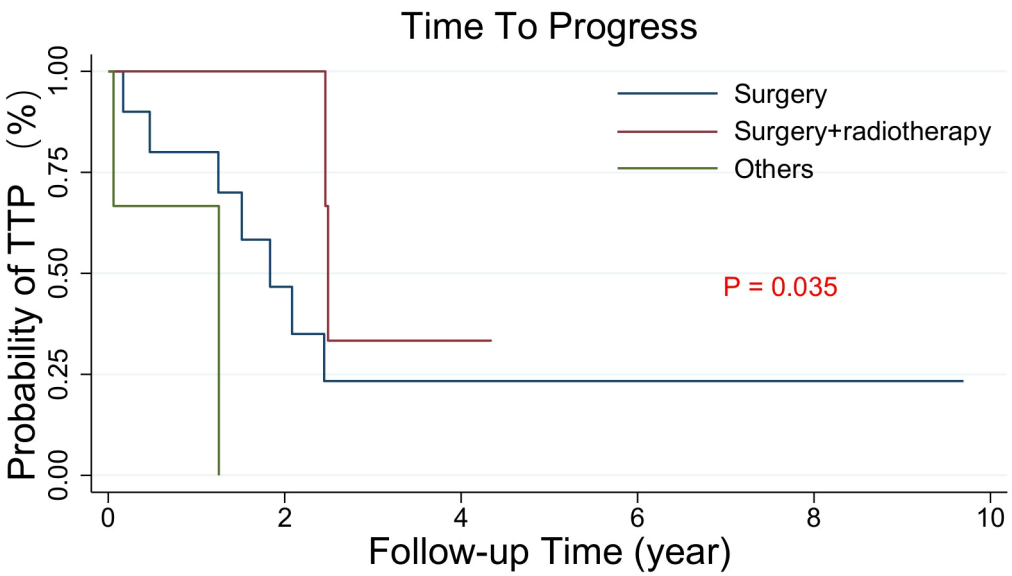

FIGURE 3
Kaplan–Meier estimated the TTP curves of 22 intracranial SFT/HPC patients with relapse after PORT who received different treatments again (Ssurgery, surgery plus radiotherapy, others). The others included 3 patients who received radiotherapy alone and 1 patient who received symptomatic treatment. The TTP of the surgery and surgery plus radiotherapy groups was similar, but different from that of the other groups (p = 0.003).

TABLE 2 COX regression analysis of factors associated with disease-free survival in patients with SFT/HPC receiving post-operative radiotherapy.

Variable	N of patient	N of events	Disease-Free Survival HR (95% CI)	p
Age	42	22	1.00 (0.96–1.06)	0.791
Treatment technique				
IMRT	20	5	1.00	
SRS	22	17	14.17 (1.78–112.63)	0.012*
Sex				
Male	25	12	1.00	
Female	17	10	0.24 (0.08–0.79)	0.019*
Tumor location				
Supratentorial	30	13	1.00	
Infratentorial	6	5	0.75 (0.19–2.96)	0.641
Both	6	4	0.61 (0.16–3.17)	0.647
Pathology grade				
II	22	12	1.00	0.180
III	20	10	0.40 (0.11–1.52)	
Recurrence times				
1	13	13	1.00	
2	4	4	2.52 (0.57–11.07)	0.729
≥ 3	5	5	1.10 (0.27–4.46)	0.896

N, number; HR, hazard ratio; CI, confidence interval; IMRT, intensity-modulated radiotherapy; SRS, stereotactic radiosurgery.
*P values are statistically significant.

had a higher survival rate (19). Our study found that compared with female patients, men had worse DFS (disease-free survival HR (95% CI) 0.24 (0.08 – 0.79), P = 0.019), which may be more related to the recurrence risk of male patients, but it is worth further investigation.

Since the World Health Organization merged SFT and HPC into a new disease called SFT/HPC in 2016, relevant research has been very limited. Furthermore, most of the previous studies on the role of PORT in intracranial HPC are based on single center analysis. The number of patients is limited, and the results are often inconsistent. Meta-analysis and research based on cumulative databases have been carried out to overcome the problems of small case series, but the results are also inconsistent (15, 20, 21). Although the role of PORT in patients with

TABLE 3 COX regression analysis of factors associated with time to progress in patients with recurrent SFT/HPC.

Variable	N of patient	N of events	Disease-Free Survival HR (95% CI)	p
Age	22	11	1.00 (0.90–1.12)	0.897
Treatment mode				
Surgery	10	7	1.00	
Surgery+radiotherapy	8	2	0.18 (0.02–1.64)	0.129
Others	4	2	10.93 (1.01–117.91)	0.049*
Sex				
Male	12	7	1.00	
Female	10	4	0.27 (0.05–1.47)	0.130
Tumor location				
Supratentorial	13	6	1.00	
Infratentorial	5	3	1.24 (0.15–10.08)	0.838
Both	4	2	0.74 (0.07–7.48)	0.796
Pathology grade				
II	12	6	1.00	0.635
III	10	5	0.66 (0.12–3.71)	

Others contain 3 cases received radiotherapy alone and 1 case received symptomatic treatment.
N, number; HR, hazard ratio; CI, confidence interval.
*P values are statistically significant.

SFT/HPC is unclear, the general consensus is that PORT is beneficial to patients undergoing surgery.

Some studies have found that compared with STR alone, PORT following STR can improve overall survival (OS) and recurrence-free survival (RFS) (20, 22, 23). Other studies have reported that PORT following GTR can also prolong OS (1, 10, 21, 24) or improve local control (25, 26). In contrast to the above, some authors report that PORT after GTR has no effect on survival (20, 27) or should not be used except for recurrent patients (28, 29). In our study, we found that different PORT strategies had a significant impact on disease-free survival. The median DFS of patients receiving PORT IMRT was 8.33 years, which was significantly different from that of patients receiving PORT SRS, which was 3.04 years (p=0.03). Compared with surgery, multivariate analysis showed that postoperative radiotherapy had no predictive effect on survival, but compared with other treatments, PORT and surgery were beneficial to DFS.

SRS has been used in patients with residual or recurrent intracranial HPC (9, 28, 30–34). It was reported that postoperative SRS can better control local tumors in patients with intracranial HPC (9). However, in our analysis, patients with SFT/HPC with SRS had poorer DFS than patients receiving IMRT. The tumor biological effective dose (BED) of the SRS and IMRT groups of SFT/HPC with an α/β ratio of 10 Gy was 33.6-41.6 Gy_{10} and 72 Gy_{10}, respectively. The biological effect of IMRT is much higher than that of SRS, which may lead to higher local control. This might be due to the higher BED inducing a greater local effect. There is no consensus on the optimal IMRT radiation dose for intracranial SFT/HPC. Some centers reported that the local control rate was improved when the tumor margin dose was not less than 60 Gy (26). In addition, the SRS radiotherapy plan mainly irradiates the tumor bed, while the IMRT plan irradiates the surrounding 1-2 cm CTV area in addition to the tumor bed. This difference in concept may lead to radiotherapy being superior to SRS in local control and recurrence prevention.

According to our analysis, PORT IMRT compared with PORT SRS seems to improve DFS. However, due to the limitations of this study, including the small sample size and its retrospective nature, caution should be taken in interpreting the current research results. To study the exact effect of PORT on local control and survival and the different effects between IMRT and SRS as PORT options, a multicenter randomized trial with a larger sample size is needed.

Conclusion

In this retrospective analysis, the DFS of PORT IMRT might be longer than that of SRS. This indicated that PORT IMRT radiotherapy technology was a feasible option. Moreover, TTP results of relapsed patients showed that, surgery and surgery combined with radiotherapy treatments have no significant difference on TTP in relapsed patients, but both of them were better than other treatments.

Data availability statement

The original contributions presented in the study are included in the article/Supplementary Material. Further inquiries can be directed to the corresponding author.

Ethics statement

The studies involving human participants were reviewed and approved by Clinical Test and Biomedical Ethics Committee at West China Hospital, Sichuan University. The ethics committee waived the requirement of written informed consent for participation.

Author contributions

Conceptualization: PA. Data curation: QG and YX. Project administration: PA. Supervision: PA. Writing-original draft: QG. Revision: QG and YX. All authors made a significant contribution to the work reported, gave final approval of the version to be published; have agreed on the journal to which the article has been submitted; and agree to be accountable for all aspects of the work.

Funding

This work was supported by National Natural Science Foundation of China (81902723), and 1·3·5 project for disciplines of excellence–Clinical Research Incubation Project, West China Hospital, Sichuan University (2021HXFH050).

Conflict of interest

The authors declare that the research was conducted in the absence of any commercial or financial relationships that could be construed as a potential conflict of interest.

Publisher's note

Supplementary material

The Supplementary Material for this article can be found online at: https://www.frontiersin.org/articles/10.3389/fonc.2022.994335/full#supplementary-material

References

1. Schiariti M, Goetz P, El-Maghraby H, Tailor J, Kitchen N. Hemangiopericytoma: Long-term outcome revisited. *J Neurosurg* (2011) 114:747–55. doi: 10.3171/2010.6.JNS091660

2. Guthrie BL, Ebersold MJ, Scheithauer BW, Shaw EG. Meningeal hemangiopericytoma: Histopathological features, treatment, and long-term follow-up of 44 cases. *Neurosurgery* (1989) 25:514–22. doi: 10.1227/00006123-198910000-00003

3. Gubian A, Ganau M, Cebula H, Todeschi J, Scibilia A, Noel G, et al. Intracranial solitary fibrous tumors: A heterogeneous entity with an uncertain clinical behavior. *World Neurosurg* (2019) 126:e48–56. doi: 10.1016/j.wneu.2019.01.142

4. Louis DN, Perry A, Reifenberger G, von Deimling A, Figarella-Branger D, Cavenee WK, et al. The 2016 world health organization classification of tumors of the central nervous system: A summary. *Acta Neuropathol* (2016) 131:803–20. doi: 10.1007/s00401-016-1545-1

5. Guan Y, Wang X, Wu N, Lu ZF, Shi QL, Wu JR. [Solitary fibrous tumor/hemangiopericytoma of central nervous system: a clinicopathological analysis of 60 cases]. *Zhonghua Bing Li Xue Za Zhi* (2019) 48:31–6. doi: 10.3760/cma.j.issn.0529-5807.2019.01.007

6. Sung KS, Moon JH, Kim EH, Kang S, Kim SH, Suh C, et al. Solitary fibrous tumor/hemangiopericytoma: Treatment results based on the 2016 WHO classification. *J Neurosurg* (2019) 130:418–25. doi: 10.3171/2017.9.JNS171057

7. Zeng L, Wang Y, Wang Y, Han L, Niu H, Zhang M, et al. Analyses of prognosis-related factors of intracranial solitary fibrous tumors and hemangiopericytomas help understand the relationship between the two sorts of tumors. *J Neuro-Oncol* (2017) 131:153–61. doi: 10.1007/s11060-016-2282-y

8. Kim BS, Kim Y, Kong D, Nam D, Lee J, Suh Y, et al. Clinical outcomes of intracranial solitary fibrous tumor and hemangiopericytoma: Analysis according to the 2016 WHO classification of central nervous system tumors. *J Neurosurg* (2018) 129:1384–96. doi: 10.3171/2017.7.JNS171226

9. Kano H, Niranjan A, Kondziolka D, Flickinger JC, Lunsford LD. Adjuvant stereotactic radiosurgery after resection of intracranial hemangiopericytomas. *Int J Radiat OncologyBiologyPhysics* (2008) 72:1333–9. doi: 10.1016/j.ijrobp.2008.03.024

10. Soyuer S, Chang EL, Selek U, McCutcheon IE, Maor MH. Intracranial meningeal hemangiopericytoma: The role of radiotherapy. *Cancer-Am Cancer Soc* (2004) 100:1491–7. doi: 10.1002/cncr.20109

11. Dufour H, Metellus P, Fuentes S, Murracciole X, Regis J, Figarella-Branger D, et al. Meningeal hemangiopericytoma: A retrospective study of 21 patients with special review of postoperative external radiotherapy. *Neurosurgery* (2001) 48:756–762, 762-763. doi: 10.1097/00006123-200104000-00011

12. Xiao J, Xu L, Ding Y, Wang W, Chen F, Zhou Y, et al. Does post-operative radiotherapy improve the treatment outcomes of intracranial hemangiopericytoma? a retrospective study. *BMC Cancer* (2021) 21:1628–36. doi: 10.1186/s12885-021-08594-x

13. Rutkowski MJ, Jian BJ, Bloch O, Chen C, Sughrue ME, Tihan T, et al. Intracranial hemangiopericytoma. *Cancer-Am Cancer Soc* (2012) 118:1628–36. doi: 10.1002/cncr.26411

14. Wang W, Zhang G, Zhang L, Li D, Wu Z, Zhang J. Long-term outcome and prognostic factors after repeated surgeries for intracranial hemangiopericytomas. *World Neurosurg* (2017) 107:495–505. doi: 10.1016/j.wneu.2017.08.027

15. Kumar N, Kumar R, Kapoor R, Ghoshal S, Kumar P, Salunke PS, et al. Intracranial meningeal hemangiopericytoma: 10 years experience of a tertiary care institute. *Acta Neurochir* (2012) 154:1647–51. doi: 10.1007/s00701-012-1442-x

16. Brunori A, Delitala A, Oddi G, Chiappetta F. Recent experience in the management of meningeal hemangiopericytomas. *Tumori* (1997) 83:856–61. doi: 10.1177/030089169708300516

17. Kabus D, Sidhu GS, Wieczorek RL, Choi HS. Metastatic meningioma. hemangiopericytoma or angioblastic meningioma? *Am J Surg Pathol* (1993) 17:1144–50. doi: 10.1097/00000478-199311000-00007

18. Fargen KM, Opalach KJ, Wakefield D, Jacob RP, Yachnis AT, Lister JR. The central nervous system solitary fibrous tumor: A review of clinical, imaging and pathologic findings among all reported cases from 1996 to 2010. *Clin Neurol Neurosurg* (2011) 113:703–10. doi: 10.1016/j.clineuro.2011.07.024

19. Arai N, Mizutani K, Takahashi S, Morimoto Y, Akiyama T, Horiguchi T, et al. Preoperative assessment of pathologic subtypes of meningioma and solitary fibrous Tumor/Hemangiopericytoma using dynamic computed tomography: A clinical research study. *World Neurosurg* (2018) 115:e676–80. doi: 10.1016/j.wneu.2018.04.132

20. Ghia AJ, Allen PK, Mahajan A, Penas-Prado M, McCutcheon IE, Brown PD. Intracranial hemangiopericytoma and the role of radiation therapy. *Neurosurgery* (2013) 72:203–9. doi: 10.1227/NEU.0b013e31827b9e68

21. Stessin AM, Sison C, Nieto J, Raifu M, Li B. The role of postoperative radiation therapy in the treatment of meningeal hemangiopericytoma–experience from the SEER database. *Int J Radiat OncologyBiologyPhysics* (2013) 85:784–90. doi: 10.1016/j.ijrobp.2012.05.042

22. Melone AG, D'Elia A, Santoro F, Salvati M, Delfini R, Cantore G, et al. Intracranial hemangiopericytoma–our experience in 30 years: A series of 43 cases and review of the literature. *World Neurosurg* (2014) 81:556–62. doi: 10.1016/j.wneu.2013.11.009

23. Staples JJ, Robinson RA, Wen BC, Hussey DH. Hemangiopericytoma–the role of radiotherapy. *Int J Radiat OncologyBiologyPhysics* (1990) 19:445–51. doi: 10.1016/0360-3016(90)90556-Y

24. Sonabend AM, Zacharia BE, Goldstein H, Bruce SS, Hershman D, Neugut AI., et al. The role for adjuvant radiotherapy in the treatment of hemangiopericytoma: A surveillance, epidemiology, and end results analysis. *J Neurosurg* (2014) 120:300–8. doi: 10.3171/2013.10.JNS13113

25. Kim JH, Jung HW, Kim YS, Kim CJ, Hwang SK, Paek SH, et al. Meningeal hemangiopericytomas: Long-term outcome and biological behavior. *Surg Neurol* (2003) 59:47–53, 53-54. doi: 10.1016/s0090-3019(02)00917-5

26. Ghia AJ, Chang EL, Allen PK, Mahajan A, Penas-Prado M, McCutcheon IE, et al. Intracranial hemangiopericytoma. *Neurosurgery* (2013) 73:624–31. doi: 10.1227/NEU.0000000000000064

27. Rutkowski MJ, Sughrue ME, Kane AJ, Aranda D, Mills SA, Barani IJ, et al. Predictors of mortality following treatment of intracranial hemangiopericytoma. *J Neurosurg* (2010) 113:333–9. doi: 10.3171/2010.3.JNS091882

28. Olson C, Yen C, Schlesinger D, Sheehan J. Radiosurgery for intracranial hemangiopericytomas: Outcomes after initial and repeat gamma knife surgery. *J Neurosurg* (2010) 112:133–9. doi: 10.3171/2009.3.JNS0923

29. Rutkowski MJ, Bloch O, Jian BJ, Chen C, Sughrue ME, Tihan T, et al. Management of recurrent intracranial hemangiopericytoma. *J Clin Neurosci* (2011) 18:1500–4. doi: 10.1016/j.jocn.2011.04.009

30. Payne BR, Prasad D, Steiner M, Steiner L. Gamma surgery for hemangiopericytomas. *Acta Neurochir* (2000) 142:527–37. doi: 10.1007/s007010050465

31. Ecker RD, Marsh WR, Pollock BE, Kurtkaya-Yapicier Ö, McClelland R, Scheithauer BW, et al. Hemangiopericytoma in the central nervous system: treatment, pathological features, and long-term follow up in 38 patients. *J Neurosurg* (2003) 98:1182–7. doi: 10.3171/jns.2003.98.6.1182

32. Sun S, Liu A, Wang C. Gamma knife radiosurgery for recurrent and residual meningeal hemangiopericytomas. *Stereot Funct Neuros* (2009) 87:114–9. doi: 10.1159/000202978

33. Cohen-Inbar O, Lee C, Mousavi SH, Kano H, Mathieu D, Meola A, et al. Stereotactic radiosurgery for intracranial hemangiopericytomas: a multicenter study. *J Neurosurg* (2017) 126:744–54. doi: 10.3171/2016.1.JNS152860

34. Kim JW, Kim DG, Chung H, Paek SH, Kim YH, Han JH, et al. Gamma knife stereotactic radiosurgery for intracranial hemangiopericytomas. *J Neuro-Oncol* (2010) 99:115–22. doi: 10.1007/s11060-010-0114-z

frontiers | Frontiers in Neurology

TYPE Case Report
PUBLISHED 17 October 2022
DOI 10.3389/fneur.2022.951054

OPEN ACCESS

EDITED BY
Ignazio Gaspare Vetrano,
IRCCS Carlo Besta Neurological Institute Foundation, Italy

REVIEWED BY
Enrico Gambatesa,
University of Milan, Italy
Lei Wu,
Zhejiang University, China

*CORRESPONDENCE
Yafeng Li
dr.yafengli@gmail.com

SPECIALTY SECTION
This article was submitted to Neuro-Oncology and Neurosurgical Oncology, a section of the journal Frontiers in Neurology

RECEIVED 23 May 2022
ACCEPTED 05 September 2022
PUBLISHED 17 October 2022

CITATION
Li Y, Xin X, Song W, Zhang X, Chen S, Wang Q, Li A and Li Y (2022) VHL syndrome without clear family history: A rare case report and literature review of Chinese patients.
Front. Neurol. 13:951054.
doi: 10.3389/fneur.2022.951054

VHL syndrome without clear family history: A rare case report and literature review of Chinese patients

Yaheng Li[1,2], Xiaohong Xin[3,4], Wenzhu Song[5], Xuan Zhang[6], Shengli Chen[6], Qian Wang[1,2], Aizhong Li[1,2] and Yafeng Li[1,2,3,4]*

[1]Department of Nephrology, Shanxi Provincial People's Hospital (Fifth Hospital) of Shanxi Medical University, Taiyuan, China, [2]Shanxi Provincial Key Laboratory of Kidney Disease, Taiyuan, China, [3]Core Laboratory, Shanxi Provincial People's Hospital (Fifth Hospital) of Shanxi University, Taiyuan, China, [4]Academy of Microbial Ecology, Shanxi Medical University, Taiyuan, China, [5]School of Public Health, Shanxi Medical University, Taiyuan, China, [6]Department of Neurosurgery, Shanxi Provincial People's Hospital (Fifth Hospital) of Shanxi Medical University, Taiyuan, China

Objective: To analyze the clinical manifestations and imaging features of a hospitalized patient with intermittent headache who was finally diagnosed with von Hippel–Lindau (VHL) syndrome and to perform whole-exon gene detection to improve the understanding of the diagnosis and treatment strategies of the disease.

Methods: A case of suspected VHL syndrome in Shanxi Provincial People's Hospital was analyzed. Proband DNA was also extracted for whole exome sequencing and screened for causative mutation sites, which were validated by Sanger sequencing. The literature about *VHL* gene mutations in Chinese patients in the past 10 years were also reviewed.

Results: There is a heterozygous mutation site c.499C > G on the *VHL* gene on the short arm of chromosome 3 of the patient, which is a missense mutation. The mutation results in the substitution of arginine with glycine at amino acid 167 of the encoded protein, which may be primarily responsible for the disease in the patient with VHL syndrome. However, the mutation did not occur in other family members.

Conclusion: Early recognition and treatment of VHL syndrome can be available with genetic testing technology. Strengthening the understanding of this complex genetic disease and improving the diagnostic rate of VHL syndrome are helpful for the precise treatment of patients with this disease, which may help prolong the survival time of patients to a certain extent and improve their quality of life.

KEYWORDS

Von Hippel–Lindaut syndrome, whole exome sequencing, gene mutation, literature, genetic testing

Introduction

Von Hippel–Lindau (VHL) syndrome is a rare clinical familial autosomal dominant tumor syndrome involving multiple body systems. Characteristic tumors in VHL syndrome include central nervous system hemangioblastomas (CNS HBs), renal cell carcinomas (RCCs), pheochromocytomas (PHEOs), and pancreatic cystadenomas. The most common tumors are retinal or CNS HBs (60–80%) and VHL syndrome-related renal lesions, which may range from simple cysts to multiple and renal cell carcinomas (RCC) (24–45%)(1). VHL syndrome-associated tumors frequently lose the function of the wild-type VHL allele in the process, which is known as loss of heterozygosity (LOH). According to statistics, about 1/36,000–53,000 people have *VHL* gene mutations (2). The majority of VHL syndrome affected have a positive family history, whereas sporadic cases of VHL syndrome with possible *de novo* mutations are rare (about 20%) and may occur during germ cell formation or early embryogenesis (3, 4). The patient with a mild clinical phenotype may be considered a sporadic case in this setting. Now, we present the genomic findings in a 50-year-old man with multiple CNS HBs, RCCs, and pancreatic neuroendocrine tumors (PNETs) diagnosed as suspected VHL syndrome without a clear positive family history. It was finally confirmed that the patient with VHL syndrome had a mutation site on the pathogenic gene *VHL*, which may be the cause of the disease.

Case presentation

Primary concerns and symptoms

A 50-year-old man presented with a 3-month history of frequent headaches associated with vomiting, nausea, and dizziness was admitted to the hospital for intermittent headache for more than half a month, aggravated with dizziness, nausea, and vomiting for 3 days. The patient had normal diet and sleep, normal urine and defecation, no significant weight loss, and no other discomforts.

Physical examination

The patient was generally in good condition. The systemic superficial lymph nodes were not palpable and enlarged, and the cardiopulmonary abdominal examination showed no abnormality. The patient had bilateral pupils of equal size and round, 2.5 cm in diameter, and sensitivity to light, and fundus examination showed no abnormality. Auxiliary examination: blood routine and urine routine were normal, fecal occult blood (-); serum amylase and urine amylase were normal; liver and kidney function, tumor markers, and coagulation showed no significant abnormality.

Laboratory tests

Contrast-enhanced MRI of the head and cervicothoracic spine (Figure 1) showed nodular enhancement in the lesions of the right cerebellar hemisphere, about 1.0 × 0.6 cm, with clear contour; the fourth ventricle crushed and narrowed, enlargement of the lateral and third ventricles; multiple nodular and tortuous linear enhancement lesions at C5-T2 of the spinal cord, with blurred contour; and round abnormal enhancement shadows of the C6 vertebral body, with blurred contour, which presented suspected radiological diagnosis of HB. Contrast-enhanced abdominal CT scan showed multiple low-density lesions of different sizes in the pancreas and partially fused; pancreatic duct dilatation; calcification of the pancreatic head; and after enhancement, a significant round enhanced nodule of about 1.1 cm in diameter was observed on the pancreatic head, which was considered a neuroendocrine tumor. Multiple round soft tissue density lesions were observed in both kidneys, the larger one was about 3.7 cm in diameter, and the enhancement in the arterial phase was higher than that in the adjacent renal cortex and renal cancer was considered. Multiple low-density lesions were observed in both kidneys, some of which were accompanied by septum and calcification, and multiple cysts were considered.

Operation and postoperative course

The patient underwent a large solid cerebellar cystic mass resection. Pathological diagnosis confirmed the lesion as HB.

After 2 years of follow-up, the condition of the patient was relieved and relatively stable.

Gene analysis

To detect the *VHL* gene mutation in the patient and his family, we collected peripheral blood from the patient, his daughter, his son, and his only younger brother. Exons of *VHL* gene were amplified from genomic DNA by polymerase chain reaction. Primer pairs are shown in Table 1.

Sanger DNA sequencing was performed and each exon was identified and confirmed by forward and reverse analysis. A heterozygous mutation (c.499 C > G) in exon 3 of *VHL* gene was detected in genomic DNA from a peripheral blood sample collected from the patient. This mutation was not detected in the peripheral blood of any other family member (Figure 2).

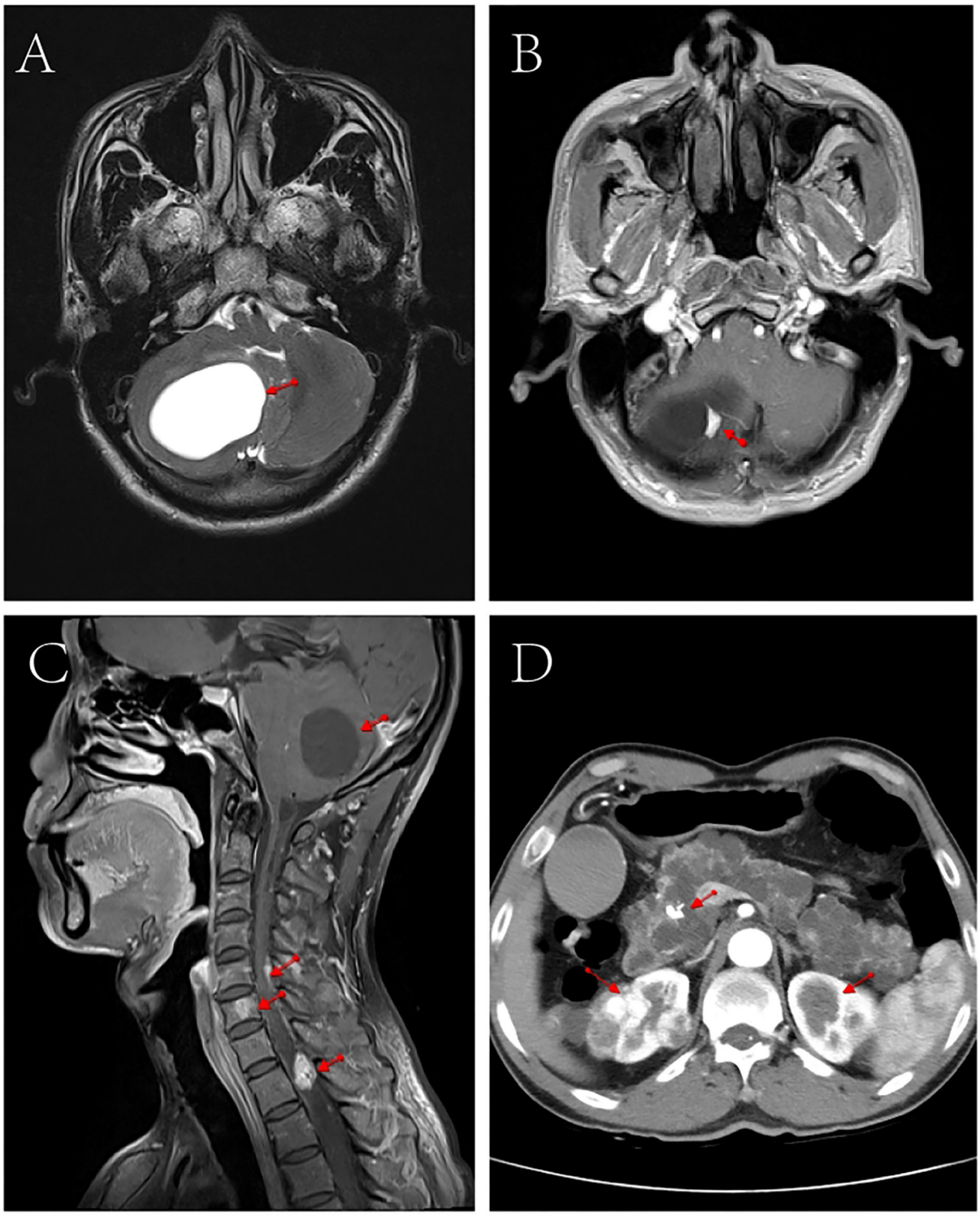

FIGURE 1
CT and MRI scan images of the patient. **(A)** Cranial MRI showed space- occupying lesions in the right cerebellar hemisphere. **(B)** Cranial enhanced MRI showed nodular enhancement in the right cerebellar hemisphere lesion (1.0 cm × 0.6 cm). **(C)** Contrast-enhanced MRI of the head and neck showed narrowing of the space in the fourth ventricle, multiple nodular and tortuous line-like enhancement in the spinal cord from C5 to T2, and round abnormal enhancement in the C6 vertebrae. **(D)** Abdominal enhanced CT showed multiple round soft tissue density lesions and multiple cystic low-density lesions in both kidneys, multiple low-density lesions of different sizes in the pancreas, and calcifications in the head of the pancreas.

After investigating the family history of the patient, it was found that his parents, grandparents, and maternal grandparents had died. The proband's father died of chronic heart disease, and the mother was healthy before her death; however, she died unexpectedly due to a car accident. None of them had a clear history of VHL syndrome-related disease.

Discussion

Von Hippel–Lindau syndrome is a progressive multisystem familial tumor syndrome characterized by phenotypically similar vascular tumors in the CNS and viscera. It's usually caused by germline mutations in the VHL tumor suppressor gene located on the short arm of chromosome 3 (3p25–26) (3).

At present, gene mutation types such as missense mutations, frameshift mutations, and in-frame deletions/insertional mutations have been detected in VHL syndrome patients. Depending on the presence or absence of PHEO, it can be divided into two clinical types. Patients with VHL type I have a low risk of developing PHEO (5). Most cases of VHL type I might be caused by missense mutations affecting the hydrophobic core of the protein, and the mutations lead to protein truncation, and partial gene deletions, which may be associated with VHL instability and high HIF activity, resulting in complete defects in protein function. In contrast, while type II is often subdivided into type IIA (with low risk of clear cell RCC (ccRCC)), type IIB (with increased risk of ccRCC), and IIC (pheochromocytoma only).VHL type II is often associated with missense mutations affecting the binding site of VHL protein (6).

Patients with VHL disease are subjected to an increased risk of developing HBs, which may affect 60–80% of patients (7). These tumors are usually multiple and no more than 50% of HBs will enlarge when followed up for more than 5 years of follow-up (8). The most common HBs are cerebellar or retinal capillary HBs, which can also occur in the spinal cord or brainstem (1). Although the tumor is benign, HB may also greatly increase morbidity and mortality in patients with VHL syndrome due to its significant impact on central nervous system architecture, and retinal edema, hemorrhage, detachment, and visual loss due to tumor exudation (9). The results of enhanced MRI examination of the cranial and cervicothoracic spine as well as CT examination showed that HB was present in the cerebellar of our reported case and cerebellar mass resection was performed. A fundus examination of the patient was not performed at that time because the eye examination showed normal vision, and the fundus examination showed no abnormality at the reexamination of the patient 1 year later. Since retinal capillary HB is the most common manifestation of VHL disease, the patient should be advised to examine the fundus at each reexamination to prevent the progression of the disease and delay in treatment. Multiple renal cysts were frequently found to coexist with RCC in 60% of patients with VHL syndrome (10), and CT diagnostic results showed renal carcinoma with multiple cysts, as described in our report. The frequency of RCC increases with age, with up to 70% of VHL patients developing RCC at age 60 and ultimately leading to death (11). About 10–20% of patients with VHL develop PHEO which can cause systemic paragangliomas. It has been associated with secondary hypertension or stroke and ultimately with death in 5% of patients with VHL syndrome (12). Approximately 35–70% of VHL syndrome patients have pancreatic manifestations (13), and as in this patient, CT examination showed multiple cysts of different sizes in the pancreas, with calcifications in the pancreatic head, which are considered neuroendocrine tumors. Although pancreatic neuroendocrine tumors are rarely responsible for morbidity and mortality, tumor transformation to malignancy or metastasis may result in a poor prognosis.

VHL syndrome can be clinically diagnosed in patients with positive family history and with central nervous system HB, RCC, or PHEO. Those without a family history must have two or more HBs or one HB and one visceral tumor (RCC, PHEO, or pancreatic tumor). In this case report, a 50-year-old patient was found to have multiple CNS HBs, multiple pancreatic and renal cysts, and RCC. Although the patient we reported had no clear family history of VHL syndrome, he still met the diagnostic criteria for VHL syndrome.

The c.499 C > G mutation of our reported case is expected to result in a mutation of amino acid 167 of the encoded protein from arginine to glycine. The arginine residue is highly conserved, with a moderate physicochemical difference between arginine and glycine. Algorithms developed to predict the impact of missense changes on protein structure and function (SIFT, PolyPhen-2, Align-GVGD) suggest that this variant may be disruptive, but these predictions require further confirmation by functional studies. Most patients with VHL syndrome inherit a germline mutation from one copy of the *VHL* gene in affected parents and one normally functioning wild-type allele from unaffected parents. Two studies have reported that the c.499 C > G mutation in *VHL* gene was associated with VHL syndrome (14, 15). However, one

TABLE 1 Primer sequences of exons of *VHL* gene.

Exons	Primer direction	Primer sequences
Exon 1	Forward	5′-GCGAAGACTACGGAGGTC-3′
	Reverse	5′-ATGTGTCCTGCCTCAAGG-3′
Exon 2	Forward	5′-CCTAGACCTCATGATCCGC-3′
	Reverse	5′-TTGGATAACGTGCCTGACATC-3′
Exon 3	Forward	5′-GGTAGTTGTTGGCAAAGCCTC-3′
	Reverse	5′-GAAACTAAGGAAGGAACCAGTCC-3′

patient had sporadic PHEO, and the other patient had a positive family history of VHL syndrome, but there was no PHEO and no clear family history of VHL syndrome in this patient. Due to the death of his parents and the absence of VHL syndrome-related conditions, first-generation sequencing verification showed that his asymptomatic younger brother, daughter, and son did not carry the heterozygous mutation. The heterozygous mutation may be *de novo*. In addition, we searched the relevant literature in PubMed, Web of Science, Embase, and other literature databases for the past 10 years (January 2012–August 2022) by using keywords such as "VHL syndrome", "VHL disease", "gene mutation", and "case report", and selected the literature with more complete clinical data for summary, and 26 cases met the conditions. We summarized the *VHL* gene mutation reports of the Chinese population in Table 2. Of the 26 Chinese patients we summarized, 16 cases belonged to VHL type I and 10 cases belonged to VHL type II, and the gene mutation types involved missense mutations, frameshift mutations, deletions and duplications of bases, and alternative splicing of introns. These mutations often occurred in the second half of exon 1 (14 cases), the first half of exon 2 (3 cases), and exon 3 (6 cases). The study has shown that *VHL* gene mutations often occurred at codons 75 and 82, cleavage sites between exon 2 and exon 3, and codons 157–189, and the hotspot of mutations was at codon 167 (CpG island region) (35). In addition to the common VHL syndrome-related neoplasms, our summary also showed that nonobstructive azoospermia, clear cell peritoneal epithelioid mesothelioma, and familial polycythemia type 2 were also associated with VHL syndrome, and the basic main treatment modalities were surgical resections or chemoradiotherapy. They are mainly based on point mutation and splice mutation. By detecting the characteristics of gene mutations and comprehensively considering family characteristics, clinical manifestations, and pathological diagnosis, it is helpful to deeply study the pathogenesis and pathogenic characteristics of VHL syndrome, thereby enriching the knowledge of this disease.

The protein pVHL encoded by the *VHL* gene is a master regulator of hypoxia-inducible factor-α (HIF-α). pVHL consists mainly of α domain and β domain. The α domain mainly forms a VCB-CUL2 complex with elongin B and elongin C, further constituting E3 ubiquitinase (36). The β domain mainly interacts with the hypoxia-inducible factor HIF-α (37). Under normoxic conditions, the VCB-CUL2 complex directly acts on HIF-α for polyubiquitination and degradation. Mutations in the *VHL* gene may reduce the degradation ability of E3 ubiquitinase, resulting in the accumulation of HIF-1α protein, which in turn activates key carcinogenic pathways such as angiogenesis, glycolysis, glucose transport, and erythropoiesis (38, 39). The upregulated cytokines such as vascular endothelial growth factor (VEGF), platelet-derived growth factor (PDGF), erythropoietin, and transforming growth factor alpha (TGF-α) (40, 41) may lead to abnormal proliferation

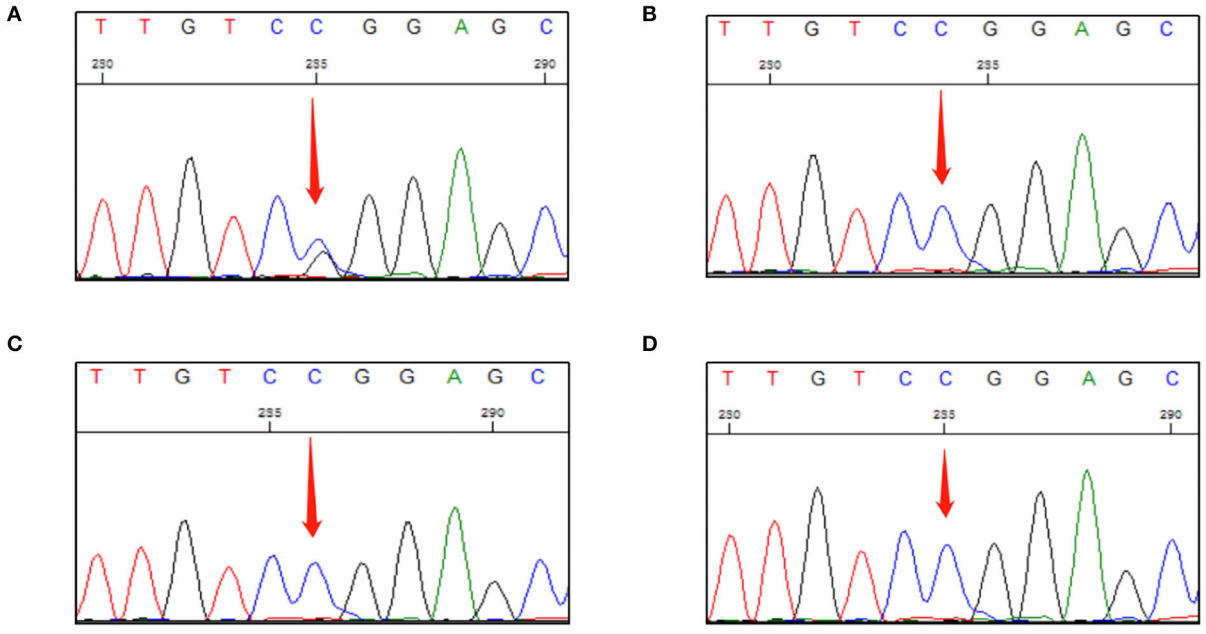

FIGURE 2
First-generation sequencing peak diagram. **(A)** The proband carried a heterozygous variant at the VHL c.499C>G site. **(B)** The proband's daughter did not carry this heterozygous mutation. **(C)** The proband's son did not carry this heterozygous mutation. **(D)** The proband's only younger brother did not carry this heterozygous mutation.

TABLE 2 *VHL* gene mutations in Chinese patients.

VHL mutations	Locations	Consequences	Clinical features	Therapies	VHL type	References
c.193 T > C	Exon 1	p.Ser65Pro	CNS HBs, multiple RCC, and pancreatic cysts	Surgical resections	VHL I	(16)
c.194 C > G	Exon 1	p.Ser65Trp	Multiple RCC and pancreatic cysts	Surgical resections	VHL I	(16)
c.208 G > A	Exon 1	p.Glu70Lys	CNS HBs, RCC, colorectal adenocarcinomas.	Surgical resection or radiation therapy	VHL I	(17)
c.227_229 del TCT	Exon 1	p.Phe76del	CNS HBs, solid kidney tumor	Surgical resection for HBs	VHL I	(18)
c.232 A > T	Exon 1	p.Asn78Tyr	Right RCC	Radical nephrectomy and molecular targeted drug Sunitinib	VHL I	(19)
c.233 A > G	Exon 1	p.Asn78Ser	Right PHEO and right RCC, bilateral epididymal cyst	Right PHEO and RCC resection and bilateral epididymal cyst resection	VHL IIB	(20)
c.239 G > T	Exon 1	p.Ser80Ile	RCC, HBs, PHEO	Surgical resection for HBs and PHEO	VHL IIB	(19)
c.254 dup T	Exon 1	p. Leu85fs	Peritoneal epithelioid mesothelioma of clear cell type	Cytoreductive surgery (CRS) and hyperthermic intraperitoneal chemotherapy (HIPEC) operation	VHL I	(21)
c.256 C> T	Exon 1	p.Pro86Ser	CNS HBs, RCC, PHEOs, multiple cysts in the pancreas and liver	Tumor resections	VHL IIB	(22)
c. 257 C > T	Exon 1	p.Pro86Leu	Optic nerve HB, pancreatic cysts	Surgical resection for HB	VHL I	(23)
c.262 T > C	Exon 1	p.Try88Arg	RCC, nonobstructive azoospermia, bilateral renal cysts, and pancreatic cysts	Not described	VHL I	(24)
c.264 G > A	Exon 1	p.Trp88Trp	PHEOs, RCC	Surgical resections	VHL IIB	(25)
c.293 A > G	Exon 1	p.Try98Cys	PHEOs	Not described	VHL IIC	(19)
327 del C	Exon 1	p.Gly39Alafs*26	CNS HBs	Surgical resection for HBs	VHL I	(26)
c.340+5 G > C	Intron 1	Abnormal splicing	Cerebral HB, PHEOs, liver cysts	Surgical resections	VHL IIA	(22)
c.349 T > A	Exon 2	p.Trp117Arg	Cerebellar and retinal HBs	Surgical resection for HBs	VHL I	(27)
c.386 T >G	Exon 2	p.Leu129Pro	PHEO, PNET	Tumor resections	VHL IIA	(28)
c.451 A > T	Exon 2	p.Ile151Phe	Cyst-solitary papilloma, pancreatic cysts, RCC, Polycystic kidney, cystadenoma in the bilateral adnexal nodes	Multiple tumor resections, Clarithromycin	VHL I	(29)
c.464T > A	Exon 3	p.Val155Glu	CNS HBs, PHEOs	Surgical resection for HBs	VHL I	(30)

(Continued)

TABLE 2 (Continued)

VHL mutations	Locations	Consequences	Clinical features	Therapies	VHL type	References
c.464-1G > C	Intron 2	Abnormal splicing	CNS HBs, multiple cysts in the pancreas and kidneys	surgical resection for cerebellar HBs	VHL I	(31)
c.464-2A > G	Intron 2	Abnormal splicing	Multiple HBs, RCC, and multiple renal and pancreatic cysts	surgical resection for HBs in the bilateral cerebellum	VHL I	(31)
c.482 G > A	Exon 3	p.Arg161Gln	Right PHEO	Right PHEO resection	VHL-IIB	(20)
c.499 C > T	Exon 3	p.Arg167Trp	Bilateral renal tumor, bilateral renal cyst CNS HBs, RCC, PHEO	Surgical resections	VHL IIB	(32)
c.500G > A	Exon 3	p.Arg167Gln	PHEO and left renal cyst	Laparoscopic surgery	VHL-II	(19)
c530 536delGACTGGA	Exon 3	P.Arg177fs	HB in the cerebellum, bilateral polycystic kidney disease, multiple hepatic cysts, and pulmonary nodules	Ventriculoperitoneal shunt and postoperative radiotherapy	VHL-I	(33)
c.598C > T	Exon 3	p.Arg200Trp	Familial erythrocytosis type 2	Not described	VHL I	(34)

of tumor cells, inhibit cell apoptosis, and promote the tumor occurrence. The c.499 C > G mutation we reported is located in the α domain and may affect the binding of VHL to elongin C and affect a series of downstream biological responses (42, 43), leading to the onset and progression of disease.

The treatment of VHL syndrome is mainly based on the surgical treatment of lesions in various organ systems to remove the lesion and relieve symptoms, but it cannot fundamentally improve the prognosis. With precision medicine and sequencing technology springing up, the diagnosis and treatment of VHL syndrome have gradually opened a new chapter. The use of drugs that block the pro-angiogenesis of VEGF signal transduction pathway can block the occurrence and development of the disease to a certain extent. Studies have shown that the use of anti-VEGF drug bevacizumab in patients with metastatic renal cancer can improve the survival rate of patients to some extent (44). However, bevacizumab may have a moderate impact on retinal HBs (45, 46). The use of the receptor tyrosine kinase inhibitor sunitinib can reduce the volume of PHEOs as well as renal and pancreatic tumors (47). In 2018, Zhang et al. discovered a new *VHL* target ZHX2 (zinc fingers and homeoboxes 2). ZHX2 may regulate nuclear factor B (NF-KB) signaling in VHL-deficient tissues to promote RCC tumorigenesis, potentially becoming a new target for the treatment of RCC (48). In 2021, the US FDA approved HIF-2α inhibitor Belzutifan (Welireg) for the treatment of CNS HBs, RCCs, or PNET associated with VHL syndrome that does not require immediate surgery (49). With the approval of Belzutifan, the evolving technology of next-generation sequencing (NGS) may power impetus for the precision medicine of VHL syndrome-related tumors (50). With the continuous deepening of the clinical treatment of *VHL* gene and VHL syndrome, surgical treatment, targeted drug therapy, gene therapy, and other methods will enable patients with VHL syndrome to obtain a wider treatment space and more effective symptomatic treatment options.

The *VHL* gene mutation c.499 C > G in the patient we reported had no clear family history of VHL syndrome. Additionally, this patient had only a mild clinical phenotype of VHL disease. Even if there is no evidence of other VHL-related lesions or a positive family history of VHL disease, clinicians should consider the possibility of sporadic VHL in such patients. Attention should be paid to differential diagnosis and regular review to try to avoid reducing misdiagnosis and missed diagnoses. Meanwhile, molecular genetic testing of such patients and family members should be considered to help identify at-risk family members to improve diagnostic certainty and advance appropriate treatment and prevent disease progression. To improve the treatment of tumors such as CNS HBs and RCCs associated with VHL syndrome, it is necessary to continuously study new pathogenesis, discover new molecular targets, and ultimately improve the quality of life of patients.

Data availability statement

The datasets presented in this article are not readily available because of ethical and privacy restrictions. Requests to access the datasets should be directed to the corresponding author.

Ethics statement

The studies involving human participants were reviewed and approved by Ethics Committee of Shanxi Provincial People's Hospital. The patients/participants provided their written informed consent to participate in this study. Written informed consent was obtained from the individual(s) for the publication of any potentially identifiable images or data included in this article.

Author contributions

YahL and XX were responsible for the drafting of the manuscript. WS helped polish the manuscript. XZ and SC offered precious knowledge on medical imaging. QW and AL were responsible for acquisition of the relevant clinical data. YafL was responsible for the conception and design of the article. All authors contributed to the manuscript and approved the submitted version.

Conflict of interest

The authors declare that the research was conducted in the absence of any commercial or financial relationships that could be construed as a potential conflict of interest.

Publisher's note

All claims expressed in this article are solely those of the authors and do not necessarily represent those of their affiliated organizations, or those of the publisher, the editors and the reviewers. Any product that may be evaluated in this article, or claim that may be made by its manufacturer, is not guaranteed or endorsed by the publisher.

References

1. Chittiboina P, Lonser RR. Von Hippel-Lindau disease. *Handb Clin Neurol.* (2015) 132:139–56. doi: 10.1016/B978-0-444-62702-5.00010-X

2. Chou A, Toon C, Pickett J, Gill AJ. Von Hippel-Lindau syndrome. *Front Horm Res.* (2013) 41:30–49. doi: 10.1159/000345668

3. Ben-Skowronek I, Kozaczuk S. Von Hippel-Lindau syndrome. *Horm Res Paediatr.* (2015) 84:145–52. doi: 10.1159/000431323

4. Murro V, Lippera M, Mucciolo DP, Canu L, Ercolino T, De Filpo G, et al. Outcome and genetic analysis of patients affected by retinal capillary hemangioblastoma in Von Hippel Lindau syndrome. *Mol Vis.* (2021) 27:542–54. Available online at: http://www.molvis.org/molvis/v27/542

5. Maher ER, Webster AR, Richards FM, Green JS, Crossey PA, Payne SJ, et al. Phenotypic expression in Von Hippel-Lindau disease: correlations with germline Vhl gene mutations. *J Med Genet.* (1996) 33:328–32. doi: 10.1136/jmg.33.4.328

6. Varshney N, Kebede AA, Owusu-Dapaah H, Lather J, Kaushik M, Bhullar JS, et al. Review of Von Hippel-Lindau syndrome. *J Kidney Cancer VHL.* (2017) 4:20–9. doi: 10.15586/jkcvhl.2017.88

7. Cassol C, Mete O. Endocrine manifestations of Von Hippel-Lindau disease. *Arch Pathol Lab Med.* (2015) 139:263–8. doi: 10.5858/arpa.2013-0520-RS

8. Shanbhogue KP, Hoch M, Fatterpaker G, Chandarana H. Von Hippel-Lindau Disease: review of genetics and imaging. *Radiol Clin North Am.* (2016) 54:409–22. doi: 10.1016/j.rcl.2015.12.004

9. Lonser RR, Butman JA, Huntoon K, Asthagiri AR, Wu T, Bakhtian KD, et al. Prospective natural history study of central nervous system hemangioblastomas in Von Hippel-Lindau disease. *J Neurosurg.* (2014) 120:1055–62. doi: 10.3171/2014.1.JNS131431

10. Ganeshan D, Menias CO, Pickhardt PJ, Sandrasegaran K, Lubner MG, Ramalingam P, et al. Tumors in von hippel-lindau syndrome: From head to toe -comprehensive state-of-the-art review. *Radiographics.* (2018) 38:849–66. doi: 10.1148/rg.2018170156

11. Maher ER, Yates JR, Harries R, Benjamin C, Harris R, Moore AT, et al. Clinical features and natural history of Von Hippel-Lindau disease. *Q J Med.* (1990) 77:1151–63. doi: 10.1093/qjmed/77.2.1151

12. Opocher G, Conton P, Schiavi F, Macino B, Mantero F. Pheochromocytoma in Von Hippel-Lindau disease and neurofibromatosis type 1. *Fam Cancer.* (2005) 4:13–6. doi: 10.1007/s10689-004-6128-y

13. Maher ER, Neumann HP, Richard S. Von Hippel-Lindau disease: a clinical and scientific review. *Eur J Hum Genet.* (2011) 19:617–23. doi: 10.1038/ejhg.2010.175

14. Gergics P, Patocs A, Toth M, Igaz P, Szucs N, Liko I, et al. Germline Vhl gene mutations in hungarian families with Von Hippel-Lindau disease and patients with apparently sporadic unilateral pheochromocytomas. *Eur J Endocrinol.* (2009) 161:495–502. doi: 10.1530/EJE-09-0399

15. Crossey PA, Richards FM, Foster K, Green JS, Prowse A, Latif F, et al. Identification of intragenic mutations in the Von Hippel-Lindau disease tumour suppressor gene and correlation with disease phenotype. *Hum Mol Genet.* (1994) 3:1303–8. doi: 10.1093/hmg/3.8.1303

16. Ma X, Tan Z, Zhang Q, Ma K, Xiao J, Wang X, et al. Vhl Ser65 mutations enhance Hif2α signaling and promote epithelial-mesenchymal transition of renal cancer cells. *Cell Biosci.* (2022) 12:52. doi: 10.1186/s13578-022-00790-x

17. Heo SJ, Lee CK, Hahn KY, Kim G, Hur H, Choi SH, et al. A case of Von Hippel-Lindau disease with colorectal adenocarcinoma, renal cell carcinoma and hemangioblastomas. *Cancer Res Treat.* (2016) 48:409–14. doi: 10.4143/crt.2014.299

18. Jia D, Tang B, Shi Y, Wang J, Sun Z, Chen Z, et al. A deletion mutation of the Vhl gene associated with a patient with sporadic Von Hippel-Lindau disease. *J Clin Neurosci.* (2013) 20:842–7. doi: 10.1016/j.jocn.2012.06.013

19. Liu Q, Yuan G, Tong D, Liu G, Yi Y, Zhang J, et al. Novel genotype-phenotype correlations in five Chinese families with Von Hippel-Lindau disease. *Endocr Connect.* (2018) 7:870–8. doi: 10.1530/EC-18-0167

20. Lin G, Zhao Y, Zhang Z, Zhang H. Clinical diagnosis, treatment and screening of the Vhl gene in three Von Hippel-Lindau disease pedigrees. *Exp Ther Med.* (2020) 20:1237–44. doi: 10.3892/etm.2020.8829

21. Du XM, Wei YP, Gao Y, Li Z, Zhang JM, Chang H, et al. Clinicopathological characteristics of primary peritoneal epithelioid mesothelioma of clear cell type: a case report. *Medicine.* (2021) 100:e25264. doi: 10.1097/MD.0000000000025264

22. Yuan P, Sun Q, Liang H, Wang W, Li L, Wang Y, et al. Germline mutations in the Vhl gene associated with 3 different renal lesions in a

Chinese Von Hippel-Lindau disease family. *Cancer Biol Ther.* (2016) 17:599–603. doi: 10.1080/15384047.2016.1167293

23. Yang B, Li Z, Wang Y, Zhang C, Zhang Z, Zhang X. Central nervous system hemangioblastoma in a pediatric patient associated with Von Hippel-Lindau disease: a case report and literature review. *Front Oncol.* (2021) 11:683021. doi: 10.3389/fonc.2021.683021

24. Man Y, Shang X, Liu C, Zhang W, Huang Q, Ma S, et al. Whole-exome sequencing identifies the Vhl mutation (C262t ≫ C, PTry88arg) in non-obstructive azoospermia-associated cystic renal cell carcinoma. *Curr Oncol.* (2022) 29:2376–84. doi: 10.3390/curroncol29040192

25. Zhang M, Wang J, Jiang J, Zhan X, Ling Y, Lu Z, et al. Von Hippel-Lindau Disease Type 2 in a Chinese Family with a Vhl PW88x truncation. *Endocrine.* (2015) 48:83–8. doi: 10.1007/s12020-014-0368-x

26. Fu XM, Zhao SL, Gui JC, Jiang YQ, Shen MN, Su DL, et al. A novel mutation links to Von Hippel-Lindau syndrome in a Chinese family with hemangioblastoma. *Genet Mol Res.* (2015) 14:4513–20. doi: 10.4238/2015.May.4.9

27. Wu X, Chen L, Zhang Y, Xie H, Xue M, Wang Y, et al. A novel mutation in the Vhl gene in a Chinese family with Von Hippel-Lindau Disease. *BMC Med Genet.* (2018) 19:204. doi: 10.1186/s12881-018-0716-4

28. Dagdeviren Çakir A, Turan H, Aykut A, Durmaz A, Ercan O, Evliyaoglu O. Two childhood pheochromocytoma cases due to Von Hippel-Lindau Disease, one associated with pancreatic neuroendocrine tumor: a very rare manifestation. *J Clin Res Pediatr Endocrinol.* (2018) 10:179–82. doi: 10.4274/jcrpe.5078

29. Ma X, Jing Y, Liu Y, Yu L. Effect of clarithromycin in Von Hippel-Lindau syndrome: a case report. *J Int Med Res.* (2019) 47:973–81. doi: 10.1177/0300060518792368

30. Lu Y, Lu J, Liu Q, Niu J, Zhang SM, Wu QY, et al. A C464t>a mutation in Vhl gene in a Chinese family with Vhl syndrome. *J Neurooncol.* (2013) 111:313–8. doi: 10.1007/s11060-012-1015-0

31. Liu Z, Zhou J, Li L, Yi Z, Lu R, Li C, et al. Intronic mutation of the Vhl gene associated with central nervous system hemangioblastomas in two Chinese families with Von Hippel-Lindau disease: case report. *BMC Med Genet.* (2020) 21:191. doi: 10.1186/s12881-020-01126-7

32. Zhang J, Ma J, Du X, Wu D, Ai H, Bai J, et al. Clinical and genetic investigation of a multi-generational chinese family afflicted with Von Hippel-Lindau disease. *Chin Med J.* (2015) 128:32–8. doi: 10.4103/0366-6999.147802

33. Wang J, Cao W, Wang Z, Zhu H. Novel gene mutation in Von Hippel-Lindau disease - a report of two cases. *BMC Med Genet.* (2019) 20:194. doi: 10.1186/s12881-019-0930-8

34. Zhang W, Bao S, Jiang LJ, Ma YP. A case of familial erythrocytosis type 2 caused by Vhl gene mutation. *Zhonghua Xue Ye Xue Za Zhi.* (2020) 41:1047–9.

35. Kolomeyer AM, Eller AW, Martel JN. Spontaneous resolution of macular epiretinal membranes after fluorescein potentiated argon laser treatment of Von Hippel-Lindau associated retinal hemangiomas: case report and review of literature. *Retin Cases Brief Rep.* (2016) 10:145–50. doi: 10.1097/ICB.0000000000000206

36. Hudler P, Urbancic M. The role of Vhl in the development of Von Hippel-Lindau disease and erythrocytosis. *Genes.* (2022) 13:362. doi: 10.3390/genes13020362

37. Kaelin WG Jr. Molecular basis of the Vhl hereditary cancer syndrome. *Nat Rev Cancer.* (2002) 2:673–82. doi: 10.1038/nrc885

38. Gossage L, Eisen T, Maher ER. Vhl, the story of a tumour suppressor gene. *Nat Rev Cancer.* (2015) 15:55–64. doi: 10.1038/nrc3844

39. He W, Batty-Stuart S, Lee JE, Ohh M. Hif-1α hydroxyprolines modulate oxygen-dependent protein stability via single Vhl interface with comparable effect on ubiquitination rate. *J Mol Biol.* (2021) 433:167244. doi: 10.1016/j.jmb.2021.167244

40. Maher ER. Von Hippel-Lindau disease. *Curr Mol Med.* (2004) 4:833–42. doi: 10.2174/1566524043359827

41. Gläsker S, Vergauwen E, Koch CA, Kutikov A, Vortmeyer AO. Von Hippel-Lindau disease: current challenges and future prospects. *Onco Targets Ther.* (2020) 13:5669–90. doi: 10.2147/OTT.S190753

42. Hacker KE, Lee CM, Rathmell WK. Vhl type 2b mutations retain Vbc complex form and function. *PLoS ONE.* (2008) 3:e3801. doi: 10.1371/journal.pone.0003801

43. Jung YS, Lee SJ, Yoon MH, Ha NC, Park BJ. Estrogen receptor ? is a novel target of the Von Hippel-Lindau protein and is responsible for the proliferation of Vhl-deficient cells under hypoxic conditions. *Cell Cycle.* (2012) 11:4462–73. doi: 10.4161/cc.22794

44. Semenza GL. Targeting Hif-1 for cancer therapy. *Nat Rev Cancer.* (2003) 3:721–32. doi: 10.1038/nrc1187

45. Tano R, Kakurai K, Sakurai T, Fujiwara R, Mano T, Maeno T. Intravitreal bevacizumab (avastin) combined with vitrectomy for recurrences of proliferative vitreoretinopathy in Von Hippel-Lindau disease. *Acta Ophthalmol.* (2012) 90:e157–8. doi: 10.1111/j.1755-3768.2011.02108.x

46. Hrisomalos FN, Maturi RK, Pata V. Long-term use of intravitreal bevacizumab (avastin) for the treatment of Von Hippel-Lindau associated retinal hemangioblastomas. *Open Ophthalmol J.* (2010) 4:66–9. doi: 10.2174/1874364101004010066

47. Jimenez C, Cabanillas ME, Santarpia L, Jonasch E, Kyle KL, Lano EA, et al. Use of the tyrosine kinase inhibitor sunitinib in a patient with Von Hippel-Lindau disease: targeting angiogenic factors in pheochromocytoma and other Von Hippel-Lindau disease-related tumors. *J Clin Endocrinol Metab.* (2009) 94:386–91. doi: 10.1210/jc.2008-1972

48. Sanchez DJ, Simon MC. transcriptional control of kidney cancer. *Science.* (2018) 361:226–7. doi: 10.1126/science.aau4385

49. Deeks ED. Belzutifan: first approval. *Drugs.* (2021) 81:1921–7. doi: 10.1007/s40265-021-01606-x

50. Cao J, Chen L, Li H, Chen H, Yao J, Mu S, et al. An accurate and comprehensive clinical sequencing assay for cancer targeted and immunotherapies. *Oncologist.* (2019) 24:e1294–e302. doi: 10.1634/theoncologist.2019-0236

frontiers | Frontiers in Oncology

TYPE Original Research
PUBLISHED 24 October 2022
DOI 10.3389/fonc.2022.1001959

OPEN ACCESS

EDITED BY
Laura Gatti,
IRCCS Carlo Besta Neurological Institute Foundation, Italy

REVIEWED BY
Debajyoti Chatterjee,
Post Graduate Institute of Medical Education and Research (PGIMER), India
Junya Fujimura,
Juntendo University, Japan

*CORRESPONDENCE
Wenbin Guan
xkl17211220116@163.com

†These authors contributed equally to this work and share first authorship

SPECIALTY SECTION
This article was submitted to Neuro-Oncology and Neurosurgical Oncology, a section of the journal Frontiers in Oncology

RECEIVED 24 July 2022
ACCEPTED 07 October 2022
PUBLISHED 24 October 2022

CITATION
Xu K, Sun Z, Wang L and Guan W (2022) Embryonal tumors with multilayered rosettes, *C19MC*-altered or not elsewhere classified: Clinicopathological characteristics, prognostic factors, and outcomes of 17 children from 2018 to 2022. *Front. Oncol.* 12:1001959. doi: 10.3389/fonc.2022.1001959

Embryonal tumors with multilayered rosettes, *C19MC*-altered or not elsewhere classified: Clinicopathological characteristics, prognostic factors, and outcomes of 17 children from 2018 to 2022

Kailun Xu[1†], Zhaoyun Sun[2†], Lifeng Wang[1] and Wenbin Guan[1*]

[1]Department of Pathology, Xin Hua Hospital Affiliated to Shanghai Jiao Tong University School of Medicine, Shanghai, China, [2]Department of Cardiothoracic Surgery, Second Clinical Medical College, Nanjing Medical University, Nanjing, China

Objective: Embryonal tumors with multilayered rosettes (ETMRs) are a histologically heterogeneous entity and gather embryonal tumors with abundant neuropil and true rosettes (ETANTRs), ependymoblastoma, and medulloepithelioma. ETMRs are highly aggressive and associated with poorer clinical courses. However, cases of this entity are rare, and advances in molecular genetics and therapy are minor. The purpose of our study was to retrospectively analyze the clinical, pathological features, and prognostic factors of ETMRs.

Methods: Our cohort consisted of 17 patients diagnosed with ETMRs in our hospital from 2018 to 2022, and two of them were lost to follow-up. Clinical data were retrieved, and immunohistochemistry and genetic analyses were performed.

Results: Among 17 cases, 16 were ETANTRs, and one was medulloepithelioma. Morphologically, tumor cells of ETANTRs could transform into anaplasia and lose the biphasic architecture during tumor progression. Immunohistochemistry of LIN28A revealed positive expression in 17 cases, and the expression of LIN28A was more intense and diffuse in the recurrent lesions than in primaries. The increased *N-MYC* copy numbers were detected in the primary tumor and recurrence of patient 8. Moreover, the incidence of metastatic disease was 100% in patients aged > 4 years and 18% in the younger group. For patients receiving chemotherapy, the median overall survival time was 7.4 months, while that of those who didn't receive it was 1.2 months. Nevertheless, surgical approaches, radiotherapy, age at presentation, gender, tumor location, and metastatic status were not associated with independent prognosis.

Conclusion: ETANTR might not present as the typical morphologies during tumor progression, so analyses of *C19MC* amplification and Lin28A antibody

are indispensable for diagnosing ETMRs accurately. Children aged > 4 years tend to have a higher rate of metastasis in ETMRs. Chemotherapy is the only prognostic factor for ETMRs patients with a favorable prognosis. The biological nature and clinical patterns for recurrent diseases need to be further demonstrated to predict prognosis and guide treatment.

KEYWORDS

embryonal tumors with multilayered rosettes, immunohistochemistry, molecular genetics, *C19MC*, Lin28A

Introduction

Embryonal tumors with multilayered rosettes are a novel entity that is extremely rare and predominantly affects children aged ≤ 2 years old (1). In the 2007 WHO classification of the central nervous system (CNS), these tumors were not well classified and were still under the broad umbrella of the CNS-primitive neuroectodermal tumors (PNET) (2). Large-scale studies subsequently showed that ETANTRs, ependymoblastoma, and medulloepithelioma (ME) shared alterations in the *C19MC* locus at the Chr 19q13.42 (3–6). Therefore, these three histologic subtypes were merged into ETMRs in the 2016 WHO classification of tumors of the CNS (7), and the 2021 WHO also follows this classification standard (1).

Histologically, these subgroups share multilayered (ependymoblastoma) rosettes and small embryonal tumors. ETMRs could develop through the CNS but mainly involve the cerebral hemisphere (8, 9). They correspond to WHO grade 4 and are associated with an aggressive clinical course. However, standard and optimal treatment has not been established, and the effects of current therapies remain unclear in ETMRs (8, 10). Moreover, the histopathological features of ETMRs have not yet been demonstrated during tumor progression, including recurrence and metastasis. Our study aimed to review and collect the cases diagnosed with ETMRs in our hospital to identify the clinical and pathologic characteristics, pathogenesis, and diagnostic factors of ETMRs.

Materials and methods

Study cohort

Seventeen patients with ETMRs were diagnosed at our hospital from January 2018 to January 2022, including ETANTRs and medulloepithelioma. All diagnoses were made according to the 2021 WHO CNS tumor classification criteria and reviewed by two expertized neuropathologists. Surgery approaches were divided into biopsy, partial resection, and complete resection. Two patients were lost to follow-up; therefore, fifteen were included in our statistical analysis. Besides, we collected 31 patients with atypical teratoid/rhabdoid tumors (AT/RTs) and 50 patients with medulloblastomas (MB) as control groups.

Immunohistochemistry and fluorescence *in situ* hybridization

Immunohistochemistry (IHC) was performed on 10% neutral buffered formalin-fixed, paraffin-embedded (FFPE) 4-um-thick tissue sections using the two-step Envision standard. The primary antibodies included: Lin28A (Cell Signaling Technology, USA), INI1 (BAF47/INI-1; Santa Cruz, USA), glial fibrillary acidic protein (GFAP; Dako, Denmark), oligodendrocyte transcription factor 2 (Olig2; Dako), synaptophysin (Syn; Novocastra, UK), neuronal nuclei (NeuN; Dako), and Ki-67 (Dako). Dual-color fluorescence *in situ* hybridization (FISH) using an intermittent microwave irradiation method was performed on 4-um-thick FFPE tissue sections (11). The *C19MC*/19q13.42 probe and a controlled 19p13.11 probe were prepared from bacterial artificial chromosome (BAC) clones as previously described (6). Lin28 IHC and INI1 IHC were performed on all ETMRs and controls, while other stains and *C19MC* FISH were performed on ETMRs.

Statistical analysis

Log-rank analysis using the Kaplan Meier and Chi-square analysis was applied to compare survival time, including overall survival (OS) and event-free survival (EFS). Cox regression analysis was performed to identify independent predictors. The level of significance was $p = 0.05$. The statistical analyses were performed using SPSS 26.0 (IBM, USA) and Prism 9.1.1 (Graphpad Software, USA).

Results

Clinical characteristics and neuroimaging features

The clinical data of all 17 patients are listed in Table 1. The age at diagnosis ranged from 16 months to 55 months (median age, 29 months); 76% (13/17) of the patients were ≤ 4 years old, and the male: female ratio was 1.83:1. Progressive-sided weakness (6/17) and vomiting (6/17) were the main symptoms, while strabismus and convulsion occurred in 3 and 2 patients, respectively.

The initial site was supratentorial in 10 patients and infratentorial in 7 patients, with a ratio of 1.4:1. Initial magnetic resonance imaging (MRI) information was available for 15 cases, and the other two were unavailable as MRI was performed at a local hospital. In 15 cases, tumors were isointense or hypointense on T1-weighted imaging (T1WI) and isointense or hyperintense on T2 WI. In contrast, tumors exhibited slight or partial contrast enhancement and hyperintensity on diffusion-weighted imaging (DWI) (Figure 1). Three of these tumors contained single or multiple partially cystic appearances. Calcification was not found in our cohort.

Histopathological features

Among the 17 patients, tumor sizes varied from 0.5 to 10cm, with a median size of 2.5cm. Sixteen patients had ETANTRs, 1 had medulloepithelioma (case 9), and no ependymoblastoma. The pathological features of the 17 cases are listed in Table 2. Morphologically, medulloepithelium was characterized by papillary, tubular, and trabecular arrangements (Figure 2), as well as sheets of poorly differentiated cells. ETANTRs showed biphasic architecture featuring dense clusters of small embryonal cells (or multilayered rosettes) and paucicellular neuropil-like areas (Figure 3). In ETANTRs, the neuropil-like areas were stained strongly and diffusely for the neuronal markers such as NeuN and Syn. In contrast, only a few positive cells were found within the multilayered rosettes and small cell areas (Figures 4D, E). The glial markers GFAP and Olig2 focally expressed in some embryonal cells but were negative in the neuron differentiated cells (Figures 4B, C). The Ki67 index ranged from 40% to 90%, which was relatively high in embryonal cells and lowered in the neuropil-like areas (Figure 4F). All tumors demonstrated diffused nuclear expression of INI1 throughout all components. Lin28A expression was found in all cases (17/17), and its immunoreactivity was more predominant and intense in multilayered rosettes and poorly differentiated small cell areas compared with neuropil-like regions (Figure 4A). In our three relapsed cases, the expression of LIN28A was much stronger and more intense in the recurrent lesions compared with primary tumors (Figure 5). Conversely, tumor cells of AT/RTs were partially or focally positive for Lin28A in13 cases (13/31, 42%), but all cases showed a nuclear loss of INI-1. In 50 cases of medulloblastoma, all tumor cells were negative for Lin28A and positive for INI-1. Besides, the

TABLE 1 Clinical details of 17 patients of ETMRs.

Number	Age (y)	Gender	Therapy	Chemotherapy	Radiotherapy	EFS (m)	OS (m)	outcome
1	2.7	F	Surg (Biopsy)	/	/	0.3	0.3	DOD
2	2.6	M	Surg (Biopsy) + RT + ChT	VCR + Carbo+ VP	32Gy CSI/22Gy focal boost	43	43	AWD
3*	2.0	M	Surg (PR) + RT + ChT	CTX + VCR	36Gy CSI/54Gy focal boost	5.3	6.3	DOD
4*c	3.4	F	Surg (CR) + RT + ChT	CTX + DDP + VCR	54Gy focus	6.5	9.5	DOD
5*	4.2	M	Surg (PR)	/	/	0.9	1.2	DOD
6*	4.3	F	Surg (CR) + RT + ChT	CTX + DDP + VCR	54Gy focus	4.8	16	DOD
7*	4.6	M	Surg (PR)	/	/	0.8	0.9	DOD
8[c]	1.9	M	Surg (CR)	/	/	1.3	1.4	DOD
9	2.0	F	Surg (PR)	/	/	0.8	0.8	DOD
10	1.3	M	Surg (CR) + ChT	CDDP + VCR + VP + CTX + MTX	/	5.8	5.8	DOD
11*	4.1	M	Surg (CR) + RT	/	54Gy focus	7.0	8.9	DOD
12	1.9	M	Surg (PR) + ChT	VCR + Carbo + VP	/	1.4	1.4	AWD
13	2.1	M	Surg (CR) + ChT	VCR + Carbo + VP	/	0.6	0.6	NED
14	2.2	F	Surg (Biopsy)	/	/	1.2	1.2	DOD
15	2.5	M	Surg (PR) + ChT	VCR + Carbo+ VP	/	8.5	8.5	DOD
6[ac]	1.4	F	Surg (PR)	lost	lost	lost	lost	lost
17[b]	3.6	M	Surg (Biopsy)	lost	lost	lost	lost	lost

/: patients did not receive the treatment; n*, patients occurred with intracranial or spinal metastasis; n[C], patients occurred with relapse; 16[a] and 17[b] were patients who were lost to follow-up. DOD, die of disease; AWD, alive with disease; NED, no evidence of disease; y, years; m, months; Surg, surgery; PR, partial resection; CR, complete resection; ChT, chemotherapy; RT, radiotherapy; OS, overall survival; EFS, event-free survival.

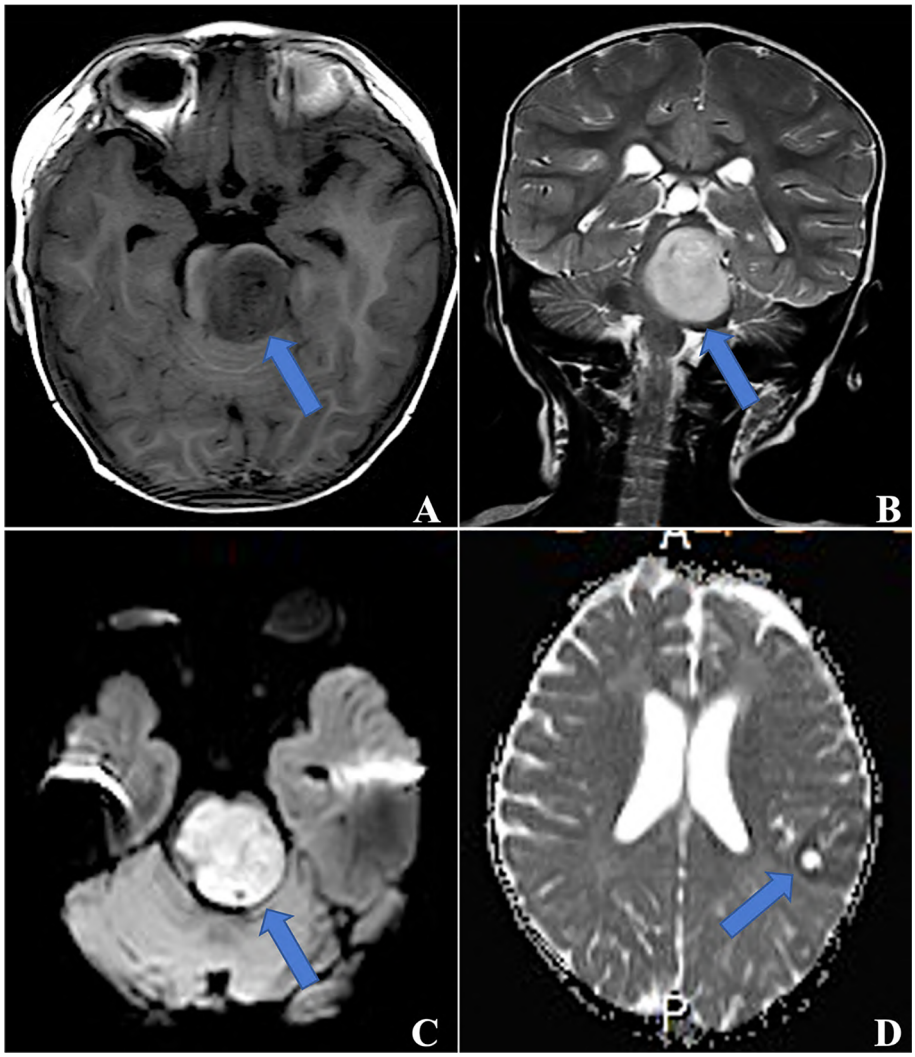

FIGURE 1
MRI for ETMRs, **(A)** TIWI showed a hypointense mass in the brainstem, which was hyperintense on both T2WI **(B)** and DWI **(C)** (blue arrows, case 5); **(D)** a 3×2×1 mass in the left parietal and occipital lobes with ringlike contrast enhancement (blue arrow, case 6).

increased copy number of *MYC* (*N*) was found in case 8 of both primary and recurrent lesions (Figure 6A), whereas no *NRAS* and *CDK6* aberrations were detected (Table 3). The amplification of the locus 19q13.42, analyzed in 17 ETMRs, was presented in 16 patients (Figure 6B). For the patient without the amplification of *C19MC* (case 9), we performed the FISH analysis of *DICER1*, and mutations were not detected.

One case (1/8) occurred with the histological evolution towards anaplasia during tumor progression (case 4). At first surgery, histopathology revealed a biphasic architecture featuring small embryonal cells with round or polygonal nuclei and scant cytoplasm and neuropil-like areas with sparse neoplastic neurocytic and ganglion cells (Figure 7A), confirming the diagnosis of ETMR. IHC showed the diffuse expression of Lin28A (Figure 7B) and focal expression of SYN and NeuN in tumor cells. FISH analysis revealed the amplification of *C19MC*. After 6.5 months, the tumor presented with recurrence demonstrated by MRI and undertook the complete resection. Histopathology showed tumor cells were three times larger than their neighboring cells with cellular pleomorphism and prominent nucleoli, indicating the anaplastic progression, but neither neuropils nor ependymoblastic rosettes were observed (Figure 7C). Amplification at 19q13.42 and immunopositivity of LIN28A (Figure 7D) still existed in the tumor cells, which demonstrated the recurrence of ETMRs.

10.3389/fonc.2022.1001959

TABLE 2 Histopathologic features of 17 patients of ETMRs.

Number	Morphology	Mitoses/10 HPFs	Ki67 index	LIN28A IHC	*C19MC* amplification	GFAP	NeuN	Specimen obtained method
1	ETANTR	8	40%	+	yes	–	+	at diagnose
2	ETANTR	15	60%	+	yes	+	–	at diagnose
3*	ETANTR	35	80%	+	yes	+	+	at diagnose
4*c	ETANTR	28 (primaries) 30 (relapse)	60% (primaries) 80% (relapse)	+	yes	+	+	at diagnose
5*	ETANTR	38	90%	+	yes	+	+	at diagnose
6*	ETANTR	30	80%	+	yes	+	–	at diagnose
7*	ETANTR	39	70%	+	yes	+	+	at diagnose
8[c]	ETANTR	35 (primaries) 37 (relapse)	70% (primaries) 75% (relapse)	+	yes	+	+	at diagnose
9	ME	28	80%	+	no	+	+	at diagnose
10	ETANTR	39	40%	+	yes	+	–	at diagnose
11*	ETANTR	32	80%	+	yes	+	–	at diagnose
12	ETANTR	26	70%	+	yes	+	+	at diagnose
13	ETANTR	45	60%	+	yes	+	+	at diagnose
14	ETANTR	42	70%	+	yes	+	–	at diagnose
15	ETANTR	36	80%	+	yes	+	–	at diagnose
16[ac]	ETANTR	15 (primaries) 35 (relapse)	40% (primaries) 50% (relapse)	+	yes	+	+	relapse
17[b]	ETANTR	30	80%	+	yes	+	+	at diagnose

/: patients did not receive the treatment; n*: patients occurred with intracranial or spinal metastasis; n[C]: patients occurred with relapse; 16[a] and 17[b] were patients who were lost to follow-up. ETANTR, embryonal tumors with abundant neuropil and true rosettes; ME, medulloepithelioma.

Treatment and outcome

All 17 patients received surgery, with five undergoing complete resections, four biopsies, and eight partial resections. Two patients were lost to follow-up. Therefore, therapy and follow-up data were only available for 15 patients (Table 1).

Five patients occurred with metastatic disease, two with recurrence, and one presented with both metastasis and recurrence. Among the six patients with metastatic disease, one developed spinal metastasis from the fourth ventricle, and two occurred with intracranial metastasis at initial presentation. All the metastatic lesions were visible by MRI, while no metastatic cells

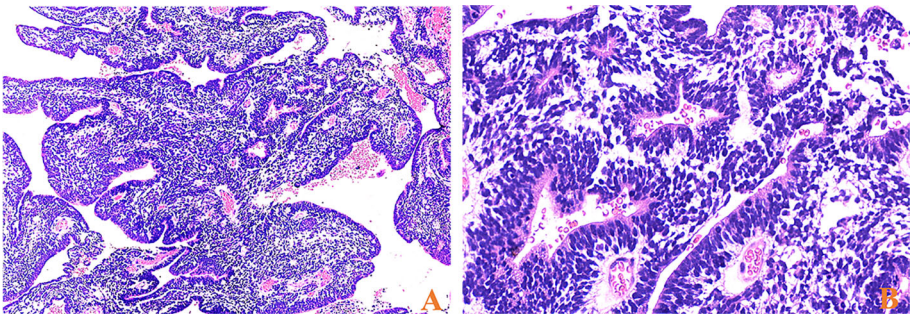

FIGURE 2
HE stainings of medulloepithelium for case 9, **(A)** papillary-like and tubular structures resembling the primitive neural tube (×40) and **(B)** on the luminal surface of these tubules, cilia, and blepharoplasts were absent (×400).

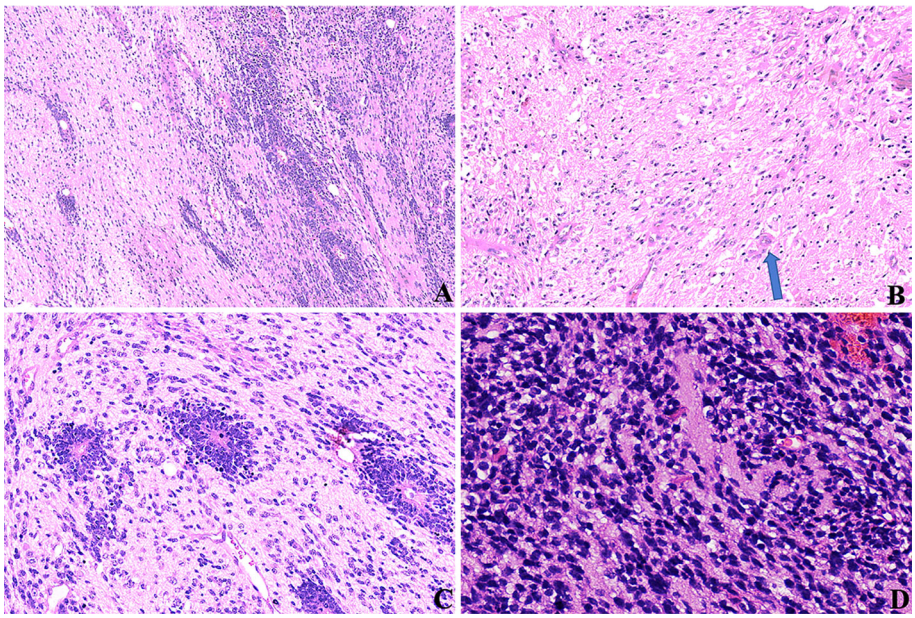

FIGURE 3
HE stainings of ETMRs for case 1, **(A)** tumor cells were in a biphasic architecture featuring dense clusters of mall embryonal cells/multilayered rosettes and paucicellular neuropil-like areas (×100); **(B)** Sparse neoplastic neurocytic and ganglion cells could be observed in the neuropil-like matrix (blue arrow, ×200); **(C)** Multilayered rosettes comprised embryonal cells in a pseudostratified neuroepithelium with a central round or slit-like lumen; The cells facing the lumen have a defined apical surface with a prominent internal limiting membrane; The nuclei of the rosette-forming cells tended to be located away from the lumen towards the outer cell border (×200); **(D)** small embryonal cells were with round or polygonal nuclei and scant cytoplasm (×400).

were found in the cerebrospinal fluid. The 2021 WHO indicates that ETMRs occur in children ≤ 4 years of age, and analyses performed with stratification for periods ≤ and > 4 years showed that two patients had intracranial metastasis in the younger group (18%, 2/11) and four in the elder group (100%, 4/4). The incidence of metastasis was significantly different between the two groups ($p = 0.025$, $\chi 2 = 9.76$; Table 4), demonstrating that children aged > 4 years were prone to occur with metastasis.

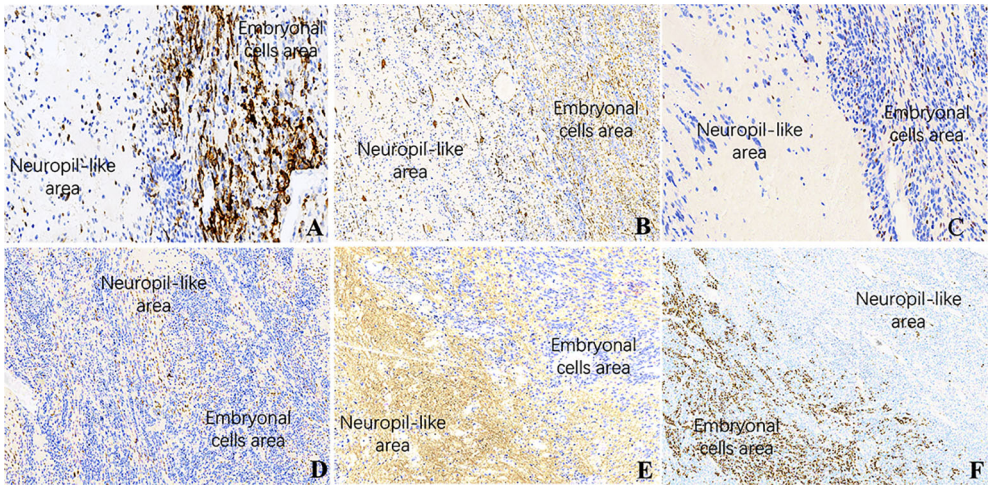

FIGURE 4
IHC of ETMRs for case 1, the expressions of **(A)** LIN28A, **(B)** GFAP, **(C)** OLIG2, and **(F)** Ki67 were stronger and more diffuse in the embryonal cell areas than in the neuropil-like matrix (×200); Neuronal makers, including NeuN **(D)** and Syn **(E)**, expressed in the neuron differentiated cells but were negative in embryonal cells (×200).

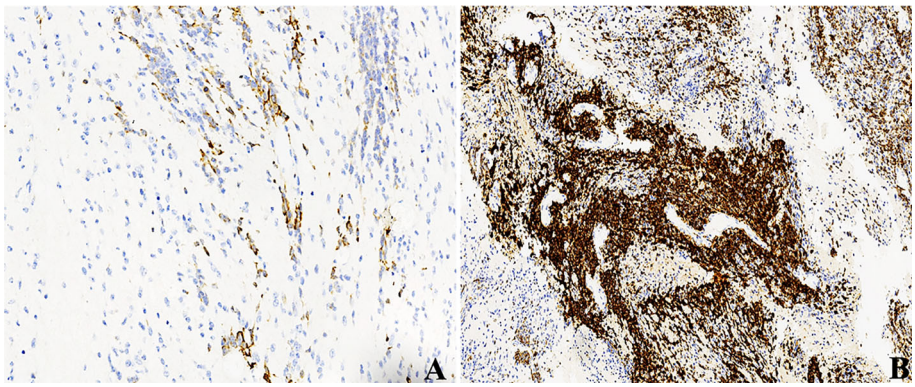

FIGURE 5
LIN28A IHC in primary and relapsed ETMRs for case 8, **(A)** LIN28A cytoplasmic immunopositivity was weaker and focal in primary tumors compared with **(B)** in recurrent counterparts (×200).

Among the 15 patients, only three are alive, and the other 12 died of tumor progression. Six patients were without adjuvant therapy after initial surgery and died within a short time (0.3-1.3 months). Nine patients were treated with adjuvant treatment following surgery (1 biopsy, 3 partial, and 5 total resections); one patient received radiotherapy alone, four received chemotherapy alone, and four received radiotherapy plus chemotherapy. The median durations of OS and EFS were both 1.4 months. Analyses of OS and EFS showed patients who were treated with radiation treatment exhibited a higher survival rate than those who were not (p = 0.03 for OS, Figure 8A; p = 0.007 for EFS, Figure 9A). However, patients who underwent complete resection didn't differ significantly from their partial resection or biopsy counterparts (p = 0.90 for OS, Figure 8F; p = 0.92 for EFS, Figure 9F). Additionally, tumor location, age, gender, and metastasis were not significantly associated with OS or EFS (respectively for OS, p = 0.50, p = 0.29, p = 0.86, p = 0.79, Figures 8C, D, E, G; respectively for EFS, p = 0.65, p = 0.56, p = 0.07, p = 0.55, Figures 9C, D, E, G).

The types of chemotherapeutic agents in our study were different between patients with and without complete resection, including vincristine, carboplatin, prednisone, cyclophosphamide, and cisplatin (see Table 1). Eight patients received chemotherapy, and one experienced long-term survival of greater than 36 months. Among them, the median OS and EFS were 7.4 and 5.6 months, respectively, while that of the patients without chemotherapy were 1.2 and 0.8 months, respectively (p = 0.04 for OS, Figure 8B; p = 0.01 for EFS, Figure 9B). We then removed age and other potential treatment biases on survival, and the multivariate analysis revealed that chemotherapy with a relative risk (RR) of 0.172 CI 95% (0.032-0.910) p = 0.038 was the only prognostic factor associated with better overall survival.

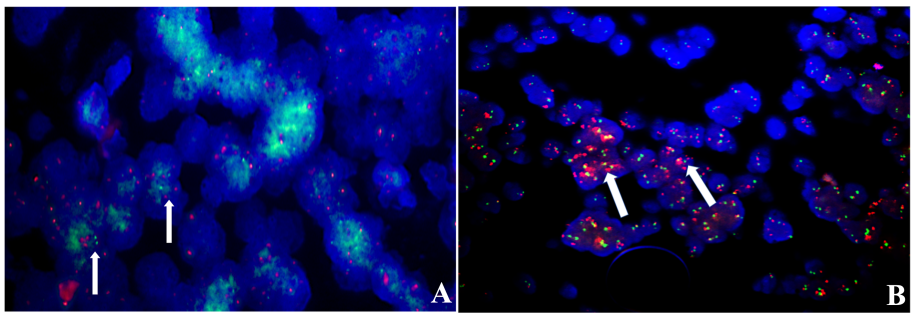

FIGURE 6
FISH analysis, **(A)** *N-MYC* for relapsed case 8 showed increased copy numbers, green signals (white arrows); **(B)** case 12 showed amplification in the GSP *C19MC* probe, red signals (white arrows).

10.3389/fonc.2022.1001959

TABLE 3 Pathological and molecular features of case 8.

markers / lesions	KI67	P53 IHC	*TP53* gene	*N-MYC*	*NRAS*	*CDK6*
primary	70%+	–	wild-type	increased copy numbers	no mutation	no amplification
relapsed	75%+	–	wild-type	increased copy numbers	no mutation	no amplification

Discussion

ETMRs are extremely rare, and their true incidence is difficult to calculate; about 100 cases have been reported in the English medical literature since its first description in 2000 by Eberhart et al. (12). However, some patients may have been misdiagnosed or missed before its defining genetic alteration was established. The tumor mainly affects infants aged < 4 years old, and 76% of patients were under the age of 4 years in our analysis, but patients aged > 18 years have also been reported (10). Our data indicated that the male-to-female ratio was 1.8:1, which is consistent with the male predominance in CNS embryonal tumors. Supratentorial tumors are more often than infratentorial tumors (6, 8, 13, 14), as observed in our cohort, while rare cases arising in the spine have been reported (8, 15). On neuroimaging, these tumors were demarcated and large. MRI demonstrated that tumors were usually hypointense on T1WI and hyperintense on T2WI and DWI, with minimal or partial contrast enhancement (16, 17 ,13). Tumors may contain cysts or calcification (18). Of note, the imaging features of ETMRs are similar to that of AT/RTs and MB. Nevertheless, accurate diagnosis is crucial due to their distinct treatment protocols and biology, leading to a dismal prognosis of ETMRs that differs significantly from AT/RTs and MB. The average OS of ETMRs after intensive therapies is approximately 12 months (6, 8, 13), compared with a 37% of 4-year OS rate in AT/RTs (19) and the 5-year survival rate of MB is 85% (20).

Histologically, poorly differentiated small cells and multilayered (ependymoblastic) rosettes are the characteristic and standard features of ETMRs (12, 13, 21). Some tumor cells in ETMRs exhibit osteoid, myeloid, epithelial, mesenchymal, or muscular differentiation or contain cytoplasmic melanin pigment (21, 22). The morphological progression between the primary and recurrent lesions in patient 4 indicates the diagnostic histology of ETMRs is not always present and might result in misdiagnosis. Tumor progression towards anaplasia may be caused by genetic aberrations like *TP53* (13, 23, 24), and it is interesting to consider whether anaplasia is of prognostic significance (as it is for medulloblastoma). However, more case numbers will need to be collected to explore it. Besides, glial and neuronal differentiation/maturation in ETMRs after combination therapies have been

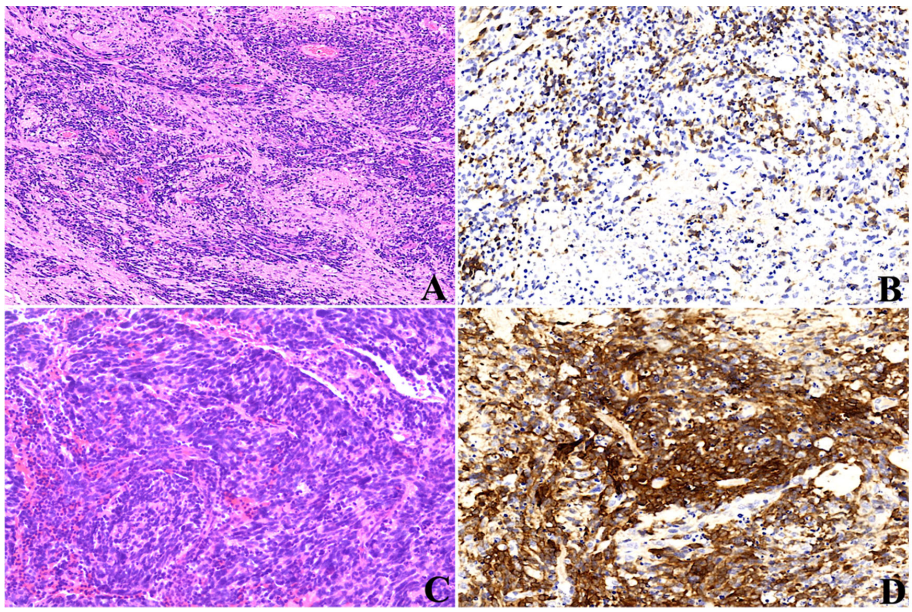

FIGURE 7
Histopathological progression of case 4, the tumor presented as the biphasic pattern of ETANTRs at the initial surgery **(A)**, and Lin28A expression was positive **(B)**; recurrent tumor after surgery showed anaplasia in large cells with cellular pleomorphism and prominent nucleoli **(C)**; the expression of Lin28A was stronger and more intense **(D)** than that of the primary lesion.

TABLE 4 Correlations between metastatic status and age in ETMRs.

age (years) / Metastatic status	aged ≤ 3 (n = 11)	aged > 3 (n = 6)	$X^2 = 9.97$ $P = 0.002$
metastasis (n = 6)	1	5	
without metastasis (n = 6)	10	1	
Total (n = 17)	11	6	

reported, and the significance of treatment and prognosis remains to be further demonstrated (25). Therefore, the analyses of *C19MC* amplification and Lin28A immunoreactivity are indispensable and should be performed in all CNS embryonal tumors in children to diagnose of ETMRs accurately. Though *C19MC* alterations are specific for ETMRs, LIN28A immunopositivity is not. Our result revealed that all cases showed positive expression of LIN28A while 16 cases had altered *C19MC*.

Immunohistochemical staining for Lin28A is more intense and prominent in the small cells and multilayered rosettes compared with neuron-differentiated cells in ETMRs irrespective of histological subgroups (13, 26). In the present study, the staining for Lin28A was more diffuse and prominent in the relapsed lesions than in primaries, which is supported by Andrey (27) as the recurrent ETMRs may be composed of hypercellular but lacked neuropil areas. Lin28A immunopositivity is not unique to ETMRs (10, 27); our study found it was also expressed focally in AT/RTs but was negative in MB. According to a large study, the strong expression of Lin28A in ETMRs statistically relates to poorer outcomes than those of negative or focal expression in other CNS embryonal tumors (27). Collectively, Lin28A IHC is of both diagnostic and prognostic significance in ETMRs (28, 29). The limitation of our study is that we didn't compare the prognosis of ETMRs with the control groups.

The origin cells and biology of ETMRs remain poorly elucidated. Recently, the *C19MC* amplification at the Chr 19q 13.42 and the LIN28A/Let-7 signaling pathways are considered crucial hallmarks for tumorigenesis (5, 26, 27). 90% of ETMRs are characterized by amplification of the polycistronic microRNA (miRNA) cluster *C19MC* on chromosome 19q13.42, one of the largest miRNA clusters that contain 60 kb and 46 miRNA genes (30, 31). Compared with supratentorial ETMRs, infratentorial tumors typically have a higher frequency of *C19MC* amplification. Approximately half of the *C19MC*-negative ETMRs, representing 5% of all ETMRs, harbor biallelic *DICER1* mutations and are mutually exclusive to *C19MC* amplification. Moreover, ETMRs characteristically express the RNA binding protein LIN28A, which could downregulate the let-7 family of miRNAs and is further associated with activating mTOR, WNT, and *MYCN* signaling pathways involving oncogenesis (27, 32). Of note, the LIN28A/let-7 pathway is the common downstream of alterations of *C19MC* and *DICER1*, which *C19MC* may affect LIN28A indirectly by downregulating Tristetraprolin (TTP). At the same time, WNT and *MYCN* signaling are downstream of the RNase III domain in *DICER1* mutations, so ETMRs are molecularly similar whether they have *C19MC* amplification (33–35). Our case 9, which had a tumor in the frontal lobe, harbored neither *C19MC* amplification nor *DICER1* mutation and should be classified as ETMR, not elsewhere classified (NEC), according to the 2021 WHO CNS classification (7). One explanation is that other genetic abnormalities, such as amplification of the miR17HG on chromosome 13, might drive the tumorgenesis of ETMRs, NEC (26). Moreover, our data showed the aberrant expression of *N-MYC* in case 8, which might play a role in tumor relapse (27), and the molecular genotyping didn't change at recurrence. Therefore, more cases and research are needed to explore the biological nature and clinical patterns of the recurrent diseases to guide the therapy better.

To date, no standard therapeutic approaches have been established for ETMRs. The treatment now includes surgery, radiotherapy, and chemotherapy, but the prognosis of ETMRs remains poorer. In our analysis, the extent of surgical resection was not associated with overall survival. This result was different from the finding reported by Kirti et al. (10), in which total resection was a positive indicator of survival in ETMRs. The limitation of our study lies in that the extent of resection was not quantitated exactly. However, it indicated that there is no obligation for surgeons to conduct the total resection of the tumor, and biopsy is adequate for pathologic diagnosis and avoiding neurocognitive impairment. Besides, we found radiotherapy was not the prognostic factor in a multivariate analysis, similar to Alexiou's research (36). However, Horwitz et al. (8) found radiotherapy was associated with a better outcome using both univariate and multivariate analyses. The bias in the literature may be introduced by the fact that radiotherapy was treated after chemotherapy and surgery, which could screen patients. The radiation volumes have not been identified in ETMR; as the younger age in the ETMRs population (median age: 2 years), radiotherapy should be administrated with caution because of the late effects. Our findings revealed that radiotherapy might not be recommended for ETMRs and could decrease neurocognitive impairment. Due to the limitation of tumor samples, the prognosis was not compared among the three subtypes of ETMRs.

The effectiveness and prognostic role of chemotherapy have not been reliably identified hitherto. Due to the lack of established protocols, the type of chemotherapeutic agents varies among patients. Our data found that patients who received chemotherapy tend to have a statistically better prognosis than those who weren't treated with chemotherapy, similar to some findings (8, 37). The favorable prognosis of chemotherapy is possible because it accelerates the neuron maturation of tumor

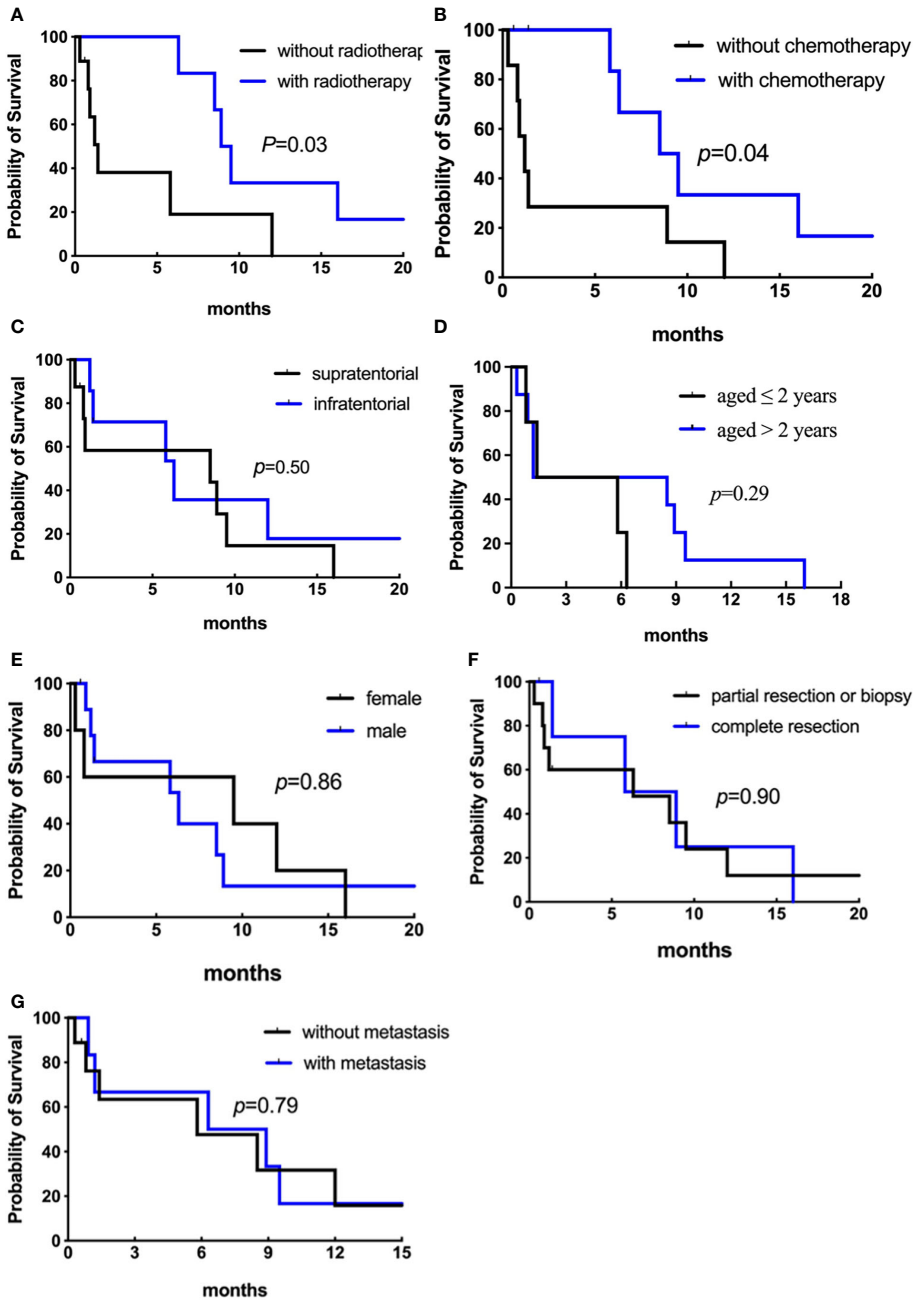

FIGURE 8
Analyses of overall survival (Kaplan–Meier method) according to **(A)** radiotherapy (p = 0.03); **(B)** chemotherapy (p = 0.04); **(C)** primary tumor location (p = 0.50); **(D)** age at diagnosis (p = 0.29). Figure 8.2 Analyses of overall survival (Kaplan–Meier method) according to **(E)** gender (p = 0.86); **(F)** surgical resection (p = 0.90); **(G)** metastatic status (p = 0.79).

cells (37). However, long-time OS of chemotherapy has not been identified in both our cohort and literature as a result of the small sample size and short duration. Therefore, more cases and long-time follow-ups are needed to explore the survival data of chemotherapy. Moreover, our results revealed that patients aged > 4 years had a higher likelihood of metastasis, as shown in other CNS embryonal tumors (38). One explanation is that tumor progression (i.e., tumor spread through the neuraxis) in an older child simply because cancer has had (presumably) more time to grow and disseminate.

Due to the limited effects of the current therapeutic strategy for ETMRs, novel treatment options are needed. Tara et al. (5) found

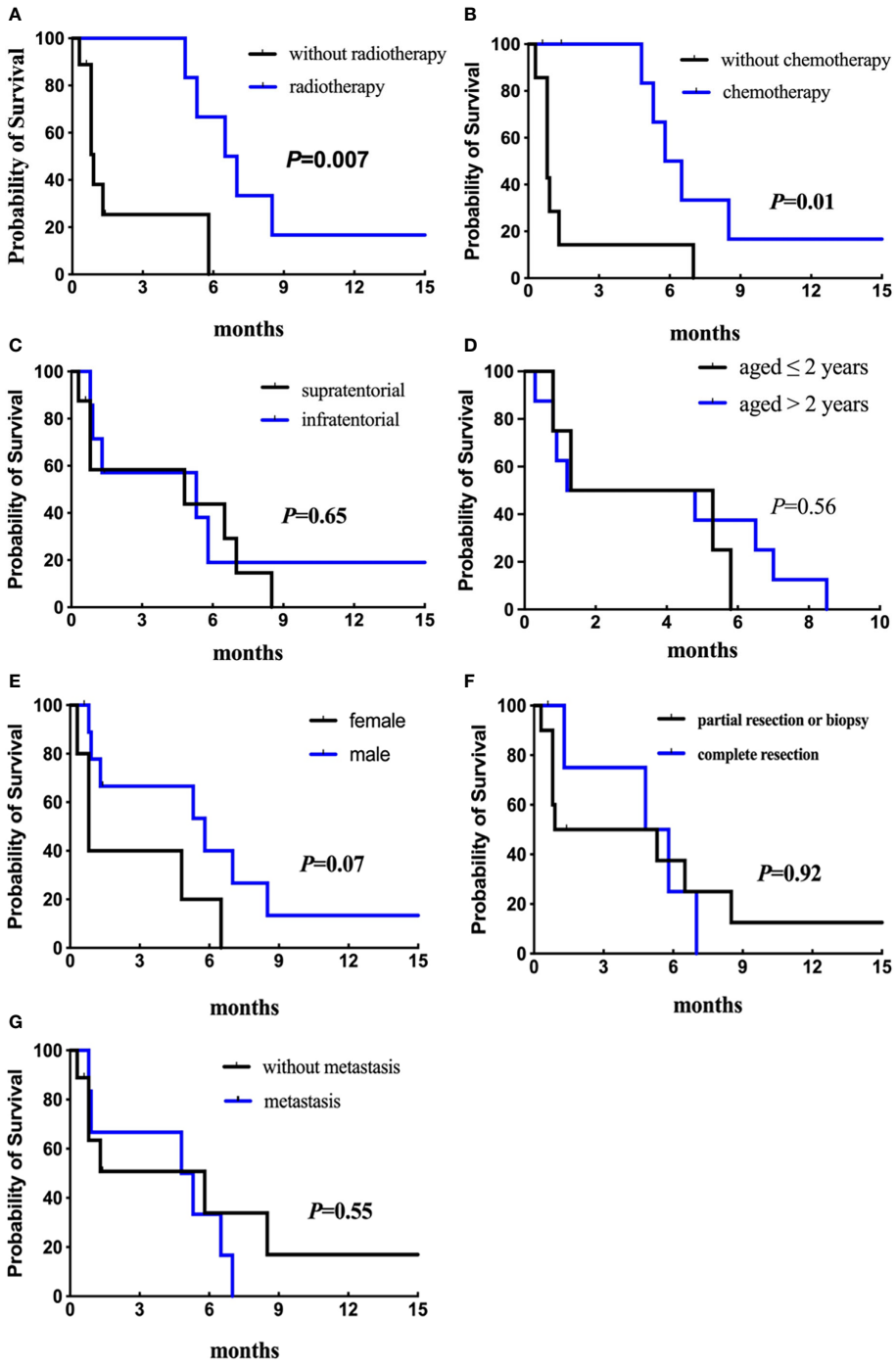

FIGURE 9
Analyses of event-free survival (Kaplan–Meier method) according to **(A)** radiotherapy (p = 0.007); **(B)** chemotherapy (p = 0.01); **(C)** primary tumor location (p = 0.65); **(D)** age at diagnosis (p = 0.56). Figure 9.2 Analyses of event-free survival (Kaplan–Meier method) according to **(E)** gender (p = 0.07); **(F)** surgical resection (p = 0.92); **(G)** metastatic status (p = 0.55).

that the ETMRs cell line, BT183, is more sensitive to inhibitors of the IGF/PI3K/mTOR pathway. Another study proposed that *SHH* inhibitors could benefit ETMRs by activating the WNT pathway and upregulating the SHH pathway (39). Large-scale research and rigorous preclinical testing are required to support these drug targets to guide the molecularly targeted medicine further. Though LIN28/let-7 pathway is a possible promising target, the mechanisms among *C19MC* amplification, *DICER1* mutations, and

LIN28 expression remain unclear. A more in-depth understanding of tumor biology is needed as well in ETMRs.In conclusion, our study covers the impressive number of patients diagnosed with ETMRs in a short time frame. Our data revealed that children over four years old have a higher rate of metastasis. The morphology of ETMRs varies, and characteristic features are not always presented along with tumor progression, which reminds us of the combination of the *C19MC* FISH and LIN28A IHC when making the diagnosis. Patients treated with chemotherapy tend to have a better prognosis. Since *C19MC* aberration has been detected for more than two decades, the understanding of ETMRs biology has improved as well as better diagnostic tools, more driving aberrations, and possible downstream targets. However, the survival of ETMRs patients has only minimally improved due to the lack of effective therapies; therefore, more case numbers and further studies are needed to demonstrate the involved signaling pathways and develop targeted molecular therapies.

Data availability statement

The raw data supporting the conclusions of this article will be made available by the authors, without undue reservation.

Ethics statement

The studies involving human participants were reviewed and approved by the Research Ethics Committee of the Shanghai Jiao Tong University School of Medicine. Written informed consent to participate in this study was provided by the patient/participants legal guardian/next of kin.

Author contributions

KX contributed to the investigation and was a significant contributor to writing the manuscript; ZS designed the project and collected data; LW performed the data analysis and designed experiments; WG revised the manuscript; KX and ZS contributed equally to the work and share first authorship. All authors read and approved the final manuscript.

Conflict of interest

The authors declare that the research was conducted in the absence of any commercial or financial relationships that could be construed as a potential conflict of interest.

Publisher's note

All claims expressed in this article are solely those of the authors and do not necessarily represent those of their affiliated organizations, or those of the publisher, the editors and the reviewers. Any product that may be evaluated in this article, or claim that may be made by its manufacturer, is not guaranteed or endorsed by the publisher.

References

1. Cree. IA, Lokuhetty. D, Peferoen. LAN, White. VA. *WHO classificaiton of umours of the central nervous system. 5th edition*. Lyon: IARC (2021).

2. Louis DN, Ohgaki H, Wiestler OD, Cavenee WK, Burger PC, Jouvet A, et al. The 2007 WHO classification of tumours of the central nervous system. *Acta Neuropathol* (2007) 114:97–109. doi: 10.1007/s00401-007-0243-4

3. Pfister S, Remke M, Castoldi M, Bai AH, Muckenthaler MU, Kulozik A, et al. Novel genomic amplification targeting the microRNA cluster at 19q13.42 in a pediatric embryonal tumor with abundant neuropil and true rosettes. *Acta Neuropathol* (2009) 117:457–64. doi: 10.1007/s00401-008-0467-y

4. Li M, Lee KF, Lu Y, Clarke I, Shih D, Eberhart C, et al. Frequent amplification of a chr19q13.41 microRNA polycistron in aggressive primitive neuroectodermal brain tumors. *Cancer Cell* (2009) 16:533–46. doi: 10.1016/j.ccr.2009.10.025

5. Spence T, Perotti C, Sin-Chan P, Picard D, Wu W, Singh A, et al. A novel C19MC amplified cell line links Lin28/let-7 to mTOR signaling in embryonal tumor with multilayered rosettes. *Neuro Oncol* (2014) 16:62–71. doi: 10.1093/neuonc/not162

6. Korshunov A, Sturm D, Ryzhova M, Hovestadt V, Gessi M, Jones DT, et al. Embryonal tumor with abundant neuropil and true rosettes (ETANTR), ependymoblastoma, and medulloepithelioma share molecular similarity and comprise a single clinicopathological entity. *Acta Neuropathol* (2014) 128:279–89. doi: 10.1007/s00401-013-1228-0

7. Louis DN, Ohgaki H, Wiestler OD, Cavenee WK, Burger PC, Jouvet A, et al. *WHO classificaiton of tumours of the central nervous system (revised 4th edition)*. Lyon: IARC (2016).

8. Horwitz M, Dufour C, Leblond P, Bourdeaut F, Faure-Conter C, Bertozzi AI, et al. Embryonal tumors with multilayered rosettes in children: The SFCE experience. *Childs Nerv Syst* (2016) 32:299–305. doi: 10.1007/s00381-015-2920-2

9. Adamek D, Sofowora KD, Cwiklinska M, Herman-Sucharska I, Kwiatkowski S. Embryonal tumor with abundant neuropil and true rosettes: An autopsy case-based update and review of the literature. *Childs Nerv Syst* (2013) 29:849–54. doi: 10.1007/s00381-013-2037-4

10. Gupta K, Sood R, Salunke P, Chatterjee D, Madan R, Ahuja CK, et al. Clinicopathological characteristics and outcomes in embryonal tumor with multilayered rosettes: A decade long experience from a tertiary care centre in north India. *Ann Diagn Pathol* (2021) 53:151745. doi: 10.1016/j.anndiagpath.2021.151745

11. Nigro JM, Takahashi MA, Ginzinger DG, Law M, Passe S, Jenkins RB, et al. Detection of 1p and 19q loss in oligodendroglioma by quantitative microsatellite analysis, a real-time quantitative polymerase chain reaction assay. *Am J Pathol* (2001) 158:1253–62. doi: 10.1016/S0002-9440(10)64076-X

12. Eberhart CG, Brat DJ, Cohen KJ, Burger PC. Pediatric neuroblastic brain tumors containing abundant neuropil and true rosettes. *Pediatr Dev Pathol* (2000) 3:346–52. doi: 10.1007/s100249910049

13. Gessi M, Giangaspero F, Lauriola L, Gardiman M, Scheithauer BW, Halliday W, et al. Embryonal tumors with abundant neuropil and true rosettes: A distinctive CNS primitive neuroectodermal tumor. *Am J Surg Pathol* (2009) 33:211–7. doi: 10.1097/PAS.0b013e318186235b

14. Gupta K, Singh V, Aggarwal A, Salunke P. Embryonal tumor with multilayered rosettes: Diagnosis on intra-operative squash smear. *Neuropathology* (2018) 38:387–91. doi: 10.1111/neup.12460

15. Wang B, Gogia B, Fuller GN, Ketonen LM. Embryonal tumor with multilayered rosettes, C19MC-altered: Clinical, pathological, and neuroimaging findings. *J Neuroimaging* (2018) 28:483–9. doi: 10.1111/jon.12524

16. Fuller C, Fouladi M, Gajjar A, Dalton J, Sanford RA, Helton KJ. Chromosome 17 abnormalities in pediatric neuroblastic tumor with abundant neuropil and true rosettes. *Am J Clin Pathol* (2006) 126:277–83. doi: 10.1309/tfbx-1lwq-93mx-qbaw

17. La Spina M, Pizzolitto S, Skrap M, Nocerino A, Russo G, Di Cataldo A, et al. Embryonal tumor with abundant neuropil and true rosettes. A new entity or only variations of a parent neoplasms (PNETs)? this is the dilemma. *J Neurooncol* (2006) 78:317–20. doi: 10.1007/s11060-005-9105-x

18. Nowak J, Seidel C, Berg F, Pietsch T, Friedrich C, von Hoff K, et al. MRI Characteristics of ependymoblastoma: Results from 22 centrally reviewed cases. *AJNR Am J Neuroradiol* (2014) 35:1996–2001. doi: 10.3174/ajnr.A4002

19. Wang RF, Guan WB, Yan Y, Jiang B, Ma J, Jiang MW, et al. Atypical teratoid/rhabdoid tumours: Clinicopathological characteristics, prognostic factors and outcomes of 22 children from 2010 to 2015 in China. *Pathology* (2016) 48:555–63. doi: 10.1016/j.pathol.2016.05.010

20. Biegel JA. Molecular genetics of atypical teratoid/rhabdoid tumor. *Neurosurg Focus* (2006) 20:E11. doi: 10.3171/foc.2006.20.1.12

21. Buccoliero AM, Castiglione F, Rossi Degl'Innocenti D, Franchi A, Paglierani M, Sanzo M, et al. Embryonal tumor with abundant neuropil and true rosettes: Morphological, immunohistochemical, ultrastructural and molecular study of a case showing features of medulloepithelioma and areas of mesenchymal and epithelial differentiation. *Neuropathology* (2010) 30:84–91. doi: 10.1111/j.1440-1789.2009.01040.x

22. Al-Hussaini M, Abuirmeileh N, Swaidan M, Al-Jumaily U, Rajjal H, Musharbash A, et al. Embryonal tumor with abundant neuropil and true rosettes: A report of three cases of a rare tumor, with an unusual case showing rhabdomyoblastic and melanocytic differentiation. *Neuropathology* (2011) 31:620–5. doi: 10.1111/j.1440-1789.2011.01213.x

23. Woehrer A, Slavc I, Peyrl A, Czech T, Dorfer C, Prayer D, et al. Embryonal tumor with abundant neuropil and true rosettes (ETANTR) with loss of morphological but retained genetic key features during progression. *Acta Neuropathol* (2011) 122:787–90. doi: 10.1007/s00401-011-0903-2

24. Korshunov A, Remke M, Gessi M, Ryzhova M, Hielscher T, Witt H, et al. Focal genomic amplification at 19q13.42 comprises a powerful diagnostic marker for embryonal tumors with ependymoblastic rosettes. *Acta Neuropathol* (2010) 120:253–60. doi: 10.1007/s00401-010-0688-8

25. Lafay-Cousin L, Hader W, Wei XC, Nordal R, Strother D, Hawkins C, et al. Post-chemotherapy maturation in supratentorial primitive neuroectodermal tumors. *Brain Pathol* (2014) 24:166–72. doi: 10.1111/bpa.12089

26. Lambo S, von Hoff K, Korshunov A, Pfister SM, Kool M. ETMR: A tumor entity in its infancy. *Acta Neuropathol* (2020) 140:249–66. doi: 10.1007/s00401-020-02182-2

27. Korshunov A, Ryzhova M, Jones DT, Northcott PA, van Sluis P, Volckmann R, et al. LIN28A immunoreactivity is a potent diagnostic marker of embryonal tumor with multilayered rosettes (ETMR). *Acta Neuropathol* (2012) 124:875–81. doi: 10.1007/s00401-012-1068-3

28. Laurent LC, Chen J, Ulitsky I, Mueller FJ, Lu C, Shamir R, et al. Comprehensive microRNA profiling reveals a unique human embryonic stem cell signature dominated by a single seed sequence. *Stem Cells* (2008) 26:1506–16. doi: 10.1634/stemcells.2007-1081

29. Ren J, Jin P, Wang E, Marincola FM, Stroncek DF. MicroRNA and gene expression patterns in the differentiation of human embryonic stem cells. *J Transl Med* (2009) 7:20. doi: 10.1186/1479-5876-7-20

30. de Rie D, Abugessaisa I, Alam T, Arner E, Arner P, Ashoor H, et al. An integrated expression atlas of miRNAs and their promoters in human and mouse. *Nat Biotechnol* (2017) 35:872–8. doi: 10.1038/nbt.3947

31. Kim YK, Kim VN. Processing of intronic microRNAs. *EMBO J* (2007) 26:775–83. doi: 10.1038/sj.emboj.7601512

32. Heo I, Joo C, Cho J, Ha M, Han J, Kim VN. Lin28 mediates the terminal uridylation of let-7 precursor MicroRNA. *Mol Cell* (2008) 32:276–84. doi: 10.1016/j.molcel.2008.09.014

33. Kim CW, Vo MT, Kim HK, Lee HH, Yoon NA, Lee BJ, et al. Ectopic over-expression of tristetraprolin in human cancer cells promotes biogenesis of let-7 by down-regulation of Lin28. *Nucleic Acids Res* (2012) 40:3856–69. doi: 10.1093/nar/gkr1302

34. Sin-Chan P, Mumal I, Suwal T, Ho B, Fan X, Singh I, et al. A C19MC-LIN28A-MYCN oncogenic circuit driven by hijacked super-enhancers is a distinct therapeutic vulnerability in ETMRs: A lethal brain tumor. *Cancer Cell* (2019) 36:51–67.e7. doi: 10.1016/j.ccell.2019.06.002

35. Rakheja D, Chen KS, Liu Y, Shukla AA, Schmid V, Chang TC, et al. Somatic mutations in DROSHA and DICER1 impair microRNA biogenesis through distinct mechanisms in wilms tumours. *Nat Commun* (2014) 2:4802. doi: 10.1038/ncomms5802

36. Alexiou GA, Stefanaki K, Vartholomatos G, Sfakianos G, Prodromou N, Moschovi M. Embryonal tumor with abundant neuropil and true rosettes: A systematic literature review and report of 2 new cases. *J Child Neurol* (2013) 28:1709–15. doi: 10.1177/0883073812471434

37. Antonelli M, Korshunov A, Mastronuzzi A, Diomedi Camassei F, Carai A, Colafati GS, et al. Long-term survival in a case of ETANTR with histological features of neuronal maturation after therapy. *Virchows Arch* (2015) 466:603–7. doi: 10.1007/s00428-015-1736-5

38. Picard D, Miller S, Hawkins CE, Bouffet E, Rogers HA, Chan TS, et al. Markers of survival and metastatic potential in childhood CNS primitive neuro-ectodermal brain tumours: An integrative genomic analysis. *Lancet Oncol* (2012) 13:838–48. doi: 10.1016/s1470-2045(12)70257-7

39. Neumann JE, Wefers AK, Lambo S, Bianchi E, Bockstaller M, Dorostkar MM, et al. A mouse model for embryonal tumors with multilayered rosettes uncovers the therapeutic potential of sonic-hedgehog inhibitors. *Nat Med* (2017) 23:1191–202. doi: 10.1038/nm.4402

frontiers | Frontiers in Oncology

TYPE Original Research
PUBLISHED 27 October 2022
DOI 10.3389/fonc.2022.1007236

OPEN ACCESS

EDITED BY
Laura Gatti,
IRCCS Carlo Besta Neurological Institute Foundation, Italy

REVIEWED BY
Jacopo Falco,
IRCCS Carlo Besta Neurological Institute Foundation, Italy
Shan Lei,
Guizhou Medical University, China

*CORRESPONDENCE
Su Yue Zheng
16659734@qq.com
Tao Hong
ht2000@vip.sina.com

†These authors have contributed equally to this work

SPECIALTY SECTION
This article was submitted to Neuro-Oncology and Neurosurgical Oncology, a section of the journal Frontiers in Oncology

RECEIVED 30 July 2022
ACCEPTED 06 October 2022
PUBLISHED 27 October 2022

CITATION
Fang C, Zhou L, Huang H, Xu HT, Hong T and Zheng SY (2022) Bioinformatics analysis and validation of the critical genes associated with adamantinomatous craniopharyngioma.
Front. Oncol. 12:1007236.
doi: 10.3389/fonc.2022.1007236

Bioinformatics analysis and validation of the critical genes associated with adamantinomatous craniopharyngioma

Chao Fang[1†], Lin Zhou[2†], Hui Huang[3†], Hai Tong Xu[1], Tao Hong[4*] and Su Yue Zheng[4*]

[1]Department of Neurosurgery, Shenzhen Key Laboratory of Neurosurgery, the First Affiliated Hospital of Shenzhen University, Shenzhen Second People's Hospital, Shenzhen, China, [2]Department of Neurosurgery, Shanghai Tenth People's Hospital, Tongji University School of Medicine, Shanghai, China, [3]Department of Neurosurgery, The Second Affiliated Hospital of Nanchang University, Nanchang, China, [4]Department of Neurosurgery, The First Affiliated Hospital of Nanchang University, Nanchang, China

Adamantinomatous craniopharyngioma (ACP) is an epithelial tumor that arises when Rathke's pouch remains during embryonic development. The pathogenesis of ACP remains unclear, and treatment options are limited. Here, we reveal the critical genes expressed in ACP and provide a basis for further research and treatment. The raw dataset GSE94349 was downloaded from the GEO database. We selected 24 ACP and 27 matched samples from individuals with no documented tumor complications (control group). Then, we screened for differentially expressed genes (DEGs) to identify key signaling pathways and associated DEGs. A total of 470 DEGs were identified (251 upregulated and 219 downregulated). Hierarchical clustering showed that the DEGs could precisely distinguish the ACP group from the control group (CG). Gene Ontology (GO) enrichment analysis indicated that the upregulated DEGs were mainly involved in cell adhesion, inflammatory responses, and extracellular matrix management. The downregulated DEGs were primarily involved in cell junction and nervous system development. Kyoto Encyclopedia of Genes and Genomes (KEGG) pathway enrichment analysis indicated that the critical pathway was pathways in cancer. In the PPI network, *CDH1*, *SHH*, and *WNT5A* had the highest degrees of interaction and were associated with the formation of ACP. *CDH1* was verified as a critical gene by quantitative reverse transcription–polymerase chain reaction (qRT-PCR) in ACP and CG samples. We found that *CDH1* may play an important role in the pathways in cancer signaling pathway that regulates ACP development. The *CDH1* gene may be a target for future research and treatment of ACP.

KEYWORDS

craniopharyngioma, pathways in cancer, *CDH1*, *SHH*, *WNT5A*

Introduction

Craniopharyngioma (CP) is a complex and diverse congenital intracranial tumor, and surgical resection is the primary treatment strategy at present. Because this tumor is located near essential brain structures, such as the optic nerve and hypothalamus, it poses significant challenges for surgery. Damage to the hypothalamus and other important brain tissue structures can lead to high fever, electrolyte disorder, obesity, and other severe complications and seriously harm patients' quality of life after surgery (1). Treatment options for CPs are difficult to determine because the balance of risks and benefits of surgery varies significantly from patient to patient. The close, heterogeneous relationship to the hypothalamus makes surgical removal of CPs challenging even though this remains the primary treatment strategy (1, 2).

The incidence of CPs is 4.6% of all intracranial tumors, and its exact pathogenesis remains unclear (1). There are two theories regarding the origin of CP cells: embryogenetic theory and metaplastic theory (3). There are two histological types of CPs, ACP and papillary craniopharyngioma (PCP), of which ACP is the most common (4). As PCP is rare in clinical practice, all subjects in this study had ACP. Exome sequencing studies have demonstrated that PCP and ACP have distinct genetic origins, primarily driven by mutually exclusive alterations; *BRAFV600E* is observed in 95% of PCPs, and *CTNNB1* is observed in 75%–96% of ACPs (5). For PCPs with *BRAFV600E* mutations, targeted therapy with *BRAF* inhibitors combined with MEK inhibitors can reduce tumor volume by 85% to 91% (6, 7). However, no similar clinical studies have been conducted on ACPs. In addition to *CTNNB1*, *CDH1* and *SHH* may play essential roles in the occurrence of ACP (8, 9).

Gene expression microarrays can be used to identify differentially expressed genes (DEGs) in ACP tissues, providing high-throughput gene expression data. Gene expression microarrays are an essential approach for studying the pathogenesis of CP. The National Center of Biotechnology Information GEO database comprises a large amount of genetic data, providing a rich resource for the study and analysis of differential gene expression levels (10).

Zou et al. (11) analyzed CP data in the USA, revealing that the mechanisms of ACP occurrence and development might involve the regulation of the RNA polymerase II promoter and glutamate receptor binding. Li et al. (12) also analyzed sample data and identified MMP12 as a potential therapeutic target in ACP. The present study examined the GSE94349 dataset, comprising a large number of samples obtained from American patients (13).

GSE94349, submitted by Donson et al. on 31 January 2017 (13), contains genetic data from 168 samples, analyzed by microarray technology using the Affymetrix Human Genome U133 Plus 2.0 array GPL570 platform.

We selected 24 ACP surgical tumor samples and 27 samples from individuals with no documented tumor complications (control group, CG) from GSE94349. However, as Donson et al. (13) was a clinical trial, the researchers did not quickly achieve a perfect match between the two groups. Although these two studies have implications for ACP, our study further contributed GSEA data. Finally, we used the intersection of the Database for Annotation, Visualization, and Integrated Discovery (DAVID) and GSEA to determine the key genes. No relevant article has been published regarding the critical genes involved in ACP by using the intersection of DAVID and GSEA.

By analyzing the gene expression data of GSE94349, DAVID and GSEA were used to conduct GO and KEGG pathway enrichment analyses. Then, the intersection of the two methods was obtained, namely, crucial pathways and genes. Finally, STRING and Cytoscape software were used to construct protein–protein interaction (PPI) networks of critical pathways and genes. The present study identified critical genes in the pathogenesis of CP, which will provide new insight into the treatment of CP.

Materials and methods

Gene annotation and missing value supplementation

The gene expression microarray data of GSE94349_series_matrix.txt were downloaded from the GEO (http://www.ncbi.nlm.nih.gov/geo/) database. The quality control and standardization of these data were completed prior to the current study. The data were processed using R software (version3.6; http://www.r-project.org/). First, we searched and downloaded GPL570, the corresponding platform of GSE94349, from the official GEO website. GSE94349 was matched with GPL570 in R language to complete gene ID conversion and annotation. Next, the missing values were calculated by KNN in R language to supplement the missing values.

Identification of the DEGs

DEGs were filtered by using the limma package in R (http://limma.org) (14). Only genes with | log2-fold change (Fc) | > 4 and p-values < 0.01 were considered DEGs. Finally, we obtained upregulated and downregulated DEGs. Volcano mapping was performed in R language; heatmaps were drawn using the R package gplot 2.

GO enrichment analysis of DEGs

The upregulated and downregulated DEGs were input into the online tool DAVID (DAVID 6.8 version) for GO enrichment

analysis. The results were analyzed according to biological process (BP), cellular component (CC), and molecular function (MF), and $p < 0.01$ was considered statistically significant.

KEGG pathway enrichment analysis

DEGs were imported into the DAVID online tool for KEGG pathway enrichment analysis, and $p < 0.01$ was considered statistically significant. We imported all the gene data for the GSEA. The Kolmogorov–Smirnov test was used to calculate the value of DEGs in each KEGG pathway by 1,000 repeated permutation tests to conduct the KEGG pathway enrichment analysis of DEGs in GSEA. $p < 0.01$ was considered statistically significant. Then, the upregulated and downregulated DEG KEGG pathway enrichment analysis results were derived. Finally, the intersection of the results of the two analysis methods was obtained to determine the target DEGs.

DAVID was used to conduct KEGG pathway enrichment analysis for all the different genes, yielding more comprehensive results. However, GSEA is a KEGG pathway enrichment analysis of all genes, yielding a complete dataset. The intersection of the two may be more valuable for further research (15). We used Venn diagrams to show the common KEGG pathways after the intersection of the DAVID and GSEA results.

PPI network

The KEGG pathway-related DEGs from the intersection of the DAVID and GSEA results were imported into the Search Tool for the Retrieval of Interacting Genes (STRING). The gene interaction relationship was derived with a confidence score >0.7 as the cutoff standard. Then, Cytoscape software (Version 3.5.1) was used to construct the PPI network between the KEGG pathway and its related DEGs. CytoHubba was used to predict the top 10 key genes. Three critical genes (*CDH1*, *WNT5A*, and *SHH*) were selected.

Patients and sample collection

ACP and CG samples were provided by the Department of Neurosurgery at The First Affiliated Hospital of Nanchang University (Nanchang, China). ACP samples were collected after endoscopic nasal resection, stored at 4°C for transport and then preserved in liquid nitrogen. Samples from individuals with no documented tumor complications [control group (CG)] were collected from patients undergoing surgery for epilepsy. The mean age of the four epileptic patients was 20 years (age range, 8–34 years), including two men and two women. A total of four ACP samples from two men and two women were obtained. The mean age of the ACP patients was 25.5 years (age range, 8–35 years). Patients pathologically diagnosed with ACP were included in the present study, while patients with other diagnoses were excluded. All specimens were pathologically and clinically diagnosed as ACP by three pathologists. The present study was approved by the Research Ethics Committee of Nanchang University [Nanchang, China; First Affiliated Hospital of Nanchang University (2020) Medical Research Ethics Review (No. 160)], and written informed consent was provided by all patients prior to the start of the study.

Sample inclusion criteria

ACP samples

1. Clinical diagnosis of craniopharyngioma and consent to surgery;
2. Han nationality, Chinese, right-handed;
3. No history of chronic cardiovascular diseases; no history of infectious diseases; previously healthy, no history of kidney disease and liver disease;
4. Normal hearing and language functions, no metal implants in the body, no history of surgery for heart, lung, or other vital organs, no history of major diseases such as brain disorders, and no history of mental illness; and
5. At least two pathologists diagnosed ACP.
6. Only when the above five items meet the requirements can they be included in the sample database of this study.

CG samples

1. Clinically diagnosed epilepsy and consent to surgery;
2. Han nationality, Chinese, right-handed;
3. No history of chronic cardiovascular diseases or infectious diseases;
4. No history of kidney and liver diseases;
5. Normal hearing, no metal implants in the body; and
6. No history of mental illness.

Only when the above six items meet the requirements can they be included in the sample database of this study.

Sample exclusion criteria

1. Oral hormone medication within 2 weeks;
2. Speech and hearing impairment;
3. Patients who cannot cooperate with researchers in information collection (e.g., coma patients with severe illness);

4. Lost contact or refused to answer the phone during the follow-up period so that postoperative information could not be collected; and
5. Patients with anemia, cachexia, and other blood cells or low hemoglobin.
6. Any one of the above five items should be excluded from this study.

Exit criteria

1. Patients or their family members voluntarily withdraw from the study after surgery;
2. Non-craniopharyngioma patients were diagnosed after preoperative collection of craniopharyngioma patient specimens;
3. Postoperative complications that require hormone and other related treatments;
4. Postoperative complications and inability to cooperate with follow-up investigators; and
5. Patients who cannot cooperate with postoperative follow-up.
6. If any of the above five criteria are met, the study will automatically stop by default.

RT-PCR

Three critical genes (*CDH1*, *WNT5A*, and *SHH*) were validated in ACP tissues and compared with CG tissues by qRT-PCR using the QuantStudio 7 Flex real-time PCR system (Bio-Rad, Nanchang, China). The primer sequences used are shown in Table 1. The $2^{-\Delta\Delta Ct}$ method was used, and the PCR results were normalized to the ACTIN gene (16).

Total RNA was extracted from ACP samples according to the instructions of the RNA Extraction Kit (Servicebio, China). Then, the total RNA of ACP samples was reverse transcribed according to the steps of the Servicebio®RT First Strand cDNA Synthesis Kit (Servicebio, China). The total RNA and cDNA of CG samples were obtained by the same method. Finally, 7.5 µl of 2×qPCR Mix, 1.5 µl of 2.5 µm primer (upstream + downstream), 2.0 µl of reverse transcription product (cDNA), and 4.0 µl of ddH_2O were added to a 200-µl PCR tube. After the PCR solution was prepared, it was gently mixed by pipetting up and down. A 96-well PCR plate was placed into a special bracket. The researchers avoided touching the bottom of the reaction plate to avoid affecting the data reading. Three wells were prepared for each reaction, and qPCR was conducted using the following reaction conditions: predenaturation at 95°C for 10 min, denaturation at 94°C for 15 s, and annealing at 60°C for 30 s for 40 cycles. When the temperature rose from 65°C to 95°C, the fluorescence signal was collected every 0.5°C to form a melting curve. RT-PCR (Bio-Rad, China) was performed on CG samples and ACP samples according to the above steps. Each experiment was repeated three times.

Data analysis

The ΔΔCT method was used as follows: A = CT (target gene, sample to be tested) − CT (internal marker gene, sample to be tested); B = CT (target gene, control sample) − CT (internal standard gene, control sample); K = A − B; express multiple = 2^{-K}. All experimental data are expressed as the mean ± SD and were statistically analyzed by *t*-test. $p < 0.05$ was considered to be statistically significant.

Results

Gene annotation and missing value supplement

The gene expression microarray data of GSE94349_series_matrix.txt were downloaded from GEO, comprising 168 samples. The ACP and control groups were selected from GSE94349_series_matrix.txt, and other samples were removed. Quality control and standardization of these data were completed, and all chip data reached comparable levels.

Identification of DEGs

Twenty-four ACP samples and 27 control samples in the GSE94349 dataset were analyzed. The volcano plot in Figure 1 shows all genetic differences with a threshold of $-\log_{10} p > 2$

TABLE 1 Primers used in present study.

Gene	Forward primer	Reverse primer
SHH	AGGAGTGAAACTGCGGGTGA	CACCGAGCAGTGGATATGTGC
CDH1	ATTGCTCACATTTCCCAACTCC	CTCTGTCACCTTCAGCCATCCT
WNT5A	TGCAATGTCTTCCAAGTTCTTCCT	ATTCATACCTAGCGACCACCAAG
ACTIN	CACCCAGCACAATGAAGATCAAGAT	CCAGTTTTTAAATCCTGAGTCAAGC

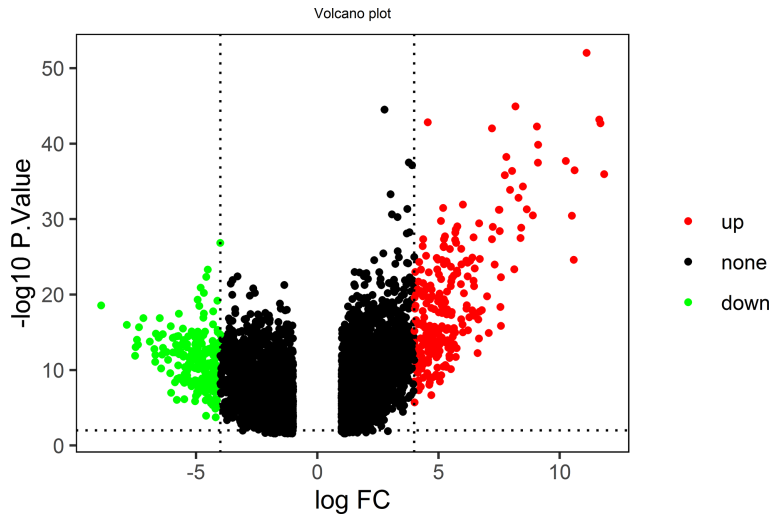

FIGURE 1
The volcano plot shows all genetic differences with a threshold of –log10 $p > 2$ ($p < 0.01$) and |log2 Fc| > 4; red dots represent upregulated genes, and green dots represent downregulated genes.

($p < 0.01$) and $|\log_2 Fc| > 4$. Red dots represent upregulated genes, and green dots represent downregulated genes. Then, based on the cutoff criteria ($p < 0.01$ and |log2 Fc| > 4), a total of 470 DEGs were identified, including 251 upregulated and 219 downregulated DEGs.

All DEGs were analyzed. DEGs were also divided into upregulated and downregulated components for separate analyses. This study aimed to identify the upregulation and downregulation of target DEGs; thus, we divided the upregulated and downregulated genes for analysis. The expression heatmap of the DEGs is shown in Figure 2. Hierarchical cluster analysis accurately distinguished ACP samples from control samples.

GO enrichment analysis

The DEGs were imported, DAVID was used for functional enrichment analysis, and the results were obtained according to the three functions of MF, CC, and BP. The GO analysis results of upregulated and downregulated DEGs are listed in the top 10 items in order of *p*-value in Figure 3.

Figure 3A shows the detailed results of the MF analysis of DEGs. The upregulated DEGs were mainly related to the activation of structural molecules and the binding of calcium ions; downregulated DEGs were mainly associated with calcium ions and calmodulin binding. Figure 3B shows the detailed results of the CC analysis of DEGs. The upregulated DEGs were mainly concentrated in exosomes, extracellular regions, and extracellular spaces; downregulated DEGs were mainly enriched in cell junctions, neuron projections, and neuronal cell bodies.

Figure 3C shows the detailed results of the BP analysis of DEGs. The upregulated DEGs were mainly associated with cell adhesion, inflammatory responses, and extracellular matrix organization, and the downregulated DEGs were mainly associated with chemical synaptic transmission and nervous system development.

The results showed that the upregulated genes were mainly involved in cell adhesion, inflammatory responses, and extracellular matrix management. The downregulated genes were mainly involved in cell junction and nervous system development.

Pathway enrichment analysis

Figure 4A shows the results of the DEG KEGG pathway analysis by DAVID. Seven KEGG pathways were enriched in the upregulated DEGs ($p < 0.01$). Twelve KEGG pathways were enriched among the downregulated DEGs ($p < 0.01$).

The upregulated pathway comprised pathways in cancer, the PI3K-Akt signaling pathway, the extracellular matrix (ECM)–receptor interaction, and the Wnt signaling pathway. The downregulated pathways were mainly associated with pathways related to retrograde endocannabinoid signaling, the synaptic vesicle cycle, morphine addiction, and neuroactive ligand–receptor interactions.

Figure 4B and Table 2 show the results of DEG analyses obtained by GSEA KEGG pathway analysis. Using $p < 0.01$ as the standard, there were seven upregulated and no downregulated pathways. Detailed results of the 7 KEGG pathways are shown in Table 2.

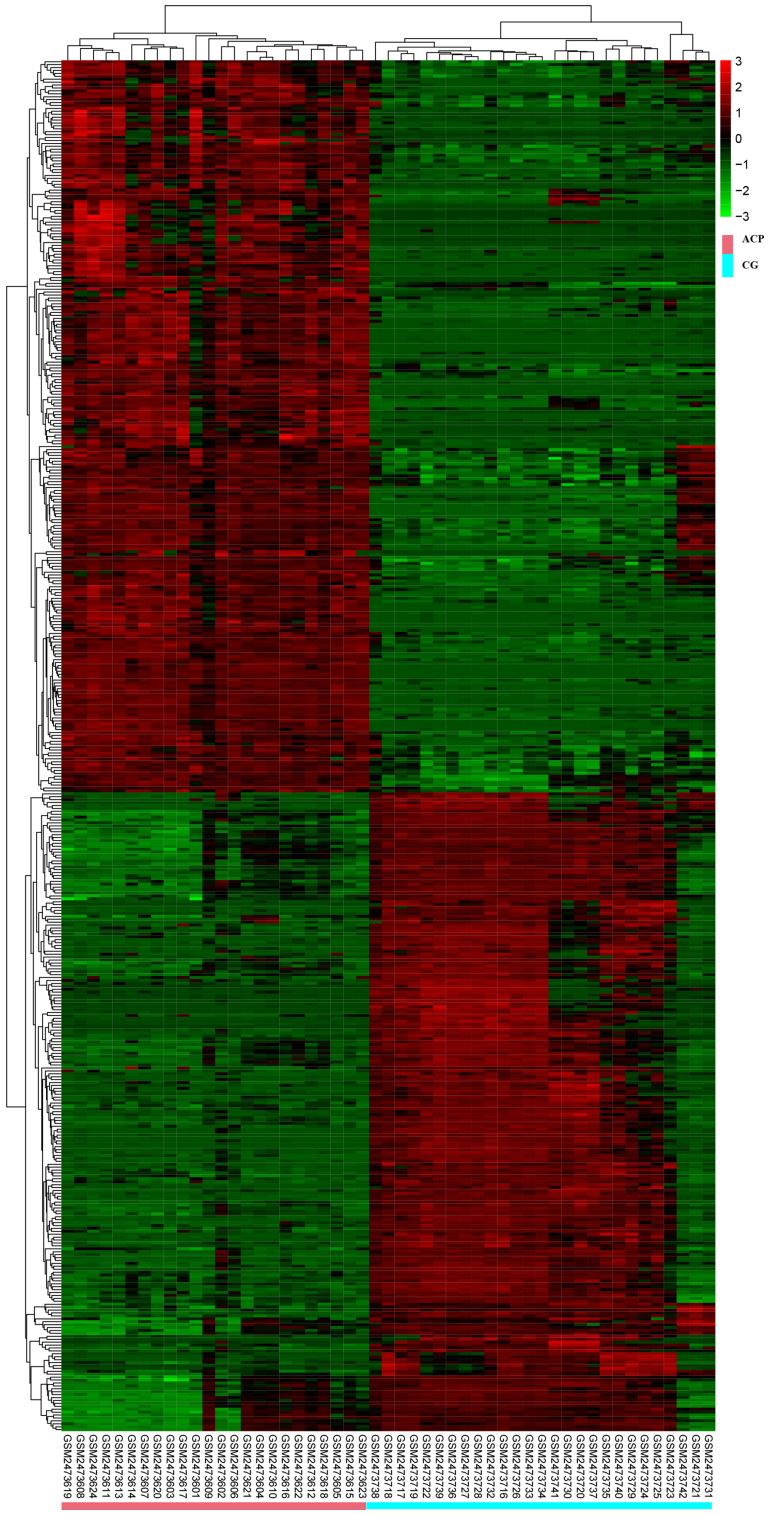

FIGURE 2
Hierarchical cluster analysis could accurately distinguish ACP samples from control samples. CGs, individuals with no documented tumor complication samples; ACP, adamantinomatous craniopharyngioma.

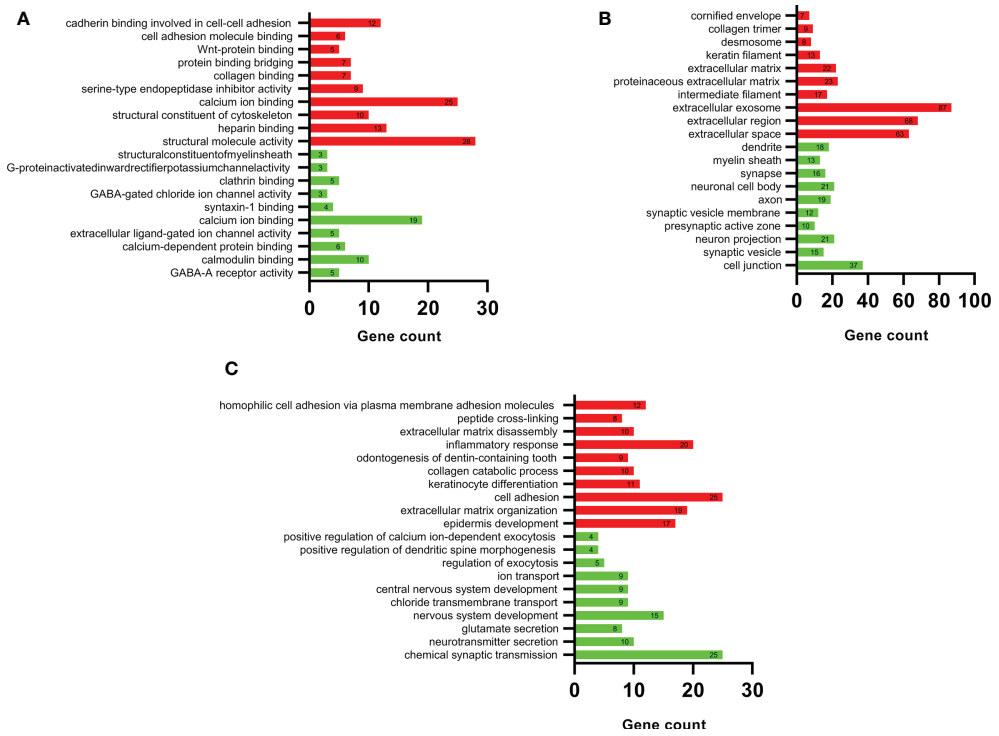

FIGURE 3
DAVID GO enrichment analysis results. According to the three functions of **(A)** molecular function, **(B)** cellular component, and **(C)** biological process, the top 10 upregulated (red) and top 10 downregulated (green) terms in each category.

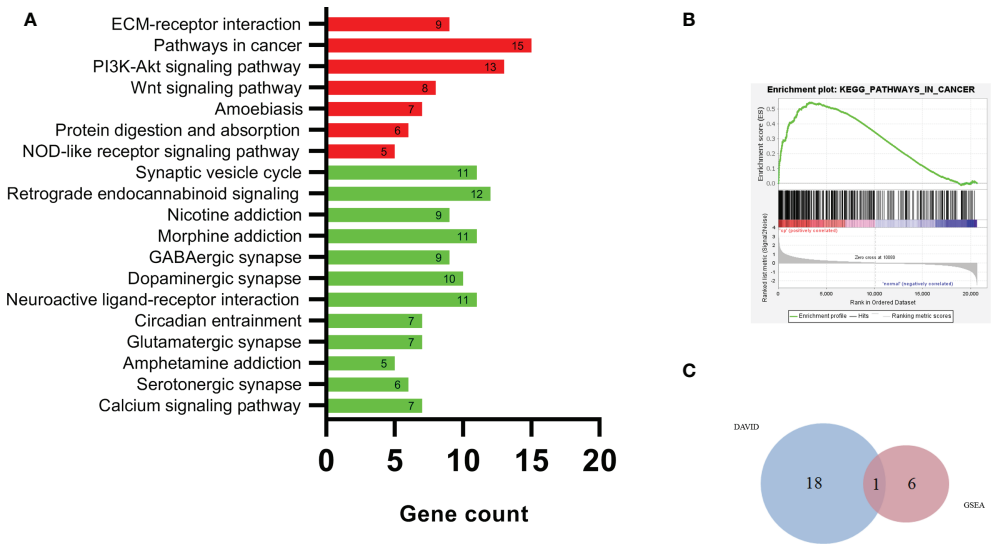

FIGURE 4
The DEG KEGG pathway analysis by DAVID **(A)**, pathways in cancer **(B)**, and Venn plot of DAVID and GSEA **(C)**. KEGG, Kyoto Encyclopedia of Genes and Genomes; DAVID, Database for Annotation Visualization and Integrated Discovery; GSEA, Gene Set Enrichment Analysis.

TABLE 2 KEGG enrichment analysis results (GSEA).

Pathway name	Gene number of pathway	ES	NES	NOM *p*-value	FDR *q*-value
Small cell lung cancer	82	0.652	1.628	0.000	0.605
Pathways in cancer	311	0.545	1.604	0.000	0.516
P53 signaling pathway	63	0.675	1.579	0.002	0.328
Steroid hormone biosynthesis	45	0.506	1.550	0.004	0.234
Cytokine–cytokine receptor interaction	240	0.656	1.548	0.004	0.200
Tgf beta signaling pathway	82	0.568	1.523	0.008	0.217
Riboflavin metabolism	15	0.621	1.572	0.009	0.299

KEGG, Kyoto Encyclopedia of Genes and Genomes; GSEA, gene set enrichment analysis; ES, enrichment score; NES, normalized enrichment score; NOM, nominal; FDR, false discovery rate.

Upregulated pathways were mainly associated with pathways in cancer and cytokine–cytokine receptor interactions.

The KEGG pathway analyses identified 19 significant pathways from DAVID and seven significant pathways from GSEA. The results of the two methods intersected, and only one common upregulated pathway was found, as shown in the Venn diagram in Figure 4C. The only upregulated pathway was "pathways in cancer". The relationship between this unique pathway and related pathways and genes is shown in Figure 5.

PPI network analysis

All of the 15 DEGs in the one common pathway were collected using STRING, and a PPI analysis was performed. The 15 DEGs were imported into the STRING database, and their interactions were identified. If the interaction score was >0.7, the PPI network could be formed with 14 nodes and 32 edges. The PPI networks presented in Figure 6 show that all DEGs were upregulated. As shown in Figure 7, the cytoHubba plug-in was used in Cytoscape software to search for the top 10 key genes among the 15 DEGs in the PPI network map. Finally, the top three critical genes (*CDH1*, *WNT5A*, and *SHH*) were selected from the 10 genes for RT-PCR verification.

RT-PCR results

Quantitative reverse-transcription polymerase chain reaction (qRT-PCR) was used to measure and compare the expression levels of the key genes in the ACP and control groups (Figure 8). The expression levels of three key genes were significantly increased in ACP *vs.* the control group, including *CDH1*, *WNT5A*, and *SHH*, but only CDH1 had statistical significance ($p < 0.05$) (Figure 8).

Discussion

A total of 470 DEGs were identified in the present study, including 251 upregulated and 219 downregulated DEGs. GO enrichment analysis indicated that the upregulated genes were mainly located in the extracellular exosome, extracellular region, and extracellular space and were involved in structural molecule activation and the binding of calcium ions, cell adhesion, inflammatory responses, and extracellular matrix organization bioprocesses. Another study showed that proinflammatory mediators drive the phosphorylation and activation of STAT3 (17). Persistent signaling through this pathway in cancer can result in a chronic inflammatory phenotype and suppression of antitumor immunity (13). Other studies have shown that cholesterol crystals in ACP activate the inflammasome, leading to the secretion of inflammatory cytokines that drive the inflammatory response (18). In addition, ECM proteins mediate epithelial–mesenchymal transformation (EMT) in ACP cells (19). The downregulated genes were mainly involved in cell junction and nervous system development. Research has shown that epithelial cell adhesion molecule (Ep-CAM) expression in craniopharyngioma could be a predictive marker of relapse (20). Additionally, ACP cells originate from remnants of Rathke's cleft, which is neuroepithelial (1, 21).

The KEGG pathway enrichment analysis in this study showed that "pathways in cancer" (https://www.kegg.jp/pathway/hsa05200) was the major pathway involved in ACP.

There was only one common pathway and all 15 DEGs in this pathway were collected using STRING, and a PPI analysis was performed. In the DAVID KEGG analysis, these 15 DEGs were mainly involved in the following five signaling pathways: Wnt signaling pathway, ECM–receptor interaction, amoebiasis, PI3K-Akt signaling pathway, and pathways in cancer. Among these signaling pathways, the association between amoebiasis and ACP was not previously reported. The other four signaling pathways have been associated with ACP.

The Wnt signaling pathway is an important aspect of ACP pathogenesis. *CTNNB1*-Mut has been shown to promote ACP primary cell proliferation by activating Wnt/β-catenin signaling (22). On the other hand, reducing the expression of β-catenin can significantly inhibit the proliferation of ACP cells, and β-catenin can promote the expression of Fascin mRNA and Fascin by acting on Fascin genes in the nucleus, thus promoting the migration and invasion ability of ACP cells (23).

The ECM can mediate EMT in ACP cells (19). EMT plays an important role in ACP development. ECM can facilitate the migration and differentiation of cells and trigger EMT, which is important for the progression and metastasis of various tumors (24, 25). Overexpression of ECM in ACP cells can promote

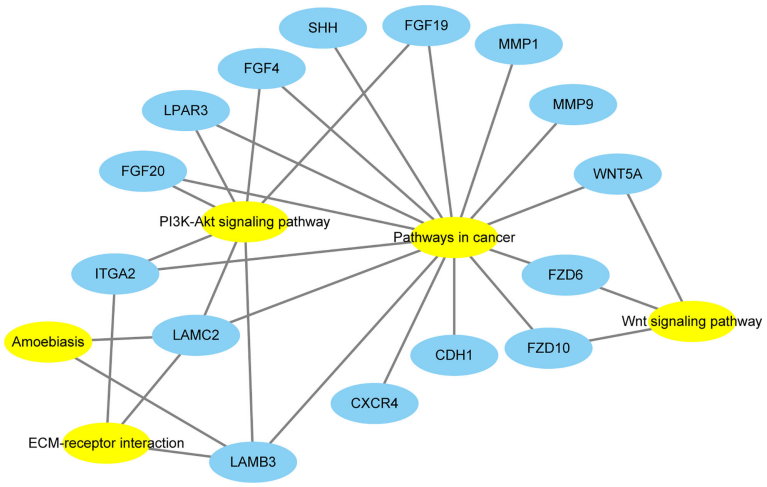

FIGURE 5
The relationship between this unique pathway (Pathway in cancer) and related pathways and genes. Yellow represents the pathways, and blue represents the genes.

tumor proliferation, migration, and invasion (19). Although the association between the PI3K-Akt signaling pathway and ACP has not been reported, Andoniadou et al. showed that fibroblast growth factors (FGFs) could induce β-catenin cells to actively divide (26). As shown in Figure 5, three FGF members (*FGF4*, *FGF19*, and *FGF20*) of the 15 DEGs were involved in the PI3K-Akt signaling pathway. The FGF family proteins are key regulators of several biological processes, and together with their receptors, they affect the development of many human cancers (27). Overactivation mutations in FGF receptors have been identified in several human cancers, including breast, bladder, and prostate cancers (28, 29). It is tempting to speculate that FGFs induce active division of β-catenin cells through the PI3K-Akt signaling pathway. However, three FGF members of the 15 DEGs were also involved in pathways in cancer; therefore, FGFs induce active division of β-catenin cells through the PI3K-Akt signaling pathway or pathways in cancer, which requires confirmation in further experiments.

Similarly, the association between pathways in cancer and ACPs has not been reported, but the three most significant key genes (*CDH1*, *WNT5A*, and *SHH*) have been closely/positively associated with craniopharyngioma. One report showed that *SHH* is highly expressed in ACPs (9). After the formation of Rathke's sac, the expression of SHH in this region gradually decreases (30). SHH can promote β-catenin overexpression in ACP animal and cell models by paracrine and autocrine effects, respectively (26). In addition, studies have shown that the expression of *VEGF* in ACP cells can promote tumor angiogenesis and increase microvascular density (31); however, whether the *SHH* pathway affects tumor blood supply in ACP

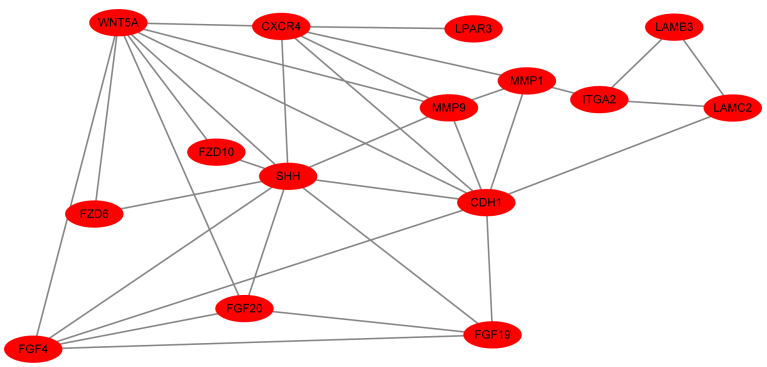

FIGURE 6
The interaction score was >0.7, and the PPI network of all upregulated DEGs (15 nodes and 33 edges) is shown.

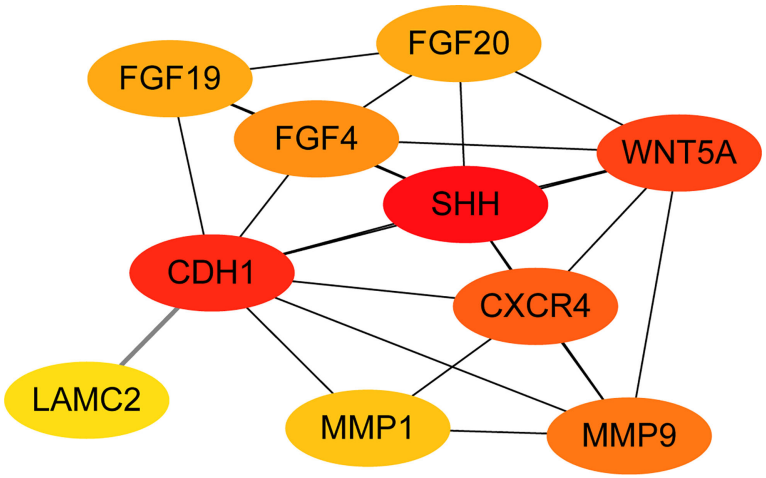

FIGURE 7
The PPI network diagram was constructed from the top 10 key genes among the 15 DEGs.

through *VEGF* has not been clarified. This result provides new directions for future research on ACPs.

As a sequestering protein of β-catenin, E-cadherin (*CDH1*) plays an important role in canonical Wnt signaling (32). Previous studies have reported conflicting results regarding the expression of E-cadherin, encoded by the *CDH1* gene, in ACP. Preda et al. found that *CDH1* expression in ACPs was not correlated with β-catenin (33). However, Qi et al. found that β-catenin was positively correlated with *CDH1* expression in ACP; β-catenin might regulate *CDH1* expression in ACPs, and decreased *CDH1* expression in ACPs has been associated with tumor recurrence (34). However, Barros et al. found that *CDH1* expression in ACPs was not associated with tumor recurrence (32). All these findings need to be further verified. However, our results provide a new direction for the future treatment of ACP.

Cancer-associated fibroblasts (CAFs) are a major component of the cancer stroma and promote cancer cell aggressiveness by secreting multiple factors (35). *WNT5A* was found to be highly expressed in tumor stromal fibroblast gastric cancer studies and was associated with poor prognosis (36). Wnt/β-Catenin and

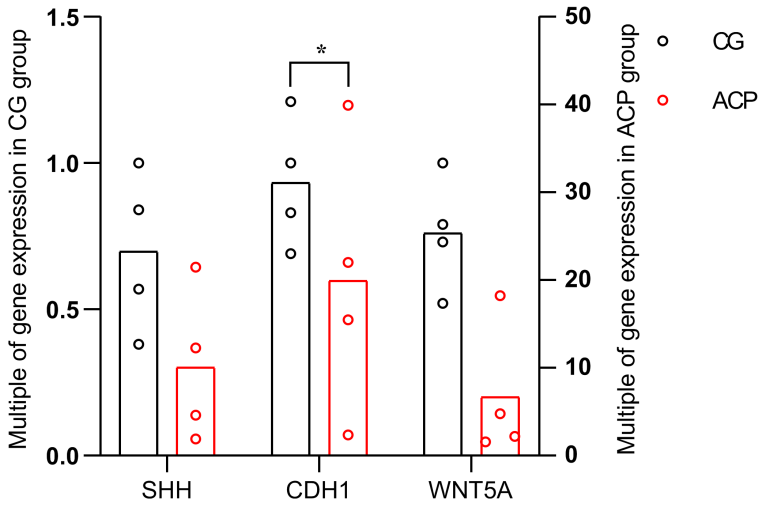

FIGURE 8
The horizontal axis shows the three key genes in the ACP and control groups. The vertical axis shows the mean value of $2^{-\Delta\Delta CT}$ of the three key genes in the ACP and control groups. CGs, individuals with no documented tumor complication samples; ACPs, adamantinomatous craniopharyngioma samples; *$p < 0.05$.

WNT5A/Ca pathways regulate proliferation and apoptosis of keratinocytes in psoriasis lesions (37). It is tempting to speculate that the Wnt/β-Catenin and *WNT5A*/Ca pathways regulate the proliferation and apoptosis of cells, representing a potential new therapeutic target for treating ACP in the future. However, no similar study has been performed for ACP. Although the key genes revealed by RT-PCR in this study are relatively clear, the sample size was small. A larger number of samples are needed for validation. The roles of the three key genes remain unclear and require verification in future studies. WNT5A could be used as a target for the treatment of ACP in the future.

In conclusion, we hope that these methods can be applied in future studies. DAVID was used to thoroughly analyze the DEGs, while GSEA was performed to comprehensively analyze the genes. The main aim of our study was to analyze the KEGG pathways of all genes, including the DEGs, using GSEA. The analysis of large amounts of ACP gene data requires substantial work, and the analysis results are likely to change as the major databases are updated.

Our results suggest that the 15 DEGs, including *CDH1*, *WNT5A*, and *SHH* genes and "pathways in cancer", may be associated with ACP. According to the cytoHubba statistical results in Cytoscape software, the first three DEGs were selected for RT-PCR verification. Our results suggest that CDH1 may play an important role in the pathways in cancer signaling pathway that regulate ACP development. However, its specific role in ACP remains to be confirmed in further experiments. Brastianos et al. showed that in PCPs with the *BRAFV600E* mutation, a *BRAF* inhibitor combined with MEK inhibitor targeted therapy can reduce tumor volume by 85%–91% (6, 7). We expect that ACP can be eliminated by similar treatments in the future. The limitation of this study is that most of the conclusions were drawn from bioinformatics analyses, and previous experimental results are lacking in in-depth research.

Clinical craniopharyngioma is rare. Our neurosurgery department treats approximately 12 patients with craniopharyngioma annually, among which 2–3 have PCP and 1–2 decline surgical treatment. Therefore, it is difficult to obtain a large number of samples for validation in a short time period. In addition, at present, methods for craniopharyngioma cell culture are in the early stages; thus, the characteristics of these tumors are challenging to verify in cell experiments.

In addition, no other analytical methods were used in this study; thus, more reliable conclusions may be obtained by integrating other analytical methods, such as ingenuity pathway analysis and WebGestalt analysis. For the three key genes selected in this study, we hope to further verify these three critical genes identified in this study and explore their specific mechanisms of action in ACP. In particular, we expect that CDH1 will be studied in the future to determine how it regulates the occurrence and development of ACP through the pathways in cancer signaling pathway.

According to the results of this study, we concluded that pathways in cancer signaling pathway is an important signaling pathway in the development of ACP. CDH1, WNT5A, and SHH regulate ACP formation through this pathway. Although this study concludes that CDH1 is the most critical gene, due to the small sample size of this study, we will expand the sample size in the future to further verify this result. For the study of ACP, in addition to CTNNB1 mutation expressing β-catenin to activate the classical Wnt signaling pathway and promote the proliferation and migration of tumor cells, current studies have confirmed that SHH in ACP can also participate in the regulation of the Wnt signaling pathway by promoting the expression of β-catenin through autocrine or paracrine. At the same time, β-catenin can regulate the expression of EGFR and promote the migration of tumor cells (38–40). Unfortunately, these studies have only been carried out in animals and cells and have not been confirmed in clinical trials. In addition, due to the lack of stable ACP cell lines, although many researchers have extracted primary ACP cells from fresh ACP tissues, no stable ACP cell lines have been constructed, so the results of these cell experiments are difficult to accept by the public.

Data availability statement

Publicly available datasets were analyzed in this study. This data can be found here: https://www.ncbi.nlm.nih.gov/geo/query/acc.cgi?acc=GSE94349.

Ethics statement

This study was reviewed and approved by The Research Ethics Committee of Nanchang University [NanChang, China; First Affiliated Hospital of Nanchang University (2020) Medical Research Ethics Review (No. 160)]. Written informed consent to participate in this study was provided by the participants' legal guardian/next of kin.

Author contributions

TH and SZ conceived the study and supervised the research. CF performed the bioinformatics analysis and was a major contributor to the writing of the manuscript. LZ prepared the figures and edited the manuscript. HH performed the PCR validation experiments. All authors contributed to the article and approved the submitted version.

Funding

This study was supported by the National Natural Science Foundation of China (grant no. 82060246), the Natural Science Foundation of Jiangxi Province, and the Science and Technology

Research Project of Jiangxi Provincial Education Department (grant nos. 20202BABL206059 and GJJ190128).

Conflict of interest

The authors declare that the research was conducted in the absence of any commercial or financial relationships that could be construed as a potential conflict of interest.

Publisher's note

References

1. Lehrich BM, Goshtasbi K, Hsu FPK, Kuan EC. Characteristics and overall survival in pediatric versus adult craniopharyngioma: A population-based study. *Childs Nerv Syst* (2021) 37:1535–45. doi: 10.1007/s00381-021-05094-y

2. Yang L, Xie SH, Fang C, EM Z, Tang B, Hong T. Preservation of hypothalamic function with endoscopic endonasal resection of hypothalamus-invaded craniopharyngiomas. *World Neurosurg* (2019) 132:e841–51. doi: 10.1016/j.wneu.2019.07.225

3. Michael. Craniopharyngioma Treasure Island (FL: StatPearls Publishing) (2021).

4. Müller HL, Merchant TE, Warmuth-Metz M, Martinez-Barbera JP, Puget S. Craniopharyngioma. *Nat Rev Dis Primers* (2019) 5(1):75. doi: 10.1038/s41572-019-0125-9

5. Omay SB, Chen YN, Almeida JP, Ruiz-Treviño AS, Boockvar JA, Stieg PE, et al. Do craniopharyngioma molecular signatures correlate with clinical characteristics? *J Neurosurg* (2018) 128(5):1473–8. doi: 10.3171/2017.1.JNS162232

6. Brastianos PK, Shankar GM, Gill CM, Taylor-Weiner A, Nayyar N, Panka DJ, et al. Dramatic Response of BRAF V600E Mutant Papillary Craniopharyngioma to Targeted Therapy. *J Natl Cancer Inst* (2015) 108(2): djv310. doi: 10.1093/jnci/djv310

7. Rostami E, Witt Nyström P, Libard S, Wikström J, Casar-Borota O, Gudjonsson O. Recurrent papillary craniopharyngioma with BRAFV600E mutation treated with neoadjuvant-targeted therapy. *Acta Neurochir (Wien)* (2017) 159(11):2217–21. doi: 10.1007/s00701-017-3311-0

8. Yang J, Hou Z, Wang C, Wang H, Zhang H. Gene expression profiles reveal key genes for early diagnosis and treatment of adamantinomatous craniopharyngioma. *Cancer Gene Ther* (2018) 25(9-10):227–39. doi: 10.1038/s41417-018-0015-4

9. Gomes DC, Jamra SA, Leal LF, Colli LM, Campanini ML, Oliveira RS, et al. Sonic hedgehog pathway is upregulatedin adamantinomatous craniopharyngiomas. *Eur J Endocrinol* (2015) 172(5):603–8. doi: 10.1530/EJE-14-0934

10. Edgar R, Barrett T. NCBI GEO standards and services for microarray data. *Nat Biotechnol* (2006) 24(12):1471–2. doi: 10.1038/nbt1206-1471

11. Zou YF, Meng LB, Wang QQ, He ZK, Hu CH, Shan MJ, et al. Identification and functionalenrichment analysis of potential diagnostic and therapeutic targets in adamantinomatous craniopharyngioma. *J Comput Biol* (2020) 27(1):55–68. doi: 10.1089/cmb.2019.0184

12. Li M, Zhou L, Li S, Fang L, Yang L, Wu X, et al. MMP12 is a potential therapeutic target for Adamantinomatous craniopharyngioma: Conclusions from bioinformatics analysis and *in vitro* experiments. *Oncol Lett* (2021) 22(1):536. doi: 10.3892/ol.2021.12797

13. Donson AM, Apps J, Griesinger AM, Amani V, Witt DA, Anderson RCE, et al. Molecular analyses revealinflammatory mediators in the solidcomponent and cyst fluid of human adamantinomatous craniopharyngioma. *J Neuropathol Exp Neurol* (2017) 76(9):779–88. doi: 10.1093/jnen/nlx061

14. Benjamini Y, Yekutieli D. The control of the false discovery rate in multiple testing under dependency. *Ann Statist* (2001) 29:1165–88. doi: 10.1214/aos/1013699998

15. Guo T, Hou D, Yu D. Bioinformatics analysis of gene expression profile datato screen key genes involved in intracranial aneurysms. *Mol Med Rep* (2019) 20 (5):4415–24. doi: 10.3892/mmr.2019.10696

16. Li Z, Zhong L, Du Z, Chen G, Shang J, Yang Q, et al. Network analyses of differentially expressed genes in osteoarthritis to identify hub genes. *BioMed Res Int* (2019) 2019:8340573. doi: 10.1155/2019/8340573

17. Yu H, Pardoll D, Jove R. STATs in cancer inflammation and immunity: A leading role for STAT3. *Nat Rev Cancer* (2009) 9:798–809. doi: 10.1038/nrc2734

18. Apps JR, Carreno G, Gonzalez-Meljem JM, Haston S, Guiho R, Cooper JE, et al. Tumour compartmenttranscriptomics demonstrates the activation of inflammatory and odontogenic programmes in human adamantinomatous craniopharyngioma and identifies theMAPK/ERK pathway as a novel therapeutic target. *Acta Neuropathol* (2018) 135(5):757–77. doi: 10.1007/s00401-018-1830-2

19. Chen M, Zheng SH, Liu Y, Shi J, Qi ST. Periostin activates pathways involve dinepithelial-mesenchymal transition in adamantinomatous craniopharyngioma. *Neurol Sci* (2016) 360:49–54. doi: 10.1016/j.jns.2015.11.042

20. Tena-Suck ML, Ortiz-Plata A, Galán F, Sánchez A. Expression of epithelial celladhesion molecule and pituitary tumor transforming gene in adamantinomatous craniopharyngioma and its correlation with recurrence of the tumor. *Ann DiagnPathol* (2009) 13(2):82–8. doi: 10.1016/j.anndiagpath.2008.12.004

21. Ganz JC. Craniopharyngiomas. *Prog Brain Res* (2022) 268(1):217–27. doi: 10.1016/bs.pbr.2021.10.033

22. He J, Zeng Z, Wang Y, Deng J, Tang X, Liu F, et al. Characterization of novel CTNNB1 mutation incraniopharyngioma by whole-genome sequencing. *Mol Cancer* (2021) 20(1):168. doi: 10.1186/s12943-021-01468-7

23. Hölsken A, Buchfelder M, Fahlbusch R, Blümcke I, Buslei R. Tumour cell migration inadamantinomatous craniopharyngiomas is promoted by activated wnt-signalling. *Acta Neuropathol* (2010) 119(5):631–9. doi: 10.1007/s00401-010-0642-9

24. Morra L, Moch H. Periostin expression and epithelial-mesenchymal transition in cancer: A review and an update. *Virchows Arch* (2011) 459(5):465–75. doi: 10.1007/s00428-011-1151-5

25. Kim CJ, Sakamoto K, Tambe Y, Inoue H. Opposite regulation of epithelial-to-mesenchymal transition and cell invasiveness by periostin between prostate and bladder cancer cells. *Int J Oncol* (2011) 38(6):1759–66. doi: 10.3892/ijo.2011.997

26. Andoniadou CL, Gaston-Massuet C, Reddy R, Schneider RP, Blasco MA, Le Tissier P, et al. Identificationof novel pathways involved in the pathogenesis of human adamantinomatous craniopharyngioma. *Acta Neuropathol* (2012) 124 (2):259–71. doi: 10.1007/s00401-012-0957-9

27. Kumar V, Goutam RS, Park S, Lee U, Kim J. Functional Roles of FGF Signaling in Early Development of Vertebrate Embryos. *Cells* (2021) 10(8):2148. doi: 10.3390/cells10082148

28. Wesche J, Haglund K, Haugsten EM. Fibroblast growth factors and their receptors in cancer. *Biochem J* (2011) 437(2):199–213. doi: 10.1042/BJ20101603

29. Bao Y, Gabrielpillai J, Dietrich J, Zarbl R, Strieth S, Schröck F, et al. Fibroblast growth factor (FGF), FGFreceptor (FGFR), and cyclin D1 (CCND1) DNA methylation in head and necksquamous cell carcinomas is associated with transcriptional activity, geneamplification, human papillomavirus (HPV) status, and sensitivity to tyrosinekinase inhibitors. *Clin Epigenet* (2021) 13(1):228. doi: 10.1186/s13148-021-01212-4

30. Treier M, Gleiberman AS, O'Connell SM, Szeto DP, McMahon JA, McMahon AP, et al. Multistep signalingrequirements for pituitary organogenesis in vivo. *Genes Dev* (1998) 12(11):1691–704. doi: 10.1101/gad.12.11.1691

31. Hu C, Chen J, Meng Y, Zhang J, Wang Y, Liu R, et al. Phosphorus-32 interstitial radiotherapy forrecurrent craniopharyngioma: Expressions of vascular endothelial growth factorand its receptor-2 and imaging features of tumors are associated with tumorr adi os ensitivi ty. *Med (Bal timor e)* (2018) 97(26):e11136. doi: 10.1097 /MD.0000000000011136

32. Jucaá CEB, Colli LM, Martins CS, Campanini ML, Paixão B, Jucá RV, et al. Impact of the canonical wnt pathwayactivati on on the pa thogenesis and prognosis of adamantinomatous craniopharyngiomas. *Horm Metab Res* (2018) 50(7):575–81. doi: 10.1055/a-0593-5956

33. Preda V, Larkin SJ, Karavitaki N, Ansorge O, Grossman AB. The wnt signalling cascade and theadherens junction complex in craniopharyngioma tumorigenesis. *Endocr Pathol* (2015) 26(1):1–8. doi: 10.1007/s12022-014-9341-8

34. Qi ST, Zhou J, Pan J, Zhang C, Silky C, Yan XR. Epithelial-mesenchymal transition andclinicopathological correlation in craniopharyngioma. *Histopathology* (2012) 61(4):711–25. doi: 10.1111/j.1365-2559.2012.04297.x

35. Kalluri R. The biology and function of fibroblasts in cancer. *Nat Rev Cancer* (2016) 16(9):582–98. doi: 10.1038/nrc.2016.73

36. Maeda M, Takeshima H, Iida N, Hattori N, Yamashita S, Moro H, et al. Cancer cell niche factors secretedfrom cancer-associated fibroblast by loss of H3K27me3. *Gut* (2020) 69(2):243–51. doi: 10.1136/gutjnl-2018-317645

37. Zhang Y, Tu C, Zhang D, Zheng Y, Peng Z, Feng Y, et al. Wnt/b-catenin and Wnt5a/Ca pathwaysregulate proliferation and apoptosis of keratinocytes in psoriasis lesions. *CellPhysiol Biochem* (2015) 36(5):1890–902. doi: 10.1007/s11102-018-0890-6

38. Prieto R, Pascual JM. Can tissue biomarkers reliably predict the biological behavior of craniopharyngiomas? a comprehensive overview. *Pituitary* (2018) 21:431–42. doi: 10.1007/s11102-018-0890-6

39. Hölsken A, Gebhardt M, Buchfelder M, Fahlbusch R, Blümcke I, Buslei R. EGFR signaling regulatestumor cell migration in craniopharyngiomas. *Clin Cancer Res* (2011) 17(13):4367–77. doi: 10.1158/1078-0432.CCR-10-2811

40. Buslei R, Hölsken A, Hofmann B, Kreutzer J, Siebzehnrubl F, Hans V, et al. Nuclear beta-catenin accumulationassociates with epithelial morphogenesis in craniopharyngiomas. *Acta Neuropathol* (2007) 113(5):585–90. doi: 10.1007/s00401-006-0184-3

frontiers | Frontiers in Oncology

TYPE Original Research
PUBLISHED 14 November 2022
DOI 10.3389/fonc.2022.1009796

OPEN ACCESS

EDITED BY
Maria Caffo,
University of Messina, Italy

REVIEWED BY
Yubo Wang,
First Affiliated Hospital of Jilin University, China
Kristin Huntoon,
University of Texas MD Anderson Cancer Center, United States
Mirza Pojskic,
University Hospital of Giessen and Marburg, Germany

*CORRESPONDENCE
Francesco Acerbi
francesco.acerbi@istituto-besta.it

SPECIALTY SECTION
This article was submitted to Neuro-Oncology and Neurosurgical Oncology, a section of the journal Frontiers in Oncology

RECEIVED 02 August 2022
ACCEPTED 19 October 2022
PUBLISHED 14 November 2022

CITATION
Falco J, Broggi M, Vetrano IG, Rubiu E, Schiariti M, Restelli F, Mazzapicchi E, Bonomo G, La Corte E, Ferroli P and Acerbi F (2022) Fluorescein sodium in the surgical treatment of pleomorphic xanthoastrocytomas: Results from a retrospective study.
Front. Oncol. 12:1009796.
doi: 10.3389/fonc.2022.1009796

Fluorescein sodium in the surgical treatment of pleomorphic xanthoastrocytomas: Results from a retrospective study

Jacopo Falco[1], Morgan Broggi[1], Ignazio G. Vetrano[1,2], Emanuele Rubiu[1], Marco Schiariti[1], Francesco Restelli[1], Elio Mazzapicchi[1], Giulio Bonomo[1], Emanuele La Corte[1], Paolo Ferroli[1] and Francesco Acerbi[1]*

[1]Department of Neurosurgery, Fondazione IRCCS Istituto Neurologico Carlo Besta, Milan, Italy, [2]Department of Biomedical Sciences for Health, Università degli Studi di Milano, Milan, Italy

Objective: Pleomorphic xanthoastrocytoma (PXA) is a rare brain tumor, most commonly affecting children and young adults. Surgical resection represents the mainstay of treatment, and extent of resection is associated with improved survival. In this study, we analyzed the role of sodium fluorescein (SF) in improving intraoperative visualization easing resection.

Methods: Surgical database of FLUOCERTUM study (Besta Institute, Milan, Italy) was retrospectively reviewed to find pleomorphic xanthoastrocytomas and anaplastic xanthoastrocytomas, according to WHO-2016/2021 classification, surgically removed by a fluorescein-guided technique from March 2016 to February 2022. SF was intravenously injected (5mg/kg) immediately after induction of general anesthesia. Tumors were removed using a microsurgical technique with the YELLOW 560 filter (*Carl Zeiss Meditec, Oberkochen, Germany*).

Results: Twelve patients (7 males and 5 females; 3 pediatric patients, mean age 10 years, range 5 to 13 years and 9 adult patients, mean age 50.6 years, range 35 to 63 years) underwent fluorescein-guided surgery. No side effects related to SF occurred. In all tumors, contrast enhancement on preoperative MRI correlated with intense, heterogeneous yellow fluorescence with bright fluorescent cystic fluid. Fluorescein was considered helpful in distinguishing tumors from viable tissue in all cases. Gross total resection was achieved in 8 cases (66.7%); in 4 cases, otherwise, the resection was subtotal with fluorescent residual spots to avoid neurological worsening (33.3%).

Conclusions: The use of SF is a valuable method for safe fluorescence-guided tumor resection. Our data documented a positive effect of fluorescein-guided surgery on intraoperative visualization, suggesting a probable role in improving the extent of resection during yellow surgery of PXA.

KEYWORDS

central nervous system tumors, neuro-oncology, yellow 560 filter, fluorescence-guided neurosurgery, pleomorphic xanthoastrocytoma (PXA), sodium fluorescein (SF)

Introduction

Pleomorphic xanthoastrocytoma (PXA) is a rare, low-grade glial tumor, commonly affecting young adults and children (1); no gender predilection was reported. According to the 2016 (2) and 2021 (3) World Health Organization (WHO) tumors classification, PXA are classified as grade II/2 or III/3 tumors; the latter, previously designated as pleomorphic xanthoastrocytoma with anaplastic features, are characterized by a mitotic index ≥ 5/10 high-power fields and are currently considered anaplastic gliomas. According to 2016 classification, pleomorphic xanthoastrocytomas and anaplastic pleomorphic xanthoastrocytomas were considered two different entities; conversely, according to WHO CNS5 version (3), PXA is a single tumor type, anaplastic has been excluded as a modifier term in favor of a grading diagnosis relative to the tumor type (i.e. grade 2 or 3) to provide more flexibility in categorization and to emphasize biological similarities within tumor types rather than approximate clinical behavior. Pleomorphic xanthoastrocytomas have a relatively favorable prognosis when compared with diffusely infiltrative astrocytomas (4).

PXA presented at MRI (5) with a heterogeneous contrast enhancement due to blood brain barrier (BBB) disruption, with peritumoral infiltrative/vasogenic brain edema; these tumors sometimes consist of solid and cystic components: the cystic fluid is generally isointense as compared with cerebrospinal fluid. Leptomeningeal enhancement is seen in a subset of patients.

Among circumscribed gliomas, PXA can present some infiltrative features: indeed, it can be difficult to distinguish between circumscribed and diffuse astrocytic gliomas. They can look very similar to epithelioid glioblastomas, especially for grade 3 PXA. Genomic methylation profiling (BRAF V600E, CDKN2A/B) is particularly helpful in such circumstances (6), as many tumors thought to be epithelioid glioblastomas actually map either to PXA or pediatric high-grade glioma.

Surgical resection is considered the cornerstone of therapy (1, 4, 7, 8); furthermore, recent reports suggest a prolonged survival in patient treated with a gross total resection (GTR). The role of adjuvant treatment in grade II/2 tumors has not been agreed upon and clinical practice varies widely; otherwise, patients affected by grade III/3 astrocytomas are generally scheduled for adjuvant Stupp protocol. Patients are usually followed up by regular imaging, as re-resection is advised at recurrence.

Sodium fluorescein (SF) is a dye that, when intravenously injected, has the peculiar characteristic to accumulate in cerebral areas presenting a damage of the BBB (9, 10). The use of a dedicated filter in the surgical microscope, with specific wavelength for fluorescein (540-690nm), allows to improve the tumor-brain discrimination intraoperatively, reducing also the dosage needed to obtain this effect (11–13). In particular, this has been shown to be associated to a better tumor identification and resection in different tumors of the central nervous system (CNS) such as high-grade gliomas (14, 15), gangliogliomas (16), cerebral metastasis (17), and primary CNS lymphomas (18), both in adult and pediatric population (19).

In July 2015, based upon preliminary scientific results from different studies published in the international literature (20, 21), including a prospective phase II trial from our group, the Italian Medicine Agency (AIFA) has extended the indications for the utilization of fluorescein molecule (https://www.gazzettaufficiale.it/atto/serie_generale/caricaDettaglioAtto/originario;jsessionid=izVcTOmnjOzfNRjjw56kAA:.ntc-as2-guri2b?atto.dataPubblicazioneGazzetta=2015-07-22&atto.codiceRedazionale=15A05620&elenco30giorni=false). According to this determination, the intravenous (i.v.) injection of SF as a neurosurgical tracer during oncological procedures for aggressive tumors of the CNS is approved and its cost is totally reimbursed by the Italian National Health System (15). A low dose (5 mg/kg) of fluorescein is i.v. administrated at the end of patient intubation (around one hour before dural opening). Since our first experience in 2011 in HGG resection (20) by means of YELLOW 560 filter (*Carl Zeiss Meditec, Oberkochen, Germany*), we have used the low dosage of 5 mg/kg for our subsequent studies and surgical procedures; this protocol has standardized SF usage independently from the characteristics of the patients or of the tumors.

In March 2016, the authors started a new prospective observational study, called FLUOCERTUM (FLUOrescein in CERebral TUMors), regarding the use of SF as a fluorescent intra-operative tracer in patients with suspected aggressive tumors of the CNS (15).

Due to the characteristics MRI contrast uptake in PXA, the use of SF as a fluorescent tracer could allow a better intraoperative discrimination of the tumoral tissue even in this tumor subtype, with beneficial effect during the surgical resection (22). The foundation of our study lays upon the intrinsic staining potential of fluorescein and the radiological features of PXA, characterized by an intense contrast-enhanced pattern (5). Since fluorescein molecule presents a slightly lower molecular weight than that of the contrast medium, the rational of its utilization is to selectively stain the contrast-enhanced areas of PXA to improve the intraoperative visualization of the tumor and its borders, better delineating even the components where contrast enhancement was not prominent (23). The principal aim of this paper consists in showing the advantages and the valuable role of fluorescein in visualization and resection of pleomorphic xanthoastrocytomas in our case series.

Methods

Patients and inclusion criteria

In this study, we retrospectively reviewed the database of the prospective observational FLUOCERTUM study, started in March 2016 and approved by the Institutional Review Board, to identify the cohort of patients affected by pleomorphic xanthoastrocytoma until February 2022. The FLUOCERTUM inclusion criteria were as follows: patients of both genders, at any age; patients with suspected aggressive lesions of the CNS, as suggested by preoperative MRI or CT with i.v. contrast agent administration. The exclusion criteria were: impossibility to give consent due to cognitive deficits or language disorders; known allergy to contrast agents or history of previous anaphylactic shocks; known severe previous adverse reactions to SF; acute myocardial infarction or stroke in the last 90 days; severe organ failure; women in their first trimester of pregnancy or lactation. The retrospective case series revision aims to identify all those consecutive patients scheduled for fluorescein-guided surgery with a histopathologically confirmed PXA according to 2016/2021 WHO CNS5 tumors classification.

Clinical and radiological management

Preoperative assessment included physical and neurological examination (Karnofsky Performance Status [KPS] (24) in adult patients and Lansky Play-Performance status [LPS] (25) in pediatric ones), laboratory tests results and contrast-enhanced MRI for neuronavigation. In preoperative MRI, patients were categorized based on preoperative contrast enhancement characteristics. To evaluate the extent of resection (EOR), a volumetric MRI examination was performed for each patient within 72 hours after surgery; in particular, to calculate the residual pathological volume, the hyperintense alterations in volumetric basal T1 acquisitions were subtracted from the volume of hyperintense tissue in post-contrast volumetric T1 images, to avoid the incidental inclusion of blood or blood product (26). The EOR was calculated as a percentage of tumor resection based on early contrast-enhanced postoperative MRI; according to the entity of resection, we distinguished four main categories: GTR (EOR 100%), sub-total resection (STR, with an EOR of 90–100%), partial resection (PR, 30–90%) and biopsy. The postoperative clinical evaluation included a standard neurological examination as above as well as laboratory test (kidney function) and exclusion of occurrence of any side effect related to fluorescein injection. Clinical and neuroradiological long-term follow-up was performed for postoperative period as part of normal clinical practice, including telephonic interview.

Surgical protocol

The standardized surgical protocol of fluorescein-guided technique, as already described in previous papers (11, 12, 15, 20, 21), is based on i.v. SF (*Monico S.p.A., Venice, Italy*) injection at standard dose of 5mg/kg, by a central or peripheral venous line, immediately upon completion of the induction of general anesthesia. Surgery was performed with the aid of a surgical microscope equipped with an integrated fluorescent filter tailored to the excitation and emission wavelength of sodium fluorescein (YELLOW 560 – *Pentero 900* and *Kinevo; Carl Zeiss Meditec, Oberkochen, Germany*). Surgical procedures were executed by different surgeons with the same philosophy regarding the importance and evaluation of SF and with the principle of the maximal safe resection. During resection, the microscope could be switched alternatively from fluorescent to white-light illumination; neuronavigation, intraoperative contrast enhanced ultrasounds or other tools could be used according to the surgeon's preference. In tumors located adjacent to eloquent areas, intraoperative neurophysiological monitoring was used. Tumors were removed in an inside-out fashion until all fluorescent tissue was removed, as considered feasible by the surgeon.

Intraoperative fluorescence characteristics and side effects

Fluorescence intensity was graded by the surgeon as intense, moderate, slight or absent; surgeons were also asked to classify the use of SF per each procedure as useful, useless or not essential to achieve surgical aims. Furthermore, medical reports were evaluated for any possible adverse effect or allergic reaction to fluorescein administration.

Statistical analysis

The heterogeneous sample was described by means of the usual descriptive statistics: mean, median and standard deviation for continuous variables and proportions for categorical ones. PRISM software for Macintosh was used for the statistical analysis.

Results

Patients population

We enrolled 12 patients (7 males and 5 females; 3 pediatric patients, mean age 10 years, range 5 to 13 years and 9 adult patients, mean age 50.6 years, range 35 to 63 years) affected by pleomorphic xanthoastrocytomas (Table 1).

All patients presented with variable contrast enhancement pattern on the preoperative MRI: predominantly, PXA showed a heterogeneous enhancement (6/12 – 50%) with different degree of intensity and occasional presence of cystic components; in 2 cases (16.7%), the tumor presented a homogeneous and intense contrast enhancement whereas in other 2 cases (16.7%) the contrast uptake resulted peripheral and heterogeneous with central cystic-necrotic areas. Finally, 2 PXA (16.7%) appeared characterized by an intense enhancement of the solid, mural component with a large, satellite cyst (Table 1).

Most patients underwent surgery until 2021; 4 out of 12 cases (33.3%) resulted pleomorphic xanthoastrocytoma (grade II, WHO 2016), 6 of them (50.0%) were diagnosed anaplastic pleomorphic xanthoastrocytoma whereas 1 patient (8.3%) was affected by pleomorphic xanthoastrocytoma (grade 2, WHO CNS5 2021) and another (8.3%) by pleomorphic xanthoastrocytoma (grade 3, WHO CNS5 2021). Data on the clinical condition at admission, discharge, and follow-up and intraoperative findings were available for all patients (Table 1).

Intraoperative fluorescence characteristics and surgeon's opinion

Intense fluorescent staining was reported in 10/12 cases (83.3%) whereas a moderate fluorescence enhancement was detected in 2 patients (16.7%). In 2 multicystic tumors, independently from specific fluorescein enhancement, we observed a bright fluorescent cystic fluid (Table 1). Five patients of our series (41.7%) were taking presurgical corticosteroid as a mild anti-edema (dexamethasone 4-8mg/day) and as a symptomatic relief; according to our case analysis, preoperative corticosteroid therapy did not affect fluorescence characteristics, as subjectively judicable by the surgeons. In all cases, intraoperative fluorescence was deemed helpful (Table 1) in achieving GTR by means of a better delineation of the borders of the tumor tissue from the health parenchyma, as compared to the conventional microsurgical technique using white-light illumination (Figure 1). Intraoperative fluorescence corresponded to preoperative MRI documented contrast enhancement. No technical difficulties regarding the use of the microscope filter nor switching between white and yellow light were encountered during the surgical resections.

Extent of resection

GTR was achieved in 8 cases out of 12 patients scheduled for tumor removal (66.7%); in 2 cases (16.7%) the resection was planned as subtotal (planned STR) due to the volume of the lesion and the relationship with eloquent areas whereas in other 2 patients (16.7%), an intended STR was the consequence of the intraoperative identification of fluorescent residual spots in the context of eloquent tissue identified by means of intraoperative neurophysiological monitoring and due to tenacious adherences with MCA branches, in order to avoid neurological worsening (Table 1).

Side effects and outcome

No adverse drug reaction related to SF injection was reported in this cohort of patients; the only remarkable and visible effect was the transient yellowish staining of urine which disappeared in about 24 hours.

At baseline, 9/12 (75%) of patients had KPS/LPS scores of 80-100, indicating good clinical and neurological conditions. Surgical morbidity led to a postoperative mild decline of KPS/LPS score in 5 patients; 6 patients were discharged with an unchanged KPS/LPS score whereas 1 patient presented a clinical improvement by means of surgical treatment. At discharge, 5/12 (41.7%) of patients had KPS/LPS scores of 80-100 (Table 1).

In addition to minor neurological complications related to the surgical manipulation of the specific eloquent structures, in 1 patient (n.5) a hemorrhagic complication requiring a re-craniotomy occurred (extradural hematoma); no significant neurological impairment derived from this emergency condition. Two patients with periventricular tumoral localization (n.6 and n.10) developed, in the postoperative course, a subacute obstructive hydrocephalus which required surgical management through positioning of a ventriculoperitoneal shunt.

The follow-up period ranged between 2 and 55 months, with a median follow-up of 24.1 months.

Tumor grading significantly influenced patient outcome; indeed, anaplastic PXA were characterized by a worst prognosis. Grade II/2 tumors were followed-up both clinically and radiologically whereas grade III/3 tumors were scheduled for Stupp protocol; no target or other pilot therapy was administered as a first line: B-Raf-inhibitor (Vemurafenib) was

TABLE 1 Characteristics of the patients and main results.

Nr.	Age	Gender	Clinical presentation	KPS/ LPS pre-op	Tumor location	Tumor enhancement	Fluorescence intensity	Intra-op side effects	Surgeon's opinion	Residual fluorescence (Y/N - explanation)	EOR (GTR, intended STR, unintended STR, PR-debulking, biopsy)	Histology	KPS/ LPS post-op	FU (Months)	FU (Radiological)	FU (KPS/ LPS)
1	5	F	visual deficit	60	left temporo-parieto-occipital	heterogeneous and intense with cystic components	moderate	no	useful	N	GTR	anaplastic pleomorphic xanthoastrocytoma (WHO III)	70	55	tumor free	80
2	37	M	seizure	90	right temporal	heterogeneous and intense	intense	no	useful	N	GTR	pleomorphic xanthoastrocytoma (WHO II)	90	52	tumor free	100
3	12	F	seizure	90	left temporal	homogeneous and intense	intense	no	useful	N	GTR	pleomorphic xanthoastrocytoma (WHO II)	90	43	tumor free	90
4	51	F	worsening headache	100	left occipital	heterogeneous and intense with cystic components	intense (bright cystic fluid)	no	useful	N	GTR	pleomorphic xanthoastrocytoma (WHO II)	100	38	tumor free	100
5	41	M	left hemiplegia, headache	60	left fronto-temporo-insular	peripheral with central necrosis	intense	no	useful	Y – fluorescent tissue adherent to insular branches of MCA and to CST	iSTR	anaplastic pleomorphic xanthoastrocytoma (WHO III)	50	20	progression disease (–> CHT)	70
6	57	M	headache	80	left fronto-mesial, lateral ventricle	homogeneous and intense	intense	no	useful	N	GTR	anaplastic pleomorphic xanthoastrocytoma (WHO III)	70	31	tumor free	90
7	63	F	confusion	80	left temporal	peripheral with central necrosis	intense	no	useful	N	GTR	anaplastic pleomorphic xanthoastrocytoma (WHO III)	70	25	progression disease (–> palliative CHT)	30
8	54	F	right hand motor impairment	80	left frontal	heterogeneous and intense	intense	no	useful	N	GTR	anaplastic pleomorphic xanthoastrocytoma (WHO III)	70	10	progression disease (–> CHT)	80
9	57	M	right hemiparesis, disphasya, confusion	60	left temporo-insular	intense enhancement of the solid component with a large cyst	intense	no	useful	Y – fluorescent tissue infiltrating MCA perforators and CST	iSTR	anaplastic pleomorphic xanthoastrocytoma (WHO III)	60	5	progression disease (–> CHT)	80
10	35	M	headache	80	left peritrigonal	heterogeneous and intense with cystic components	intense fluorescence	no	useful	Y – fluorescent tissue adherent to CST and to arcuate fascicle	planned iSTR	pleomorphic xanthoastrocytoma (WHO II)	80	5	stable tumor	90
11	60	M	right arm and leg motor deficit	80	left front-parietal	heterogeneous and faint	intense fluorescence	no	useful	Y – fluorescent tissue adherent to CST	planned iSTR	pleomorphic xanthoastrocytoma (WHO 3)	60	3	progression disease (–> palliative CHT)	0
12	13	M	headache	100	left frontal	intense enhancement of the solid component with a large cyst	moderate (bright cystic fluid)	no	useful	N	GTR	pleomorphic xanthoastrocytoma (WHO 2)	100	2	tumor free	100

10.3389/fonc.2022.1009796

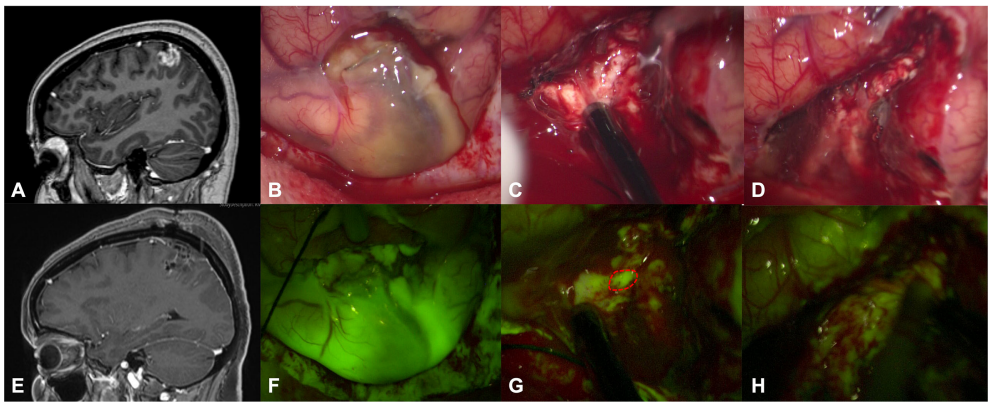

FIGURE 1
Preoperative T1 with contrast sagittal scan **(A)** in a 54-year-old female (patient n.8) shows a left frontal anaplastic pleomorphic xanthoastrocytoma with a gross-total resection, as detectable by postoperative post-contrast T1 MRI in **(E)**. After dural opening, it was possible to appreciate a greyish and pale lesion **(B)** that was better highlighted after activation of YELLOW 560 filter **(F)**. The tumor was removed with an inside-out fashion with the aid of a monopolar suction probe, showing a bleeding, friable tissue **(C)**. During surgical resection, fluorescein helps the surgeon to identify residual pathological tissue (dotted lines in **G**), not clearly visible under white light **(C)**. At the end of resection **(D, H)**, no more fluorescent/pathological areas were detectable with the YELLOW 560 filter activated or with white light illumination.

purposed in case of progression disease (27). Follow-up data were available for all patients.

Regarding grade II/2 PXA, all 5 patients were neuroradiologically stable (tumor free or stable remnant tumor) with substantially unchanged clinical status (Table 1).

Otherwise, regarding anaplastic PXA (7 cases), only 2 patients (28.6%) were neuroradiological stable (tumor free) presenting a clinical improvement measured by means of the KPS/LPS score. Three patients (42.9%) presented progression disease although Stupp protocol and are prosecuting with a chemotherapeutic approach with the possibility of performing a re-do surgery; finally, in 2 cases (28.6%), progression disease was so quick and clinically worsening leaving space only for palliative therapies (Table 1).

Discussion

To our knowledge, this is the first report evaluating the advantages of fluorescein-guided surgery in PXA resection. Given that the contrast uptake at the preoperative T1-weighted MRI reflects the fluorescent staining pattern of the tumor (9, 15), we hypothesized that the use of the SF would have positively affected the intraoperative magnification of these neoplasms. Indeed, the use of SF could improve tumor visualization and, therefore, the entity of tumor removal (14): our observation was associated with contrast enhancement on preoperative MRI, which was present in almost all tumors of our series.

Ten patients enrolled in the study were scheduled for surgery with a previous planning of macroscopic resection but keeping in mind the philosophy of maximal safe resection: in this series, we obtained GTR in more than half of the patients (8/10, 80.0%); this data can be explained by the fact that many tumors were located in such eloquent regions in which a sub-total resection is sometimes advisable, in order to avoid permanent neurological deficits. As a matter of fact, minimal residual tumor (lower than 10% of preoperative tumor volume) at postoperative MRI was expected in 4 cases out of the total 12 patients (33.3%), as it was involving eloquent areas (sensorimotor region, corticospinal tract, and arcuate fascicle) or due to the adherences to MCA insular or perforating branches and was therefore independent from the fluorescence visualization. Therefore, in these cases, the EOR was related to the identification of eloquent subcortical tissue during resection, by means of neurophysiological monitoring, that allowed obtaining a maximal safe resection. In fact, in all cases, surgeon-reported visibility of pathologic tissue was clearly enhanced by SF and YELLOW 560 filter view and almost always judged helpful for complete tumor resection.

Pleomorphic xanthoastrocytoma is an astrocytic tumor thought to originate from subpial astrocytes or their precursors (1, 7). It is a rare entity accounting for < 1% and it is mostly seen in children and adolescents, with a median age of onset of 22 years old (22). They can arise anywhere along the neuroaxis, but they usually originate in the temporal lobe inducing epilepsy as a presenting symptom. PXA is a relatively recent entity with variable clinical outcome and still current dilemma regarding the optimum treatment (1); the rarity of this disease precludes conducting a strong trial: currently, aggressive surgical resection is the more effective therapeutic intervention because of its irrefutable correlation with both overall survival

(OS) and progression-free survival (PFS). The role of supramaximal resection is discussed but no evidence is present.

According to WHO CNS5 classification (3), pleomorphic astrocytomas are considered as circumscribed astrocytic gliomas in consideration of their more solid growth pattern, as opposed to the strongly infiltrative behavior of diffuse astrocytomas; they are include in the same group of the more frequent pilocytic astrocytomas (PA), though, at the same time and as discussed above, PXA present some infiltrative features which make them like adult-type diffuse astrocytoma. In relation to mitotic index and specific mutations, PXA are classified as a grade II/2 or III/3 tumors. Pediatric PXA patients have improved survival outcomes compared to their adult counterparts. PXA have a higher tendency to recur than other gliomas; indeed, PFS is similar between grade II/2 and grade III/3 tumors, whereas anaplastic pleomorphic xanthoastrocytomas, having a more aggressive behavior, present a worse prognosis with a significative impact on OS. Therefore, the WHO grading is still important, remaining a strong predictor of overall survival.

Few recent published series regarding this argument show that GTR was achievable in about half of the patients operated with white-light illumination (7, 22, 28). In this perspective, the application of new technical tools aiming at improving the EOR could be beneficial in the management of PXA. During the last years SF has emerged as intraoperative tracer able to improve brain-tumor visualization (14–16), due to its vascular, non-specific mechanism of action related to the accumulation in brain regions with BBB disruption (9, 12): these areas present an altered permeability that seems to correlate consistently with the contrast enhanced portions of T1-weighted MRI sequences, accounting for the staining capacity of this fluorescent tracer with tumors that uptake contrast (21). Previous experiences had suggested that the use of SF could be associated with a bright fluorescence of the tumor area in primary and recurrent high-grade gliomas (14, 15, 20, 29), in brain metastases (17), in primary CNS lymphomas (18), in gangliogliomas (16), and recently in the similar entity of circumscribed astrocytic gliomas which are the pilocytic astrocytomas (30): this was also associated with good results in term of extent of resection as well as PFS and OS. In particular, in the heterogeneous group of PA, a maximal safe resection was reached in more than 80% of cases. Use of the fluorophore 5-aminolevulinic acid (5-ALA), a biochemical precursor of hemoglobin that provokes the synthesis and accumulation of fluorescent porphyrins in different tumors, has been reported but with inconsistent results: in a recent systematic review by Schwake et al. (31), 5-ALA was evaluated in different pediatric tumors, including 3 PXA, and strong fluorescence enhancement could be detected in 1 case (32), therefore accounting for a judgment of usefulness only in the 33.3% of the entire series. No comparative study for this specific tumoral histotype are available in the current literature.

In addition, the recent introduction of a dedicated filter integrated on the surgical microscope, specific for the excitation and emission wavelength of sodium fluorescein, has further improved the intraoperative visualization of the tumor and the surrounding brain parenchyma (11, 12). This technological adjunct significantly affected the development of fluorescein-guided surgery having increased the discrimination of tumoral tissue from the surrounding viable brain parenchyma. Our results seem to suggest that fluorescein-guidance for surgical resection may improve the intraoperative discrimination of the tumor margin and potentially increase the GTR rate. As stated by Xue et al. (33), we want to underline that our opinion is that only the combination of the largest number of tools, also including fluorophores, can guarantee an optimal surgical radicality in CNS surgery.

Although intraoperative evaluation of the fluorescence was subjective in this study, the report of helpful fluorescence in all cases, particularly at the tumor margins, taken together with the rate of GTR, suggests a reproducible effect (Figure 1). Fluorescein is still undergoing feasibility tests, especially in combination with the specific YELLOW 560 filter. It is important to stress that, in most of the Countries, the use of SF as a tracer in neuro-oncology should still be considered off-label; thus, a widespread utilization of fluorescence-guided surgery will depend on the definitive approval by the competent authorities (12, 15). Optimal dosage and timing of SF in PXA surgery is neither known nor experienced in this study: also in this cohort of tumors, we have used the low dosage of 5mg/kg, intravenously injected at the time of patient intubation (11), as originally proposed by our group in January 2012 (20).

The main limitation of the presented study is represented by the lack of data about overall survival in grade II/2 tumors: given the rarity of PXA, a long-term follow-up is not available in our data; for this reason, along with the inclusion of both anaplastic and not PXA, a proper patient evaluation from a prognostic perspective was not possible. Another selection bias in addition to different tumor grading inclusion, is the association in a single cohort of both adult and pediatric cases. Moreover, we did not make any comparison between the use of SF and white-light illumination or other available fluorophores, like 5-ALA. The current state, it is difficult to compare these two important fluorophores since the different mode of action, administration and visualization (34). Despite these weaknesses, our study could represent a proof of concept that may indicate that fluorescein utilization is potentially useful in the identification of tumoral tissue and in achieving a high rate of GTR of PXA. As previously demonstrated with other lesions, further studies could better elucidate the contribution of

fluorescein-guided technique in improving the intraoperative visualization during surgical resection of this tumor subtype. Furthermore, the effect of fluorescein on PFS and OS needs to be evaluated in a randomized, controlled clinical trial with adequate power to precisely assess the outcomes within a predefined observation period.

Conclusion

Our data suggested a positive effect of fluorescein-guided surgery during resection of PXA with contrast enhancement on preoperative MRI. We assert that SF is a safe and feasible tool: the use of fluorescein and YELLOW 560 filter is a readily available method for fluorescence-guided tumor resection, allowing intraoperative tumor visualization similarly to contrast enhancement in brain MRI.

Data availability statement

The raw data supporting the conclusions of this article will be made available by the authors, without undue reservation.

Ethics statement

The studies involving human participants were reviewed and approved by the Ethical Committee of the Fondazione IRCCS Istituto Neurologico Carlo Besta. Written informed consent to participate in this study as well as for the publication of any potentially identifiable images or data included in this article was obtained from the individual(s), and minor(s)' legal guardian/next of kin.

Author contributions

JF, MB and FA: study concept and design. JF, ER and FA: critical revision of the manuscript for intellectual content. All authors: acquisition of data, data analysis and interpretation. PF and FA: study supervision. All authors contributed to the article and approved the submitted version.

Funding

This study was partially supported by Associazione Paolo Zorzi per le Neuroscienze, ONLUS and by the Italian Ministry of Health (RRC).

Conflict of interest

Francesco Acerbi received honoraria from the Carl Zeiss Meditec Company for lectures at International Congresses.

The remaining authors declare that the research was conducted in the absence of any commercial or financial relationship that could be constructed as a potential conflict of interest.

Publisher's note

References

1. Shaikh N, Brahmbhatt N, Kruser TJ, Kam KL, Appin CL, Wadhwani N, et al. Pleomorphic xanthoastrocytoma: A brief review. *CNS Oncol* (2019) 8(3):CNS39. doi: 10.2217/cns-2019-0009

2. Louis DN, Perry A, Reifenberger G, von Deimling A, Figarella-Branger D, Cavenee WK, et al. The 2016 world health organization classification of tumors of the central nervous system: A summary. *Acta Neuropathol* (2016) 131(6):803–20. doi: 10.1007/s00401-016-1545-1

3. Louis DN, Perry A, Wesseling P, Brat DJ, Cree IA, Figarella-Branger D, et al. The 2021 WHO classification of tumors of the central nervous system: A summary. *Neuro Oncol* (2021) 23(8):1231–51. doi: 10.1093/neuonc/noab106

4. Dono A, Lopez-Rivera V, Chandra A, Lewis CT, Abdelkhaleq R, Sheth SA, et al. Predictors of outcome in pleomorphic xanthoastrocytoma. *Neuro Oncol Pract* (2021) 8(2):222–9. doi: 10.1093/nop/npaa076

5. She D, Liu J, Xing Z, Zhang Y, Cao D, Zhang Z. MR imaging features of anaplastic pleomorphic xanthoastrocytoma mimicking high-grade astrocytoma. *Am J Neuroradiol* (2018) 39(8):1446–52. doi: 10.3174/ajnr.A5701

6. Vaubel R, Zschernack V, Tran QT, Jenkins S, Caron A, Milosevic D, et al. Biology and grading of pleomorphic xanthoastrocytoma–What have we learned about it? *Brain Pathol* (2021) 31(1):20–32. doi: 10.1111/bpa.12874

7. Mallick S, Benson R, Melgandi W, Giridhar P, Rath GK. Grade II pleomorphic xanthoastrocytoma; A meta-analysis of data from previously reported 167 cases. *J Clin Neurosci* (2018) 54:57–62. doi: 10.1016/j.jocn.2018.05.003

8. Ida CM, Rodriguez FJ, Burger PC, Caron AA, Jenkins SM, Spears GM, et al. Pleomorphic xanthoastrocytoma: Natural history and long-term follow-up. *Brain Pathol* (2015) 25(5):575–86. doi: 10.1111/bpa.12217

9. Diaz RJ, Dios RR, Hattab EM, Burrell K, Rakopoulos P, Sabha N, et al. Study of the biodistribution of fluorescein in glioma-infiltrated mouse brain and histopathological correlation of intraoperative findings in high-grade gliomas resected under fluorescein fluorescence guidance. *J Neurosurg* (2015) 122 (6):1360–9. doi: 10.3171/2015.2.JNS132507

10. Moore GE. Fluorescein as an agent in the differentiation of normal and malignant tissues. *Science (80-)* (1947) 106(2745):130–1. doi: 10.1126/science.106.2745.130-a

11. Acerbi F, Broggi M, Broggi G, Ferroli P. What is the best timing for fluorescein injection during surgical removal of high-grade gliomas? *Acta Neurochir (Wien)* (2015) 157(8):1377–8. doi: 10.1007/s00701-015-2455-z

12. Cavallo C, De Laurentis C, Vetrano IG, Falco J, Broggi M, Schiariti M, et al. The utilization of fluorescein in brain tumor surgery: A systematic review. *J Neurosurg Sci* (2018) 62(6):690–703. doi: 10.23736/S0390-5616.18.04480-6

13. Vetrano IG, Acerbi F, Falco J, Devigili G, Rinaldo S, Messina G, et al. Fluorescein-guided removal of peripheral nerve sheath tumors: A preliminary analysis of 20 cases. *J Neurosurg* (2021) 1–10. doi: 10.3171/2019.9.JNS19970

14. Acerbi F, Broggi M, Schebesch KM, Höhne J, Cavallo C, De Laurentis C, et al. Fluorescein-guided surgery for resection of high-grade gliomas: A multicentric prospective phase II study (FLUOGLIO). *Clin Cancer Res* (2018) 24 (1):52–61. doi: 10.1158/1078-0432.CCR-17-1184

15. Falco J, Cavallo C, Vetrano IG, de Laurentis C, Siozos L, Schiariti M, et al. Fluorescein application in cranial and spinal tumors enhancing at preoperative MRI and operated with a dedicated filter on the surgical microscope: Preliminary results in 279 patients enrolled in the FLUOCERTUM prospective study. *Front Surg* (2019) 6:49. doi: 10.3389/fsurg.2019.00049

16. Höhne J, Acerbi F, Falco J, Akçakaya MO, Schmidt NO, Kiris T, et al. Lighting up the tumor–fluorescein-guided resection of gangliogliomas. *J Clin Med* (2020) 9(8):2405. doi: 10.3390/jcm9082405

17. Schebesch KM, Hoehne J, Hohenberger C, Proescholdt M, Riemenschneider MJ, Wendl C, et al. Fluorescein sodium-guided resection of cerebral metastases–experience with the first 30 patients. *Acta Neurochir (Wien)* (2015) 157(6):899–904. doi: 10.1007/s00701-015-2395-7

18. Schebesch KM, Hoehne J, Hohenberger C, Acerbi F, Broggi M, Proescholdt M, et al. Fluorescein sodium-guided surgery in cerebral lymphoma. *Clin Neurol Neurosurg* (2015) 139:125–8. doi: 10.1016/j.clineuro.2015.09.015

19. de Laurentis C, Höhne J, Cavallo C, Restelli F, Falco J, Broggi M, et al. The impact of fluorescein-guided technique in the surgical removal of CNS tumors in a pediatric population: Results from a multicentric observational study. *J Neurosurg Sci* (2019) 63:679–87. doi: 10.23736/S0390-5616.19.04601-0

20. Acerbi F, Broggi M, Eoli M, Anghileri E, Cuppini L, Pollo B, et al. Fluorescein-guided surgery for grade IV gliomas with a dedicated filter on the surgical microscope: Preliminary results in 12 cases. *Acta Neurochir (Wien)* (2013) 155(7):1277–86. doi: 10.1007/s00701-013-1734-9

21. Acerbi F, Cavallo C, Schebesch KM, Akçakaya MO, de Laurentis C, Hamamcioglu MK, et al. Fluorescein-guided resection of intramedullary spinal cord tumors: Results from a preliminary, multicentric, retrospective study. *World Neurosurg* (2017) 108:603–9. doi: 10.1016/j.wneu.2017.09.061

22. Rodrigues A, Bhambhvani H, Medress ZA, Malhotra S, Hayden-Gephart M. Differences in treatment patterns and overall survival between grade II and anaplastic pleomorphic xanthoastrocytomas. *J Neurooncol* (2021) 153(2):321–30. doi: 10.1007/s11060-021-03772-0

23. Neira JA, Ung TH, Sims JS, Malone HR, Chow DS, Samanamud JL, et al. Aggressive resection at the infiltrative margins of glioblastoma facilitated by intraoperative fluorescein guidance. *J Neurosurg* (2017) 127(1):111–22. doi: 10.3171/2016.7.JNS16232

24. Mor V, Laliberte L JNM, Wiemann M. The karnofsky performance status scale. *Cancer* (1984) 53(9):2002–7. doi: 10.1002/1097-0142(19840501)53:9<2002::aid-cncr2820530933>3.0.co;2-w.

25. Lansky SB, List MA, Lansky LL, Ritter-Sterr C, Miller DR. The measurement of performance in childhood cancer patients. *Cancer* (1987) 60(7):1651–6. doi: 10.1002/1097-0142(19871001)60:7<1651::AID-CNCR2820600738>3.0.CO;2-J

26. Grabowski MM, Recinos PF, Nowacki AS, Schroeder JL, Angelov L, Barnett GH, et al. Residual tumor volume versus extent of resection: predictors of survival after surgery for glioblastoma. *J Neurosurg* (2014) 121(5):1115–23. doi: 10.3171/2014.7.JNS132449

27. Finch EA, Elton SW, Huang BY, Trembath DG, Blatt J. Long-term efficacy of single-agent vemurafenib for pleomorphic xanthoastrocytoma. *J Pediatr Hematol Oncol* (2020) 42(2):152–5. doi: 10.1097/MPH.0000000000001395

28. Wu W, Zuo P, Li C, Gong J. Clinical features and surgical results of pediatric pleomorphic xanthoastrocytoma: Analysis of 17 cases with a literature review. *World Neurosurg* (2021) 151:e778–85. doi: 10.1016/j.wneu.2021.04.129

29. Höhne J, Schebesch KM, de Laurentis C, Akçakaya MO, Pedersen CB, Brawanski A, et al. Fluorescein sodium in the surgical treatment of recurrent glioblastoma multiforme. *World Neurosurg* (2019) 125:e158–64. doi: 10.1016/j.wneu.2019.01.024

30. Falco J, Höhne J, Broggi M, Rubiu E, Restelli F, Vetrano IG, et al. Fluorescein-guided surgery for the resection of pilocytic astrocytomas: A multicentric retrospective study. *Front Oncol* (2022) 12:943085. doi: 10.3389/fonc.2022.943085

31. Schwake M, Schipmann S, Müther M, Köchling M, Brentrup A, Stummer W. 5-ALA fluorescence–guided surgery in pediatric brain tumors–a systematic review. *Acta Neurochir (Wien)* (2019) 161(6):1099–108. doi: 10.1007/s00701-019-03898-1

32. Ruge JR, Liu J. Use of 5-aminolevulinic acid for visualization and resection of a benign pediatric brain tumor. *J Neurosurg Pediatr* (2009) 4:484–6. doi: 10.3171/2009.6.PEDS08428

33. Xue Z, Kong L, Hao S, Wang Y, Jia G, Wu Z, et al. Combined application of sodium fluorescein and neuronavigation techniques in the resection of brain gliomas. *Front Neurol* (2021) 12:747072. doi: 10.3389/fneur.2021.747072

34. Cramer Ahrens L, Green Krabbenhøft M, Würgler Hansen R, Mikic N, Pedersen CB, Poulsen FR, et al. Effect of 5-aminolevulinic acid and sodium fluorescein on the extent of resection in high-grade gliomas and brain metastasis. *Cancers (Basel)* (2022) 14:1–16. doi: 10.3390/cancers14030617

frontiers | Frontiers in Oncology

TYPE Case Report
PUBLISHED 24 November 2022
DOI 10.3389/fonc.2022.1007651

OPEN ACCESS

EDITED BY
Ignazio Gaspare Vetrano,
IRCCS Carlo Besta Neurological Institute Foundation, Italy

REVIEWED BY
Maria Guadalupe Moreno Treviño,
University of Monterrey, Mexico
Debora Garozzo,
Mediclinic Parkview Hospital, United Arab Emirates

*CORRESPONDENCE
Zhi-Chao Wang
shmuwzc@163.com
Bin Wang
Wangb1435@sh9hospital.org.cn

†These authors have contributed equally to this work and share first authorship

SPECIALTY SECTION
This article was submitted to Neuro-Oncology and Neurosurgical Oncology, a section of the journal Frontiers in Oncology

RECEIVED 30 July 2022
ACCEPTED 02 November 2022
PUBLISHED 24 November 2022

CITATION
Wei C-J, Peng L-L, Chuang M-H, Wang Z-C and Wang B (2022) Case Report: Differential diagnosis for tuberous sclerosis and neurofibromatosis type 1 diagnostic pitfall of aggressively enlarged right upper limb.
Front. Oncol. 12:1007651.
doi: 10.3389/fonc.2022.1007651

Case Report: Differential diagnosis for tuberous sclerosis and neurofibromatosis type 1 diagnostic pitfall of aggressively enlarged right upper limb

Cheng-Jiang Wei[1†], Li-Ling Peng[2†], Man-Hon Chuang[1†], Zhi-Chao Wang[1*] and Bin Wang[1*]

[1]Department of Plastic and Reconstructive Surgery, Shanghai Ninth People's Hospital, Shanghai Jiao Tong University School of Medicine, Shanghai, China, [2]Shanghai Universal Medical Imaging Diagnostic Center, Huaxin Business Center, Shanghai, China

Tuberous sclerosis complex (TSC) is an inherited disorder that typically presents with seizures, developmental delay, cutaneous lesions, and facial angiomas. Clinical diagnosis of TSC based on symptoms is sometimes challenging due to its clinical similarities with neurofibromatosis type 1 (NF1), another type of neurogenetic tumor syndrome. Differential diagnosis should be carefully performed on the basis of clinical presentations, imaging, laboratory, and genetic testing. Here, we presented a case of a patient with an aggressively enlarged right upper limb in the NF1 clinic, who was initially suspected of a giant plexiform neurofibroma. However, differential diagnosis revealed TSC as the final diagnosis. The treatments for NF1 and TSC vary significantly, and misdiagnoses can lead to serious threat to the patients' health. We also systematically reviewed all previous cases regarding differential diagnoses between NF1 and TSC. This case report can help clinicians make more accurate diagnoses and benefit the potential patient community.

KEYWORDS

tuberous sclerosis complex (TSC), neurofibromatosis type 1 (NF1), differential diagnosis, treatment, follow-up recommendation, case report

Introduction

Tuberous sclerosis complex (TSC) is a rare genetic disease characterized by seizures, developmental delay, and facial angiomas (Vogt's triad) (1). Neurofibromatosis type 1 (NF1) is another neurogenetic tumor syndrome caused by the mutation of the *NF1* gene (2). There are similarities in clinical symptoms between TSC with NF1, which might cause misdiagnosis. Here, we described a case of a young patient with TSC with an

enlarged right arm who was first diagnosed as NF1 during first visit to the clinic. Genetic testing revealed the *TSC1* mutation, and TSC was confirmed as the final diagnosis. Furthermore, the radiological imaging showed lung lymphangioleiomyoma and poor blood supply in the right arm. Last, we discussed the clinical treatment and follow-up recommendation for this patient (Figure 1).

Case presentation

A 20-year-old man presented to our institution, complaining that the right upper limb was much thicker than the left from birth, along with the enlargement of his left index finger and middle finger (Figures 2A–C). The volume of the right upper limb increased significantly during puberty. Five months before this visit, the patient suffered from an ulcer on the right hand that had failed to heal. He did not pay much attention to the enlarged right arm as he has got used to the condition for over 20 years. The main complaint for this visit was the non-healing right-hand ulcer, which he thought could be solved after simple debridement. He showed little awareness and had limited knowledge regarding the disease. Upon questioning, the patient declared no history of seizures and showed no signs of amentia. His parents also reported that the patient had no history of autism.

On clinical examination, the right arm was significantly more prominent than the left, with the soft tissue being much thicker than the opposite side. Meanwhile, there were sebaceous adenomas on the back, depigmented macules on the face, and fibromas under the nail bed (periungual fibromas) and gingiva (Figures 2D–G). Other skin lesions of tuberous sclerosis such as ash-leaf spots and shagreen patches were not evident. The physical examinations of cardiovascular and central nervous systems were also normal.

We initially suspected the case as plexiform neurofibroma with NF1 due to the enlargement of the right arm. However, the facial spots described by the patient as "café' au lait spots" are actually depigmented macules. Whole-body imaging was then conducted for the patient. The head CT revealed subependymal, cortical, and subcortical nodules (Figure 3A). Meanwhile, we found lymphangioleiomyomatosis on the chest CT, focal sclerosis, and bone cysts in multiple bone regions such as the spine (Figures 3B, C). Although MRI might help clarify the nature of the enlarged right arm, it could not be conducted as the volume of the patient's right arm exceeded the maximum size limit of our MRI machine. No hemorrhage and retinal hamartomas were found on ophthalmic examination, and mild mitral regurgitation was found on echocardiography.

Genetic testing was conducted for further differential diagnosis. No *NF1* mutation was found. Furthermore, there was a heterozygous mutation on the TSC1 gene.

On the basis of these features, a diagnosis of TSC was established, and the non-healing ulcer was considered to be associated with the vascular blockage caused by the thickened soft tissue. Digital subtraction angiography (DSA) was used to analyze the blood flow condition of the right arm (Supplementary File 1). The result showed insufficient blood supply in the distal

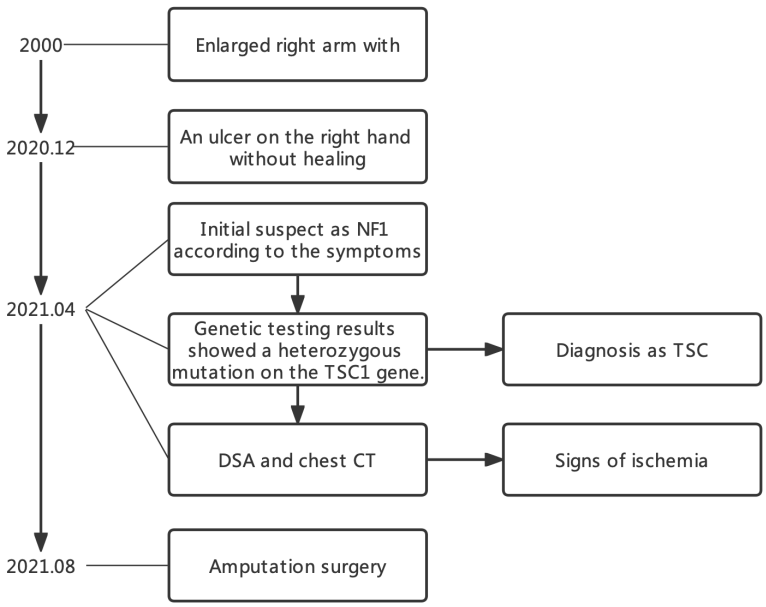

FIGURE 1
Timeline of this case.

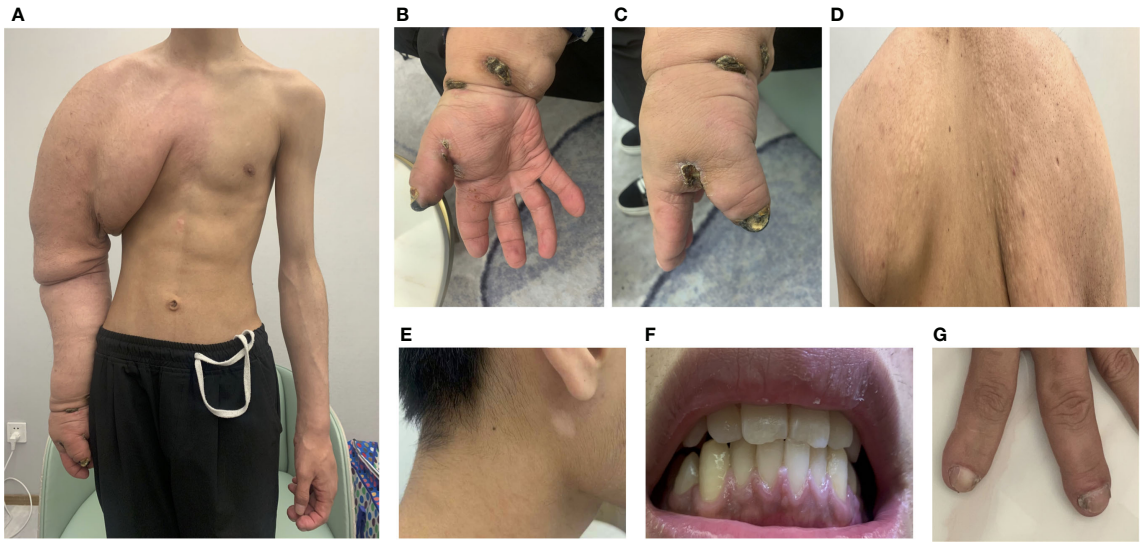

FIGURE 2
Clinical symptoms. **(A)** Enlarged right arm; **(B, C)** unhealing ulcer; **(D)** adenoma sebaceous; **(E)** depigmented macule; **(F)** gingiva; **(G)** periungal fibromas.

right upper limb, and amputation appeared to be the only treatment plan for the patient. During consultation, the patient showed difficulties accepting this treatment plan and stated that he needed time for consideration. Approximately 4 months later, he finally accepted the amputation surgery of the right arm as the ulcer condition barely improved. After the surgery, we recommended life-long follow-up and monitoring of potentially fatal complications. Annual ophthalmology examination was also essential for the risk of hemorrhage. As the patient also presented with lung lymphangioleiomyoma and cyst, high-resolution CT should be performed every year and the annual pulmonary function examination was necessary.

Discussion and conclusions

TSC is caused by the pathogenic variants in either the *TSC1* or *TSC2* tumor suppressor genes, located on chromosomes 9q34 and 16p13, respectively (3). *TSC1* and *TSC2* encode the protein hamartin and tuberin, which together suppress the activity of the mammalian target of rapamycin (mTOR) pathway (4). Loss of their function leads to continuous activation of the mTOR pathway, which results in cell proliferation (4). Typical clinical symptoms of TSC include periungual fibromas, renal angiomyolipoma, benign interstitial expansion of lung pulmonary smooth muscle cells, and neurological symptoms like seizures and neurodevelopmental delay (1).

Neurofibromatosis type 1 (NF1) is also an autosomal dominant genetic disorder caused by another tumor suppressor gene *NF1* (2). The *NF1* gene encodes neurofibromin, a negative regulator of the RAS–mitogen-activated protein kinase pathway. The loss of *NF1* contributes to the activation of this pathway and finally leads to tumor growth and development (5). Classic clinical features include café-au-lait macules, skinfold freckling, benign neurofibromas like cutaneous neurofibroma and plexiform neurofibroma, brain tumors, iris hamartomas, and typical bony lesions. Meanwhile, there are also reports of neurological manifestations such as epilepsy (6).

Comparing these two diseases, both may have vague and overlapping clinical presentations that can lead to missed diagnosis and finally cause delayed treatment. Coincidentally, both NF1 and TSC were first described by Von Recklinghausen, which proved from the side that these two diseases have some similar symptoms (7, 8). The major clinical diagnostic criteria of TSC such as hypomelanotic macule, angiofibroma, and shagreen patch are sometimes difficult to distinguish from typical NF1 phenomenon like café-au-lait macules, skinfold freckling, and benign neurofibroma (Table 1). Although NF1 and TSC are the first and second most common neurogenetic tumor syndromes, NF1 only has a prevalence of approximately 1:2,500 to 1:3,500, whereas TSC is even rarer and affects 1 in 5,500 to 1 in 10,000 live births (9). The limited amount of clinical cases further caused difficulties in clinical differential diagnosis, especially for doctors in remote areas. Moreover, it was shown that, in some cases, both NF1 and TSC could occur in a single individual, which might further confuse the diagnosis. We performed an extensive review of the literature using PubMed search including the words (NF1 and tuberous sclerosis) from the year 2000 until 2021 (Table 2) (10–14). Interestingly, Wheeler and Sadeghi-Nejad reported a case of a 4-month girl

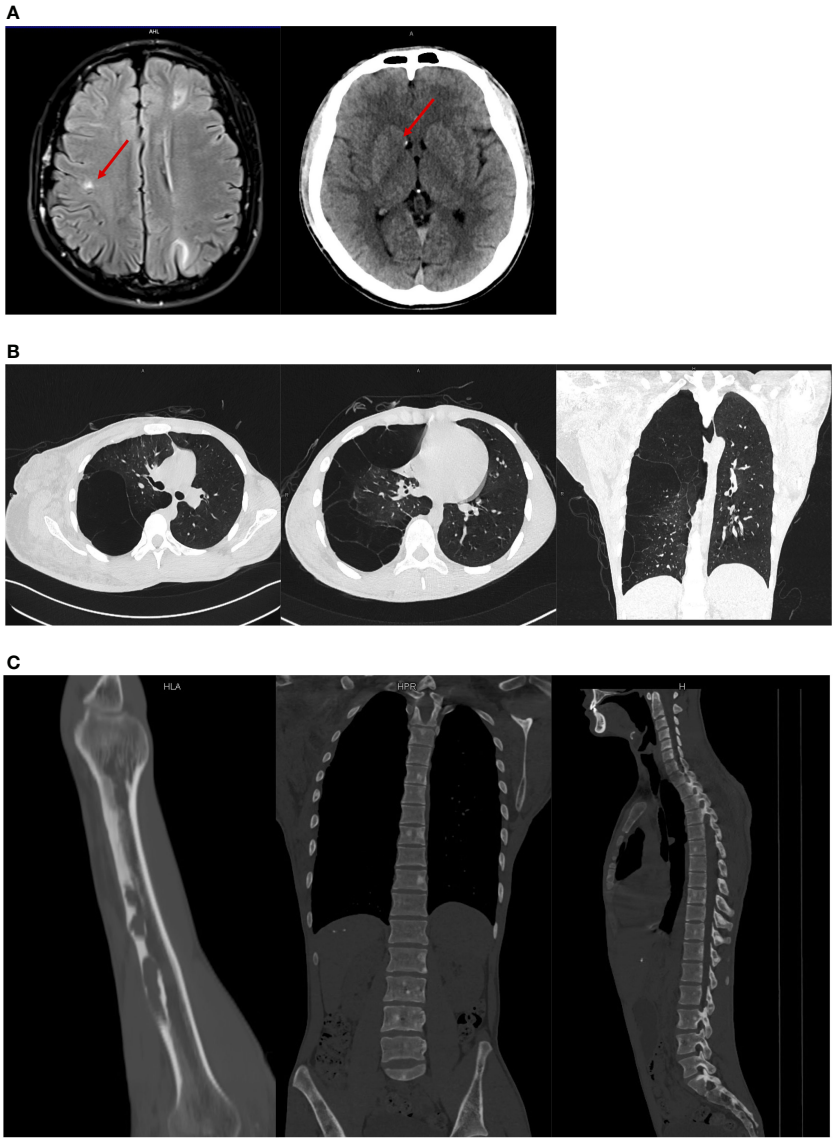

FIGURE 3
Medical imaging results. **(A)** Nodules showed on the head CT; **(B)** lymphangioleiomyomatosis on the chest CT and bone cysts in the different regions; **(C)** lymphangioleiomyomatosis on the chest CT and bone cysts in the different regions.

that suffered from both NF1 and TSC but reported a family history of NF1 only (12). After a definite diagnosis of TSC was made for this girl, her parents were carefully re-examined and also confirmed the diagnosis of TSC (12). This case further indicates the similarities of some clinical symptoms, and one definite diagnosis might further inhibit the recognition of another. Genetic testing and pathological biopsy may be necessary for a definite diagnosis of TSC. Moreover, as TSC and NF1 are both hereditary diseases, first-degree relatives should undergo a clinical assessment and a three-generation family history is required.

Current clinical management of TSC is insufficient as most of them are symptomatic treatments, especially for seizures. Early therapeutic intervention for children who present with infantile spasms correlated with TSC is essential, and the first-line treatment is vigabatrin (15). Furthermore, the mTOR inhibitors such as everolimus have provided great therapeutic promise. A clinical study showed that treatment with everolimus in patients with TSC resulted in a sustained decrease in seizure frequency in children and adolescents (16). Nonetheless, this patient did not have any history of seizures. As he reached the age of 20 and presented with vascular blockage indicated by the non-healing

TABLE 1 Comparison of diagnosis criteria or neurofibromatosis type 1 and tuberous sclerosis complex.

	Neurofibromatosis type 1	Tuberous sclerosis complex
Major Features	1. Six or more café-au-lait macules (>5 mm in diameter in pre-pubertal children or >15mm in post-pubertal children); 2. Freckling in the axillary or groin; 3. Two or more neurofibromas of any type or one plexiform neurofibroma; 4. Optic glioma; 5. Two or more Lisch nodules; 6. A distinct osseous lesion such as sphenoid dysplasia; 7. A first-degree relative with neurofibromatosis type 1; 8. A pathogenic NF1 variant revealed by genetic testing.	1. Facial angiofibromas or forehead plaque; 2. Two or more non-traumatic ungual or periungual fibroma; 3. Three or more hypomelanotic macules (≥5 mm diameter); 4. Shagreen patch; 5. Three or more cortical dysplasias (includes tubers and perebral while matter radial migration lines); 6. Two or more subependymal nodules; 7. Two or more subependymal giant cell astrocytoma; 8. Multiple retinal nodular hamartomas; 9. Cardiac rhabdomyoma (single or multiple); 10. Lymphangioleiomyomatosis (LAM); 11. Angiomylipoma.
Minor Features	/	1. "Confetti" skin lesions; 2. Hamartomatous rectal polyps; 3. Gingival fibromas; 4. Pits in dental enamel; 5. Cerebral white matter radial "migration tracts"; 6. Retinal achromic patches; 7. Bone cysts.
Diagnosis Criteria	An individual must have two or more of these features.	Definite TSC: Two major features or a major feature with two minor features; probable TSC: one major feature and one minor feature; possible TSC: one major feature or two or more minor features.

ulcer, surgical approaches were considered according to the 2021 updated TSC international recommendations (17). DSA examination further showed signs of ischemia. As a result, amputation was the only surgical choice for him. Compared to the limited drug choices for patients with TSC, the development of drug therapies for patients with NF1 progressed rapidly. Selumetinib, a Mitogen-activated extracellularsignal-regulated kinase (MEK) inhibitor, was reported effective for plexiform neurofibroma and was approved for clinical usage by FDA (18). Early distinguishment of these two diseases is essential for further proper clinical treatment.

Another essential issue for the treatment of patients with TSC is life-long follow-up recommendations. TSC influences multiple organs in the body, and some manifestations are life-threatening. For example, our patient has lymphangioleiomyoma, which might cause respiratory dysfunction. According to the 2021 updated TSC international recommendations, we recommended routine serial pulmonary function test annually on chest CT (17). Meanwhile, we had several recommendations regarding other possible TSC features, including continuous sun protection for depigmented macules, detailed dental examination every 6 months, electrocardiography every 3 years for mild mitral regurgitation, annual ophthalmic evaluation, and renal function assessment. For patients with NF1, life-long follow-up is also essential, but they are less concerned with respiratory dysfunction. A definite diagnosis is essential for further proper follow-up.

Definite and accurate diagnosis is the basis for proper and effective treatment, and misdiagnosis might cause further damage to the patients and waste medical resources. It is far

TABLE 2 List of published case reports of patients with both NF-1 and TSC from 2000 to 2021.

Case (ref.)	Age (years)/ sex	Publication year	TSC phenomena	NF1 phenomena	Therapy
1 (10)	15/female	2013	Facial angiofibroma; hypopigmented macule; shagreen patch; ungual fibroma	Café-au-lait macules; segmental freckling	None report
2 (11)	infant/ female	2004	Hypopigmented macules; shagreen patch; family history	Café-au-lait macules; optic glioma; family history	Closely follow-up
3 (12)	infant/ female	2005	Subependymal glial nodules; cutaneous hypopigmented patches; shagreen patch; family history; delayed cognitive development	Family history; Café-au-lait macules; right orbit superior (suspect of plexiform neurofibroma); delayed cognitive development	None report
4 (13)	20/female	2009	Shagreen patches; periungual fibroma; subependymal glial nodules; family history.	Café-au-lait macules; plexiform neurofibroma; axillary freckling	None report
5 (14)	24/male	2007	Seizure; shagreen patches; subependymal giant cell astrocytoma	Lisch nodules; Café-au-lait macules; plexiform neurofibroma	Right frontal craniotomy

more essential for relatively rare diseases as most doctors might have relatively less experience with them. This case introduced the possible pitfall and similarities of clinical phenomena between TSC and NF1, which might be helpful for future clinical diagnosis and management of these diseases in this area.

Data availability statement

The original contributions presented in the study are included in the article/Supplementary Material. Further inquiries can be directed to the corresponding authors.

Ethics statement

The studies involving human participants were reviewed and approved by the institutional review board of Shanghai Ninth People's Hospital, Shanghai Jiaotong University School of Medicine. The patients/participants provided their written informed consent to participate in this study. Written informed consent was obtained from the individual(s) for the publication of any potentially identifiable images or data included in this article.

Author contributions

C-JW wrote the manuscript and was involved in the diagnostic and therapeutic clinical processes. L-LP analyzed radiology medical images and contributed to the diagnostic and therapeutic processes. M-HC made substantial contribution during revision. Z-CW and BW helped in the diagnostic process and critically revised the manuscript and were responsible for the diagnosis and treatment of the patient. All authors read and approved the final manuscript.

Funding

This work was supported by grants from National Natural Science Foundation of China (82102344; 82172228; 81772115); Shanghai Rising Star Program supported by Science and Technology Commission of Shanghai Municipality (20QA1405600); Science and Technology Commission of Shanghai Municipality (19JC1413, 22MC1940300) ; Natural Science Foundation of Shanghai (22ZR1422300); "Chenguang Program" supported by Shanghai Education Development Foundation (SHEDF) (19CG18); Innovative research team of high-level local universities in Shanghai (SSMU-ZDCX20180700); the Project of Biobank (YBKA201901) from Shanghai Ninth People's Hospital, Shanghai Jiao Tong University School of Medicine; Research Project of Multi-Disciplinary Team of Shanghai Ninth People's Hospital (201907).

Conflict of interest

The authors declare that the research was conducted in the absence of any commercial or financial relationships that could be construed as a potential conflict of interest.

Publisher's note

All claims expressed in this article are solely those of the authors and do not necessarily represent those of their affiliated organizations, or those of the publisher, the editors and the reviewers. Any product that may be evaluated in this article, or claim that may be made by its manufacturer, is not guaranteed or endorsed by the publisher.

Supplementary material

The Supplementary Material for this article can be found online at: https://www.frontiersin.org/articles/10.3389/fonc.2022.1007651/full#supplementary-material

References

1. Randle SC. Tuberous sclerosis complex: A review. *Pediatr Ann* (2017) 46: e166–71. doi: 10.3928/19382359-20170320-01

2. Huson SM, Compston DA, Harper PS. A genetic study of von recklinghausen neurofibromatosis in south east wales. II. guidelines for genetic counselling. *J Med Genet* (1989) 26:712–21. doi: 10.1136/jmg.26.11.712

3. Portocarrero LKL, Quental KN, Samorano LP, Oliveira ZNP, Rivitti-Machado M. Tuberous sclerosis complex: review based on new diagnostic criteria. *Bras Dermatol* (2018) 93:323–31. doi: 10.1590/abd1806-4841.20186972

4. Kwiatkowski DJ. Rhebbing up mTOR: new insights on TSC1 and TSC2, and the pathogenesis of tuberous sclerosis. *Cancer Biol Ther* (2003) 2:471–6. doi: 10.4161/cbt.2.5.446

5. Ratner N, Miller SJ. A RASopathy gene commonly mutated in cancer: the neurofibromatosis type 1 tumour suppressor. *Nat Rev Cancer* (2015) 15:290–301. doi: 10.1038/nrc3911

6. Nix JS, Blakeley J, Rodriguez FJ. An update on the central nervous system manifestations of neurofibromatosis type 1. *Acta Neuropathol* (2020) 139:625–41.

doi: 10.1007/s00401-019-02002-2

7. Anderson JL, Gutmann DH. Neurofibromatosis type 1. *Handb Clin Neurol* (2015) 132:75–86. doi: 10.1016/B978-0-444-62702-5.00004-4

8. Gomez MR. History of the tuberous sclerosis complex. *Brain Dev* (1995) 17 Suppl:55–7. doi: 10.1016/0387-7604(94)00130-8

9. Strowd RE3rd, Plotkin SR. Familial nervous system tumor syndromes. *Continuum (Minneap Minn)* (2020) 26:1523–52. doi: 10.1212/CON.0000000000000950

10. Murakami Y, Wataya-Kaneda M, Tanaka M, Katayama I. Case of tuberous sclerosis complex complicated by mosaic localized neurofibromatosis type 1. *J Dermatol* (2013) 40:413–4. doi: 10.1111/1346-8138.12074

11. Erbay SH, Oljeski SA, Bhadelia R. Rapid development of optic glioma in a patient with hybrid phakomatosis: neurofibromatosis type 1 and tuberous sclerosis. *AJNR Am J Neuroradiol* (2004) 25:36–8. doi: 10.1016/S1076-6332(03)00599-3

12. Wheeler PG, Sadeghi-Nejad A. Simultaneous occurrence of neurofibromatosis type 1 and tuberous sclerosis in a young girl. *Am J Med Genet A 133A* (2005) 133A(1):78–81. doi: 10.1002/ajmg.a.30530

13. Suttur MS, Mysore SR, Krishnamurthy B, Nallur RB. Rare association of turner syndrome with neurofibromatosis type 1 and tuberous sclerosis complex. *Indian J Hum Genet* (2009) 15:75–7. doi: 10.4103/0971-6866.55220

14. Alaraj AM, Valyi-Nagy T, Roitberg B. Double phakomatosis; neurofibromatosis type-1 and tuberous sclerosis. *Acta Neurochir (Wien)* (2007) 149:505–9; discussion 509. doi: 10.1007/s00701-007-1140-2

15. Strzelczyk A, Grau J, Bast T, Bertsche A, Bettendorf U, Hahn A, et al. Prescription patterns of antiseizure drugs in tuberous sclerosis complex (TSC)-associated epilepsy: a multicenter cohort study from Germany and review of the literature. *Expert Rev Clin Pharmacol* (2021) 14:749–60. doi: 10.1080/17512433.2021.1911643

16. Franz DN, Lawson JA, Yapici Z, Ikeda H, Polster T, Nabbout R, et al. Everolimus for treatment-refractory seizures in TSC: Extension of a randomized controlled trial. *Neurol Clin Pract* (2018) 8:412–20. doi: 10.1212/CPJ.0000000000000514

17. Northrup H, Aronow ME, Bebin EM, Bissler J, Darling TN, de Vries PJ, et al. Updated international tuberous sclerosis complex diagnostic criteria and surveillance and management recommendations. *Pediatr Neurol* (2021) 123:50–66. doi: 10.1016/j.pediatrneurol.2021.07.011

18. Dombi E, Baldwin A, Marcus LJ, Fisher MJ, Weiss B, Kim A, et al. Activity of selumetinib in neurofibromatosis type 1-related plexiform neurofibromas. *N Engl J Med* (2016) 375:2550–60. doi: 10.1056/NEJMoa1605943

frontiers | Frontiers in Oncology

TYPE Original Research
PUBLISHED 09 January 2023
DOI 10.3389/fonc.2022.1070878

OPEN ACCESS

EDITED BY
Alireza Mansouri,
The Pennsylvania State University (PSU), United States

REVIEWED BY
Mirza Pojskic,
University Hospital of Giessen and Marburg, Germany
Kristin Huntoon,
University of Texas MD Anderson Cancer Center, United States
Xiaodong Tang,
Peking University People's Hospital, China
Maria Teresa Pedro,
Universitaetsklinikum Ulm, Germany

*CORRESPONDENCE
Ignazio G. Vetrano
Ignazio.vetrano@istituto-besta.it

†These authors share last authorship

‡These authors have contributed equally to this work and share first authorship

SPECIALTY SECTION
This article was submitted to Neuro-Oncology and Neurosurgical Oncology, a section of the journal Frontiers in Oncology

RECEIVED 15 October 2022
ACCEPTED 12 December 2022
PUBLISHED 09 January 2023

CITATION
Nazzi V, Innocenti N, Castelli N, Tramacere I, Eoli M, Cojazzi V, Gatti L, Acerbi F, Falco J and Vetrano IG (2023) Assessing the role of sodium fluorescein in peripheral nerve sheath tumors and mimicking lesions surgery: An update after 142 cases. *Front. Oncol.* 12:1070878. doi: 10.3389/fonc.2022.1070878

Assessing the role of sodium fluorescein in peripheral nerve sheath tumors and mimicking lesions surgery: An update after 142 cases

Vittoria Nazzi[1‡], Niccolò Innocenti[1‡], Nicolò Castelli[1], Irene Tramacere[2], Marica Eoli[3], Vittoria Cojazzi[1], Laura Gatti[4], Francesco Acerbi[1], Jacopo Falco[1†] and Ignazio G. Vetrano[1,4,5*†]

[1]Department of Neurosurgery, Fondazione IRCCS Istituto Neurologico Carlo Besta, Milan, Italy, [2]Department of Research and Clinical Development, Scientific Directorate, Fondazione IRCCS Istituto Neurologico Carlo Besta, Milan, Italy, [3]Molecular Neuro-Oncology Unit, Fondazione IRCCS Istituto Neurologico Carlo Besta, Milan, Italy, [4]Neurobiology Laboratory, Fondazione IRCCS Istituto Neurologico Carlo Besta, Milan, Italy, [5]Department of Biomedical Sciences for Health, Università degli Studi di Milano, Milan, Italy

Objective: Peripheral nerve sheath tumors (PNST) include mainly schwannomas and neurofibromas. Surgical resection represents the mainstay of treatment but due to their pathogenesis, distinguishing between intact functional nerve and the fibers from whence the PNST arose may not always be easy to perform, constituting the most relevant risk factor in determining a worsening in neurological condition. The introduction of intraoperative tools to better visualize these tumors could help achieve a gross-total resection. In this study, we analyzed the effect of sodium fluorescein (SF) on the visualization and resection of a large cohort of PNST.

Methods: Between September 2018 and December 2021, 142 consecutive patients harboring a suspected PNST underwent fluorescein-guided surgery at the Department of Neurosurgery of the Fondazione IRCCS Istituto Neurologico Carlo Besta, Milan, Italy. All patients presented with a different degree of contrast enhancement at preoperative MRI. SF was intravenously injected after intubation at 1 mg/kg. Intraoperative fluorescein characteristics and postoperative neurological and radiological outcomes were collected, analyzed, and retrospectively compared with a historical series.

Results: 142 patients were included (42 syndromic and 100 sporadic); schwannoma was the predominant histology, followed by neurofibroma (17 neurofibroma e 12 plexiform neurofibroma) and MPNST. Bright fluorescence was present in all cases of schwannomas and neurofibromas, although with a less homogeneous pattern, whereas it was significantly less evident for malignant PNST; perineurioma and hybrid nerve sheath tumors were characterized by a faint fluorescence enhancement. The surgical resection

rate in the general population and even among the subgroups was about 66.7%; from the comparative analysis, we found a consistently higher rate of complete tumor removal in plexiform neurofibromas, 66% in the "fluorescent" group vs 44% in the "historical" group (p-value < 0.05). The rate of complications and mean surgical time were superimposable among the two populations.

Conclusions: SF is a valuable method for safe fluorescence-guided PNST and mimicking lesions resection. Our data showed a positive effect of fluorescein-guided surgery in increasing the rate of surgical resection of plexiform neurofibromas, suggesting a possible role in improving the functional and oncological outcome of these lesions.

KEYWORDS

fluorescein-guided surgery, peripheral nerve sheath tumors, PNST, schwannoma, neurofibroma, sodium fluorescein (SF), YELLOW560 filter

1 Introduction

Peripheral nerve sheath tumors (PNST) constitute a miscellaneous group that counts for 10-15% of all soft tissue primary tumors (1). Among the histopathologic entities within the PNST (2), benign lesions, i.e., schwannomas and neurofibromas, are the most common overall and more frequently affect adults (3, 4). PNST can be sporadic lesions or associated with neurocutaneous syndromes characterized by multisystemic manifestations, prominently affecting structures primarily derived from the ectoderm (5, 6). Syndromic PNST affect young adults and children and are generally present in multiple localizations, including several subcutaneous lesions; although it is a rare subgroup, malignant PNST are more frequent in syndromic diseases than sporadic conditions. Neurofibromas are mainly related to neurofibromatosis type 1 (NF1), and they present the risk of malignant transformation into aggressive and infiltrative sarcomas (7, 8), with severe morbidity and also mortality (9). The role of adjuvant radiotherapy and traditional chemotherapy remains unclear for such tumors. The mainstay of treatment is surgical enucleation which should not lead to neurological impairment (3, 10, 11); gross-total resection is a pivotal predictor of local control and recurrence and could prevent possible malignant behavior (12). A relevant tool to reduce surgical morbidity on neurological functions is the use of intraoperative neurological monitoring (IOM) (13) which has an impact on identifying functional nerves, localizing the safest entry point inside the tumor capsule, and recognizing anatomical structures in case of large and destructive tumors. Nevertheless, the role of IOM is still an argument of debate among different groups involved in PNST surgery (14). Moreover, distinguishing between functional intact nerves and the silent fibers from whence the PNST arose is not always easy to perform (10). As already studied in central nervous system (CNS) tumors surgery, using intraoperative fluorophores could represent a valuable method to visualize pathological tissue better and possibly improve tumor resection (15–18).

Fluorescein is a green fluorescent synthetic organic compound with countless medical applications, mainly as fluorescein sodium salt (SF), a water-soluble dye. Although some pioneering applications in neuro-oncology (19), its use has been initially limited to ophthalmology (20). However, introducing a dedicated and integrated filter in the surgical microscope has exponentially increased SF applications in neurosurgery. After the first prospective phase II trial to evaluate the safety and efficacy of fluorescein-guided resection of high-grade gliomas by the use of a dedicated fluorescence filter in the surgical microscope (17), the Italian Medicine Agency (AIFA) has extended the indications for the utilization of fluorescein molecule (905/2015) (21). According to this determination, the use of SF as a neurosurgical tracer during oncological procedures is approved, and the Italian National Health System reimburses its cost.

The potential role of SF in PNST surgery is still little explored, despite some preliminary clinical reports (22–25). Experimental models have demonstrated that SF causes endoneurial extravasation, like blood-brain barrier extravasation, confirming the behavior of fluorescein as an unspecific vascular dye (26–28). In 2019, we presented our preliminary experience in a series of 20 patients with different PNST, in which fluorescein was used for intraoperative visualization and guidance in tumor removal (25), and we demonstrated that fluorescein is a feasible, safe, and helpful

intraoperative adjunct to better identify and distinguish PNST from intact functional nerves, with a possible impact on tumor resection, particularly in diffuse neurofibromas (29, 30). Then we started a prospective analysis on a broader series regarding the use of SF as an intraoperative tracer for peripheral nerve tumors. We present our experience and benefits of intraoperative SF application during surgical removal of different PNST.

2 Methods

2.1 Patients and inclusion criteria

The inclusion criteria were: (1) patients of both genders, excluding pediatric patients (2) patients with suspected PNST, as suggested by preoperative ultrasound and MRI with paramagnetic contrast agent administration. The exclusion criteria were: (1) impossibility to give consent due to cognitive deficits or language disorders; (2) known allergy to contrast agents or history of previous anaphylactic shocks or known severe previous adverse reactions to SF; (3) acute myocardial infarction or stroke in the last 90 days; (4) severe organ failure; (5) women in their first trimester of pregnancy or lactation. Patients harboring mimicking lesions at histopathological examination but who had required a similar microsurgical treatment including the role of intraoperative neuromonitoring to preserve neurological function have not been excluded. The study started in September 2018, when the first patient was enrolled. All patients gave written informed consent for the surgical procedure, including the use of fluorescein, and were included in the prospective study about the use of fluorescein in neurosurgical procedures. The protocol has been approved by the Ethical Committee of the Fondazione IRCCS Istituto Neurologico Carlo Besta. To identify a comparative cohort of patients affected by PNST undergoing surgery before SF diffusion, we systematically and retrospectively reviewed our departmental surgical and neuropathological databases between March 2015 and August 2018. The Institutional review board approved the retrospective analysis.

2.2 Clinical and radiological management

The preoperative assessment included physical and neurological examination, laboratory test results, preoperative contrast-enhanced MRI of the region of interest, and ultrasonography. The postoperative clinical evaluation comprises neurological examination as above, laboratory test (kidney function), and exclusion of any side effect related to fluorescein injection. Patients with sporadic PNST received standard radiological follow-up with a first MRI of the nerve and body segment of interest three months after surgery; on the contrary, patients affected by neurofibromatosis or schwannomatosis underwent a more accurate neuro-oncological follow-up, also comprising brain and spinal MRI. Gross total resection was defined as the absence of residual hyperintense tissue on postoperative postcontrast volumetric T1 images after subtraction of the volume of spontaneous hyperintense tissue in volumetric T1 images without contrast; the T2 sequence was further analyzed and compared to preoperative one to exclude residual pathological tissue.

2.3 Surgical protocol

The standardized surgical protocol of fluorescein-guided technique is based on intravenous (i.v.) SF (*Monico S.p.A., Venice, Italy*) injection at the standard dose of 1mg/kg immediately upon completion of the induction of general anesthesia. Surgery was performed under microscopic view through surgical microscopes equipped with an integrated fluorescent filter tailored to sodium fluorescein excitation and emission wavelength (YELLOW 560 – *Pentero 900; Carl Zeiss Meditec, Oberkochen, Germany*). During resection, the microscope could be switched alternatively from fluorescent to white-light illumination. The safest surgical technique forecasts a sufficiently large tumor exposure, followed by inspection and pseudocapsule or true capsule direct electrophysiological stimulation to identify possible functional fascicles running inside. To guarantee an accurate IOM, general anesthesia is administered in a totally intravenous way with a targeted controlled infusion (TIVA-TCI) of a combination of propofol and remifentanil, maintained at a constant plasma concentration due to pharmacokinetic models; muscle relaxants are only used during intubation and, when necessary, a curare antagonist is administered before starting the electrostimulation. The subsequent surgical step is, therefore, the incision of a safe, silent entry zone, followed by intraneural and longitudinal dissection allowing progressive isolation and tumor removal *via* en bloc enucleation. In the case of huge tumors or neurofibromas, neoplastic tissue is usually removed piecemeal when an en-bloc enucleation is not feasible. Current neurophysiological protocol for peripheral nerve surgery comprises continuous free-running and stimulus-triggered electromyography to verify during and at the end of the procedure the functional integrity of the nerve.

2.4 Intraoperative fluorescence characteristics and side effects

Fluorescence intensity was subjectively graded by the surgeon as bright (homogeneous or inhomogeneous), faint or absent during surgical procedure; in addition, it was reported by the surgeon whether fluorescein was considered useful for

removing the tumor. Furthermore, medical reports were evaluated for any possible adverse effect or allergic reaction to fluorescein administration.

2.5 Histological analysis

Histopathological analysis was performed in each case; tumors were classified according to the 2016 and 2021 WHO classification of nervous tissue tumors (31, 32) by the neuropathology group of our Institute as part of the daily clinical practice.

2.6 Statistical analysis

The sample was described by means of the usual descriptive statistics: mean, median, and standard deviation for continuous variables and proportions for categorical ones. PRISM software for Macintosh was used for the statistical analysis.

3 Results

A total of 142 consecutive patients (75 females and 67 males) admitted at our Institution between September 2018 and December 2021 for a suspected PNST were included in the analysis. The mean age of presentation was 45.1 years, with a median age of 47.8 years (ranging from 18 to 82 years). The median follow-up in our cohort was 6.5 months, with a minimum of 3 months and a maximum of 35 months. Patients with neurocutaneous syndromes represented 29.6% of our cohort (42/142): 21 patients (14.8%) were affected by NF1, 15 patients (10.6%) by schwannomatosis, and 6 (4.2%) by NF2. The most common neoplasms were schwannomas (92/142 – 64.8%), followed by neurofibromas (17/142 – 12%) and plexiform neurofibromas (12/142 – 8.5%); MPNST were the fourth most represented histology (5/142 – 3.5%). The remaining neoplasms were a heterogeneous group with less common PNST, such as hybrid peripheral nerve tumors, perineurioma, lymphomas, and others. Histopathological and intraoperative fluorescein findings are reported in Table 1.

TABLE 1 Clinical characteristics of the Sodium Fluorescein series.

Histology	N°	Neurocutaneous syndromes	Location	Resection	Complications
Schwannoma	91 (64%)	9 Schwannomatosis 7 NF2 3 NF1	39 Inferior Limbs 21 Superior limbs 18 Intracanalar 12 Brachial Plexus	87/91 Total (95,6%) 4/91 Subtotal (4,4%)	4 transient sensory deficits 2 transient motor deficits 1 dural tear
Neurofibroma	17 (12%)	10 NF1	7 Intracanalar 4 Head 3 Superior limbs 2 Back 1 Inferior limbs	15/17 Total (88%) 2/17 Subtotal (12%)	1 transient sensory deficit 1 permanent motor deficit
Plexiform Neurofibroma	12 (8.5%)	8 NF1 3 Rasopathy	5 Head 5 Inferior limbs 1 Brachial plexus 1 Superior limbs	8/12 Total (66%) 4/12 Subtotal 34%)	1 worsening of a pre-existing hypostenia
Malignant Peripheral Nerve Sheath Tumor (MPSNT)	5 (3.5%)	1 NF2	4 Brachial Plexus 1 Intracanalar	1/5 Total (20%) 4/5 Subtotal (80%)	no
Hybrid PNS tumor	3	2 Schwannomatosis 1 Rasopathy	2 Superior limbs 1 Inferior limbs	1/3 Total (33%) 2/3 Subtotal (66%)	1 transient motor deficit

(Continued)

10.3389/fonc.2022.1070878

TABLE 1 Continued

Histology	N°	Neurocutaneous syndromes	Location	Resection	Complications
Follicular lymphoma	2	none	2 Superior limbs	Total	no
LN hyperplasia	1	none	Superior limbs	Total	no
Plexiform Schwannoma	1	none	Inferior limbs	Total	no
Ganglioneuroma	1	none	Intracanalar	Subtotal	no
Lypomatosis of the nerve	1	none	Superior limbs	Subtotal	no
Perineurioma	1	none	Intracanalar	Subtotal	no
Steatonecrosis	1	none	Inferior limbs	Subtotal	no
Ganglion cyst	1	none	Inferior limbs	Total	no
Epithelioid hemangioendothelioma	1	none	Superior limbs	Total	no
Mesenchymal tissue tumor	1	none	Brachial Plexus	Total	no
Nodular tenosynovitis	1	none	Inferior limbs	Total	no
Solitary fibrous tumor	1	none	Superior limbs	Total	no
Mixopapillary Ependimoma	1	none	Intracanalar	Total	no
Total	142	21 NF1 12 Schwannomatosis 8 NF2 4 Rasopathies	49 Inferior limbs 33 Superior limbs	122/142 Total (86%) 20/142 Subtotal (14%)	11/142 (7.7%)

In 117 out of 142 patients (82.4%), we achieved a complete tumor removal (Figure 1), defined as radiological (at 3-months MRI) and histological radical excision without border infiltration at the histological specimen. We then analyzed these results concerning tumor histopathology. Similar complete resection rates in schwannomas (81/92) and neurofibromas (15/17) were achieved. In plexiform neurofibromas, the complete removal rate was 66.7% (8/12), while in MPSNT, 40% (2/5). In 6 cases of neurofibromas and in two schwannomas (Figure 2), the final YELLOW 560 visualization showed the presence of small remnants not visible under white-light illumination; this occurred more frequently in plexiform neurofibromas (4 of these 6 cases). The overall complication rate was 7.7% (11/142), considering both transient and permanent new neurological deficits. In 5 cases, a postoperative transient sensitive deficit was recorded, whereas all recovered completely at the three months follow-up. In four cases, postoperative worsening of a pre-existing motor deficit was present; after physio-kinesiotherapy, the patients partially recovered: in 2 cases, at the first follow-up visit, the neurological status was superimposable with the preoperative one, while in the other 2 cases a mild worsened motor deficit remained. A cerebrospinal fluid leak occurred in a sacral schwannoma with intradural extension, requiring revision surgery but without neurological impairment. Only one patient with a large cervical neurofibroma had a new motor deficit after surgery with left arm hyposthenia that persisted after physio-kinesiotherapy.

We finally compared these results retrospectively with a historical cohort of patients submitted to surgery between 2015 and 2018, matched for age, gender, and lesion characteristics. The "fluorescein" group (2018-2021) and the "standard of care (SOC)" group were comparable in terms of overall complete tumor removal and complication rates, the primary endpoints of our study. Looking at histological subgroups, we found a consistently higher rate of complete tumor removal in plexiform neurofibromas, 66% in the "fluorescent" group vs. 44% in the "SOC" group (p-value < 0.05, Fisher's exact test, CI 95%) (Table 2).

4 Discussion

In our surgical series, the utilization of SF has represented a helpful adjunct in most of the PNST, mainly in neurofibromas. Compared to the retrospective analysis of a historical cohort well-matched for demographic and clinical characteristics, the use of SF could add significant advantages to tumor

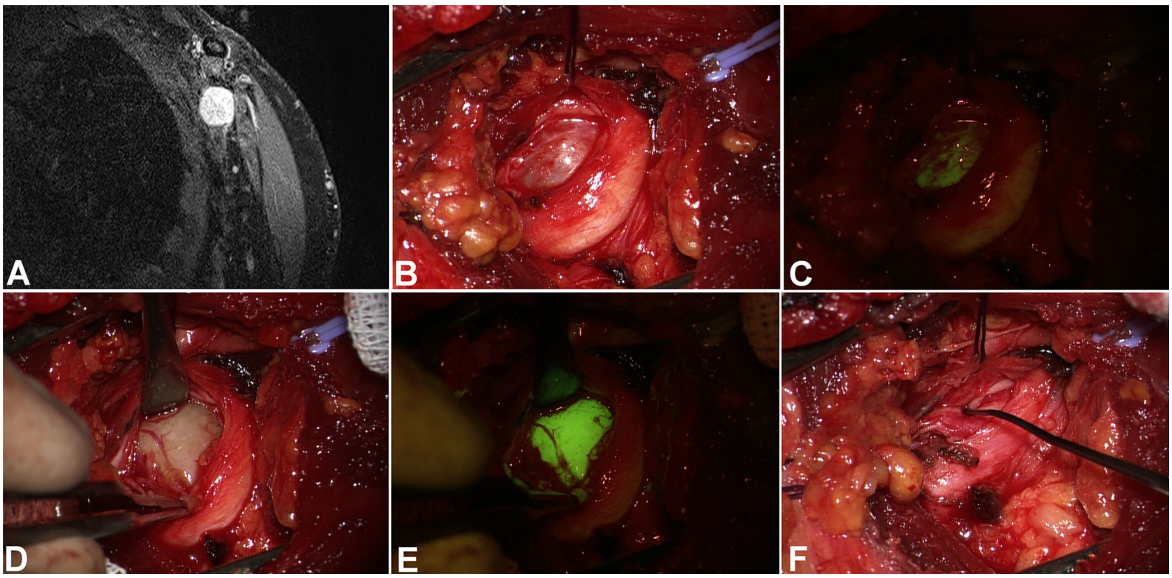

FIGURE 1
Left brachial plexus schwannoma (coronal MRI scan in **A**). After skin incision and subcutaneous tissues dissection, the tumor appeared surrounded by the nerve **(B)**. The first examination under YELLOW 560 filter **(C)** showed a slight and diffuse fluorescence both of the tumor and the nerve covering the tumor. However, after pseudocapsule incision **(D)**, the tumor showed an intense and homogeneous fluorescence **(E)**, whereas the nerve was only slightly fluorescent. Tumor removal was performed under intraoperative neurophysiological monitoring **(F)**.

visualization. In particular, SF constituted a valuable tool in increasing the extent of resection in plexiform neurofibromas. During the last years, SF has emerged as an intraoperative tracer able to improve brain-tumor visualization (16–18, 33, 34), due to its non-specific, vascular mechanism of action related to the accumulation in brain regions with blood-brain barrier (BBB) disruption, as it happens with MRI contrast enhancement (35). The availability of integrated and specific filters in the surgical microscope has contributed to the wide diffusion of fluorescein (36). Therefore, based on our extensive experience with CNS tumors, we empirically started this experience of fluorescent PNST using a low dosage of 1mg/kg of sodium fluorescein, i.v. injected during the patient intubation to achieve optimal discrimination between the tumor and normal surrounding nerves (25, 29). Moreover, another factor that led us to evaluate the role of SF in PNST was that other diffused intraoperative dye as 5-ALA has demonstrated, in few cases of spinal neurinomas, the lack of positive fluorescence pattern, in relation to its specific mechanism of action (37, 38).

In our preliminary analysis comprising only 20 lesions, we discussed that fluorescein plays a valuable role during surgical resection of schwannomas by highlighting the pathological tissue with a brighter fluorescent appearance than the surrounding nerves (25). Nevertheless, we noted that the most relevant advantage of SF was obtained mainly in neurofibromas helping identify diffuse tumor remnants (Figure 3). The German group led by Pedro found similar results: the authors examined 21 cases of PNST during surgery under SF at the low dosage of 0.5-1mg/kg (22, 23). An optimal distinction between tumor and surrounding nerves was observed in all 17 schwannomas scheduled for fluorescein-guided surgery, in 1 neurofibroma, and 1 MPNST. The authors also experienced the role of SF in fascicular biopsy of lesions involving the whole nerve segment (23, 39), finding usefulness in a case of B-cell lymphoma, whereas the fluorescein uptake in the MPNST was so widespread that the SF-contrast was judged useless (23). Moreover, they stressed the role of ImageJ, an open platform for digital video analysis, in objectifying SF enhancement, confirming the intraoperative impression of increased fluorescence of the PNST compared to healthy tissue. After these experiences, SF was established as a standard visualization tool in PNST surgery at the authors' Institution (23). Some case reports have also demonstrated the application and usefulness of SF in other peripheral nerve diseases, such as intraneural ganglion cysts (24). In contrast to all the previously mentioned findings, Kalamarides et al. examined five schwannomas with a fluorescein dosage of 0.5mg/kg (40) without noticing any benefit deriving from filter activation in tumor visualization or pathological tissue discrimination from nerve fascicles, except for only 1 case. However, these different results could partially be explained by the dose and timing of SF administration: as for CNS tumors, the high discrimination assured by SF appears to

10.3389/fonc.2022.1070878

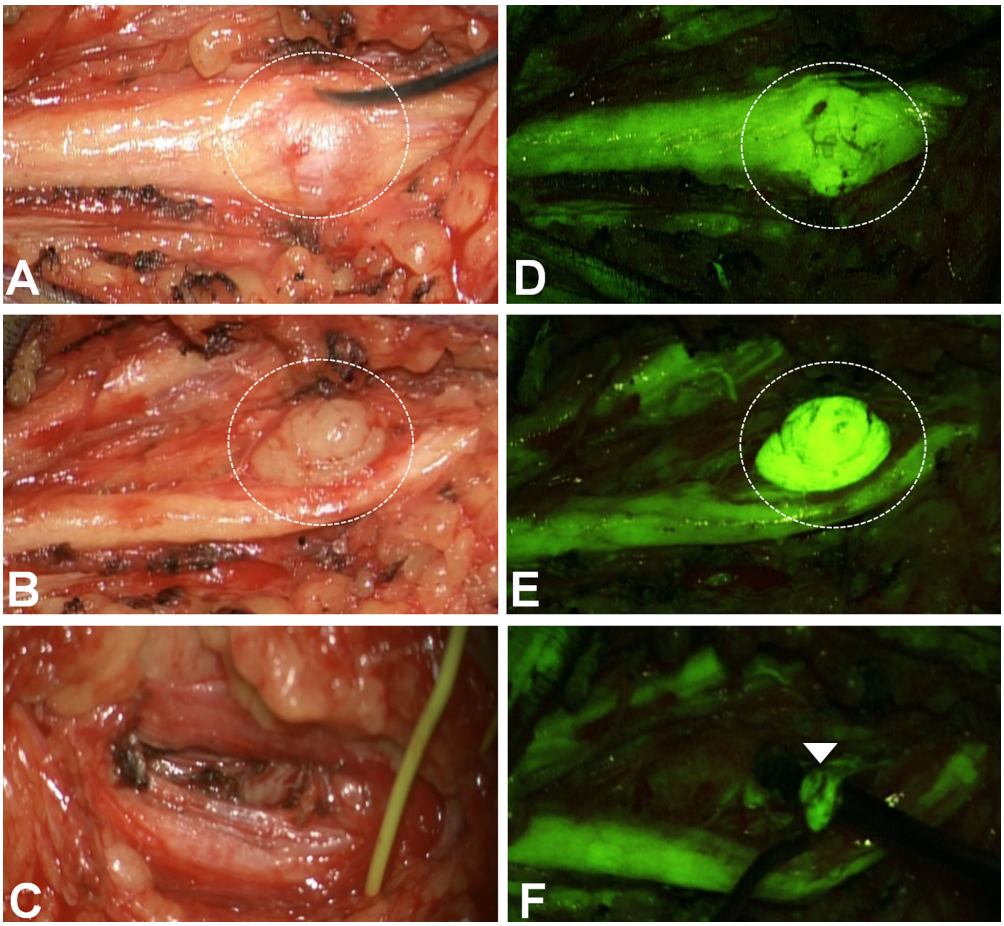

FIGURE 2
Remnants identification in a left superficial peroneal schwannoma (**A–C**: white light; **D–F**: YELLOW560). After the popliteal fascia opening, the sciatic-superficial popliteal nerve was identified and followed distally: one 1,5 cm schwannoma was visible (*dotted circle* in A). The first fluorescein examination **(D)** depicted a corresponding area of more slight fluorescence than the nerve. Therefore the capsule was opened **(B)**. However, the tumor appeared intensely fluorescent, more than the nerve **(E)**. After tumor removal **(C)**, the last examination under YELLOW560 evidenced a small remnant (*arrowhead*) non-clearly visible under white light, then removed to obtain a gross-total resection.

TABLE 2 Clinical characteristics of the comparison historical cohort of PNST.

Histology	N°	Neurocutaneous syndromes	Location	Resection	Complications
Schwannoma	86 (60%)	5 Schwannomatosis 2 NF1 1 NF2	36 Inferior Limbs 23 Superior limbs 15 Intracanalar 12 Brachial Plexus	79/86 Total (92%) 7/86 Subtotal (8%)	1 permanent sensory deficit 1 permanent motor deficit 3 transient sensory deficits 2 transient motor deficits 2 dural tear
Neurofibroma	37 (26%)	27 NF1 1 Schwannomatosis	13 Superior limbs 7 Inferior limbs 5 Chest 4 Head	36/37 Total (97%) 1/37 Subtotal (3%)	1 permanent sensory deficit

(Continued)

10.3389/fonc.2022.1070878

TABLE 2 Continued

Histology	N°	Neurocutaneous syndromes	Location	Resection	Complications
			3 Brachial Plexus 3 Back 2 Intracanalar		
Plexiform Neurofibroma	9 (6%)	9 NF1	4 Inferior limbs 3 Superior limbs 1 Chest 1 Intracanalar	4/9 Total (44 %) 5/9 Subtotal (56 %)	1 permanent motor deficit
Plexiform Schwannoma	3 (2%)	none	2 Superior limbs 1 Inferior limbs	3 Total (100%)	1 transient sensory deficit
Malignant Peripheral Nerve Sheath Tumor (MPSNT)	2 (1.5%)	2 NF1	2 Brachial Plexus	2 Subtotal (100%)	no
Fibrolipoma	1 (0.7%)	none	Superior limbs	Total	no
Branchial cyst	1 (0.7%)	none	Brachial plexus	Total	no
Lipoma	1 (0.7%)	none	Neck	Total	no
Nodular fascitis	1 (0.7%)	none	Inferior limbs	Total	no
Lymphoma	1 (0.7%)	none	Neck	Total	no
Total	142	40 NF1 6 Schwannomatosis 1 NF2	49 Inferior limbs 42 Superior limbs 18 Brachial Plexus 18 Intracanalar 6 Chest 4 Head 3 Back 2 Neck	127/142 Total (89%) 15/142 Subtotal (11%)	12/142 (8.5%)

depend on the injection time and dosage (30). Regarding other commercially available fluorophores, 5-aminolevulinic acid (5-ALA) has been employed in spinal tumors but without any positive fluorescence pattern in the case of schwannomas (37). To date, no other study has been reported regarding using 5-ALA in PNST surgery, including MPNST.

A bright fluorescence was present in all schwannomas (Figure 4) and neurofibromas of the present series; on the contrary, the fluorescence pattern was significantly less evident for malignant PNST, as also reported by other groups (23). Perineurioma and hybrid nerve sheath tumors were instead characterized by a faint fluorescence enhancement, although the rarity of these histotypes cannot allow a strong generalization. Other tumors and lesions such as B-cell lymphomas, solitary fibrous tumors, or other malignant entities appeared highly fluorescent with an inhomogeneous pattern due to sporadic necrotic regions. Pedro and coworkers discussed about the role of a digitalized and video analysis of fluorescein enhancement: in our experience, comprising also CSN tumor oncology, we were used to evaluate a broad range of fluorescein enhancement due to several characteristics besides the specificity of the tumor, such as the timing of injection, previous radiation therapy or corticosteroid administration. Therefore, after an appropriate learning curve, we consider that an adequate subjective evaluation can overcome the software elaboration since the role of fluorescein magnification consists in allowing a discrimination between health and pathological fluorescent tissue, not based upon absolute uptake value how much rather on enhancement compared to the baseline of the surgical cavity.

These uptake findings correlate to the characteristic's enhancement of tumors at preoperative MR, and the concentration of SF depends on endoneurial extravasation. The key point is the disruption of the blood-nerve barrier (BNB), which shares some structural features with the BBB (26, 41). The interaction between blood and nerve sheath justifies our clinical findings, in particular the increase of fluorescent enhancement after pseudocapsule opening and during tumor resection: this evidence can be explained considering that tumor growth disrupts the tight junctions, a

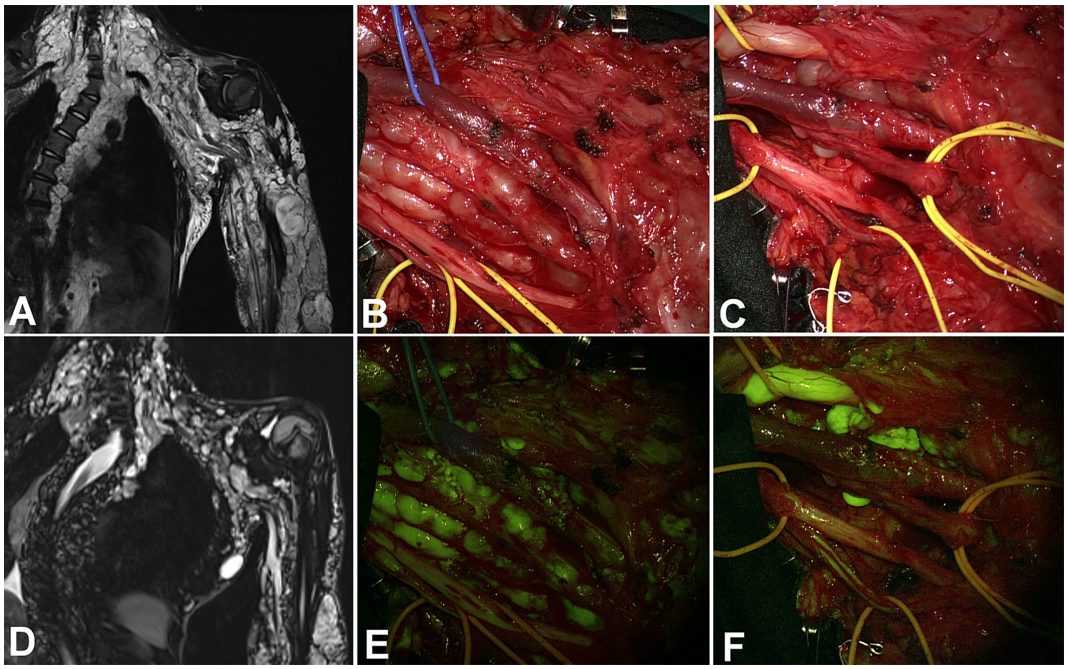

FIGURE 3
Coronal view in a huge plexiform neurofibroma of the whole upper left arm. Due to the rapid increase of a nodular lesion between radial and median nerves, the patients underwent partial surgery (coronal view in **(A)** – preoperative – and **D** – postoperative), with progressive exposure of the nerves by alternating the white light **(B, C)** and the YELLOW560 filter activation **(E, F)**. The tumor showed intense fluorescence if compared to the moderate fluorescein uptake of the nerve, whereas the neurofibroma partially substituted the radial nerve **(F)**.

network of transmembrane and peripheral proteins, altering BNB structure and leading to fluorescein extravasation and accumulation inside neoplastic nodules (28). In particular, a stratified analysis of our results revealed that the contribution of fluorescein is more significant for schwannomas and neurofibromas: the former presented a bright fluorescence with intense delineation of tumor borders which made more straightforward surgery, especially for large lesions which need a piecemeal removal. In the case of neurofibromas, especially for the plexiform variant, the role of SF can be judged fundamental in increasing the resection rate, as demonstrated by the comparison to our historical institutional series. Differently from schwannomas, due to various entering and exiting fascicles in neurofibromas, SF facilitates progressive dissection and piecemeal resection, thus allowing further identification of small remnants not visible under white-light illumination. Most of surgery can be performed under YELLOW 560 visualization which allows to visualize the surgical field in similar natural color with an adequate brightness: therefore, we cannot be able to quantify the specific cases in which SF could have increased resection; this datum can be indirectly derived by means a comparison with the historical series. On the contrary, the use of fluorescein remains questionable for other rarer tumors, such as MPNST, showing a minimal or heterogeneous pattern of SF uptake (Figure 5) and widespread involvement of healthy and functional structures; further studies including specifically a single-tumor entity could determine the real potentiality of this methodic.

The complication rate is similar in the current series and the historical cohort. These findings can be explained by the role of IOM, employed for several years at our Institution, comprising both the control and the SF cohort. Intraoperative fascicular mapping and monitoring is still a surgical milestone; the use of SF represents, in our experience, an intraoperative adjunct without rejecting the standard principles of PNST microsurgical resection to preserve neurological function. We hypothesize the role of SF in selecting yellow nervous fibers silent at direct stimulation, probably due to tumor infiltration, to potentially increase surgical radicality. We did not report fluorescein-related side effects or adverse reactions. The only visible manifestation of fluorescein administration is the onset of a transient and harmless yellowish urinary stain that rapidly disappears after 24 hours. Despite the very high safety profile of SF, as also reported for ophthalmological applications that usually employ a dose of 500 mg (20, 42), the lack

10.3389/fonc.2022.1070878

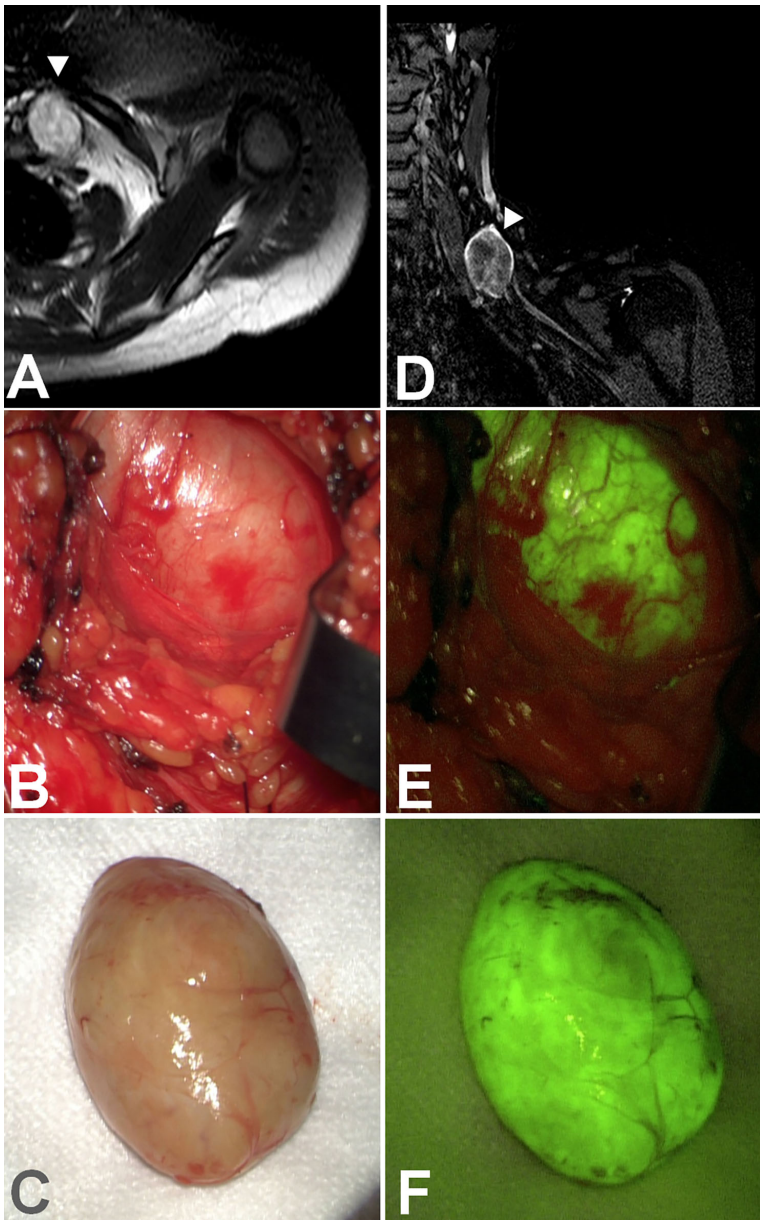

FIGURE 4
Axial **(A)** and coronal **(D)** view of a schwannoma of the suprascapular nerve. Under white light **(B)**, the tumor capsule was, in some parts, indistinguishable from the nerve, but the schwannoma showed intense fluorescein uptake **(E)** compared to the nerve lying lower. The tumor was removed en bloc **(C)** entirely, and intense and homogeneous fluorescence was still visible **(F)**.

of side effects may be related to the low dosage used in this study, thanks to the dedicated filter into the microscope, that allowed more accurate identification of fluorescent tissue. Nonetheless, the main limitation of the presented study is represented by the heterogeneous histology of PNST included. In addition, the lack of a significant long-term follow-up prevents the elucidation of a possible correlation between the use of SF, the extent of resection, and survival. Another selection bias is the association of both sporadic and syndromic tumors. Future prospective studies could better address these limitations by stratifying the cohorts according to the major predicting factors of PNST removal, including tumor histology.

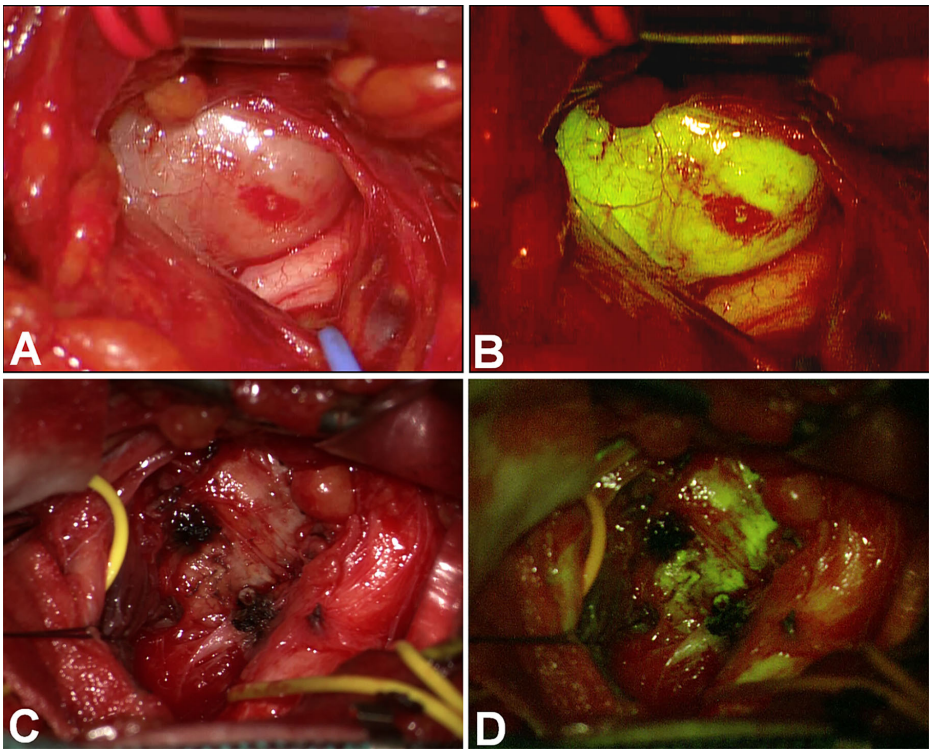

FIGURE 5
Comparison among the intense and homogeneous fluorescein uptake of a brachial plexus schwannoma **(A, B)** and a MPNST of the upper limb **(C)**, which showed inhomogeneous and slightly fluorescence **(D)**, compared to the surrounding nerve.

5 Conclusion

Fluorescein-guided surgery seems to be a safe and effective technique that can be used during the surgical resection of PNST to identify better and distinguish the most frequent subtypes of PNST from intact functional nerves. Prospective studies with long-term follow-up and designed for specific histologies could provide significant insights into the effects of fluorescein application on PNST patients' outcomes.

Data availability statement

Publicly available datasets were analyzed in this study. This data can be found here: https://zenodo.org/.

Ethics statement

The studies involving human participants were reviewed and approved by Ethics Committee Fondazione IRCCS Istituto Neurologico Carlo Besta. The patients/participants provided their written informed consent to participate in this study.

Author contributions

VN, NI, JF, NC, and IV: study concept and design. VN, NI, JF, IT, and IV: critical revision of the manuscript for intellectual content. All authors: acquisition of data, data analysis, and interpretation. VN and IV: study supervision. All authors contributed to the article and approved the submitted version.

Funding

This study was partially supported by *Associazione Paolo Zorzi per le Neuroscienze, ONLUS*, and by the Italian Ministry of Health (RRC).

Acknowledgments

ME is a member of ERN Genturis and ERN Euracan.

Conflict of interest

FA received honoraria from the Carl Zeiss Meditec Company for lectures at International Congresses.

The remaining authors declare that the research was conducted in the absence of any commercial or financial relationships that could be construed as a potential conflict of interest.

Publisher's note

References

1. Tiel R, Kline D. Peripheral nerve tumors: Surgical principles, approaches, and techniques. *Neurosurg Clin N Am* (2004) 15:167–75. doi: 10.1016/j.nec.2004.02.003

2. Rodriguez FJ, Folpe AL, Giannini C, Perry A. Pathology of peripheral nerve sheath tumors: Diagnostic overview and update on selected diagnostic problems. *Acta Neuropathol* (2012) 123:295–319. doi: 10.1007/s00401-012-0954-z

3. Kim DH, Murovic JA, Tiel RL, Moes G, Kline DG. A series of 397 peripheral neural sheath tumors: 30-year experience at Louisiana state university health sciences center. *J Neurosurg* (2005) 102:246–55. doi: 10.3171/jns.2005.102.2.0246

4. Montano N, D'Alessandris QG, D'Ercole M, Lauretti L, Pallini R, Di Bonaventura R, et al. Tumors of the peripheral nervous system: Analysis of prognostic factors in a series with long-term follow-up and review of the literature. *J Neurosurg* (2016) 125:363–71. doi: 10.3171/2015.6.JNS15596

5. Guan J, Riva-Cambrin J, Brockmeyer DL. Chiari-related hydrocephalus: Assessment of clinical risk factors in a cohort of 297 consecutive patients. *Neurosurg Focus FOC* (2016) 41:E2. doi: 10.3171/2016.8.FOCUS16203

6. Akshintala S, Baldwin A, Liewehr DJ, Goodwin A, Blakeley JO, Gross AM, et al. Longitudinal evaluation of peripheral nerve sheath tumors in neurofibromatosis type 1: growth analysis of plexiform neurofibromas and distinct nodular lesions. *Neuro Oncol* (2020) 22:1368–78. doi: 10.1093/neuonc/noaa053

7. Tucker T, Wolkenstein P, Revuz J, Zeller J, Friedman JM. Association between benign and malignant peripheral nerve sheath tumors in NF1. *Neurology* (2005) 65:205–11. doi: 10.1212/01.wnl.0000168830.79997.13

8. Fisher MJ, Blakeley JO, Weiss BD, Dombi E, Ahlawat S, Akshintala S, et al. Management of neurofibromatosis type 1-associated plexiform neurofibromas. *Neuro Oncol* (2022) 24(11):1827-1844. doi: 10.1093/neuonc/noac146

9. Martin E, Pendleton C, Verhoef C, Spinner RJ, Coert JH. Morbidity and function loss after resection of malignant peripheral nerve sheath tumors. *Neurosurgery* (2022) 90:354–64. doi: 10.1093/neuros/nyab342

10. Stone JJ, Spinner RJ. Go for the gold: A "plane" and simple technique for resecting benign peripheral nerve sheath tumors. *Oper Neurosurg* (2020) 18:60–8. doi: 10.1093/ons/opz034

11. Russell SM. Preserve the nerve: Microsurgical resection of peripheral nerve sheath tumors. *Neurosurgery* (2007) 61:113–7; discussion 117-8. doi: 10.1227/01.neu.0000289724.89588.bc

12. Guha D, Davidson B, Nadi M, Alotaibi NM, Fehlings MG, Gentili F, et al. Management of peripheral nerve sheath tumors: 17 years of experience at Toronto Western hospital. *J Neurosurg* (2018) 128:1226–34. doi: 10.3171/2017.1.JNS162292

13. Safaee MM, Lyon R, Barbaro NM, Chou D, Mummaneni PV, Weinstein PR, et al. Neurological outcomes and surgical complications in 221 spinal nerve sheath tumors. *J Neurosurg Spine* (2017) 26:103–11. doi: 10.3171/2016.5.SPINE15974

14. Wilson TJ, Hamrick F, Alzahrani S, Dibble CF, Koduri S, Pendleton C, et al. Analysis of the effect of intraoperative neuromonitoring during resection of benign nerve sheath tumors on gross-total resection and neurological complications. *J Neurosurg* (2021), 1–10. doi: 10.3171/2020.8.JNS202885

15. Rey-Dios R, Cohen-Gadol AA. Intraoperative fluorescence for resection of hemangioblastomas. *Acta Neurochir (Wien)* (2013) 155:1287–92. doi: 10.1007/s00701-013-1723-z

16. Falco J, Cavallo C, Vetrano IG, de Laurentis C, Siozos L, Schiariti M, et al. Fluorescein application in cranial and spinal tumors enhancing at preoperative MRI and operated with a dedicated filter on the surgical microscope: Preliminary results in 279 patients enrolled in the FLUOCERTUM prospective study. *Front Surg* (2019) 6:49. doi: 10.3389/FSURG.2019.00049

17. Acerbi F, Broggi M, Eoli M, Anghileri E, Cuppini L, Pollo B, et al. Fluorescein-guided surgery for grade IV gliomas with a dedicated filter on the surgical microscope: Preliminary results in 12 cases. *Acta Neurochir (Wien)* (2013) 155:1277–86. doi: 10.1007/s00701-013-1734-9

18. Acerbi F, Broggi M, Schebesch KM, Höhne J, Cavallo C, De Laurentis C, et al. Fluorescein-guided surgery for resection of high-grade gliomas: A multicentric prospective phase II study (FLUOGLIO). *Clin Cancer Res* (2018) 24:52–61. doi: 10.1158/1078-0432.CCR-17-1184

19. Moore GE. Fluorescein as an agent in the differentiation of normal and malignant tissues. *Sci (80-)* (1947) 106:130–1. doi: 10.1126/science.106.2745.130-a

20. Kornblau IS, El-Annan JF. Adverse reactions to fluorescein angiography: A comprehensive review of the literature. *Surv Ophthalmol* (2019) 64:679–93. doi: 10.1016/j.survophthal.2019.02.004

21. *Determination 905/2015* . Available at: www.gazzettaufficiale.it/eli/id/2015/07/22/15A05620/sg.

22. Pedro MT, Eissler A, Schmidberger J, Kratzer W, Wirtz CR, Antoniadis G, et al. Sodium fluorescein–guided surgery in peripheral nerve sheath tumors: First experience in 10 cases of schwannoma. *World Neurosurg* (2019) 124:e724–32. doi: 10.1016/j.wneu.2019.01.010

23. Pedro MT, Grübel N, Durner G, Pala A, Wirtz CR, Koenig RW. Intraoperative sodium-fluorescence imaging in peripheral nerve sheath tumors (PNST)-a new additional promising diagnostic tool. *Front Oncol* (2021) 11:655392. doi: 10.3389/fonc.2021.655392

24. Stone JJ, Graffeo CS, de Ruiter GCW, Rock MG, Spinner RJ. Intraoperative intravenous fluorescein as an adjunct during surgery for peroneal intraneural ganglion cysts. *Acta Neurochir (Wien)* (2018) 160:651–4. doi: 10.1007/s00701-018-3477-0

25. Vetrano IG, Acerbi F, Falco J, Devigili G, Rinaldo S, Messina G, et al. Fluorescein-guided removal of peripheral nerve sheath tumors: A preliminary analysis of 20 cases. *J Neurosurg* (2019), 1–10. doi: 10.3171/2019.9.JNS19970

26. Abram SE, Yi J, Fuchs A, Hogan QH. Permeability of injured and intact peripheral nerves and dorsal root ganglia. *Anesthesiology* (2006) 105:146–53. doi: 10.1097/00000542-200607000-00024

27. Perez ER, Bracho O, Ein L, Szczupak M, Monje PV, Fernandez-Valle C, et al. Fluorescent detection of merlin-deficient schwann cells and primary human vestibular schwannoma cells using sodium fluorescein. *Otol Neurotol* (2018) 39:1053–9. doi: 10.1097/MAO.0000000000001895

28. Malmgren LT, Olsson Y. Differences between the peripheral and the central nervous system in permeability to sodium fluorescein. *J Comp Neurol* (1980) 191:103–17. doi: 10.1002/cne.901910106

29. Vetrano IG, Saletti V, Nazzi V. Fluorescein-guided resection of plexiform neurofibromas: How I do it. *Acta Neurochir (Wien)* (2019) 161:2141–5. doi: 10.1007/s00701-019-04038-5

30. Vetrano IG, Nazzi V, Acerbi F. What is the advantage of using sodium fluorescein during resection of peripheral nerve tumors? *Acta Neurochir (Wien)* (2020) 162:1153–5. doi: 10.1007/s00701-019-04209-4

31. Louis DN, Perry A, Reifenberger G, von Deimling A, Figarella-Branger D, Cavenee WK, et al. The 2016 world health organization classification of tumors of the central nervous system: A summary. *Acta Neuropathol* (2016) 131:803–20. doi: 10.1007/s00401-016-1545-1

32. Louis DN, Perry A, Wesseling P, Brat DJ, Cree IA, Figarella-Branger D, et al. The 2021 WHO classification of tumors of the central nervous system: A summary. *Neuro Oncol* (2021) 23:1231–51. doi: 10.1093/neuonc/noab106

33. Acerbi F, Cavallo C, Schebesch KM, Akçakaya MO, de Laurentis C, Hamamcioglu MK, et al. Fluorescein-guided resection of intramedullary spinal cord tumors: Results from a preliminary, multicentric, retrospective study. *World Neurosurg* (2017) 108:603–9. doi: 10.1016/j.wneu.2017.09.061

34. de Laurentis C, Höhne J, Cavallo C, Restelli F, Falco J, Broggi M, et al. The impact of fluorescein-guided technique in the surgical removal of CNS tumors in a pediatric population: Results from a multicentric observational study. *J Neurosurg Sci* (2019) 63:679–87. doi: 10.23736/S0390-5616.19.04601-0

35. Cavallo C, De Laurentis C, Vetrano IG, Falco J, Broggi M, Schiariti M, et al. The utilization of fluorescein in brain tumor surgery: A systematic review. *J Neurosurg Sci* (2018) 62:690–703. doi: 10.23736/S0390-5616.18.04480-6

36. Acerbi F, Restelli F, de Laurentis C, Falco J, Cavallo C, Broggi M, et al. Fluorescent tracers in neurosurgical procedures: A European survey. *J Neurosurg Sci* (2021) 65:618–25. doi: 10.23736/S0390-5616.18.04494-6

37. Millesi M, Kiesel B, Woehrer A, Hainfellner JA, Novak K, Martínez-Moreno M, et al. Analysis of 5-aminolevulinic acid-induced fluorescence in 55 different spinal tumors. *Neurosurg Focus* (2014) 36:E11. doi: 10.3171/2013.12.FOCUS13485

38. Wainwright JV, Endo T, Cooper JB, Tominaga T, Schmidt MH. The role of 5-aminolevulinic acid in spinal tumor surgery: A review. *J Neurooncol* (2019) 141:575–84. doi: 10.1007/s11060-018-03080-0

39. Pedro MT, Eissler A, Scheuerle A, Schmidberger J, Kratzer W, Wirtz CR, et al. Sodium fluorescein as intraoperative visualization tool during peripheral nerve biopsies. *World Neurosurg* (2020) 133:e513–21. doi: 10.1016/j.wneu.2019.09.081

40. Kalamarides M, Bernat I, Peyre M. Extracapsular dissection in peripheral nerve schwannoma surgery using bright light and fluorescein sodium visualization: Case series. *Acta Neurochir (Wien)* (2019) 161:2447–52. doi: 10.1007/s00701-019-04071-4

41. Peltonen S, Alanne M, Peltonen J. Barriers of the peripheral nerve. *Tissue barriers* (2013) 1:e24956. doi: 10.4161/tisb.24956

42. Danis RP, Wolverton S, Steffens T. Phototoxicity from systemic sodium fluorescein. *Retina* (2000) 20:370–3. doi: 10.1097/00006982-200004000-00008

frontiers | Frontiers in Oncology

TYPE Original Research
PUBLISHED 09 January 2023
DOI 10.3389/fonc.2022.1055046

OPEN ACCESS

EDITED BY
Pierpaolo Alongi,
ARNAS Ospedali Civico Di Cristina Benfratelli, Italy

REVIEWED BY
Jacopo Falco,
Carlo Besta Neurological Institute Foundation (IRCCS), Italy
Giulio Bonomo,
Carlo Besta Neurological Institute Foundation (IRCCS), Italy

*CORRESPONDENCE
Fang Peng
pengfang@csu.edu.cn

SPECIALTY SECTION
This article was submitted to Neuro-Oncology and Neurosurgical Oncology, a section of the journal Frontiers in Oncology

RECEIVED 21 October 2022
ACCEPTED 05 December 2022
PUBLISHED 09 January 2023

CITATION
Yang Z, Li Z, Fu C, Zhu Y, Lin Y, Deng Y, Li N and Peng F (2023) Development and validation of a nomogram to predict overall survival and cancer-specific survival in patients with primary intracranial malignant lymphoma: A Retrospective study based on the SEER database. *Front. Oncol.* 12:1055046. doi: 10.3389/fonc.2022.1055046

Development and validation of a nomogram to predict overall survival and cancer-specific survival in patients with primary intracranial malignant lymphoma: A Retrospective study based on the SEER database

Ziyue Yang[1,2], Zhenfen Li[1,2], Chunmeng Fu[1,2], Yuanyuan Zhu[1,2], Ying Lin[3], Ying Deng[4], Ning Li[1] and Fang Peng[1,2]*

[1]Department of Blood Transfusion, Xiangya Hospital, Central South University, Changsha, Hunan, China, [2]National Health Commission (NHC) key Laboratory of Cancer Proteomics, Xiangya Hospital, Central South University, Changsha, Hunan, China, [3]Department of Nuclear Medicine, Xiangya Hospital, Central South University, Changsha, China, [4]Department of Scientific Research Management, Ningxiang People's Hospital, Hunan University Traditional Chinese Medicine, Ningxiang, Changsha, Hunan, China

Introduction: Primary intracranial malignant lymphoma (PIML) is a rare form of lymphoma that most often occurs in the brain and has an extremely low 5-year survival rate. Although chemotherapy and radiotherapy are widely used in the clinical management of PIML, the choice of treatment regimen and the actual circumstances of patients remain challenges when assessing survival rates in different patients.

Methods: Considering this, we obtained clinical treatment and survival information from the Surveillance, Epidemiology, and End Results database (SEER) on patients with lymphoma, the primary site of which was the brain, and performed statistical analyses of the demographic characteristics. Survival analyses were performed using the Kaplan–Meier method, and univariate and multivariate Cox proportional hazards regression analyses were performed to identify independent prognostic factors.

Result: We identified age, pathology, the Ann Arbor stage, and treatment as the risk factors affecting patient prognosis. The areas under the curve (AUCs) for

overall survival at 1, 3, and 5 years were 0.8, 0.818, and 0.81, respectively. The AUCs for cancer-specific survival at 1, 3, and 5 years were 0.8, 0.79, and 0.79. The prediction ability in the development and verification cohorts was in good agreement with the actual values, while we plotted the clinical decision curves for the model, suggesting that the nomogram can provide benefits for clinical decision-making.

Conclusion: Our model provides a prognostic guide for patients with PIML and a reliable basis for clinicians.

KEYWORDS

primary intracranial malignant lymphoma, neurological tumors, diffuse large B lymphoma, SEER database, nomogram

Introduction

Primary intracranial malignant lymphoma (PIML) is an uncommon form of lymphoma, accounting for 1% of all non-Hodgkin's lymphomas (1). Its incidence has increased over the last 30 years and is closely related to the immune function of patient (2). PIML has become the most common neurological tumor because of the increase in patients with acquired immunodeficiency syndrome and the use of immunosuppressive drugs following transplantation (3). Although PIML is relatively rare, it is more common than the secondary spread of primary extracranial lymphoma (4).

PIML is treated with a combination of chemotherapy, radiotherapy, and surgery in clinical practice (5). Of these, chemotherapy is the most conventional treatment (6), and experts in the field agree that high doses of methotrexate are the backbone of multimodal therapy (7), including other chemotherapeutic agents. However, there are many controversies regarding the treatment of PIML. The impact of surgical resection on PIML remains controversial, with one clinical study suggesting that for intracranial lymphoma, surgical resection improves PFS (progression-free survival) but not OS (1). Other controversies include the optimal upfront chemotherapy regimen, the status of radiotherapy, the risks and benefits of surgical treatment, and treatment involving the cerebrospinal fluid space (8).

To explore the impact of different demographic characteristics and treatment on the prognosis of patients with PIML, we performed a retrospective analysis of data corresponding to patients with PIML based on the Surveillance, Epidemiology and End Result (SEER) database (9). SEER database, supported by a project of the National Cancer Institute (NCI), is a real-world database of clinical oncology literature that has been widely used for epidemiological investigations and statistical analyses (10), especially for a rare tumor type such as PIML. With a total of 1245 patients diagnosed with lymphoma of the brain origin between 1975 and 2019, this is the most comprehensive retrospective study to analyze clinicopathological features. Using these data and establishing a nomogram model that predicts OS and CSS (Cancer Specific Survival), which will provide an excellent reference for future clinical decisions.

Method

Data acquisition

The SEER Program of the NCI contains retrospective data on the demographic characteristics, disease classification, pathological features, and treatment of tumors in patients from different states in the USA (10). In its official data retrieval SEER* Stat software, the "Incidence-SEER Research Plus Data, Nov 2021 sub (1975–2019)" dataset corresponded to patients with PIML from 1975-2019. The primary site label identified the brain (code C71.9), and the behavior code ICD-0-3 was used to identify the malignance. The disease was identified as a lymphoid neoplasm after the 2021 revision. We collected information on sex, age, the time of diagnosis, the primary tumor site, pathological staging of the lymphoma, radiotherapy, chemotherapy, surgical treatment, survival time, marital status, the cause of death, and survival status. A total of 919 patients were included after screening based on the following exclusion criteria (1): Ann Arbor stage information was unknown (2), treatment information was unknown (3), survival time was unknown. The graphical abstract of this study is presented in Figure 1.

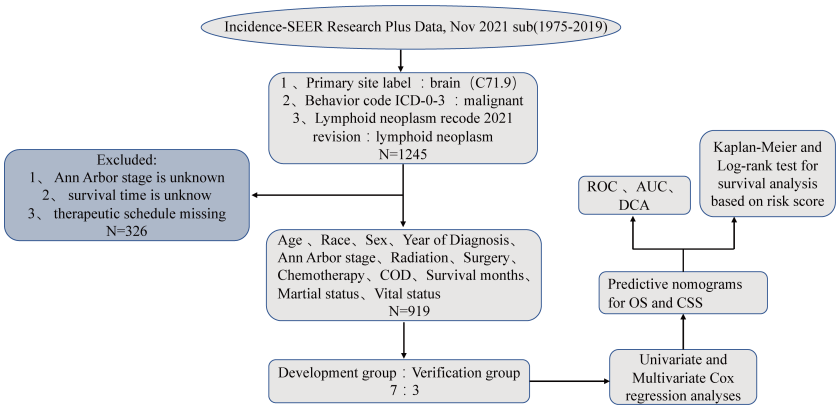

FIGURE 1
The flowchart of this study which was including and dividing patients.

Statistical analysis

All statistical analyses were performed using R Studio (version 4.1.2) and SPSS (version 36.0). First, the 919 samples were randomly divided in a 7:3 ratio into development and verification groups using the sample statement in R Studio (11). These groups were used to develop and validate the model. Statistical analysis between the two groups was performed using the R package "CompareGroups," and chi-square tests were used for comparisons between the groups. The R package "survival," "rms," "survivalROC," "survminer," and "ggplot2" were used for survival analysis and to develop nomogram models and plot Kaplan–Meier (KM) curves.

OS (Overall survival) and CSS (cancer-specific survival) are commonly used indicators to assess the prognostic status of tumor patients. First, OS and CSS were used as the outcome variables. Using the KM method, OS and CSS were calculated using SPSS software. We obtained the Cox regression model parameters using maximum likelihood estimation with the help of the partial likelihood function. We included all variables in the development cohort in the univariate Cox regression analysis separately, and P values < 0.05 were considered statistically significant. Variables that were statistically and clinically significant were included in the multivariate Cox analysis, while hazard risk ratios were calculated, with a value > 1 being considered a risk factor for survival. The independent prognostic factors affecting OS and CSS in patients with PIML were identified. A nomogram prediction model was developed based on the established Cox regression results. All the above was also verified in the verification cohort.

A risk score formula was constructed based on multivariate Cox regression. All the patients were divided into high and low risk groups according to the risk scores, and the probability of poor survival was quantified for each patient. A nomogram model was constructed based on the multivariate Cox regression analysis. To further evaluate the predictive performance of the nomogram model, the area under the subject working characteristic curve (AUC) and correction curve for OS and CSS at 1, 3, and 5 years were calculated (11). A higher AUC and smoother correction curves indicated that the models had a greater ability to predict patient prognosis (12). Decision curve analysis (DCA) also demonstrated that our models could deliver greater patient benefits (13). Finally, the KM method was used to plot survival curves with different variables.

Result

Patients' characteristics

A total of 919 patients diagnosed with lymphoma between 1975 and 2019 with the primary site in the brain and documented survival time and clinical staging were included in the study. Table 1 summarizes the demographic and clinical characteristics of all the patients. The patients were randomly distributed into a developmental group (n = 643) and a verification group (n = 276), and the chi-square test was used to confirm the significant internal differences between the two groups. The International Prognostic Index (IPI) stage of lymphoma scores 60 years as 0 points and age >60 years as 1 point (14). In this study, all patients were classified according to the IPI scoring system using the age of 60 years as the cutoff value. Of these, 573 patients (62%) were younger than 60 years at the time of diagnosis. Caucasian ethnicity predominated (n = 735, 80%), and there were 609 (66%) male patients.

Diffuse large B-cell lymphoma was the most common histological subtype, with 462 cases (50%), which is sufficient to establish that the most common pathological type of intracranial lymphoma is the same as the systemic lymphoma

10.3389/fonc.2022.1055046

TABLE 1 The demographic and clinical features of patients with PIML.

	Total	Development Cohort	Verification Cohort	*P Value*
	N=919	N=643(70%)	N=276 (30%)	
Age				0.202
<60	573(62.3%)	410 (63.8%)	163 (59.1%)	
>=60	346(37.7%)	233 (36.2%)	113 (40.9%)	
Race				0.981
Black	103(11.2%)	71 (11.0%)	32 (11.6%)	
Other	80(8.8%)	56 (8.71%)	24 (8.70%)	
Unknown	1(0.10%)	1 (0.16%)	0 (0.00%)	
White	735(80.0%)	515 (80.1%)	220 (79.7%)	
Sex:				0.005
Female	310(33.7%)	198 (30.8%)	112 (40.6%)	
Male	609(66.3%)	445 (69.2%)	164 (59.4%)	
Year of Diagnosis:				0.005
1989-1983	66(7.2%)	49 (7.62%)	17 (6.16%)	
1990-1999	398(43.3%)	292 (45.4%)	106 (38.4%)	
2000-2009	265(28.8%)	189 (29.4%)	76 (27.5%)	
2010-2015	190(20.8%)	113 (17.6%)	77 (27.9%)	
Histology:				0.387
DLBCL	462(50.3%)	316 (49.1%)	146 (52.9%)	
HL	2(0.2%)	2 (0.31%)	0 (0.00%)	
Lymphoid neoplasm*	346(37.6%)	252 (39.2%)	94 (34.1%)	
NHL	109(11.9%)	73 (11.4%)	36 (13.0%)	
Ann Arbor stage:				0.921
Stage I	729(79.3%)	512 (79.6%)	217 (78.6%)	
Stage II	11(1.2%)	7 (1.09%)	4 (1.45%)	
Stage III	6(0.7%)	4 (0.62%)	2 (0.72%)	
Stage IV	173(18.8%)	120 (18.7%)	53 (19.2%)	
Surgery:				0.977
NO	767(83.4%)	536 (83.4%)	231 (83.7%)	
YES	152(16.6%)	107 (16.6%)	45 (16.3%)	
Radiation:				0.303
NO	465(50.6%)	333 (51.8%)	132 (47.8%)	
YES	454(49.4%)	310 (48.2%)	144 (52.2%)	
Chemotherapy:				0.974
No/Unknown	547(59.5%)	382 (59.4%)	165 (59.8%)	
Yes	372(40.5%	261 (40.6%)	111 (40.2%)	

(Continued)

TABLE 1 Continued

	Total	Development Cohort	Verification Cohort	*P Value*
	N=919	N=643(70%)	N=276 (30%)	
COD:				0.342
Alive	98(10.7%)	66 (10.3%)	32 (11.6%)	
NHL	371(40.4%)	252 (39.2%)	119 (43.1%)	
other	450(49.0%)	325 (50.5%)	125 (45.3%)	
Marital status:				0.141
Divorced	75(8.2%)	49 (7.62%)	26 (9.42%)	
Married	387(42.1%)	275 (42.8%)	112 (40.6%)	
Separated	6(0.7%)	3 (0.47%)	3 (1.09%)	
Single (never married)	361(39.3%)	262 (40.7%)	99 (35.9%)	
Unknown	21(2.3%)	11 (1.71%)	10 (3.62%)	
Unmarried or Domestic Partner	1(0.10%)	1 (0.16%)	0 (0.00%)	
Widowed	78(7.3%)	42 (6.53%)	26 (9.42%)	
Status:				0.63
Alive	98(10.7%)	66 (10.3%)	32 (11.6%)	
Dead	821(89.3%)	577 (89.7%)	244 (88.4%)	
Overall Survival				
1-year	270(29.5%)			
3-year	190(21.0%)			
5-year	131(16.1%)			
Cancer-specific Survival				
1-year	225(27.5%)			
3-year	156(19.3%)			
5-year	104(14.6%)			

*Lymphoid neoplasm is a group of malignant neoplasm originated from all lymphocytes.

(15). This was followed by lymphoid tumors in 346 cases (38%). Hodgkin's lymphoma was the least common, with only 2 cases (0.2%). For lymphoma, Ann Arbor staging guided clinical diagnosis and treatment was used, with stages I and IV accounting for the majority of the 919 patients included in the study, 729 (80%) and 173 (19%), respectively. For treatment, 152 (17%) patients underwent surgery, with some of the remaining patients treated for surgery due to patients' refusal and the lack of indications for surgery. Radiotherapy and chemotherapy were administered to 454 (49%) and 372 (40%) patients, respectively. Due to the limitations of the database, it was not possible to know about the specific treatment regimens of the patients or the chemotherapeutic drugs used.

Meanwhile, the median survival time for the entire cohort was 3 months. As shown in the survival curves in Figure 2, the OS rates for the entire cohort were 29.5%, 21.0%, and 16.1% at 1, 3, and 5 years. The CSS rates were 27.5%, 19.3%, and 14.6% at 1, 3, and 5 years, respectively.

Survival analysis of OS and CSS

Univariate and multivariate Cox regression analyses were performed to predict prognostic factors affecting OS and CSS. First, all variables in the development cohort, including age, sex, race, the time of diagnosis, the type of pathology, the Ann Arbor stage, radiotherapy, surgical treatment (other than biopsy), chemotherapy, and marital status were included in the statistical analysis. The results shown in Table 2 indicate that age was a potential risk factor affecting OS. Marital status is also

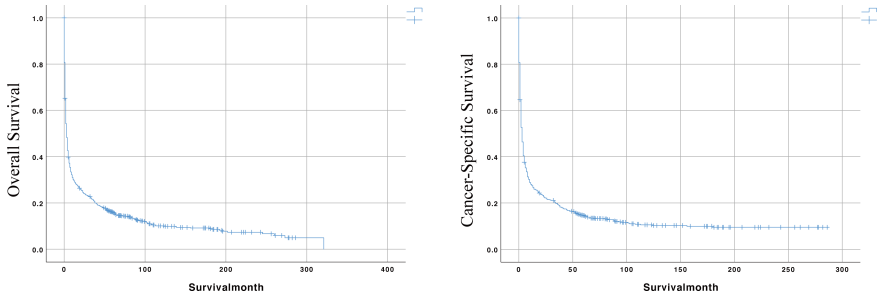

FIGURE 2
The Kaplan-Meier (KM) curves for predicting the OS and CSS of PIML patients in the whole cohort.

TABLE 2 The result of Univariate and Multivariate COX regression analyses of OS and CSS in development group.

	Overall Survival using COX regression						Cancer-Specific Survival using COX regression					
	Univariate Analysis (Development)			Multivariate Analysis (Development)			Univariate Analysis (Development)			Multivariate Analysis (Development)		
	HR	95% CI	*P value*	HR	95%CI	*P value*	HR	95% CI	*P value*	HR	95%CI	*P value*
Age												
<60	ref			ref			ref			ref		
>=60	1.766	1.491-2.092	4.65e-11 ***	1.73282	1.4514-2.0688	1.2e-09 ***	0.9427	0.7904-1.124	0.512			
Sex												
Female	ref						ref					
Male	1.055	0.8829-1.26	0.556				1.538	1.271-1.861	9.44e-06 ***	1.1581	0.9264-1.4477	0.19739
Race												
Black	ref						ref					
Other	1.1644	0.89644-1.513	0.254				0.6149	0.4644-0.8143	0.000688 ***	0.872	0.6504-1.1691	0.35986
Unknown	0.6803	0.09432-4.906	0.702				/	/	/	/	/	/
White	1.061	0.72963-1.543	0.756				0.4892	0.3264-0.7331	0.000532 ***	0.7858	0.5147-1.1997	0.26418
Year of Diagnosis												
1989-1983	ref						ref					
1990-1999	0.881	0.6473-1.199	0.42				1.1361	0.8113-1.5910	0.457764	1.1478	0.8074-1.6319	0.44247
2000-2009	0.9062	0.6565-1.251	0.549				0.5657	0.3940-0.8123	0.002026**	0.8158	0.5572-1.1943	0.29509
2010-2015	1.2022	0.8530-1.694	0.293				0.48	0.3282-0.7022	0.000156***	0.7686	0.5117-1.1545	0.20483
Histology												
NHL	ref			ref			ref			ref		

(Continued)

TABLE 2 Continued

	Overall Survival using COX regression						Cancer-Specific Survival using COX regression					
	Univariate Analysis (Development)			Multivariate Analysis (Development)			Univariate Analysis (Development)			Multivariate Analysis (Development)		
	HR	95% CI	*P value*	HR	95%CI	*P value*	HR	95% CI	*P value*	HR	95%CI	*P value*
DLBCL	0.8227	0.2046-3.3077	0.78339	1.0005	0.2461-4.0669	0.99945	1.4161	0.1985-10.105	0.729	1.5833	0.2123-11.8074	0.65398
Lymphoid neoplasm	0.8143	0.6832-0.9707	0.02192	1.1401	0.9261-1.4037	0.21648	1.7262	1.4346-2.077	7.34e-09***	1.0552	0.8609-1.2932	0.60494
HL	1.4194	1.0899-1.8485	0.00936 **	1.325985	1.0124-1.7368	0.04045 *	0.9117	0.6677-1.245	0.561	0.883	0.6391-1.2200	0.45065
Ann Arbor stage												
Stage I	ref						ref					
Stage II	1.7901	0.8481-3.778	0.127				0.5465	0.2262-1.320	0.179			
Stage III	0.8278	0.3092-2.216	0.707				0.8944	0.2872-2.785	0.847			
Stage IV	0.949	0.7688-1.171	0.626				1.0607	0.8468-1.329	0.608			
Radiation												
NO	ref						ref					
YES	0.861	0.7311-1.014	0.0728				0.9552	0.8783-1.248	0.609			
Surgery												
NO	ref			ref			ref			ref		
YES	0.5511	0.4372-0.6947	4.57e-07 ***	0.654283	0.4963-0.8626	0.00263 **	0.5614	0.4365-0.7222	7.03e-06 ***	0.6895	0.5280-0.9004	0.00633 **
Chemotherapy												
No/Unknown	ref			ref			ref			ref		
Yes	0.3635	0.3048-0.4336	<2e-16 ***	0.4078	0.3374-0.4930	< 2e-16 ***	0.3474	0.2875-0.4197	<2e-16 ***	0.4494	0.3572-0.5653	8.42e-12 ***
Marital status												
Single	ref			ref			ref			ref		
Married	0.7795	0.5648-1.076	0.1298	0.8982	0.6471-1.2468	0.52114	0.8492	0.6022-1.197	0.35115	1.1182	0.7783-1.6066	0.54563
Separated	2.0409	0.6324-6.586	0.2327	1.1564	0.3551-3.7661	0.80938	1.9232	0.6862-5.390	0.2136	1.3042	0.4549-3.7388	0.62115
Unknown	1.4244	1.0319-1.966	0.0315*	1.1808	0.8508-1.6388	0.32039	1.6273	1.1561-2.291	0.00525 **	1.1999	0.8370-1.7201	0.32125
Widowed	1.054	0.5304-2.095	0.8807	1.0101	0.5069-2.0129	0.97728	1.2469	0.6385-2.435	0.51813	1.2103	0.6127-2.3907	0.58271
Divorced	1.5957	0.2195-11.599	0.6443	1.8864	0.2563-13.8841	0.53317	1.6645	0.2283-12.138	0.61523	2.0404	0.2694-15.4506	0.48995
Unmarried or Domestic Partner	1.2492	0.8183-1.907	0.3026	1.2287	0.8011-1.8845	0.34534	1.3386	0.8582-2.088	0.19856	1.2886	0.8176-2.0309	0.27459

*P<0.05, **p<0.005, ***p<0.0005.

a potential prognostic factor. In addition, the pathological type of Hodgkin's lymphoma, surgery, and chemotherapy were significantly associated with OS. However, our results showed that radiotherapy was not significantly associated with OS.

Variables that were statistically significant in the univariate Cox analyses were then included in the multivariate Cox regression analysis. The data showed that age was an independent risk factor affecting the prognosis of patients, with patients 60 years or older having a poor prognosis. The pathology type of Hodgkin's lymphoma was also an independent factor affecting OS, with patients with Hodgkin's lymphoma having worse OS. Chemotherapy and surgery were independent prognostic factors, with the risk of death being 0.41 times higher for those who received chemotherapy than for those who did not, and 0.65 times higher for those who received surgery than for those who did not, suggesting that patients treated with chemotherapy and surgery had better OS. Cox regression analysis showed that the Ann Arbor stage was not a prognostic factor. This may be related to the distribution of the data, as lymphoma is an insidious malignancy with high heterogeneity, and all data were distributed closer to stages I and IV. Nonetheless, the Ann Arbor stage remains the preferred assessment criterion in clinical decision-making.

Meanwhile, CSS is one of the most important predictors of prognosis in patients with malignancy. The impact of the 10 aforementioned variables on CSS was further explored. In contrast to OS, the results of univariate Cox analysis showed that age did not have the potential to influence CSS. Sex and age were able to influence CSS, and the time to diagnosis was a potential predictor of CSS. As previously described, these statistically significant differences in the univariate analysis were further included in the multivariate Cox analysis, which showed that age and sex had a P value greater than 0.05 and failed to show independent predictive power. Like OS, surgery (P = 0.00633) and chemotherapy (P = 8.42e-12) remained highly significant independent prognostic factors. In summary, both statistically and in clinical practice, treatment significantly influenced the prognostic survival of patients, but statistical analysis showed that radiotherapy did not demonstrate superiority. Next, the KM method was used to calculate the probability of survival for OS (Figure 3) and CSS (Figure 4) in PIML, and all cohorts were categorized by variables, showing a significant correlation with prognosis.

Establishment and evaluation of prognostic nomogram

To assess the survival probability in individual patients, the nomogram models for predicting patients' OS and CSS were

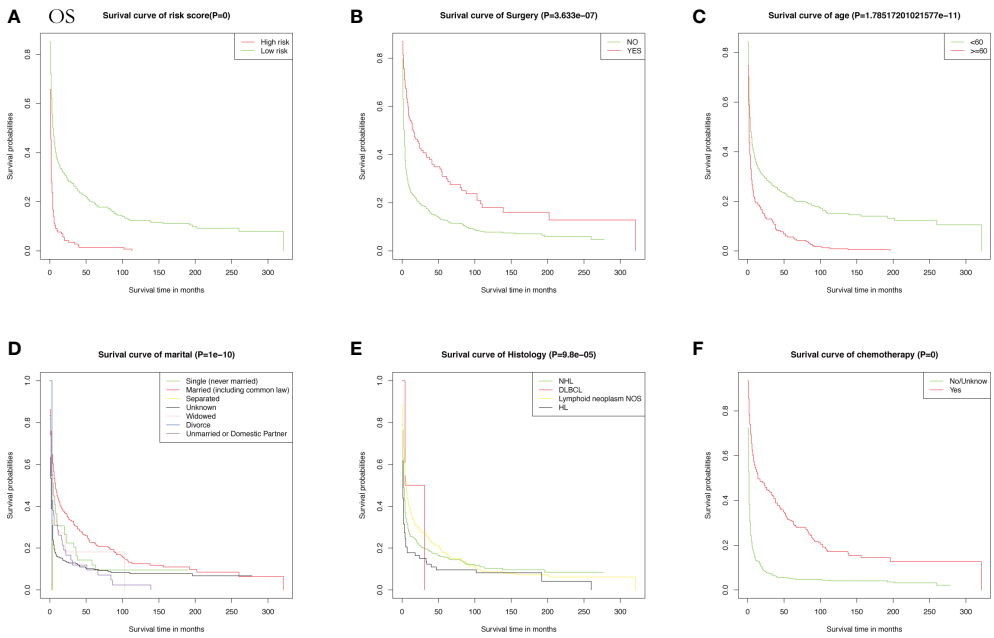

FIGURE 3
The Kaplan-Meier (KM) method was performed to calculate the OS classified by clinical pathologic factors for patients with PIML. The clinical pathologic factors including risk score **(A)**, Surgery **(B)**, Age **(C)**, Marital status **(D)**, Histology **(E)**, Chemotherapy **(F)**.

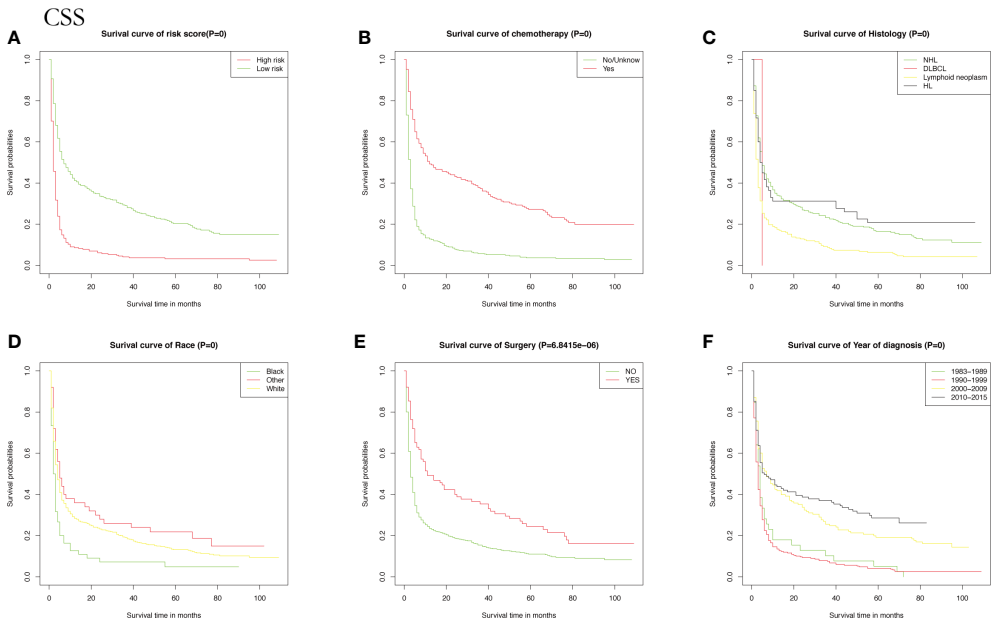

FIGURE 4
The Kaplan-Meier (KM) method was performed to calculate the CSS classified by clinical pathologic factors for patients with PIML. The clinical pathologic factors including risk score **(A)**, Chemotherapy **(B)**, Histology **(C)**, Race **(D)**, Surgery **(E)**, Year of diagnosis **(F)**.

developed in the development cohort. Factors of significant prognostic and clinical significance were screened using multivariate Cox regression analysis, including age, the type of pathology, treatment, and Ann Arbor staging (Figure 5). Detailed scores for each factor are shown in the nomogram, and by calculating these scores against the total score on the bottom axis, OS and CSS could be predicted at 1, 3, and 5 years. To verify the feasibility of these models, receiver-operating characteristic curves were used to assess the accuracy of the nomogram models. The AUC values for OS at 1, 3, and 5 years were 0.8, 0.818, and 0.81. In the development cohort (Figure 6), and the AUC values for CSS were 0.8, 0.799, and 0.798, respectively (Figure 7). These data demonstrated the predictive power of the nomogram based on the development cohort. Next, the effectiveness of the nomogram was validated in the verification cohort to further demonstrate its reliability, with AUC values of 0.8, 0.832, and 0.809 for OS (Figure 8) and 0.8, 0.845, and 0.788 for CSS (Figure 9) in the verification cohort at 1, 3, and 5 years, respectively, demonstrating the potential ability of the established nomogram to predict 1-, 3- and 5-year survival rates

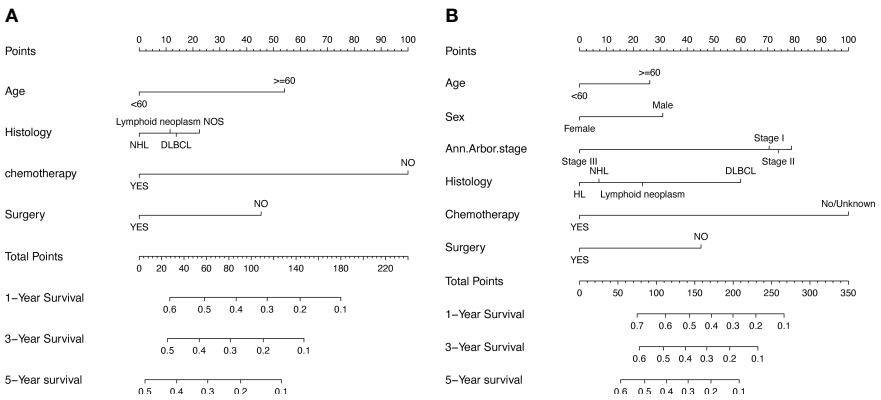

FIGURE 5
The prognostic nomogram models to predict 1-year, 3-year, and 5-year of OS and CSS for patients *via* development cohort **(A, B)**.

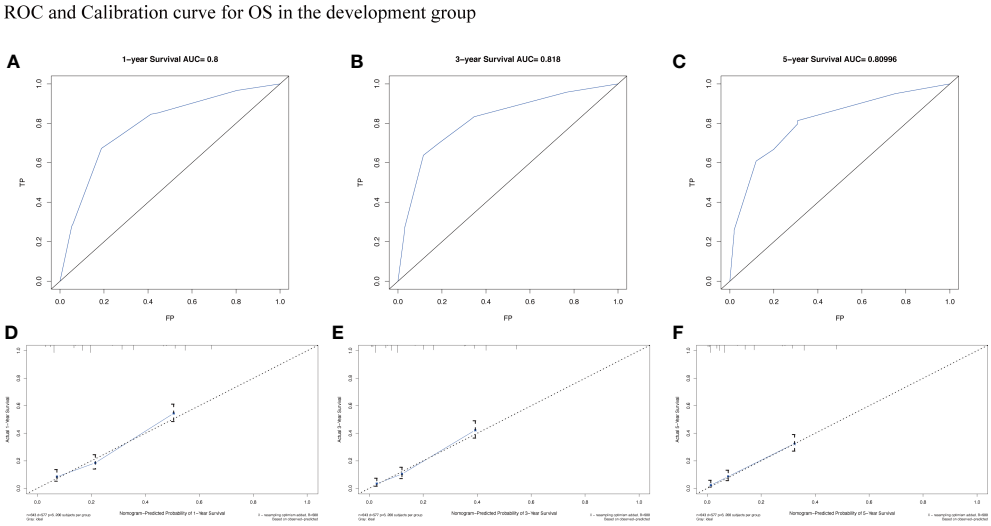

FIGURE 6
The AUC **(A-C)** and calibration curve **(D-F)** of 1-year, 3-year, and 5-year to assess the performance of predictive models for OS in the development group.

in patients with PIML (Figure 10). Analysis of the AUC and calibration curves in these validated cohorts showed consistent results in the development cohort, and these results confirmed the strong relevance and value of the multi-established nomogram in predicting the prognosis of patients with intracranial lymphoma in clinical practice. The model built by the nomogram was further subjected to DCA, a simple method for evaluating clinical prediction models. The data showed that the model built according to the nomogram yielded good benefits, allowing patients to achieve higher benefits for the same risk.

Next, risk scores for patients with intracranial lymphoma were quantified based on the patients' clinicopathological factors, age, sex, type of pathology, and treatment. To further illustrate whether risk scores could be considered independent prognostic factors, we determined the median risk score as a basis for classifying high-risk subgroups and low-risk wind

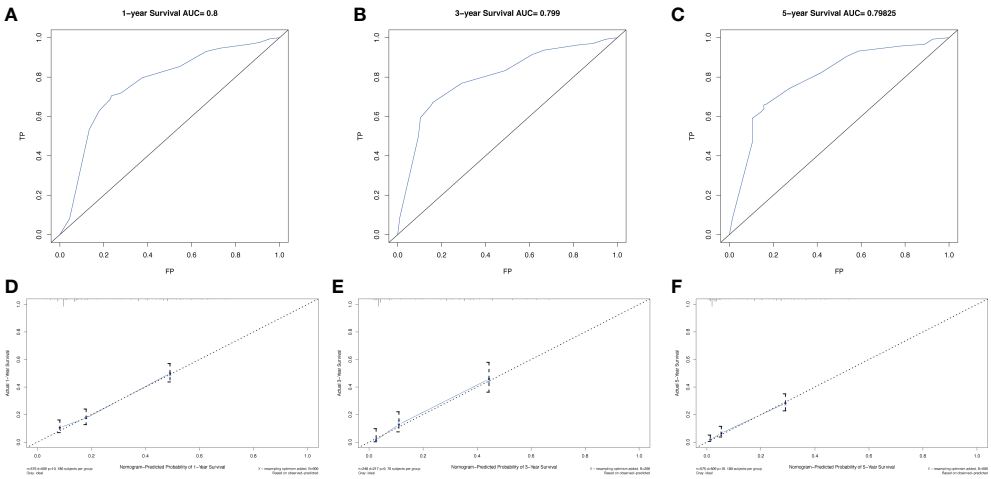

FIGURE 7
The AUC **(A-C)** and calibration curve **(D-F)** of 1-year, 3-year, and 5-year to assess the performance of predictive models for CSS in the development group.

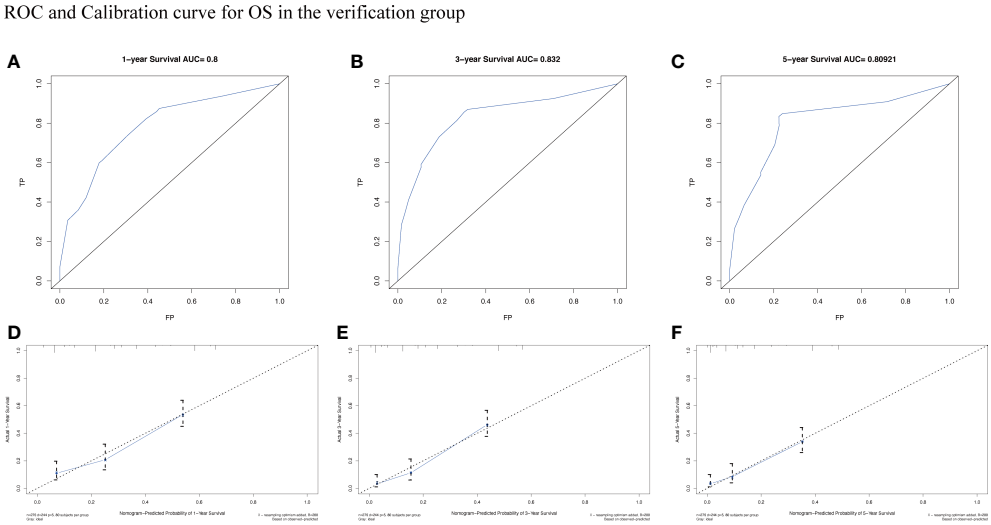

FIGURE 8
The AUC **(A-C)** and calibration curve **(D-F)** of 1-year, 3-year, and 5-year to assess the performance of predictive models for OS in the verification group.

resistance, with KM curves showing better survival rates in the low-risk group.

Discussion

To our knowledge, PIML is a relatively rare intracranial malignancy that accounts for approximately 1.5% of all primary intracranial tumors (16). PIML can initially present with optic nerve damage, increased intracranial pressure, a high degree of malignancy, a specific release site, and a poor prognosis (17). The prognosis of this rare type of lymphoma, in which non-Hodgkin's lymphoma is the main type, has improved over the last decade due to the use of high doses of methotrexate (18). However, the prognosis of PIML depends on several other factors, such as the time of diagnosis, histological and

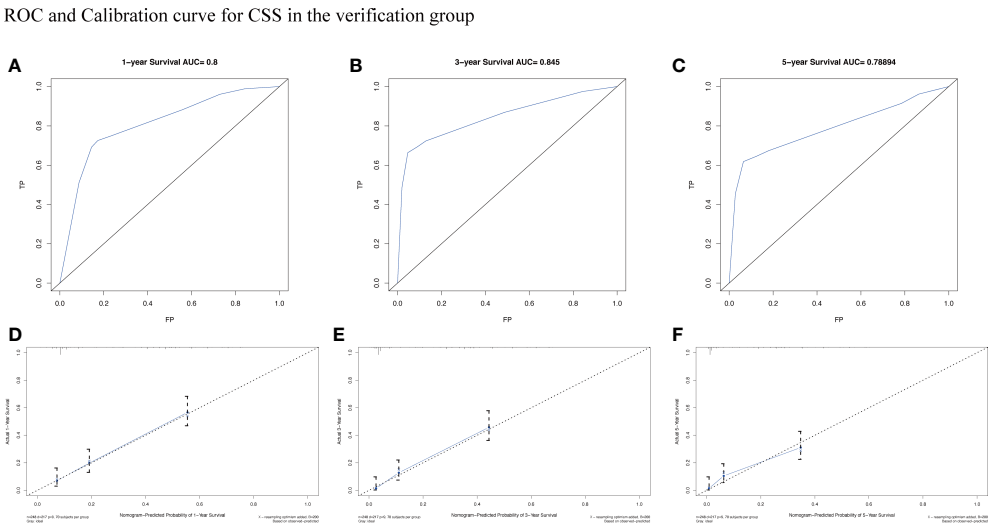

FIGURE 9
The AUC **(A-C)** and calibration curve **(D-F)** of 1-year, 3-year, and 5-year to assess the performance of predictive models for CSS in the verification group.

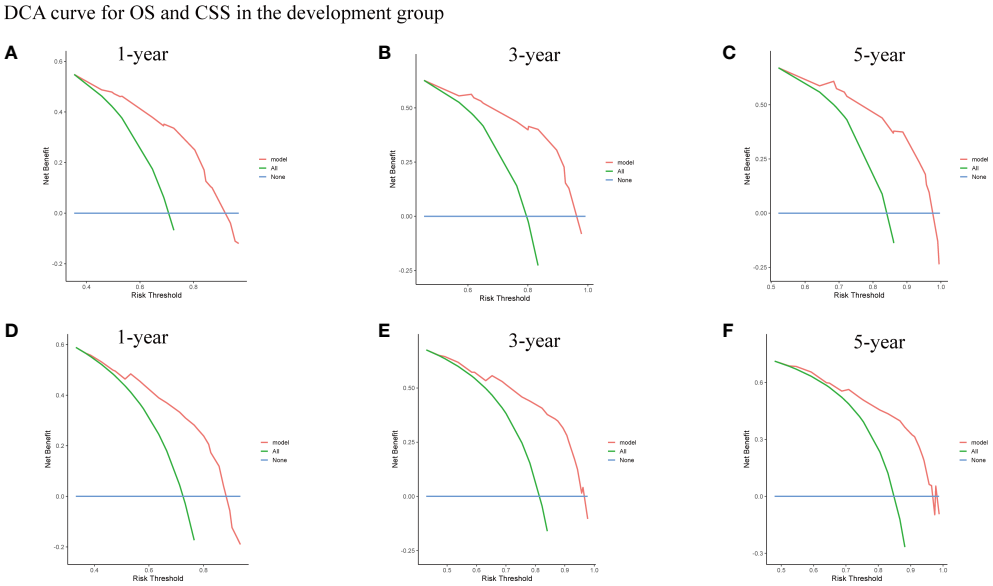

FIGURE 10
The DCA curve for OS **(A-C)** and CSS **(D-F)** of 1-year, 3-year, and 5-year in the development group.

biological characteristics of the tumor, and the appropriateness of the treatment (19). In conclusion, after more than a decade of development, the prognosis of PLML remains unsatisfactory (20). Routine physical examinations are unable to assess intracranial conditions, and most intracranial abnormalities detected on magnetic resonance imaging, as well as their specific anatomical location, prevent clinicians from obtaining a specifically determined (21). Therefore, there is a need to explore sensitive and specific tumor markers and diagnostic methods. Owing to the rarity of intracranial lymphoma, there are only a few related clinical studies (22). According to the literature, there are no randomized clinical trials for recurrent, refractory PIML, and no prognostic models for PIML have been developed (23). To better understand the clinical demographic characteristics and risk factors of PIML, we investigated the largest sample of data corresponding to patients with PIML retrieved from the SEER database, and these data were used to develop and validate prognostic OS and CSS nomograms for patients with PIML. These models can be applied in clinical practice to provide advice to physicians when making clinical decisions.

This study included 919 patients who were diagnosed with lymphoma between 1975 and 2019 with an intracranial primary site and documented survival time and clinical staging. Detailed data on demographic characteristics were obtained and statistically analyzed, with OS rates of 29.5%, 21.0%, and 16.1% at 1, 3, and 5 years, respectively, for the entire cohort. Univariate Cox regression analysis was performed to identify potential risk factors, and multivariate Cox regression analysis was performed to identify independent prognostic factors. The patients were categorized according to IPI staging using a cut-off of 60 years of age, with 62.3% of patients <60 years. Age was one of the most notable risk factors for prognosis in patients with PIML; patients >60 years had worse OS, although 60 years of age was statistically insignificant for CSS based on the results. In addition, there appeared to be no statistically significant difference in the effect of sex on intracranial lymphoma, with a potentially significant difference in incidence by sex. Meanwhile, the pathology was consistent with that of lymphoma, with diffuse large B-cell type remaining the most common type, whereas patients with a pathological type of Hodgkin's lymphoma had a worse prognosis, in line with the results of previous studies (24).

Ann Arbor staging was not significant based on the statistical analysis of this study. This may be strongly related to the distribution of data, with most patients (98.1%) having stages I and IV, which could have biased the results of the regression analysis. This reflects the following two extremes in the staging of patients with PIML: early onset of symptoms causing discomfort, leading to earlier medical intervention, or early onset of no obvious symptoms, and an advanced stage by the time of the first medical examination (25). However, the results of the statistical analysis do not negate the role of Ann Arbor staging in guiding clinical practice.

Meanwhile, treatment options are the most important factors affecting the prognosis of patients with PIML (26),and patients who have not undergone systemic treatment generally have a worse survival time. Management of patients with PIML

included surgical tumor resection (other than biopsy), chemotherapy and radiation therapy. This multimodal treatment, including chemotherapy and aggressive surgery can convey a survival advantage in patients with PIML (27).However, radiotherapy does not show a unique superiority over chemotherapy and surgery, contrary to our conventional understanding (28).Patients treated with chemotherapy and surgery generally have longer life expectancy (29). These data confirm the importance of chemotherapy in the treatment regimen for PIML. However, owing to the limitations of the database, it is not possible to obtain information on the specific options for treatment, including surgery, the drug regimens for chemotherapy, and the choice of dose and irradiation target area for radiotherapy, all of which largely influence the patient outcomes (30).

A nomogram to predict patient prognosis was further developed based on a risk-based coefficient. Given the importance of age for patient staging, we included age in the creation of the nomogram. Firstly, time-dependent receiver-operating characteristic curves indicated that the nomogram had high sensitivity and specificity. Second, the small deviation from the reference line demonstrated the high reliability of the established nomogram, and the DCA curve showed that the nomogram contributed to better clinical decision-making (31).

For lymphomas of the central nervous system, MRI (magnetic resonance imaging) is the diagnostic method of choice. The T2-weighted (T2W) signal usually indicates intracranial edema and lesions of vascular origin, while the T1-weighted (T1W) signal shows intracranial parenchymal lesions or occupancies (32). For patients with PIML, there is no substitute for MRI in assessing the anatomical localization of the tumor, tumor size, and edema of the brain parenchyma. Meanwhile, positron emission tomography combined with computed tomography (PET/CT) is increasingly being demonstrated in clinical trials as the center of gravity in the evaluation of lymphoma. Gradually, a diagnostic approach with MRI and PET/CT as the core has been developed. In particular, the sensitivity of PET/CT has increased dramatically in patients with lymphoma involving bone marrow involvement (33). However, a subset of lymphoma patients exhibits low ^{18}F fluorodeoxyglucose (FDG) avidity (34). Also, PET/CT based staging is prognostically instructive in most clinical explorations, suggesting that imaging can give direct evidence in tumor morphology, infiltration, and metastasis. These significantly influence the treatment choice and prognostic evaluation of patients.

The study tracked all records of PIML patients in the SEER database from 1979-2019, building a prognostic model over a forty-year cohort. This model is reliable in terms of sample size. And it can provide a basis for subsequent multicenter clinical studies or prospective studies. At the same time, imaging information was missing from the data we collected, and this absence is understandable. The first publication on ^{18}F FDG PET in lymphoma was in 2007 (32). Also, medical imaging system is evolving very rapidly, it is difficult to document with quantifiable information, and imaging changes in patients at different pathological stages are dynamic. Therefore, this study focuses more on quantifiable factors in the data and uses different factors: gender, age, stage, and type of pathology to build models that predict the prognosis of different patients. Most of these factors can be obtained in the admission records, which is faster and more specific. Also imaging evidence can be used as valid evidence of prognosis, which, together with the results of this study, allows a better management and assessment of the prognosis and treatment of patients. In other words, with our prognostic model as a basis, we can combine imageomics and molecular diagnostics to build a multimodal prognostic model (35). It is a big challenge that requires more clinical studies and further molecular research.

In summary, this study obtained comprehensive clinical data from the SEER database and assessed the actual situation of individual patients from different perspectives, using uniform criteria and methods. This allowed us to comprehensively analyze the clinicopathological features of intracranial lymphomas. However, this study had several limitations. First, the treatment-specific information in the cohort was not sufficiently comprehensive, which prevented us from further targeting the benefits of different treatment. Due to the limitations of the database, we do not have access to a definitive treatment plan, which is the factor that has the greatest impact on patient prognosis. This includes the surgical procedure, the size and extent of tumor resection, the management of metastases including lymph nodes, and postoperative management. This information can be more specific and refined for assessing the prognosis of patients. At the same time, more large multicenter clinical trials are needed to explore the details of these treatment factors, which have positive implications for improving the prognosis of patients with intracranial lymphoma. Second, the SEER database contains qualitative or semi-quantitative data, and the statistical reliability was, to some extent, impaired. Finally, the nature of retrospective studies inevitably results in bias (36). Although our findings and new models require further in-depth studies, our results can provide new insights for treating patients with PIML and can assist oncology hematologists.

Conclusion

We constructed a new nomogram to predict OS and CSS in patients with PIML. In addition, we found that age, surgery, chemotherapy, Ann Arbor staging, and histological type are independent risk factors for PIML. The identification of risk factors and construction of nomograms can provide new insights for patients with PIML and oncology hematologists, allowing doctors to make better choices during clinical decision-making.

Data availability statement

The original contributions presented in the study are included in the article/supplementary material. Further inquiries can be directed to the corresponding author.

Author contributions

ZY and FP had the idea and wrote the main manuscript texts. CF ,ZL and YZ performed the literature search and data analysis. YL, YD, and NL drafted and critically revised the work. All authors contributed to the article and approved the submitted version.

Funding

This work was supported by National Natural Science Foundation of China (82270633, 81602527), and Natural Science Foundation of Hunan Province, China (2020JJ5949).

Acknowledgments

We thank all the staff members of SEER database for their hard work.

Conflict of interest

The authors declare that the research was conducted in the absence of any commercial or financial relationships that could be construed as a potential conflict of interest.

Publisher's note

References

1. Ouyang T, Wang L, Zhang N, Zhang Z, Xiong Y, Li M, et al. Clinical characteristics, surgical outcomes, and prognostic factors of intracranial primary central nervous system lymphoma. *World Neurosurg* (2020) 139:e508–e16. doi: 10.1016/j.wneu.2020.04.049

2. Bhagavathi S, Wilson JD. Primary central nervous system lymphoma. *Arch Pathol Lab Med* (2008) 132(11):1830–4. doi: 10.5858/132.11.1830

3. Hochberg FH, Miller DC. Primary central nervous system lymphoma. *J Neurosurg* (1988) 68(6):835–53. doi: 10.3171/jns.1988.68.6.0835

4. Jiddane M, Nicoli F, Diaz P, Bergvall U, Vincentelli F, Hassoun J, et al. Intracranial malignant lymphoma. report of 30 cases and review of the literature. *J Neurosurg* (1986) 65(5):592–9. doi: 10.3171/jns.1986.65.5.0592

5. Kamihara J, Bourdeaut F, Foulkes WD, Molenaar JJ, Mossé YP, Nakagawara A, et al. Retinoblastoma and neuroblastoma predisposition and surveillance. *Clin Cancer Res* (2017) 23(13):e98–e106. doi: 10.1158/1078-0432.CCR-17-0652

6. Franchino F, Rudà R, Soffietti R. Mechanisms and therapy for cancer metastasis to the brain. *Front Oncol* (2018) 8:161. doi: 10.3389/fonc.2018.00161

7. Naiman JL, Rupprecht LM, Tanyeri G, Philippidis P. Intrathecal methotrexate. *Lancet.* (1970) 1(7646):571. doi: 10.1016/s0140-6736(70)90812-3

8. Grommes C, DeAngelis LM. Primary CNS lymphoma. *J Clin Oncol* (2017) 35 (21):2410–8. doi: 10.1200/JCO.2017.72.7602

9. Doll KM, Rademaker A, Sosa JA. Practical guide to surgical data sets: Surveillance, epidemiology, and end results (SEER) database. *JAMA Surg* (2018) 153(6):588–9. doi: 10.1001/jamasurg.2018.0501

10. Duggan MA, Anderson WF, Altekruse S, Penberthy L, Sherman ME. The surveillance, epidemiology, and end results (SEER) program and pathology: Toward strengthening the critical relationship. *Am J Surg Pathol* (2016) 40(12): e94–e102. doi: 10.1097/PAS.0000000000000749

11. Verbakel JY, Steyerberg EW, Uno H, De Cock B, Wynants L, Collins GS, et al. Erratum to "ROC curves for clinical prediction models part 1. ROC plots showed no added value above the AUC when evaluating the performance of clinical prediction models" [J clin epidemiol. 126C(2020):207-16]. *J Clin Epidemiol.* (2021) 130:171–3. doi: 10.1016/j.jclinepi.2020.11.013

12. Janssens A, Martens FK. Reflection on modern methods: Revisiting the area under the ROC curve. *Int J Epidemiol.* (2020) 49(4):1397–403. doi: 10.1093/ije/dyz274

13. Van Calster B, Wynants L, Verbeek JFM, Verbakel JY, Christodoulou E, Vickers AJ, et al. Reporting and interpreting decision curve analysis: A guide for investigators. *Eur Urol.* (2018) 74(6):796–804. doi: 10.1016/j.eururo.2018.08.038

14. Ruppert AS, Dixon JG, Salles G, Wall A, Cunningham D, Poeschel V, et al. International prognostic indices in diffuse large b-cell lymphoma: A comparison of IPI, r-IPI, and NCCN-IPI. *Blood.* (2020) 135(23):2041–8. doi: 10.1182/blood.2019002729

15. Sukswai N, Lyapichev K, Khoury JD, Medeiros LJ. Diffuse large b-cell lymphoma variants: An update. *Pathology.* (2020) 52(1):53–67. doi: 10.1016/j.pathol.2019.08.013

16. Svendsen FH, Heegaard S. Lymphoma of the eyelid. *Surv Ophthalmol* (2017) 62(3):312–31. doi: 10.1016/j.survophthal.2016.11.009

17. Dermarkarian CR, Kini AT, Al Othman BA, Lee AG. Neuro-ophthalmic manifestations of intracranial malignancies. *J Neuroophthalmol.* (2020) 40(3):e31–48. doi: 10.1097/WNO.0000000000000950

18. Ferry JA. Scientific advances and the evolution of diagnosis, subclassification and treatment of lymphoma. *Arch Med Res* (2020) 51(8):749–64. doi: 10.1016/j.arcmed.2020.05.022

19. Ansell SM. Non-Hodgkin lymphoma: Diagnosis and treatment. *Mayo Clin Proc* (2015) 90(8):1152–63. doi: 10.1016/j.mayocp.2015.04.025

20. Shankland KR, Armitage JO, Hancock BW. Non-Hodgkin lymphoma. *Lancet* (2012) 380(9844):848–57. doi: 10.1016/S0140-6736(12)60605-9

21. Slone HW, Blake JJ, Shah R, Guttikonda S, Bourekas EC. CT and MRI findings of intracranial lymphoma. *AJR Am J Roentgenol.* (2005) 184(5):1679–85. doi: 10.2214/ajr.184.5.01841679

22. Jahr G, Broi MD, Holte HJr., Beiske K, Meling TR. Evaluation of memorial Sloan-Kettering cancer center and international extranodal lymphoma study group prognostic scoring systems to predict overall survival in intracranial primary CNS lymphoma. *Brain Behav* (2018) 8(3):e00928. doi: 10.1002/brb3.928

23. Karls S, Shah H, Jacene H. PET/CT for lymphoma post-therapy response assessment in other lymphomas, response assessment for autologous stem cell transplant, and lymphoma follow-up. *Semin Nucl Med* (2018) 48(1):37–49. doi: 10.1053/j.semnuclmed.2017.09.004

24. Ansell SM. Hodgkin Lymphoma: Diagnosis and treatment. *Mayo Clin Proc* (2015) 90(11):1574–83. doi: 10.1016/j.mayocp.2015.07.005

25. Algazi AP, Kadoch C, Rubenstein JL. Biology and treatment of primary central nervous system lymphoma. *Neurotherapeutics.* (2009) 6(3):587–97. doi: 10.1016/j.nurt.2009.04.013

26. Ansell SM. Hodgkin Lymphoma: A 2020 update on diagnosis, risk-stratification, and management. *Am J Hematol* (2020) 95(8):978–89. doi: 10.1002/ajh.25856

27. Karschnia P, Batchelor TT, Jordan JT, Shaw B, Winter SF, Barbiero FJ, et al. Primary dural lymphomas: Clinical presentation, management, and outcome. *Cancer.* (2020) 126(12):2811–20. doi: 10.1002/cncr.32834

28. Hoskin P, Popova B, Schofield O, Brammer C, Robinson M, Brunt AM, et al. 4 gy versus 24 gy radiotherapy for follicular and marginal zone lymphoma (FoRT): Long-term follow-up of a multicentre, randomised, phase 3, non-inferiority trial. *Lancet Oncol* (2021) 22(3):332–40. doi: 10.1016/S1470-2045(20)30686-0

29. Bataille B, Delwail V, Menet E, Vandermarcq P, Ingrand P, Wager M, et al. Primary intracerebral malignant lymphoma: Report of 248 cases. *J Neurosurg* (2000) 92(2):261–6. doi: 10.3171/jns.2000.92.2.0261

30. Zain JM. Aggressive T-cell lymphomas: 2019 updates on diagnosis, risk stratification, and management. *Am J Hematol* (2019) 94(8):929–46. doi: 10.1002/ajh.25513

31. Vickers AJ, Holland F. Decision curve analysis to evaluate the clinical benefit of prediction models. *Spine J* (2021) 21(10):1643–8. doi: 10.1016/j.spinee.2021.02.024

32. Barrington SF, Mikhaeel NG, Kostakoglu L, Meignan M, Hutchings M, Mueller SP, et al. Role of imaging in the staging and response assessment of lymphoma: consensus of the international conference on malignant lymphomas imaging working group. *J Clin Oncol* (2014) 32(27):3048–58. doi: 10.1200/JCO.2013.53.5229

33. El-Galaly TC, Villa D, Gormsen LC, Baech J, Lo A, Cheah CY. FDG-PET/CT in the management of lymphomas: current status and future directions. *J Intern Med* (2018) 284(4):358–76. doi: 10.1111/joim.12813

34. Cerci JJ, Pracchia LF, Linardi CC, Pitella FA, Delbeke D, Izaki M, et al. 18F-FDG PET after 2 cycles of ABVD predicts event-free survival in early and advanced Hodgkin lymphoma. *J Nucl Med* (2010) 51(9):1337–43. doi: 10.2967/jnumed.109.073197

35. Lee SY, Jeon SI, Jung S, Chung IJ, Ahn CH. Targeted multimodal imaging modalities. *Adv Drug Delivery Rev* (2014) 76:60–78. doi: 10.1016/j.addr.2014.07.009

36. Yang M, Li Z, Dou D. Can retrospective studies confirm causes of drug-induced liver injury? *Gastroenterology* (2019) 157(5):1436–7. doi: 10.1053/j.gastro.2019.03.078

frontiers | Frontiers in Oncology

TYPE Review
PUBLISHED 13 January 2023
DOI 10.3389/fonc.2022.1084404

OPEN ACCESS

EDITED BY
Ignazio Gaspare Vetrano,
IRCCS Carlo Besta Neurological Institute Foundation, Italy

REVIEWED BY
Andrea Saladino,
IRCCS Carlo Besta Neurological Institute Foundation, Italy
Mervyn Lim,
National University Hospital, Singapore

*CORRESPONDENCE
Georges N Abi Lahoud
icvns@clinique-bizet.com

†These authors have contributed equally to this work

SPECIALTY SECTION
This article was submitted to Neuro-Oncology and Neurosurgical Oncology, a section of the journal Frontiers in Oncology

RECEIVED 30 October 2022
ACCEPTED 22 December 2022
PUBLISHED 13 January 2023

CITATION
Serratrice N, Lameche I, Attieh C, Chalah MA, Faddoul J, Tarabay B, Bou-Nassif R, Ali Y, Mattar JG, Nataf F, Ayache SS and Abi Lahoud GN (2023) Spinal meningiomas, from biology to management - A literature review. *Front. Oncol.* 12:1084404. doi: 10.3389/fonc.2022.1084404

Spinal meningiomas, from biology to management - A literature review

Nicolas Serratrice[1], Imène Lameche[1], Christian Attieh[1], Moussa A Chalah[1,2,3], Joe Faddoul[1,4], Bilal Tarabay[1], Rabih Bou-Nassif[5], Youssef Ali[6], Joseph G Mattar[1], François Nataf[7], Samar S Ayache[1,2,3,8†] and Georges N Abi Lahoud[1,3†*]

[1]Institut de la Colonne Vertébrale et des Neurosciences (ICVNS), Centre Médico-Chirurgical Bizet, Paris, France, [2]EA 4391, Excitabilité Nerveuse et Thérapeutique, Faculté de Santé, Université Paris Est, Créteil, France, [3]Gilbert and Rose-Marie Chagoury School of Medicine, Lebanese American University, Byblos, Lebanon, [4]Service de Neurochirurgie, Centre Hospitalier de la Côte Basque, Bayonne, France, [5]Department of Neurosurgery, Memorial Sloan Kettering Cancer Center, New York, NY, United States, [6]Institut de Chirurgie Osseuse et de Neurochirurgie, Médipole-Montagard, Avignon, France, [7]Service de Neurochirurgie, Hôpital Lariboisière, Paris, France, [8]Service de Physiologie-Explorations Fonctionnelles, DMU FIxIT, Hôpital Henri Mondor, Créteil, France

Meningiomas arise from arachnoidal cap cells of the meninges, constituting the most common type of central nervous system tumors, and are considered benign tumors in most cases. Their incidence increases with age, and they mainly affect females, constituting 25-46% of primary spinal tumors. Spinal meningiomas could be detected incidentally or be unraveled by various neurological symptoms (*e.g.*, back pain, sphincter dysfunction, sensorimotor deficits). The gold standard diagnostic modality for spinal meningiomas is Magnetic resonance imaging (MRI) which permits their classification into four categories based on their radiological appearance. According to the World Health Organization (WHO) classification, the majority of spinal meningiomas are grade 1. Nevertheless, they can be of higher grade (grades 2 and 3) with atypical or malignant histology and a more aggressive course. To date, surgery is the best treatment where the big majority of meningiomas can be cured.

Abbreviations: AKT1, alpha serine/threonine-protein kinase 1; ALPL, alkaline phosphatase; AR, androgen receptors; CCA, chlormadinone acetate; CDKN2A, cyclin-dependent kinase inhibitor 2A; CNS, central nervous system; CPA, cyproterone acetate; CSF, cerebrospinal fluid; *e.g.*, *exempli gratia*; EMM, extracranial meningioma metastases; ER, estrogen receptor; GTR, gross total resection; HRT, hormonal replacement therapy; *i.e.*, *id est*; IMRT, image-modulated radiation therapy; KLF4, Kruppel like factor 4; LATS1, large tumor suppressor kinase 1; MEP, motor evoked potentials; MIS, minimally invasive surgery; MMP9, matrix metallopeptidase 9; MRI, magnetic resonance imaging; NF2, neurofibromatosis type 2; PCNA, proliferating cell nuclear antigen; PI3K, phosphoinositide 3-kinases; SBRT, stereotactic body radiation therapy; SEP, somatosensory evoked potentials; SMARCB1, SWI/SNF related, matrix associated, actin dependent regulator of chromatin, subfamily B, member 1; SMARCE1, SWI/SNF related, matrix associated, actin dependent regulator of chromatin, subfamily E, member 1; SMO, smoothened; T1-WI, T1-weighted images; T2-WI, T2-weighted images; TRAF7, TNF receptor-associated factor 7; *vs.*, *versus*; WHO, World Health Organization.

Advances in surgical techniques (ultrasonic dissection, microsurgery, intraoperative monitoring) increase the complete resection rate. Operated patients have a satisfactory prognosis, even in those with poor preoperative neurological status. Adjuvant therapy has a growing role in treating spinal meningiomas, mainly in the case of subtotal resection and tumor recurrence. The current paper reviews the fundamental epidemiological and clinical aspects of spinal meningiomas, their histological and genetic characteristics, and their management, including the various surgical novelties and techniques.

KEYWORDS

gross total resection (GTR), meningiomas, spinal meningiomas, stereotactic body radiation therapy (SBRT), minimally invasive (MIS), microsurgery (MS), ultrasonic dissection, central nervous system

Introduction

Meningiomas are lesions that arise from arachnoidal cap cells, the outer part of the arachnoid layer and villi (1). They usually form dural attachments and are marked by meningothelial hyperplasia (1).

Spinal meningiomas are relatively rare, accounting for approximately 3% of all meningiomas of the central nervous system (CNS) (2) and 25-46% of all primary intraspinal neoplasms (2, 3). 90% of intradural extramedullary spinal tumors are either meningiomas or schwannomas and constitute nearly 25% of primary spinal neoplasia (3).

Spinal meningiomas mainly affect people in their fifth decade of life and are more frequent in women (given their estrogen receptors) (4). In case they occur in young patients, or if they cause multiple lesions, a genetic disorder like neurofibromatosis type 2 (NF2) or aggressive histological subtypes should be suspected (2, 4). Spinal meningiomas most commonly occur in the posterior, posterolateral, or lateral thoracic region, followed by the anterior cervical and lumbosacral regions. The main treatment is surgery, which can be performed in (a) a classical open microsurgical approach in the vast majority of cases, (b) a minimally invasive surgery (MIS), or (c) through an endoscopic intervention (5). The choice of the most appropriate surgical method could be challenging, especially in the case of aggressive meningiomas and in some difficult access tumors (*e.g.*, location anterior to the spinal cord in the thoracic region). For instance, ventral/ventrolateral cervical meningiomas within the upper cervical region, may envelop the vertebral artery (6), and thus require precise presurgical calculations to adopt the safest approach.

The scientific knowledge regarding spinal meningiomas has evolved over the past twenty years. This evolution concerns multiple aspects, including clinical evaluation, molecular and radiological specificities, and microsurgical management techniques. Therefore, the main goal of this paper is to come up with an updated review of spinal meningiomas, with a particular focus on their clinical presentation, biological and imaging aspects, and neurosurgical strategies.

Selection criteria

A review of the literature was carried out using PubMed/Medline and Scopus databases. The following keywords were used: "spinal meningioma" AND ("biology" OR "molecular" OR "genetic" OR "endocrine" OR "imaging" OR "grading" OR "prognosis" OR "surgery" OR "resection" OR "intraoperative monitoring" OR "adjuvant therapy" OR "recurrence" OR "psychology" OR "anxiety" AND "depression"). Original papers published in English and French were included in the analysis. The references of the selected papers were manually scanned in order to identify any additional references. To note, papers on intracranial meningiomas were also scanned and relevant papers were included since some research on spinal meningiomas stem from studies carried out on intracranial meningiomas.

Clinical features

Spinal meningiomas are typically solitary, well-circumcised, slow-growing, intradural extramedullary tumors (Figure 1) (7) that usually respect the surrounding normal tissue (1). Hence, they are often perceived as noninvasive. However, they could be aggressive in some cases by seeding other parts of the CNS or the surgical site.

As stated above, meningiomas are more frequently seen at the thoracic level and tend to expand slowly without any clinical

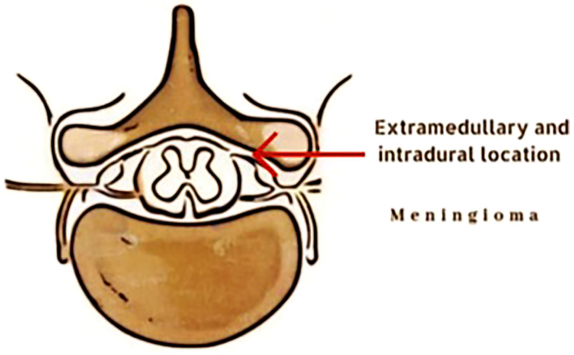

FIGURE 1
Illustration of extramedullary and intradural location of a spinal meningioma.

manifestation initially. Around 9% of cases are asymptomatic and report no complaints (8). At an advanced stage, meningiomas compromise spinal elements, resulting in various neurological symptoms and signs, such as pain, motor, and sensory disturbances, gait abnormality, and sphincter dysfunction. Complaints can vary from one person to another depending on the size of the meningioma and the exact site of the spinal compression (8). Clinical manifestations depend also on the initial size of the spinal canal as large constitutional ones can tolerate the development of large sized tumors while remaining asymptomatic.

The most frequent presentation is pain, ranging from 42% in some case series to as high as 87% in other reports (8, 9). Pain is more frequently described as local or radicular. Apart from pain, patients often report sensory and motor symptoms. Sensory manifestations can have many aspects, such as aching, burning, tingling, numbness, hypoesthesia, paresthesia, and anesthesia. These symptoms can be present in 16% to 84% of cases (4, 10). However, the most alarming sign for patients is motor deficit. It can start as a slight weakness and evolves later into a complete motor deficit. Motor symptoms are present in 33% to 93% of patients with spinal meningiomas (2, 4). Moreover, some patients could complain of gait and balance disturbances in 47% to 93% of cases (8, 11). Finally, sphincter dysfunction is reported in some series but less frequently than other symptoms. Sphincter dysfunction can be seen in 6 to 60% of patients seeking medical opinion (8, 11). A summary of the clinical manifestations is depicted in Table 1.

Pathology

Many histological subtypes of meningiomas have been described, among which meningothelial, fibroblastic, and transitional meningiomas are the most frequent ones. The histological analysis of meningiomas defines the histological type and grade of the tumor according to the 2021 World Health Organization (WHO) classification, as illustrated in Figure 2 (16). It classifies meningiomas into three grades, where each grade correlates with different potential for growth, metastatic spread, recurrence, and prognosis.

Many histologic subtypes are observed in both intracranial and spinal meningiomas. Meningothelial, metaplastic, psammomatous, transitional, atypical, and clear cell subtypes are the most common subtypes of intracranial meningiomas. As for spinal meningiomas, the psammomatous, meningothelial and transitional subtypes distinguish them, and they have a lower risk of recurrence than the intracranial ones for reasons yet to be determined.

The WHO divides meningiomas into three grades from 1 to 3 (benign, atypical and malignant, respectively) based on their malignancy degree (17). In the case of "mixed" tumors, the diagnosis of the dominant histological type (*i.e.*, the type forming more than 50% of the tumor) is retained. However, the presence of a minority contingent with more aggressive potential should be reported.

Genetic alterations

Advances in molecular biology have greatly improved the understanding of the various mechanisms at the origin of meningiomas development. Molecular profiles of spinal meningiomas are similar to their intracranial counterparts (18). These alterations account for 3% of reported cases only. Chromosomal instability is a widespread molecular alteration that characterizes recurrent or poor prognosis meningiomas. Accumulation of cytogenetic aberrations is associated with higher-grade meningiomas and a higher risk of recurrence, which explains why high-grade meningiomas have more altered cytogenetic profiles than benign meningiomas (19). Table 2 summarizes the different gene mutations implicated in meningiomas and their prognosis.

Among the multiple mechanisms of oncogenesis, the increased cell proliferation was considered as the most important one. In brain tumors, the typical immunohistochemically marker Ki-67/MIB-1 for cell proliferation is more predictive of survival than the expression of proliferating cell nuclear antigens p53 and PCNA. In meningiomas, a high expression level of Ki-67 is directly associated with significant worse prognostic, especially with Ki-67 index higher than 4% (24). A close follow-up is recommended in this population.

Chromosomal abnormalities

Among the chromosomal abnormalities found to be related to spinal meningiomas, chromosomal 22q deletion seems to be

TABLE 1 Summary of clinical manifestations in spinal meningiomas.

Authors	Patients	Meningiomas location	Symptoms/Signs
Levy et al., 1982 (12)	n=97 (mean age 53, 80% females)	Cervical (n=17) Thoracic (n=73) Lumbar (n=7)	Back and/or limb pain 72% Motor deficit 66% Sensory symptoms +/- signs 32% Bowel and/or bladder dysfunction 40% Gait disturbances NP
Solero et al., 1989 (13)	n=174 (mean age 56, 82% females)	Cervical (n=26) Thoracic (n=144) Lumbar (n=4)	Back and/or limb pain 53% Motor deficit 93% Sensory symptoms +/- Signs 61% Bowel and/or bladder dysfunction 50% Gait disturbances NP
Gezen et al., 2000 (14)	n=36 (mean age 49, 75% females)	Cervical (n=8) Thoracic (n=20) Lumbar (n=8)	Back and/or limb pain 83% Motor deficit 83% Sensory symptoms +/- signs 50% Bowel and/or bladder dysfunction 36% Gait disturbances NP
Cohen-Gadol et al., 2003 (15)	n=40 (mean age 34.5, 87.5% females)	Cervical (n=16) Thoracic (n=23) Lumbar (n=2)	Back and/or limb pain 45% Motor deficit 40% Sensory symptoms +/- signs 80% Bowel and/or bladder dysfunction 40% and 13% respectively Gait disturbances 68%
Cohen-Gadol et al., 2003 (15)	n=40 (mean age 67.1, 82.5% female)	Cervical (n=8) Thoracic (n=32) Lumbar (n=0)	Sensory symptoms +/- signs 87% Bowel and/or bladder dysfunction 40% and 8% respectively Gait disturbances 80%
Sandalcioglu et al., 2008 (4)	n=131 (mean age 69, 87% females)	Cervical (n=21) Cervicothoracic (n=7) Thoracic (n=95) Thoracolumbar (n=6) Lumbar (n=2)	Back and/or limb pain 47% Motor deficit and sensory symptoms +/- signs 84% Gait disturbances 83%
Engelhard et al., 2010 (8)	n=430 (mean age 49.3, 56.7% females)		Back and/or limb pain 42% Motor deficit 64% Sensory symptoms +/- signs 50% Bowel and/or bladder dysfunction 16% and 6% respectively Gait disturbances 47%
Postalci et al., 2011 (9)	n=46 (mean age 52, 72% females)	Cervical (n=4) Thoracic (n=39) Lumbar (n=3)	Back and/or limb pain 87% Motor deficit 78% Bowel and/or bladder dysfunction 9% Asymptomatic 9% Gait disturbances NP
Riad et al., 2013 (11)	n=15 (mean age 67.6, 86.7% females)	Cervical (n=2) Thoracic (n=11) Lumbar (n=2)	Back and/or limb pain 60% Motor deficit 80% Sensory symptoms +/- signs 80% Bowel and/or bladder dysfunction 60% Gait disturbances 93%
Zhang et al., 2020 (10)	n=84 (mean age NP, 63.1% females)	Cervical (n=10) Cervicothoracic (n=1) Thoracic (n=4) Thoracolumbar (n=13) Lumbar (n=56)	Back and/or limb pain 75% Motor deficit 33% Sensory symptoms +/- signs 16% Bowel and/or bladder dysfunction 11% Gait disturbances NP

N, number; NP, Not Provided; age is expressed in years.

the most important one (25). In addition, one study on sixteen patients with spinal meningiomas showed an allelic loss of the 1p chromosomal arm - involving several genes such as the ALPL (Alkaline phosphatase) gene - and a homozygous loss of 9p that results in inactivation of tumor suppressor genes such as the CDKN2A (Cyclin-dependent kinase inhibitor 2A) (19, 21). Other chromosomal abnormalities have also been described, such as the loss of 10q and the gain of 5p and 17q (26).

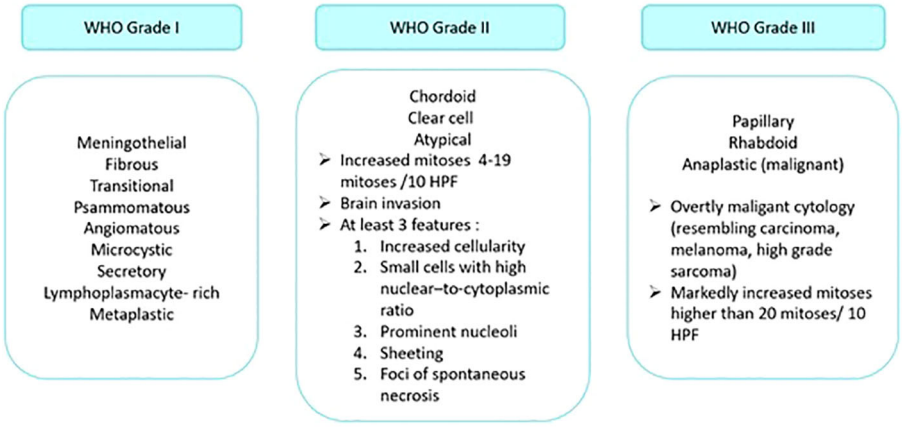

FIGURE 2
Grading of meningiomas according to the 2021 WHO classification system. HPF: high power field.

NF2-mutated meningiomas

In Schwann cells, the NF2 gene on chromosome 22q12.2 leads to the production of merlin, a protein also known as schwannomine, that provides myelin insulation for nerves. Merlin is also involved in the regulation of several key signaling pathways implied in cytoskeletal remodeling and cell motility. In addition, this protein is a tumor suppressor that

TABLE 2 Main molecular alteration and their prognosis in meningiomas.

Authors	Genes	Products	Gene alterations	Prognosis
Mota et al., 2020 (20)	NF2	Merlin	Downregulation Several mutations	Early event in tumorigenesis
Weber et al., 1997 (19), Goutagny et al., 2010(21)	CDKN2A/ p14ARF	P14	Downregulation Hypermethylation	Associated with high-grade tumors
Weber et al., 1997 (19), Goutagny et al., 2010(21)	ALPL	Alkaline phosphatase	Downregulation	Associated with high-grade tumors and recurrence
Lee & Lee, 2020 (22)	PI3K	Catalytic subunit of kinase, PI3K	Upregulation	Associated with tumorigenesis of non-NF2 meningiomas
Lee & Lee, 2020 (22)	AKT1	Serine/threonine-protein kinase	Upregulation E17K mutation	Associated with tumorigenesis of non-NF2 meningiomas
Lee & Lee, 2020 (22)	TRAF7	TNF receptor-associated factor 7	Several mutations	Associated with tumorigenesis of non-NF2 meningiomas
Lee & Lee, 2020 (22)	KLF4	Kruppel-like factor 4	Upregulation K409Q mutation	Associated with tumorigenesis of non-NF2 and secretory meningiomas
Lee & Lee, 2020 (22)	SMO	Smoothened, G protein-coupled receptor	Upregulation Several mutations	Associated with tumorigenesis of non-NF2 meningiomas
Tauziede-Espariat et al., 2018 (15)	SMARCE1	Subunit of the SWI/SNF complex	Downregulation Several mutations	Associated with high-grade tumors
Tauziede-Espariat et al., 2018 (15)	SMARCB1	Subunit of the SWI/SNF complex	Several mutations	Associated with high-grade tumors
Barresi et al., 2012 (23)	MMP9	Matrix metalloproteinase-9	Upregulation	Associated with tumorigenesis and edema

AKT1, Alpha serine/threonine-protein kinase 1; ALPL, Alkaline phosphatase; CDKN2A, Cyclin-dependent kinase inhibitor 2A; KLF4, Kruppel-like factor 4; MMP9, Matrix metallopeptidase 9; NF2, Neurofibromatosis type 2; PI3K, Phosphoinositide 3-kinases; SNF, Sucrose Non-Fermentable; SWI, SWItch; SMARCB1, SWI/SNF related, matrix associated, actin dependent regulator of chromatin, subfamily B, member 1; SMARCE1, SWI/SNF related, matrix associated, actin dependent regulator of chromatin, subfamily E, member 1; SMO, Smoothened; TNF, Tumor necrosis factor; TRAF7, TNF receptor-associated factor 7.

prevents cell proliferation (20). The loss of merlin expression is characteristic of all NF2-associated meningiomas and nearly half of sporadic cases. Mutations in the NF2 gene produce an abnormally shortened protein altering its functional condition (20). NF2 mutation is also known to activate several oncogenic signaling pathways such as PI3K/AKT1 (20).

NF2-non-mutated meningiomas

Approximately 40% of sporadic meningiomas are independent of NF2 inactivation and are linked to other mutations discovered in high-throughput sequencing studies of large cohorts of meningiomas (27). For grade I meningiomas, mutations in AKT1 (v-akt murine thymoma viral oncogene homolog 1, leading to activation of the PI3K pathway), TRAF7 (Tumor necrosis factor receptor-associated factor 7, encoding the pro-apoptotic E3 ubiquitin ligase), KLF4 (Krupple-like factor 4, a pluripotency-inducing transcription factor) and SMO (Smoothened, frizzled family receptor, leading to activation of the Hedgehog pathway) have been identified and appear to be mutually exclusive of NF2 alterations (22). In addition, mutations in the SMARCE1 gene (SWI/SNF related, matrix associated, actin dependent regulator of chromatin, subfamily E, member 1) have been reported in clear cell meningioma, and mutations in the SMARCB1 gene (SWI/SNF related, matrix associated, actin dependent regulator of chromatin, subfamily B, member 1) are involved in multiple meningiomas. These mutations are further associated with tumor location and histological subtype (Tauziede-Espariat et al., 2017). In spinal schwannoma, one study reported a mutation in the large tumor suppressor kinase 1 gene (LATS1), a downstream mediator of NF2, but the clinical relevance of these alterations remains unknown in spinal meningiomas (28).

Other additional mutations

Comparative microarray analysis between spinal and intracranial meningiomas confirmed that spinal meningiomas are associated to a higher rate of chromosome 22 deletion (23). Moreover, 35 genes out of 1555 reported were more highly expressed in spinal than in intracranial meningiomas (23). Barresi et al. reported that spinal meningiomas showed an increased expression of the matrix metalloproteinase family, a group of proteins also involved in cell growth and invasion (23).

Meningiomas and sex hormones

Multiple reasons suggest the association between sexual hormones and the development of meningiomas. Meningiomas are more common in females, even more for spinal meningiomas than intracranial meningiomas, and are positively correlated with breast cancer (29, 30). Most meningiomas express progesterone and somatostatin receptors (31). Spinal meningiomas expressed more androgen receptors (AR+) and estrogen receptors (ER+) than intracranial meningiomas (30).

Many studies have investigated the impact of sex hormone medication, such as oral contraception or hormonal replacement therapy (HRT), on meningiomas development. Results were inconclusive still recently (32–34). A dose-dependent relationship between the incidence and growth of meningiomas and hormonal treatment with progestin cyproterone acetate (CPA) has recently been established (35). A similar but lower risk of meningiomas has been recently reported with the use of chlormadinone acetate and nomegestrol acetate as progestin treatments (35).

Concerning HRT in menopausal patients, evidence from epidemiological studies seem to favor an increased risk of meningiomas in treated patients although a recent study failed to show an increased growth of meningiomas in HRT treated *vs.* nontreated patients (36). Until larger studies are available, it seems wise to recommend avoiding HRT in patients with meningiomas (37).

Based on studies demonstrating the expression of hormonal receptors in meningiomas, therapies targeting these receptors have been tried but have failed to show an overall favorable clinical outcome in meningioma treatment (37).

To the best of our knowledge, there are no published data on spinal meningiomas in pregnant women. However, data arising from intracranial meningiomas research suggest that the latter may enlarge during pregnancy, as noted by Cushing and Eisenhardt (38). But the rarity of this condition does not allow to clearly define the risk and the need for surgery during pregnancy. Usually, urgent neurosurgery can be indicated during pregnancy in case of neurological symptoms such as motor deficit or visual impairment (39, 40). For asymptomatic meningiomas, a multidisciplinary approach is always useful to better evaluate the pros and cons of surgery during pregnancy and following management both for maternal and fetal health, the aim being, as far as possible, to organize the surgery away from childbirth (41).

Neuroimaging

Magnetic resonance imaging aspect

Magnetic resonance imaging (MRI) is currently the preferred diagnostic modality of intradural spinal tumors (Figure 3). On MRI, most spinal meningiomas show intermediate to hypo intensity on T1-weighted images (WI) and are iso- to hyperintense on T2-WI (42, 43). In fact, on T2-WI, these tumors present with a higher signal than the spinal cord but a lower signal than the surrounding fat tissue (44). They are usually well-circumscribed, with an intermediate to strong homogeneous enhancement after gadolinium injection (45). Tumors with heterogeneous enhancement seldom present with a decreased intratumoral signal on T2-WI due to calcifications, hemorrhage, or necrosis (46).

Intratumoral calcifications are reported in less than 5% of spinal meningiomas (46) but are associated with poor functional outcomes after surgical resection (4).

Characteristic radiological features

As previously mentioned, spinal meningiomas are most commonly found in the thoracic region, in the lateral and anterolateral aspects of the spinal cord (in front of the denticulate ligament). Although a dural tail is a characteristic feature of meningiomas, it is less frequently seen in spinal than in cranial meningiomas (47).

Radiological classification

Yeo et al. classify spinal meningiomas into four categories depending on their MRI appearance (44): Type A includes tumors with a dural attachment (with and without dural tail) that shows homogeneous enhancement after gadolinium injection; type B consists of oval-shaped tumors with hypo intense component on T2WI; type C consists of "*en plaque*" meningioma, that grows in a diffuse sheet-like aspect along with the dura mater; and type D for the rest of spinal meningiomas that could not type A, B nor C.

A unique presentation of "en plaque" meningioma

"*En plaque*" or type C meningioma is a subgroup of spinal meningiomas. It is frequently associated with intramedullary signal changes on T2WI (44), although myelomalacia is a rare

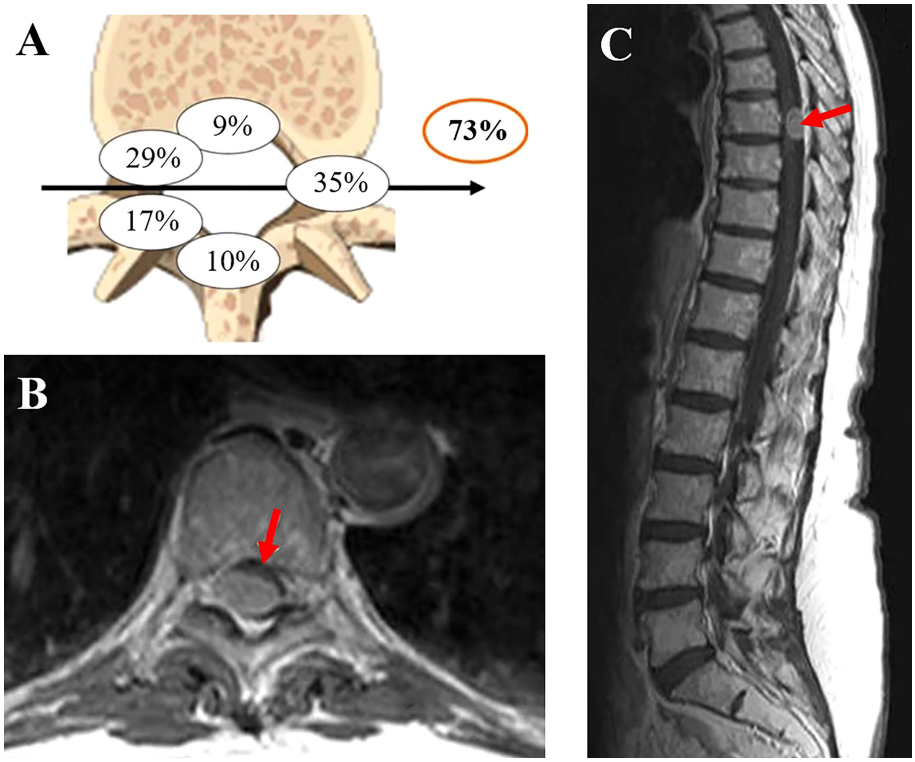

FIGURE 3
(A) Localization of the dural attachment (73% located ventrally to the dentate ligament). **(B, C)** Spinal meningioma aspects on MRI. The figure is adapted from reference 4 and reproduced with permission from SNCSC.

finding in spinal meningiomas (47). Moreover, type C meningioma has a larger size at diagnosis compared to well-encapsulated tumors (44). Thus, it has an increased risk of worse surgical outcomes, with postoperative arachnoiditis and higher recurrence rates after surgical resection. This might be explained by the diffuse growth pattern of these tumors, which delays clinical manifestations (44).

Observation

More available neuroimaging modalities as MRI scans facilitated the discovery of incidental meningiomas. These lesions represent of 0.9% to 1.0% of the general population (48). Depending on the growth of the lesions, a follow-up plan is set for every individual patient. Presently, it is agreed that annual MRI scans are recommended in meningiomas of WHO grade 1 for five years. After that period, biannual MRIs can be performed.

During pregnancy, a close follow-up is recommended in patients known to have meningiomas (40).

Management

Unlike intracranial meningiomas, spinal meningiomas do not generally invade the pia and rarely result in spinal cord edema, compared to small intracranial meningiomas that can cause significant vasogenic edema thus becoming symptomatic (49). Spinal meningiomas tend to manifest clinically once they exhibit a direct mass effect on the neural elements (50). For incidentally discovered meningiomas, clinical and radiographical observation is essential to select the best management strategy, even in the case of a documented tumor growing on serial imaging. Several factors should be considered in asymptomatic spinal meningioma before proposing tumor resection. Those factors include the patient's age, comorbidities, and tumor size.

Surgery

Surgery is the gold standard therapy for spinal meningiomas (51). Pseudomeningoceles or CSF leakage are the most common complications occurring in nearly 4% of cases (52). In neurosurgical practice, spinal meningiomas location and growing patterns may affect surgical results (9). The tumor location in the canal was classified into four types depending on the location of the dural attachment of the tumor and their shape (53): dorsal, lateral and ventral; dumbbell-shaped spinal meningioma being extremely rare. Ventrally attached large tumors causing spinal cord signal changes are linked with poor functional outcomes and increased risk of spinal cord traction during surgery. Severe preoperative impairment (McCormick grades III, IV, and V) that may reflect the plasticity and a vulnerable spinal cord, is significantly related to neurological deterioration postoperatively (54). Location of the meningioma throughout the spine is also important, as lumbar location gives more freedom for gross total resection (GTR) than dorsal or cervical locations, due to the absence of the spinal cord. Thoracic location is most critical as the vascularization of the spinal cord is frail (54).

Surgical removal of dorsal or lateral lesions is usually not difficult, and complete surgical resection can be achieved in 97% of cases (13). Ventrally located are less accessible, and "*en plaque*" meningiomas may not be removed totally (9).

A posterior midline approach with laminectomy can be used in the majority of dorsal or dorsolateral spinal meningiomas. Bilateral laminectomy, one level above and below the lesion, is usually sufficient for exposure in open surgery for small lesions (6, 55). The integrity of the surrounding vertebral structures should be mandatory to preserve biochemical stability, especially in cases of multilevel laminectomy or facet join disruption (56).

Anterior or anterolateral approaches are exceptional (56, 57), and must be reserved to complex anterior spinal meningiomas, because complications are more frequent, especially for CSF leakage (58). These techniques generally require a corpectomy, preferably with a unilateral approach, which implies a complementary vertebral fixation and fusion for the preservation of biomechanical stability. In some cases of anterolateral localization, when costotransversectomy and pediculectomy are needed to safely access the spinal canal and expose the lateral and anterior parts of the tumor, unilateral instrumented fusion should be done.

Excision of spinal meningiomas follows the Simpson grading (Table 3) regarding the totality of the resection and the treatment of the dural tail attachment (59). One of the most critical surgical steps is to define a dissection plane between the lesion and the neural elements. To access to the anterior compartment, it might be required to separate the dentate ligaments during debulking to ensure a convenient area of manipulation of the spinal cord (7). Tumor excision is accomplished using micro scissors, rongeurs, bipolar cauterization and/or ultrasonic cavitation aspirator (7, 55). Hemostasis of the epidural plexus can be achieved using surgical compression, low-intensity electrocoagulation, or hemostatic agents (55). Dural attachment resection with a patch graft suturing must be systematically performed to limit postoperative complications such as pseudomeningoceles or CSF leakage (52, 60). Finally, Kaplan-Meier survival curves

TABLE 3 Simpson grading in meningiomas.

Grade I	GTR of the tumor as well as its dural attachments and the underlying abnormal bone
Grade II	GTR of the tumor with coagulation of the dural attachments
Grade III	GTR of the tumor without resection or coagulation of the dural attachments
Grade IV	Subtotal resection of the tumor
Grade V	Simple decompression with or without biopsy
GTR, Gross total resection.	

showed that there is no significant difference between Simpson grade I and II, grade II GTR is more convenient in difficult surgical cases where access is difficult and risky (54).

Minimally-invasive techniques

In 2006, Tredway et al. reported operative success using a mini-invasive hemilaminectomy technique with a tubular retractor system (55), allowing to less manipulation of the spinal cord, thus maintaining vertebral stability, decreasing blood loss and reducing hospitalization period. Since then, numerous reports have confirmed the feasibility and safety of MIS for spinal meningiomas. However, this type of approach can only be used for small lesions limited to maximum two vertebral levels (55), and must be offered to elderly and fragile patients when possible (61). However, there is still not enough evidence to recommend MIS techniques over the classical open surgery (62), because the studies advocating for MIS had small sample sizes and mixed extra- and intra-medullary tumors, resulting in confounding biases. More inspections are needed in the near future to establish specified criteria and indications for the proper usage of MIS in the treatment of spinal meningiomas.

Intraoperative monitoring

Spinal surgery has little margin for error. Therefore, all means must be deployed to preserve the functioning of the spinal pathways and reduce the postsurgical neurological deficit. For this purpose, intraoperative neurophysiological monitoring was first introduced in 1975 by Tamaki and Yamane and has been widely used by spinal surgeons to provide information regarding the extent of tissue manipulation, tissue resection, and preservation of spinal tracts function (2, 56).

Motor evoked potentials (MEP) and somatosensory evoked potentials (SEP) are the two main neuromonitoring tools used during surgery. MEP explore the integrity of the pyramidal tracts and are primarily used in the context of anterior and anterolateral spinal lesions. SEP examine the dorsal columns and are thus mainly used in the case of posterior and posterolateral spinal lesions. The two modalities are frequently combined and offer quick and valuable surgical feedback. Intraoperative SEP and/or MEP deterioration prompt rapid surgical intervention and prevent irreversible sensory and motor pathways damage.

MEP requires stimulation of the pyramidal tracts and response recording through surface electrodes placed over a muscle of interest (for instance, intrinsic hand muscles or tibialis anterior muscle) (63–66). Direct spinal stimulation could elicit muscle responses and has been used by several groups worldwide. However, it is now known that the obtained responses could not accurately reflect the functioning and integrity of central motor pathways. Although these motor responses translate the firing of lower motor neurons, they result from the activation of various spinal tracts, including antidromic activation of dorsal column axons that have collaterals with lower motor neurons (67). Therefore, brain stimulation is recommended to monitor the integrity of corticospinal (pyramidal) tracts (64).

Brain activation could be obtained by applying magnetic or electric stimulation to the scalp. For intraoperative monitoring, electric currents are by far more practical than the magnetic field. They are delivered to the brain through "corkscrew" needles, straight needles, or surface electrodes. The latter consists of electroencephalographic (EEG) cups that could be securely fixed on the scalp (before surgery) using collodium. Anodal stimulation was more efficient than cathodal stimulation in evoking MEP. Stimulating electrodes are placed at specific sites over the motor cortex, such as C3, C4, C1, C2, Cz - 1 cm, and Cz + 6 cm (according to the 10-20 international system of electrode placement). Several montages have been proposed, like hemispheric, interhemispheric, and midline (for review, please refer to 64); each has its advantages and inconveniences that fall outside the scope of this paper and will not be discussed here.

As for SEP, this technique requires stimulation of a peripheral nerve of the upper or lower limb and response recording through electrodes positioned over the primary sensory cortex (65). Recording electrodes consist of either EEG cup electrodes fixed to the scalp using collodium or subcutaneous needle electrodes. The latter provide rapid positioning but could increase the risk of local infection or subcutaneous hemorrhage.

Concerning stimulation, median and posterior tibial nerves are usually used; other peripheral nerves can also be stimulated in certain circumstances; for instance, the ulnar nerve is chosen in lower cervical interventions. The stimuli are rectangular, of 0.2 to 0.3 ms duration, and supramaximal intensity. The latter corresponds to two times the motor threshold or three times the sensory threshold (65).

For both techniques, qualified and experimented personnel is needed to accurately detect any changes in SEP or MEP response, distinguish it from any confounder, and warn the surgical team.

Metastatic spinal meningiomas

The literature regarding spinal meningiomas metastasis is lacking. However, according to data arising from intracranial meningiomas research, extracranial meningioma metastases (EMM) occur in 0.1% of intracranial meningiomas mainly encountered in atypical and anaplastic lesions. Most common sites of metastasis are the lungs and pleura but intraspinal and vertebral EMM also occur in a lesser percentage and are poorly described in the literature. There is no standard treatment protocol for EMM although their presence might worsen the prognosis of the concerned patients (68). EMM occurrence is independent of WHO grading and can be even present before tumor recurrence.

Tumor recurrence

As stated previously, spinal meningiomas are benign tumors with a low recurrence rate independently of the histological grade of the cancer. In general, the recurrence rate in spinal meningiomas tend to be less than in intracranial meningiomas. The recurrence/progression of meningiomas after ten years can reach 13% (2, 69). The incidence was lower for convexity lesions (3%) than parasagittal (18%) and sphenoid ridge (34%) meningiomas. Multiple demographic, clinical and radiological factors have been associated with increased recurrence rates, such as patient age (recurrence rate higher in young patients (below 50)), tumor location (cervical), infiltrating meningioma, *En plaque* growth, extradural extension, arachnoid scarring, and partial resection (Simpson IV-V grades). Moreover, a recent series reported by Park et al. found that foraminal and thoracic location is associated with a higher recurrence rate (70).

In addition, histological types seem to influence the recurrence risk; for instance, spinal clear cell meningioma was found to have a greater recurrence rate (10).

The importance of dural attachment resection is controversial and contrasting results have been described. For instance, Nakamura et al. found that the recurrence rate was lower for Simpson Grade I than for Simpson Grade II resection (53). In contrast, a low recurrence rate can be found even without dural resection (71). In the same perspective, the add-on value of including the dural tail in the field of radiation therapy is still undetermined. Some data come from the domain of intracranial meningioma, where the radiation of the dural attachment was not found to be beneficial (*i.e.*, it did not reduce the recurrence rate) in a large retrospective series recently reported by Piper etal. (72). A better understanding of the dural tail (or dural attachment) pathophysiology is needed to guide and improve the management of this cancer.

Functional outcomes and complications

Spinal meningiomas are frequently associated with a favorable neurological and functional prognosis (4, 73, 74).

The patients who underwent surgical decompression experienced significant post-operative improvements in Patient Reported Outcomes as measured by the Brief Pain Index and MD Anderson Symptom Inventory (75). However, anterior or calcified lesions, recurrences, cases in which the arachnoid layer has been violated, tumors invading the spinal cord and/or the vascular structures do not have the same favorable outcome (74). Therefore, the preoperative functional and neurological evaluation using the Frankel and the McCormick scales should be carried out before and after surgery (Tables 4, 5). Complications are present due to neurological worsening that

TABLE 4 Frankel scale evaluating functional outcomes in spinal cord injuries.

A	Complete neurological injury - no motor or sensory function below the level of the injury
B	Preserved sensation only - no motor function below the level of the injury
C	Preserved motor non-functional - some motor function observed below the level of the injury
D	Preserved motor function - useful motor function below the level of the injury
E	Normal motor - no clinically detected abnormality in motor or sensory function with normal sphincter function; abnormal reflexes and subjective sensory abnormalities may be present

TABLE 5 McCormick scale evaluating neurological outcomes in spinal cord injuries.

1	Intact neurologically, normal ambulation, and minimal dysesthesia
2	Mild motor or sensory deficit and functional independence
3	Moderate deficit, limitation of function, and independent without external aid
4	Severe motor or sensory deficit, limited function, and dependent
5	Paraplegia or quadriplegia, even without flickering movement

can be caused by the surgery itself. This includes spinal epidural hematoma, CSF leakage with or without deep or superficial infections, syringomyelia, and iatrogenic instability (4, 73, 76). In the event of early postoperative neurological deterioration, epidural hematoma should be suspected, and an emergent MRI obtained, in order to rule out this complication, the other possibility being spinal cord ischemia or edema. Epidural hematoma should be evacuated in an urgent manner to obtain rapid and total neurological recovery. In the absence of epidural hematoma and the presence of spinal cord edema, high-dose intravenous steroids should be administered. There are no exact percentages in the literature for these postoperative complications, but all publications agree on their rarity and (*i.e.*, below 5% of cases). CSF leakage is treated by lumbar drainage for 4-5 days and usually resolves without surgical revision. Superficial and deep infections are rare and must be treated with antibiotic therapy and surgical revision when required. Syringomyelia is a late onset complication. If chronic neurological impairment is attributed to the development of the evolving syrinx, subarachnoidal shunting of the cavity through an intracystic catheter should be considered. This complication is usually of bad prognosis. Iatrogenic instability should be considered mainly when back pain remains an issue with the appearance of local kyphosis on control imaging. Instrumented fusion should be considered. It could be done through a minimally invasive navigated percutaneous approach.

Adjuvant therapy

Surgery remains the primary treatment modality for spinal meningiomas, although radiotherapy may be used as an adjuvant treatment in some cases.

Postoperative radiotherapy role is not well understood yet (14). Radiotherapy and radiosurgery are the two best substitutes for surgery in specific situations described in the literature (77–79).

Both therapeutic strategies are depicted in Table 6. Patients with WHO grade 1 meningiomas do not necessarily need adjuvant treatment after resection that might be sufficient for short-term tumor control (80).

TABLE 6 Indication for adjuvant treatment in spinal meningiomas.

Radiotherapy	WHO grade 3 meningioma
	WHO grade 2 meningioma with recurrence
	Subtotal resection
Radiosurgery	Elderly patients who cannot tolerate surgery
	Patients with recurrent tumors without spinal cord compression and who are not candidates for surgery
WHO, World Health Organization.	

Upfront radiosurgery is usually not an option, given that small, non-compressive lesions usually require a close observation strategy, and large symptomatic lesions should undergo surgery. It may be used in fragile patients who cannot be operated. In addition, a 2-3 mm margin between the meningioma and the spinal cord is required for an effective tumoricidal dose (81). Thus, stereotactic body radiation therapy (SBRT) can be proposed for operated patients within a safe margin. The definitive SBRT dose consisted of delivering 21 Gray in three fractions. Five-year control rates with stereotactic therapy for meningiomas, varied between 70% and 100% (82). Adjuvant therapy can also be considered in WHO grade 3 meningiomas, given that these lesions are more aggressive and have a higher recurrence rate (83). Image-modulated radiation therapy (IMRT) and conventional fractionated radiation therapy have also been used to treat spinal meningioma, but SBRT is the preferred modality (77).

Chemotherapy is not used in the management of spinal meningiomas. In invasive atypical meningiomas (WHO grade 3), multiple agents have been used, including hydroxyurea, interferon α-2B, long-acting Sandostatin, and even multidrug sarcoma protocols (84). Chemotherapy can also have a role as a salvage therapy in cases of highly aggressive tumors.

Specific situation: Spinal meingioma in pediatric population

When a spinal meningioma is diagnosed in children, a strictly follow-up must be adopted because of the high risk of developing other tumors, particularly in the context of NF2 (52). Complete surgical resection is the primary treatment modality of

spinal meningiomas (85). Adjuvant radiotherapy should be recommended only for children with recurrence (85).

Psycho-oncological aspects

Neuropsychiatric symptoms could be observed in oncology wards, including neuro-oncology. They could result either from the direct effect of the tumoral processes affecting the CNS (such in the case of intracranial meningiomas) and/or secondary to the stressful events or the adjustment processes that arise from the announcement of potentially life-threatening conditions and the related workup, surgical interventions, prognosis, and follow-up (86–88). Although these manifestations might affect patients with meningiomas, as in those with other tumors, they remain overlooked and sometimes forgotten. The majority of the few available studies published on this matter focused on intracranial meningiomas and reported the frequent occurrence of fatigue, anxiety, and depression symptoms (89, 90), as well as the lack of effect of pharmacological therapies (Methylphenidate or Modafinil) on these symptoms, compared to placebo in the randomized clinical trials that recruited patients with primary brain tumors including meningiomas (91, 92).

Fewer data are available on this matter in spinal meningiomas and involve anxiety, depression, and quality of life. For instance, in one study that considered patients with intradural extramedullary spinal tumors (of which 31.8% were meningiomas), some (50%) or extreme (14.3%) problems with anxiety and depression according to a quality-of-life questionnaire (EQ-5D-3L) were reported before the surgical intervention; the rates started to decrease from less than 1-month following the surgery to 3-12 months later, but they increased back to baseline values after one-year follow-up (93). Moreover, in another study involving patients with intradural extramedullary spinal tumors, of which 4.2% had meningiomas, 22.9% met the diagnostic and statistical manual of mental disorder criteria (DSM IV-TR) of a psychiatric disorder. In comparison, 37.5% and 12.5% of patients had mild and moderate depression symptoms according to Beck Depression Inventory, respectively (94). Furthermore, in a third study that addressed the previous limitation by including a homogeneous cohort of patients with spinal meningiomas (n=84), some or extreme problems with anxiety and depression were reported by 31% and 3.6% of patients, respectively, according to a quality-of-life questionnaire (EQ-5D-3L; 95). Here, no significant differences in problems related to anxiety and depression were found in gender or neurological status.

These facts warrant more research to further understand this clinical population's affective and cognitive outcomes. A thorough investigation of these variables would help to (a) understand such outcomes (depression and anxiety symptoms, fear of recurrence, fatigue, coping strategies) and their clinical predictors, (b) subsequently develop specific screening tools to quantify the symptoms and identify patients at risk, and (c) implement psycho-oncological interventions that could be ideally offered in a patient-tailored manner (psychoeducation, psychosocial support, pharmacotherapeutics or psychotherapies if justified) (96). Lastly, informal caregivers of patients with spinal meningiomas seem to be still forgotten (97), and future studies are needed to evaluate and help these "hidden patients" (98), which might contribute to its turn in improving patients' outcomes.

Conclusion

Spinal meningiomas are intradural, slow-growing tumors, classified as a WHO grade 1 lesion in more than 70% of the cases. There is no histological difference between spinal and intracranial meningiomas.

Since intradural spinal tumors are not frequent, multicenter studies are required to fully understand and materialize the promise of targeted genetic therapies that will widen the treatment options in the future with a better clinical decision-making.

Observation should be implemented when suitable. Surgical treatment is the gold standard solution, with a principal goal of a GTR (Simpson grade I). If this GTR cannot be achieved, a SIMPSON II is advised, if possible, given the low recurrence rates. In cases of the ventral tumor where GTR is hardly achievable, small amounts of the tumor should be left. If interval growth is seen, the residual tumor can be observed and/or treated with adjuvant therapy, mainly SBRT.

Advances in surgical approaches, especially endoscopic and minimally invasive techniques, are still ongoing to minimize the risks with a better postoperative prognosis with a complete resection as a primary treatment modality.

Psycho-oncological interventions might be beneficial in patients presenting with spinal meningiomas. More research is needed to optimize screening and support patients and their informal caregivers.

Author contributions

SA and GL: Conceptualization and methodology. NS, IL, CA, BT, FN, JF, JM, MC, RB-N and YA: Data analysis, writing-original draft preparation. MC and SA: Review and editing. SA and GL: supervision. All authors contributed to the article and

approved the submitted version.

Conflict of interest

SA declares having received compensation from ExoNeural Network AB, Sweden. MC declares having received compensation from Janssen Global Services LLC, ExoNeural Network AB, Sweden, and Ottobock, France.

The remaining authors declare that the research was conducted in the absence of any commercial or financial relationships that could be construed as a potential conflict of interest.

Publisher's note

References

1. Perry A, Gutmann DH, Reifenberger G. Molecular pathogenesis of meningiomas. *J Neurooncol.* (2004) 70(2):183–202. doi: 10.1007/s11060-004-2749-0

2. Ravindra VM, Schmidt MH. Management of spinal meningiomas. *Neurosurg Clin N. Am* (2016) 27(2):195–205. doi: 10.1016/j.nec.2015.11.010

3. Saraceni C, Harrop JS. Spinal meningioma: chronicles of contemporary neurosurgical diagnosis and management. *Clin Neurol Neurosurg* (2009) 111 (3):221–6. doi: 10.1016/j.clineuro.2008.10.018

4. Sandalcioglu IE, Hunold A, Müller O, Bassiouni H, Stolke D, Asgari S. Spinal meningiomas: critical review of 131 surgically treated patients. *Eur Spine J* (2008) 17(8):1035–41. doi: 10.1007/s00586-008-0685-y

5. Arima H, Takami T, Yamagata T, Naito K, Abe J, Shimokawa N, et al. Surgical management of spinal meningiomas: A retrospective case analysis based on preoperative surgical grade. *Surg Neurol Int* (2014) 5(Suppl 7):S333–8. doi: 10.4103/2152-7806.139642

6. Parsa AT, Lee J, Parney IF, Weinstein P, McCormick PC, Ames C. Spinal cord and intradural-extraparenchymal spinal tumors: current best care practices and strategies. *J Neurooncol.* (2004) 69(1-3):291–318. doi: 10.1023/b:neon.0000041889.71136.62

7. Gottfried ON, Gluf W, Quinones-Hinojosa A, Kan P, Schmidt MH. Spinal meningiomas: surgical management and outcome. *Neurosurg Focus.* (2003) 14(6): e2. doi: 10.3171/foc.2003.14.6.2

8. Engelhard HH, Villano JL, Porter KR, Stewart AK, Barua M, Barker FG, et al. Clinical presentation, histology, and treatment in 430 patients with primary tumors of the spinal cord, spinal meninges, or cauda equina. *J Neurosurg Spine.* (2010) 13 (1):67–77. doi: 10.3171/2010.3.SPINE09430

9. Postalci L, Tugcu B, Gungor A, Guclu G. Spinal meningiomas: recurrence in ventrally located individuals on long-term follow-up; a review of 46 operated cases. *Turk. Neurosurg* (2011) 21(4):449–53.

10. Zhang H, Ma L, Shu C, Dong LQ, Ma YQ, Zhou Y. Spinal clear cell meningiomas: Clinical features and factors predicting recurrence. *World Neurosurg* (2020) 134:e1062–76. doi: 10.1016/j.wneu.2019.11.093

11. Riad H, Knafo S, Segnarbieux F, Lonjon N. Spinal meningiomas: surgical outcome and literature review. *Neurochirurgie.* (2013) 59(1):30–4. doi: 10.1016/j.neuchi.2012.10.137

12. Levy WJ, Bay J, Dohn D. Spinal cord meningiomas. *J Neurosurg* (1982) 57:804– 812.

13. Solero CL, Fornari M, Giombini S, Lasio G, Oliveri G, Cimino C, et al. Spinal meningiomas: review of 174 operated cases. *Neurosurgery.* (1989) 25(2):153–60.

14. Gezen F, Kahraman S, Canakci Z, Bedük A. Review of 36 cases of spinal cord meningioma. *Spine* (2000) 25(6):727–31. doi: 10.1097/00007632-200003150-00013

15. Cohen-Gadol AA, Zikel OM, Koch CA, Scheithauer BW, Krauss WE. Spinal meningiomas in patients younger than 50 years of age: a 21-year experience. *J Neurosurg* (2003) 98(3 Suppl):258–63.

16. Birzu C, Peyre M, Sahm F. Molecular alterations in meningioma: prognostic and therapeutic perspectives. *Curr Opin Oncol* (2020) 32(6):613–22. doi: 10.1097/CCO.0000000000000687

17. Holleczek B, Zampella D, Urbschat S, Sahm F, von Deimling A, Oertel J, et al. Incidence, mortality and outcome of meningiomas: A population-based study from Germany. *Cancer Epidemiol.* (2019) 62:101562. doi: 10.1016/j.canep.2019.07.001

18. Moussalem C, Massaad E, Minassian GB, Ftouni L, Bsat S, Houshiemy MNE, et al. Meningioma genomics: a therapeutic challenge for clinicians. *J Integr Neurosci* (2021) 20(2):463–9. doi: 10.31083/j.jin2002049

19. Weber RG, Boström J, Wolter M, Baudis M, Collins VP, Reifenberger G, et al. Analysis of genomic alterations in benign, atypical, and anaplastic meningiomas: toward a genetic model of meningioma progression. *Proc Natl Acad Sci U. S. A.* (1997) 94(26):14719–24. doi: 10.1073/pnas.94.26.14719

20. Mota M, Shevde LA. Merlin regulates signaling events at the nexus of development and cancer. *Cell Commun Signal* (2020) 18(1):63. doi: 10.1186/s12964-020-00544-7

21. Goutagny S, Yang HW, Zucman-Rossi J, Chan J, Dreyfuss JM, Park PJ, et al. Genomic profiling reveals alternative genetic pathways of meningioma malignant progression dependent on the underlying NF2 status. *Clin Cancer Res* (2010) 16 (16):4155–64. doi: 10.1158/1078-0432.CCR-10-0891

22. Lee YS, Lee YS. Molecular characteristics of meningiomas. *J Pathol Transl Med* (2020) 54(1):45–63. doi: 10.4132/jptm.2019.11.05

23. Barresi V, Alafaci C, Caffo M, Barresi G, Tuccari G. Clinicopathological characteristics, hormone receptor status and matrix metallo-proteinase-9 (MMP-9) immunohistochemical expression in spinal meningiomas. *Pathol Res Pract* (2012) 208(6):350–5. doi: 10.1016/j.prp.2012.02.013

24. Liu N, Song SY, Jiang JB, Wang TJ, Yan CX. The prognostic role of ki-67/MIB-1 in meningioma: A systematic review with meta-analysis. *Med (Baltimore).* (2020) 99(9):e18644. doi: 10.1097/MD.0000000000018644

25. Sayagués JM, Tabernero MD, Maíllo A, Trelles O, Espinosa AB, Sarasquete ME, et al. Microarray-based analysis of spinal versus intracranial meningiomas: different clinical, biological, and genetic characteristics associated with distinct patterns of gene expression. *J Neuropathol Exp Neurol* (2006) 65(5):445–54. doi: 10.1097/01.jnen.0000229234.13372.d8

26. Boetto J, Peyre M, Kalamarides M. Meningiomas from a developmental perspective: exploring the crossroads between meningeal embryology and tumorigenesis. *Acta Neurochir. (Wien).* (2021) 163(1):57–66. doi: 10.1007/s00701-020-04650w

27. Youngblood MW, Duran D, Montejo JD, Li C, Omay SB, Özduman K, et al. Correlations between genomic subgroup and clinical features in a cohort of more than 3000 meningiomas. *J Neurosurg* (2019) 25:1–10. doi: 10.3171/2019.8.JNS191266

28. Kim YH, Ohta T, Oh JE, Le Calvez-Kelm F, McKay J, Voegele C, et al. TP53, MSH4, and LATS1 germline mutations in a family with clustering of nervous system tumors. *Am J Pathol* (2014) 184(9):2374–81. doi: 10.1016/j.ajpath.2014.05.017

29. Ostrom QT, Patil N, Cioffi G, Waite K, Kruchko C, Barnholtz-Sloan JS. CBTRUS statistical report: Primary brain and other central nervous system tumors diagnosed in the united states in 2013-2017. *Neuro Oncol* (2020) 22(12 Suppl 2): iv1–iv96. doi: 10.1093/neuonc/noaa200

30. Portet S, Banor T, Bousquet J, Simonneau A, Flores M, Ingrand P, et al. New insights into expression of hormonal receptors by meningiomas. *World Neurosurg* (2020) 140:e87–96. doi: 10.1016/j.wneu.2020.04.168

31. Miyagishima DF, Moliterno J, Claus E, Günel M. Hormone therapies in meningioma-where are we? *J Neurooncol.* (2022). doi: 10.1007/s11060-022-04187-1

32. Benson VS, Pirie K, Green J, Casabonne D, Beral VMillion Women Study Collaborators. Lifestyle factors and primary glioma and meningioma tumours in

the million women study cohort. *Br J Cancer.* (2008) 99(1):185–90. doi: 10.1038/sj.bjc.6604445

33. Blitshteyn S, Crook JE, Jaeckle KA. Is there an association between meningioma and hormone replacement therapy? *J Clin Oncol* (2008) 26(2):279–82. doi: 10.1200/JCO.2007.14.2133

34. Benson VS, Kirichek O, Beral V, Green J. Menopausal hormone therapy and central nervous system tumor risk: large UK prospective study and meta-analysis. *Int J Cancer.* (2015) 136(10):2369–77. doi: 10.1002/ijc.29274

35. Samoyeau T, Provost C, Roux A, Legrand L, Dezamis E, Plu-Bureau G, et al. Meningioma in patients exposed to progestin drugs: results from a real-life screening program. *J Neurooncol.* (2022) 160(1):127–36. doi: 10.1007/s11060-022-04124-2

36. Dresser L, Yuen CA, Wilmington A, Walker M, Vogel TJ, Merrell RT, et al. Estrogen hormone replacement therapy in incidental intracranial meningioma: a growth-rate analysis. *Sci Rep* (2020) 10(1):17960. doi: 10.1038/s41598-020-74344-x

37. Hage M, Plesa O, Lemaire I, Raffin Sanson ML. Estrogen and progesterone therapy and meningiomas. *Endocrinology* (2022) 163(2):bqab259. doi: 10.1210/endocr/bqab259

38. Chakravarthy V, Kaplan B, Gospodarev V, Myers H, De Los Reyes K, Achiriloaie A. Houdini Tumor: Case report and literature review of pregnancy-associated meningioma. *World Neurosurg* (2018) 114:e1261–5. doi: 10.1016/j.wneu.2018.03.187

39. Antolínez Ayala VE, García Arias MD, Bautista Vargas SE, Báez Cárdenas LM, Castellanos Peñaranda C. Paraplegia due to spinal meningioma during the third trimester of pregnancy: case report and literature review. *Spinal. Cord. Ser Cases.* (2021) 7(1):31. doi: 10.1038/s41394-020-00368-0

40. Carbone L, Somma T, Iorio GG, Vitulli F, Conforti A, Raffone A, et al. Meningioma during pregnancy: what can influence the management? a case series and review of the literature. *J Matern. Fetal. Neonatal. Med* (2022) 35(25):8767–77. doi: 10.1080/14767058.2021.2004585.C

41. Dumitru AE, Panaitescu A, Iancu G, Paslaru FG, Paslaru AC, Gorgan RM, et al. Management strategies and clinical follow-up of pregnant women with intracranial meningioma. *J Med Life* (2021) 14(1):2–6. doi: 10.25122/jml-2021-0012

42. Liu WC, Choi G, Lee SH, Han H, Lee JY, Jeon YH, et al. Radiological findings of spinal schwannomas and meningiomas: focus on discrimination of two disease entities. *Eur Radiol* (2009) 19(11):2707–15. doi: 10.1007/s00330-009-1466-7

43. Hoover JM, Morris JM, Meyer FB. Use of preoperative magnetic resonance imaging T1 and T2 sequences to determine intraoperative meningioma consistency. *Surg Neurol Int* (2011) 2:142. doi: 10.4103/2152-7806.85983

44. Yeo Y, Park C, Lee JW, Kang Y, Ahn JM, Kang HS, et al. Magnetic resonance imaging spectrum of spinal meningioma. *Clin Imaging.* (2019) 55:100–6. doi: 10.1016/j.clinimag.2019.02.007

45. De Verdelhan O, Haegelen C, Carsin-Nicol B, Riffaud L, Amlashi SF, Brassier G, et al. MR imaging features of spinal schwannomas and meningiomas. *J Neuroradiol* (2005) 32(1):42–9. doi: 10.1016/s0150-9861(05)83021-4

46. Doita M, Harada T, Nishida K, Marui T, Kurosaka M, Yoshiya S. Recurrent calcified spinal meningioma detected by plain radiograph. *Spine* (2001) 26(11):E249–52. doi: 10.1097/00007632-200106010-00005

47. Abul-Kasim K, Thurnher MM, McKeever P, Sundgren PC. Intradural spinal tumors: current classification and MRI features. *Neuroradiology.* (2008) 50(4):301–14. doi: 10.1007/s00234-007-0345-7

48. Goldbrunner R, Stavrinou P, Jenkinson MD, Sahm F, Mawrin C, Weber DC, et al. EANO guideline on the diagnosis and management of meningiomas. *Neuro Oncol* (2021) 23(11):1821–34. doi: 10.1093/neuonc/noab150

49. Hou J, Kshettry VR, Selman WR, Bambakidis NC. Peritumoral brain edema in intracranial meningiomas: the emergence of vascular endothelial growth factor-directed therapy. *Neurosurg Focus.* (2013) 35(6):E2. doi: 10.3171/2013.8.FOCUS13301

50. Corell A, Cerbach C, Hoefling N, Björkman-Burtscher IM, Jakola AS. Spinal cord compression in relation to clinical symptoms in patients with spinal meningiomas. *Clin Neurol Neurosurg* (2021) 211:107018. doi: 10.1016/j.clineuro.2021.107018

51. Jecko V, Weller J, Houston D, Champeaux-Depond C. Epidemiology and survival after spinal meningioma surgery: A nationwide population-based study. *Asian Spine J* (2022). doi: 10.31616/asj.2021.0213

52. Maiti TK, Bir SC, Patra DP, Kalakoti P, Guthikonda B, Nanda A. Spinal meningiomas: clinicoradiological factors predicting recurrence and functional outcome. *Neurosurg Focus.* (2016) 41(2):E6. doi: 10.3171/2016.5.FOCUS16163

53. Nakamura M, Tsuji O, Fujiyoshi K, Hosogane N, Watanabe K, Tsuji T, et al. Long-term surgical outcomes of spinal meningiomas. *Spine* (2012) 37(10):E617–23. doi: 10.1097/BRS.0b013e31824167f1

54. Kobayashi K, Ando K, Matsumoto T, Sato K, Kato F, Kanemura T, et al. Clinical features and prognostic factors in spinal meningioma surgery from a multicenter study. *Sci Rep* (2021) 11:11630. doi: 10.1038/s41598-021-91225-z

55. Tredway TL, Santiago P, Hrubes MR, Song JK, Christie SD, Fessler RG. Minimally invasive resection of intradural-extramedullary spinal neoplasms. *Neurosurgery* (2006) 58(1 Suppl):ONS52–8. doi: 10.1227/01.neu.0000192661.08192.1c

56. Misra SN, Morgan HW. Avoidance of structural pitfalls in spinal meningioma resection. *Neurosurg Focus.* (2003) 14(6):e1. doi: 10.3171/foc.2003.14.6.1

57. Payer M. The anterior approach to anterior cervical meningiomas: review illustrated by a case. *Acta Neurochir. (Wien).* (2005) 147(5):555–60. doi: 10.1007/s00701-005-0502-x

58. Albanese V, Platania N. Spinal intradural extramedullary tumors. personal experience. *J Neurosurg Sci* (2002) 46(1):18–24.

59. Simpson D. The recurrence of intracranial meningiomas after surgical treatment. *J Neurol Neurosurg Psychiatry* (1957) 20(1):22–39. doi: 10.1136/jnnp.20.1.22

60. Iacob G. Spinal meningiomas. personal experience and review of literature. *Roman. Neurosurg* (2014) 21:146–60.

61. Dauleac C, Leroy HA, Karnoub MA, Obled L, Mertens P, Assaker R. Minimally invasive surgery for intradural spinal meningioma: A new standard? a comparative study between minimally invasive and open approaches. *Neurochirurgie.* (2022) 68(4):379–85. doi: 10.1016/j.neuchi.2022.01.006

62. Caballero-García J, Linares-Benavides YJ, Leitão ULS, Aparicio-García C, López-Sánchez M. Minimally invasive removal of extra- and intradural spinal tumors using full endoscopic visualization. *Global Spine J* (2022) 12(1):121–9. doi: 10.1177/2192568220948806

63. Groppa S, Oliviero A, Eisen A, Quartarone A, Cohen LG, Mall V, et al. A practical guide to diagnostic transcranial magnetic stimulation: report of an IFCN committee. *Clin Neurophysiol* (2012) 123(5):858–82. doi: 10.1016/j.clinph.2012.01.010

64. MacDonald DB, Skinner S, Shils J, Yingling CAmerican Society of Neurophysiological Monitoring. Intraoperative motor evoked potential monitoring - a position statement by the American society of neurophysiological monitoring. *Clin Neurophysiol* (2013) 124(12):2291–316. doi: 10.1016/j.clinph.2013.07.025

65. MacDonald DB, Dong C, Quatrale R, Sala F, Skinner S, Soto F, et al. Recommendations of the international society of intraoperative neurophysiology for intraoperative somatosensory evoked potentials. *Clin Neurophysiol* (2019) 130(1):161–79. doi: 10.1016/j.clinph.2018.10.008

66. Rossini PM, Burke D, Chen R, Cohen LG, Daskalakis Z, Di Iorio R, et al. Non-invasive electrical and magnetic stimulation of the brain, spinal cord, roots and peripheral nerves: Basic principles and procedures for routine clinical and research application. an updated report from an IFCN committee. *Clin Neurophysiol* (2015) 126(6):1071–107. doi: 10.1016/j.clinph.2015.02.001

67. Langeloo DD, Journée HL, de Kleuver M, Grotenhuis JA. Criteria for transcranial electrical motor evoked potential monitoring during spinal deformity surgery a review and discussion of the literature. *Neurophysiol. clinique. = Clin neurophysiol.* (2007) 37(6):431–9. doi: 10.1016/j.neucli.2007.07.007

68. Singh R, Ryan C, Chohan MO, Tisnado J, Hadjigeorgiou GF, Bilsky MH. Intracranial meningioma with vertebral or intraspinal metastasis: report of 2 cases and review of the literature. *J Neurosurg Spine.* (2016) 25(6):775–81. doi: 10.3171/2016.5.SPINE151457

69. Mirimanoff RO, Dosoretz DE, Linggood RM, Ojemann RG, Martuza RL. Meningioma: analysis of recurrence and progression following neurosurgical resection. *J Neurosurg* (1985) 62(1):18–24. doi: 10.3171/jns.1985.62.1.0018

70. Park BJ, Dougherty MC, Noeller J, Nourski KV, Gold CJ, Menezes AH, et al. Spinal meningioma in adults: Imaging characteristics, surgical outcomes, and risk factors for recurrence. *World Neurosurg* (2022) 164:e852-e860. doi: 10.1016/j.wneu.2022.05.054

71. King AT, Sharr MM, Gullan RW, Bartlett JR. Spinal meningiomas: a 20-year review. *Br J Neurosurg* (1998) 12(6):521–6. doi: 10.1080/02688699844367

72. Piper K, Yu S, Taghvaei M, Fernandez C, Mouchtouris N, Smit RD, et al. Radiation of meningioma dural tail may not improve tumor control rates. *Front Surg* (2022) 9:908745. doi: 10.3389/fsurg.2022.908745

73. Westwick HJ, Yuh SJ, Shamji MF. Complication avoidance in the resection of spinal meningiomas. *World Neurosurg* (2015) 83(4):627–34. doi: 10.1016/j.wneu.2014.12.015

74. Raco A, Pesce A, Toccaceli G, Domenicucci M, Miscusi M, Delfini R. Factors leading to a poor functional outcome in spinal meningioma surgery: Remarks on 173 cases. *Neurosurgery.* (2017) 80(4):602–9. doi: 10.1093/neuros/nyw092

75. Newman WC, Berry-Candelario J, Villavieja J, Reiner AS, Bilsky MH, Laufer I, et al. Improvement in quality of life following surgical resection of benign

intradural extramedullary tumors: A prospective evaluation of patient-reported outcomes. *Neurosurgery.* (2021) 88(5):989–95. doi: 10.1093/neuros/nyaa561

76. McGirt MJ, Garcés-Ambrossi GL, Parker SL, Sciubba DM, Bydon A, Wolinksy JP, et al. Short-term progressive spinal deformity following laminoplasty versus laminectomy for resection of intradural spinal tumors: analysis of 238 patients. *Neurosurgery.* (2010) 66(5):1005–12. doi: 10.1227/01.NEU.0000367721.73220.C9

77. Gerszten PC, Chen S, Quader M, Xu Y, Novotny JJr, Flickinger JC. Radiosurgery for benign tumors of the spine using the synergy s with cone-beam computed tomography image guidance. *J Neurosurg* (2012) 117(Suppl):197–202. doi: 10.3171/2012.8.GKS12981

78. Lee KD, DePowell JJ, Air EL, Dwivedi AK, Kendler A, McPherson CM. Atypical meningiomas: is postoperative radiotherapy indicated? *Neurosurg Focus.* (2013) 35(6):E15. doi: 10.3171/2013.9.FOCUS13325

79. Saade R, Hessel A, Ginsberg L, Fuller G, Bell D. Primary extradural meningioma presenting as a neck mass: Case report and review of the literature. *Head Neck.* (2015) 37(8):E92–5.

80. Sun SQ, Cai C, Ravindra VM, Gamble P, Yarbrough CK, Dacey RG, et al. Simpson Grade I-III resection of spinal atypical (World health organization grade II) meningiomas is associated with symptom resolution and low recurrence. *Neurosurgery.* (2015) 76(6):739–46. doi: 10.1227/NEU.0000000000000720

81. Tseng CL, Eppinga W, Charest-Morin R, Soliman H, Myrehaug S, Maralani PJ, et al. Spine stereotactic body radiotherapy: indications, outcomes, and points of caution. *Global Spine J* (2017) 7(2):179–97. doi: 10.1177/2192568217694016

82. Kalash R, Glaser SM, Flickinger JC, Burton S, Heron DE, Gerszten PC, et al. Stereotactic body radiation therapy for benign spine tumors: is dose de-escalation appropriate? *J Neurosurg Spine.* (2018) 29(2):220–5. doi: 10.3171/2017.12.SPINE17920

83. Noh SH, Kim KH, Shin DA, Park JY, Yi S, Kuh SU, et al. Treatment outcomes of 17 patients with atypical spinal meningioma, including 4 with metastases: a retrospective observational study. *Spine J* (2019) 19(2):276–84. doi: 10.1016/j.spinee.2018.06.006

84. Moazzam AA, Wagle N, Zada G. Recent developments in chemotherapy for meningiomas: a review. *Neurosurg Focus.* (2013) 35(6):E18. doi: 10.3171/2013.10.FOCUS13341

85. Piątek P, Kwiatkowski S, Milczarek O. Spinal meningiomas in pediatric patients - a case series and literature review. *Surg Neurol Int* (2022) 13:445. doi: 10.25259/SNI_365_2022

86. Mukand JA, Blackinton DD, Crincoli MG, Lee JJ, Santos BB. Incidence of neurologic deficits and rehabilitation of patients with brain tumors. *Am J Phys Med Rehabil.* (2001) 80(5):346–50. doi: 10.1097/00002060-200105000-00005

87. Lidstone V, Butters E, Seed PT, Sinnott C, Beynon T, Richards M. Symptoms and concerns amongst cancer outpatients: identifying the need for specialist palliative care. *Palliat. Med* (2003) 17(7):588–95. doi: 10.1191/0269216303pm814oa

88. Pranckeviciene A, Deltuva VP, Tamasauskas A, Bunevicius A. Association between psychological distress, subjective cognitive complaints and objective neuropsychological functioning in brain tumor patients. *Clin Neurol Neurosurg* (2017) 163:18–23. doi: 10.1016/j.clineuro.2017.10.007

89. van der Vossen S, Schepers VP, Berkelbach van der Sprenkel JW, Visser-Meily JM, Post MW. Cognitive and emotional problems in patients after cerebral meningioma surgery. *J Rehabil Med* (2014) 46(5):430–7. doi: 10.2340/16501977-1795

90. Kalasauskas D, Keric N, Abu Ajaj S, von Cube L, Ringel F, Renovanz M. Distress and quality of life do not change over time in patients with operated and conservatively managed intracranial meningioma. *Acta Neurochir. (Wien).* (2021) 163(12):3417–24. doi: 10.1007/s00701-021-05004-w

91. Boele FW, Douw L, de Groot M, van Thuijl HF, Cleijne W, Heimans JJ, et al. The effect of modafinil on fatigue, cognitive functioning, and mood in primary brain tumor patients: a multicenter randomized controlled trial. *Neuro Oncol* (2013) 15(10):1420–8. doi: 10.1093/neuonc/not102

92. Reijneveld JC, Klein M.) the effect of modafinil on fatigue, cognitive functioning, and mood in primary brain tumor patients: a multicenter randomized controlled trial. *Neuro Oncol* (2013) 15(10):1420–8.

93. Viereck MJ, Ghobrial GM, Beygi S, Harrop JS. Improved patient quality of life following intradural extramedullary spinal tumor resection. *J Neurosurg Spine.* (2016) 25(5):640–5. doi: 10.3171/2016.4.SPINE151149

94. Luzzati F, Giusti EM, Scotto GM, Perrucchini G, Cannavò L, Castelnuovo G, et al. Quality of life, pain, and psychological factors in patients undergoing surgery for primary tumors of the spine. *Support. Care Cancer.* (2020) 28(3):1385–93. doi: 10.1007/s00520-019-04965-0

95. Pettersson-Segerlind J, von Vogelsang AC, Fletcher-Sandersjöö A, Tatter C, Mathiesen T, Edström E, et al. Health-related quality of life and return to work after surgery for spinal meningioma: A population-based cohort study. *Cancers (Basel).* (2021) 13(24):6371. doi: 10.3390/cancers13246371

96. Sperner-Unterweger B. Psychoonkologie - psychosoziale onkologie: Integration in ein onkologisches behandlungskonzept [Psycho-oncology - psychosocial oncology: integration in a concept of oncological treatment]. *Nervenarzt.* (2011) 82(3):371–8. doi: 10.1007/s00115-010-3163-9

97. Boele FW, Rooney AG, Bulbeck H, Sherwood P. Interventions to help support caregivers of people with a brain or spinal cord tumour. *Cochrane Database Syst Rev* (2019) 7(7):CD012582. doi: 10.1002/14651858.CD012582.pub2

98. Hill J. The hidden patient. *Lancet.* (2003) 362(9396):1682. doi: 10.1016/S0140-6736(03)14820-9

frontiers | Frontiers in Oncology

TYPE Case Report
PUBLISHED 19 January 2023
DOI 10.3389/fonc.2023.1099618

OPEN ACCESS

EDITED BY
Ignazio Gaspare Vetrano,
IRCCS Carlo Besta Neurological Institute Foundation, Italy

REVIEWED BY
Murat Gokden,
University of Arkansas for Medical Sciences, United States
Jens Schittenhelm,
University of Tübingen, Germany
Jacopo Falco,
IRCCS Carlo Besta Neurological Institute Foundation, Italy
Eyas M. Hattab,
University of Louisville, United States

*CORRESPONDENCE
Marta Penas-Prado
marta.penas-prado@nih.gov

SPECIALTY SECTION
This article was submitted to Neuro-Oncology and Neurosurgical Oncology, a section of the journal Frontiers in Oncology

RECEIVED 16 November 2022
ACCEPTED 09 January 2023
PUBLISHED 19 January 2023

CITATION
Frederico SC, Vera E, Abdullaev Z, Acquaye A, Aldape K, Boris L, Briceno N, Choi A, Christ A, Cooper D, Grajkowska E, Kunst T, Leeper HE, Levine J, Lollo N, Pratt D, Quezado M, Shah R, Wall K, Gilbert MR, Armstrong TS and Penas-Prado M (2023) Heterogeneous clinicopathological findings and patient-reported outcomes in adults with *MN1*-altered CNS tumors: A case report and systematic literature review. *Front. Oncol.* 13:1099618. doi: 10.3389/fonc.2023.1099618

Heterogeneous clinicopathological findings and patient-reported outcomes in adults with *MN1*-altered CNS tumors: A case report and systematic literature review

Stephen C. Frederico[1,2], Elizabeth Vera[1], Zied Abdullaev[3], Alvina Acquaye[1], Kenneth Aldape[3], Lisa Boris[1], Nicole Briceno[1], Anna Choi[1], Alexa Christ[1], Diane Cooper[4], Ewa Grajkowska[1], Tricia Kunst[1], Heather E. Leeper[1], Jason Levine[5,6], Nicole Lollo[1], Drew Pratt[3], Martha Quezado[3], Ritu Shah[7], Kathleen Wall[1], Mark R. Gilbert[1], Terri S. Armstrong[1] and Marta Penas-Prado[1*]

[1]Neuro-Oncology Branch, Center for Cancer Research (CCR), National Cancer Institute (NCI), National Institutes of Health (NIH), Bethesda, MD, United States, [2]University of Pittsburgh School of Medicine, Pittsburgh, PA, United States, [3]Laboratory of Pathology, National Cancer Institute (NCI), National Institutes of Health (NIH), Bethesda, MD, United States, [4]Office of Research Services, National Institutes of Health (NIH), Bethesda, MD, United States, [5]Pediatric Oncology Branch, Center for Cancer Research (CCR), National Cancer Institute (NCI), National Institutes of Health (NIH), Bethesda, MD, United States, [6]IT and Clinical Informatics, Center for Cancer Research (CCR), National Cancer Institute (NCI), National Institutes of Health (NIH), Bethesda, MD, United States, [7]Department of Radiology and Imaging Sciences, National Cancer Institute (NCI), National Institutes of Health (NIH), Bethesda, MD, United States

The uncommon *MN1*-altered primary central nervous system (CNS) tumors were recently added to the World Health Organization 2021 classification under the name Astroblastoma, *MN1*-altered. Another term used to describe them, "High-grade neuroepithelial tumor with *MN1* alteration" (HGNET-MN1), makes reference to their distinct epigenetic profile but is currently not a recommended name. Thought to occur most commonly in children and predominantly in females, *MN1*-altered CNS tumors are associated with typical but not pathognomonic histological patterns and are characterized by a distinct DNA methylation profile and recurrent fusions implicating the *MN1* (meningioma 1) gene. Diagnosis based on histological features alone is challenging: most cases with morphological features of astroblastoma (but not all) show these molecular features, whereas not all tumors with *MN1* fusions show astroblastoma morphology. There is large variability in reported outcomes and detailed clinical and therapeutic information is frequently missing. Some patients experience multiple recurrences despite multimodality treatment, whereas others experience no recurrence after surgical resection alone, suggesting large clinical and biological heterogeneity despite unifying epigenetic features and recurrent fusions. In this report, we present the demographics, tumor characteristics, treatment, and outcome (including patient-reported outcomes) of three adults with *MN1*-altered primary CNS tumors diagnosed *via* genome-wide DNA methylation and RNA sequencing. All three patients were females and two of them were diagnosed as young adults. By

reporting our neuropathological and clinical findings and comparing them with previously published cases we provide insight into the clinical heterogeneity of this tumor. Additionally, we propose a model for prospective, comprehensive, and systematic collection of clinical data in addition to neuropathological data, including standardized patient-reported outcomes.

KEYWORDS

CNS, HGNET-*MN1*, astroblastoma, MN1, rare CNS tumor, adult

Introduction

The term high-grade neuroepithelial tumor with *MN1* alteration (HGNET-MN1) was first introduced in 2016 as one of four novel tumors with a distinct DNA methylation profile that emerged after analysis of CNS PNETs (central nervous system primitive neuroectodermal tumors) (1, 2). In addition, the presence of a recurrent fusion implicating the *MN1* (meningioma 1) gene was described; however, the specific mechanism by which *MN1* fusions drive tumor development is still unknown (1, 3). Due to histopathological overlap with other CNS tumors and a lack of a uniform immunohistochemical profile, the diagnosis of MN1-altered tumors with conventional methods remains challenging. Quite often, tumors with the HGNET-MN1 epigenetic profile are diagnosed histologically as either ependymomas or astroblastomas (1, 2), and most tumors histologically diagnosed as astroblastoma belong to this molecular entity (2). In recognition of this association, the 2021 World Health Organization (WHO) classification of CNS Tumors updated the previous morphological diagnosis of astroblastoma to reflect these molecular findings, and renamed this tumor as astroblastoma, *MN1*-altered, simultaneously recommending against the use of the term HGNET-MN1. However, this latest WHO classification also comments on the need for future work to establish clear histopathological and molecular criteria by which astroblastomas with *MN1* alterations can be distinguished from morphologically comparable neuroepithelial tumors with similar genetic alterations (4). In most cases this tumor arises in the supratentorial region and is thought to primarily affect children (1, 3). Unfortunately, available clinical and outcome data is quite limited due to the rarity of this tumor. Additionally, there is a lack of universally available molecular testing required for diagnosis which creates a challenge for retrospective data collection. Few publications provide information about the clinical outcomes for patients diagnosed with astroblastoma MN1-altered or HGNET-MN1, collectively referred to within this manuscript as MN1-altered CNS tumors.

Given their rarity, recent description, and heterogeneous outcome, evidence-based treatment guidelines are not available and prospective studies that would help determine optimal therapy are difficult to implement. In this report, we present three patients with *MN1*-altered CNS tumors, two initially diagnosed as young adults, and one presenting with a late recurrence after being diagnosed in childhood. *MN1*-altered CNS tumors in adults are even a more uncommon clinical presentation for which only anecdotal experience has been reported to date.[6–7,12,15] In addition to discussing these adult patients' demographics, clinical presentation, imaging, pathological and molecular findings, we also discuss their treatment and outcome, including patient-reported outcomes (PROs). Our cases and those previously reported highlight the clinical heterogeneity of this tumor and potential management options. Additionally, we propose a model for longitudinal, comprehensive, and systematic collection of clinical data, including standardized patient-reported outcomes, that is aimed at improving the understanding of these and other newly described rare CNS tumors for which prospective clinical data is often impossible to obtain, and retrospective data collection is often limited to basic demographic and survival data.

Methods

The three cases discussed in this manuscript were retrieved from enrollees in an IRB-approved Natural History Study (NHS) at the Neuro-Oncology Branch, National Cancer Institute (NCI), National Institutes of Health (NIH) (NCT02851706), which allows longitudinal evaluation of adult patients with primary CNS tumors who are probable future candidates for NCI Phase I and II protocols, including tumors that are understudied or have indeterminate natural history. Of 950 participants enrolled in this study as of October 21, 2021, only three were found to be diagnosed with *MN1*-altered tumors. NHS longitudinal data collection includes comprehensive, structured clinical information, PROs (MDASI-BT and/or SP, Patient-Reported Outcome Measurement Information System

Abbreviations: CNS, Central Nervous System; HGNET-MN1, High-Grade Neuroepithelial Tumor with *MN1* Alteration; PNET, Primitive Neuroectodermal Tumor; GFAP, Glial Fibrillary Acidic Protein; INI1, Integrase interactor 1; L1CAM, L1 Cell Adhesion Molecule; NeuN, Neuronal Nuclear Protein; BRAF, v-Raf murine sarcoma viral oncogene homolog B; EMA, Epithelial Membrane Antigen; OLIG2, Oligodendrocyte Transcription Factor 2; PLAP, Placental Alkaline Phosphatase; HMB-45, Human Melanoma Black – 45; TERT, Telomerase Reverse Transcriptase; IDH, Isocitrate Dehydrogenase; MGMT, O[6]-methylguanine-DNA methyltransferase; PARP1, Poly(ADP-Ribose) Polymerase 1; RB1, RB Transcriptional Corepressor 1; KPS, Karnofsky Performance Status; MRI, Magnetic Resonance Imaging; CT, Computed Tomography; CLIA, Clinical Laboratory Improvement Amendments; NCI, National Cancer Institute; NIH, National Institutes of Health; NHS, Natural History Study; MDASI-BT, MD Anderson Symptom Inventory-Brain Tumor.

[PROMIS], NeuroQOL Cognition Function, and EQ-5D-3L) completed at baseline and each subsequent clinic visit, and collection of peripheral blood and tumor tissue samples.

Patient-reported outcomes

Symptom occurrence has been shown to predict treatment course and survival in patients with solid tumors. PROs provide information directly from patients about their symptoms, quality of life, and functional status associated with their tumor and/or treatment. PROs can help optimize patient care, provide information that goes beyond mere survival, and have not been previously reported for those diagnosed with *MN1*-altered CNS tumors.

The MD Anderson Symptom Inventory-Brain Tumor (MDASI-BT) is a validated instrument that allows self-reporting of symptom severity and interference with daily activities (5). The inventory utilizes a scoring system with 0 representing a symptom which was not present/did not interfere with the patient's life over the last 24 hours, to 10 which represents a symptom that is as bad as you could imagine and interfered completely with a patient's life. Scores of greater than or equal to 5 are considered moderate to severe.

Emotional state was assessed with "PROMIS-depression short form 8a" and "Anxiety short form 8a." Mean *t*-scores for depression and anxiety were calculated based on the general U.S. population mean *t*-score of 50. Mean *t*-scores greater than 60 indicate moderate to severe depression or anxiety.

Neuro-QoL Cognition Function measures self-perceived cognition; a mean *t*-score of 50 is considered average for the general U.S. population. Mean *t*-scores less than 40 are considered moderate to severe impairment of cognitive function.

EQ-5D-3L measures general health status. Responses can be described as health states, where each digit of the five-digit health state reflects the severity of its corresponding dimension. The "11111" health state reflects no problems in any dimension. An index score is calculated based on U.S. population weights and reflects the patient's perception of their own health. An index score of 1 indicates the patient perceives their health as perfect; an index score of 0 indicates they perceive their health as bad as death; and a negative index score indicates they perceive their health as worse than death.

Tumor testing

All tumor specimens were reviewed histologically, and molecular analysis was performed at the Laboratory of Pathology, NCI, Bethesda, Maryland. Methods are summarized in Supplementary Tables 4, 5. Final interpretation of each case was based on integration of methylation-based classification, histopathological findings, clinical history, and data reported in the biomedical literature.

Literature review

We performed a systematic review of the literature following the Preferred Reporting Items for Systematic Review and Meta-Analysis (PRISMA). In consultation with an NIH biomedical research librarian, a search was performed in PubMed (NLM), EMBASE (Elsevier), Web of Science (Clarivate), and Scopus (Elsevier) from December 2022 back to the start of each database. Due to few studies, we searched broadly for studies using only the key terms HGNET-MN1, astroblastoma, and MN1-altered in the topic fields and in the title/abstract fields. PubMed retrieval was 16 citations; EMBASE retrieval was 36 citations, Web of Science retrieval was 18 citations, and Scopus retrieval was 13 citations (Supplementary Figure 2). The total from all four databases was 83 citations. Of the 83 citations, 43 citations were duplicates. The remaining 40 citations were reviewed in full text based on our inclusion and exclusion criteria. Studies were included if they discussed the clinical management of the initial malignancy, provided patient OS and PFS, and there was a molecular diagnosis of HGNET-MN1 or astroblastoma-MN1 altered, at a minimum. Studies were excluded either due to there being a lack of molecular and/or detailed clinical data (reason 1), or due to the tumor being an extracranial lesion (reason 2). Of the 40 citations reviewed in full text, 9 of these studies were included in our manuscript, collectively describing 27 cases.

Patient 1

The patient is a 25-year-old female who was first diagnosed with a left fronto-parietal tumor at 5 years of age after presenting emergently with right-sided facial weakness and urinary incontinence. She underwent surgical resection outside the United States, and pathology was informed as "ependymoma". The tumor recurred when she was 7 years old, and she underwent additional surgical resection at that time and again one year later, then receiving 59.4 Gy involved brain field radiotherapy. After completing radiotherapy, she experienced her first seizure.

Her imaging remained stable for 16 years until medically refractory epilepsy prompted repeat imaging. A brain MRI with and without gadolinium at age 24 revealed a right fronto-parietal enhancing nodule within the resection cavity (Figure 1A). She underwent a gross total resection of this new enhancing nodule. Histopathology showed a tumor with moderate cellularity, composed of monomorphic cells with round/oval nuclei and rhabdoid appearance. Mitoses were rare. No areas of hemorrhage or tumor necrosis were observed. The tumor had discrete interface with surrounding brain parenchyma (Figure 2A). The neoplastic cells were positive for GFAP (subset) and INI (retained); while negative for L1CAM, NeuN, and BRAF V600E. Olig2 staining was not performed. Synaptophysin showed focal, often dot-like staining, of unclear significance; Ki67 proliferation index was low. Additional molecular analysis including genome-wide DNA methylation and gene panel *via* Oncomine Comprehensive Assay v3 were performed. Methylation class was "CNS high-grade neuroepithelial tumor with *MN1* alteration" (Figure 2D). MGMT promoter methylation was negative. Copy number variations can be found in Supplementary Figure 1. *SLX4* (p.Ala1755Val) and *ESR1* (p.Leu23Val) mutations were identified and classified as variants of uncertain significance (variant allele frequency 52.9% and 49.3%, respectively). Homozygous CDKN2A deletion was not observed. RNA sequencing was performed as a research test and a *MN1::BEND2* fusion was found. Tissue from the patient's two prior recurrences during her childhood were analyzed *via* DNA methylation and found to be also consistent with HGNET-MN1.

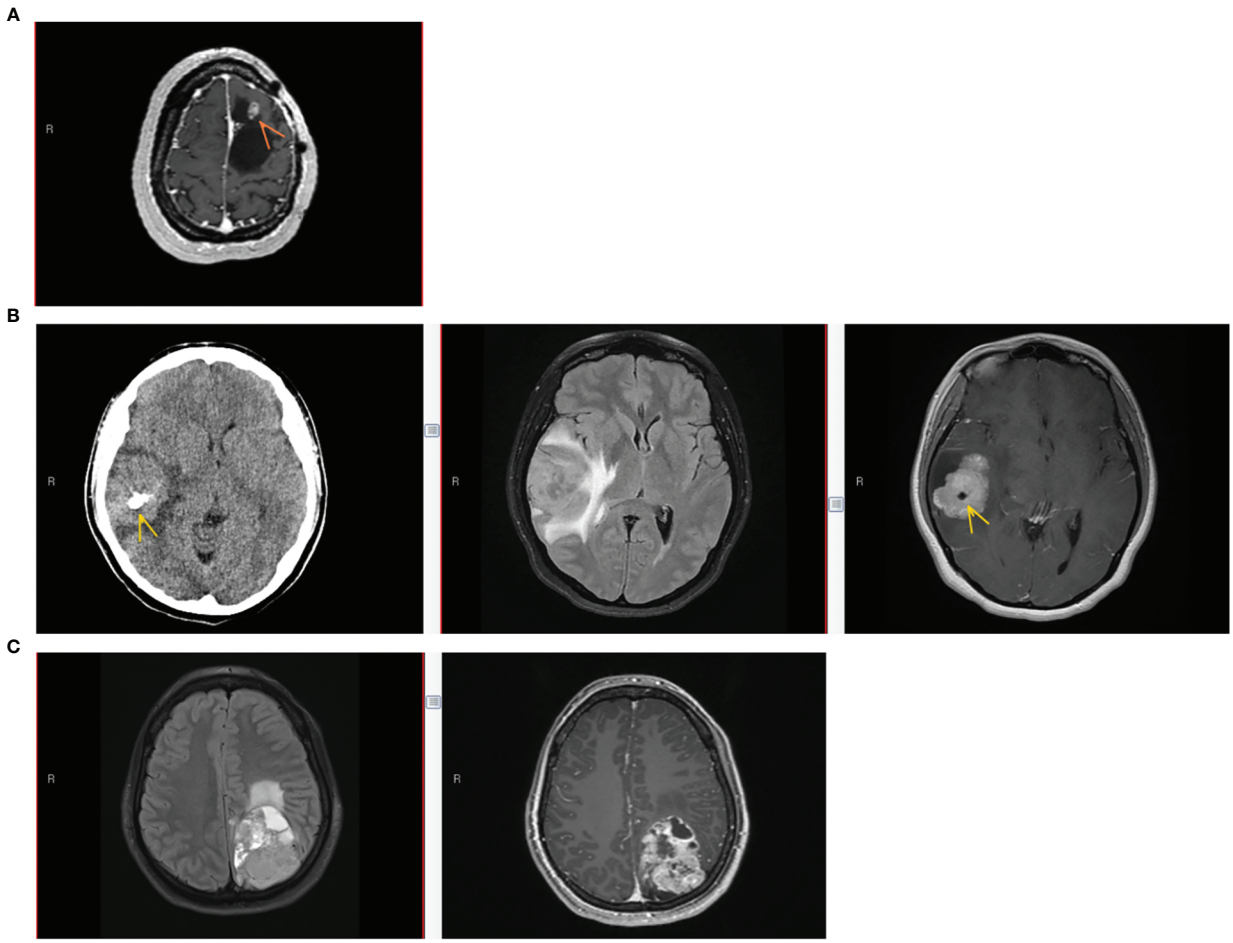

FIGURE 1
Patient imaging findings. **(A)** Patient #1 imaging findings at 3rd recurrence. Axial T1-weighted MRI with gadolinium showing an enhancing nodule (arrow) along the anterior-superior margin of the previous left frontal resection cavity. **(B)** Patient #2 imaging at initial presentation. Left to right: Axial CT without contrast, Axial T2/FLAIR MRI, and Axial T1-weighted MRI with gadolinium. Lobular homogeneously enhancing mass with cystic component in the right frontotemporal region, with vasogenic edema, mass effect, midline shift, and intratumoral calcification (arrow). **(C)** Patient #3 imaging at initial presentation. Left to right, Axial T2/FLAIR MRI, and Axial T1-weighted MRI with gadolinium. Large heterogeneously enhancing left parieto-occipital mass with perilesional edema and midline shift.

Following her most recent resection, she continued MRI surveillance, and her imaging has remained without evidence of recurrent or residual tumor for the last 3 years. Her most recent neurologic exam revealed weakness of her right hand and foot. She described having partial seizures occurring typically twice per month and lasting from 1 to 10 minutes, and generalized seizures occurring typically twice per year. She was receiving levetiracetam and lacosamide. In contrast with the stable imaging findings, PROs obtained during surveillance revealed seven symptoms rated as moderate to severe and with moderate to severe interference with daily activities (MDASI-BT), moderate to severe depressive symptoms (PROMIS), and an index score of 0.67 on EQ-5D-3L with some problems with walking and self-care and moderate pain/discomfort and moderate anxiety/depression (Table 1; Supplementary Tables 1–3).

Patient 2

This patient is a 29-year-old right-handed female who presented 2 years prior with worsening headaches, nausea and vomiting. A brain MRI revealed a right frontal-temporal mass (Figure 1B). She underwent surgical resection with pathology revealing a tumor composed of epithelioid cells forming vague rosettes and with patchy hyalinization of vessel walls, suggestive of a morphological diagnosis of astroblastoma (Figure 2B). No areas of hemorrhage or tumor necrosis were observed. The tumor was diffusely positive for vimentin but showed only patchy stain for GFAP. Only rare cells were positive for S-100. There was cytoplasmic staining for EMA, and synaptophysin showed dot-like positivity in the cytoplasm of tumor cells. Neuron-specific enolase also showed patchy staining within the tumor. INI-1 staining was retained by the tumor cells, and Olig2 staining was negative. Immunohistochemical stain for Ki-67 demonstrated a focal elevated labeling index of 10%–20%. Additional molecular analysis included genome-wide DNA methylation and next generation sequencing using a Primary CNS Tumor panel. Methylation class was "CNS high-grade neuroepithelial tumor with MN1 alteration" (Figure 2D). Copy number variations can be found in Supplementary Figure 1. *PARP1* (p.Trp481Cys) and *RB1* (p.Gin436Lys) mutations of uncertain significance with variant

10.3389/fonc.2023.1099618

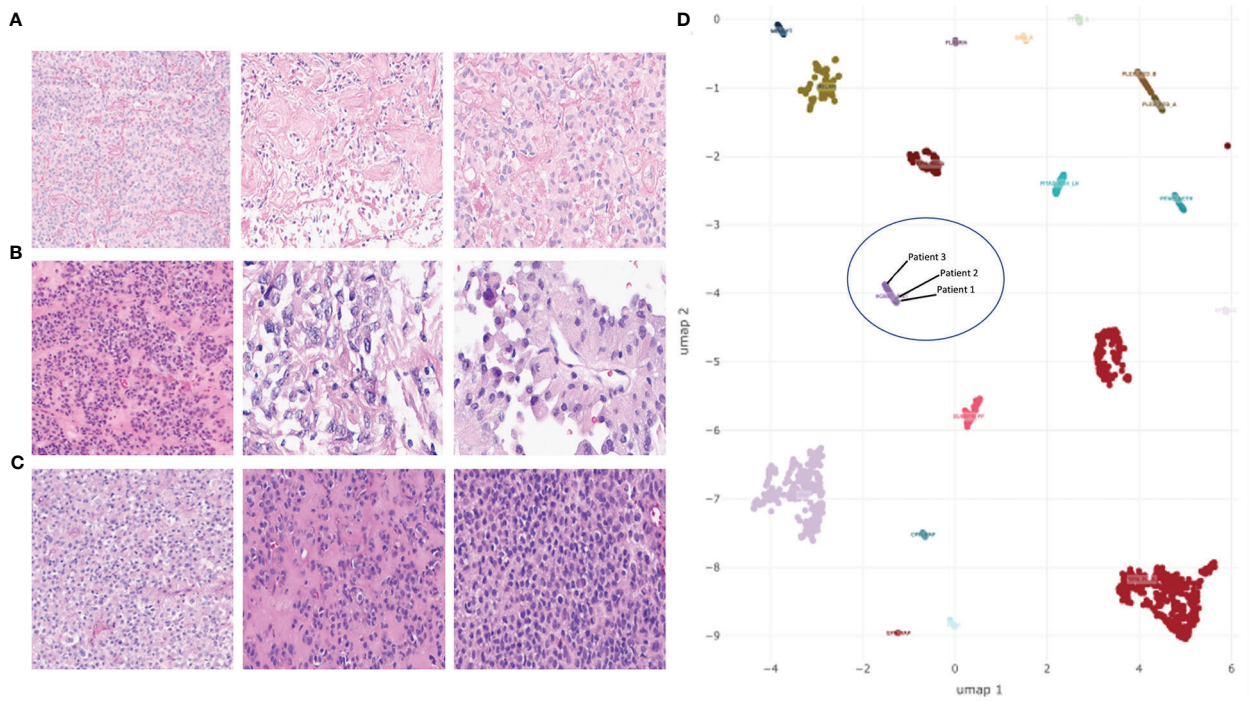

FIGURE 2
H&E-stained sections of tumors and UMAP embedding of DNA methylation array data for select tumor types. **(A–C)** H&E-stained sections showing the range of histologic characteristics of astroblastoma (wide-tapered perivascular pseudorosettes and prominent hyalinization) for patient 1 **(A)**, patient 2 **(B)**, and patient 3 **(C)**. **(D)** UMAP embedding of *MN1*-altered astroblastoma samples (HGNET-MN1), embedded among select groups of CNS tumors. Three samples from *MN1*-fused patients discussed in this study are included in a blue circle.

TABLE 1 MDASI-BT measurement of symptom burden and interference for Patients 1–3.

	Patient 1	Patient 2	Patient 3
Timing	Surveillance	Surveillance	Treatment initiation
Overall symptom factor	3.7	1.4	3.4
Affective factor	8.4	1.6	5.2
Cognitive factor	1.5	2.8	4.5
Neurologic factor	4.5	0.8	3.5
Treatment-related factor	4.0	1.3	2.0
General disease factor	1.0	1.0	2.5
Gastrointestinal factor	0.0	0.0	0.5
Number of moderate-severe symptoms	7	0	6
Overall interference	5.3	1.0	5.8
Activity-related interference	4.0	1.3	6.7
Mood-related interference	6.6	0.7	5.0
Moderate-severe interference	Yes	No	Yes

allele frequency of 53% and 49%, respectively, were identified. Homozygous CDKN2A deletion was not observed. RNA sequencing *via* CLIA testing revealed a *MN1::BEND2* fusion.

Following tumor resection, she underwent involved-field radiotherapy (unknown dose) with concurrent temozolomide completed 3 months after resection. Her imaging remained stable without evidence of recurrent or residual tumor at her last visit 2 years after treatment. As of the patient's most recent physical exam, her KPS score was rated as 90 with no major neurological deficit. PROs obtained during surveillance revealed no symptoms rated as moderate to severe, no moderate to severe interference with daily activities (MDASI-BT), no moderate to severe depressive or anxiety symptoms

(PROMIS), and an index score of 1.00 on EQ-5D-3L (Table 1; Supplementary Tables 1–3). She was not on any medications and continues brain MRI surveillance every 4–6 months.

Patient 3

This patient is a 36-year-old female who had presented emergently 3 years prior reporting bilateral headaches, right-sided blurry vision, and intermittent diplopia. She had right incomplete homonymous hemianopsia and a right cranial nerve VI palsy on exam. A brain MRI revealed a left parieto-occipital enhancing mass (Figure 1C). She underwent a complete surgical resection and outside pathology was reported as "CNS embryonal tumor with rhabdoid features". Histopathology revealed a malignant and infiltrative neoplasm composed of sheets of cells with abundant eosinophilic to clear cytoplasm, eccentric nuclei, and prominent nucleoli with associated areas of hemorrhage and tumor necrosis, but also perivascular pseudorosettes (Figure 2C). The neoplastic cells were positive for vimentin and glypican3 while negative for synaptophysin, GFAP, keratin and inhibin. EMA staining was focally positive. Olig2 staining was not performed. DNA methylation performed in two independent CLIA certified laboratories revealed a methylation class of "CNS high-grade neuroepithelial tumor with MN1 alteration" (Figure 2D). Copy number variations can be found in Supplementary Figure 1. No clinically relevant variants were detected *via* Primary CNS Tumor gene panel. Homozygous CDKN2A deletion was not observed. RNA sequencing *via* CLIA testing revealed a *MN1::BEND2* fusion.

She received craniospinal radiation to a total dose of 30.6 Gy in 17 fractions with a 30 Gy boost in 15 fractions to the left parietal surgical bed completed 3.5 months following resection. She experienced her first disease progression 7 months after the initial tumor resection and began receiving cisplatin and lomustine. She required dose reduction after 3 cycles due to myelosuppression. About 12 months following her initial diagnosis imaging showed a second tumor progression. She then underwent a second gross total resection followed by Gamma Knife radiosurgery (5 fractions to the left parietal region; dose unknown). Seven months later, imaging showed enlarging enhancement adjacent to the left parietal cavity with increased perilesional edema and enhancement extension into the craniotomy defect. Another subtotal resection confirmed tumor recurrence. She began exploring potential clinical trials at our center.

At the time of her first visit, her KPS score was rated as 80. She had dysarthric speech, a slow and cautious gait and was unable to perform tandem gait. She was on multiple medications including dexamethasone, oxycodone, docusate, pantoprazole, levetiracetam, ondansetron, aripiprazole, trazadone, benzonatate, albuterol inhaler, melatonin, and acetaminophen.

Her MRI revealed nodular contrast enhancement in the walls of the most recent resection cavity. She was tapered off dexamethasone and enrolled in a clinical trial on which she began receiving a checkpoint inhibitor. PROs obtained prior to treatment initiation revealed 6 symptoms rated as moderate to severe and with moderate to severe interference with daily activities (MDASI-BT), moderate to severe depressive symptoms (PROMIS), moderate to severe impairment in perceived cognition, and an index score of 0.71 on EQ-5D-3L with some problems with walking and performing usual activities, moderate pain/discomfort, and moderate anxiety/depression (Table 1; Supplementary Tables 1–3). Two months after starting experimental treatment her MRI showed increased T1 contrast enhancement in the occipital resection site with associated T2/FLAIR hyperintensity, extending into the left thalamus and left parietal lobe. With this imaging progression, the patient stopped receiving trial therapy and underwent surgical resection followed by treatment with bevacizumab. She continued to decline and died one year following her clinical trial enrollment and less than 3 years after initial diagnosis.

TABLE 2 Demographic, treatment, and outcome data of patients with *MN1*-altered CNS tumors.

Citation	Patient	Age at diagnosis (years)	Sex	Pathological diagnosis (morphological)	Initial treatment	Method used to diagnose *MN1*-altered CNS tumors	Recurrence	Treatment for recurrence	PFS	OS
(6)	1	6	Female	Anaplastic astroblastoma	GTR	DNA and RNA sequencing, RT-PCR, FISH Patient determined to have MN1: BEND2 fusion	Yes	Multiple resections; RT and TMZ for 2nd recurrence; CCNU/TMZ for 3rd recurrence.	7 Months	10 Years
(7)	2	9	Female	Recurrent astroblastoma	SR	DNA Methylation, FISH	Yes	RT	Unknown	+27 Years
(7)	3	10	Female	Anaplastic astroblastoma	SR with RT and TMZ	DNA Methylation, FISH	No	N/A	+2.8 Years	+2.8 Years

(Continued)

TABLE 2 Continued

Citation	Patient	Age at diagnosis (years)	Sex	Pathological diagnosis (morphological)	Initial treatment	Method used to diagnose *MN1*-altered CNS tumors	Recurrence	Treatment for recurrence	PFS	OS
(7)	4	31	Female	Malignant glioma, features suggestive of astroblastoma	SR with RT and TMZ	DNA Methylation, FISH	No	N/A	+1 Year	+1 Year
(8)	5	4	Female	Low-grade astroblastoma	GTR	DNA Methylation	No	N/A	+21 Months	+21 Months
(9)	6	4.8	Female	"Four of 10 supratentorial lesions were initially diagnosed morphologically as anaplastic ependymoma. Other diagnoses included peripheral primitive neuroectodermal tumors (one), embryonal tumor not otherwise specified (NOS) (one), atypical glial neoplasia (two), malignant tumor with rhabdoid characteristics (one), and astroblastoma (two). All three spinal tumors were morphologically consistent with ependymoma." **	GTR with RT (Focal, 59.4 Gy)	Genome-wide methylation arrays/RT-PCR 2 patients determined to have MN1: BEND2 fusion **	No	N/A	+11 Months	+11 Months
(9)	7	5.8	Female	see above "**"	GTR	Genome-wide methylation arrays/RT-PCR see above "**"	No	N/A	+24 Months	+24 Months
(9)	8	8.9	Female	see above "**"	GTR with RT (Focal, 50 Gy) and VAC/VAdriaC	Genome-wide methylation arrays/RT-PCR see above "**"	No	N/A	+9.6 Years	+9.6 Years
(9)	9	5	Female	see above "**"	STR	Genome-wide methylation arrays/RT-PCR see above "**"	Yes	STR with RT (Focal, 45 Gy)	15 Months	+18 Months
(9)	10	4.5	Female	see above "**"	GTR with RT (Focal, 54 Gy)	Genome-wide methylation arrays/RT-PCR see above "**"	Yes	GTR with CP/celecoxib	26.4 Months	35.4 Months

(Continued)

TABLE 2 Continued

Citation	Patient	Age at diagnosis (years)	Sex	Pathological diagnosis (morphological)	Initial treatment	Method used to diagnose *MN1*-altered CNS tumors	Recurrence	Treatment for recurrence	PFS	OS
(9)	11	7	Female	see above "**"	GTR with RT (Focal, 59.4 Gy)	Genome-wide methylation arrays/RT-PCR see above "**"	Yes	GTR with RT (CSI, 36 Gy + Boost)	3 Years	6 Years
(9)	12	3.6	Female	see above "**"	STR	Genome-wide methylation arrays/RT-PCR see above "**"	Yes	GTR with RT (Focal, 54 Gy) and VCR/VP/CP	6 Months	+16 Years
(9)	13	6.7	Female	see above "**"	GTR with RT (CSI, 36 Gy + Boost) and SJMB12	Genome-wide methylation arrays/RT-PCR see above "**"	No	N/A	+25 Months	+25 Months
(9)	14	14.6	Male	see above "**"	STR with RT (Focal, 45 Gy)	Genome-wide methylation arrays/RT-PCR see above "**"	Yes	RT (CSI, 36 Gy + Boost) and Oral VP	23 Months	7.3 Years
(9)	15	13	Female	see above "**"	GTR	Genome-wide methylation arrays/RT-PCR see above "**"	No	N/A	+24 Months	+24 Months
(9)	16	36	Male	see above "**"	STR with RT (CyberKnife)	Genome-wide methylation arrays/RT-PCR see above "**"	Yes	STR	5 Years	+11 Years
(9)	17	10	Female	see above "**"	GTR	Genome-wide methylation arrays/RT-PCR see above "**"	No	N/A	+8.3 Years	+8.3 Years
(9)	18	8	Female	see above "**"	GTR with RT (CSI, 23.5 Gy + Boost) and SJMB-96	Genome-wide methylation arrays/RT-PCR see above "**"	Yes	GTR with RT (Focal, 50.4 Gy) and 5D	5.2 Years	+7.5 Years

(Continued)

TABLE 2 Continued

Citation	Patient	Age at diagnosis (years)	Sex	Pathological diagnosis (morphological)	Initial treatment	Method used to diagnose *MN1*-altered CNS tumors	Recurrence	Treatment for recurrence	PFS	OS
(9)	19	14	Female	see above "**"	GTR	Genome-wide methylation arrays/RT-PCR see above "**"	No	N/A	+5.3 Years	+5.3 Years
(10)	20	9	Female	Yolk sac carcinoma	STR with chemotherapy	RT-PCR Patient determined to have MN1: BEND2 fusion	Yes	Gamma knife radiosurgery and chemotherapy - GTR following recurrence	8 Months	+12 Months
(11)	21	24	Female	High-grade astroblastoma	GTR with RT (Local, 50 Gy)	FISH Patient determined to have MN1: BEND2 fusion	Yes	GTR	12 Years	+13 Years
(12)	22	36	Female	Low-grade astroblastoma	GTR	Not Reported	Yes	RT for 1st progression STR for 2nd progression Hypo-fractionated stereotactic radiosurgery for 3rd progression, followed by Temozolomide x 6 cycles. GTR for 4th progression followed by bevacizumab and lomustine x 4 cycles.	24 Months	+15 Years
(13)	23	13	Female	Astroblastoma	GTR	Whole Genome Sequencing (WGS) Patient determined to have MN1:GTSE1 and EWSR1: PATZ1 fusions	No	N/A	+36 Months	+36 Months
(14)	24	9	Female	Malignant tumor with papillary and rhabdoid pattern	GTR with RT (Focal, 50 Gy) and VAC/ VAdriaC	DNA methylation Patient determined to have MN1: BEND2 fusion	No	N/A	+10 Years	+10 Years

(Continued)

TABLE 2 Continued

Citation	Patient	Age at diagnosis (years)	Sex	Pathological diagnosis (morphological)	Initial treatment	Method used to diagnose *MN1*-altered CNS tumors	Recurrence	Treatment for recurrence	PFS	OS
(14)	25	10	Female	Gliofibroma	GTR	RT-PCR Patient determined to have MN1: BEND2 fusion	No	N/A	+2 Years	+2 Years
(14)	26	6	Female	PXA vs ABM; non-typical tumor	GTR	DNA methylation Patient determined to have MN1: BEND2 fusion	No	N/A	+3 Years	+3 Years
(14)	27	4.9	Female	Ependymoma vs ABM vs HGNET-MN1 tumor	GTR with RT (Focal, 59.4 Gy)	RT-PCR Patient determined to have MN1: BEND2 fusion	No	N/A	+2 Years	+2 Years
This Manuscript	28	5	Female	Ependymoma	SR	DNA methylation, RNA sequencing Patient determined to have MN1: BEND2 fusion	Yes	SR for 1st recurrence, RT (59.4 Gy) for 2nd recurrence, GTR for 3rd recurrence.	~24 Months	+21 Years
This Manuscript	29	27	Female	Astroblastoma	SR with RT and TMZ	DNA methylation, RNA sequencing Patient determined to have MN1: BEND2 fusion	No	N/A	+28 Months	+28 Months
This Manuscript	30	33	Female	CNS embryonal tumor with rhabdoid features	SR with RT (30.6 Gy + Boost)	DNA methylation, RNA sequencing Patient determined to have MN1: BEND2 fusion	Yes	GTR, CIS and CCNU, and RT for 1st recurrence. STR for 2nd recurrence with checkpoint inhibitor	~7 Months	2.9 Years

SR, Surgical Resection; GTR, Gross Total Resection; STR, Subtotal Resection; TMZ, Temozolomide; RT, Radiation Therapy; VAC, vincristine-actinomycin D-cyclophosphamide; VAdriaC, vincristine-adriamycin-cyclophosphamide; VCR, vincristine; VP, etoposide; SJMB12, St Jude medulloblastoma regimen; SJMB-96, St Jude medulloblastoma-96 regimen; CP, cyclophosphamide; 5D, five drugs; CIS, cisplatin; CCNU, lomustine; FISH, Fluorescence In Situ Hybridization.

Literature review

Table 2 summarizes the demographic, diagnostic, treatment, and outcome data of previously published cases of astroblastoma *MN1*-altered and HGNET-MN1 from the 9 studies meeting our inclusion criteria. A total of 30 cases are included in the table (27 previously published plus the three reported in this manuscript). Among these cases, the median age at diagnosis was 9 years with a range of 3.6 to 36 years old. Only six of the 30 patients were diagnosed as adults (18 years of age and older), including 2 of our patients. Only two of the 30 patients were male.

The most common morphological diagnoses prior to a molecular diagnosis of an *MN1*-altered tumor were astroblastoma or ependymoma. During follow up of variable duration, 14 of the 30 patients (46.7%) experienced at least one recurrence of their disease; however, 25 of the 30 (83.3%) were still alive at the time of their last follow up. The shortest progression-free survival (PFS) was 6 months whereas the longest was 12 years. The shortest surviving patient died 35 months (2.9 years) after diagnosis. The longest survival was 27 years, with the patient still alive at the last follow up. We did not identify any other manuscript reporting PROs in patients with this diagnosis.

Discussion

MN1-altered CNS tumors are a newly described and uncommon diagnostic entity. Our NHS, which enrolls adults with primary CNS tumors and routinely incorporates tumor testing with DNA methylation and next generation sequencing panels, identified three participants (all female) with this diagnosis whose comprehensive longitudinal clinical information including PROs, imaging findings and tumor analysis are presented in this manuscript. Two of our patients were diagnosed as young adults, and one experienced a late recurrence as an adult after a prolonged period of stabilization of a tumor diagnosed in her childhood.

Our systematic literature review identified 40 publications of which only 9 provided sufficient information for inclusion. Only four of the 27 cases identified in these 9 publications were diagnosed as adults, indicating the very uncommon presentation in this age group, although this may also reflect a general paucity of advanced molecular testing of primary CNS tumors in adults outside of specialized centers. Few publications discuss the detailed clinical features, management, and outcome of these tumors in adults, and we provide valuable information on the clinical course, diagnosis, and management of this disease.

Our three patients received an integrated diagnosis of HGNET-MN1 before the publication of the latest 2021 WHO classification recommending the term astroblastoma, *MN1*-altered. We found, that despite sharing the same DNA methylation profile and *MN1::BEND2* gene fusion, survival and functional outcomes were quite heterogenous, as reflected by their variable clinical course and our patient's self-reported symptom burden. Two of our three patients were highly symptomatic, including depression and anxiety and reported an impact on their general health status (one reported this despite the context of prolonged tumor control), highlighting the importance of understanding the patient's experience in addition to simply analyzing survival data.

Furthermore, the limited existing literature also suggests that outcomes measured as either OS or PFS do not appear to correlate with factors such as age at diagnosis, sex, or initial treatment. Some patients experience a short PFS and multiple recurrences despite treatment with surgery, radiation, and chemotherapy, while others experience years long PFS and OS after only having undergone surgical resection. The determinants of this vast difference in outcomes despite the unifying molecular diagnosis remain unknown and likely include clinical features, tumor genomics and treatment modalities. Table 2 also highlights a discrepancy between PFS and OS as many patients experience short PFS yet prolonged OS with some experiencing late recurrences (9, 11). Sturm and colleagues reported that of the eight patients diagnosed with HGNET-MN1 in their study, 100% experienced an overall survival (OS) beyond 8 years, but only two had a progression-free survival (PFS) that extended beyond 6 years (2). This discrepancy between PFS and OS was also noted by Lehman and colleagues, who found that patients with MN1-rearranged CNS tumors had a clear and significant survival advantage compared to $BRAF^{V600E}$-mutant tumors, and patients bearing MN1-rearrangements were all alive at the time of publication despite multiple recurrences in some cases (15).

The presence of specific interchromosomal gene fusions may impact survival in patients diagnosed with *MN1*-altered tumors as five of the patients included in our review possessed an *MN1::BEND2* fusion with two of these patients having an OS surpassing 100 months (8.3 years). However, one of our patients with an *MN1::BEND2* fusion (Patient 3) experienced her first recurrence only 7 months after her original diagnosis despite intensive therapy and died in 3 years. We acknowledge that the number of cases with reported gene fusions is very small as a comprehensive molecular profile likely remains unexplored in many patients. Systematic analysis of the presence of specific interchromosomal gene fusions and detailed prospective collection of treatment data may provide further insight into whether specific fusions impact OS and PFS.

Although a specific type of interchromosomal gene fusion may be a contributing factor to these differences in outcome, it is likely not the only one. Of four tumors analyzed using RNA sequencing by Sturm and colleagues, gene fusions between *MN1* and *BEN domain containing 2* (*BEND2*) were observed in three samples (2). An additional gene fusion was observed between *MN1* and *CXXC-type zinc finger protein 5* (*CXXC5*) in another sample (2). High expression levels of BEND2 (a fusion partner) were uniquely observed in HGNET-MN1 tumors distinct from other CNS tumor types (2). Moreover, a set of samples including the tumor harboring the *MN1::CXXC5* fusion formed a distinctly separate cluster *via* t-SNE analysis (t-distributed stochastic neighbor embedding), while all three tumors harboring *MN1::BEND2* fusion were found in a larger homogenous cluster, potentially indicating differences in underlying biology, and therefore outcomes, depending on the *MN1* fusion partner. These findings indicate not only the need for further molecular characterization of these tumors, but also the collection of detailed clinical and treatment data as these may act as other important factors determining outcome.

Currently, only advanced methods such as DNA methylation profiling and targeted next generation sequencing can confirm this

diagnosis both in tumors morphologically diagnosed as astroblastomas, and in tumors with histological features that resemble other diagnoses or are insufficient for a specific morphological diagnosis. Hopefully, with the increased recognition of the utility of advanced molecular testing, these tests will be more accessible enabling more accurate diagnosis of a variety of primary CNS cancers. This increase in diagnostic precision will allow better characterization of the natural history of this tumor, ultimately providing important prognostic information and guiding therapy. However, it is essential to collect large series of well annotated and comprehensive clinical, treatment, and outcome data to help decipher prognostic and predictive factors of this and other emergent rare CNS tumors defined by their molecular features.

Data availability statement

The datasets presented in this study can be found in online repositories. The names of the repository/repositories and accession number(s) can be found in the article/Supplementary Material.

Ethics statement

The three cases discussed in this manuscript were retrieved from enrollees in an IRB-approved Natural History Study at the Neuro-Oncology Branch, National Cancer Institute, National Institutes of Health (NCT02851706; Natural History of and Specimen Banking for People with Tumors of the CNS). The patients/participants provided their written informed consent to participate in this study. Written informed consent was obtained from the individual(s) for the publication of any potentially identifiable images or data included in this article.

Author contributions

This study was conceptualized and designed by SF and MP-P. A review of the literature was performed by SF and DC. TA is the PI and AA, NB, AnC, AlC, EG, TK, HL, and JL are the core team of the study from which clinical data was collected. LB, NL, KW, MP-P and MG provided direct clinical care to patients included in this manuscript. The data was analyzed and interpreted by SF, MP-P, EV, KA, DP, MQ, RS, TA and MG. SF and MP-P wrote the initial draft of the manuscript. SF, ZA and MP-P created the figures for the manuscript, and MP-P supervised the study. All coauthors reviewed and agreed with the final manuscript. All authors contributed to the article and approved the submitted version.

Funding

This research was supported by the Intramural Research Program of the National Institutes of Health (NIH), National Cancer Institute, NIH Library, and the Center for Cancer Research.

Acknowledgments

The authors thank Yolanda L. Jones, NIH Library, for editing assistance.

Conflict of interest

The authors declare that the research was conducted in the absence of any commercial or financial relationships that could be construed as a potential conflict of interest.

Publisher's note

All claims expressed in this article are solely those of the authors and do not necessarily represent those of their affiliated organizations, or those of the publisher, the editors and the reviewers. Any product that may be evaluated in this article, or claim that may be made by its manufacturer, is not guaranteed or endorsed by the publisher.

Supplementary material

The Supplementary Material for this article can be found online at: https://www.frontiersin.org/articles/10.3389/fonc.2023.1099618/full#supplementary-material

SUPPLEMENTARY FIGURE 1
Copy number variations obtained *via* DNA methylation analysis in patients 1 (A), 2 (B), and 3 (C). A range of copy number patterns were observed in these tumors. Patient 3 showed both whole-chromosome and partial chromosome gains and losses. Patient 3 also showed alterations in chromosome 22q and X, possibly related to a chromosomal rearrangement leading to MN1::BEND2 fusion.

SUPPLEMENTARY FIGURE 2
PRISMA Flow Diagram Highlighting Included and Excluded Studies. A total of 83 citations were identified from four databases using the search terms HGNET-MN1, astroblastoma, and MN1-altered. 43 of these citations were removed due to being duplicated. 40 studies were assessed for eligibility. 28 studies were excluded due to there being a lack of molecular and/or clinical data (reason 1), and 3 studies were excluded due to the tumor being an extracranial lesion (reason 2). Of the 40 studies assessed for eligibility, a total of 9 were included in our review.

References

1. Tauziède-Espariat A, Pagès M, Roux A, Siegfried A, Uro-Coste E, Nicaise Y, et al. Pediatric methylation class HGNET-MN1: Unresolved issues with terminology and grading. *Acta Neuropathol Commun* (2019) 7(1):176. doi: 10.1186/s40478-019-0834-z

2. Sturm D, Orr BA, Toprak UH, Hovestadt V, Jones DTW, Capper D, et al. New brain tumor entities emerge from molecular classification of CNS-PNETs. *Cell* (2016) 164 (5):1060–72. doi: 10.1016/j.cell.2016.01.015

3. Board WCoTE. Central nervous system tumours. *Int Agency Res Cancer* (2021) 6(5).

4. Louis DN, Perry A, Wesseling P, Brat DJ, Cree IA, Figarella-Branger D, et al. The 2021 WHO classification of tumors of the central nervous system: A summary. *Neuro Oncol* (2021) 23(8):1231–51. doi: 10.1093/neuonc/noab106

5. Armstrong TS, Mendoza T, Gning I, Coco C, Cohen MZ, Eriksen L, et al. Validation of the M.D. Anderson symptom inventory brain tumor module (MDASI-BT). *J Neurooncol* (2006) 80(1):27–35. doi: 10.1007/s11060-006-9135-z

6. Burford A, Mackay A, Popov S, Vinci M, Carvalho D, Clarke M, et al. The ten-year evolutionary trajectory of a highly recurrent paediatric high grade neuroepithelial tumour with MN1:BEND2 fusion. *Sci Rep* (2018) 8(1):1032. doi: 10.1038/s41598-018-19389-9

7. Wood MD, Tihan T, Perry A, Chacko G, Turner C, Pu C, et al. Multimodal molecular analysis of astroblastoma enables reclassification of most cases into more specific molecular entities. *Brain Pathol* (2018) 28(2):192–202. doi: 10.1111/bpa.12561

8. Petruzzellis G, Alessi I, Colafati GS, Diomedi-Camassei F, Ciolfi A, Pedace L, et al. Role of DNA methylation profile in diagnosing astroblastoma: A case report and literature review. *Front Genet* (2019) 10:391. doi: 10.3389/fgene.2019.00391

9. Baroni LV, Rugilo C, Lubieniecki F, Sampor C, Freytes C, Nobre L, et al. Treatment response of CNS high-grade neuroepithelial tumors with MN1 alteration. *Pediatr Blood Cancer* (2020) 67(12):e28627. doi: 10.1002/pbc.28627

10. Chen W, Soon YY, Pratiseyo PD, Sutanto R, Hendriansyah L, Kuick CH, et al. Central nervous system neuroepithelial tumors with MN1-alteration: An individual patient data meta-analysis of 73 cases. *Brain Tumor Pathol* (2020) 37(4):145–53. doi: 10.1007/s10014-020-00372-0

11. Ujihara M, Mishima K, Sasaki A, Adach JI, Shirahata M, Suzuki T, et al. Unique pathological findings of astroblastoma with MN1 alteration in a patient with late recurrence. *Brain Tumor Pathol* (2021) 38:243–249. doi: 10.1007/s10014-021-00401-6

12. Gopakumar S, McDonald MF, Sharma H, Tatsui CE, Fuller GN, Rao G. Recurrent HGNET-MN1 altered (astroblastoma MN1-altered) of the foramen magnum: Case report and molecular classification. *Surg Neurol Int* (2022) 13:139. doi: 10.25259/SNI_1208_2021

13. Chadda KR, Holland K, Scoffings D, Dean A, Pickles JC, Behjati S, et al. A rare case of paediatric astroblastoma with concomitant MN1-GTSE1 and EWSR1-PATZ1 gene fusions altering management. *Neuropathol Appl Neurobiol* (2021) 47(6):882–8. doi: 10.1111/nan.12701

14. Lubieniecki F, Vazquez V, Lamas GS, Camarero S, Nuñez FJ, Baroni L, et al. The spectrum of morphological findings in pediatric central nervous system MN1-fusion-positive neuroepithelial tumors. *Childs Nervous System* (2022). doi: 10.1007/s00381-022-05741-y

15. Lehman NL, Usubalieva A, Lin T, Allen SJ, Tran QT, Mobley BC, et al. Genomic analysis demonstrates that histologically-defined astroblastomas are molecularly heterogeneous and that tumors with MN1 rearrangement exhibit the most favorable prognosis. *Acta Neuropathol Commun* (2019) 7(1):42. doi: 10.1186/s40478-019-0689-3

frontiers | Frontiers in Oncology

TYPE Case Report
PUBLISHED 07 February 2023
DOI 10.3389/fonc.2023.1087232

OPEN ACCESS

EDITED BY
Laura Gatti,
IRCCS Carlo Besta Neurological Institute Foundation, Italy

REVIEWED BY
Tao Wu,
Henan University of Traditional Chinese Medicine, China
Ignazio Gaspare Vetrano,
IRCCS Carlo Besta Neurological Institute Foundation, Italy

*CORRESPONDENCE
Xintao Huang
xintaoh@hotmail.com

SPECIALTY SECTION
This article was submitted to Neuro-Oncology and Neurosurgical Oncology, a section of the journal Frontiers in Oncology

RECEIVED 02 November 2022
ACCEPTED 25 January 2023
PUBLISHED 07 February 2023

CITATION
Wang Y, Yang Y, Wang Q, Wang C, Xu X, Wang D, Bai F, Li P and Huang X (2023) Sellar B lymphoblastic lymphoma mimics pituitary apoplexy with newly discovered gene mutations in TP53 and PAX5: A case report.
Front. Oncol. 13:1087232.
doi: 10.3389/fonc.2023.1087232

Sellar B lymphoblastic lymphoma mimics pituitary apoplexy with newly discovered gene mutations in TP53 and PAX5: A case report

Yi Wang[1], Yajun Yang[1], Qiuxia Wang[2], Ce Wang[1], Xinjuan Xu[3], Dongao Wang[4], Feirong Bai[4], Panpan Li[1] and Xintao Huang[4]*

[1]Department of Neurosurgery, First Hospital of Shanxi Medical University; and The First School of Clinical Medicine, Shanxi Medical University, Taiyuan, Shanxi, China, [2]Department of Gastroenterology, Affiliated Hospital of Southwest Medical University, Luzhou, Sichuan, China, [3]Department of Neurosurgery, Shanxi Cardiovascular Disease Hospital, Taiyuan, Shanxi, China, [4]Department of Neurosurgery, First Hospital of Shanxi Medical University, Taiyuan, Shanxi, China

Lymphoblastic lymphoma (LBL) is a rare tumor that accounts for approximately 2-4% of all non-Hodgkin lymphomas, and less than 20% of LBLs are derived from B cells. B- Lymphoblastic lymphoma (B-LBL) often presents as bone marrow and peripheral blood lesions, and is very rare to present as a seller mass. We report a case of sellar B lymphoblastic lymphoma mimicking pituitary apoplexy, and review its diagnosis and treatment process, combined with the literature to deepen the understanding of sellar tumors.

KEYWORDS

B-LBL, sellar tumor, rare, gene mutation, Pax5, TP53

Introduction

Lymphoblastic lymphoma (LBL) is a rare type of aggressive non-Hodgkins lymphoma (NHL). In the 2017 WHO classification, LBL is classified together with acute lymphoblastic leukemia (ALL) as ALL/LBL, and LBL is conventionally distinguished from ALL by less than 20–25% marrow infiltrating blasts cells (1). LBL represents 2-4% of adult NHL, divided into B cell LBL (B-LBL) and T cell LBL (T-LBL), but only 20% of them are derived from precursor B cells (2). The global incidence of B-LBL/ALL is about 1-5/100000 persons per year (3). Up to now, only one case of B-LBL in sellar has been reported and diagnosed as primary pituitary stalk B-LBL (4). Due to the extreme rarity of sellar B-LBL, its incidence and prevalence cannot be estimated.

Case presentation

A 22-year-old male was presented to our hospital in May 2022 with “sudden drop of left eye vision for one week.” The patient had been healthy prior to the onset of his illness, and denied family history of genetic disease. Visual assessment: visual acuity was 0.2 in the left eye and 1.0 in the right eye. Fundus examinations disclosed optic disc edema in

the left eye. Acuity examinations showed inferonasal sector hemianopia in the left eye and superonasal sector hemianopia in the right eye. He underwent MRI at another hospital 2 days before admission; Results showed that the sella was expanded, with an oval slightly long T1 and long T2 abnormal signal, and there was uneven enhancement and a clear boundary; The lesion size was 2.16x1.60x2.16cm (Figures 1A–C). A diagnosis of a large pituitary macroadenoma with compression of the left optic chiasm was considered. His disease progressed rapidly. On the afternoon of admission, he presented with a sudden decrease in visual acuity in his right eye, and his visual acuity of the right eye improved slightly after rapid infusion of mannitol and dexamethasone. CT of the head showed that a hyperdense nodules can be seen inside the pituitary fossa (Figure 1D). We considered it to be a pituitary apoplexy. Then, an emergency craniotomy was performed. Preoperative tests: 1. Blood routine examination: leucocyte [8.6×10^9/L (3.5-9.5)], absolute value of lymphocytes [1.22×10^9/L (1.1-3.2)], lymphocyte percentage [14.3% (20-50)]; 2. endocrine tests: cortisol [1174nmol/L (171-536)] was elevated, and other hormones were normal; 3. HIV (-). We found the tumor had an outer envelope, with tough texture and a very rich blood supply during surgery (Figure 1E). All eyes had significantly improved vision without diabetes insipidus and electrolyte disturbance after surgery. Pathological results: B-lymphoblastic lymphoma (Figure 1F). Immunohistochemistry results: CD10(+ +), CD79A (+), KI67(+ 90%), P53(10% +), TDT (65%), Syn (+), BCL-6(+), BCL-2(> 90% +), LMO2(+), PAX5(+), CD99(+), CD20(-). Bone marrow specimens were evaluated by flow cytometry, and we found that B lymphocytes with CD19+CD20+ accounted for about 19.8% of lymphocytes, with polyclonal expression of Kappa and Lambda (Figures 1G, H), but no obvious abnormal immunophenotype cells were found. Next-generation sequencing was performed on tumor tissue to detect of 93 gene variants associated with lymphoma, and six variations in five genes were found (Table 1). *PAX5* c.913_923delCGTGACTTGGC (p.R305Efs*32) and *TP53* c.969_971delGGAinsAGGC (p.D324Gfs*13) are not recorded in COSMIC, MSK database, and both of them are new discoveries. One month after surgery, he underwent a PET/CT examination, which showed that the tumor had invaded both kidneys, ureters, prostate, pelvis, and left femoral head and neck. There was no tumor recurrence when he had his

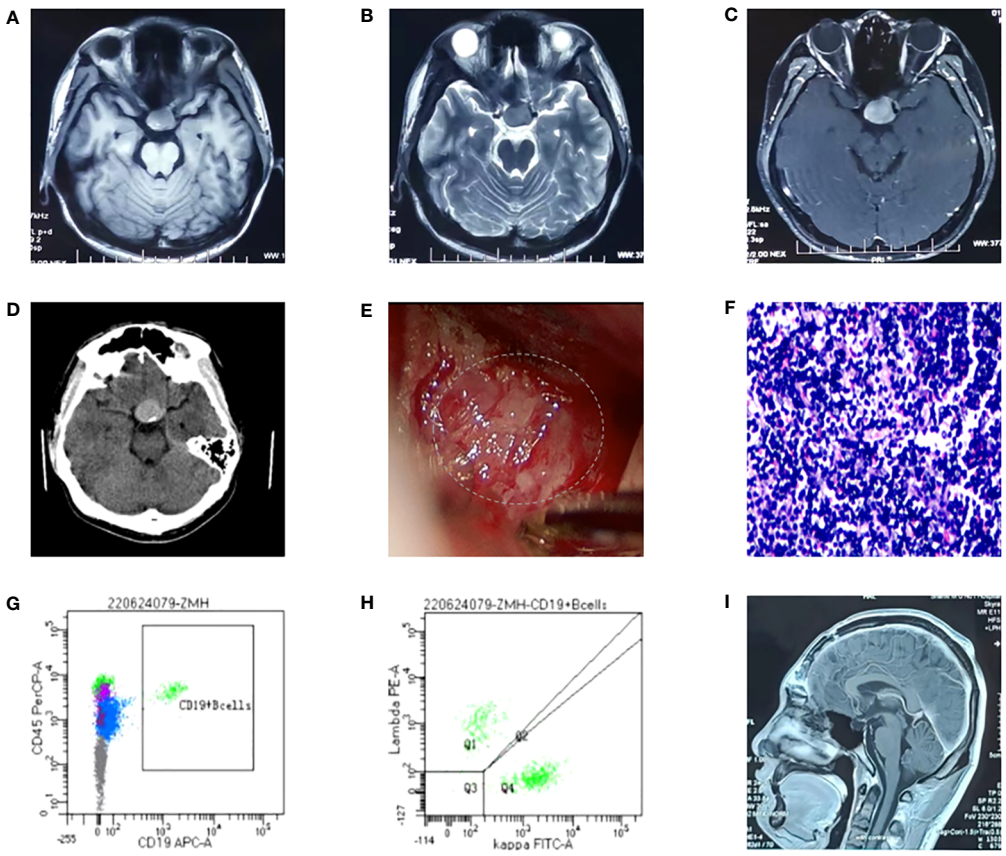

FIGURE 1
(A-C) Head MRI: the sella was expanded, with an oval slightly long T1 and long T2 abnormal signal, and there was uneven enhancement and a clear boundary. The neurohypophysis is clearly shown, the left optic chiasm is compressed, and the internal carotid artery in the left cavernous sinus is partially surrounded. The intracranial segment of the left optic nerve were compressed and slightly thinned, and the enhanced scan showed mild enhancement; **(D)** Head CT: the sella is enlarged, high-density nodules are seen in the pituitary fossa, the size is about 2.1*2.8cm, and the CT value is about 56HU; **(E)** The tumor was found to have abundant blood supply during the operation; **(F)** Pathological section: Proliferating tumor cells and have a starry sky appearance and they are dense, with medium cell volume, thin cytoplasm, large and slightly irregular nuclei, and fine chromatin; **(G, H)** Flow cytometry, and we found that B lymphocytes with CD19+CD20+ accounted for about 19.8% of lymphocytes, with polyclonal expression of Kappa and Lambda; **(I)** Postoperative re-examination of head MRI showed no tumor recurrence.

TABLE 1 Genome variation detection results.

Gene	Transcript	Base changes	Amino acid changes	Functional regions	Variation frequency/copy number
PAX5	NM_016734.1	c.77T>G	p.V26G	EX2	45.8%
PAX5	NM_016734.1	c.913_923del CGTGACTTGGC	p.R305Efs*32	EX8	33.8%
TP53	NM_000546.5	c.969_971del GGAinsAGGC	p.D324Gfs*13	EX9	3.8%
XPO1	NM_003400.3	c.1711G>A	p.E571K	EX15	1.3%
CDKN2A	NM_000077.4	missing	-	9p21.3	0.5
CDKN2B	NM_004936.3	missing	-	9p21.3	0.4

1. The table only lists the functional variations in the coding regions of important genes; 2. Mutation frequency refers to the proportion of mutations found at this locus in the total of wild type and mutant alleles during allele testing; 3. The normal value of copy number is 1.
"*" is used for nucleotide numbering and indicates the translation termination codon.
"-" means blank.

second MRI in October 2022 (Figure 1I). On October 26, 2022, the patient had a re-examination of PET/CT and found that the increased FDG uptake in his both kidneys, ureters, prostate, pelvis, and left femoral head and neck were reduced compared with the previous range, and the extent of lymphoma involvement was relieved. Until mid-December, he had been receiving 4 rounds of hyper-CVAD chemotherapy at our institution, and complications such as acute pancreatitis and anemia occurred. The patient now claims that his left eye vision is worse than postoperative and cannot take care of himself. Next step he is going to undergo stem cell transplant treatment.

Discussion

Initially, we considered the sudden loss of vision in his right eye as pituitary apoplexy, but we found that the tumor had invaded the right optic canal and did not find any evidence of pituitary apoplexy during the surgery. Reviewing the diagnosis and treatment process of this case, his medical history, clinical symptoms, signs, laboratory findings and radiological characteristics were consistent with pituitary adenoma, so it was easy to be misdiagnosed as pituitary apoplexy. A retrospective study showed that the clinical manifestations of pituitary lymphoma were similar to those of invasive pituitary adenoma, and half of patients show clinical and/or laboratory evidence of hypopituitarism at diagnosis. In addition, 50% of the patients had visual field defects and 40% had symptoms of cranial nerve involvement (5). Clinical studies have shown that most B-LBL patients present with lower stage lesions, mainly consisting of osteolytic bone lesions (26%) and skin lesions (23%), and rare findings included mediastinal or pleural disease (11%), isolated bone marrow disease (13%), isolated lymph node (13%), or visceral disease (4%). Only a minority of patients (6%) have central nervous system manifestations (6). Meyer et al. used molecular inversion probe technology to analyze the genetic data of 23 B-LBL patients, and found that *CDKN2A/B* deletions were the most common alteration identified in 6/23 (26%) B-LBL cases. IKZF1 and *PAX5* deletions were observed in 13% and 17% of B-LBL (7). *TP53* is the most frequently mutated gene in human cancer, and is closely related to the occurrence and development of tumors (8). Mutations in the *TP53* gene detected in multiple NHL patients, and the detection frequencies in diffuse large B-cell lymphoma (DLBCL), transformed follicular lymphoma (tFL) and Burkitt lymphoma (BL) patients were 21%-31.7% (9–11), 29%-80% (12) and 33%(12), respectively. Mutations in the TP53 gene are extremely rare in patients with B-LBL (13).

PAX5 is a member of the PAX transcription factor family. The main feature of this gene family is the highly conserved DNA binding motif paired box. *PAX5* plays an important role in B cell differentiation, and participates in the regulation of B lymphocyte specific target gene - CD19 gene. B cell-specific activator protein (BSAP) encoded by Pax5 gene plays a decisive role in the early directed differentiation of B cells. In the process of hepatocarcinogenesis, *PAX5* inhibits hepatocarcinogenesis by inhibiting cell proliferation and regulating p53 signaling pathway to induce apoptosis. It can be used as an auxiliary marker in diagnosing classical Hodgkin lymphoma and B-NHL (14, 15). Studies have shown that in B lymphoma, *PAX5* promotes lymphomagenesis through stimulation of B cell receptor signaling (16). However, other studies have shown that *PAX5* silencing promotes mantle cell lymphoma (MCL) cell proliferation and that *PAX5* overexpression induces MCL cell death (17). Mutations in the *PAX5* gene are detected at a frequency of 7% in patients with B-cell progenitor acute lymphoblastic leukemia (BCP-ALL) (18). *PAX5* c.913_923delCG TGACTTGGC (p.R305Efs*32) is a frameshift mutation, which leads to a substitution of the arginine at position 305 to glutamic and termination at position 336 and causes the transcription to end prematurely (Figure 2), resulting in functionally impaired proteins, or loss of protein expression through nonsense-mediated mRNA degradation (NMD).

TP53 (tumor protein P53) is a tumor suppressor gene. The protein it encodes, P53, is a DNA binding protein involved in a variety of biological processes. P53 protein regulates target gene expression in response to various cellular stresses, thereby inducing cell cycle arrest, cell apoptosis and senescence, DNA repair, or changes in metabolism. In the cell cycle, when the DNA in the cell is damaged or defective, the P53 protein will arrest the cell cycle in G1 and G2 phases, and start the corresponding repair mechanism to repair the damaged or defective DNA. If the repair fails, the P53 protein initiates the apoptosis mechanism to clear the damaged cells, thus achieving the regulatory function. *TP53* c.969_971delGGAinsAGGC (p.D324Gfs*13) is also a frameshift mutation, which leads to a substitution of the aspartic at

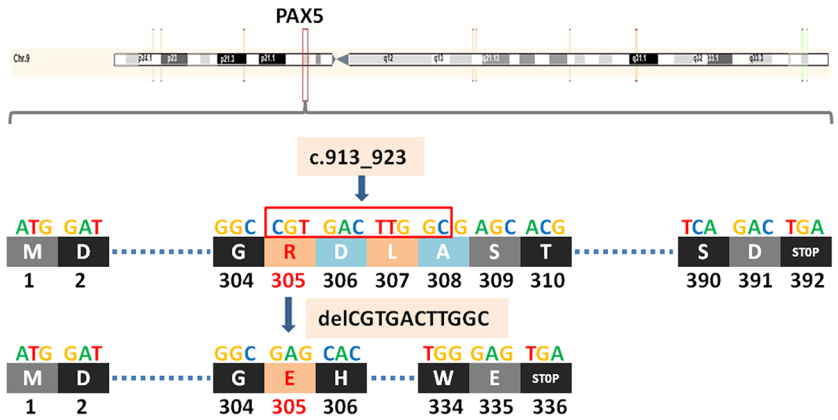

FIGURE 2
A newly discovered frameshift mutation in PAX5, which leads to a substitution of the arginine at position 305 to glutamic and termination at position 336. ATG (base sequence) transcription translates to methionine (M,start codon); GAT/GAC transcription translates to aspartic acid (D); GGC transcription translates to glycine (G); CGT transcription translates to arginine (R); GAG transcription translates to glutamic acid (E); CAC transcription translates to histidine (H); TTG transcription translates to leucine (L); GCG transcription translates to alanine (A); AGC/TCA transcription translates to serine (S); ACG transcription translates to threonine (T); TCA transcription translates to serine (S); TGG transcription translates to tryptophane (W); TGA transcription translates to stop codon.

position 324 to glycine and termination at position 336 and causes the transcription to end prematurely(Figure 3), resulting in functionally impaired proteins, or loss of protein expression through nonsense-mediated mRNA degradation (NMD).

PAX5 c.77T>G (p.V26G) is a missense mutation, which leads to a substitution of the valine at position 26 to glycine. SIFT and PolyPhen-2 provide an in silico prediction of the functional consequences of missense mutations. The former appears to be harmless, while the latter is on the opposite side. *XPO1* is a proto-oncogene and Involved in the regulation of mitosis. *XPO1* c.1711G>A (p.E571K) is a missense mutation, which leads to a substitution of the glutamic at position 571 to lysine. It can be used as a novel biomarker for classical Hodgkin lymphoma and helps to capture the pathogenesis of classical Hodgkin lymphoma (19). *CDKN2A* and *CDKN2B* are tumor suppressor genes. Loss of *CDKN2A* may lead to the loss of p16ink4a which is a CDK4/6 inhibitor. In turn, CDK4/6 will be activated, resulting in dysregulation of cell proliferation (20, 21). *CDKN2B* copy number variation is the result of deletion of the *CDKN2A-CDKN2B* locus.

Conclusion

Sellar lymphoma has no special imaging features, which presents a huge challenge to both accurate diagnosis and personalized therapy. Although sellar lymphoma is extremely rare, it should always be considered in the diagnosis of sellar tumors, and early diagnosis and systematic treatment are the key to improve the prognosis of B-LBL patients.

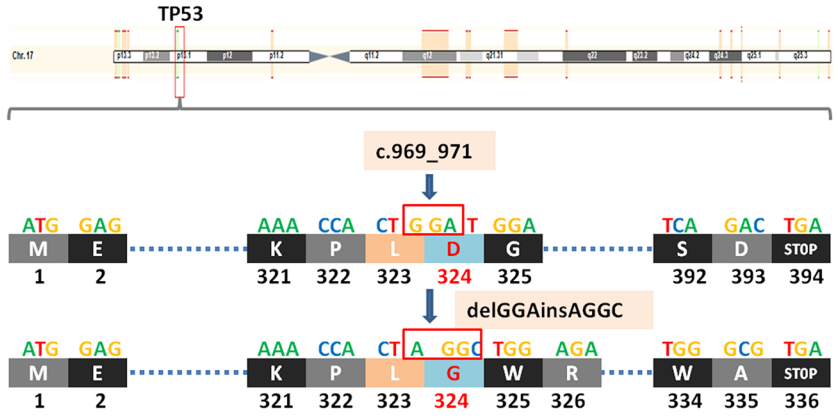

FIGURE 3
A newly discovered frameshift mutation in TP53, which leads to a substitution of the aspartic at position 324 to glycine and termination at position 336. ATG (base sequence) transcription translates to methionine (M,start codon); GAG transcription translates to glutamic acid (E); AAA transcription translates to lysine (K); CCA transcription translates to proline (P); CTG/CTA transcription translates to leucine (L); GAT/GAC transcription translates to aspartic acid (D); GGA/GGC transcription translates to glycine (G); TCA transcription translates to serine (S); TGG transcription translates to tryptophane (W); AGA transcription translates to arginine (R); GCG transcription translates to alanine (A); TGA transcription translates to stop codon.

Data availability statement

The datasets presented in this study can be found in online repositories. The names of the repository/repositories and accession number(s) can be found in the article/supplementary material.

Ethics statement

Written informed consent was obtained for the publication of this case report.

Author contributions

XH, YW, DW and FB were involved in the surgery. PL, XX and CW did literature search. YW, YY and QW drafted the paper. XH revised the paper. All authors contributed to the article and approved the submitted version.

Funding

This work was funded by: 1. Research Project Supported by Shanxi Scholarship Council of China(2020-169); 2. Fund Program for the Scientific Activities of Selected Returned Overseas Professionals in Shanxi Province(20210023); 3. Fundamental Research Program of Shanxi Province (202203021211017).

Acknowledgments

I am grateful to all those who devoted much time to reading this thesis and giving me much advice, which will benefit me in my later study.

Conflict of interest

The authors declare that the research was conducted in the absence of any commercial or financial relationships that could be construed as a potential conflict of interest.

Publisher's note

References

1. Arber DA, Orazi A, Hasserjian R, Thiele J, Borowitz MJ, Le Beau MM, et al. The 2016 revision to the world health organization classification of myeloid neoplasms and acute leukemia. *Blood* (2016) 127(20):2391–405. doi: 10.1182/blood-2016-03-643544

2. Intermesoli T, Weber A, Leoncin M, Frison L, Skert C, Bassan R. Lymphoblastic lymphoma: a concise review. *Curr Oncol Rep* (2022) 24(1):1–12. doi: 10.1007/s11912-021-01168-x

3. Borowitz M. B lymphoblastic leukaemia/lymphoma, not otherwise specified. *Who Classification Tumours Haematopoietic Lymphoid Tissues* (2008).

4. Yang D, Bu X, Yan Z, Cheng X, Wu T. Primary lymphoma of the pituitary stalk presenting as diabetes insipidus and visual deterioration: a case report and literature review. *Int J Clin Exp Med* (2018) 11(10):11289–93.

5. Gola M, Doga M, Bonadonna S, Velardo A, Giustina A. Primary pituitary lymphoma. *Endocrinol* (2004) 14(5):288–92. doi: 10.1097/01.ten.0000139004.32317.4c

6. Ducassou S, Ferlay C, Bergeron C, Girard S, Laureys G, Pacquement H, et al. Clinical presentation, evolution, and prognosis of precursor b-cell lymphoblastic lymphoma in trials LMT96, EORTC 58881, and EORTC 58951. *Br J Haematol* (2011) 152(4):441–51. doi: 10.1111/j.1365-2141.2010.08541.x

7. Meyer JA, Zhou D, Mason CC, Downie JM, Rodic V, Abromowitch M, et al. Genomic characterization of pediatric b-lymphoblastic lymphoma and b-lymphoblastic leukemia using formalin-fixed tissues. *Pediatr Blood Cancer* (2017) 64(7):e26363. doi: 10.1002/pbc.26363

8. Kastenhuber E, Lowe S. Putting p53 in context. *Cell* (2017) 170(6):1062–78. doi: 10.1016/j.cell.2017.08.028

9. Schiefer A, Kornauth C, Simonitsch-Klupp I, Skrabs C, Masel E, Streubel B, et al. Impact of single or combined genomic alterations of TP53, MYC, and BCL2 on survival of patients with diffuse Large b-cell lymphomas: A retrospective cohort study. *Medicine* (2015) 94(52):e2388. doi: 10.1097/md.0000000000002388

10. Young K, Leroy K, Møller M, Colleoni G, Sánchez-Beato M, Kerbauy F, et al. Structural profiles of TP53 gene mutations predict clinical outcome in diffuse large b-cell lymphoma: an international collaborative study. *Blood* (2008) 112(8):3088–98. doi: 10.1182/blood-2008-01-129783

11. Zainuddin N, Berglund M, Wanders A, Ren Z, Amini R, Lindell M, et al. TP53 mutations predict for poor survival in de novo diffuse large b-cell lymphoma of germinal center subtype. *Leukemia Res* (2009) 33(1):60–6. doi: 10.1016/j.leukres.2008.06.022

12. Cheung K, Horsman D, Gascoyne R. The significance of TP53 in lymphoid malignancies: mutation prevalence, regulation, prognostic impact and potential as a therapeutic target. *Br J haematol* (2009) 146(3):257–69. doi: 10.1111/j.1365-2141.2009.07739.x

13. Krieger D, Moericke A, Oschlies I, Zimmermann M, Schrappe M, Reiter A, et al. Frequency and clinical relevance of DNA microsatellite alterations of the CDKN2A/B, ATM and p53 gene loci: a comparison between pediatric precursor T-cell lymphoblastic lymphoma and T-cell lymphoblastic leukemia. *Haematologica* (2010) 95(1):158–62. doi: 10.3324/haematol.2009.007526

14. Feldman AL, Dogan A. Diagnostic uses of Pax5 immunohistochemistry. *Adv Anatom Pathol* (2007) 14(5):323–34. doi: 10.1097/PAP.0b013e3180ca8a49

15. Johri N, Patne S, Tewari M, Kumar M. Diagnostic utility of PAX5 in Hodgkin and non-Hodgkin lymphoma: A study from northern India. *J Clin Diagn Res JCDR* (2016) 10 (8):XC04–XC7. doi: 10.7860/jcdr/2016/21476.8352

16. Cozma D, Yu D, Hodawadekar S, Azvolinsky A, Grande S, Tobias J, et al. B cell activator PAX5 promotes lymphomagenesis through stimulation of b cell receptor signaling. *J Clin Invest* (2007) 117(9):2602–10. doi: 10.1172/jci30842

17. Teo A, Chen Z, Miranda R, McDonnell T, Medeiros L, McCarty N. Differential PAX5 levels promote malignant b-cell infiltration, progression and drug resistance, and predict a poor prognosis in MCL patients independent of CCND1. *Leukemia* (2016) 30 (3):580–93. doi: 10.1038/leu.2015.140

18. Familiades J, Bousquet M, Lafage-Pochitaloff M, Béné M, Beldjord K, De Vos J, et al. PAX5 mutations occur frequently in adult b-cell progenitor acute lymphoblastic leukemia and PAX5 haploinsufficiency is associated with BCR-ABL1 and TCF3-PBX1 fusion genes: a GRAALL study. *Leukemia* (2009) 23(11):1989–98. doi: 10.1038/leu.2009.135

19. Camus V, Stamatoullas A, Mareschal S, Viailly P, Sarafan-Vasseur N, Bohers E, et al. Detection and prognostic value of recurrent exportin 1 mutations in tumor and cell-free circulating DNA of patients with classical Hodgkin lymphoma. *Haematologica* (2016) 101(9):1094–101. doi: 10.3324/haematol.2016.145102

20. LaPak K, Burd C. The molecular balancing act of p16(INK4a) in cancer and aging. *Mol Cancer Res MCR* (2014) 12(2):167–83. doi: 10.1158/1541-7786.Mcr-13-0350

21. Sharpless N. INK4a/ARF: a multifunctional tumor suppressor locus. *Mutat Res* (2005) 576:22–38. doi: 10.1016/j.mrfmmm.2004.08.021

frontiers | Frontiers in Oncology

TYPE Original Research
PUBLISHED 07 February 2023
DOI 10.3389/fonc.2023.1007393

OPEN ACCESS

EDITED BY
Ignazio Gaspare Vetrano,
Carlo Besta Neurological Institute Foundation (IRCCS), Italy

REVIEWED BY
Maria Luisa Garrè,
Giannina Gaslini Institute (IRCCS), Italy
Pierpaolo Alongi,
ARNAS Ospedali Civico Di Cristina Benfratelli, Italy

*CORRESPONDENCE
Ya'ou Liu
liuyaou@bjtth.org
Liwei Zhang
zhangliweittyy@163.com

†These authors have contributed equally to this work

SPECIALTY SECTION
This article was submitted to Neuro-Oncology and Neurosurgical Oncology, a section of the journal Frontiers in Oncology

RECEIVED 30 July 2022
ACCEPTED 16 January 2023
PUBLISHED 07 February 2023

CITATION
Zhang P, Duan Y, Gu G, Qu L, Xiao D, Xi T, Pan C, Liu Y and Zhang L (2023) Clinical, pathological, and radiological features of 80 pediatric diffuse intrinsic pontine gliomas: A single-institute study. *Front. Oncol.* 13:1007393. doi: 10.3389/fonc.2023.1007393

Clinical, pathological, and radiological features of 80 pediatric diffuse intrinsic pontine gliomas: A single-institute study

Peng Zhang[1,2,3†], Yunyun Duan[2,4†], Guocan Gu[1†], Liying Qu[4], Dan Xiao[2], Tianshu Xi[2], Changcun Pan[1,2,3], Ya'ou Liu[2,4*] and Liwei Zhang[1,2,3*]

[1]Department of Neurosurgery, Beijing Tiantan Hospital, Capital Medical University, Beijing, China, [2]China National Clinical Research Center for Neurological Diseases, Beijing, China, [3]Beijing Neurosurgical Institute, Beijing, China, [4]Department of Radiology, Beijing Tiantan Hospital, Capital Medical University, Beijing, China

Objective: Diffuse intrinsic pontine gliomas (DIPGs) are rare but devastating diseases. This retrospective cross-sectional study aimed to investigate the clinical, radiological, and pathological features of DIPGs.

Materials and methods: The clinical data of 80 pediatric DIPGs under clinical treatment in Beijing Tiantan Hospital from July 2013 to July 2019 were retrospectively collected and studied. A follow-up evaluation was performed.

Results: This study included 48 men and 32 women. The most common symptoms were cranial nerve palsy (50.0%, 40/80 patients) and limb weakness (41.2%, 33/80 patients). Among the 80 patients, 24 cases were clinically diagnosed, 56 cases were pathologically verified, and 45 cases were tested for H3K27 alteration status, with 34 H3K27 alteration cases confirmed. Radiological results indicated that enhancement was common (65.0%, 52/80 patients). Cho/Cr was of predictive value for H3K27 alteration status (P = 0.012, cutoff value = 2.38, AUC = 0.801). Open cranial surgery followed by further chemotherapy and radiotherapy was beneficial for patients' overall survival. Cox regression analysis indicated H3K27 alteration to be the independent prognostic influencing factor for DIPGs in this series (P = 0.002).

Conclusion: DIPGs displayed a wide spectrum of clinical and imaging features. Surgery-suitable patients could benefit from postoperative comprehensive therapy for a better overall survival. H3K27 alteration was the independent prognostic influencing factor for DIPGs.

KEYWORDS

diffuse intrinsic pontine glioma, H3K27 alteration, overall survival, MRS, radiomics

Introduction

Brainstem gliomas (BSGs) are defined as a heterogeneous group of gliomas that arise from the midbrain, pons, or medulla. BSGs show a bimodal peak of age distribution, with the first peak in the latter half of the first decade and the second peak in the fourth decade (1). BSGs account for approximately 20% of central nervous system tumors in children, and 80% of them are diffuse intrinsic pontine gliomas (DIPGs) (2).

The prognosis for diffuse BSGs has been very poor, compared with a better prognosis in focal low-grade gliomas of the midbrain or focal gliomas in the dorsal bulbo-medullary or pons. Pediatric DIPGs, with a median overall survival of 9–12 months, have been a main research focus for the past 50 years due to their inoperability and resistance to chemotherapy and radiotherapy (3). Whether chemotherapy and radiotherapy could improve prognosis is still controversial. Approximately 80% of pediatric DIPGs harbor H3K27 alterations. Brain tumors that harbor H3K27 alterations seem to have a particularly poor prognosis. In order to classify this new biological feature of brain tumors, a new subtype "diffuse midline glioma, H3K27 altered (DMG-H3K27-alt)" was termed (4). However, the radiomics features of DIPGs, as a pretreatment non-invasive measurement, especially for the DMG-H3K27-alt types, are less known.

DIPGs are a wide range of diseases defined by MR imaging. Histopathology with molecular features is the gold standard for diagnosis. A new study indicated the histone alteration status of predictive value for prognosis (3). Due to the risks of biopsy or open cranial surgery for DIPGs, MRI has been used for the diagnosis of DIPGs for decades. Whether MR features are correlated with histone alteration status and prognosis in DIPGs is still unknown. Furthermore, whether DIPG patients could benefit from chemotherapy and radiotherapy still needs more exploration. In order to obtain a better understanding of the clinical and imaging features of DIPGs, we conducted this retrospective cross-sectional study.

Materials and methods

This study was approved by the Scientific Review Board of the IRB in our hospital. All DIPGs with intact clinical data and MR imaging data were included from July 2013 to July 2019. Clinical information, including age, sex, symptom duration before diagnosis, neurological findings, pathological findings, natural history, treatment with chemotherapy, and treatment with radiotherapy, was retrospectively collected. Patients were diagnosed with DIPG according to MRI images, clinical manifestations, and intact clinical records. Patients without magnetic resonance spectrum results or without intact clinical data were excluded. All the histopathological results and molecular pathological results were reviewed by an experienced team of neuropathologists at Beijing Tiantan Hospital, Capital Medical University.

Imaging review

Imaging evaluation was independently performed by two senior radiologists and one neurosurgeon. A consensus opinion was utilized if there were discrepancies among the reviewers; all images were reviewed again and an agreement among the reviewers was reached. Imaging information included maximum tumor size in the cross section, percentage of pons involved in the cross section, tumor margin, eccentric position, T2 hypointensity, heterogeneity, diffuse restriction, hemorrhage, peritumoral edema, necrosis, cystic, enhancement characteristics, spectroscopy features, hydrocephalus, supratentorial peri-ventricular edema, presence of stripes in non-necrotic T2 hyperintensity regions in the cross section of the pons, location of medulla involvement, and location of midbrain involvement. Diffuse intrinsic pontine glioma was defined as having its epicenter in the pons and typically involving more than 50% of its surface according to the imaging features in MRI. Only diffuse intrinsic pontine gliomas were included in this study for further analysis. Quantitative analysis of diffusion, spectroscopy data, and correlation with other variables was performed.

Histone alteration status

Cases were pathologically verified through stereotactic biopsy or open cranial biopsy. In addition to histopathological diagnosis, immunohistochemistry (IHC) assessment of histone alteration status was also performed. The IHC method utilizes a polyclonal, mutant-specific antibody that recognizes the product of all H3K27 variants, and a positive result was visualized microscopically as strong nuclear staining of the tumor cells (5).

Statistical analysis

Univariable and multivariable analyses of imaging features (quantitative value of diffuse restriction and spectroscopy data, external pontine tumor location, and T2 pontine stripe features), clinical data, and histone status relative to overall survival (OS, diagnosis until death) were performed using Cox proportional hazards regression. The hazard ratio (HR) and odds ratio (OR) for OS and histone status were summarized. Variables with P <0.05 in the univariable analysis were chosen for multivariable analysis when applicable. Correlation analysis between histone status and other variables was also performed. Correlations with a value of $P < 0.05$ were considered to be of statistical significance. Paired t-tests or independent sample t-tests were used for quantitative data; P <0.05 was considered to be of statistical significance. The chi-square test was used for nominal data, and P <0.05 was considered to be of statistical significance.

Results

Demographics, clinical, and imaging features

Demographics and overall survival

A total of 80 patients who met the criteria were included, consisting of 48 men and 32 women. The median age was 7 years old (range between 2 and 14 years). The demographic data and correlation with OS are summarized in Table 1.

Clinical data and overall survival

Prediagnostic symptom duration time ranged from 1 week to 3 years (with a median duration time of 1 month, Table 1). The most common first symptom before diagnosis was lower cranial nerve palsy, followed by limb weakness and ataxia. A shorter prediagnostic symptom duration time indicated a much shorter overall survival ($P = 0.048$).

Among the 80 patients, 56 cases were pathologically verified through stereotactic biopsy or open cranial biopsy. Pathology results were reviewed back-to-back by two senior pathologists to reach an agreement. Totally, 56 cases were verified with pathology and a total of 45 cases were tested for H3K27 alteration status with 31 alteration-positive cases. The correlation between overall survival and pathological results is listed in Table 2. Higher tumor grade was correlated with the presence of necrosis on MRI imaging ($P = 0.024$) and indicated a much shorter overall survival time ($P = 0.043$).

Histone alteration status and correlation

Among the 56 cases, H3K27 alteration status was identified in 45 cases, consisting of 31 H3K27 alterations and 14 wild-type cases Table 2). Among the 45 cases with H3K27 alteration assessment results, a shorter overall survival was correlated with H3K27 alteration status ($P = 0.003$). Furthermore, H3K27 alteration was identified to be statistically correlated with the presence of stripes in the pontine ($P = 0.035$) and cerebellum involvement ($P = 0.044$). H3K27 alteration status showed no correlation with ADC, Cho/NAA, Cho/CR, or NAA/CR (Table S1). Pontine stripes in MR T2 were commonly observed in DIPGs (55%, 44/80 cases) and correlated with H3K27 alteration status ($P = 0.006$).

TABLE 1 Clinical parameters correlated with OS of 80 DIPGs.

Characteristics		No. (%) of patients	*P*-value
Sex			0.684
	Male	48 (60.0)	
	Female	32 (40.0)	
Symptom duration time before diagnosis			0.048
	≤1 month	29 (51.8)	
	>1 month	27 (48.2)	
Neurological findings			
	Cranial nerve palsy	40 (50.0)	0.731
	Limb weakness	33 (41.2)	0.839
	Limb sensory disturbance	10 (12.5)	0.249
	Ataxia	26 (32.5)	0.452
Treatment			0.00*
	Clinical observation	24	
	Open cranial cytoreductive surgery or stereotactic biopsy	18	
	Stereotactic biopsy plus radiotherapy and/or chemotherapy	6	
	Open cranial cytoreductive surgery plus radiotherapy and/or chemotherapy	32	

*Indicates P <0.01.

TABLE 2 Pathological parameters correlated with OS of 56 DIPGs.

Characteristics		No. (%) of patients	*P*-value
Pathological findings			0.043*
	Astrocytoma (WHO grade II)	8 (14.3)	
	Oligodendroastrocytoma(WHO grade II)	5 (8.9)	
	Anaplastic oligodendroastrocytoma (WHO grade III)	12 (21.4)	
	Diffuse midline glioma with H3K27 alteration (WHO grade IV)	31 (68.9)	
H3K27M			0.003
	Alteration	31 (68.9)	
	Wild type	14 (31.1)	

*Indicates overall survival was significantly different between low-grade glioma (WHO grade II) and high-grade glioma (WHO grades III and IV).

Treatment protocols and overall survival

Among the 80 patients, 24 were clinically diagnosed as having DIPG according to MRI imaging and received no other clinical treatment. Another 18 patients only received stereotactic biopsy or open cranial surgery without subsequent radiotherapy and/or chemotherapy, another 6 patients received radiotherapy and/or chemotherapy after stereotactic biopsy, and the other 32 patients received open cranial tumor burden reduction surgery followed by radiotherapy and/or chemotherapy. Survival analysis indicated that patients receiving stereotactic biopsy or open cranial tumor burden reduction surgery plus radiotherapy and/or chemotherapy had a longer overall survival ($P < 0.001$, Figure 1A; Table 3), compared with the clinical observation group and the stereotactic biopsy/open cranial cytoreductive surgery group. The overall survival between the clinical observation group and the stereotactic biopsy or open cranial cytoreductive surgery group was of no statistical significance. The overall survival was significant between the other three groups ($P < 0.001$, Table 3).

MRI features and overall survival

MRI imaging of the 80 cases was reviewed independently by two senior radiologists, and disagreement cases were reviewed again to reach an agreement. The detailed features of MRI images of the 80 cases are listed in Table 4. The medulla was involved in 58 cases, in which the pontomedullary sulcus was involved in 53 cases and the fundus of the fourth ventricle was involved in 33 cases. The midbrain was involved in 68 cases, in which the tectum was involved in 34 cases, the tegmentum was involved in 63 cases, and the cerebral

peduncle was involved in 10 cases. The thalamus was involved in four cases, mainly involving the central-median part of the thalamus. The brachium was involved in 70 cases and the cerebellum was involved in 19 cases. Cerebellum involvement was identified to correlate with OS ($P = 0.045$, Table 4). No statistical significance was found between OS and other involved parts of the brainstem.

According to the shape and growth features of tumors in the pons, we divided DIPGs into two types: tropism growth and exophytic growth. The correlation between this classification and OS was of statistical significance ($P = 0.023$, Table 5), and tropism growth tumor had a much shorter overall survival.

Imaging features that correlated with overall survival were calculated separately (Table 5). No statistical significance was found between OS and these MRI features. Quantitative analysis was performed between OS and the spectrum as well as diffuse restriction parameters. A lower rate of Cho/CR indicated a worse prognosis ($P = 0.023$, cutoff value = 1.66, AUC = 0.709, Figure S1). Furthermore, a lower rate of Cho/CR was also correlated with H3K27 alteration status (Figure 2) and a higher tumor grade ($P = 0.002$, Table S2). The ADC value, representing diffuse restriction feature, failed to identify any statistical correlation with OS.

With Cox analysis, H3K27 alteration indicated a worse prognosis and was an independent prognosis indicator for cases with H3K27 alteration test results ($P = 0.004$, Figure 1B).

TABLE 3 Treatment protocols correlated with OS of 80 DIPGs.

Parameters	Group A	Group B	Group C	Group D
$X \pm S$	4.54 ± 5.69	6.15 ± 3.65	13.60 ± 10.58	16.71 ± 15.89
Group A	–	0.24	0.002	0.000*
Group B	0.24	–	0.000*	0.000*
Group C	0.002	0.000*	–	0.000*
Group D	0.000*	0.000*	0.000*	–

Group A, clinical observation; group B, stereotactic biopsy or open cranial surgery; group C, stereotactic biopsy plus radiotherapy and/or chemotherapy; group D, open cranial cytoreductive surgery plus radiotherapy and/or chemotherapy.
*Indicates P <0.001.

Discussion

Correlation between clinical treatment and overall survival

Not all DIPGs were suitable for surgical removal. The exophytic portion of DIPGs could be safely resected with the use of intraoperative multimodal monitoring and neuronavigation techniques (6) (Figure 3). DIPGs with exophytic portions were more suitable for surgical resection and had a longer overall survival in this series.

Chemotherapy and radiotherapy have been recommended for DIPGs as treatment protocols for decades (7). However, resistance to chemotherapy and radiotherapy widely exists among DIPGs. Whether DIPG patients could benefit from chemotherapy and radiotherapy is still controversial. Within this series, through clinical observation, the overall survival was approximately 11 months, which was in accordance with previous reports (8). For DIPG patients who received chemotherapy and/or radiotherapy in this series, the overall survival was much longer than in the comparative groups ($P < 0.001$), which indicated that DIPG patients could benefit from chemotherapy and/or radiotherapy. Furthermore, we noticed from clinical practice that performing radiotherapy could induce the presence of enhancement and focal changes of DIPGs in MRI imaging, due to radiation-induced vascular changes within the tumor, which was noticed in previous case reports and needs further investigation (9).

The latest published study by our team indicates that the different locations of the brainstem tumor correlated with histone status and prognosis (3). This phenomenon did not exist in DIPGs in this series, which may be attributable to DIPGs mainly located in the pontine rather than in other parts of the brainstem.

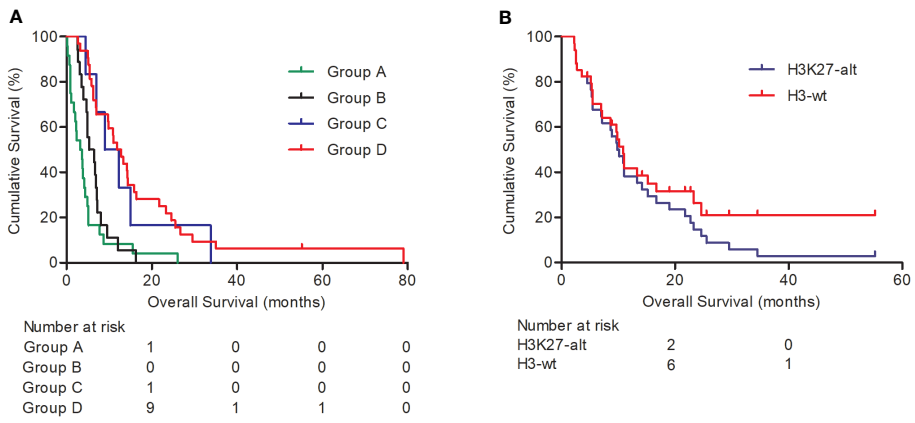

FIGURE 1
Kaplan–Meier survival analysis for DIPGs. Graph **(A)** shows the overall survival of DIPG patients in different treatment groups: Group A, clinical observation group; group B, stereotactic biopsy or open cranial surgery; group C, stereotactic biopsy plus radiotherapy and/or chemotherapy; group D, open cranial cytoreductive surgery plus radiotherapy and/or chemotherapy. Graph **(B)** indicates H3K27 alteration status predicts shorter overall survival ($P = 0.004$).

10.3389/fonc.2023.1007393

TABLE 4 Imaging parameters correlated with OS of 80 DIPGs.

Characteristics		No. (%) of patients	*P*-value
MRS parameters			
	Cho/Cr	–	0.037
	Cho/NAA	–	0.138
	NAA/Cr	–	0.840
ADC value			0.055
Enhancement			0.571
	Yes	52 (65.0)	
	No	28 (35.0)	
Necrosis			0.696
	Yes	25 (31.3)	
	No	55 (68.7)	
Intratumoral bleed			0.777
	Yes	7 (8.8)	
	No	73 (91.2)	
Cystic changes			0.793
	Yes	10 (12.5)	
	No	70 (87.5)	
Peritumoral edema			0.425
	Yes	25 (31.3)	
	No	55 (68.7)	
Hydrocephalus			0.681
	Yes	68 (85.0)	
	No	12 (15.0)	
Paraventricular edema			0.571
	Yes	62 (77.5)	
	No	18 (22.5)	
Pontine stripes			0.556
	Yes	44 (55.0)	
	No	36 (45.0)	

Correlation between MRI imaging and clinical features

With the development of stereotactic techniques and open cranial techniques, stereotactic biopsy or surgical biopsy is available for many DIPG patients under acceptable risks (10). However, due to the non-invasive advantages, DIPG is still mainly diagnosed based on MRI imaging and clinical manifestation. Furthermore, many features of the tumor can be identified through MRI images, for example, tumor growth pattern, enhancement, necrosis, hemorrhage, peritumoral edema, and hydrocephalus (11, 12). A survival prediction model as well as classification systems were also mentioned in previous reports (13, 14). These MRI features could provide rather important information for clinical diagnosis and therapy.

TABLE 5 Tumor growth features in MRI imaging correlated with OS of 80 DIPGs.

Characteristics	No. (%) of patients	*P*-value
Midbrain involvement	68 (85.0)	0.320
Tectum	34 (50.0)	0.385
Tegmentum	63 (92.6)	0.816
Crus cerebri	10 (14.7)	0.381
Medulla involvement	59 (73.8)	0.205
Pontomedullary sulcus	53 (89.8)	0.079
Fourth ventricle fundus	33 (55.9)	0.433
Thalamus involvement	4 (5.0)	0.556
Brachium involvement	70 (87.5)	0.527
Cerebellum involvement	19 (23.8)	0.045
Classification based on growth pattern in MRI imaging		0.023
Without exophytic growth part	26 (32.5)	
With exophytic growth part	54 (67.5)	

DIPG was defined as a tumor body mainly located in the pons. Within this study, we identified that DIPGs could also have different growth patterns with an extrapontine lesion on MRI imaging, which was also identified in a recently published article (15). In this series, at least 54 extrapontine lesions were observed in 80 cases (67.5%), which was similar to the report by Makepeace et al. (15). Among this series, more than 70% (58/80) of the DIPGs were found to involve the medulla, with the pontomedullary sulcus as the main affected part of the medulla, indicating that the tumor may involve the medulla mainly through the ventral part of the medulla. More than 80% (68/80) of the DIPGs in this series were found to involve the midbrain, with the tectum and tegmentum as the main affected parts of the midbrain, indicating that the tumor may involve the midbrain mainly through the dorsal part of the midbrain. These involved areas were the main locations where cranial nerves start over from the brainstem. In contrast to Makepeace's report, we failed to identify a statistical correlation between overall survival and extrapontine lesion numbers or involvement of the middle cerebellar peduncles. We suggest that

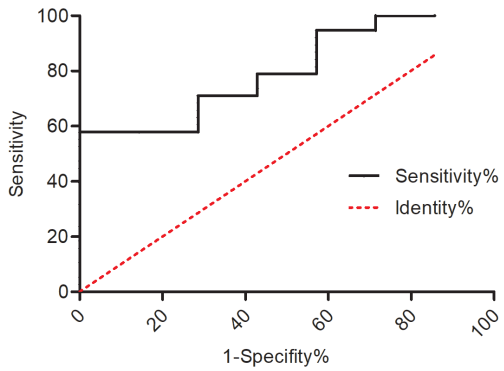

FIGURE 2
ROC curve of the predictive value of Cho/Cr for H3K27 alteration status (P = 0.012, cutoff value = 2.38, AUC = 0.801).

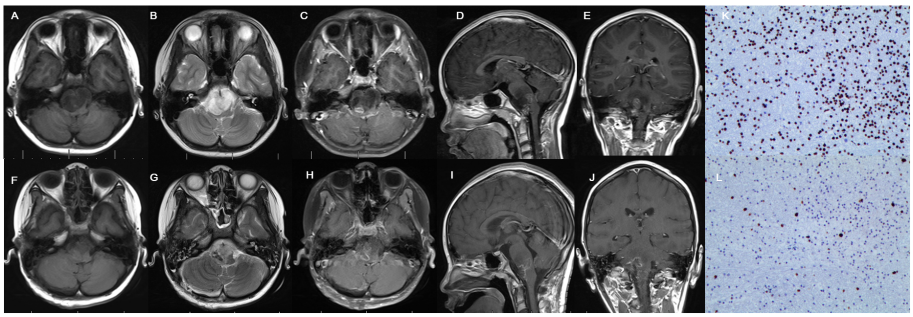

FIGURE 3
Cranial MRI examination revealed glioma located in the brainstem with extrapontine lesion, showing mixed hypointense and hyperintense in T1 **(A)** and hyperintense signal in T2 **(B)** and irregular enhancement **(C–E)** in preoperative images. Postoperative MRI confirmed partial resection **(F–J)**. Immunohistochemistry indicates H3K27M positive **(K)** and Ki-67 positive **(L)**.

these findings may be valuable for risk stratification and radiation therapy planning in future clinical trials. Furthermore, these findings could be helpful in explaining why the lower cranial nerves as well as the long-tract defection signs were commonly identified as the early main clinical manifestations of DIPG patients.

Correlation between MRI imaging and overall survival

Pontine stripes were distinct in the T2 series of many DIPGs, which have been mentioned previously (16) but not analyzed. This characteristic feature of DIPG was identified in more than 50% (44/80) of the cases in this study, indicating it to be a common MRI imaging feature in DIPG. We identified that the performance of pontine stripes was statistically correlated with H3K27 alteration ($P = 0.006$), although pontine stripes did not correlate with OS in this study.

Quantitative assessment of the spectrum and diffusion restriction has been used for the diagnosis of glioma and for the prediction of prognosis in supratentorial glioma studies (17–19). MRS was also used for differentiating brainstem glioma from non-tumoral diseases (20) and for indicating clinical progression (21). In this series, we identified that the lower rate of Cho/CR was correlated with a higher tumor grade and a shorter overall survival in DIPGs, with the tumor pathology grade an independent prognostic factor. These results indicate that a lower Cho/CR reflects malignant tumor growth features and could be used as a diagnostic indicator and a prognostic predictor.

Exophytic tumor growth has been recommended as a feature for brainstem tumor resectable indication in previous reports (22, 23). Exophytic tumor growth of DIPG accounts for 32.5% of the cases in this series (similar to 28% in previous reports (22)) and indicates a longer overall survival ($P = 0.023$). The reason for this may be because the exophytic growth pattern of the tumor causes less pressing or destruction of the brainstem, or because the exophytic tumor was more suitable for accepting neurosurgical resection, which provides tumor burden reduction and more tissue for pathological identification, allowing the generation of more effective, comprehensive therapy protocols. Other MRI imaging features, including enhancement, necrosis, cystic changes, and hemorrhage, did not correlate with the overall survival. Hydrocephalus and supratentorial periventricular edema were not correlated with overall survival.

Conclusion

Some DIPGs were suitable for surgical removal for the purpose of diagnosis and cytoreductive surgery of the lesion. Postoperative comprehensive therapy is beneficial for the overall survival of the patients. H3K27 alteration status was correlated with overall survival. Cho/Cr was of predictive value for H3K27 alteration status; also, pontine stripes in the MR T2 series were commonly observed and were correlated with H3K27 alteration status, which needs further study with larger samples.

Data availability statement

The raw data supporting the conclusions of this article will be made available by the authors, without undue reservation.

Ethics statement

Written informed consent was obtained from the individual(s), and minor(s)' legal guardian/next of kin, for the publication of any potentially identifiable images or data included in this article.

Author contributions

PZ, YD, and GG carried out the clinical data collection, statistical analysis, and manuscript drafting and modification. DX and TX helped in the clinical data collection and statistical analysis. LQ and CP helped in the clinical data collection. YL and LZ conceived the study and participated in the design of the study and modified the manuscript. All authors contributed to the article and approved the submitted version.

Funding

This study was supported by the Science and Technology Innovation 2030—Brain Science and Brain-Inspired Intelligence Project of China (2021ZD0200201), National Natural Science Foundation of China (81872048), the Beijing Municipal Natural Science Foundation (7214214), and the Beijing Health Commission (JingCaiKeWenZhi (2019)2348).

Conflict of interest

The authors declare that the research was conducted in the absence of any commercial or financial relationships that could be construed as a potential conflict of interest.

Publisher's note

Supplementary material

The Supplementary Material for this article can be found online at: https://www.frontiersin.org/articles/10.3389/fonc.2023.1007393/full#supplementary-material

References

1. Purohit B, Kamli AA, Kollias SS. Imaging of adult brainstem gliomas. *Eur J Radiol* (2015) 84(4):709–20. doi: 10.1016/j.ejrad.2014.12.025

2. Green AL, Kieran MW. Pediatric brainstem gliomas: new understanding leads to potential new treatments for two very different tumors. *Curr Oncol Rep* (2015) 17(3):436. doi: 10.1007/s11912-014-0436-7

3. Chen LH, Pan C, Diplas BH, Xu C, Hansen LJ, Wu Y, et al. The integrated genomic and epigenomic landscape of brainstem glioma. *Nat Commun* (2020) 11(1):3077. doi: 10.1038/s41467-020-16682-y

4. Louis DN, Perry A, Wesseling P, Brat DJ, Cree IA, Figarella-Branger D, et al. The 2021 WHO classification of tumors of the central nervous system: a summary. *Neuro Oncol* (2021) 23(8):1231–51. doi: 10.1093/neuonc/noab106

5. Hoffman LM, Veldhuijzen van Zanten SEM, Colditz N, Baugh J, Chaney B, Hoffmann M, et al. Clinical, radiologic, pathologic, and molecular characteristics of long-term survivors of diffuse intrinsic pontine glioma (DIPG): A collaborative report from the international and European society for pediatric oncology DIPG registries. *J Clin Oncol* (2018) 36(19):1963–72. doi: 10.1200/JCO.2017.75.9308

6. Xiao X, Kong L, Pan C, Zhang P, Chen X, Sun T, et al. The role of diffusion tensor imaging and tractography in the surgical management of brainstem gliomas. *Neurosurg Focus* (2021) 50(1):E10. doi: 10.3171/2020.10.FOCUS20166

7. El-Khouly FE, Veldhuijzen van Zanten SEM, Santa-Maria Lopez V, Hendrikse NH, Kaspers GJL, Loizos G, et al. Diagnostics and treatment of diffuse intrinsic pontine glioma: where do we stand? *J Neurooncol* (2019) 145(1):177–84. doi: 10.1007/s11060-019-03287-9

8. Cohen KJ, Jabado N, Grill J. Diffuse intrinsic pontine gliomas-current management and new biologic insights. Is there a glimmer of hope? *Neuro Oncol* (2017) 19(8):1025–34. doi: 10.1093/neuonc/nox021.

9. Chen H, Li X, Zhang X, Xu W, Mao F, Bao M, et al. Late delayed radiation-induced cerebral arteriopathy by high-resolution magnetic resonance imaging: A case report. *BMC Neurol* (2019) 19(1):232. doi: 10.1186/s12868-019-0505-9

10. Puget S, Beccaria K, Blauwblomme T, Roujeau T, James S, Grill J, et al. Biopsy in a series of 130 pediatric diffuse intrinsic pontine gliomas. *Childs Nerv Syst* (2015) 31 (10):1773–80. doi: 10.1007/s00381-015-2832-1

11. Poussaint TY, Vajapeyam S, Ricci KI, Panigrahy A, Kocak M, Kun LE, et al. Apparent diffusion coefficient histogram metrics correlate with survival in diffuse intrinsic pontine glioma: A report from the pediatric brain tumor consortium. *Neuro Oncol* (2016) 18(5):725–34. doi: 10.1093/neuonc/nov256

12. Leach JL, Roebker J, Schafer A, Baugh J, Chaney B, Fuller C, et al. MR imaging features of diffuse intrinsic pontine glioma and relationship to overall survival: Report from the international DIPG registry. *Neuro Oncol* (2020) 22(11):1647–57. doi: 10.1093/neuonc/noaa140

13. Jansen MH, Veldhuijzen van Zanten SE, Sanchez Aliaga E, Heymans MW, Warmuth-Metz M, Hargrave D, et al. Survival prediction model of children with diffuse intrinsic pontine glioma based on clinical and radiological criteria. *Neuro Oncol* (2015) 17(1):160–6. doi: 10.1093/neuonc/nou104

14. Barkovich AJ, Krischer J, Kun LE, Packer R, Zimmerman RA, Freeman CR, et al. Brain stem gliomas: a classification system based on magnetic resonance imaging. *Pediatr Neurosurg* (1990) 16(2):73–83. doi: 10.1159/000120511

15. Makepeace L, et al. MRI Patterns of extrapontine lesion extension in diffuse intrinsic pontine gliomas. *AJNR Am J Neuroradiol* (2020) 41(2):323–30. doi: 10.3174/ajnr.A6391

16. Castel D, Philippe C, Calmon R, Le Dret L, Truffaux N, Boddaert N, et al. Histone H3F3A and HIST1H3B K27M mutations define two subgroups of diffuse intrinsic pontine gliomas with different prognosis and phenotypes. *Acta Neuropathol* (2015) 130 (6):815–27. doi: 10.1007/s00401-015-1478-0

17. Wang Q, Scoggins M, Mitrea B, Li Y, Edwards A, Tinkle CL, et al. The diagnostic performance of magnetic resonance spectroscopy in differentiating high-from low-grade gliomas: A systematic review and meta-analysis. *Eur Radiol* (2016) 26(8):2670–84. doi: 10.1007/s00330-015-4046-z

18. Molloy AR, Najac C, Viswanath P, Lakhani A, Subramani E, Batsios G, et al. MR-detectable metabolic biomarkers of response to mutant IDH inhibition in low-grade glioma. *Theranostics* (2020) 10(19):8757–70. doi: 10.7150/thno.47317

19. Toh CH, Castillo M, Wei KC, Chen PY. MRS as an aid to diagnose malignant transformation in low-grade gliomas with increasing contrast enhancement. *AJNR Am J Neuroradiol* (2020) 41(9):1592–8. doi: 10.3174/ajnr.A6688

20. Porto L, Hattingen E, Pilatus U, Kieslich M, Yan B, Schwabe D, et al. Proton magnetic resonance spectroscopy in childhood brainstem lesions. *Childs Nerv Syst* (2007) 23(3):305–14. doi: 10.1007/s00381-006-0221-5

21. Panigrahy A, Nelson MD Jr, Finlay JL, Sposto R, Krieger MD, Gilles FH, et al. Metabolism of diffuse intrinsic brainstem gliomas in children. *Neuro Oncol* (2008) 10 (1):32–44. doi: 10.1215/15228517-2007-042

22. Lesniak MS, Klem JM, Weingart J, Carson BS Sr. Surgical outcome following resection of contrast-enhanced pediatric brainstem gliomas. *Pediatr Neurosurg* (2003) 39 (6):314–22. doi: 10.1159/000075260

23. Hankinson TC, Campagna EJ, Foreman NK, Handler MH.. Interpretation of magnetic resonance images in diffuse intrinsic pontine glioma: A survey of pediatric neurosurgeons. *J Neurosurg Pediatr* (2011) 8(1):97–102. doi: 10.3171/2011.4.PEDS1180

frontiers | Frontiers in Oncology

TYPE Case Report
PUBLISHED 24 February 2023
DOI 10.3389/fonc.2023.1100532

OPEN ACCESS

EDITED BY
Pierpaolo Alongi,
ARNAS Ospedali Civico Di Cristina Benfratelli, Italy

REVIEWED BY
Vadim Byvaltsev,
Irkutsk State Medical University, Russia
Zhichao Wang,
Shanghai Jiao Tong University, China

*CORRESPONDENCE
Giulio Bonomo
dott.giuliobonomo@gmail.com

†These authors have contributed equally to this work

SPECIALTY SECTION
This article was submitted to Neuro-Oncology and Neurosurgical Oncology, a section of the journal Frontiers in Oncology

RECEIVED 16 November 2022
ACCEPTED 06 February 2023
PUBLISHED 24 February 2023

CITATION
Bonomo G, Gans A, Mazzapicchi E, Rubiu E, Alimonti P, Eoli M, Paterra R, Pollo B, Iess G, Restelli F, Falco J, Acerbi F, Schiariti MP, Ferroli P and Broggi M (2023) Sporadic spinal psammomatous malignant melanotic nerve sheath tumor: A case report and literature review.
Front. Oncol. 13:1100532.
doi: 10.3389/fonc.2023.1100532

Sporadic spinal psammomatous malignant melanotic nerve sheath tumor: A case report and literature review

Giulio Bonomo[1,2,3*†], Alessandro Gans[1,2†], Elio Mazzapicchi[1,2], Emanuele Rubiu[1,2], Paolo Alimonti[1], Marica Eoli[4], Rosina Paterra[4], Bianca Pollo[5], Guglielmo Iess[1,2], Francesco Restelli[1,2], Jacopo Falco[1,2], Francesco Acerbi[1], Marco Paolo Schiariti[1], Paolo Ferroli[1] and Morgan Broggi[1]

[1]Department of Neurosurgery, Fondazione IRCCS Istituto Neurologico C. Besta, Milan, Italy, [2]School of Medicine, University of Milan, Milan, Italy, [3]Department of Neurological Surgery, Policlinico "G. Rodolico-S. Marco" University Hospital, Catania, Italy, [4]Molecular Neuro-Oncology Unit, Fondazione IRCCS Istituto Neurologico C. Besta, Milan, Italy, [5]Neuropathology Unit, Fondazione IRCCS Istituto Neurologico C. Besta, Milan, Italy

Background: Sporadic Spinal Psammomatous Malignant Melanotic Nerve Sheath Tumor (SSP-MMNST) is a rare subgroup of peripheral nerve sheath tumors arising along the spine. Only a few reports of SSP-MMNST have been described. In this paper, we review the literature on SSP-MMNST focusing on clinical, and diagnostic features, as well as investigating possible pathogenetic mechanisms to better implement therapeutic strategies. We also report an illustrative case of a young female presenting with cervicobrachial pain due to two SSP-MMNSTs arising from C5-6 right spinal roots.

Case description: We report a case of a 28-year-old woman presenting with right arm weakness and dysesthesia. Clinical examination and neuroimaging were performed, and, following surgical removal of both lesions, a histological diagnosis of SSP-MMNST was obtained.

Results: The literature review identified 21 eligible studies assessing 23 patients with SSP-MMNST, with a mean onset age of 41 years and a slight male gender preference. The lumbar district was the most involved spinal segment. Gross-total resection (GTR) was the treatment of choice in all amenable cases, followed in selected cases with residual tumor by adjuvant radiotherapy or chemotherapy. The metastatic and recurrence rates were 31.58% and 36.8%, respectively.

Conclusion: Differently from common schwannomas, MMNST represents a rare disease with known recurrence and metastatization propensity. As reported in our review, SSP-MMNST has a greater recurrence rate when compared to other forms of spinal MMNST, raising questions about the greater aggressiveness of the former. We also found that residual disease is related to a higher risk of systemic

disease spreading. This metastatic potential, usually associated with primary lumbar localization, is characterized by a slight male prevalence. Indeed, whenever GTR is unachievable, considering the higher recurrence rate, adjuvant radiation therapy should be taken into consideration.

KEYWORDS

malignant melanotic nerve sheath tumor, spinal, nerve sheath, tumor, psammomatous, sporadic, case report, melanotic schwannoma

Introduction

Malignant melanotic nerve sheath tumor (MMNST) represents a rare variant of nerve sheath neoplasms and accounts for less than 1% of all primary peripheral nerve sheath tumors (1). MMNST predominantly develops from spinal or visceral autonomic nerves (2). Considering its histological and ultrastructural traits of schwannomian differentiation, MMNST was historically considered an atypical variant of schwannoma, hence the definition of "Melanotic schwannoma" (3). However, given its recently uncovered different genetic profile, MMNST now represents a distinct malignant entity, as reported in the 2020 World Health Organization (WHO) classification of soft tissue tumors and in the 2021 WHO classification of central nervous system (CNS) tumors (4, 5). Psammomatous MMNST is an even rarer variant of MMNST, often arising along with the gastrointestinal tract-related nerves or in the extremities (6). The first reported case of MMNST was that by Millar et al. in 1932. The Authors described an uncommon pigmented neural tumor stemming from a sympathetic nerve in the thoracic region (7). The coining of the term would come later, with the 1975 Fu et al. publication (8).

MMNSTs are categorized according to two main groups. The first one is represented by its association with Carney Complex (CC). This entity features autosomal dominant inheritance and is characterized by patchy skin pigmentation, endocrine hyperactivity, and cardiac, mammary, and cutaneous myxomas (9, 10). About 50% of all MMNSTs are associated with CC (9). The second group of MMNSTs includes the presence of round concentric calcifications, known as psammoma bodies. Around 50% of all MMNSTs are psammomatous, and about half of these cases are CC-related (11). Therefore, it is crucial to rule out CC in MMNST patients and consider the possibility of sporadic cases of the disease. Additionally, few reported cases were associated with neurofibromatosis (12).

MMNST displays both malignant and metastatic potential depending on its histology. Microscopically, MMNST features spindle-shaped and epithelioid cells in intertwining fascicles, with a significant concentration of melanin both in the neoplastic cells and in the associated melanophages (1).

Clinical presentation depends on anatomical location. MMNST typically arises along the spinal nerve sheath (13), thus explaining frequent symptoms such as pain and paraesthesia (14–17).

To date, the literature has reported approximately 150 cases of MMNST. In this paper, we review the literature on SSP-MMNST in order to improve the knowledge of this disease, focusing on clinical, and diagnostic data, as well as investigating possible pathogenetic mechanisms to better implement therapeutic strategies. We also report a case of a young female presenting with cervicobrachial pain due to two SSP-MMNSTs arising from C5 and C6 right roots.

Results

A PRISMA flowchart is presented in Figure 1. A primary search returned 449 records. After excluding 192 duplicates, 257 records were screened. After screening titles and abstracts and removing articles without full-text, 85 full-text articles were left and evaluated for eligibility. Given that 64 of them were ineligible for inclusion, we selected 21 full-text papers for the review. We identified 23 cases of SSP-MMNST, including 9 (39.13%) females and 14 (60.87%) males. The male-to-female ratio was 1.56:1, suggesting a slight male prevalence of the disease. The mean age of onset of the disease was 40.39 ± 13.11 years. Spinal localization was as follows: 4 cervical (16.67%), 7 thoracic (29.17%), 9 lumbar (37.5%), and 4 sacral (16.67%). Metastases were reported in 6 cases (4 male, 2 female) with a metastatic rate of 31.58%. Lungs were the main site of metastatization (50%), followed by spinal cord, meninges, bone, chest wall, lymph nodes, and brain parenchyma. In 83.33% of the metastatic cases, the primary tumor site was in the lumbar region, particularly in L4/L5. The mean age of metastatic patients was 37.33 ± 9.09 years. There was no significant difference between the mean age of metastatic and non-metastatic patients (p=0.519). Nonetheless, males appeared slightly more at risk of developing metastasis, with a relative risk (RR) of 1.45 (p=0.6082). Treatment approaches in patients included gross-total resection (GTR) in 17

Abbreviations: CC, Carney's complex; CNS, central nervous system; CT, Computed Tomography; EMG, Electromyography; FDG-PET/CT, Fluorodeoxyglucose-Positron Emission Tomography/Computed Tomography; GTR, Gross-Total Resection; MMNST, Malignant Melanotic Nerve Sheath Tumor; MRI, magnetic resonance imaging; PAS, periodic acid-Schiff; SSP-MMNST, Sporadic Spinal Psammomatous Malignant Melanotic Nerve Sheath Tumor; STR, Sub-Total Resection; RR, Relative risk; WHO, World Health Organization.

cases (73.91%), and subtotal resection in 5 cases (22.73%), while one refused the treatment. Patients underwent adjuvant radiotherapy in 4 cases (18.18%), with only one without any recurrence. The disease recurrence rate among the 19 patients with known data was 36.84% (7/19). Of these 7 patients, 4 succumbed to the disease (57.14%), 2 were alive with disease stability (28.57%), and 1 was not reported. Of these 7 patients with disease recurrence, 4 had metastatic locations (57.14%). Finally, 3 of 5 (60%) patients who underwent subtotal resection (STR) developed disease recurrence. On the other hand, only 4 of the 17 patients that underwent GTR suffered a recurrence (23.53%). Considering all 23 patients with SSP-MMNST, the outcome was unknown in 6 patients, 9 were disease-free (52.94%), 6 died, and 2 were still affected by the disease at the time of follow-up. Follow-up was different for each of the cases.

Case presentation

A 28-year-old woman presented with a one-year history of cervical pain radiating to the right arm. She had no history of other illnesses, surgeries, related traumas, or a family history of spinal diseases. No skin pigmentary abnormalities were observed. Neurological examination revealed mild weakness in the right arm and dysesthesia in the C5-C6 right dermatome. Electromyography (EMG) testing was performed and did not disclose any abnormality. Spinal cord Magnetic Resonance Imaging (MRI) demonstrated two right intracanal extradural and intra/extra-foraminal lesions at the cervical level: the first lesion measured 20x10mm and was located at the C6-C7 level with paravertebral extension and "dumbbell" shape; the other smaller one was located at C5-C6 level (Figure 2).

The case was discussed by a multidisciplinary team which set the indication for surgical removal of the lesions. The patient gave written informed consent for the procedure. On the day of surgery, the patient was positioned supine, and a laminectomy was performed at the C5-C7 levels. Through a microscopic technique and an extended transcanalar approach, a GTR of intracanal, intra-foraminal, and paravertebral components of the two lesions was performed. Fat tissue was placed to reinforce the dural closure. The postoperative course was uneventful and characterized by strength recovery. On the other hand, dysesthesia slightly improved, but never recovered completely. The patient underwent a postoperative cervical MRI, which confirmed radical excision of both lesions (Figure 2). Surgical specimen underwent histopathological examination, which showed spindle-shaped epithelioid cells with eosinophilic cytoplasm carrying abundant melanin and scattered psammoma bodies. Neoplastic cells featured nuclear polymorphisms and evident nucleoli as well (Figure 3). Immunochemistry showed cellular positivity for " HMB-45, S100,

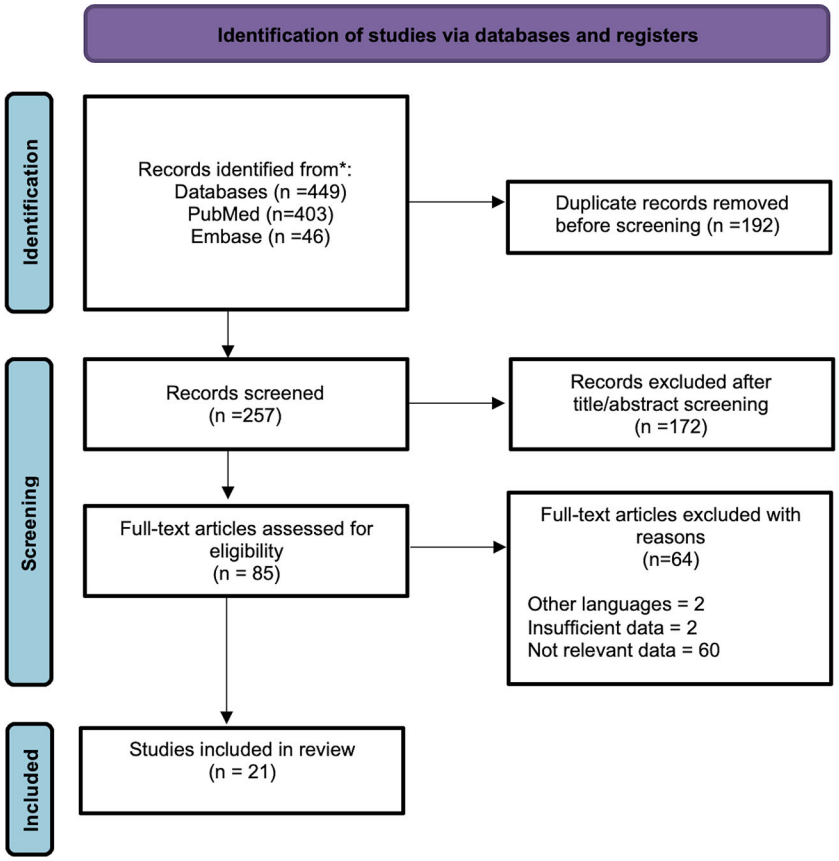

FIGURE 1
PRISMA flowchart diagram.

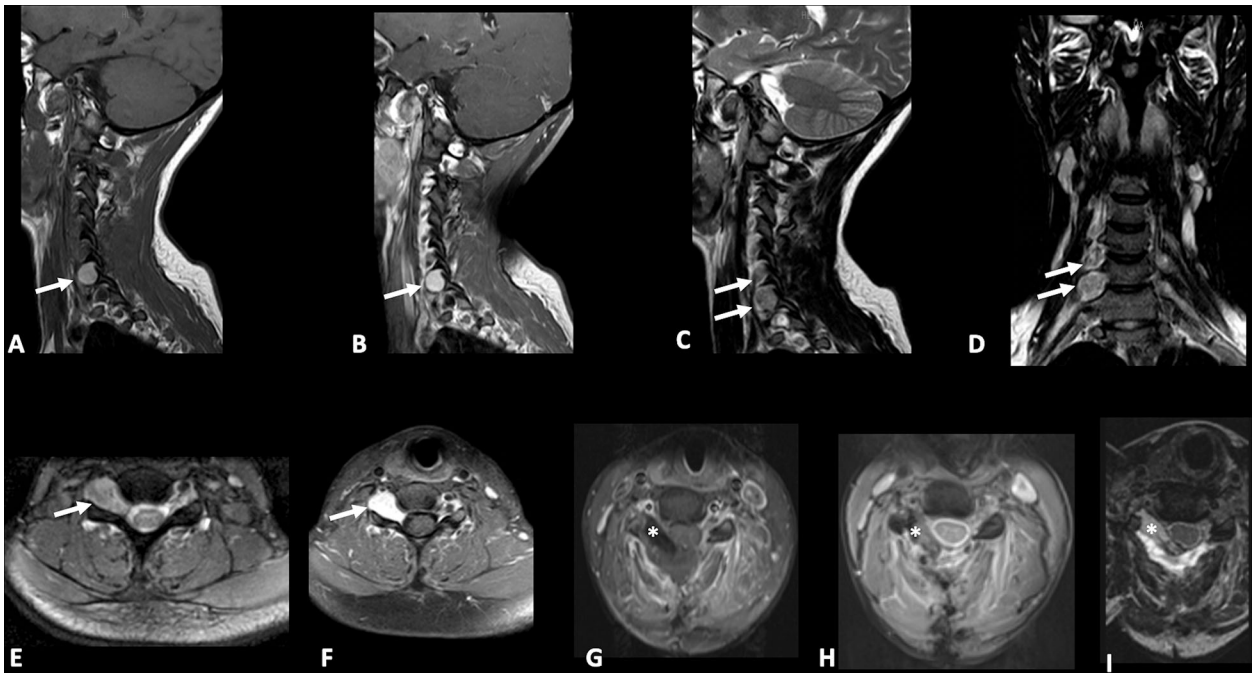

FIGURE 2
Pre-operative sagittal T1-weighted **(A)**, sagittal **(B)** and axial **(F)** post-gadolinium T1-weighted, sagittal **(C)**, coronal **(D)**, axial **(E)** T2-weighted Nuclear Magnetic Resonance (MRI) images demonstrating the presence of two right sided extradural spinal lesions (arrows) at C5-C7 levels one of which is larger with intraforaminal and paravertebral extension and "dumbbell" shape. Postoperative axial post-gadolinium T1-weighted and fat suppression **(G)**, Gradient echo (GRE) **(H)**, and T2-weighted **(I)** MRI images demonstrating gross total resection (GTR) of lesions and placement of fat tissue (asterisk) to reinforce dural closure.

Synaptophysin, Melan-A and Collagen-IV ", thereby confirming a diagnosis of MNNST. MIB-1 proliferative index was 4-5%. To rule out CC, molecular screening on *PRKAR1A* gene was performed using Sanger sequencing, and no germline pathogenic variant in *PRKAR1A* was identified. Concerning the young age of the patient, research on the pathogenic variant in phacomatosis susceptibility genes (*NF1, NF2, SPRED1, SMARCB1, LZTR1)* and other 24 genes relevant in the pathogenesis of nervous system tumors (*TP53, EGFR, PDGFRA, PTEN, PIK3CA, PIK3R, RB1, NOTCH1, CDK4, CDKN2A, CDKN2B, IDH1, IDH2, FUBP1 CIC, TACC3, TERTp, ATRX, DAXX, FGFR3, ACVR1, H3F3A, KIAA1549 BRAF)*, was performed using a customized gene panel on lymphocyte DNA and tumor tissue. No pathogenic variants of those genes were detected in both tissues. 30 days after the surgical procedure, a whole-body Fluorodeoxyglucose-positron emission tomography/computed tomography (FDG-PET/CT) was performed, showing no residual focal pathology nor metastasis, and an echocardiogram revealed no cardiac myxoma. One year after surgery, the patient was in clinical and radiological remission without any signs of recurrence of the disease as confirmed by a recent one-year FDG-PET/CT.

Discussion

SSP-MMNST is a rare, aggressive, and diagnostically challenging tumor of spinal nerves. We reviewed cases of SSP-MMNST by performing a literature search on PubMed and Embase databases. Their features are summarized in Table 1. It should be noted that some case reports did not include complete clinical, treatment, and genetic data of patients.

MMNST, formerly known as Melanotic Schwannoma or Schwannian melanotic tumor, was classified as a malignant lesion in the 2020 WHO classification of soft tissue tumors (4). The neoplasm rarely affects children and most commonly arises in adults, presenting as a sporadic lesion or as part of CC. The mean age of presentation is 38 years and no geographic, racial, ethnic, or gender preferences have been reported so far (35, 36). MMNST development in younger patients may be related to Carney syndrome (24). Psammomatous variants may be seen in patients with CC and arise a decade earlier than isolated sporadic cases, with a prevalence peak in the third decade of life (24, 37). In our analysis, the average disease age of onset for SSP-MMNSTs was 40±13 years (range 17 to 65 years), with slight male prevalence (1.56:1, M:F ratio). This is in contrast with previous studies in which no significant sex predilection was reported.

MMNST generally arises from spinal nerves and sympathetic ganglia as a single lesion (6, 9, 23). Nonetheless, literature reports scarce occurrences in other sites such as sympathetic chains, cranial nerve roots, peripheral nerves, cerebellum, orbit, choroids, soft tissue, alveolar nerves, palate, parotid gland, heart, oral cavity, oesophageal wall, pancreas, trachea, and bones (2, 10, 38–45). Spinal MMNST occurs in the lumbosacral region in 47.2% of cases, in the thoracic tract in 30.5%, and in the cervical region in 22.2%. The tumor may grow both in an intramedullary and extramedullary pattern. Furthermore, the lesion usually moves into the vertebral foramen or paravertebrally mainly affecting the

posterior nerve roots (6, 7, 20, 46–48). Our review focused on SSP-MMNST and showed that the lumbar district is the most affected one, with no significant difference between the right and left sides.

The clinical presentation of spinal MMNST is related to its anatomical location. Approximately one-third of cases are asymptomatic (9). On the contrary, symptoms of spinal nerve and spinal cord involvement, which are observed in 35.5% of patients, include radicular and back pain, dysesthesia, progressive sensory and motor deficits, ataxia, and sphincter disorders (38). The peculiar combination of radicular and back pain leads to misdiagnosis, with discopathy being the most frequent one. Mechanical dysfunction of adjacent organs due to compression is reported in 13% of cases (49). Complications vary according to tumor location and may include CC sequelae such as heart failure and stroke (1). Our case was characterized by mild weakness in the right arm and dysesthesia in the C5-C6 right dermatome with progressive deterioration within a year.

Unlike common schwannomas, MMNST is prone to local recurrence and displays metastatic potential (6, 9, 39). Metastases primarily occur in the lung and pleura but may also involve mediastinum, diaphragm, pericardium, endocardium, bone, liver, and spleen (6, 9, 38). In their studies, Torres-Mora et al. and Alexiev et al. showed local recurrence in 15 to 35% of cases and a metastasis rate of 26% to 44% (1, 6).

Our review on SSP-MMNST demonstrated metastasis occurrence in 31.58% of cases, with male prevalence (66.6%) and with no statistically significant difference from the metastatic rate of spinal MMNST (p=0.463) (40). The main metastatic site was lung parenchyma, consistent with previous literature.

In 83% of cases of metastasis, the primitive tumor developed in the lumbar region with a slightly greater risk in males (RR=1.45, p=0.608). The mean age in patients with metastatic disease was lower than non-metastatic ones (37.33 ± 9 vs 42 ± 15 years), with no significant difference.

Comparing whole-body MMNST data (6) with ours on SSP-MMNST, we observed no significant difference in the metastasic rate (44% vs 31.58%, p= 0.563) nor in the recurrence rate (35% vs 36.84%, p = 0.8833). Furthermore, when considering only sporadic spinal MMNSTs (40) and comparing them with our SSP-MMNSTs, we did not find a significant difference in the rate of metastasis (32.7% vs 31.58%, p= 0.9273) nor recurrence (25% vs 36.8%, p= 0.2639). These results seem to support the hypothesis that this histological type has no greater local or distant aggressiveness than sporadic and spinal non-psammomatous cases and whole-body MMNST. We believe that the lack of significant difference between the spinal sporadic MMNST cases and our SSP-MMNST ones may arise from the small sample size available. Nevertheless, the recurrence rate of 36.8% in SSP-MMNST versus 25% in sporadic spinal MMNST appears to be an interesting finding that, if confirmed, could reveal a greater aggressiveness of the former.

Histologically, MMNST generally consists of a single ovoid lesion, and it is rarely multifocal. Adjacent bone erosion may be observed (6, 9, 23, 41). Although being a circumscribed tumor, MMNST does not feature any capsule, in contrast to the typical schwannoma. This characteristic may reflect the potential aggressiveness of the disease. Microscopically, spindle-shaped and plump epithelioid cells appear in intertwined fascicles or nests (1). Melanin accretions in the neoplastic cells and associated melanophages are usually identified. Cytoplasmic pigmentation is highly variable. The pigment is positive for silver Fontana-Masson melanin staining and negative for Prussian blue and periodic acid-Schiff (PAS) staining (50). Rare mitoses are discernible in most lesions. MMNSTs typically lack Verocay bodies, microcysts and thick-walled hyalinized blood vessels (42). The criteria for malignancy in MMNST are not yet fully established. Nonetheless, histological characteristics like large vesicular nuclei with macronucleoli, intense mitotic activity, and necrosis point towards aggressive behavior (6, 38). Immunohistochemical staining for S100, SOX10, HMB-45, Melan-A, p16 and vimentin yields positive results, whereas GFAP, EMA, and CK staining are mostly negative (6, 9, 20, 41–45, 49, 50). All MMNST cases

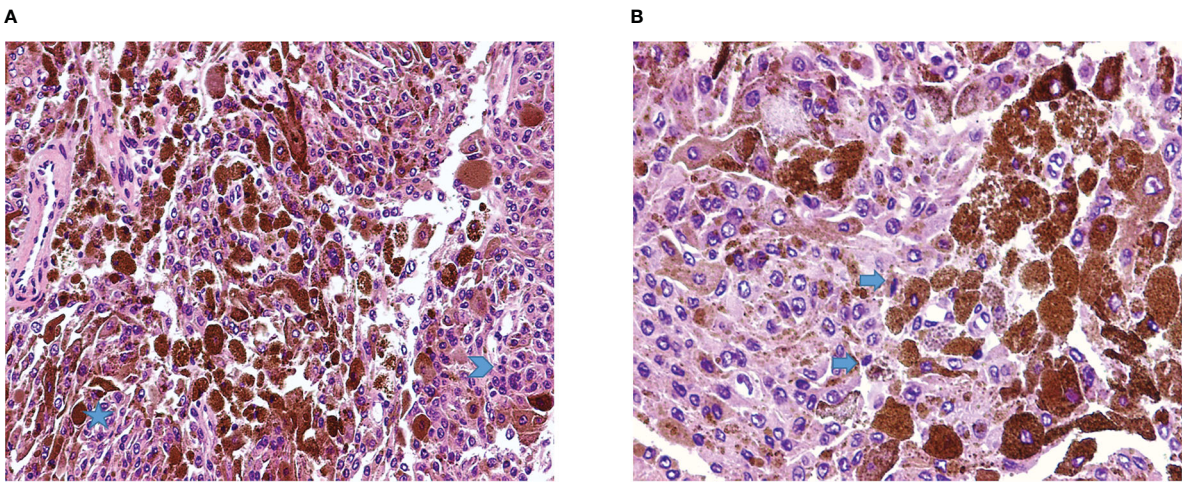

FIGURE 3
(A) Malignant melanotic nerve sheath tumor (MMNST) composed by pleomorphic cells, with spindle to polygonal shape, organized on fascicles (star) or sheets of roughly syncytial epithelioid cells (arrowhead), and numerous elements with heavy pigment deposits (H&E, magnification 20x).
(B) Cellular details show the presence of occasional mitoses (arrows) and brown finely granular melanin pigment (H&E, magnification 40x).

TABLE 1 Reported cases of sporadic spinal psammomatous melanotic schwannoma.

Authors	Year	Sex	Age	L	NR	Clinical	Met	T	R	O
Killeen et al. (18)	1988	F	26	S	S1	5-year lombalgia and leg pain	NA	GTR	NO	Resolution
Hollinger et al. (19)	1999	M	47	T	T12	3-year back and leg pain	NO	GTR	NO	Resolution
Vallat-Decouvelaere et al. (20)	1999	F	35	L	L4	3-year lombalgia	Bone, lymph nodes	GTR	6-year	72/DOD
Vallat-Devouvelaere et al. (20)	1999	M	27	L	L5	lombalgia	Lung, pleura	GTR	NO	72/DOD
Cummings et al. (21)	2000	M	51	S	S2	8-month lombalgia	NA	Declined Surgery	NA	NA
Kuchelmeister et al.(22)	2004	F	53	C	C6	2-year brachialgia with radicular radiation of pain into the right digits I-III	NO	GTR	NO	Resolution
Buhl et al.(23)	2006	M	28	L, S	L5-S1 + multiple small lesions	4-week lombalgia and sciatalgia	NO	GTR	2,5-year	30/AWD
Marton et al. (24)	2007	F	30	C	C3	6-month neck pain and spasms	NO	GTR	12-month	12/AWD
Azarpira et al.(25)	2009	M	37	L	L2	8-month lombalgia	NA	GTR	NA	NA
Arvanitis (14)	2010	M	36	L	L3	Back pain, weakness, weight loss	NA	STR x2	NA	NA
Izquierdo et al.(26)	2010	F	29	T	T8	Leg paresthesia, gait disturbance, muscle spasms	NO	GTR	NO	Resolution
Zhao et al. (27)	2011	M	46	C	C7	1-year neck pain, hand weakness	NO	GTR +RAD	NO	Resolution
Shields et al. (11)	2011	F	65	T	T7	Back pain	NO	STR +RAD	8-month	8/DOD
Shields et al. (11)	2011	M	33	L	L5	Lombalgia with radicular irradiation on the leg	Lung	STR +RAD	2-year	48/DOD
Mahesh et al. (28)	2014	M	67	T	T8-T12	2-week paraparesis, constipation, dysuria	NO	GTR	NO	Resolution
Bakan et al. (15)	2015	F	31	T	T4	Back pain	NO	GTR	NO	Resolution
Shabani et al. (29)	2015	M	54	C	C5	Incidental, on monitoring developed cervicobrachialgia	Lower spinal nerve root	GTR	3-month	7/DOD
Guzel et al. (17)	2016	M	36	L	L5	3-month lombalgia	NO	GTR	NO	Resolution
Khoo et al. (30)	2016	F	36	L	L5	4-year hip and leg pain	Brain and meninges	STR x2	10-month	NA
Mahmood et al.(31)	2016	M	17	T	T3	6-months pain and discomfort in the right upper chest	NO	GTR	NO	NA
Takatori et al.(32)	2020	M	39	L	L4	Lombalgia, numbness	Lungs, spinal cord, chest wall, stomach	STR +RAD	NO	22/DOD
Nagashima et al. (33)	2020	M	48	S	S2	6-month lombosciatalgia, dysuria	NO	GTR	NO	Resolution
Yeom et al. (34)	2022	F	58	T	T11-T12	Low back pain, paresthesia and cold sensation in both legs for years	NO	GTR	NA	NA

L, location; NR, nerve root; Met, metastasis; T, treatment; R, recurrence; O, outcome; DOD, Death of Disease; AWD, Alive with Disease; RAD,Radiation; NA, Not Applicable.

display positive laminin and collagen IV linear and pericellular immunoreactions (50). Aside from our case report, we identified two other MMNST cases with a hemorrhagic presentation, one of which was a heart attack mimicker (27, 40). In our case, the histological features matched with data available in the literature (Figure 3).

MMNST pathogenesis is still poorly understood. Several theories about histogenesis of the tumor have been described. Schwann cells and melanocytes share both their neuroectodermal origin and migration routes. Given this common developmental lineage, Schwann cells may be capable of synthesizing melanin under specific circumstances (18, 51, 52). Further hypotheses point to a melanomatous transformation of neoplastic Schwann cells (53).

Genetically, MMNST features a complex karyotype with recurring 22q band monosomy, variable whole chromosomal gains, and recurrent losses usually affecting chromosomes 1 and 21 and chromosome arm 17p.45 (54). Approximately half of the psammomatous cases are associated with CC, an autosomal dominant genetic disease harboring a chromosome 17 mutation that affects the cAMP-dependent protein kinase type I regulatory subunit alpha (*PRKAR1A*) gene (9, 42). CC diagnosis requires at least two major clinical findings. However, a single finding is sufficient in cases of positivity for the inactivating *PRKAR1A* gene mutation (38). MMNST may also develop in neurofibromatosis type I (12, 48). Recent cytogenetic studies demonstrated trisomy 6p at ring chromosome 11 in MMNST, suggesting some similarities with malignant melanoma. However, MMNST lacks the prototypical BRAFV600E mutation (55).

MMNST diagnosis is based on clinical, histopathological, and instrumental findings. The histological diagnosis requires careful differential considerations between neurofibroma, pigmented dermatofibrosarcoma protuberans, melanocytoma, and malignant melanoma.

Our case matched previous literature, with both tumors being positive for HMB-45, S100, Synaptophysin, Melan-A, and Collagen-IV. MIB-1 proliferative index was 4-5%. Phacomatosis susceptibility and CNS tumorigenesis genes were also investigated with negative results. Their negativity allowed us to exclude melanoma, CC, and Neurofibromatosis.

Radiologically, SSP-MMNST is characterized by hyperintensity in T1-weighted sequences, hypointensity in T2-weighted sequences, and homogeneous post-contrast enhancement (Table 2). These features were confirmed in our case (Figure 2). By contrast, schwannomas often present hypointensity in T1 and hyperintensity in T2 (56–58). Melanin displays paramagnetic effects, leading to stable free radicals. Essentially, melanin protons have shorter T1 and T2 relaxation times. Nevertheless, melanin concentration and tumor density are not always consistent. On axial images, the tumor may appear dumbbell-shaped with varying relationships to the medulla and dura. According to the Asazuma et al. classification (59), dumbbell schwannomas are classified into 6 types with our case classified as type IIb (Extradural, inside the spinal canal, intraforaminal and paravertebral).

FDG PET/CT provides a unique contribution to: (a) the differential diagnosis of benign and malignant lesions, (b) the detection of covert metastases, (c) the monitoring of treatment response, and (d) the evaluation of MMNST prognosis (6, 9, 39, 60, 61). The patient in our case underwent two full-body FDG-PET-CT scans, the first in the immediate post-operative period and the second at one-year follow-up. In both cases, the scan was negative for focal uptake areas, ruling out disease recurrence and metastasis.

Surgery represents the cornerstone of treatment for MMNST, with GTR being the gold standard for all subtypes. During surgery, a residual tumor capsule may be left to prevent spinal cord injury if the tumor is closely adherent (62, 63).

In our review on SSP-MMNST, the most common approach was GTR in 73.91% of cases. Among these, only 23.53% developed disease recurrence, as opposed to 60% of patients who underwent STR. The total recurrence rate was 36.84%, and 57.14% of that percentage was associated with metastasis. This finding may suggest that recurrent SSP-MMNSTs tend to be more aggressive and, therefore more prone to spread systemically.

Given the limited number of cases, post-surgical management is controversial. No current guidelines for adjuvant treatment in MMNST are available (38, 50). Some studies show a beneficial role of adjuvant radiotherapy in post-operative tumor residuals, reducing the rate of relapse and metastasis during a 24-month follow-up (50). Fractionated radiotherapy is a suitable option for complex MMNST close to

TABLE 2 Comparison of Spinal MMNST and SSP-MMNST.

	Spinal MMNST	SSP-MMNST
Epidemiology	35-55 years	40±13
Associated syndromes	Carney's complex	Sporadic: PRKAR1A, NF2 and BRAFv606 negative. No evidence of skin lesions, myxomas nor endocrinological tumors.
Location	Thoracic (33.8%), lumbar (27.3%), cervical (26%), sacral (13%)	Lumbar (37.5%), thoracic (29.17%), cervical (16.67%), sacral (16.67%)
Sign and symptoms	Dysesthesia, pain	Dysesthesia, pain
Neuroradiology	T1 hyperintense, T2 hyperintense	T1 hyperintense, T2 hyperintense
Treatment	GTR if symptomatic, consider adjuvant chemotherapy or radiotherapy	GTR if symptomatic, consider adjuvant chemotherapy or radiotherapy
Recurrence	25%	36.8%
Metastasis	32.7%	31.5%

susceptible structures, such as the spinal cord, although no significant data on mortality reduction are yet available (38). Indeed, some studies have recommended 54 Gy fractionated radiation therapy applied to the spine (46). Spinal stereotactic radiosurgery may also be considered. Chemotherapy has instead demonstrated low response rates and no mortality benefit (64). In our analysis, radiotherapy was employed in only 18.18% of cases as an adjuvant treatment following STR. Given the metastatic potential of SSP-MMNST, these data seem to suggest that, whenever residual disease is left, adjuvant radiotherapy may be appropriate.

Conclusion

Differently from common schwannomas, MMNST represents a rare disease with known recurrence and metastatization propensity. As reported in our review, SSP-MMNST has a greater recurrence rate when compared to other forms of spinal MMNST, raising questions about its greater aggressiveness. We also found that residual disease is related to a higher risk of systemic spreading. This metastatic potential, usually associated with primary lumbar localization, is characterized by a slight male prevalence. Indeed, whenever GTR is unachievable, considering the higher recurrence rate, adjuvant radiation therapy should be taken into consideration.

Data availability statement

The original contributions presented in the study are included in the article/supplementary material. Further inquiries can be directed to the corresponding author.

Ethics statement

Ethical review and approval was not required for the study on human participants in accordance with the local legislation and institutional requirements. The patients/participants provided their written informed consent to participate in this study. Written informed consent was obtained from the individual(s) for the publication of any potentially identifiable images or data included in this article. Patient signed informed consent regarding publishing his data and photographs.

Author contributions

GB, EM, and MB performed the clinical assessment. GB, AG, EM, ER, PA, and GI critically reviewed the literature and drafted the manuscript. All authors were responsible for important intellectual content. All authors contributed to the article and approved the submitted version.

Funding

This work was supported by the Italian Ministry of Health (RRC).

Conflict of interest

The authors declare that the research was conducted in the absence of any commercial or financial relationships that could be construed as a potential conflict of interest.

Publisher's note

References

1. Alexiev BA, Chou PM, Jennings LJ. Pathology of melanotic schwannoma. *Arch Pathol Lab Med Allen Press* (2018) 142:1517–23. doi: 10.5858/arpa.2017-0162-RA

2. Brierley JD, Asamura H, Eycken EV, Rous B eds. *BONE AND SOFT TISSUE TUMOURS*. TNM Atlas: Wiley (2021) p. 209–25.

3. Hodson JJ. An intra-osseous tumor combination of biological importance–invasion of a melanotic schwannoma by an adamantinoma. *J Pathol Bacteriol* (1961) 82:257–66. doi: 10.1002/path.1700820203

4. Sbaraglia M, Bellan E, Dei Tos AP. The 2020 WHO classification of soft tissue tumours: news and perspectives. *Pathologica* (2020) 113:70–84. doi: 10.32074/1591-951X-213

5. Osborn AG, Louis DN, Poussaint TY, Linscott LL, Salzman KL. The 2021 world health organization classification of tumors of the central nervous system: What neuroradiologists need to know. *Am J Neuroradiology* (2022) 43:928–37. doi: 10.3174/ajnr.A7462

6. Torres-Mora J, Dry S, Li X, Binder S, Amin M, Folpe AL. Malignant melanotic schwannian tumor: A clinicopathologic, immunohistochemical, and gene expression profiling study of 40 cases, with a proposal for the reclassification of 'melanotic schwannoma'. *Am J Surg Pathol* (2014) 38:94–105. doi: 10.1097/PAS.0b013e3182a0a150

7. Millar WG. A malignant melanotic tumour of ganglion cells arising from a thoracic sympathetic ganglion. *J Pathol Bacteriol* (1932) 35:351–7. doi: 10.1002/path.1700350305

8. Fu Y-S, Kaye GI, Lattes R. Primary malignant melanocytic tumors of the sympathetic ganglia, with an ultrastructural study of one. *Cancer* (1975) 36:2029–41. doi: 10.1002/cncr.2820360917

9. Carney JA. Psammomatous melanotic schwannoma. a distinctive, heritable tumor with special associations, including cardiac myxoma and the cushing syndrome. *Am J Surg Pathol* (1990) 14:206–22. doi: 10.1097/00000478-199003000-00002

10. Aidan Carney J, Gordon H, Carpenter PC, Vittal Shenoy B, Go VLW. The complex of myxomas, spotty pigmentation, and endocrine overactivity. *Med (Baltimore)* (1985) 64:270–83. doi: 10.1097/00005792-198507000-00007

11. Shields C, Glassman S, LisaBE S, Raque G. Malignant psammomatous melanotic schwannoma of the spine: A component of Carney complex. *Surg Neurol Int* (2011) 2:136. doi: 10.4103/2152-7806.85609

12. Murakami T, Kiyosawa T, Murata S, Usui K, Ohtsuki M, Nakagawa H. Malignant schwannoma with melanocytic differentiation arising in a patient with neurofibromatosis. *Br J Dermatol* (2000) 143:1078–82. doi: 10.1046/j.1365-2133.2000.03849.x

13. Greenberg MS. *Neurology | Handbook of Neurosurgery [Internet]*. karger.com (2019). Available from: https://www.thieme.com/books-main/neurology/product/5411-handbook-of-neurosurgery.

14. Arvanitis LD. Melanotic schwannoma: A case with strong CD34 expression, with histogenetic implications. *Pathol Res Pract* (2010) 206:716–9. doi: 10.1016/j.prp.2010.02.011

15. Bakan S, Kayadibi Y, Ersen E, Vatankulu B, Ustundag N, Hasiloglu ZI. Primary psammomatous melanotic schwannoma of the spine. *Ann Thorac Surg* (2015) 99:e141–3. doi: 10.1016/j.athoracsur.2015.02.060

16. Chandran RS, Patil AK, Prabhakar RB, Balachandran K. Melanotic schwannoma of spine: Illustration of two cases with diverse clinical presentation and outcome. *Asian J Neurosurg* (2018) 13:881–4. doi: 10.4103/ajns.AJNS_353_16

17. Güzel E, Er U, Güzel A, Toktaş Z, Yaplcler Ö. Melanotic schwannoma of the L5 root. *Neuroradiol J* (2016) 29:219. doi: 10.1177/1971400916638359

18. Killeen RM DCBS. Melanocytic schwannoma. *Cancer* (1988) 62:174–83. doi: 10.1002/1097-0142(19880701)62:1<174::AID-CNCR2820620127>3.0.CO;2-G

19. Hollinger P, Godoy N, Sturzenegger M. Magnetic resonance imaging findings in isolated spinal psammomatous melanotic schwannoma [4]. *J Neurol* (1999) 246:1100–2. doi: 10.1007/s004150050522

20. Vallat-Decouvelaere AV, Wassef M, Lot G, Catala M, Moussalam M, Caruel N, et al. Spinal melanotic schwannoma: A tumour with poor prognosis. *Histopathology* (1999) 35:558–66. doi: 10.1046/j.1365-2559.1999.00786.x

21. Cummings TJ, Liu K, Jordan LK 3rd, Dodd LG. Fine-needle aspiration diagnosis of psammomatous melanotic schwannoma. *Diagn Cytopathol* (2000) 23(1):55–58. doi: 10.1002/1097-0339(200007)23:1<55::AID-DC13>3.0.CO;2-B

22. Kuchelmeister K, Lotz C, Schönmayr R, Schachenmayr W. April 2004: Woman in her early fifties with a cervical intraspinal and extraspinal mass lesion. *Brain pathology* (2004) 14(4): 453-4–458-9. doi: 10.1111/j.1750-3639.2004.tb00090.x

23. Buhl R, Barth H, Hugo HH, Mautner VF, Mehdorn HM. Intracranial and spinal melanotic schwannoma in the same patient. *J Neurooncol* (2004) 68:249–54. doi: 10.1023/B:NEON.0000033491.23654.6c

24. Marton E, Feletti A, Orvieto E, Longaitti P. Dumbbell-shaped c-2 psammomatous melanotic malignant schwannoma. case report and review of the literature. *J Neurosurg Spine* (2007) 6:591–9. doi: 10.3171/spi.2007.6.6.14

25. Azarpira N, Torabineghad S, Sepidbakht S, Rakei M, Bagheri MH. Cytologic findings in pigmented melanotic schwannoma. *Acta Cytol* (2009) 53(1):113–115. doi: 10.1159/000325096

26. Martinez Izquierdo MA, Lopez-Soto V, Saenz-Santamaria J, Lacruz-Pelea C. Intraoperative cytological findings in two cases of psammomatous melanotic schwannoma. *Cytopathology* (2011) 22:60–2. doi: 0.1111/j.1365-2303.2010.00740.x

27. Zhao QH, Zhi S, Wang Z, Tian JW. Psammomatous melanotic schwannoma with cystic changes from old hemorrhages in the cervical spinal canal: A case report. *Orthop Surg* (2011) 3:143–6. doi: 10.1111/j.1757-7861.2011.00133.x

28. Mahesh I, Karthikeyan VS, Malathi M. Spotty skin pigmentation and multiple blue naevi as cutaneous markers for spinal melanotic schwannoma. *BMJ Case Rep* (2014) 2014. doi: 10.1136/bcr-2013-201567

29. Shabani S, Fiore SM, Seidman R, Davis RP. Intraspinal psammomatous melanotic schwannoma not associated with Carney complex: Case report. *J Neurosurg Spine* (2015) 23:233–8. doi: 10.3171/2014.11.SPINE13990

30. Khoo M, Pressney I, Hargunani R, Tirabosco R. Melanotic schwannoma: An 11-year case series. *Skeletal Radiol* (2016) 45:29–34. doi: 10.1007/s00256-015-2256-8

31. Mahmood UB, Khan FW, Fatima B, Tariq MU, Fatimi SH. Primary melanotic schwannoma with typical histology. *J Coll Physicians Surgeons Pakistan* (2016) 26:707–10.

32. Takatori N, Hiyama A, Sakai D, Katoh H, Sato M, Watanabe M. A rare case of intraspinal psammomatous melanotic schwannoma: A case report. spine surg relat res. *Japanese Soc Spine Surg Related Res* (2020) 4:91. doi: 10.22603/ssrr.2019-0034

33. Nagashima Y, Nishimura Y, Eguchi K, Awaya T, Yoshikawa S, Haimoto S, et al. Intraosseous melanotic schwannoma in the sacrum mimicking primary bone tumor. NMC case rep J. *Japan Neurosurgical Soc* (2020) 7:107. doi: 10.2176/nmccrj.cr.2019-0238

34. Yeom JA, Song YS, Lee IS, Han IH, Choi KU. Malignant melanotic nerve sheath tumors in the spinal canal of psammomatous and non-psammomatous type: Two case reports. *World J Clin Cases* (2022) 10:8735–41. doi: 10.12998/wjcc.v10.i24.8735

35. Faria MHG, Dória-Netto RH, Osugue GJ, Queiroz L de S, Chaddad-Neto FE. Melanotic schwannoma of the cervical spine progressing with pulmonary metastasis: Case report. *Neurol Med Chir (Tokyo)* (2013) 53:712–6. doi: 10.2176/nmc.cr2012-0203

36. Koeller KK, Shih RY. Intradural extramedullary spinal neoplasms: Radiologic-pathologic correlation. *Radiographics Radiological Soc North America Inc.;* (2019) 39:468–90. doi: 10.1148/rg.2019180200

37. Keskin E, Ekmekci S, Oztekin O, Diniz G. Melanotic schwannomas are rarely seen pigmented tumors with unpredictable prognosis and challenging diagnosis. *Case Rep Pathol* (2017) 2017:1–4. doi: 10.1155/2017/1807879

38. Siordia JA, Golden TR. Current discoveries and management of psammomatous melanotic schwannoma. *J Cancer Tumor Int* (2016) 3:1–7. doi: 10.9734/JCTI/2016/23786

39. Kang YE, Jeong JO, Kim KH, Ki CS, Kim HJ. Malignant intercostal psammomatous melanotic schwannoma in a patient with Carney complex. *Korean J Intern Med* (2018) 33:1256. doi: 10.3904/kjim.2017.139

40. Soyland DJ, Goehner DR, Hoerschgen KM, Gust TD, Vuong SM. Hemorrhagic spinal melanotic schwannoma presenting as acute chest pain: A case report and literature review. *Surg Neurol Int* (2021) 12:164. doi: 10.25259/SNI_786_2020

41. Kurtkaya-Yapicier O, Scheithauer BW, Woodruff JM. The pathobiologic spectrum of schwannomas. *Histol Histopathol* (2003) 18(3):925–934. 10.14670/HH-18.925

42. Rodriguez FJ, Stratakis CA, Gareth D. Genetic predisposition to peripheral nerve neoplasia: diagnostic criteria and pathogenesis of neurofibromatoses. *Acta Neuropathol* (2012) 123(3):349–367. 10.1007/s00401-011-0935-7

43. Chetty R, Vajpeyi R, Penwick JL. Psammomatous melanotic schwannoma presenting as colonic polyps. *Virchows Archiv* (2007) 451:717–20. doi: 10.1007/s00428-007-0453-0

44. Choi SE, Cha YJ, Kim J, Cha H, Seo J, Kuh SU, et al. A rare case of aggressive melanotic schwannoma occurred in spinal nerve of a 59-Year-Old Male. *J Pathol Transl Med* (2017) 51:505. doi: 10.4132/jptm.2017.01.04

45. Li B, Chen Q. Melanotic schwannoma of thoracic spinal root mimics metastatic melanoma: A potential pitfall for misdiagnosis. *Int J Clin Exp Pathol* (2015) 8:8639.

46. Santaguida C, Sabbagh AJ, Guiot MC, Del Maestro RF. Aggressive intramedullary melanotic schwannoma: Case report. *Neurosurgery* (2004) 55(6):1430. doi: 10.1227/01.NEU.0000143617.25417.68

47. Solomon RA, Handler MS, Sedelli RV, Stein BM. Intramedullary melanotic schwannoma of the cervicomedullary junction. *Neurosurgery* (1987) 20:36–8. doi: 10.1227/00006123-198701000-00010

48. Zhang HY, Yang GH, Chen HJ, Wei B, Ke Q, Guo H, et al. Clinicopathological, immunohistochemical, and ultrastructural study of 13 cases of melanotic schwannoma. *Chin Med J (Engl)* (2005) 118:1451–61.

49. Merat R, Szalay-Quinodoz I, Laffitte E, Dermatopathology G–. *Psammomatous melanotic schwannoma: A challenging histological diagnosis*. karger.com (2015). Available at: https://www.karger.com/Article/Abstract/442708.

50. Gulati HK, Joshi AR, Anand M, Deshmukh SD. Non psammomatous melanocytic schwannoma presenting as a subcutaneous nodule: A rare presentation of a rare lesion. *Asian J Neurosurg* (2016) 11:317. doi: 10.4103/1793-5482.148789

51. Janzer RC, Makek M. Intraoral malignant melanotic schwannoma. ultrastructural evidence for melanogenesis by schwann's cells. *Arch Pathol Lab Med* (1983) 107:298–301.

52. Çulhaci N, Dikicioglu E, Meteoglu I, Bukru S. Multiple melanotic schwannoma. *Ann Diagn Pathol* (2003) 7(4):254–8. doi: 10.1016/s1092-9134(03)00073-x

53. Mandybur TI. Melanotic nerve sheath tumors. *J Neurosurg* (1974) 41:187–92. doi: 10.3171/jns.1974.41.2.0187

54. Koelsche C, Hovestadt V, Jones DTW, Capper D, Sturm D, Sahm F, et al. Melanotic tumors of the nervous system are characterized by distinct mutational, chromosomal and epigenomic profiles. *Brain Pathol* (2015) 25:202–8. doi: 10.1111/bpa.12228

55. Italiano A, Michalak S, Soulié P, Peyron AC, Pedeutour F. Trisomy 6p and ring chromosome 11 in a melanotic schwannoma suggest relation to malignant melanoma rather than conventional schwannoma. *Acta Neuropathol* (2011) 121:669–70. doi: 10.1007/s00401-011-0820-4

56. Bendszus M, Urbach H, Wolf HK, Schramm J, Solymosi L. Magnetic resonance imaging of intraspinal melanotic schwannoma. *Eur Radiol* (1998) 8:1197. doi: 10.1007/s003300050534

57. Küsters-Vandevelde HVN, van Engen-Van Grunsven IACH, Küsters B, van Dijk MRCF, Groenen PJTA, Wesseling P, et al. Improved discrimination of melanotic schwannoma from melanocytic lesions by combined morphological and GNAQ mutational analysis. *Acta Neuropathol* (2010) 120:755. doi: 10.1007/s00401-010-0749-z

58. Solomou G, Dulanka Silva AH, Wong A, Pohl U, Tzerakis N. Extramedullary malignant melanotic schwannoma of the spine: Case report and an up to date systematic review of the literature. *Ann Med Surg* (2020) 59:217. doi: 10.1016/j.amsu.2020.10.003

59. Asazuma T, Toyama Y, Maruiwa H, Fujimura Y, Hirabayashi K. Surgical strategy for cervical dumbbell tumors based on a three-dimensional classification. *Spine (Phila Pa 1976)* (2004) 29:E10–4. doi: 10.1097/01.BRS.0000103662.13689.76

60. Shen XZ, Wang W, Luo ZY. 18F-FDG PET/CT imaging for aggressive melanotic schwannoma of the L3 spinal root: A case report. *Med NLM (Medline)* (2021) 100: e24803. doi: 10.1097/MD.0000000000024803

61. Trufant JW, Brenn T, Fletcher CDM, Virata AR, Cook DL, Bosenberg MW. Melanotic schwannoma arising in association with nevus of ota: 2 cases suggesting a shared mechanism. *Am J Dermatopathology* (2009) 31:808–13. doi: 10.1097/DAD.0b013e3181accd0e

62. Chen D, Gu W. Subdural extramedullary melanotic schwannoma of the thoracic spinal cord: A case report. *Turk Neurosurg* (2015) 25:326–31. doi: 10.5137/1019-5149.JTN.8153-13.0

63. Xiao LL, Shun-Dong D. Melanotic schwannoma: Two cases of rare lesions. *Pathol Oncol Res* (2019) 25:1667–70. doi: 10.1007/s12253-018-0417-5

64. Watson JC, Stratakis CA, Bryant-Greenwood PK, Koch CA, Kirschner LS, Nguyen T, et al. Neurosurgical implications of Carney. *J Neurosurg* (2000) 92(3):413–418. doi: 10.3171/jns.2000.92.3.0413

Frontiers in Oncology

Advances knowledge of carcinogenesis and tumor progression for better treatment and management

The third most-cited oncology journal, which highlights research in carcinogenesis and tumor progression, bridging the gap between basic research and applications to imrpove diagnosis, therapeutics and management strategies.

Discover the latest Research Topics

See more →

Frontiers

Avenue du Tribunal-Fédéral 34
1005 Lausanne, Switzerland
frontiersin.org

Contact us

+41 (0)21 510 17 00
frontiersin.org/about/contact